Targeted Protein Degradation as a New Approach to Drug Discovery

Christopher Patrick Tinworth

A Thesis Submitted for the Degree of
Doctor of Philosophy

June 2017

Declaration

This thesis is the result of the author's original research. It has been composed by the author and has not been previously submitted for examination which has led to the award of a degree.

Signed: Date:

Abstract

Proteolysis targeting chimeras (Protacs) are heterobifunctional small molecules which induce targeted protein degradation by hijacking the natural intracellular quality control mechanism, the ubiquitin-proteasome system. Protacs simultaneously bind both a target protein and an E3 ubiquitin ligase, forming a ternary complex. The close proximity of the target protein and the E3 ligase allows transfer of the post-translational modifier ubiquitin onto the target protein, which allows the protein to be recognised and degraded into small peptidic fragments by the proteasome. The Protac approach offers several advantages over small-molecule inhibition alone as efficacy can be driven from low drug concentrations, extended duration of action can be achieved, and scaffolding functions of the target protein can be removed.

In this thesis, the application of Protac technology towards a series of disease-relevant proteins is explored. In Chapters 2 and 3, Protacs targeting the kinase ActR2B and the thyroid hormone receptor were developed as potential treatments for sarcopenia and hyperthyroidism, respectively. However, in both cases, no target degradation was observed.

Given the lack of degradation with the initial empirically selected targets, a distinct, non-selective approach to protein degradation was considered in Chapter 4. Protacs based on a highly promiscuous kinase inhibitor were designed and synthesised, then profiled using proteome-wide expression proteomics. This strategy allowed identification of several novel degradable targets, and also indicated proteins that may be more challenging to degrade. The opportunity for degradation selectivity in the absence of binding selectivity was also highlighted.

Having identified Bruton's tyrosine kinase (BTK) as one of these degradable targets, selective BTK Protacs were then studied in Chapter 5. Protacs based on the covalent inhibitor Ibrutinib led to the surprising discovery that covalent inhibition prevents Protac-mediated degradation of BTK. Protacs developed from a selective, reversible BTK inhibitor allowed rapid interrogation of the kinase as a prototypical Protac target.

Acknowledgements

This thesis would not have be possible without a great many people who have helped me through the duration of my PhD. Firstly, I am enormously grateful to my industrial supervisor Dr. John Harling for his constant guidance and direction, and for being kind enough to keep me on full-time. I thank my academic supervisor Prof. William J. Kerr for his outstanding support and backing throughout the process, and for sharing some unforgettable stories. I am also highly thankful to Dr. Harry Kelly for his support throughout the PhD programme and his dedication to my personal development over the past few years. I thank Dr. Ian Churcher for his encouragement and giving me great opportunities as DPU head.

Thank you to the Protein Degradation DPU, especially my chemistry colleagues Dr. Afjal Miah, Dr. Chris Tame, Ian Smith and Dr. Mark Rackham for sharing their invaluable advice and putting up with my music taste in the lab. I am grateful to Dr. Sebastien Campos for his support through the first year of my PhD. I would also like to acknowledge my Protein Degradation DPU biology colleagues, in particular Dr. Zuni Bassi for assistance generating biological data presented in this thesis. I thank Dr. Nico Zinn and Cellzome for carrying out expression proteomics experiments. I thank Andrea Malley and Dr. Laura Paterson for administrative support through the PhD programme, and GSK and the University of Strathclyde for funding. I also thank various analytical and screening groups across GSK for their assistance.

None of this would have ever been possible without the unconditional support and encouragement of my family. Thank you for nodding and smiling when I try to explain any of this to you, I hope this makes an adequate doorstop.

Contents

Abbreviations

Ac	Acetyl
Aq	Aqueous
ActR2B	Activin type IIB receptor
ALK	Activin receptor-like kinase
AML	Acute myeloid
ANO1	Anoctamin-1
AR	Androgen receptor
Arg	Arginine
ASC	Apoptosis-related speck-like protein containing a caspase recruitment domain
Asn	Asparagine
ATP	Adenosine triphosphate
BCR	B-cell receptor
BET	Bromodomain and Extra Terminal
BL	Burkitt's lymphoma
Boc	*tert*-Butyloxycarbonyl
BRD	Bromodomain containing protein
BTK	Bruton's tyrosine kinase
Chrom LogD	Lipophilicity measured chromatographically at pH 7.4
cIAP1	Cellular inhibitor of apoptosis protein 1
CLL	Chronic lymphocytic leukaemia
CLND	Chemiluminescent nitrogen detection
CRABPs	Cellular retinoic acid binding proteins
CRPC	Castration–resistant prostate cancer
CV	Column volumes
D_{max}	Degree of maximal substrate degradation
Da	Dalton
DBD	DNA binding domain
DBU	1,8-Diazabicyclo[5.4.0]undec-7-ene
DCE	1,2-Dichloroethane
DC_{50}	Concentration at which 50 % of substrate is degraded
DIPEA	*N*,*N*-Diisopropylethylamine

DMF	*N*,*N*-Dimethylformamide
DMSO	Dimethylsulfoxide
DNA	Deoxyribonucleic acid
dppf	1,1'- Bis(diphenylphosphino)ferrocene
DUB	Deubiquitinating enzyme
ER	Estrogen receptor
ERRα	Estrogen-related receptor alpha
ERK	Extracellular signal–regulated kinase
Et	Ethyl
FAK	Focal adhesion kinase
GFP	Green fluorescent protein
GST	Glutathione S-tranferase
h	Hour
H	Helix
HATU	1-[Bis(dimethylamino)methylene]-1*H*-1,2,3-triazolo[4,5-*b*]pyridinium 3-oxid hexafluorophosphate
HECT	Homologous to the E6-AP Carboxyl Terminus
HIF-1α	Hypoxia-inducible factor 1α
His	Histidine
HMBC	Heteronuclear multiple-bond correlation spectroscopy
HRMS	High resolution mass spectrometry
HSQC	Heteronuclear single quantum coherence spectroscopy
Hyp	Hydroxyproline
IAP	Inhibitor of apoptosis protein
IC_{50}	The compound/substance concentration required for 50 % inhibition
IL	Interleukin
IMiD	Immunomodulatory imide drugs
IR	Infrared spectroscopy
K	Lysine
LBD	Ligand binding domain
LCMS	Liquid chromatography mass spectrometry
Luc	Luciferase
m	Metre

M	Molar concentration
MAPK	Mitogen-activated protein kinase
MCL	Mantle cell lymphoma
MDAP	Mass directed automated preparative HPLC
MDM2	Human murine double minute 2
Me	Methyl
MetAP2	Methionine aminopeptidase 2
Min	Minute
MM	Multiple myeloma
MOM	Methoxymethyl
MP	Melting point
MW	Microwave
NAE	NEDD8-activating enzyme
NBS	*N*-Bromosuccinimide
NEDD8	Neural precursor cell-expressed developmentally-downregulated 8
NF-κB	Nuclear factor kappa-light-chain-enhancer of activated B cells
NHS	*N*-Hydroxysuccinimide
NIS	*N*-Iodosuccinimide
NLRP3	NOD-like receptor protein 3
NMP	*N*-Methyl-2-pyrrolidone
NMR	Nuclear magnetic resonance spectroscopy
PD	Pharmacodynamic
PEG	Polyethylene glycol
PH	Pleckstrin homology
pIC_{50}	-log (IC_{50})
PID	Primary immunological deficiency
PIP	Phosphatidylinositol (3,4,5)-trisphosphate
PK	Pharmacokinetic
PKC	Protein kinase C
PLCγ	Phospholipase C-γ
PPI	Protein-protein interaction
Protac	Proteolysis targeting chimera
PTM	Post-translational modification

RA	Rheumatoid arthritis
RING	Really interesting new gene
RIPK2	Receptor-interacting serine/threonine-protein kinase 2
RNAi	RNA interference
rt	Room temperature
RTK	Receptor tyrosine kinase
RXR	Retinoid X receptor
SAR	Structure-activity relationship
SCF	Skp Cullin F-box protein
SLP65	B cell linker protein
SERD	Selective estrogen receptor degrader
SNIPER	Specific and non-genetic IAP-dependent protein eraser
SPE	Solid phase extraction
SYK	Spleen tyrosine kinase
T_3	Triiodothyronine
T_4	Thyroxine
TBAF	Tetra-*n*-butyl ammonium fluoride
TFA	Trifluoroacetic acid
THF	Tetrahydrofuran
THPTA	Tris(3-hydroxypropyltriazolylmethyl)amine
TGFβ	Transforming growth factor beta
TI	Therapeutic index
TIPS	Triisopropylsilane
TKI	Tyrosine kinase inhibitor
TMT	Tandem mass tag
TR	Thyroid hormone receptor
TR-FRET	Time resolved fluorescence resonance energy transfer
UAE	Ubiquitin-activating enzyme
Ub	Ubiquitin
UPS	Ubiquitin-proteasome system
VEGFR	Vascular endothelial growth factor receptor
VHL	Von Hippel−Lindau protein
v/v	By volume
WM	Waldenstrom's macroglobulinaemia

w/w	By weight
xid	X-Linked immunodeficiency
XLA	X-linked agammaglobulinemia
°C	Degrees Celsius

1. Introduction

1.1 Contemporary Drug Discovery

The goal of much contemporary drug discovery is the inhibition of a biological process leading to a beneficial effect on a disease state. For intracellular targets, the predominant paradigm for achieving this is the use of synthetic small molecules which bind to and antagonise or inhibit a specific biological target through an appropriate functional binding site (Figure 1). However, for functional silencing of a specific target, this approach suffers from some key limitations.

Figure 1. Traditional small-molecule drug discovery process

Firstly, antagonistic efficacy is generally only achieved when the drug molecule is directly bound to and inhibiting the function of its target at high levels of occupancy (often >90 %).[1] Once the drug has been removed by metabolism or other clearance mechanisms, occupancy at the target site drops, biological function is restored, and the desired therapeutic effect diminishes. The requirement for high target exposure, high target occupancy along with the desired pharmacological effect has developed into a key indicator of Phase II survival of small molecules.[2]

Secondly, for a small molecule antagonist to be effective, it needs to bind with good affinity to its target with the direct consequence of inhibition of a specific biological function. This can usually be achieved when the biological target has a suitable binding site for a natural substrate or co-factor, often referred to as a ‘druggable’ target. Generating ligands for poorly tractable or ‘undruggable’ targets is particularly challenging when the protein to be modulated lacks high-affinity small molecule binding sites, or when the protein possesses multiple functions mediated through distal domains. This limits the number of proteins that may be targeted using small molecules alone; accordingly, a large proportion of the human disease-modifying proteome remains untapped by currently approved drugs.[3]

Strategies for the enhancing the pharmacodynamic efficacy of small molecule antagonists have become highly sought after in order to overcome the potential for attrition based on efficacy. One approach is modulation of binding kinetics of an inhibitor, where slowly dissociating ligands can extend target occupancy in order to sustain the desired pharmacodynamic effect (i.e. extension of k_{off}, Figure 2).[4,5] The issue with this approach is that slow dissociation can be challenging to design prospectively and such agents are often discovered through serendipitous processes.[6]

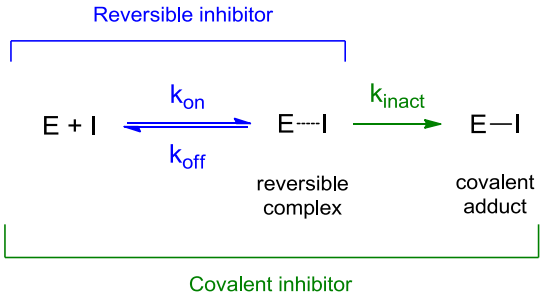

Figure 2. Comparing reversible and covalent inhibitors (E = enzyme, I = inhibitor)

The pinnacle of extended target occupancy is the use of irreversible covalent inhibitors, which form a permanent adduct with the target protein following reversible association (Figure 2). Pharmacodynamic effects are potentiated in this case since recovery of function is only possible after *de novo* cellular resynthesis of the protein, which for many targets can be slow.[7,8] This allows uncoupling of pharmacokinetics from pharmacodynamics to give extended duration of action in the absence of a freely circulating inhibitor (Figure 3).

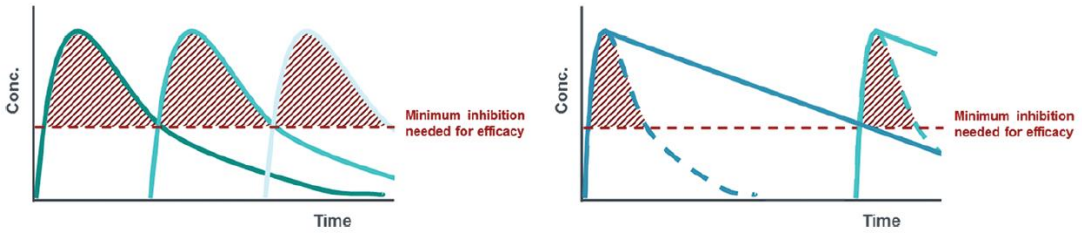

Figure 3.[9] Reversible inhibitors directly correlate drug concentration to continued efficacy (left), while covalent inhibitors do not require continued exposure to maintain efficacy (right)

While covalent inhibitors have clear advantages over reversible inhibitors, they also suffer from significant risks. Covalent protein-inhibitor adducts have the potential to induce an immunogenic response by generation of antibodies which target the epitope now rendered 'foreign' by the covalent modification, termed idiosyncratic toxicity.[10,11] High target selectivity is also required to prevent non-specific covalent binding which may compound these toxicity issues, particularly when dosing provides highly local drug exposure.

In order to overcome these limitations, new approaches are required which allow movement beyond the occupancy-based efficacy paradigm and also allow a wider range of less tractable targets to be modulated with small molecule agents. One such way of doing this is by removal of the protein target from the cell rather than inhibiting its function. Once a protein is physically removed from a cell, recovery of function will again depend on *de novo* protein resynthesis, whilst circumventing the toxicity risks associated with covalent inhibitors. Removal of the protein would also allow disruption of secondary functions not available through inhibition of a small molecule binding site.

Modulation of intracellular protein concentration can be achieved with nucleic acid-based agents that interfere with protein synthesis, such as anti-sense oligonucleotides and RNA interference (RNAi).[12–14] However, these approaches often suffer from issues with stability and delivery of nucleotides, and complexities of specific tissue targeting, with toxicity often caused by accumulation in non-target organs, such as the liver and kidney.[15] An attractive strategy is to achieve protein knockdown using synthetic small molecule agents, which offer many advantages in terms of dosing convenience, tunable biodistribution, and lower production costs. A potential approach to this is through hijacking of the physiological intracellular protein degradation pathway, namely the ubiquitin-proteasome system (UPS), to induce targeted protein degradation. This approach will be outlined and explored within this thesis.

1.2 The Ubiquitin-Proteasome System

In all cells, proteins are constantly being degraded to their constituent amino acids and replaced by newly synthesised protein.[16] The turnover rate of proteins can vary widely from a matter of minutes for regulatory proteins to a number of months for haemoglobin in red blood cells. There are two major degradative pathways in cells; the UPS is the major pathway for degradation of intracellular proteins,[17] while most other exogenous and intracellular material not targeted by the UPS are degraded through the lysosomal pathway.[18]

The UPS functions by localising targeted proteins to the 26S proteasome, a 2.5 MDa complex which induces proteolysis. This process is initiated by post-translational modification (PTM) of a protein substrate with ubiquitin, a 76 amino acid protein (Figure 4).[19–21] First, ubiquitin must be activated by an E1 ligase by formation of a thioester linkage between an E1 cysteine residue and the *C*-terminus of ubiquitin, accompanied by consumption of adenosine triphosphate (ATP).

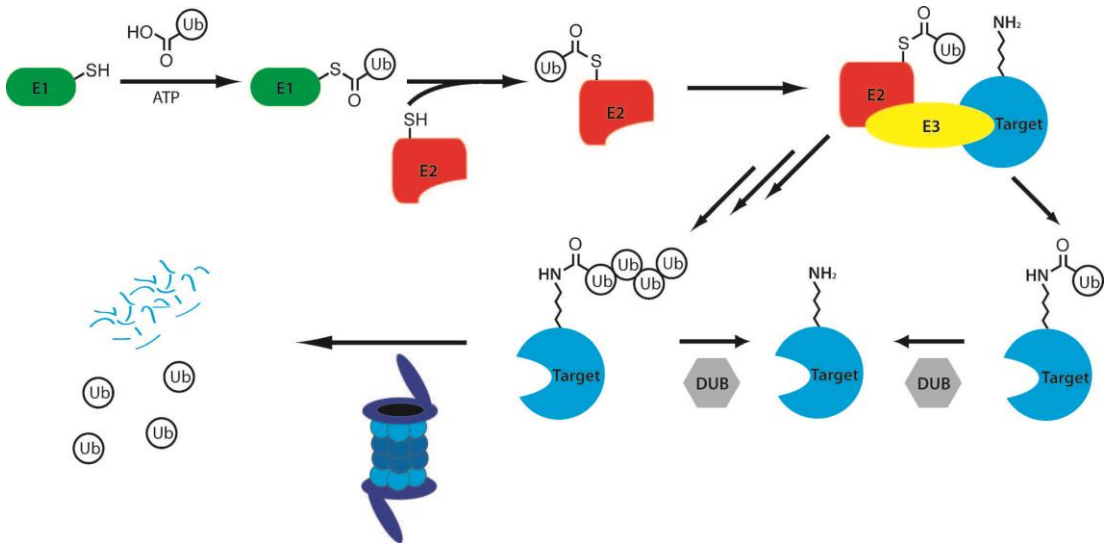

Figure 4.[22] The ubiquitin-proteasome system

The ubiquitin unit is then transferred to an E2 ligase, also known as a ubiquitin-conjugating enzyme, through a further activated thioester linkage. The E2 ligase then forms a ternary complex with an E3 ligase and the protein substrate, bringing the E2 and substrate into sufficiently close proximity to allow direct or indirect ubiquitin

transfer onto a surface-exposed lysine residue of the substrate. Direct or indirect ubiquitin transfer is dependent on the form of E3 ligase, which are either Really Interesting New Gene (RING) finger domain or Homologous to the E6-AP Carboxyl Terminus (HECT) domain type. RING finger domain proteins allow ubiquitin transfer directly onto the substrate from the E2 ligase through an E2-E3-substrate ternary complex, while HECT E3 ligases first accept ubiquitin to give a further E3 thioester intermediate, which then leads to ubiquitin transfer onto the substrate (Figure 5).[23]

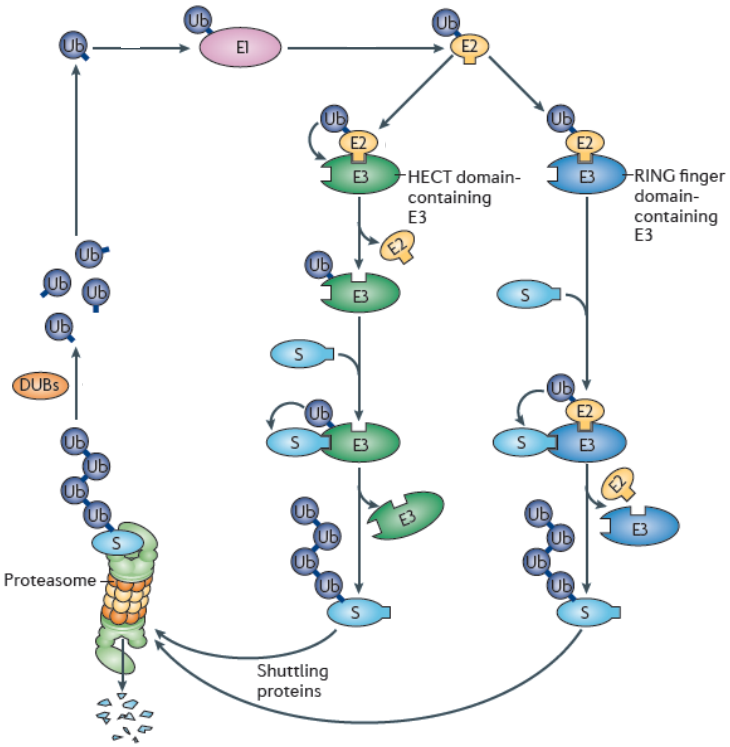

Figure 5.[24] The distinct pathways of RING and HECT E3 ligases (S = Substrate)

Although primarily recognised as a targeting signal for the UPS, ubiquitin transfer has also been implicated in other cellular processes, such as signal transduction and enzyme activation,[25,26] endocytosis,[27] chromatin rearrangement,[28] and DNA repair.[29] This is highly dependent on the form of ubiquitination, and the manner of ubiquitin chain linkage (Figure 6).[30] Traditionally, it has been shown that at least four ubiquitin units linked by K48 residues are required to allow recognition of the target protein by the proteasome,[31,32] though a series of shorter ubiquitin chains[33] and even monoubiquitination[34] have since been shown to be sufficient. Protein ubiquitination is

also a fully reversible process, and a series of proteases known as deubiquitinases (DUBs) can cause cleavage of ubiquitin.[21,35,36]

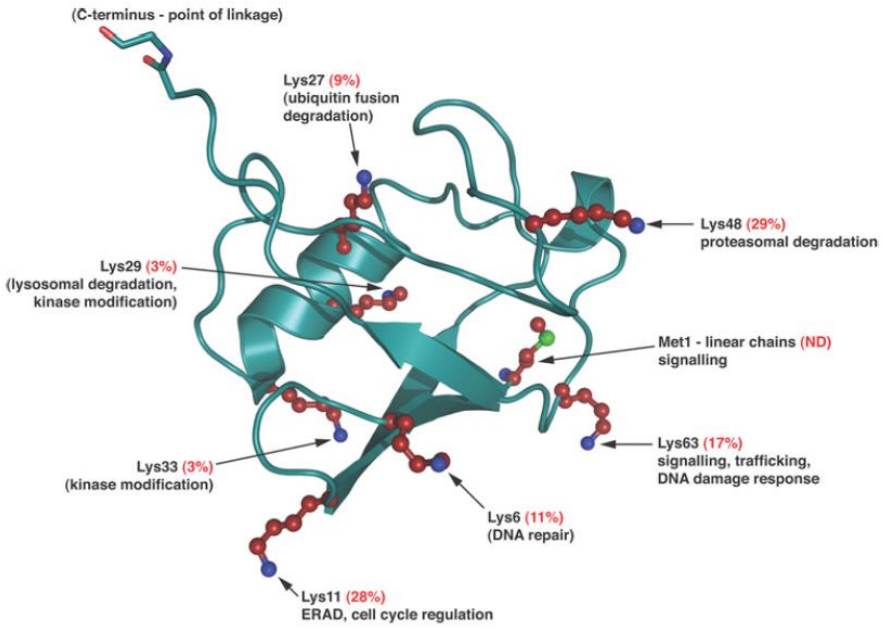

Figure 6.[30] Diverse signalling resulting from polyubiquitin linkage patterns by their relative abundance

Ubiquitin is necessary but not sufficient for protein degradation by the proteasome.[32] The 26S proteasome itself consists of two subunits; the 19S regulatory particle, responsible for recognition and commitment of substrates to the 20S core particle, which is responsible for proteolysis.[37] The ubiquitin chain is first recognised by ubiquitin receptors on the 19S proteasome (Rpn10 and Rpn13), then undergoes a conformational change to begin substrate acceptance (Figure 7).[38] In order to enter the proteasome channel, presentation of a structurally disordered region of the substrate is required with which to initiate substrate engagement and unfolding.[39,40] A further conformational change occurs and the polyubiquitin chain is cleaved by Rpn11 as the linearised protein chain enters the 20S proteasome barrel.[41,42]

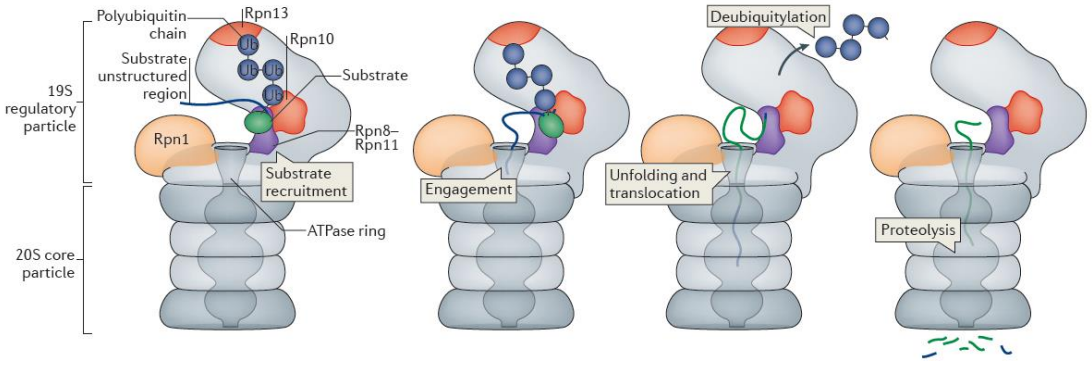

Figure 7.[43] Overview of a processing of a ubiquitinated substrate by the proteasome

After entering the gated channel of the 20S proteasome, proteolysis occurs mediated by a series of threonine proteases. The linear chain docks at Thr^1 active sites, where and is cleaved into short peptides by the mechanism outlined in Figure 8.[44] The cleaved peptides are then ejected back into the cytoplasm and may then be employed for incorporation into newly synthesised protein.

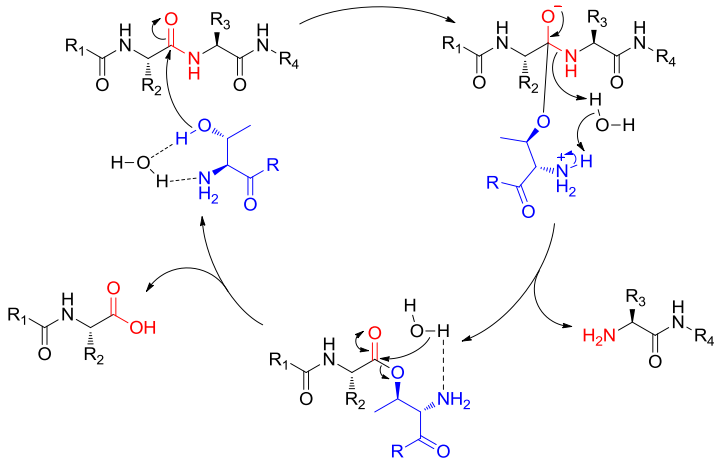

Figure 8. Thr^1-dependent proteolysis mediated by the 20S proteasome

1.3 Drug Discovery in the Ubiquitin-Proteasome System

Given the critical role of the UPS in intracellular protein regulation and cell cycle control, it has become a rich target for modulation or inhibition using small molecules. As intervention at different stages of the pathway can give varying levels of disruption to cellular homeostasis, a wide range of both clinical agents and biological tools have been generated. The key discoveries in this field will be summarised in this section.

1.3.1 Proteasome Inhibition

As the proteasome acts as a quality-control unit for newly synthesised proteins, and is responsible for degradation of key regulators of cell cycle progression, inhibition of the proteasome can rapidly perturb intracellular proteostasis. Myeloma cells are particularly sensitive to disruption of proteostasis,[45] and proteasome inhibition has evolved into a frontline treatment for multiple myeloma (MM).[46] Small molecule inhibitors mostly target the 20S proteasome and act by covalent adduct formation with the nucleophilic terminal Thr residues in the β1, β3 and β5 subunits responsible for substrate proteolysis (Figure 9).

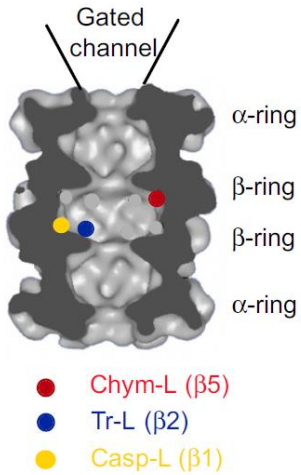

Figure 9.[47] The 20S proteasome barrel, indicating the location of proteolytic active sites

The first proteasome inhibitor to be identified was the peptidic aldehyde MG-132, which inhibits Thr^1 by reversible acetal formation (Figure 10).[17,48] This molecule has

found widespread use as a biological tool, however rapid *in vivo* oxidation of the key aldehyde group limits the therapeutic use of this structural class of proteasome inhibitors.[49]

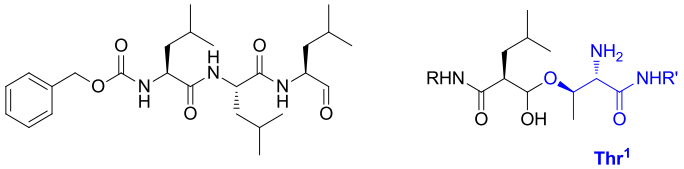

Figure 10. Aldehyde-containing proteasome inhibitor MG132 (left) and mode of action (right)

The boronate-containing dipeptide bortezomib (marketed as Velcade; Figure 11, left) was the first proteasome inhibitor to be FDA-approved for treatment of MM[50] and mantle cell lymphoma.[51] The boronate moiety reversibly inhibits the terminal Thr residues with a slower dissociation rate than aldehydes such as MG-132, due to an H-bonding interaction with the terminal Thr N-H (Figure 11, right).[52]

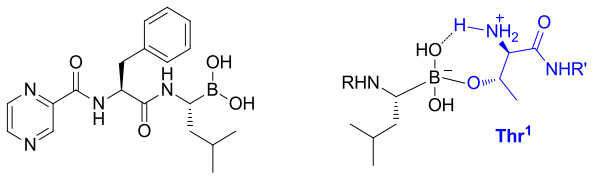

Figure 11. Clinical proteasome inhibitor Bortezomib (Velcade) and mechanism of proteasome inhibition

This interaction also results in inhibition of off-target serine proteases, believed to be the cause of dose-limiting peripheral neuropathy observed upon bortezomib treatment.[53] A further issue with the slow off-rate of bortezomib is that it rapidly inhibits the proteasome in red blood cells and does not readily dissociate, resulting in poor distribution into tissue.[54] This has led to development of second generation boronates with a faster off-rate (CEP-18770) and boronate produgs (Ixazomib), presented in Figure 12.[54,55] Ixazomib citrate is once-weekly orally bioavailable prodrug which has been recently approved for treatment of MM (marketed as Ninlaro).[56]

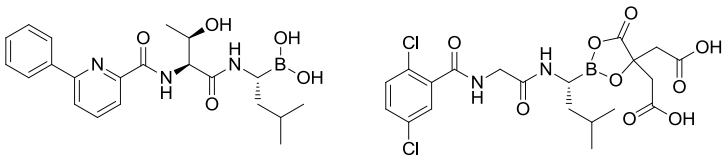

Figure 12. Second generation boronate proteasome inhibitors CEP-18770 (left) and Ixazomib citrate (right)

The tetrapeptide natural product epoxomicin was first described as an antitumour agent long before its mechanism of action was known (Figure 13, top left).[57] The origin of this activity was later uncovered, as epoxomicin was found to be a selective and potent inhibitor of the proteasome.[58] The high selectivity for proteasome inhibition over off-target serine and cysteine proteases is thought to be driven by the unique formation of a morpholine adduct with the α-amino group of Thr[1] (Figure 13, bottom).[59]

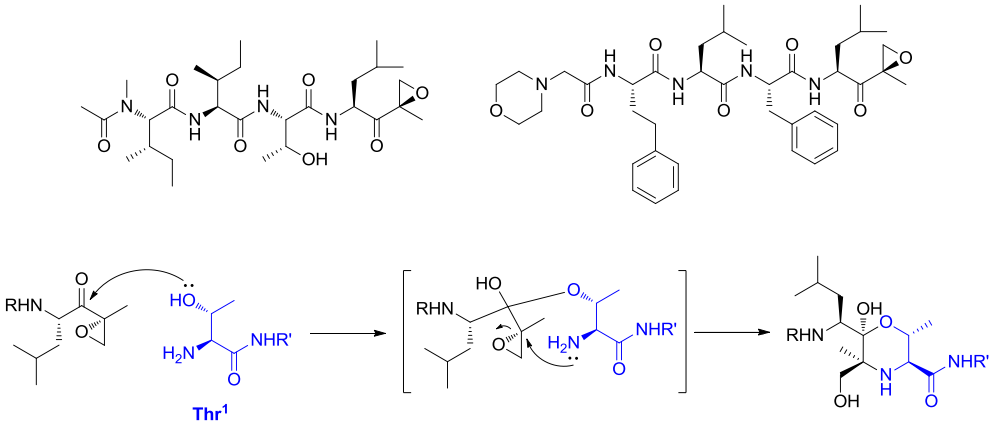

Figure 13. Natural product epoxomicin (top left) and clinical proteasome inhibitor carfilzomib (top right); mechanism of action of α-epoxyketone proteasome inhibitors (bottom)

Carfilzomib (marketed as Kyprolis) was developed by direct elaboration of epoxomicin, retaining the key epoxyketone fragment and has subsequently been approved by the FDA for treatment of MM (**Figure** 13, top right).[60] As for bortezomib, further medicinal chemistry efforts have identified orally bioavailable analogues (PR-047) for more flexible dosing strategies.[61]

1.3.2 Inhibition of E1 and E2 Ligases

As inhibition at the ubiquitin-activation (E1) stage of the UPS would prevent global ubiquitination, degradation of proteins would be prevented. This would result in effects mirroring that of proteasome inhibition, also preventing the many regulatory functions of ubiquitin. However, E1 enzymes are also responsible for transfer of further ubiquitin-like proteins, which play equally important roles in the UPS.[62] Though some ubiquitin-activating enzyme (UAE) inhibitors have been reported, few have appropriately drug-like properties for therapeutic use.[63]

The most advanced example of an E1 inhibitor does not target a UAE, rather a ubiquitin-like activating enzyme, neural precursor cell-expressed developmentally-downregulated 8 (NEDD8) activating enzyme (NAE). NEDD8 is a ubiquitin-like PTM which is essential for activation of Skp Cullin F-box (SCF) E3 ligases;[64] NAE catalyses this SCF NEDDylation event. MLN4924 (Pevonedistat, Figure 14) covalently inhibits NAE and prevents activation of SCF ligase function resulting in accumulation of its substrates, several of which play fundamental roles in cancer development.[65] MLN4924 has demonstrated potent inhibition of cancer cell proliferation in preclinical models and some clinical activity in acute myeloid leukaemia (AML) patients.[66]

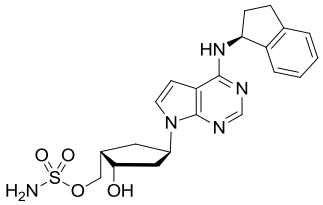

Figure 14. NAE inhibitor MLN4924

In the case of E2 ligases, even fewer inhibitors have been identified. The most prominent example is CC0651 (Figure 15), which inhibits the E2 enzyme Cdc34A.[67] The mechanism of action of CC0651 is unusual as it binds an allosteric pocket of Cdc34A, remote from the active site cysteine onto which ubiquitin is transferred. Subsequently, it has been found that CC0651 induces a conformational change which stabilises a low-affinity interaction between Cdc34A and ubiquitin, allowing priming mediated by the E1 ligase but preventing ubiquitin transfer to an E3 ligase or target protein.[68]

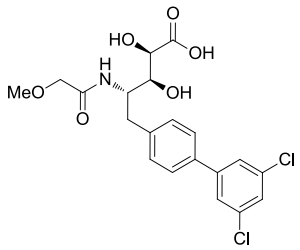

Figure 15. Structure of E2 ligase inhibitor CC0651

1.3.3 Inhibition of E3 Ligases

As E3 ligases are responsible for ubiquitination of specific substrates, small molecule intervention at this stage should allow more precise therapeutic targeting and cause less global disruption to the UPS.[36] Inhibitors developed in this area mostly target the ligase-substrate protein-protein interaction (PPI), which are often challenging to drug due to the size of the PPI interface and lack of a traditional catalytic sites, often requiring recognition of polar PTMs.[69] Development of small-molecules targeting these PPIs often begin with identification of peptide truncates, which in isolation are often not cell-permeable.[70] Rational design strategies are often employed to develop more drug-like inhibitors from these peptides, while some have been discovered serendipitously. Discovery of inhibitors for three of these E3 ligases will be described in this section.

1.3.3.1 VHL Inhibition

The transcription factor hypoxia-inducible factor 1-alpha (HIF-1α), an 850 amino acid protein) is critical in oxygen sensing and the hypoxic response.[71,72] Under hypoxic conditions HIF-1α is constitutively expressed and stable, however under normoxic conditions, HIF-1α undergoes hydroxylation (Pro564→Hyp564) mediated by prolyl hydroxylase domain enzymes. Hydroxylated HIF-1α is the primary substrate for the E3 ligase Von-Hippel Lindau protein (VHL), which polyubiquitinates HIF-1α resulting in its proteasomal degradation.[73]

As small molecule inhibition of the HIF-1α VHL PPI would result in HIF-1α accumulation, this would artificially induce the hypoxic response and could provide therapeutic benefit for conditions such as anemia.[74] Recently, some advances have

been made targeting this interaction using a small molecule approach, particularly for application in protein degradation strategies (*vide infra*). As hydroxylated HIF-1α binds VHL most strongly at the Hyp564 residue, research carried out by Crews and co-workers focusing on a hydroxyproline core and modification of the surrounding structure. This led to small molecule VHL binders with moderate potency, an example of which is presented in Figure 16.[75–77]

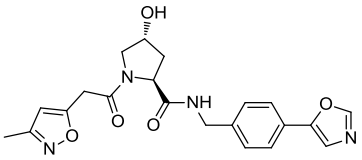

Figure 16. First-generation small molecule VHL binder (VHL pIC_{50} = 5.4)

These compounds were further optimised within our laboratories,[78] improving on potency and lipophilicity to give the sub-micromolar binding affinity ligand presented in Figure 17. Additional characterisation of this ligand has been reported subsequently.[79]

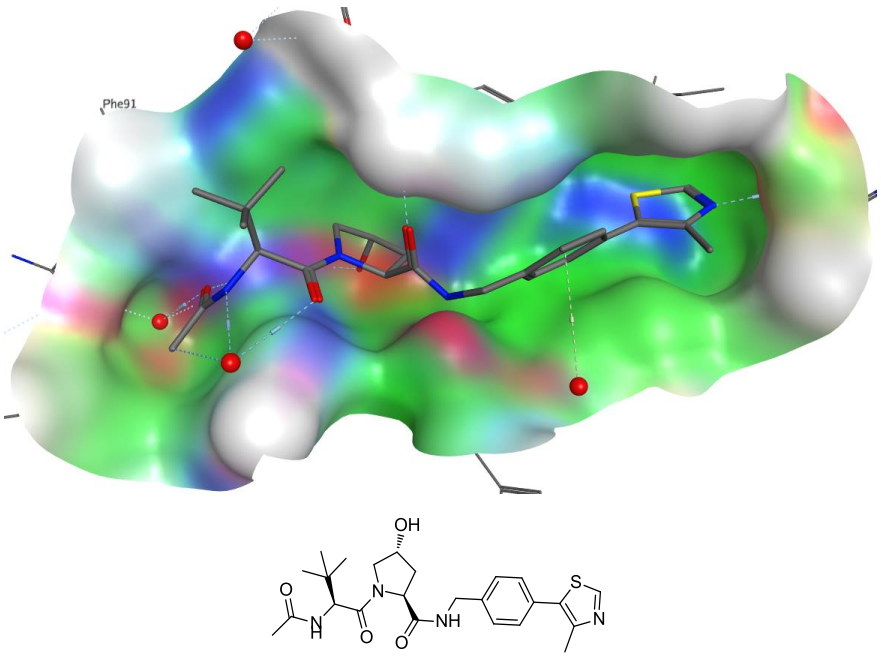

Figure 17.[79] Co-crystal structure of VHL and optimised ligand (surface coloured by pocket region: red = polar, green = hydrophobic, blue = solvent exposed)

Further research within our laboratories identified a more lipophilic isoindolinone-containing VHL binder (Figure 18), allowing physicochemical modulation whilst maintaining binding affinity.[78]

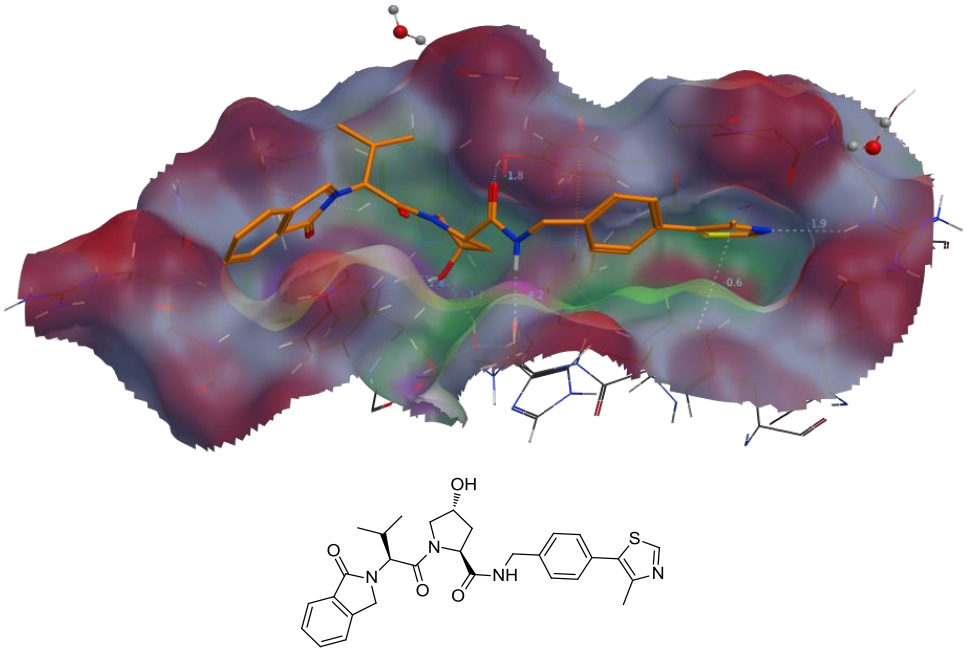

Figure 18.[80] Co-crystal structure of an isoindolinone-containing ligand and VHL, which contains an alternative exit vector accessible through the phenyl group

1.3.3.2 Cereblon Inhibition

The infamous drug thalidomide (Figure 19) was first prescribed in the late 1950s to pregnant women as an anti-nausea and sedative drug, however before its teratogenic effects were discovered, thousands of children had been inflicted with severe birth defects.[81–83] The protein cereblon, a member of the $CUL4^{CRBN}$ (Roc1-CUL4-DDB1-CRBN) E3 ligase complex, has since been identified as the primary target of thalidomide teratogenicity.[84]

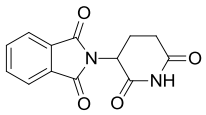

Figure 19. Structure of cereblon inhibitor thalidomide

The structural class of molecules which bind to cereblon, known as immunomodulatory imide drugs (IMiDs), also include the phthalimide analogues pomalidomide and lenalidomide (Figure 20).

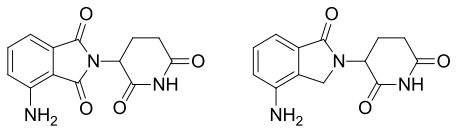

Figure 20. Structures of pomalidomide (left) and lenalidomide (right)

Upon binding to cereblon, IMiDs cause formation of a neomorphic surface allowing recruitment, ubiquitination and subsequent degradation of neosubstrates, primarily the transcription factors Ikaros and Aiolos (also known as IKZF1 and IKZF3, Figure 21).[85–87] Degradation of these neosubstrates results in IL-2 secretion and stimulation of T cells, critical for the anti-myeloma activity of IMiDs.[85,88] IMiD binding also prevents engagement of the endogenous cereblon substrate MEIS2, which then accumulates as its degradation is prevented.[89] MEIS2 is a transcription factor involved in proximal limb development, and its accumulation is one possible explanation for the teratogenic effects observed upon cereblon inhibition.

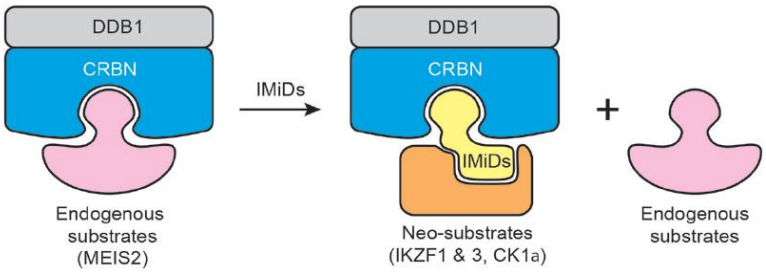

Figure 21.[90] IMiD binding prevents binding of endogenous cereblon substrates such as MEIS2 and allows degradation of neosubstrates such as Ikaros and Aiolos

Minor modification of the IMiD ligands result in formation of differentiated neomorphic surfaces which can engage and degrade diverse neosubstrates. Lenalidomide, but not pomalidomide, has been shown to induce degradation of casein kinase 1α (CK1α), indicating that neosubstrate recruitment to cereblon is highly sensitive to minor structural variation.[91] A further cereblon modulator, CC-885 (Figure 22), has been shown to selectively recruit the translation termination factor GSPT1 to

the cereblon ligase complex over pomalidomide and lenalidomide.[92] CC-885 creates an interaction hotspot for GSPT1 allowing a cereblon-GSPT1 PPI to occur, resulting in $CUL4^{CRBN}$-mediated ubiquitination and degradation.

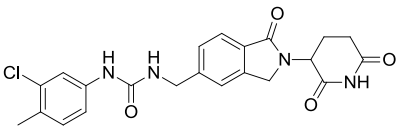

Figure 22. Cereblon modulator CC-885 which recruits neosubstrate GSPT1

As indicated in the co-crystal structure of pomalidomide displayed in Figure 23, the glutarimide ring common to all IMiDs is buried in the substrate binding site. The solvent exposure of the phthalimide ring accounts for the apparent flexibility of neosubstrate recruitment, allowing formation of distinct neomorphic surfaces.

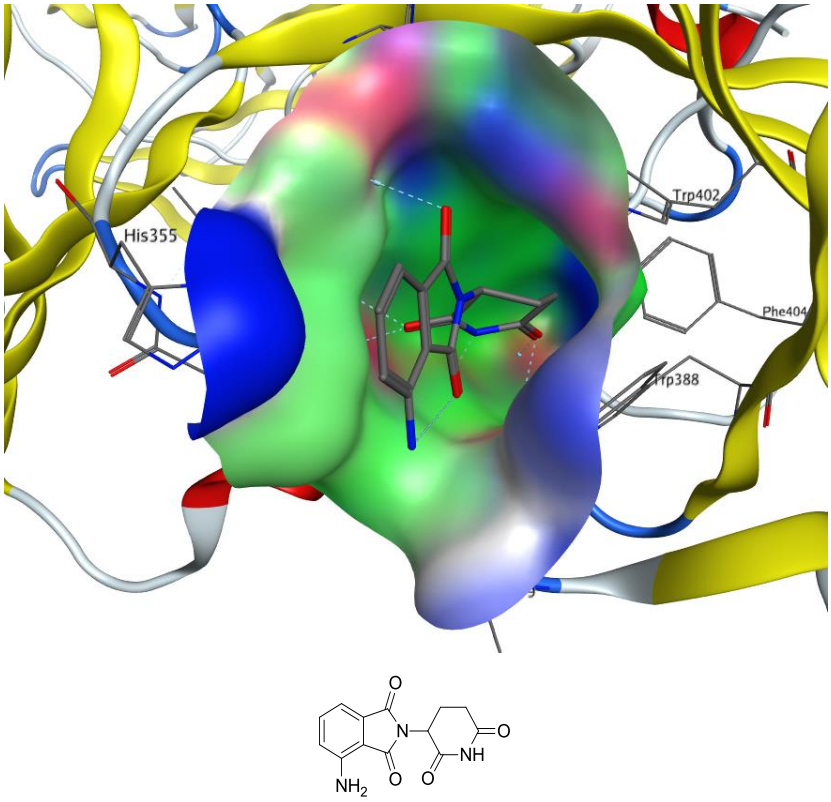

Figure 23.[89] Crystal structure of pomalidomide (surface coloured by pocket region; blue = solvent exposed, green = hydrophobic, red = polar)

1.3.3.3 IAP Inhibition

Inhibitor of apoptosis proteins (IAPs) are critical mediators of apoptosis which promote cell survival by inhibiting activation of caspases.[93,94] The most important members of the family include X-linked IAP (XIAP), cellular IAP1 (cIAP1), cIAP2 which contain three baculovirus IAP repeat (BIR) domains and a *C*-terminal RING domain which give them E3 ligase activity.[95,96] XIAP inhibits apoptosis by binding to caspase-9 through its BIR3 domain and caspase-3/7 through its BIR2 domain,[97,98] while the cIAPs prevent activation of tumour necrosis factor alpha (TNF-α) through inhibition of caspase-8.[99] The protein second mitochondria-derived activator of caspases (Smac) is the endogenous antagonist of the IAPs.[100,101] Antagonism of XIAP by Smac results in displacement of caspase-3/7/9,[102,103] while antagonism of the cIAPs activates their E3 ligase activity resulting in their autoubiquitination and degradation, releasing caspase-8 (Figure 24).[104]

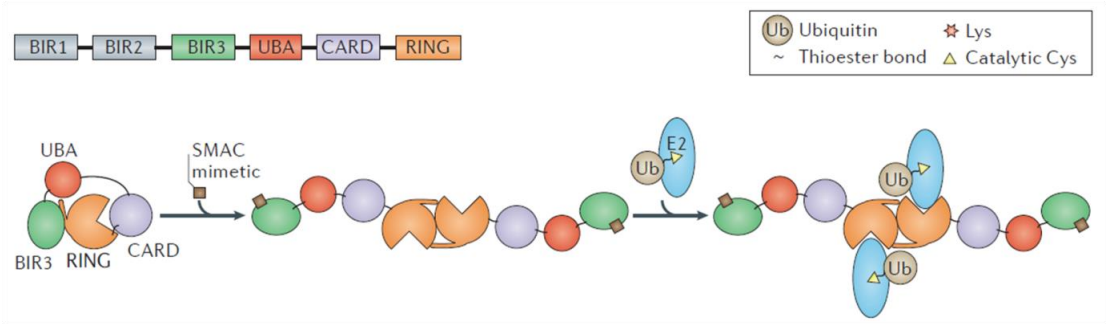

Figure 24.[105] Mechanism of cIAP1 activation. When inactivated, cIAP1 is stable in a closed conformation and the RING domain is internalised. Upon activation by a Smac mimetic, the complex opens and dimerises, exposing the RING domain. The RING domain is then available to bind to an E2 ligase

As IAPs are often overexpressed in tumour cells,[106] a number of Smac mimetics have been developed for cancer therapy in order to promote these pro-apoptotic pathways.[107] Despite its large size, the BIR binding motif of Smac consists of a short AVPI tetrapeptide, from which the majority of small-molecule IAP inhibitors have been directly developed (Figure 25).

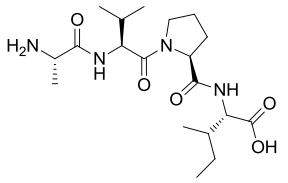

Figure 25. Structure of Smac AVPI tetrapeptide

Both monovalent and bivalent Smac mimetics have been developed, and some exemplar Smac mimetics currently in clinical trials are displayed in Figure 26.[108] In this context, bivalent IAP antagonists prove to be significantly more efficacious than monovalent pre-clinically,[109] believed to be an avidity effect driven by simultaneous engagement of both BIR2 and BIR3.[103,110]

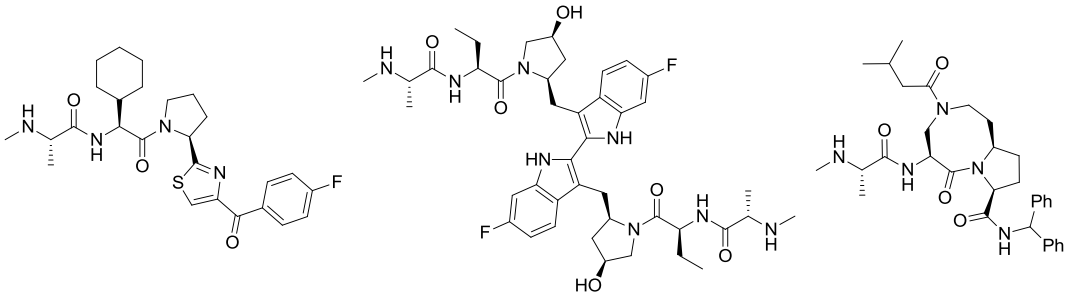

Figure 26. Examples of clinical monomeric and dimeric Smac-mimetic IAP inhibitors LCL-161 (left), Birinapant (centre), Debio1143 and (right)

1.4 Small Molecule-mediated Protein Degradation

1.4.1 Proteolysis Targeting Chimera

A proteolysis targeting chimera (Protac) is a heterobifunctional small molecule which manipulates the UPS to degrade a targeted protein.[111] This approach was originally conceived by Prof. Craig Crews and Prof. Ray Deshaies in 2001; the proposed mechanism of action is outlined in Figure 27.[112] The structure of a Protac consists of two moieties, respectively designed to bind to an E3 ligase and a target protein connected through a linker. Simultaneous interaction of the two subunits with their respective targets is thought to result in the formation of a target-Protac-ligase ternary complex.[113,114] The proximity of the E3 ligase complex to the target protein results in non-physiological polyubiquitination of the target protein on a lysine residue, leading to recognition of by the proteasome and subsequent degradation.

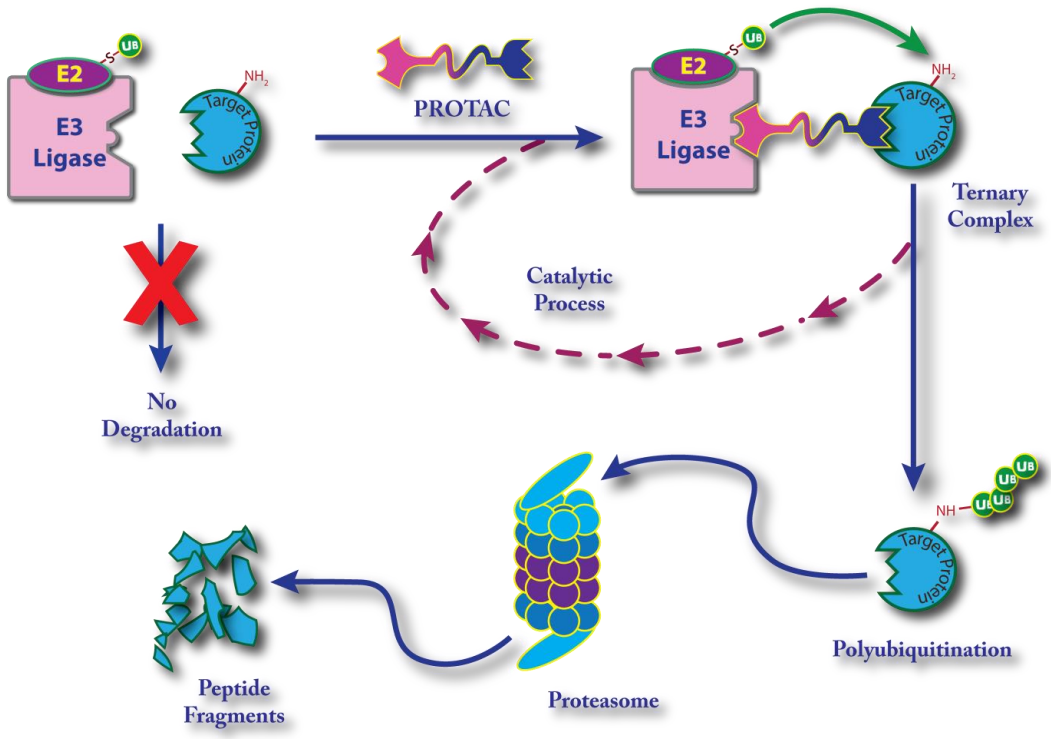

Figure 27.[115] Proposed mechanism of action of Protacs. Protac-mediated ternary complex formation allows ubiquitin transfer from the E3 ligase complex onto the target protein. Following polyubiquitination, the target protein is recognised and degraded by the proteasome.

As the role of the Protac is simply to facilitate the interaction between the E3 ligase complex and the target protein, the Protac can dissociate and is free to mediate the ubiquitination and degradation of multiple substrate molecules. This catalytic activity potentially allows efficient degradation to be driven from low drug concentrations, as only low levels of equilibrium occupancy are required to drive an efficient kinetic process.

Additionally, as the Protac need only bind to the target protein rather than inhibit a specific function, an affinity probe that binds at any orthosteric or other site could be derivatised to give an efficacious Protac. This opens up the potential to target proteins which have no classical binding site or for which functional inhibitors cannot be found. Equally, Protacs may be advantageous in cases where an inhibitor alone has insufficient potency or half-life to drive useful occupancy-driven *in vivo* efficacy. Furthermore, as the target protein is being removed from the cell rather than simply being inhibited, there is the potential to modulate secondary or scaffolding functions of a protein that cannot be altered by inhibition alone.

As the Protac mechanism proceeds through formation of a ternary complex, the associated equilibria are more complex than for a simple protein-inhibitor binary system (Figure 28).[116]

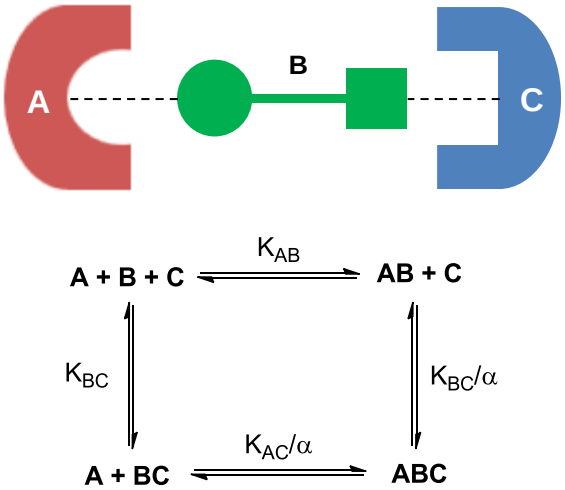

Figure 28. Ternary complex formation and associated equilibria (α = cooperativity in ABC complex formation; α > 0 = positive cooperativity, α < 0 = negative cooperativity)

In particular, ternary equilibria are subject to the 'hook effect,' often otherwise described as the 'prozone effect' or 'dose-limited activity' as a result of a bell-shaped dose response (Figure 29).[116] Increasing concentration of the intermediary species **B** first reaches an optimal concentration, where maximal degradation will occur. With increasing concentration, **B** begins to saturate occupancy at both binding partners **A** and **C**, and binary complexes dominate, decreasing the population of ternary complexes and reducing the levels of degradation.

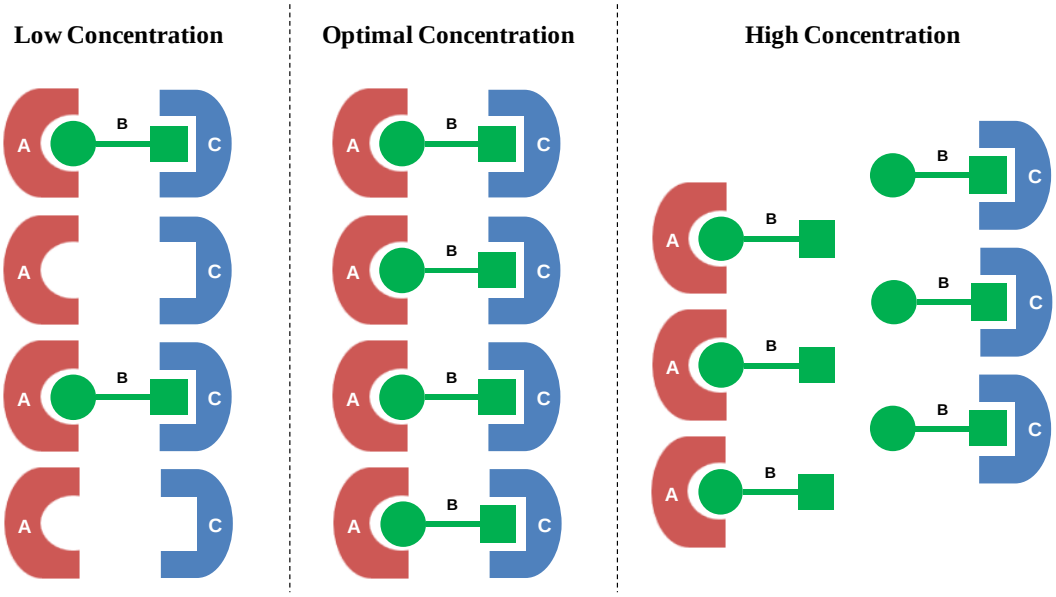

Figure 29. Rationalisation of the hook effect observed in ternary systems

The first Protacs synthesised by Crews and co-workers contained a phosphopeptide to bind the E3 ligase SCF (Figure 30). This ligase binder was linked to ligands that bind to methionine aminopeptidase 2 (MetAP2),[112] the androgen receptor (AR), and the estrogen receptor (ER), respectively.[117] However, it is likely that these compounds lacked cell permeability due to the highly polar phosphopeptide SCF binder.

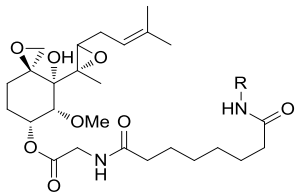

Figure 30. Crews' MetAP2-SCF Protac (R = GGGGGGRAEDS*GNES*EGE-COOH or GGGGGGDRIIDS*GLDS*M-COOH; * = phosphorylated residue)

In attempts to increase permeability, several Protacs were synthesised containing peptidic binders, derived from HIF1α, to bind to the VHL. These Protacs were targeted towards ER (Figure 31),[118–120] the aryl hydrocarbon receptor,[121,122] the *cis-trans* isomerase FKBP1A, and AR.[119] Although degradation of some of the targets was reported, this was only observed at high concentrations (>10 μM) at which competing effects due to cytotoxicity cannot be ruled out.

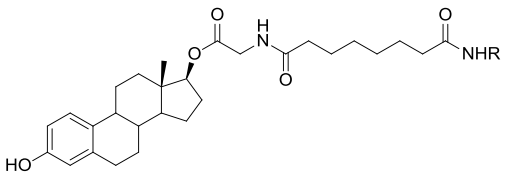

Figure 31. Structure of ER-VHL pentapeptide Protac (R = Leu-Ala-Hyp-Tyr-Ile-COOH)

It is believed that the peptidic Protacs reported in the literature fail to show degradation at physiologically useful concentrations due to the poor permeability of their E3 ligase binders. The advent of non-peptidic E3 ligase ligands has more recently allowed design of Protac molecules which overcome many of the limitations of these previous agents. Most effort has focussed on the small set of ligases VHL, cereblon, the IAP family and MDM2.

Despite a molecular weight of over 1000 Da, which places Protacs well outside more traditional areas of drug-like small molecule property space,[123] they have shown potent cellular effects and even *in vivo* activity. Progress with non-peptidic Protacs has been rapid, but no Protac molecule has yet been reported to have entered clinical development. Whether a Protac-induced protein knockdown strategy will be limited to use in chemical biology or find wider application in therapeutic development will depend on a number of factors including the pharmacokinetics, dose level, selectivity, safety and tolerability, ability to synthesise on scale and a range of other factors. In the following section the potential advantages and issues of advancing Protacs designed to recruit different E3 ligases in a drug discovery setting are discussed.

1.4.1.1 VHL Protacs

The VHL ligand described in Section 1.3.3.1 was combined with a cell-active small molecule inhibitor of the serine-threonine kinase receptor-interacting serine/threonine-protein kinase 2 (RIPK2) resulting in a RIPK2-VHL Protac (Figure 3).[124] This Protac was able to induce highly potent degradation of RIPK2 was observed, with a DC_{50} = 1.4 nM (DC_{50} is the concentration at which 50 % of substrate is degraded) and almost complete knockdown (D_{max} >95 %, where D_{max} = maximal level of degradation) in THP-1 monocytes at concentrations above 10 nM following 16 h incubation. At concentrations over 3 μM, Protac-induced reduction of protein levels was partially abrogated, consistent with the three-body binding predicted from the Protac mechanism whereby saturation of RIPK2 and VHL binding sites disfavours formation of the ternary complex required for ubiquitin transfer.[116]

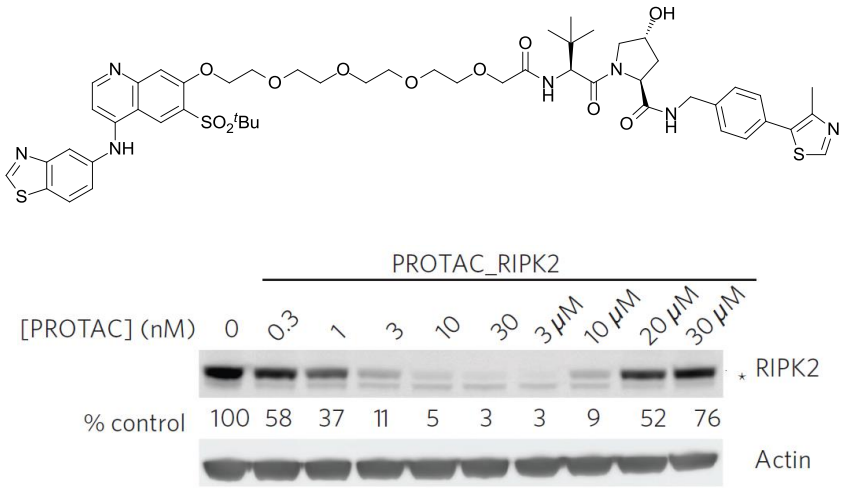

Figure 32.[124] Structure of RIPK2 Protac (above) and western blot demonstrating dose-dependent RIPK2 degradation following 16 h incubation in THP-1 cells (below) and the 'hook effect' observed at high concentrations

The rapid onset of action of RIPK2 degradation was also demonstrated, with knockdown observed as early as 1 h after treatment, and almost complete knockdown by 4 h. After complete RIPK2 knockdown and washout of the Protac from cells, protein levels were found to require around 24 h to return to basal levels, which suggests the potential for efficacy even after drug clearance.

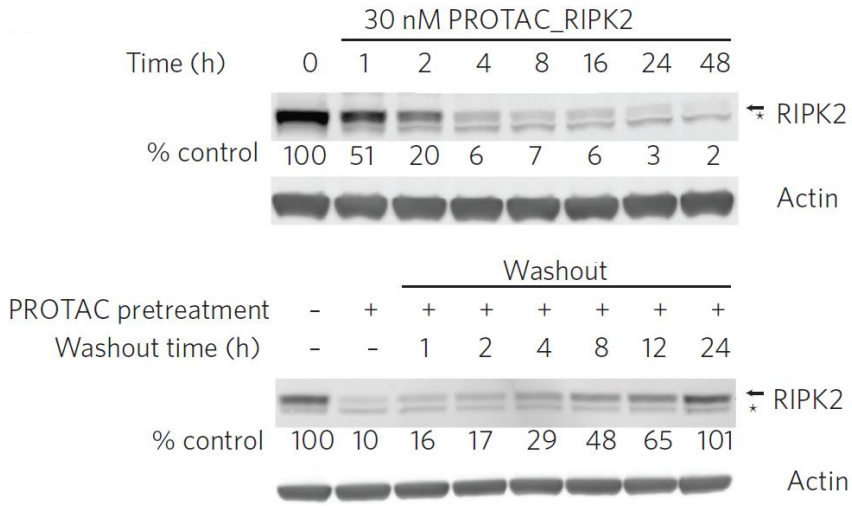

Figure 33.[124] Western blot demonstrating rapid onset of RIPK2 degradation following treatment with 30 nM RIPK2 Protac (above), and the extended duration available after Protac washout (below)

To confirm that the observed effect is proceeding by the proposed Protac mechanism, a number of controls were carried out (Figure 34). In the presence of the epimer of the RIPK2 Protac, which does not bind to VHL, no degradation was observed, indicating the effect is driven by binding to both target protein and E3 ligase. Inhibition of the proteasome with epoxomicin resulted in no change to RIPK2 levels, demonstrating that the effect is proteasome-dependent. Incubation with either parent RIPK2 or VHL ligand, or combination of both ligands, resulted in no RIPK2 degradation highlighting the necessity of ternary complex formation.

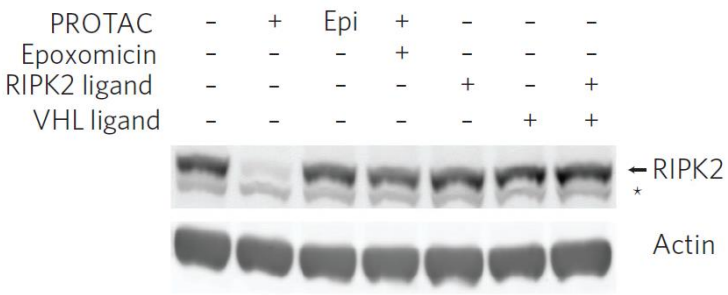

Figure 34.[124] Protac-mediated degradation of RIPK2 is dependent on the stereochemistry of the VHL binder (Epi refers to the epimer of the RIPK2-VHL Protac), the proteasome and the linkage between the RIPK2 and VHL ligand (THP-1 cells treated with 30 nM indicated compound, apart from epoxomicin which was employed at 1 μM concentration)

Cellular expression proteomics, which allows quantification of relative protein abundance before after compound treatment, was carried out using the RIPK2-VHL Protac (Figure 35). This demonstrated displayed the high levels of degradation selectivity attainable using a Protac strategy. Taking advantage of the high selectivity intrinsic to the RIPK2-binding ligand, RIPK2 was found to be one of only two proteins significantly knocked down from ~7000 quantified proteins following incubation with 30 nM of RIPK2 Protac for 18 h. Interestingly, modest knockdown of a second kinase, MAPKAPK3, was also observed, despite the Protac showing only very weak binding to this protein (K_d > 3 μM).

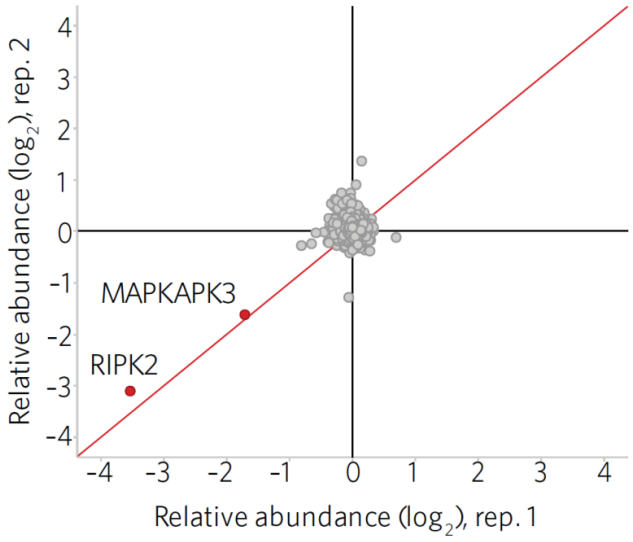

Figure 35.[124] Variation in protein level abundance following incubation with 30 nM RIPK2 Protac for 18 h in THP-1 cells indicating high degradation selectivity for RIPK2

Further characterisation of the RIPK2 Protac validated the E3-ligase-dependent nature of the degradation. The presence of a RIPK2-Protac-VHL ternary complex was confirmed by co-immunoprecipitation and, by reconstitution of the E1-E2-E3 cascade *in vitro*, Protac-mediated direct ubiquitination of RIPK2 was demonstrated. This latter system was also used to demonstrate quantitatively the catalytic nature of Protac action, with super-stoichiometric ubiquitination of RIPK2 observed. It should be noted that the system generated in this experiment is highly artificial and the Protac:protein stoichiometry is almost certainly an underestimate, given the significantly enhanced efficacy of this Protac in cells.[125] This observation of a small molecule agent acting catalytically may offer the possibility of high *in vivo* efficacy from low drug exposure, thus beginning to move beyond the limitations of current equilibrium, occupancy-based methods.

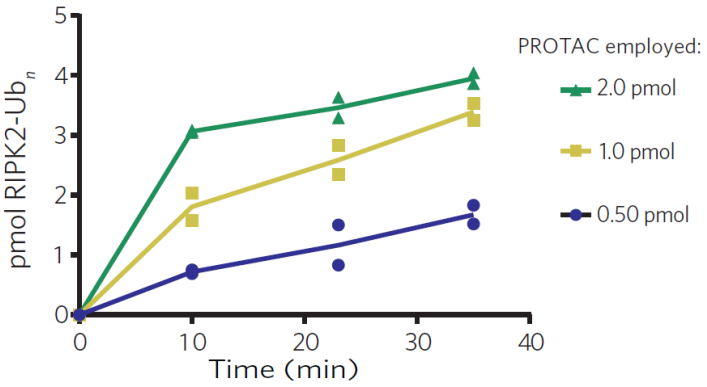

PROTAC (pmol):	0.5	1.0	2.0
RIPK2-Ub (pmol):	1.7	3.4	4.0
Stoichiometry:	3.3	3.4	2.0

Figure 36.[124] Super-stoichiometric ubiquitination is observed upon reconstitution of the E1-E2-E3 ubiquitin transfer cascade *in vitro*, indicating the catalytic nature of the Protac mechanism

Protacs are designed to redirect the function of E3 ligases towards ubiquitination of unnatural substrates, and as such carry the potential risk of unwanted modulation of endogenous ligase substrate processing. With VHL-dependent Protacs, unwanted inhibition of basal HIF-1α ubiquitination may result in its accumulation, potentially triggering the hypoxic response as an undesired ligase-dependent effect. However, using the RIPK2-VHL Protac, the increase of a hypoxic marker in an reporter model was only observed at 30 μM concentration.[124] This suggests up to a thousand fold window between cellular RIPK2 degradation and HIF-1α stabilisation, indicating minimal potential for undesired pharmacological effects *via* VHL inhibition.

Degradation of the estrogen-related receptor alpha (ERRα), an orphan nuclear receptor, has also been described.[124] The ERRα-VHL Protac (Figure 37) demonstrated dose-dependent ERRα knockdown with an observed DC_{50} ~100 nM in MCF-7 cells. This Protac was found to be efficacious *in vivo*; mice dosed with 100 mg/kg of ERRα-VHL showed reduced ERRα levels, with ~40 % knockdown observed in heart, kidney and MDA-MD-231 tumours relative to vehicle-treated mice.

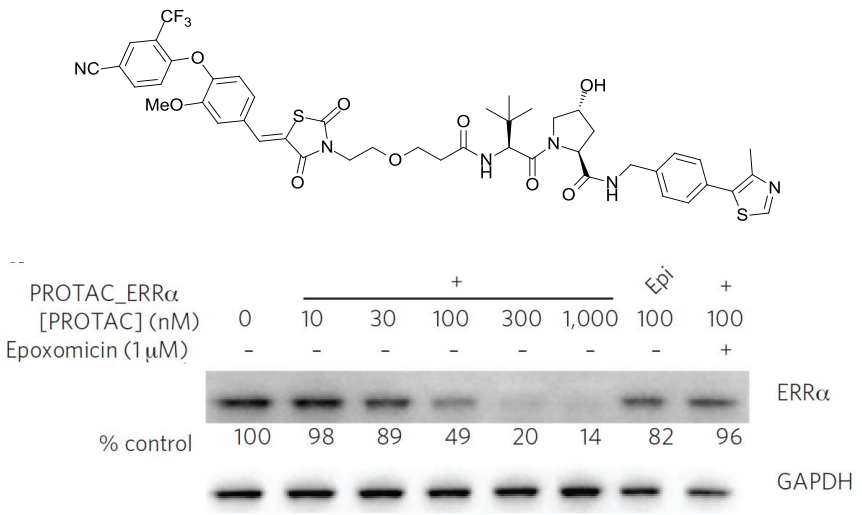

Figure 37. Structure of a VHL Protac targeting ERRα (above) and a western blot indicating dose-dependent ERRα degradation upon incubation with ERRα Protac for 8 h in MCF7 cells

VHL-mediated degradation of BET (Bromodomain and Extra Terminal) proteins has also been investigated.[126] Conjugation of the pan-BET inhibitor JQ1 to the VHL binder resulted in JQ1-VHL Protac (Figure 38), which demonstrated degradation of bromodomain containing proteins BRD2/3/4 following 24 h incubation in HeLa cells. Although this JQ1-VHL Protac showed no binding selectivity between the BRD isoforms, it was reported to show modestly selective degradation of BRD4 over BRD2/3, (though Western blot characterisation of this Protac using different antibodies failed to demonstrate any selectivity between degradation of the BRD isoforms).[127]

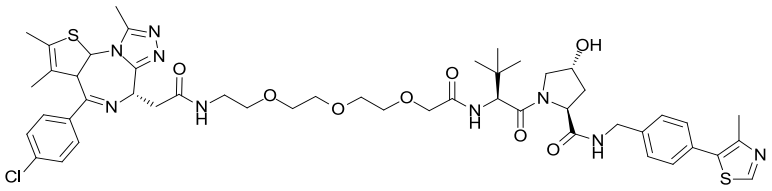

Figure 38. Structure of an initial VHL Protac targeting BET proteins

A further pan-BET VHL Protac ARV-771 (Figure 39) has been described as a potential treatment for metastatic castration-resistant prostate cancer (CRPC).[128] This JQ-1-VHL Protac, which employs a slightly modified VHL binder, induces BRD2/3/4

degradation with a DC_{50} <5 nM resulting in transcriptionally controlled c-MYC inhibition with an IC_{50} < 1 nM following 16 h incubation in 22Rv1 cells. In a 22Rv1 murine xenograft model, subcutaneous administration of ARV-771 resulted in a dose-dependent decrease in tumour size, with tumour regression after 30 mg/kg treatment. In a further VCaP xenograft model, 30 mg/kg daily dosing was not tolerated, indicating potential for significant compound-related toxicity. Dosing every 3 days resulted in 60 % tumour growth inhibition over a 16 day period, though some toxicity was also observed. The BET family of proteins appear to be susceptible to facile degradation and have also been degraded using the E3 ligase cereblon (*vide infra*).

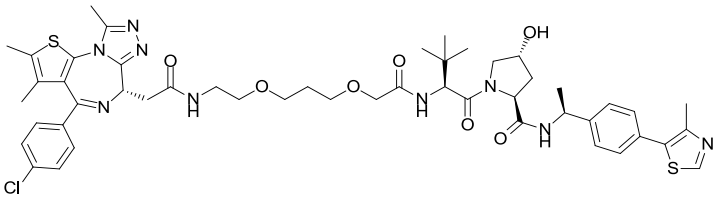

Figure 39. Structure of a further VHL Protac targeting BET proteins employing a modified VHL inhibitor

In the development of a series of Protacs exploring the degradation of oncogenic kinases, conjugation of the tyrosine kinase inhibitors (TKIs) dasatinib and bosutinib to a VHL binder gave the TKI Protacs displayed in Figure 40.[129] Whilst the dasatinib-VHL Protac (Figure 40, top) proved to be an active degrader, demonstrating ABL knockdown, the bosutinib-VHL Protac (Figure 40, bottom) gave no ABL degradation.

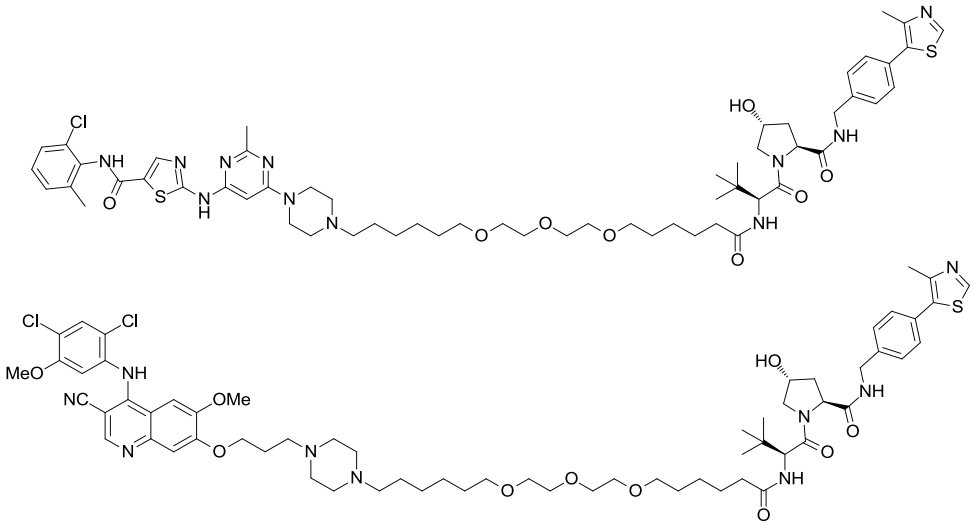

Figure 40. VHL Protacs targeting BCR-ABL employing dasatinib (above) and bosutinib (below)

Similarly, neither compound degraded the prototypical target BCR-ABL, despite evidence of cellular uptake as adjudged by inhibition of kinase function. This is in stark contrast to related Protacs utilising the same TKIs linked to the ligand for the E3 ligase cereblon (*vide infra*). This highlights a subtle interplay between target protein binder and ligase binder in Protac design, as certain combinations may result in mismatched protein orientations, preventing efficient target degradation.

In summary, recruitment of VHL as a targeted degradation strategy has demonstrated effective knockdown of a variety of both nuclear and cytoplasmic target proteins. With highly selective and potent effects also shown *in vivo*, more extensive use of VHL-dependent Protacs may offer attractive options for drug discovery.

1.4.1.2 Cereblon Protacs

While cereblon ligands themselves formally act as a Protac by allowing recruitment and degradation of neosubstrates (Section 1.3.3.2), they have also found use as a ligase-recruiting module in specifically targeted Protacs. With the knowledge that thalidomide and its analogues can effectively recruit the E3 ligase function of cereblon, several groups have successfully designed Protacs using these ligands. Bradner and co-workers conjugated a phthalimide-derived cereblon binder to the pan-BET inhibitor JQ1 to give a pan-BET Protac (dBET1, Figure 41) able to degrade BRD4 with a D_{max} > 85 % at concentrations as low as 100 nM in MV4-11 cells.[130] In a similar manner to VHL-dependent Protacs, degradation was found to have a rapid onset, with complete BRD4 knockdown observed within 2 h after incubation with 100 nM of dBET1.

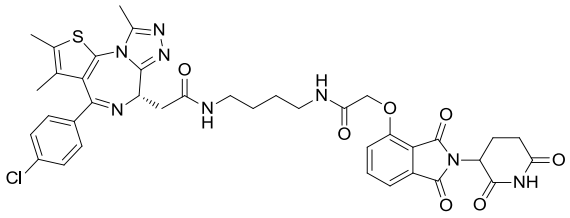

Figure 41. Structure of Bradner's JQ1-cereblon Protac dBET1

In order to delineate the effects of BRD4 inhibition and degradation, Protac dBET1 was directly compared to the parent binder JQ1. Firstly, expression proteomics were carried out to a depth of ~7400 proteins following incubation with 250 nM of JQ1 or dBET1 for 2 h. JQ1 alone was found to only cause limited knockdown of oncogenes MYC and PIM1, while incubation with dBET1 caused significant knockdown of BRD2/3/4, consistent with the pan-BET inhibition of JQ1, and induced similar downregulation of MYC and PIM1. This demonstrates the high proteome level selectivity attainable using a cereblon-recruiting Protac, as previously demonstrated by recruitment of VHL.

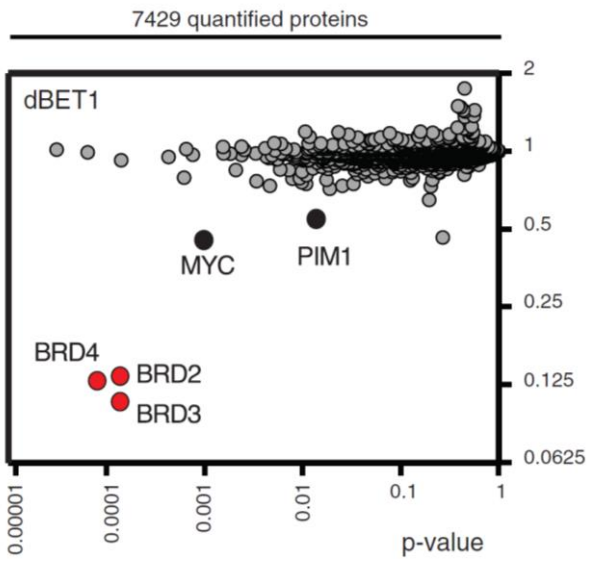

Figure 42.[130] Proteomic selectivity profile of dBET1

Pan-BET Protac dBET1 demonstrated inhibition of cell proliferation in MV4-11 cells superior to inhibitor treatment and enhanced apoptotic response in primary leukemic patient blasts, signifying the potential advantages of degradation over inhibition. In a disseminated MV4-11 xenograft model, the Protac was found to reduce the number of leukemic cells in bone marrow more potently than BET inhibitor JQ1 following daily treatment for 19 days.

An analogous approach to BRD4 degradation by Crews and co-workers also made use of JQ1 linked to a cereblon binder through an alternate linker (ARV-825, Figure 43).[131] This JQ1-cereblon Protac induced more potent degradation of BRD4, with an observed $DC_{50} < 1$ nM in Burkitt's lymphoma (BL) cell lines, demonstrating the profound effect length and physicochemical properties of the linking module can have on induced degradation and the importance of optimal linker design in achieving efficient degradation.

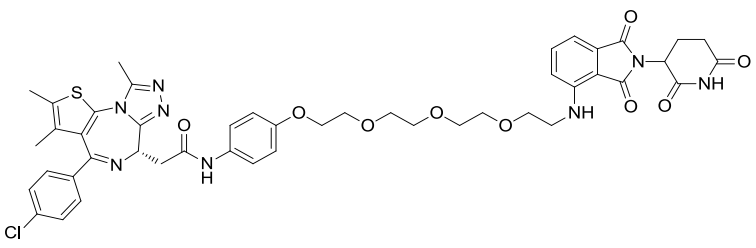

Figure 43. Crews' JQ1-cereblon Protac ARV-825

This Protac demonstrated more pronounced downregulation of the oncogene c-MYC and its downstream target SLC19A1 compared to treatment with JQ1 in BL cells, with sustained suppression of SLC19A1 after Protac washout. Again, Protac treatment was found to more effectively inhibit proliferation and induce apoptosis than the inhibitor alone. These examples of JQ1-based Protacs show how a degradation approach can significantly enhance the cellular activity of known ligands and also demonstrate effects which are sustained after drug removal, suggestive of the potential for potent *in vivo* effects from lower drug exposures and durations.

Degradation of the cis-trans isomerase FKBP12 has also been demonstrated using a FKBP12-cereblon Protac, with a DC_{50} of approximately 10 nM in MV4-11 cells (Figure 44).[130]

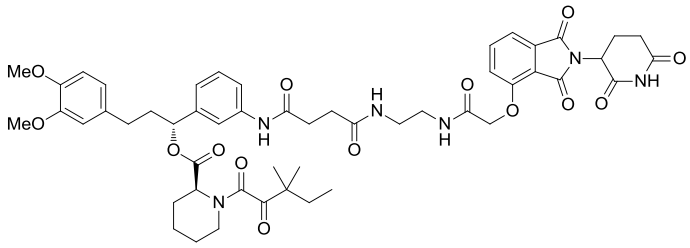

Figure 44. FKBP12-cereblon Protac

The incorporation of various tyrosine kinase inhibitors into Protacs targeting BCR-ABL has been demonstrated by recruitment of VHL (*vide supra*),[129] however stark differences were displayed upon replacement with a cereblon binder. Whilst dasatinib-VHL Protac 6 degraded ABL only, the corresponding dasatinib-cereblon Protac (Figure 45, top) degraded both ABL and BCR-ABL with a D_{max} (ABL) > 85 % and D_{max} (BCR-ABL) > 60 % after 24 h incubation at 1 μM in K562 cells. Similarly, while a bosutinib-VHL Protac was unable to degrade ABL or BCR-ABL, the corresponding bosutinib-cereblon Protac (Figure 45, bottom) induced degradation of both targets, with a D_{max} (ABL) = 90 % and D_{max} (BCR-ABL) = 80 % under the same conditions. These data demonstrate how different E3 ligases may degrade proteins with differing levels of efficiency, lending greater flexibility to apply Protac strategies to new proteins or families of proteins.

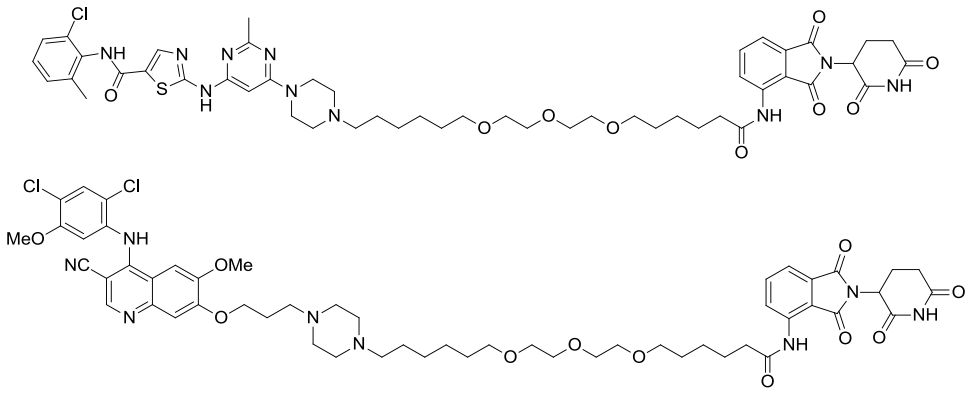

Figure 45. Cereblon Protacs targeting BCR-ABL employing dasatinib (above) and bosutinib (below)

A potential issue around using IMiD-based cereblon Protacs is their limited *in vivo* stability. Not only are the parent binders subject to facile hydrolysis *in vitro*,[132] but are prone to rapid clearance *in vivo* with the parent IMiDs having relatively short half-lives (3 – 9.5 h),[133] due in large part to oxidative metabolism and glutarimide hydrolysis.[134] Further medicinal chemistry optimisation of pharmacokinetics may be required in order to increase *in vivo* duration of action, although for Protacs which show very fast degradation, drug exposure for a relatively short period of time may be sufficient to degrade a significant amount of target protein to deliver a desired clinical response. For target proteins which are resynthesised slowly, further sustained effects may also be seen offering the possibility of long-acting drug action where the Protac may not actually be present in significant concentration for a large part of the dosing interval, leading to potential advantages in minimising unwanted pharmacology driven by high drug exposure.

Additionally, although the molecular properties which contribute to achieving oral bioavailability for molecules with molecular weights >500 are not yet fully understood,[135] the cereblon binding moiety represents one of the smallest ubiquitin E3 ligase recruiting modules, so can give Protacs with lower molecular weights, potentially increasing the chance to achieve oral bioavailability, which in turn may allow an increased range of dosing routes and clinical applications.

A further issue of using Protac derivatives of IMiDs is the potential to observe the teratogenic effects of the parent IMiDs, which may have significant implications for

the breadth of clinical application of the molecules. The exact molecular mechanism for IMiD-induced tetratogenicity has not been definitively identified, though it may be mediated by inhibition of endogenous function and accumulation of substrates such as MEIS2.[89] Further work will be required to show whether IMiD-containing Protacs do inherit these teratogenic effects and if increased therapeutic indices are possible relative to the IMiDs themselves.

1.4.1.3 IAP Protacs

A series of Protacs developed by Naito and co-workers, which have been termed Specific and Non-genetic IAP-dependent Protein ERasers (SNIPERs), contain a target protein binder conjugated to an IAP binder, recruiting its E3 ligase functionality. Early SNIPERs targeting the cellular retinoic acid binding protein II (CRABP-II) employed derivatives of the IAP ligand methyl bestatin (Figure 46). Although methyl bestatin binds the BIR3 domain of cIAP1,[136] it is also highly unselective and its significant toxicity profile limits its suitability for further development.[137]

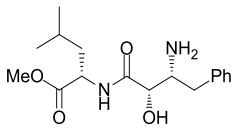

Figure 46. Structure of methyl bestatin

A CRABP-II-bestatin Protac (Figure 47, left) was effective in degrading CRABP-II, however degradation was observed only at high concentrations.[138,139] A more selective Smac-mimetic IAP ligand, MV-1,[109] has been employed as a pan-IAP antagonist in a CRABP-II SNIPER (Figure 47, right) which demonstrated complete knockdown of both CRABP-II and cIAP1 at 3 μM.

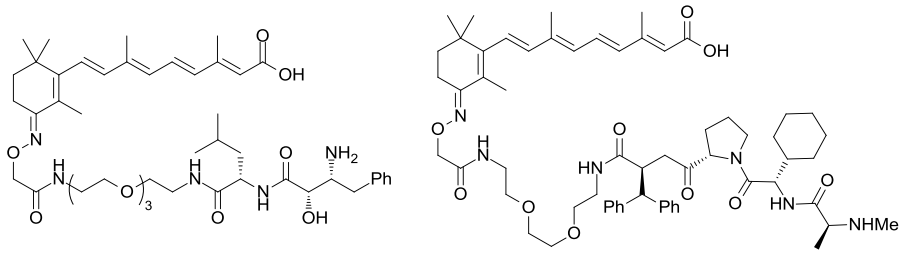

Figure 47. SNIPERs targeting CRABP-II using bestatin (left) or MV-1 (right) to recruit IAP

Further SNIPERs targeting a series of nuclear receptors (retinoic acid receptor, estrogen receptor (ER) and androgen receptor) employed bestatin to recruit cIAP1, however degradation was only observed at high concentrations (>10 μM), with retention of the potentially labile ester of bestatin.[140] An ER SNIPER was designed employing the ER antagonist Tamoxifen which demonstrated ER degradation at 10 μM concentration.[141,142] At 3 μM concentration, protein levels were observed to increase, potentially as a result of ER antagonism, however the high concentrations required for degradation prevent firm conclusions from being drawn due to the potential for cytotoxicity.

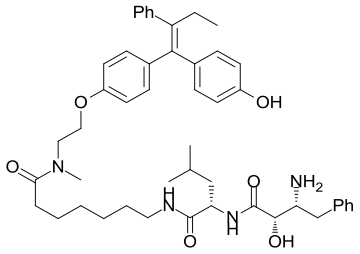

Figure 48. Bestatin-containing ERα SNIPER

Incorporation of IAP ligands into Protacs may yet be an attractive and novel strategy though reports so far have not shown the highly potent and selective cellular effects associated with use of VHL or cereblon recruitment. The vast majority of current reported SNIPERs use bestatin, which suffers from poor selectivity and moderate cIAP1 inhibition.[137] As many IAP inhibitors have been developed as potential anti-tumour agents, alternative molecules may offer new opportunities to increase the range of its application to protein degradation.

1.4.1.4 MDM2 Protacs

The tumour suppressor p53 is a is vital for the regulation of cellular processes and a common response to cellular stress is to activate and stabilise p53.[143–147] It is proposed that tumour survival in many cancers is promoted by deactivation of the p53 pathway. The E3 ligase human murine double minute 2 (MDM2), downregulates p53 by a direct PPI, one result of which is proteasomal degradation following p53 ubiquitination by MDM2.[148,149] Disruption of the MDM2-p53 interaction prevents deactivation of the p53 pathway and presents a potential therapy for multiple cancers.[150] The first report of an MDM2 antagonist was in 2004, when a subclass of molecules known as Nutlins were discovered (Nutlin-3a is presented in Figure 49).[151] Nutlin-3a was found to be a highly effective activator of the p53 pathway in cancer cells, resulting in cell cycle arrest, apoptosis and growth inhibition of tumour xenografts.

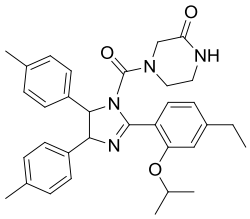

Figure 49. Nutlin-3a, an MDM2 inhibitor

In an attempt to degrade the androgen receptor (AR) by recruitment of MDM2, a nutlin inhibitor was conjugated to non-steroidal AR binder to give AR-MDM2 Protac (Figure 50).[152] Modest AR degradation was observed at 10 μM in HeLa cells, though little characterisation of the mechanism was carried out, meaning it is very difficult to assess the exact mode of action and specificity of degradation. Use of more recent MDM2 ligands may represent an attractive strategy for Protac design,[153] though currently, the utility of this E3 ligase for inducing protein degradation remains poorly described.

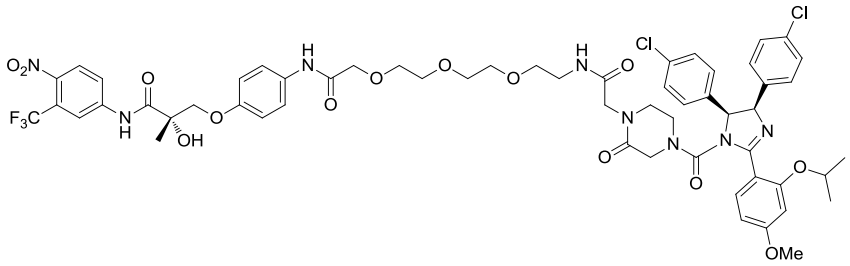

Figure 50. Structure of an AR-MDM2 Protac

1.4.2 HaloProtacs

A HaloTag is a protein tag designed to covalently bind synthetic chloroalkane ligands used to bioorthogonally label fusion proteins *in vitro*.[154] HaloProtacs are a subclass of Protacs used to degrade proteins fused to a HaloTag 7 label by recruitment of an E3 ligase. Conjugation of a VHL ligand to a hexyl chloride tag resulted in a VHL HaloProtac (Figure 51), which demonstrated dose-dependent degradation of a green fluorescent protein (GFP) - HaloTag7 fusion with a DC_{50} = 19 nM.[155] Use of the enantiomer of the VHL HaloProtac resulted in no degradation indicating the effect is dependent on ligase recruitment. This VHL HaloProtac was also able to demonstrate degradation of both ERK-1 and MEK-1 HaloTag 7 fusion proteins, indicating the potential generality of this strategy.

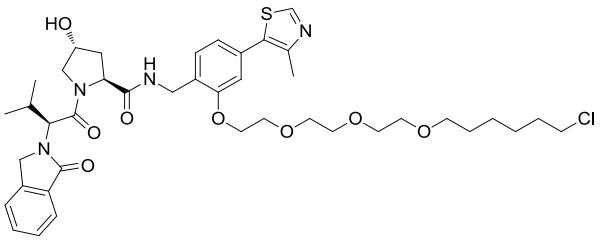

Figure 51. Structure of a VHL HaloProtac

The proposed mechanism of action of a HaloProtac is analogous to a Protac, however in this case a binary complex is formed, as the hexyl chloride tag forms a covalent bond to the HaloTag7 protein (Figure 52).[155] The HaloTag7 protein itself is thought to be resistant to ubiquitination and degradation,[156] hence it is believed that the fusion protein-ligand complex recruits VHL, allowing ubiquitin transfer onto the target protein and ultimately causing its degradation *via* the proteasome.

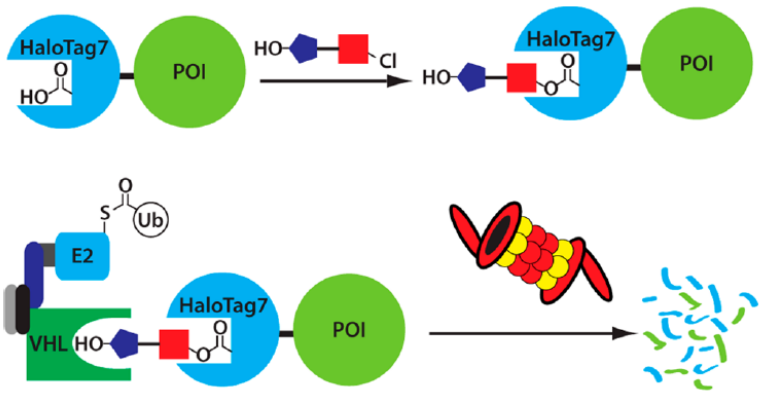

Figure 52.[155] Proposed mechanism of action of a HaloProtac (POI = protein of interest)

An analogous HaloProtac recruiting IAP has been reported employing IAP ligand MV-1 previously used in a CRABP-II IAP Protac (Figure 53),[157] however significantly higher concentrations of IAP HaloProtac were required to demonstrate any effect on protein levels.

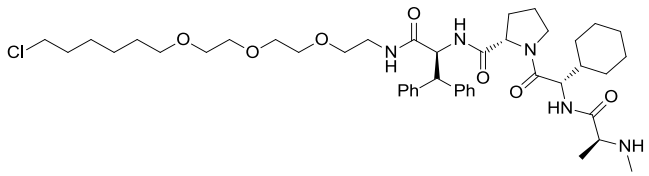

Figure 53. Structure of an IAP HaloProtac incorporating IAP ligand MV-1

1.4.3 Inhibitor-mediated Protein Degradation

Inducing direct degradation of a target protein removes the requirement for recruitment of an E3 ligase using a Protac. The most notable example of this is Fulvestrant (also known as faslodex; Figure 54, left), a selective estrogen receptor degrader (SERD), which is FDA-approved for the treatment of breast cancer.[158] Fulvestrant mediated ER degradation is believed to proceed by inducing a conformational change, resulting in exposure of a hydrophobic surface causing its ubiquitination and proteasomal degradation.[159] Fulvestrant is required to be administered by intramuscular injection and does not achieve complete ER engagement clinically.[160] Recently, a non-steroidal orally bioavailable SERD, GDC-0810 (Figure 54, right), has been described to have

superior activity over fulvestrant due to greater levels of exposure achievable using this dosing strategy.[161]

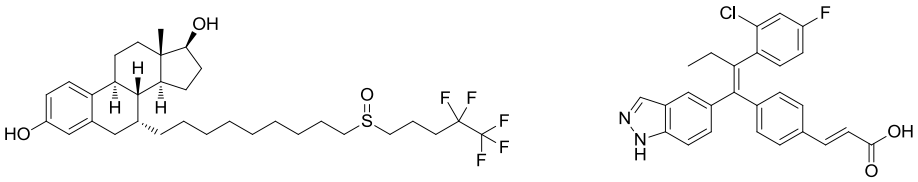

Figure 54. Structure of SERDs Fulvestrant (left) and GDC-0810 (right)

CI-1033 is a covalent inhibitor of the kinase ErbB2 (Figure 55), which also causes its degradation by the proteasome.[162] It is thought that covalent modification results in a conformational change in the ATP binding site and proteasomal degradation proceeds by a chaperone-mediated response.

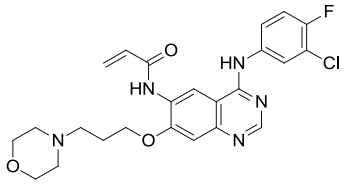

Figure 55. Structure of ErbB2 degrader CI-1033

Inhibitors that also induce protein degradation span multiple target classes. RNA polymerase I inhibitor BMH-21 (Figure 56, left) causes its proteasomal degradation by destabilisation of catalytic subunit RPA194.[163] The calcium-activated chloride channel Anoctamin-1 (ANO1) is highly expressed in cancer, however inhibition alone does not inhibit proliferation.[164] Inhibitor $CaCC_{inh}$-AO1 (Figure 56, right) was found to increase ubiquitination of ANO1, resulting in its degradation by the proteasome and inhibiting cancer cell proliferation. Again, this process is thought to proceed by causing a conformational change in ANO1.

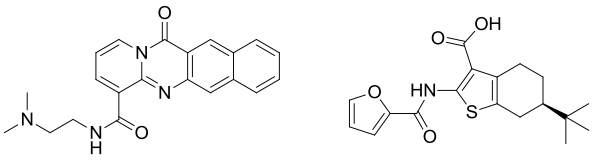

Figure 56. RNA polymerase I degrader BMH-21 (left) and ANO1 degrader $CaCC_{inh}$-AO1 (right)

The majority of inhibitors that directly induce protein degradation have been discovered serendipitously; though the attractive pharmacodynamic profile attainable using an inhibitor/degrader has triggered more targeted strategies to induce this effect. One of these strategies, known as 'hydrophobic tagging,' involves conjugation of an inhibitor to a hydrophobic group to mimic a partially misfolded protein state, resulting in degradation *via* the proteasome (as observed using Fulvestrant). This strategy was initially used to target HaloTag fusion proteins,[156,165] however has since developed into an approach amenable towards targeted proteins.

A ligand-finding strategy targeting the pseudokinase Her3 led to the discovery of the first selective Her3 covalent ligand TX1-85-1 (Figure 57, left).[166] This molecule alone was found to fully inhibit Her3 in cells, however did not inhibit Her3-dependent downstream function. Modification of this ligand with an adamantyl hydrophobic tag gave TX2-121-1 (Figure 57, right) which caused partial degradation of Her3 at 0.5 μM and 2 μM.

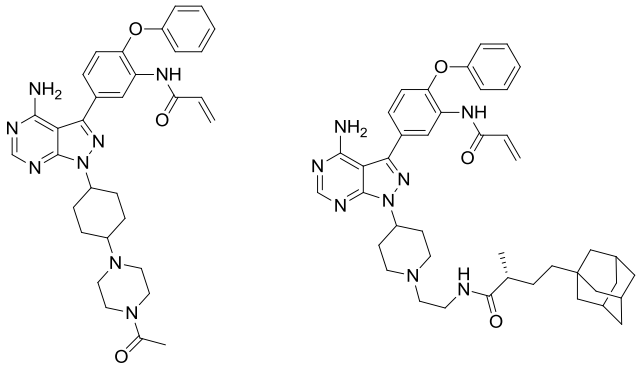

Figure 57. Her3 ligand (TX1-85-1, left) and Her3 degrader (TX2-121-1, right) generated using a hydrophobic tagging strategy

This tagged molecule was able to inhibit downstream effectors Erk and Akt, and cause cell death of Her3-dependent cell lines at 1 μM concentration.[166] Degradation was found to be dependent on the both the proteasome and molecular chaperones Hsp70 and Hsp90, which are involved in sensing protein misfolding.[167] These chaperones may recognise the hydrophobic tag and direct Her3 to the proteasome; a proposed mechanism is outlined in Figure 58.

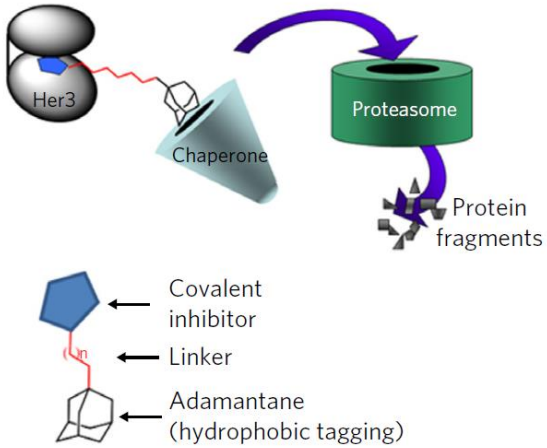

Figure 58.[166] Proposed mechanism for Her3 degradation by a hydrophobic tagging strategy

In an analogous manner to SERDs, a hydrophobic tagging approach has been taken towards AR degradation as a strategy to combat AR antagonist resistance in CRPC.[168] By modification of an AR agonist RU59063 (Figure 59, top left) with a hydrophobic tag resulted in SARD279 (Figure 59, top right), which demonstrated concentration-dependent AR degradation with a DC_{50} = 1 μM (Figure 59, bottom)

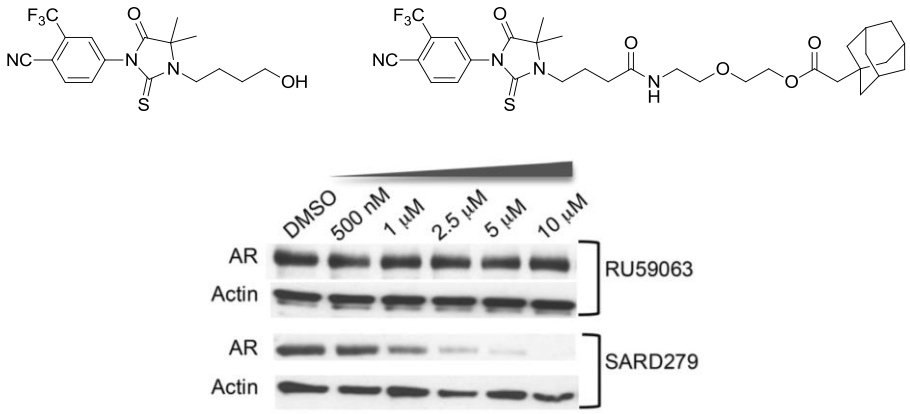

Figure 59.[168] AR agonist RU59063 (top left) and AR degrader SARD279 incorporating a hydrophobic tag (top right); western blot indicating hydrophobic tag induced AR degradation (bottom)

By a similar approach, Boc-protected arginine (Boc_3Arg) has been identified as a degron to induce protein degradation.[169] Though initially believed to proceed in a similar manner to the adamantyl conjugation strategy, the Boc_3Arg tag is now thought

to act by directly localising the target protein to the 20S proteasome and does not involve target protein ubiquitination.[170] Degradation of glutathione-S-transferase has been demonstrated by Boc_3Arg conjugation of covalent inhibitor ethacrynic acid (Figure 60, top).[169] Boc_3Arg-mediated degradation of dihydrofolate reductase has also been demonstrated by tagging of non-covalent ligand trimethoprim (Figure 60, bottom), however a higher concentration was required, suggesting that covalent inhibition may be preferable for this approach.

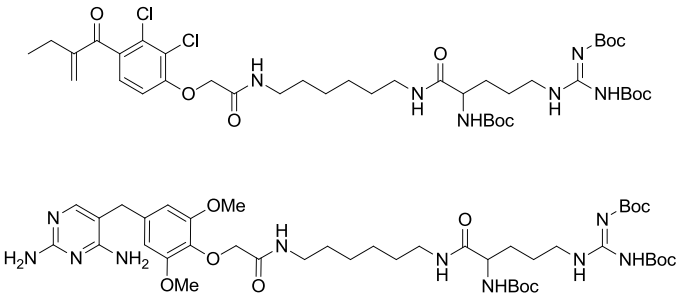

Figure 60. Boc_3Arg tagged ligands targeting glutathione-S-transferase (above) and dihydrofolate reductase (below)

1.5 Aims and Objectives

Small molecule-mediated targeted protein degradation using Protacs has recently been validated as a highly promising approach for application in drug discovery. In this thesis, development of Protacs targeting a series of disease-relevant proteins will be explored. For each protein, the biological rationale for functional inhibition will first be outlined, then the potential therapeutic benefit of targeting these proteins using a Protac-mediated degradation approach will be proposed.

Once a suitable ligand for a target protein of interest is identified, the design of Protacs based on this ligand will be described. An appropriate linking vector to the E3 ligase will be determined using available X-ray crystallography data or other literature sources, and will then be synthesised to give a sufficient amount of desired product.

The designed Protacs will then assessed to determine that biochemical inhibition of the target protein is consistent with the parent inhibitor, and that the physicochemical properties of the molecule are appropriate for further intracellular profiling. Having confirmed this, western blotting will be performed to validate target protein degradation in a relevant cell line. Identification of an active protein degrader will then allow determination of the potential advantages of target protein degradation over traditional functional inhibition.

2. ActR2B Protacs

2.1 The ActR2B Receptor

Myostatin is a protein which regulates muscle growth.[171] Myostatin null mice are viable and have a lean, muscled phenotype (Figure 61),[171,172] while knockout or overexpression of the gene in adult mice results in muscle gain or loss, respectively.[173–175] Myostatin initiates signalling by binding to type I and type II transforming growth factor beta (TGFβ) family receptors, which are transmembrane protein kinases.[176–178]

Figure 61.[172] Increased skeletal muscle mass in myostatin-null mice (right) compared to wild-type mice (left)

The primary receptor for myostatin is the Activin receptor type IIB (ActR2B), which recruits a type I acceptor, the Activin receptor-like kinase (ALK) 4 or 5, when myostatin is bound (Figure 62).[179] The type I acceptor is phosphorylated by ActR2B, leading to downstream phosphorylation of the proteins Smad2/3 inside the cell.[180,181] This is thought to be followed by translocation to the nucleus by complexation of Smad2/3 with Smad4, resulting in nuclear transcription. Hence, artificial disruption of the myostatin pathway could lead to muscle gain, which could have potential therapeutic use in the treatment of sarcopenia and other muscle wasting illnesses.

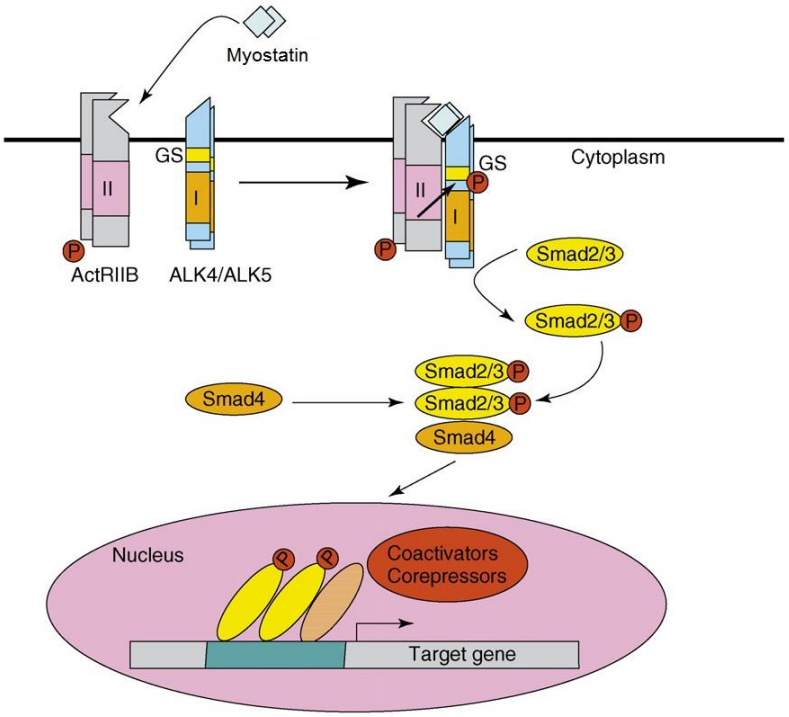

Figure 62.[178] The myostatin signalling pathway

The potential for ALK5 inhibition as a treatment for sarcopenia has been reported by Ohsawa and co-workers,[182] however ALK5 inhibitors have been reported to cause heart valve lesions in rats.[183] Therefore, inhibition of the ActR2B receptor selectively over ALK5 is required. Research undertaken within our laboratories resulted in the discovery of a series of pyridone compounds, which demonstrated good binding to ActR2B and over 100 fold selectivity over ALK5 (Figure 63).[184] Despite high levels of binding to ActR2B biochemically, none of the inhibitors from this series were able to block myostatin signalling in cells.

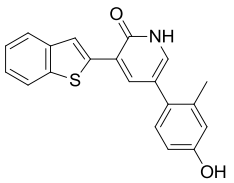

Figure 63. Small molecule ActR2B inhibitor (biochemical ActR2B pIC_{50} = 8.5, ALK5 pIC_{50} = 6.1)

As the ActR2B binder demonstrated potent biochemical binding but induced no cellular effect, it was thought that a Protac approach could exploit the high binding potency of the ligands. The target protein binder in an ActR2B Protac would not need to alter signalling by occupancy-driven kinase inhibition, it is only required to be sufficiently potent to anchor to the binding site and allow ternary complex formation, leading to ubiquitin transfer and subsequent degradation. Degradation of ActR2B should result in the same effect as siRNA-mediated ActR2B knockdown, which does antagonise myostatin signalling.[184] Therefore, degradation of ActR2B could also be a potential treatment for muscle wasting illnesses such as sarcopenia.

2.2 ActR2B Protac Design

Design of a Protac targeting ActR2B requires a combination of the VHL binding fragment and ActR2B binding fragment through a linker. The length of the linker is believed to be important as it must allow both proteins (ActR2B and VHL) to simultaneously bind to the Protac without clashing. However, designing this linker length using molecular modelling software is challenging as both proteins are extremely large in size.

The linking position to the ActR2B binder (Figure 63) was rationalised using X-ray crystal data generated from the ActR2B binder indicated in Figure 64. The pyridone and phenol fragments bind to the kinase *via* hydrogen bond interactions, while the bicyclic heterocycle extends away from the binding site and is solvent exposed. Linking as far as possible from the binding site should lead to minimal disruption of binding, thus the exit vector for the linker was chosen on the solvent front of the bicyclic heterocycle.

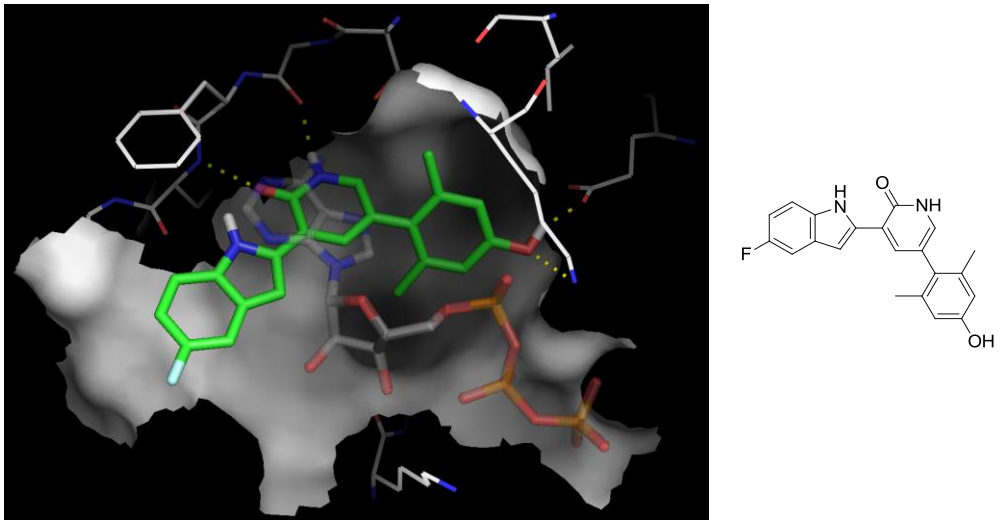

Figure 64.[184] Co-crystal structure of a lead compound and ActR2B

Two forms of VHL binder are available within our laboratories which have different linking positions.[125] This could potentially alter the angle of approach of the two proteins in the protein-Protac-protein ternary complex which may allow more efficient ubiquitination. The structures of the fragments are an amine-linked VHL binder (Figure 65, left), and a phenol-linked VHL binder (Figure 65, right).

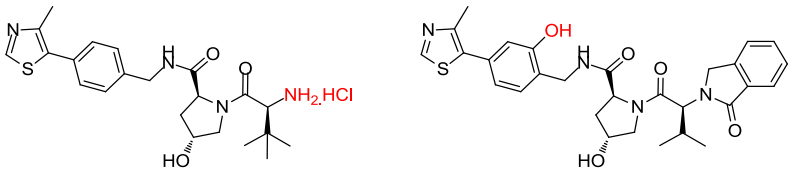

Figure 65. Active VHL binders with linking points highlighted (left, amine-linked VHL; right, phenol-linked VHL)

To confirm the mode of action of the Protacs, active and inactive VHL binding fragments are required to be linked to the ActR2B binders. Only the Protacs with the active VHL binding moiety should be able to degrade the kinase by engagement of the E3 ligase. If degradation is observed with the Protac containing the inactive VHL binding moiety, it will be concluded that this degradation does not involve the formation of the ternary complex and is related to other protein degradation pathways or cytotoxicity. The inactive VHL binders are the enantiomers of the active VHL binders (Figure 66).

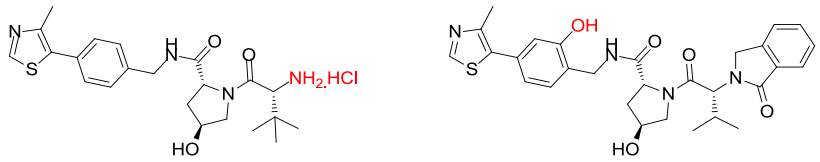

Figure 66. Inactive VHL binders with linking points highlighted (left, amine-linked VHL; right, phenol-linked VHL)

Combining these fragments resulted in the general structure of proposed ActR2B amine-linked VHL Protacs and phenol-linked VHL Protacs (Figure 67). A polyethylene glycol (PEG) linker was chosen to connect the two binding partners with an arbitrary chain length of four EG units.

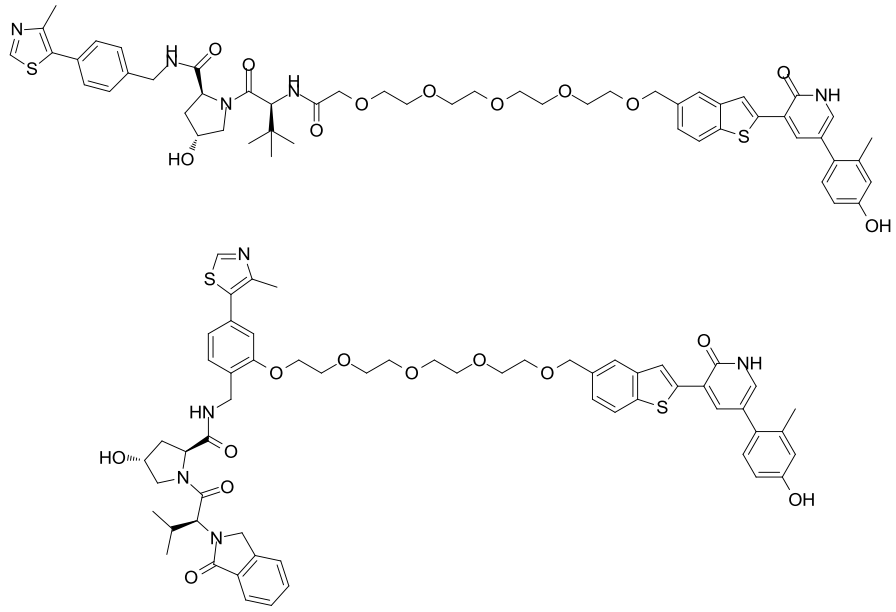

Figure 67. Structure of target active ActR2B-VHL Protacs

2.3 ActR2B Protac Synthesis

Synthesis of the ActR2B binding fragment was first investigated (Scheme 1). Commercially available 3-bromo-2-chloropyridine was treated with sodium methoxide, resulting in the formation of methoxypyridine **2** *via* nucelophilic aromatic substitution in 77 % yield. This was then treated with *N*-iodosuccinimide (NIS) in the presence of trifluoroacetic acid (TFA),[185] to give the iodinated species in 82 % yield. A Suzuki coupling was then performed using 3-bromo-5-iodo-2-methoxypyridine and commercially available (4-hydroxy-2-methylphenyl)boronic acid, selectively coupling at the iodo-substituted position over the bromo-substituted position, in line with literature precedent.[186,187] This delivered phenol **3** in 61 % yield, alongside some bis-coupled product observed during the reaction due to a second coupling at the bromo-substituted carbon.

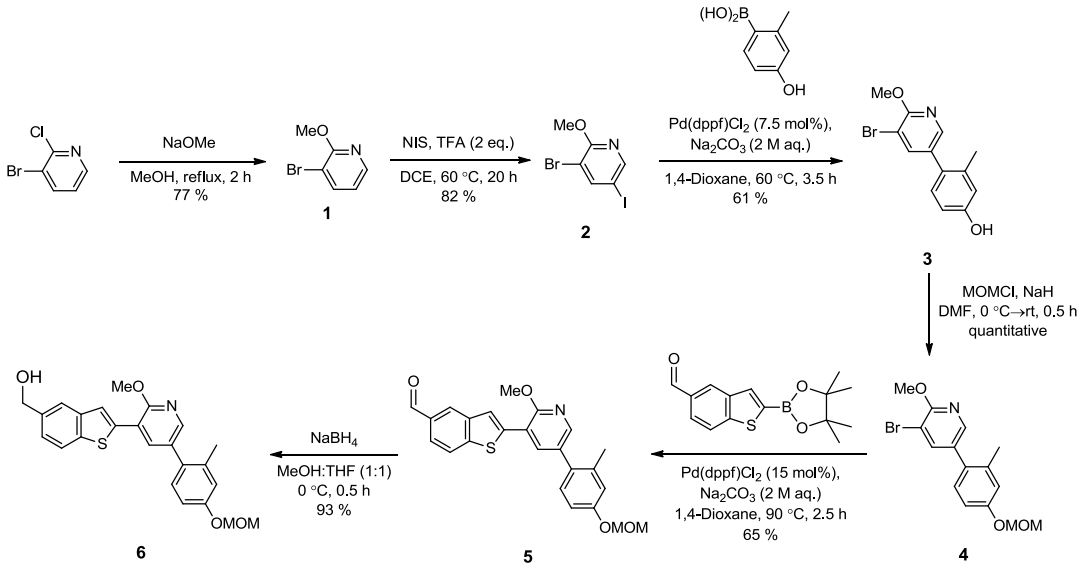

Scheme 1. Synthesis of ActR2B-binding fragment precursor

The phenol was then protected with methoxymethyl chloride (MOM-Cl) in the presence of sodium hydride to yield MOM-protected **4** quantitatively. The acid-sensitive protecting group was chosen to facilitate a late stage 3-fold acid deprotection of the phenol, 2-methoxypyridine and carboxylic acid (*vide infra*) moieties in one step. This protection reaction was also tested in the presence of weaker base *N*,*N*-diisopropylethylamine (DIPEA), however the reaction failed to reach greater than 60

% conversion, even after addition of excess MOM chloride and base. Substrate **4** was then subjected to a further Suzuki coupling using an aldehyde-containing boronic ester synthesised within our laboratories,[188] delivering aldehyde **5** in 65 % yield. Reduction of **5** with sodium borohydride generated benzylic alcohol **6** in 93 % yield.

In order to assess the binding ability of compound **7** alone (Scheme 2), a full deprotection of **6** was attempted. Using HCl (4 M in dioxane) at 70 °C or TFA in dioxane at reflux led to deprotection of the MOM group only, failing to demethylate the 2-methoxypyridine moiety. Changing the acidic media to HCl (6 M aqueous (aq.)) resulted in obtaining the fully deprotected product **6** with a 19 % yield. This low yield was the consequence of partial chlorination of the benzylic alcohol in the product and formation of the partially deprotected intermediate (compound **7a** and **7b**, Figure 68) observed during the course of the reaction (these side products were observed by LCMS and were not isolated). Compound **7** was submitted to the ActR2B binding assay and the data is presented later in Table 1.

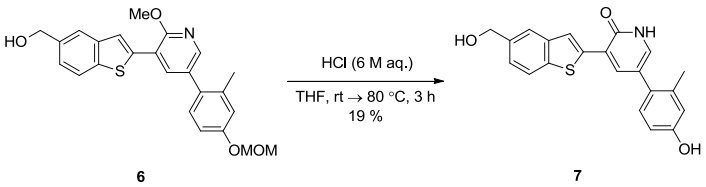

6 7

Scheme 2. Deprotection reaction yielding the ActR2B binder **7**

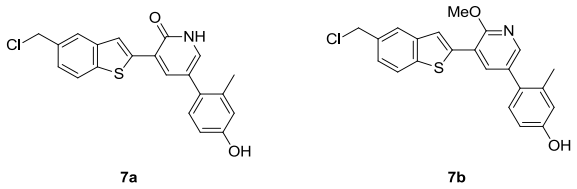

7a **7b**

Figure 68. Side products observed by LCMS during the deprotection reaction described in Scheme 2

In order to synthesise amine-linked VHL Protacs, an *O*-alkylation was carried out using sodium hydride in *N*,*N*-dimethylformamide (DMF) with a tosylated *tert*-butyl ester PEG chain linker synthesised within our laboratories.[125] This process proceeded with concomitant ester deprotection, resulting in acid **8** in 65 % yield (Scheme 3). Treatment of acid **8** with HCl (6 M aq.) afforded deprotected acid **9** in 39 % yield.

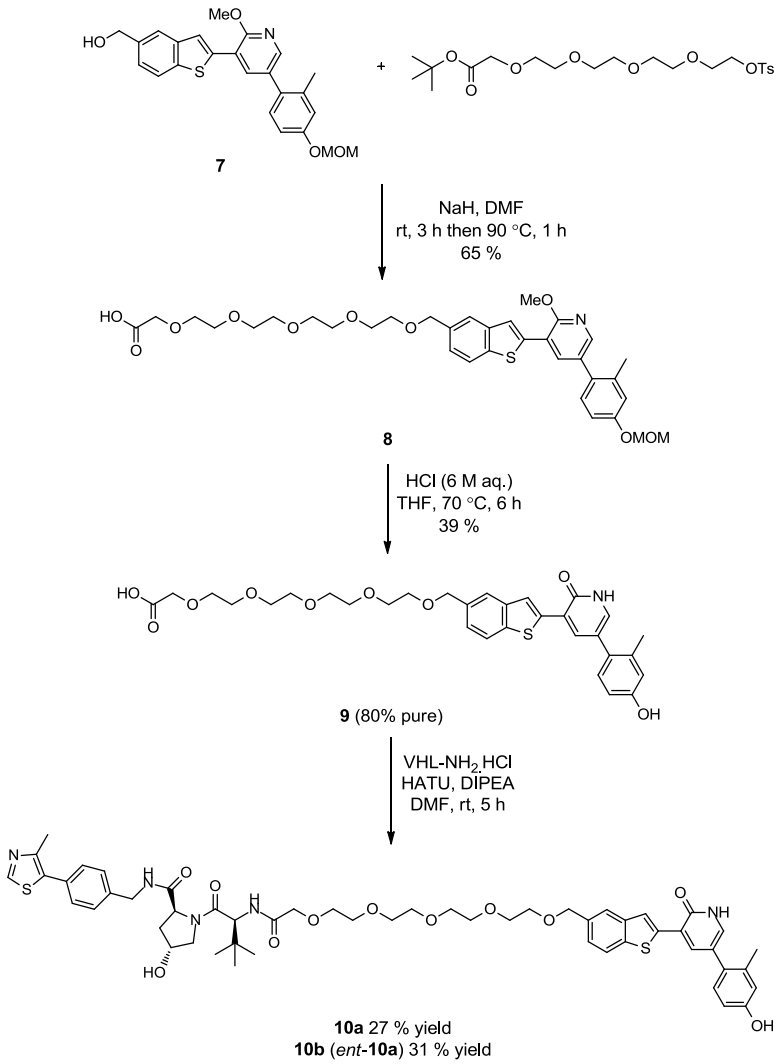

Scheme 3. Synthesis of active/inactive amine-linked VHL Protacs **10a** and **10b**

Intermediate **9** was then coupled to the active and inactive VHL amines, synthesized within our laboratories,[189] using amide coupling reagent 1-[bis(dimethylamino)methylene]-1*H*-1,2,3-triazolo[4,5-*b*]pyridinium 3-oxide hexafluorophosphate (HATU) in the presence of DIPEA.[190] This resulted in attainment of the desired Protacs **10a** and **10b** in moderate yields (27 % and 31 %, respectively).

Since the available phenol-linked VHL binders are linked through a different functional group, an alternative approach was required to synthesise the corresponding Protacs. Previously synthesised protected alcohol **6** was alkylated with a dichlorinated PEG linker to give the intermediate **11** in 61 % yield (Scheme 4). This was linked to active and inactive phenol-linked VHL binders to give precursors **12a** and **12b** in low

yield in the presence of K_2CO_3 (13 % and 22 %, respectively), followed by deprotection with HCl (4 M in dioxane) to give phenol-linked VHL Protacs **13a** and **13b** in moderate yield (63 % and 58 %, respectively). Deprotection under these conditions proceeded in improved yield compared to a previous synthesis of **13a** and **13b**, where use of HCl (6 M aq.) delivered the same product in significantly lower yields.

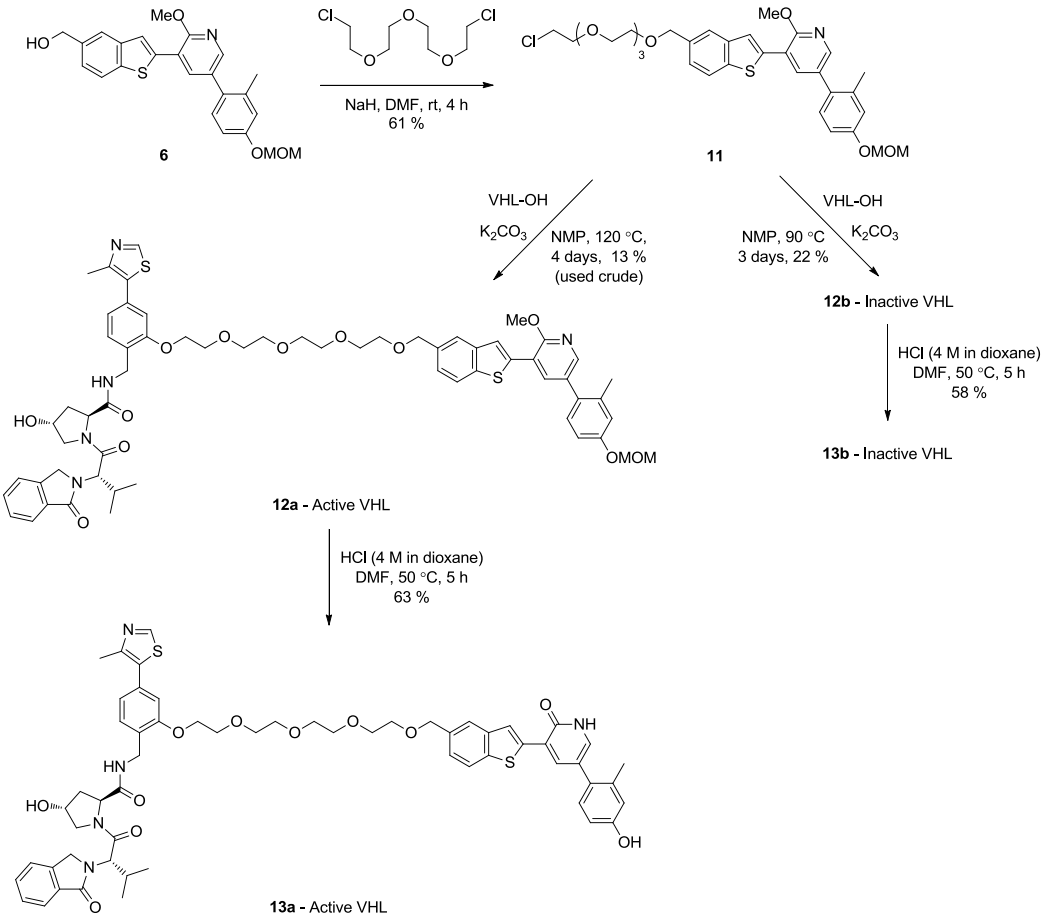

Scheme 4. Synthesis of phenol-linked VHL Protacs **13a** and **13b**

2.4 ActR2B Protac Profiling

The synthesised compounds were first tested in a biochemical ActR2B fluorescence polarisation (FP) binding assay, measuring displacement of a fluorescent ligand from the ActR2B kinase domain, and also in an ALK5 biochemical assay to assess whether binding to ActR2B was maintained and selectivity over ALK5.

Table 1. Data collected for ActR2B-related compounds

Compound	ActR2B pIC_{50}	ALK5 pIC_{50}	VHL pIC_{50}	A204 pIC_{50}[1]	Chrom LogD	Solubility (µM)[2]
7	8.2	6.9	<4	5.1	2.7	37
9	8.0	6.7	<4	<4.3	2.1	382
10a	6.8	6.0	6.4	5.6	4.3	40
10b	6.4	6.3	<4	<4.3	4.3	19
13a	6.1	5.9	nd	<4.3	4.8	≥498
13b	6.2	5.6	<4	<4.3	4.8	328

[1]6 h incubation with compound in A204 cells with 2 nM myostatin; lower limit of assay = 4.3 [2]Solubility measured by chemiluminescent nitrogen detection (CLND)

Compound **7**, the proposed ActR2B binder, proved to be potent towards ActR2B with approximately 10 fold selectivity over ALK5 in biochemical assays. Attachment of the linker in compound **9** mostly retained potency and selectivity towards ActR2B in the same assays. However, in the resulting Protacs **10a**/**10b** and **13a**/**13b**, the pIC_{50} towards ActR2B decreased by 1-1.5 log units and selectivity over ALK5 was lost. The reason for this decrease in potency is explored below. As expected, the active VHL Protac **10a** was found to be potent at VHL (pIC_{50} = 6.4) compared to the inactive VHL Protac **10b** (pIC_{50} < 4). Compounds **7** and **9** were also inactive towards VHL, which confirms no interference of the ActR2B binder at the VHL binding site.

The compounds were tested in a cellular myostatin signalling assay based on assays reported in the literature,[179–181] carried out by incubation with the compound in A204 rhabdomyosarcoma cells with 2 nM myostatin for 6 h and measuring luciferase activity

of a phospho-SMAD2/3 dependent promoter. ActR2B binder **7** was found to be weakly active in this assay; however, this is may be due to inhibition of ALK5. Protac **10a** appeared to show activity in the cellular assay (pIC_{50} = 5.6), however, the raw data indicated little difference between **10a** and **10b**. Accordingly, the registered activity is believed to be due to an artefact from the curve fitting software; therefore it was concluded that Protac **10a** was inactive in the cell assay.

The four Protacs were then tested to assess whether degradation of ActR2B would be observable by western blotting, a semiquantative measure of the level of specific proteins in a cell lysate relative to an internal control.[191–193] A204 cells were treated with increasing concentrations (0.5 µM to 18 µM) of active and inactive Protacs for 6 h and 24 h and the ActR2B levels in the cell lysates were analysed and compared to a cellular reference protein (actin), which should not be degraded by the Protac mechanism (Figure 69). The intensity of the ActR2B and actin bands remained relatively constant (within experimental error) across the various concentrations and incubation times and no significant differences were observed between the active and inactive Protacs. It was therefore concluded that none of the Protacs demonstrated significant degradation of ActR2B, which was consistent with the lack of activity observed in the A204 cell assay.

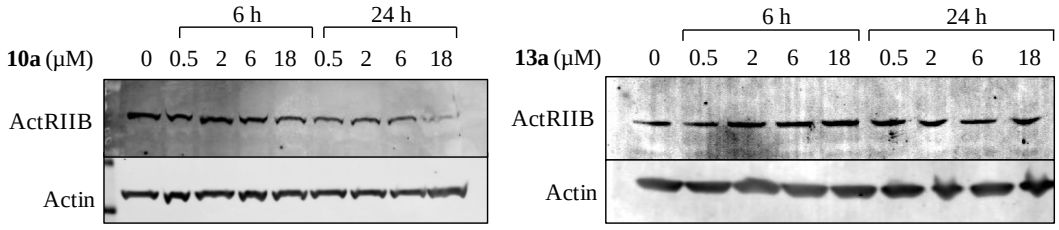

Figure 69.[194] Western blots assessing degradation of ActR2B in A204 cells using Protacs **10a** and **13a** relative to actin as an internal control

2.5 Conclusions

The synthesis of Protacs targeting ActR2B was successfully performed in 9 linear steps. These Protacs were found to have moderate potency towards ActR2B, however failed to show any functional response in cellular assays or degradation experiments. A potential reason for this lack of observable activity may depend on the subcellular localisation of the protein, which will be explored below.

At the same time as the synthesis of ActR2B Protacs was carried out, research elsewhere within our laboratories aimed to further explore kinase degradation. Vandetanib (**A**), a non-selective kinase inhibitor,[195] was modified into a Protac using the same crystal structure-based rationale used for the ActR2B Protacs.[189] The Vandetanib-based Protacs were found to have similar levels of potency at kinases RIPK2 and vascular endothelial growth factor receptor 2 (VEGFR2) as for the ActR2B Protacs, and equally comparable physicochemical properties (Table 2).

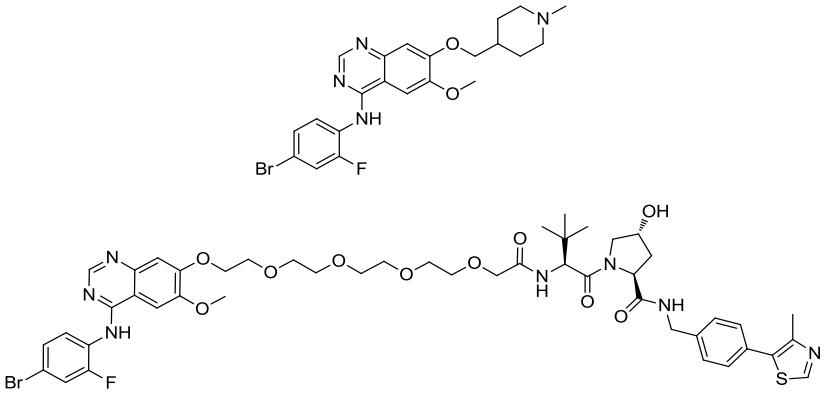

Figure 70. Vandetanib (above) and Vandetanib-VHL Protac (below)

The Vandetanib Protac demonstrated some potency in a cellular RIPK2 assay, confirming that the molecule was able to engage RIPK2 inside a cell (pIC_{50} = 6.5, Table 2).

Table 2. Profiling of Vandetanib-based compounds

Compound	RIPK2 pIC_{50}	RIPK2 cell pIC_{50}	VEGFR2 pIC_{50}	VHL pIC_{50}	Chrom LogD	Solubility (µM)[1]
Vandetanib	7.2	6.4	7.9	<4	3.1	296
Vandetanib Protac (active)	5.8	6.0	6.2	6.5	4.9	25

[1]*Solubility measured by CLND*

The Vandetanib based Protac was then tested in western blotting experiments to assess the potential degradation of RIPK2. The active VHL Vandetanib Protac demonstrated concentration-dependent degradation of RIPK2, with a DC_{50} = 800 nM following 4 h incubation in HEK293 cells (Figure 71, top). RIPK2 protein levels partially recovered at higher concentrations (10 µM), indicative of the hook effect. The corresponding inactive VHL Protac had no effect on RIPK2 protein levels (Figure 71, bottom).

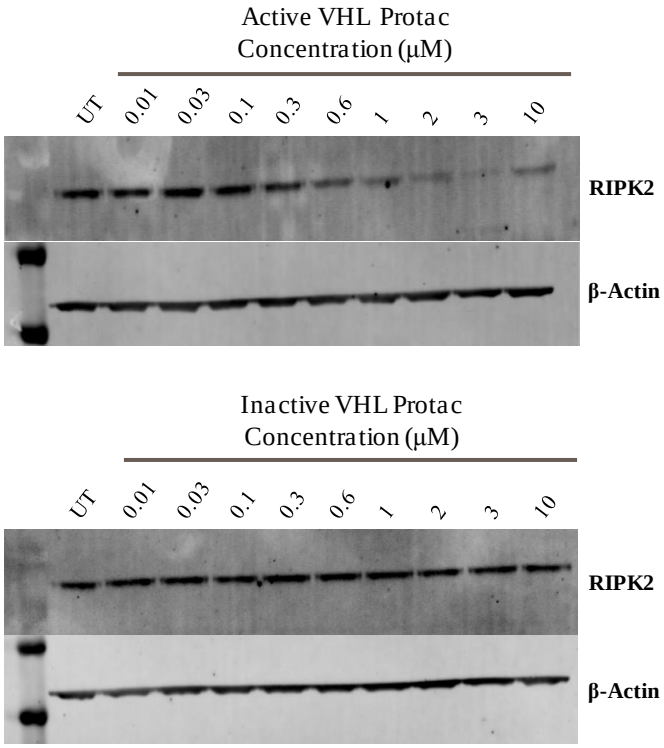

Figure 71. RIPK2 degradation observed with active VHL Vandetanib Protac (top) and not with the corresponding inactive VHL Protac (bottom) following 4 h incubation in HEK293 cells

Despite a similar binding for RIPK2 and VEGFR2 in the biochemical assays (Table 2), the Vandetanib-VHL Protac did not degrade VEGFR2 at any of the concentrations tested (Figure 72). Although both kinases are intracellular, they are located in different parts of the cell: whilst RIPK2 is mostly located in the cytoplasm,[196] VEGFR2 is a transmembrane receptor tyrosine kinase (RTK).[197]

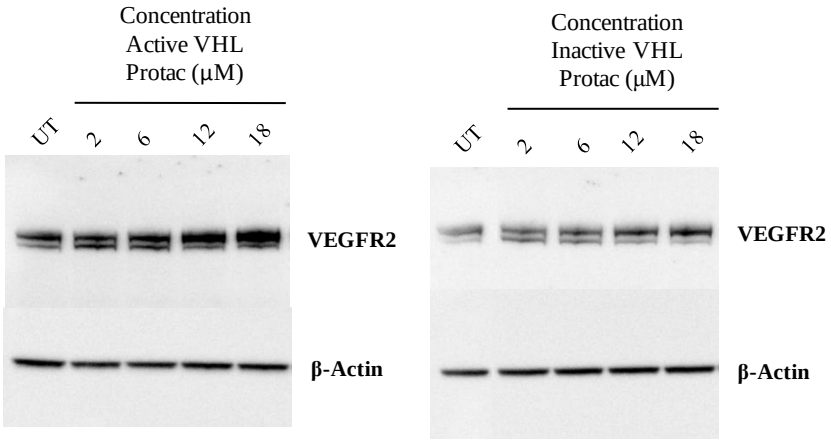

Figure 72. No degradation of transmembrane kinase VEGFR2 is observed with active/inactive VHL Vandetanib Protacs following 4 h incubation in SW579 cells

It was therefore hypothesised that the subcellular localisation of the kinase may influence whether degradation is observed. It is known that ubiquitination of transmembrane proteins is possible, and is often a signal for their endocytosis and degradation through the lysosomal pathway.[198] As ActR2B and VEGFR2 are both transmembrane kinases, and VEGFR2 is not degraded by a functioning Protac despite evidence of binding, this class of proteins may not be amenable to Protac-mediated degradation. Their localisation in the membrane may sterically hinder the approach of the E3 ligase complex, thus preventing ubiquitin transfer onto the protein. Equally, this class of proteins may not present a significant number of cytoplasm-exposed lysines when compared to cytosolic kinases, for which a greater degree of potential conformations and surface area will be accessible. Due to the lack of degradation or cellular effects observed with the synthesised ActR2B Protacs, no further experiments were conducted and an alternate disease-modifying target was selected.

3. TR Protacs

3.1 The Thyroid Hormone Receptor

3.1.1 Biological Role and Structure

The thyroid hormone receptor (TR) belongs to the nuclear receptor family, a class of intracellular, ligand-regulated transcription factors.[199–201] TR is regulated by the endogenous thyroid hormone ligands triiodothyronine (T_3) and its precursor thyroxine (T_4), which play an important role in growth, development, and homeostasis (Figure 73).[202]

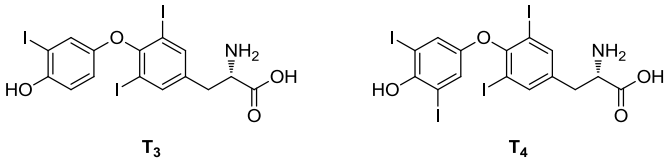

Figure 73. Structures of endogenous TR ligands T_3 (left) and T_4 (right)

There are two thyroid hormone receptor subtypes (TRα and TRβ), which are expressed by two different genes, located on chromosomes 17 and 3, respectively.[202] Each gene produces two isoforms, however only the TR isoforms α_1, β_1, and β_2 bind T_3 and T_4. Like other nuclear receptors, these TR isoforms are comprised of mostly homologous deoxyribonucleic acid (DNA) binding domains (DBDs) and ligand binding domains (LBDs). The LBDs of TRα and TRβ differ by a single amino acid residue (Ser-277 vs. Asn-311), however, their *N*-terminal domains are unconserved and are of variable length (Figure 74).[202]

The TRβ isoforms are the most predominant; $TR\beta_1$ has high expression in the brain, liver, and kidney,[203,204] while the mRNA for $TR\beta_2$ is most abundant in the anterior pituitary, yet undetectable in the liver, kidney, heart, cerebrum, and other organs of adult rats.[205] Unlike the highly localised $TR\beta_2$, $TR\alpha_1$ and $TR\beta_1$ are expressed in almost all tissues with variable distributions, with $TR\alpha_1$ showing high abundance in skeletal muscle and the brain.[206]

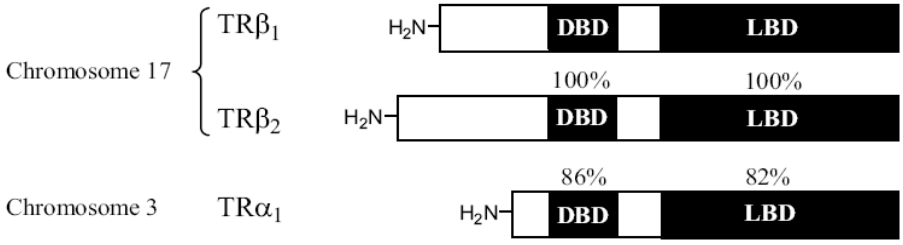

Figure 74.[207] Comparison of the TR isoforms β_1, β_2, and α_1. Amino acid homology with isoform β_1 is indicated as a percentage above each domain

TR is mostly transcriptionally active as a heterodimer with the retinoid X receptor (RXR),[208,209] and is activated or repressed by interacting with co-activators or co-repressors when T_3 is bound or unbound, respectively (Figure 75, above).[210] The TR/RXR dimer is bound to DNA at thyroid response elements (TRE) regardless of binding site occupancy, unlike steroid hormone receptors such as ER.[211] Helix 12 (H12) is relatively mobile and acts as a 'molecular switch' for the receptor. When T_3 is bound, H12 closes over and a hydrophobic cleft is formed by residues on H3, H5, and H12, acting as a docking site for the LXXLL motif of the co-activator (where L = lecuine and X = any amino acid), eventually resulting in nuclear transcription (Figure 75, below).[212]

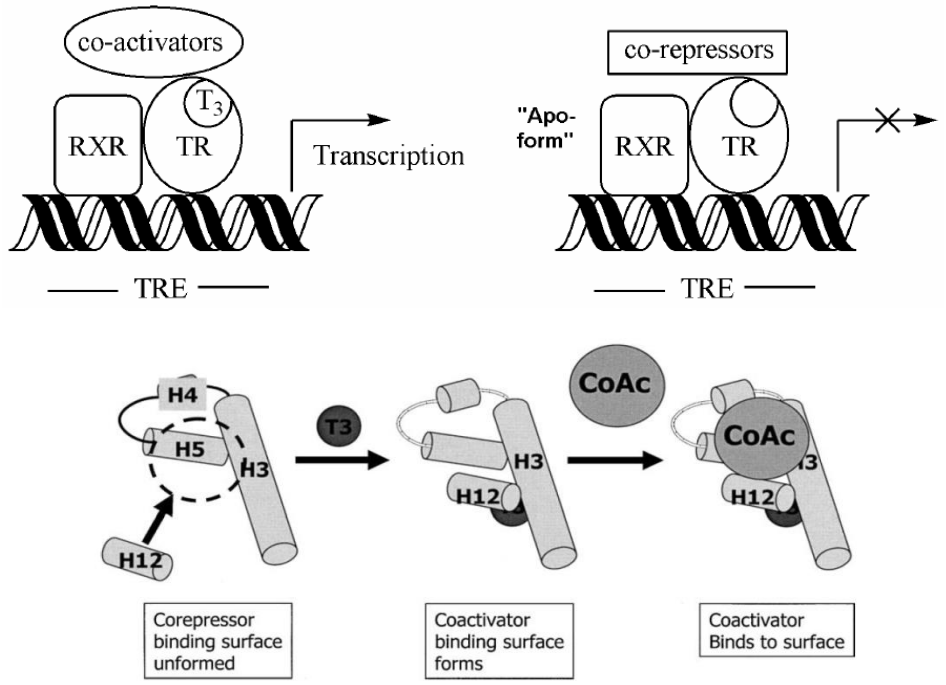

Figure 75.[207,213] Above: The RXR/TR heterodimer and the role of co-activators/co-repressors in transcription. Below: The role of T_3 and H12 in co-activator binding

The multiply halogenated structures of T_3 and T_4 are not particularly amenable to systematic modification,[214] however halogen-free thyromimetic scaffold GC-1 is a TRβ-selective agonist with sub-nanomolar affinity, offering easy access to analogues (Figure 76).[215] The solved X-ray crystal structure of GC-1 like TRβ-selective agonist KB141 in complex with TRβ indicates the key interactions made in the LBD (Figure 77).[216] A hydrogen bond between the 4'-phenol and His-435 is important for binding and activity. Substituents at the 3-, 5- and 3'- positions occupy hydrophobic pockets of the receptor, and sterically force the perpendicular conformation of the two rings.

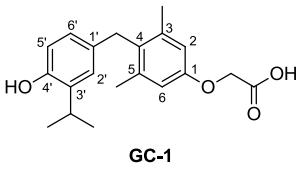

GC-1

Figure 76. Structure of thyromimetic GC-1 including ring numbering system

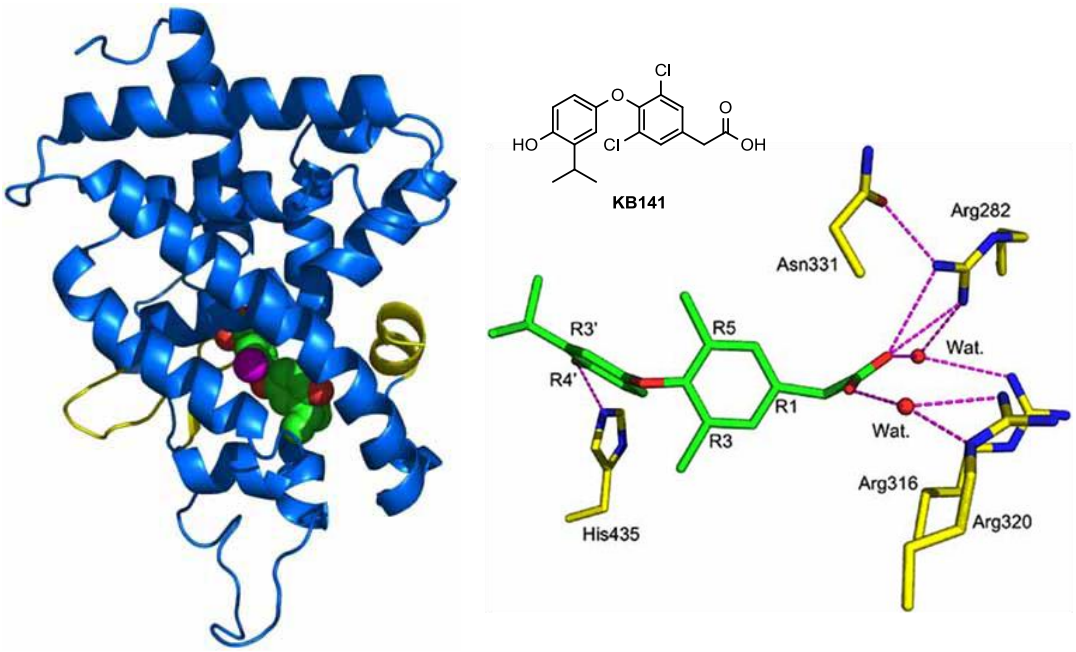

Figure 77.[216] Left: The ligand binding domain of TRβ_1 in complex with the TR agonist KB141 (green, structure inset). H12 (yellow) covers the entrance to the binding pocket. Right: Key interactions made by agonist KB141 (green) in complex with TRβ_1 (yellow).

3.1.2 TR Direct Antagonists

Although the crystal structures of several bound TR agonists have been solved, there is no crystal structure of unbound or antagonist-bound TR; thus assumptions have to be made in TR antagonist design. The structures and affinities of the most significant direct TR antagonists are outlined in Figure 78 and Table 3, respectively. All three antagonists bind to human TRα/β with $pIC_{50}/pK_d > 6.8$ and demonstrate no significant selectivity between each isoform.

Table 3. Binding affinities of TR antagonists

Name	Human TRα (nM)	Human TRβ (nM)
NH-3[217]	93 ±23	20 ±7
HY-4[218]	112 ±18	149 ±13
KK-1[219]	36 ±3	22 ±3

Data for NH-3/HY-4 expressed as mean K_Ds ±SE.

Data for KK-1 is expressed as a mean IC_{50} ±SE.

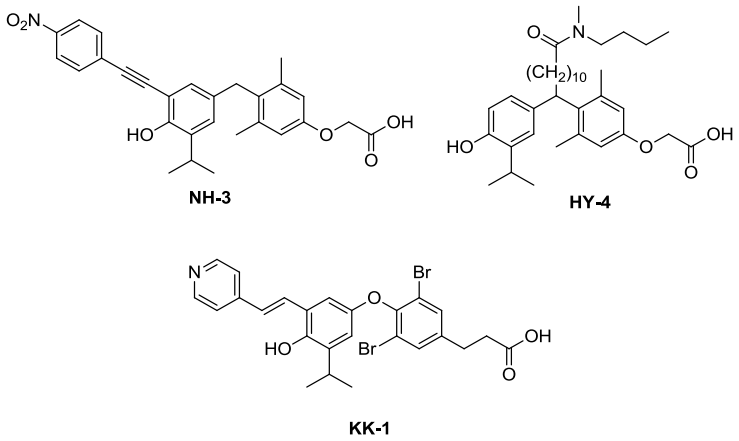

Figure 78. Literature TR antagonists

The TR antagonist NH-3 was designed following an extension hypothesis, by which direct projection from the 5' position could disturb the packing of H12 and prevent formation of the co-activator binding surface.[217] NH-3 was the first TR antagonist to exhibit inhibition of thyroid hormone *in vivo*;[220] however, pharmacological assessment of NH-3 in rats revealed that it acts as a partial agonist at higher doses.[221] It important to note that the nitro group can be metabolically activated to a nitroso species which is associated with toxicity,[222] yet also appears to be important with respect to antagonist activity. A large number of alternative substituents on the extension resulted in agonist activity.[223]

KK-1, another TR antagonist, was designed following the same extension hypothesis. A pyridyl vinyl group was selected in order to increase water solubility and molecular modelling indicated that the extension would cause a steric clash with the H12 agonist

conformation (Figure 79), promoting antagonism.[219] KK-1 was found to act as a full antagonist in a reporter assay in Chinese hamster ovary K1 cells.

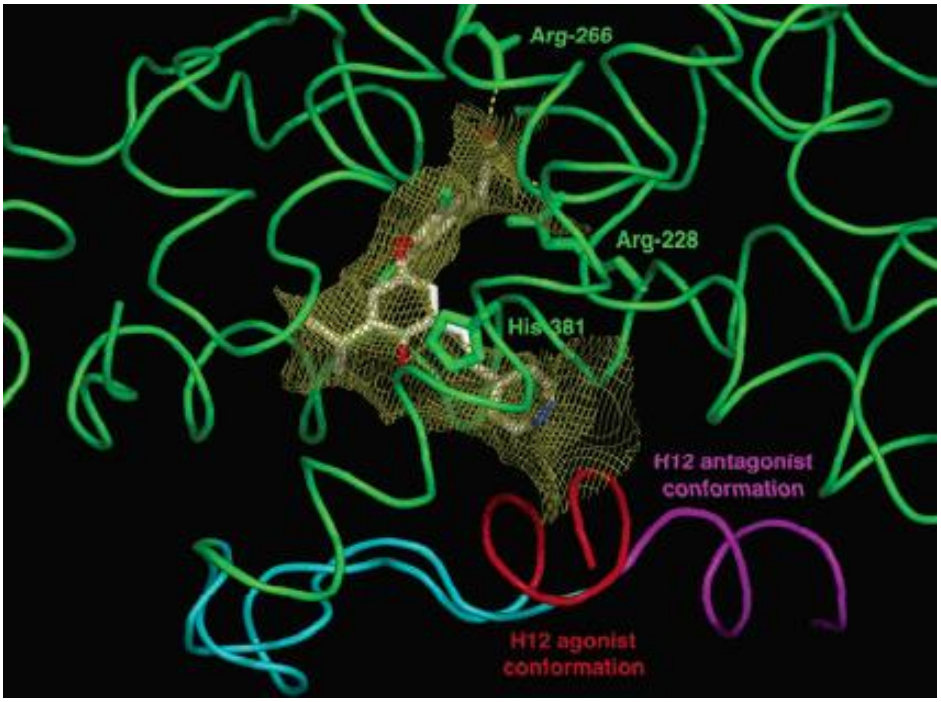

Figure 79.[219] TR antagonist KK-1 docked into the TRβ binding site indicating the agonist bound (red) and antagonist bound (purple) conformations of H12

HY-4 (Figure 78, right) was designed following the solved crystal structure of ER antagonist ICI-164,384 bound to ER (Figure 80, left);[224,225] it was believed that a similar alkylamide extension from the bridge position of GC-1 would project out in the same direction, leading to TR antagonist activity.[218] HY-4 was found to behave as a competitive antagonist, while shorter chain extensions led to weak agonist activity (Figure 80, right); hence, it is believed that the amide and long carbon chain prevents binding of co-activators.

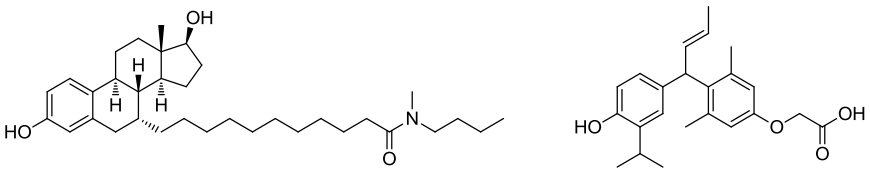

Figure 80. Left: ER antagonist ICI-164,384, used to design the TR antagonist HY-4. Right: TR agonist with a short bridge extension.

3.2 TR Protac Project Aims

3.2.1 Potential Clinical Application

Low circulating levels of thyroid hormone leads to hypothyroidism, which is commonly treated by hormone replacement using synthetic T_4 (also known as Levothyroxine).[226] Conversely, elevated levels of T_3 or T_4 result in hyperthyroidism, manifesting as weight loss, muscle wasting, tachycardia, cardiac arrhythmia, bone loss, and anxiety.[227] The underlying cause of 50-80 % of cases of hyperthyroidism is Graves' disease, where antibodies bind to the thyroid gland and promote thyroid hormone secretion.[228]

Current treatments for hyperthyroidism include treatment with methimazole (or carbimazole), propyluracil, radioiodine treatment, or complete thyroid removal. The thioamide drugs methimazole, its corresponding prodrug carbimazole, and propyluracil (Figure 81) inhibit thyroperoxidase, an enzyme involved in thyroid hormone synthesis; however these drugs take 4-8 weeks to show an effect since the existing high levels of thyroid hormone must first be depleted.[229–231] Treatment with radioiodine reduces the size of the thyroid gland, however can reduce the gland to such an extent that the patient is rendered hypothyroidic.[232] Radioiodine treatment is also not tolerable for a number of patients, including pregnant women, children, and patients with severe thyrotoxicosis. In severe cases, removal of the thyroid gland is necessary, with the patient requiring permanent treatment with thyroxine.[233]

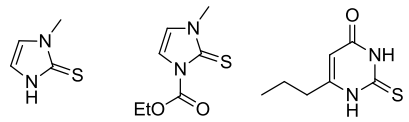

Figure 81. Marketed thioamide antithyroid agents: methimazole (left), carbimazole (middle) and propyluracil (right)

There is a clinical need for a fast-acting, titratable medicine to treat hyperthyroidism, however no described TR antagonists are adequate for this purpose; therefore a Protac approach may be relevant in this case. By reducing protein levels by degradation of TR, the amount of circulating T_3/T_4 that is recognised by the receptor would be reduced

and decrease the activity of the thyroid, therefore this approach may be a potential therapy for hyperthyroidism. Previous success with degradation of ER, another nuclear receptor, gives confidence in the prospect of inducing TR degradation.[125]

3.2.2 TR Protac Design

In order to design a TR Protac, an existing antagonist is required to be modified in order to effectively bind TR. Agonism is not desirable in this context; activation of the receptor before degradation of the target would be detrimental to a patient with hyperthyroidism. Ideally, the TR antagonist should be non-selective across TR subtypes (or TRα selective); since selective TRβ degradation could leave TRβ containing organs hypothyroidic (liver, kidneys, pituitary), while other organs would remain at basal TR levels.[207]

The structure of TR antagonist NH-3 suggests that linking to the VHL binder through the 5'-extension may result in a TR antagonist Protac (Figure 82). Preparative studies relating to potential NH-3 based Protac structures will be described in later sections.

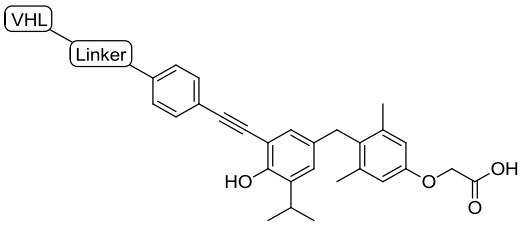

Figure 82. General structures of proposed Protacs based on TR antagonist NH-3

3.2.3 TR Assay Systems

In order to assess the potency and binding mode of the Protac, a TRα and TRβ time resolved fluorescence resonance energy transfer (TR-FRET) assay was available,[234] the principle of which is outlined in Figure 83. Recombinant TRα or TRβ ligand binding domain modified with a glutathione S-tranferase (GST) tag binds to an anti-GST tagged antibody modified with a terbium cryptate, which acts as the fluorescence donor.

The fluorescence acceptor is a streptavidin conjugate bound to an LXXLL co-activator motif; this can only bind when the co-activator binding site is formed (when H12 is closed, see Section 3.1.1). In the agonist mode of the assay, the LXXLL conjugate does not bind in the absence of an agonist ligand, however as the concentration of agonist is increased, the level of binding between the LXXLL conjugate and the receptor increases, resulting in an increased FRET signal. An antagonist would show no effect in this assay, since the co-activator binding site cannot form.

In antagonist mode, a fixed level of agonist (T_3) is present, resulting in a baseline non-zero FRET signal. As the TR ligand is titrated in, an agonist would lead to increased co-activator binding, increasing the FRET signal, while titrating an antagonist would reduce co-activator binding, reducing the FRET signal. For all the assays, potencies are derived from a dose response curve comparing FRET signal and ligand concentration and presented as EC_{50} or IC_{50} values, depending on whether the compound is an agonist or antagonist, respectively.

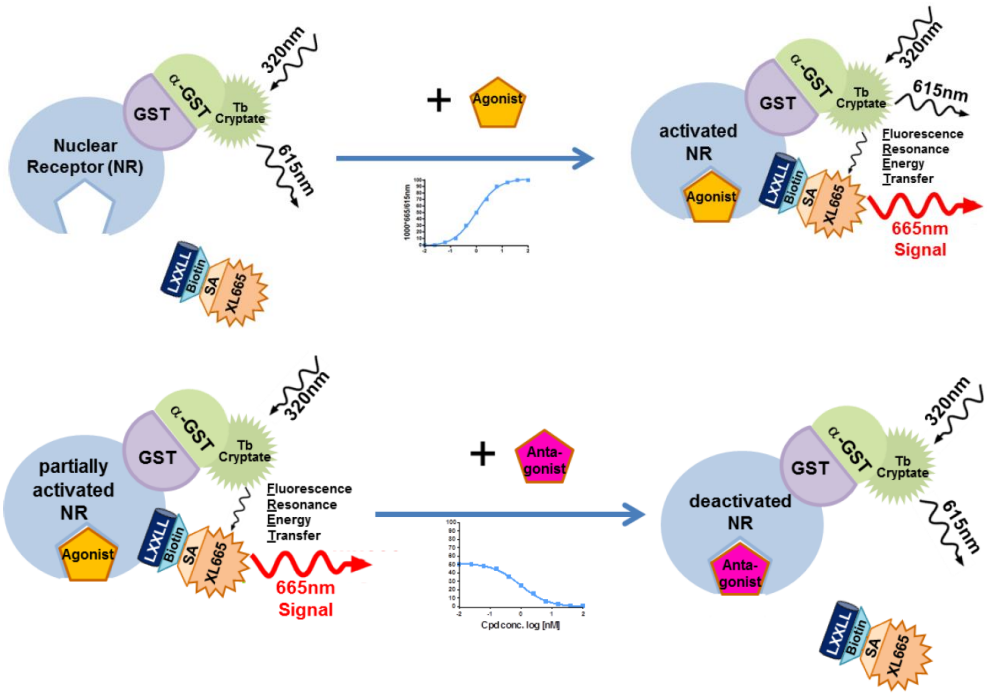

Figure 83.[234] TR TR-FRET assay in agonist mode (above) and antagonist mode (below)

To assess the cellular potency and binding mode of the Protacs, they are also tested in a Gal4 reporter gene assay, the principle of which is outlined in Figure 84. HEK293 cells are transfected with a reporter plasmid (pFR-Luc) containing a synthetic promoter with five repeats of the yeast Gal4 binding site that control expression of the firefly luciferase gene and pCMV-BD, a gene encoding the TR ligand binding domain fused to the DNA binding domain of yeast Gal4. Recruitment of the co-activator to the TR binding domain results in activation of the Gal4 promoter *via* the Gal4 DNA binding domain. This results in activation of the firefly luciferase reporter gene, leading to expression of the firefly luciferase enzyme. The firefly luciferase enzyme promotes oxidation of luciferin to oxyluciferin, which results in a luminescence signal. A control reporter (Renilla luciferase) is also included to account for any cytotoxic effects, since it constitutively expressed and should give little variability between assays.

In agonist mode, the compound is incubated in the system for 16 h before cell lysis. When the compound is titrated in, an agonist will engage with the ligand binding domain, leading to closing of H12 and co-activator recruitment (Figure 84, left). An

antagonist will give no luminescence in this mode of the assay since there is no competing agonist to give a basal signal.

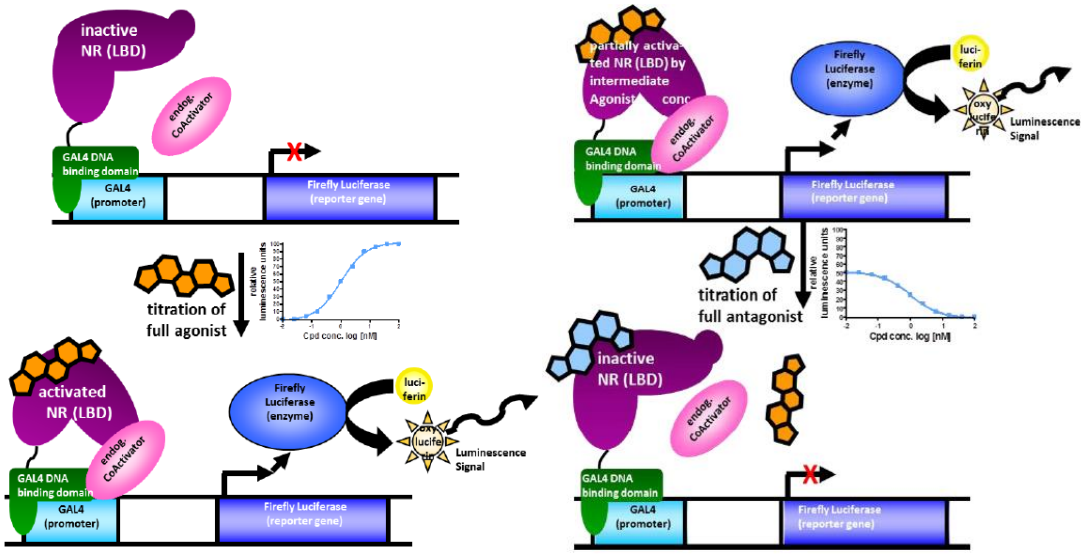

Figure 84.[234] Principle of the TRβ cell based assay in agonist mode (left) and antagonist mode (right)

In antagonist mode, T_3 is added to the system to give a baseline luminescence signal, then the compound is titrated in (Figure 84, right). If the compound acts as an antagonist then T_3 is displaced; subsequently H12 is displaced leading to disruption of the co-activator binding site, preventing transcription and reducing the luminescence signal. In this assay, an agonist will result in further agonism and increase the basal luminescence signal.

3.3 5'-Linked TR Protac Synthesis

The synthesis of 5'-substituted GC-1 based TR binders have been previously described in the literature;[217,223,235] hence, modification of these routes to incorporate the PEG linker and VHL binder would be required. The synthesis of Protacs targeting TR will be outlined within this section.

3.3.1 TR Binder Synthesis

Bromination of 2-isopropylphenol was first carried out to give phenol **14** in 68 % yield, which was subsequently protected with a MOM group to give compound **15** in 64 % yield (Scheme 5). 4-Bromo-3,5-dimethylphenol was protected with a triisopropylsilyl (TIPS) group to give bromide **16** in 95 % yield, then lithium-halogen exchange was carried out; subsequent trapping with DMF afforded the corresponding aldehyde **17** in 74 % yield. The two fragments were combined by lithium-halogen exchange of **15** and trapping with aldehyde **17** to give bridged alcohol **18** in 62 % yield, which was then deoxygenated under an atmosphere of hydrogen to give protected TR binder fragment **19** in 94 % yield.

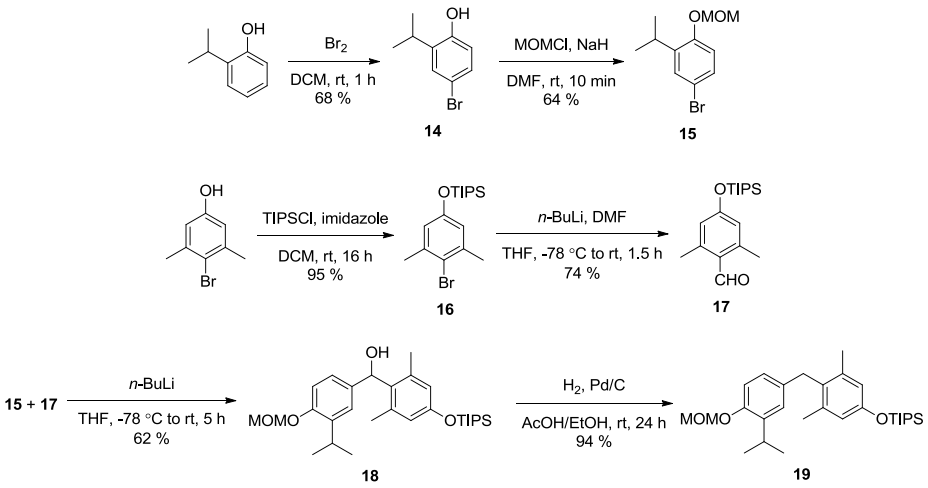

Scheme 5. Synthesis of protected TR binder fragment **19**

Iodination and subsequent silyl deprotection of compound **19** proceeded in moderate yield to give phenol **20** in 23 % yield over two steps and 50 % purity, since the desired product proved to be inseparable from the des-iodo corresponding dehalogenated

material (Scheme 6). Coupling reactions were then tested on substrate **20** to determine the viability of this route in the synthesis.

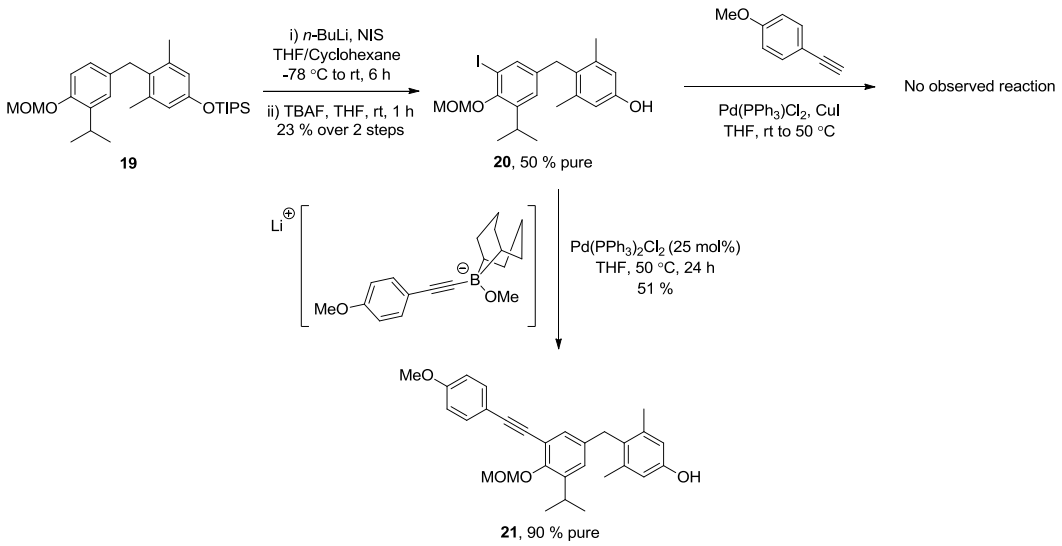

Scheme 6. Synthesis of TR binder precursor **21** (TBAF = Tetra-*N*-butyl ammonium fluoride). Yields based on amount of starting material in impure samples

Standard Sonogashira conditions led to no observed reaction of starting material. A possible explanation for this lack of reactivity is likely to involve the transmetallation of the copper acetylide; the Pd(II) intermediate formed after oxidative addition may be unreactive to transmetallation due to stabilisation by the neighbouring MOM group. Instead, a Suzuki reaction was carried out *via* an alkynyl boronate as previously reported for the synthesis of other 5'-substituted TR binders, which delivered phenol **21** in 51 % yield and 90 % purity.[217]

3.3.2 Initial TR Protac Synthesis

Synthesis of the linking fragment was first performed. Displacement of the 4-PEG tosylate was carried out to give the ester **22** in 91 % yield, followed by acidic deprotection to give acid **23** in 84 % yield (Scheme 7).

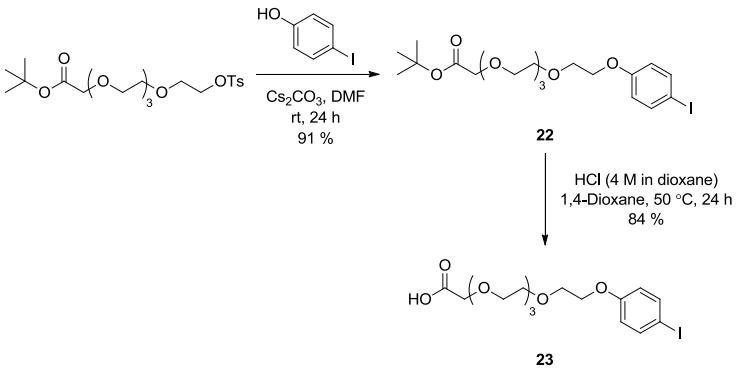

Scheme 7. Synthesis of linker **23**

Due to the poor reactivity previously observed in the attempted Sonogashira coupling of iodinated binder **20**, it was thought that extension of the alkyne out from the TR fragment would allow a subsequent Sonogashira coupling to occur. Stepwise alkyne extension of a separate batch of **20** (with 60 % purity) using trimethylsilylacetylene, alkylation, and silyl deprotection was carried out to give alkyne **24** (Scheme 8) in 30 % yield over three steps, however the product was again not separable from the corresponding alkylated des-iodo starting material impurity.

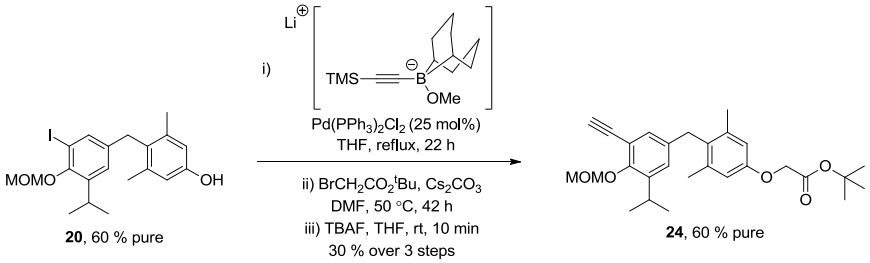

Scheme 8. Synthesis of protected TR binder **24**

Sonogashira coupling was then attempted between compounds **23** and **24**; unfortunately, this resulted in the Glaser coupled product **25** which was observed by LCMS but not isolated (Scheme 9).[236] In an attempt to avoid Glaser coupling, a copper-free Sonogashira was carried out following reported conditions,[237] however, this also resulted in undesired product **25**. Following this, the previously used Suzuki alkynyl boronate coupling was carried out leading to formation of the desired product **26**, however in only 11 % yield (Scheme 10).

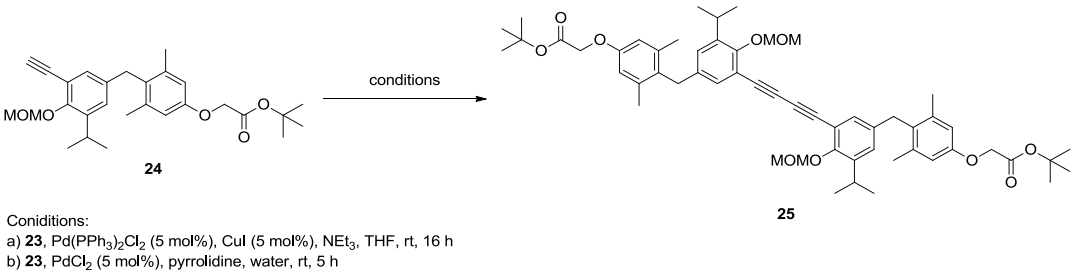

Scheme 9. Conditions leading to undesired Glaser coupled product **25**

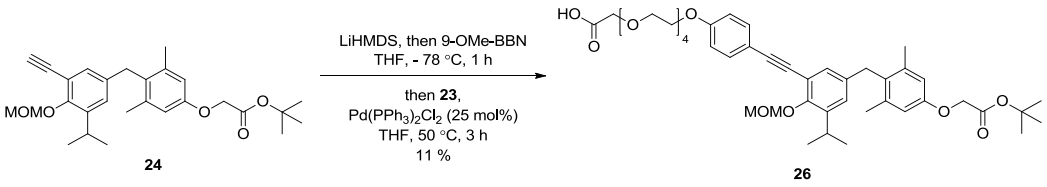

Scheme 10. Suzuki coupling of alkyne **24**

This poor yield was deemed insufficient to allow completion of the Protac synthesis, hence an alternative approach was considered, focusing on optimisation of a coupling step between compound **20** and an alkyne-containing linker.

3.3.3 Improved TR Protac Synthesis

Due to the shortcomings of the initial synthesis, it was decided that optimisation of the alkyne-iodo coupling would be most useful to allow synthesis of the TR Protacs in reasonable yield. First, Sonogashira coupling of 4-iodophenol with trimethylsilylacetylene led to phenol **27** in 92 % yield (Scheme 11). However, attempted deprotection of this using TBAF resulted in polymerisation of the product. In contrast, displacement of the 4EG tosylate with phenol **27** followed by silyl deprotection led to ester **28** without polymerisation. Basic hydrolysis using sodium hydroxide (2 M aq.) gave acid **29** in 70 % yield.

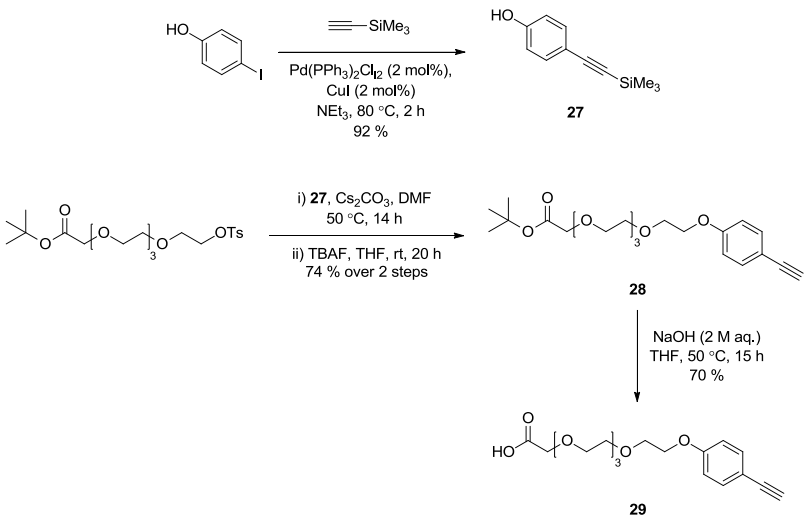

Scheme 11. Synthesis of phenylacetylene-containing linker **29**

Sonogashira coupling was attempted between iodinated binder **20** and acid **29**; the Glaser coupled product **30** was observed as in the previous synthesis (Scheme 12). Encouragingly, by switching the copper(I) catalyst to the gold(I) catalyst $Au(PPh_3)Cl$, the desired acid **31** was obtained in 34 % yield, following conditions reported by Panda and Sarkar.[238] It is believed that Glaser coupling is suppressed since Au(I) is less prone to oxidation than Cu(I); the gold acetylide may also be more amenable to transmetallation, allowing the Sonogashira coupling to occur.

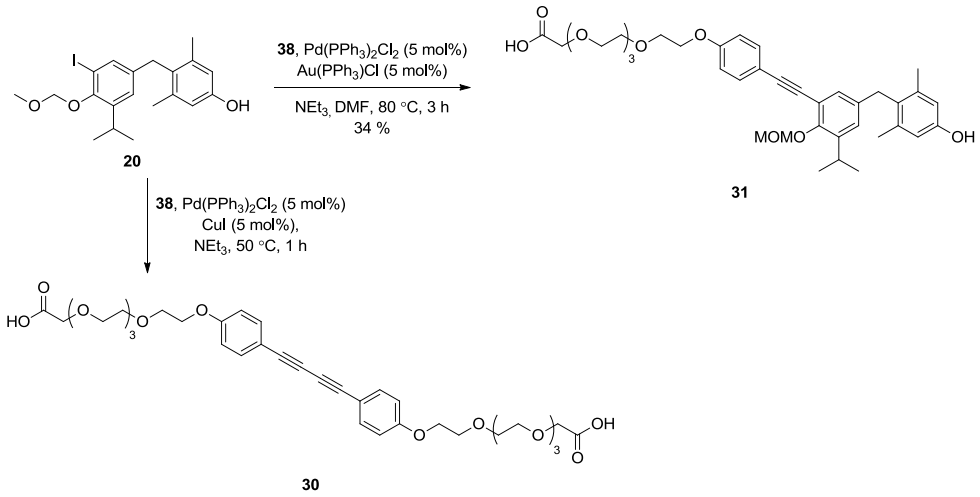

Scheme 12. Formation of Glaser coupled product **30** observed under standard Sonogashira conditions and the desired product **31** formed under Au(I) modified conditions

Although the yield of the reaction was relatively low, it was an improvement compared to the initial route (Scheme 10) and produced a sufficient amount of compound **31** to complete the synthesis. Subsequent amide coupling, alkylation, and acid/base deprotection of intermediate **31** led to the desired Protacs **32** and **33** in 16 % and 14 % yields, respectively, over three steps (Scheme 13). Acidic conditions removed the MOM protecting group (observed by LCMS), but failed to deprotect the *tert*-butyl ester, therefore basic hydrolysis was carried out *in situ*.

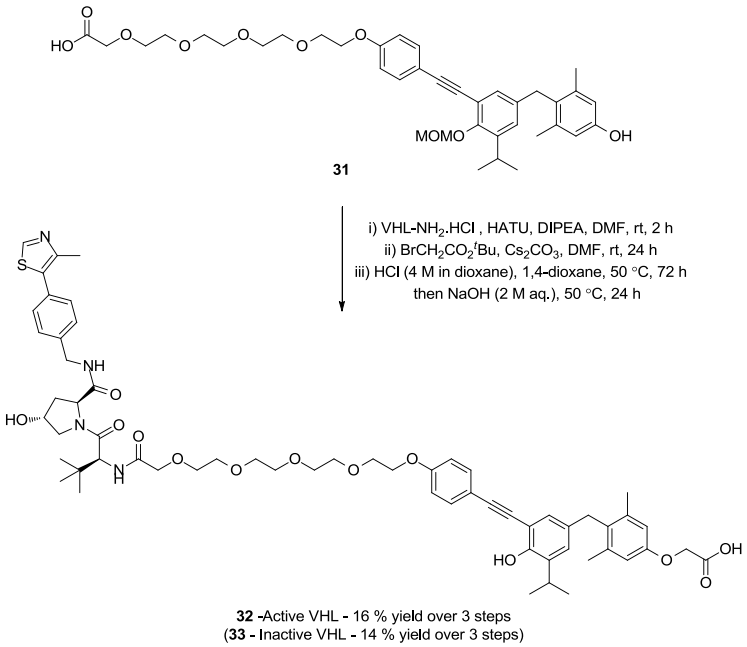

Scheme 13. Final steps of 5'-TR Protac synthesis

Protac **33** was tested in the TRα/β FRET assays, the data for which is outlined in Table 4; Protac **32** was not profiled due to insufficient material, however, it is likely to have the same TR binding profile due to high structural similarity. Protac **33** was found to act as an agonist, with sub-micromolar potency at TR (TRα/β EC_{50} = 650/840 nM), in contrast to the known TR antagonist NH-3. It was thought that the extension of the PEG chain away from the binding site would have led to displacement of H12, resulting in an antagonist response due to disruption of co-activator recruitment. As Protac **33** is observed to act as an agonist, H12 must be sufficiently mobile to compensate for the potential steric clash induced by the PEG chain extension out of the TR binding site and allow an agonist response.

Table 4. Data for Protacs **32** and **33**

Compound	Binding mode	TRα/β FRET EC_{50} agonist mode (nM)	TRα/β FRET EC_{50} antagonist mode (nM)[1]	VHL pIC_{50}
32	-	-	-	5.5
33	Full agonist	650/840	770/250	<4

[1]*Antagonist mode measured in the presence of 1 nM T_3 (TRα) or 3 nM T_3 (TRβ)*

The potency at VHL for active VHL Protac **32** was found to be reduced by ~1 log unit compared to the parent VHL binder, the reason for which is unclear. Protac **32** was then submitted to the TRβ degradation assay, however the Protac failed to show any effect on TRβ levels despite observation of biochemical target engagement. This may be caused by Protac **32** only having moderate potency at both TR, by inference from Protac **33**, and VHL.

Following on from the collection of these data, it was thought that direct modification of a TR antagonist, retaining as many structural features as possible, would lead to an antagonistic response in the corresponding Protac and improve TR potency over Protac **32**.

3.4 NH-3-based Protacs

As Protac **32** was found to be an agonist with moderate potency, it was thought that direct modification of literature antagonist NH-3 would yield a Protac which acts as a TR antagonist and retains the potency of the parent binder. Docking of the NH-3 ligand into the co-crystal structure of GC-1 and $TR\beta_1$ suggested that linking from the *ortho* or *meta* position of the 5'-phenylacetylene extension would have a minimal effect upon ligand binding (Figure 85).[239]

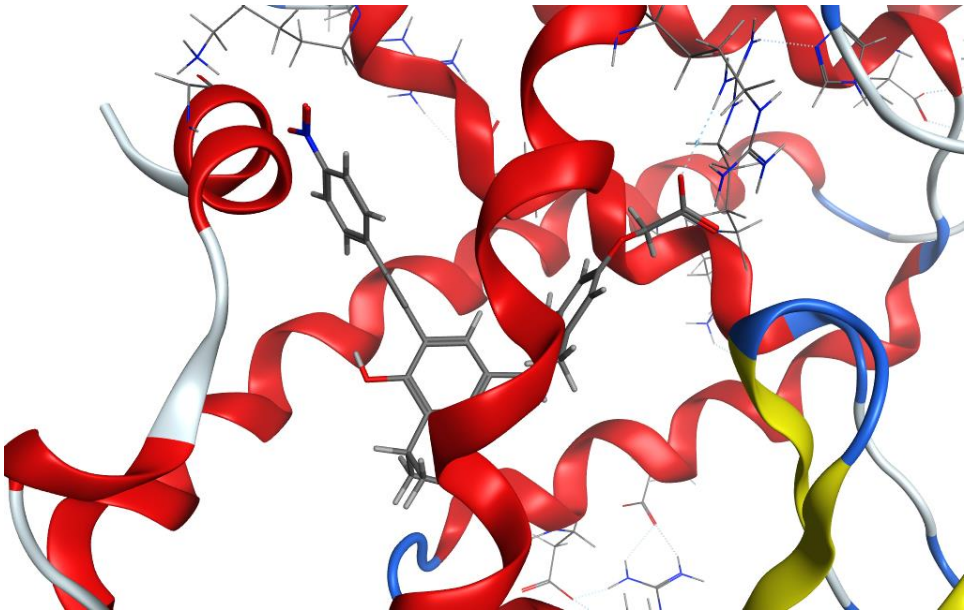

Figure 85. Docking of NH-3 ligand (based on co-crystal structure of GC-1 and TRβ_1). Note that H12 (top left) is in the closed agonist conformation

The basis for the antagonistic effect of exclusively electron-poor 5'-phenylacetylene extensions can also be inferred using this model. In the agonist conformation, H12 is primarily kept in place by a salt bridge, however, a phenylalanine residue is also present on H12 in close proximity to the phenylacetylene extension (Figure 86). Potentially, a π-stacking interaction between the phenylalanine on H12 and the electron-poor extension prevents formation of the salt bridge, resulting in an antagonistic effect. With an electron-rich extension, this interaction does not occur and H12 moves in order to tolerate the steric clash, hence H12 can close resulting in an agonistic effect, as observed with Protac **33**.

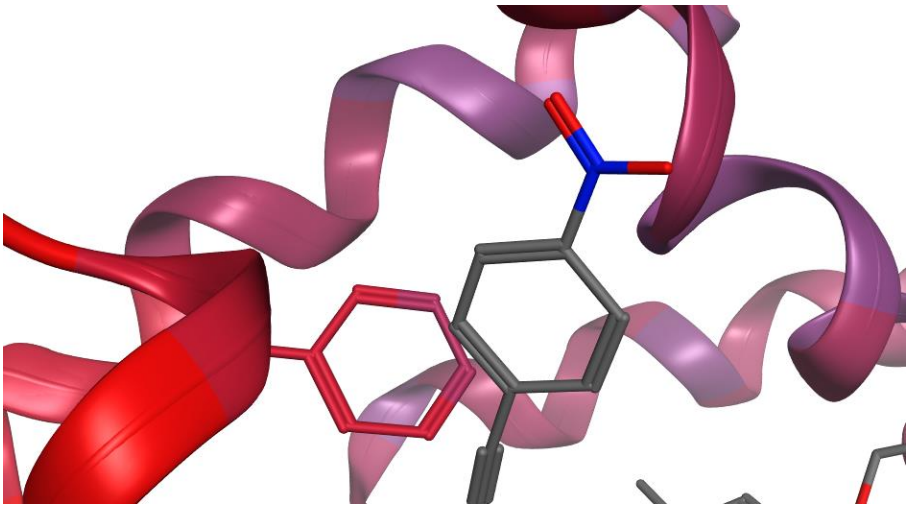

Figure 86. Docking of NH-3 indicating the close proximity of the 5' extension and pendant phenylalanine of H12 (closed conformation)

To first explore whether linking from the phenylacetylene extension of NH-3 would lead to retention of antagonism, a modified binder with a capped PEG linker was synthesised. Phenol **20** was alkylated with *tert*-butyl bromoacetate to give ester **34**, which again proved inseparable from the des-iodo impurity of **20** (Scheme 14). The capped linker extension was synthesised by tosylation of 2-(2-(2-methoxyethoxy)ethoxy)ethanol to give tosylate **35** in 80 % yield. 2-Bromo-5-nitroanisole was demethylated with boron tribromide to give phenol **36** in 84 % yield, which was then alkylated with tosylate **35** to give aryl bromide **37** in 62 % yield. Subsequent Sonogashira reaction and TMS deprotection gave alkyne **38** in 68 % yield over two steps.

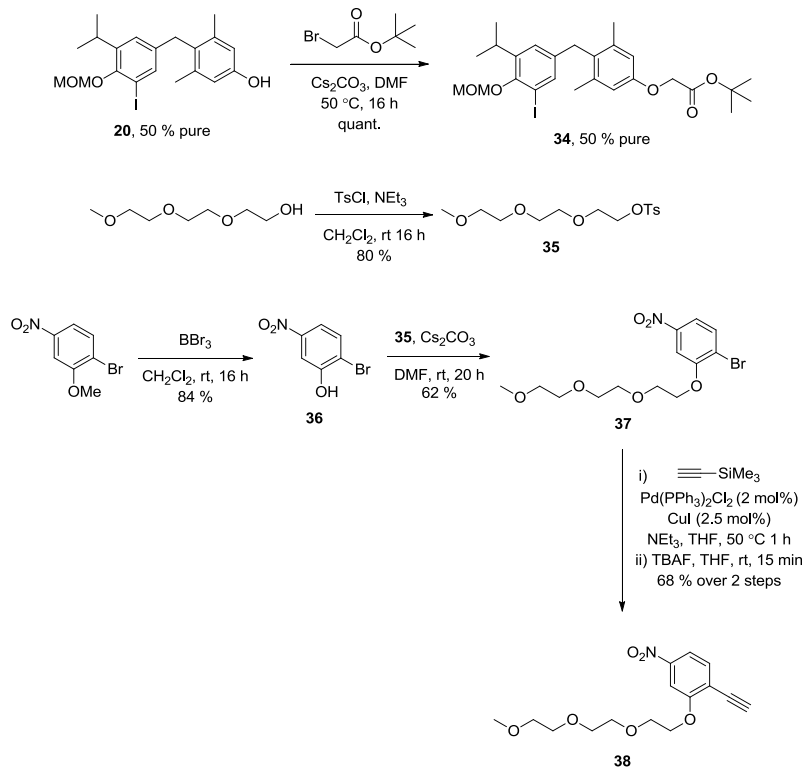

Scheme 14. Synthesis of iodinated ester **34** and alkyne **38**

Alkyne **38** was then coupled to protected iodide **34** and deprotected to give protected binder **39** in 56 % yield (Scheme 15). Deprotection of **39** was then carried out to give linked NH-3 binder **40** in 18 % yield.

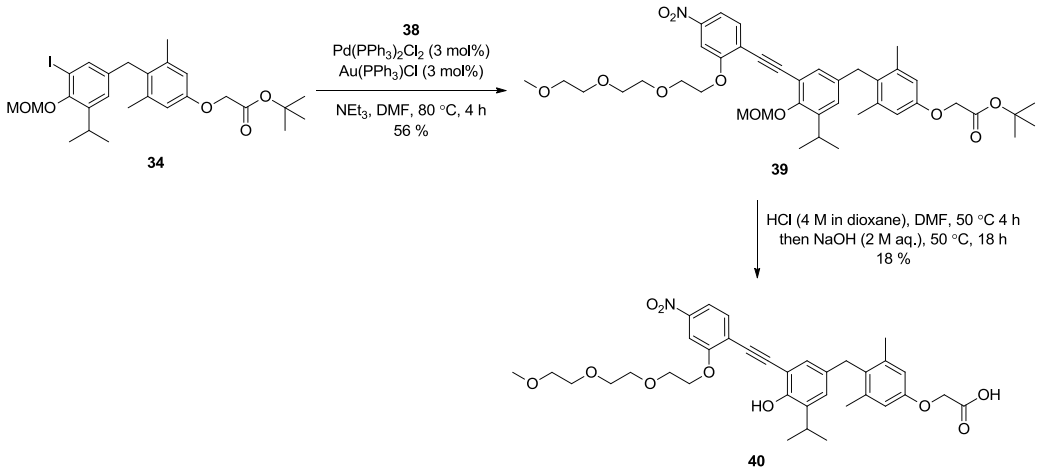

Scheme 15. Synthesis of linked NH-3 binder **40**

Synthesis of the corresponding NH-3 based Protac was then carried out following a similar procedure. Phenol **36** was alkylated with the 4EG tosylate to give bromide **41**

in 69 % yield (Scheme 16). Coupling to trimethylsilylacetylene and deprotection gave alkyne **42** in 76 % yield over two steps.

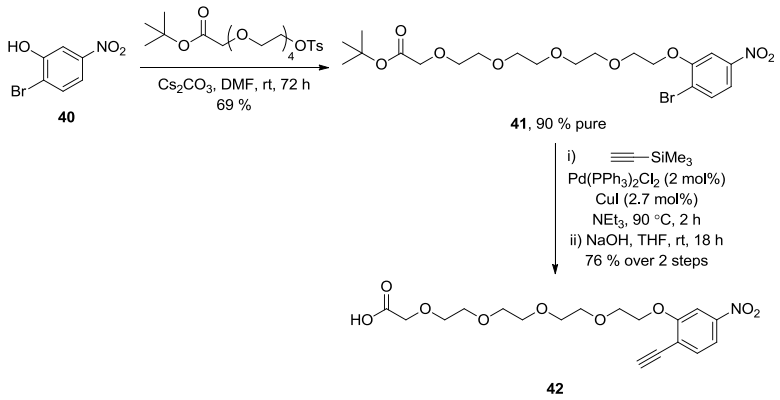

Scheme 16. Preparation of alkyne **42**

Coupling of alkyne **42** onto binder **34** gave acid **43** in 49 % yield, which was subsequently coupled onto the VHL amine and deprotected to give NH-3 based Protac **44** in 18 % yield (Scheme 17).

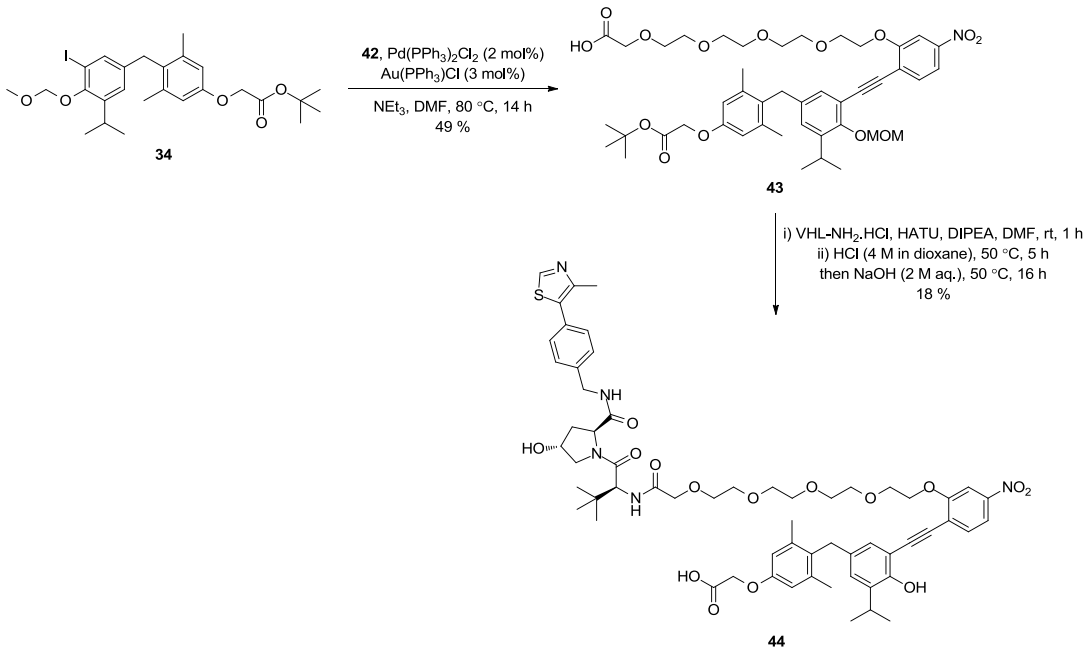

Scheme 17. Completion of NH-3 Protac synthesis

The synthesis of NH-3 was also carried out to compare its activity in the TR assay systems. Coupling of 1-ethynyl-4-nitrobenzene onto aryl iodide **34** gave protected NH-

3 **45** in 23 % yield, however deprotection of **45** under literature conditions (first acidic then basic conditions) led to benzofuran **46** by a 5-*endo*-dig cyclisation of the phenol onto the *ortho*-alkyne (Scheme 18). This accounts for the low yielding deprotections of the NH-3 linked binder and Protac as the benzofuran product would have also been formed.

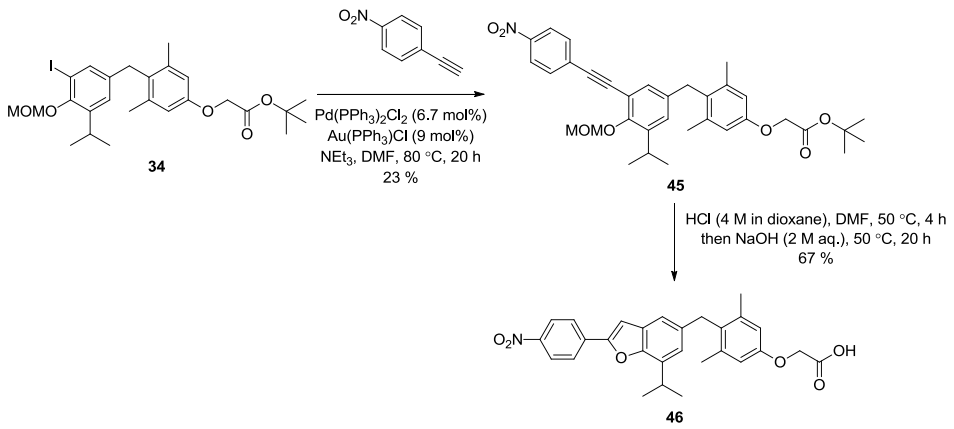

Scheme 18. Attempted synthesis of NH-3

The synthesis of NH-3 was then reattempted using an alternative deprotection strategy. Coupling of 1-ethynyl-4-nitrobenzene onto a protected methyl ester binder available within our laboratories[240] was carried out, as previously, to give protected NH-3 **47** in 26 % yield, however the order of deprotection was reversed so the phenol was not exposed to basic conditions (Scheme 19). Basic hydrolysis followed by acidification gave NH-3 (**48**) in 44 % yield.

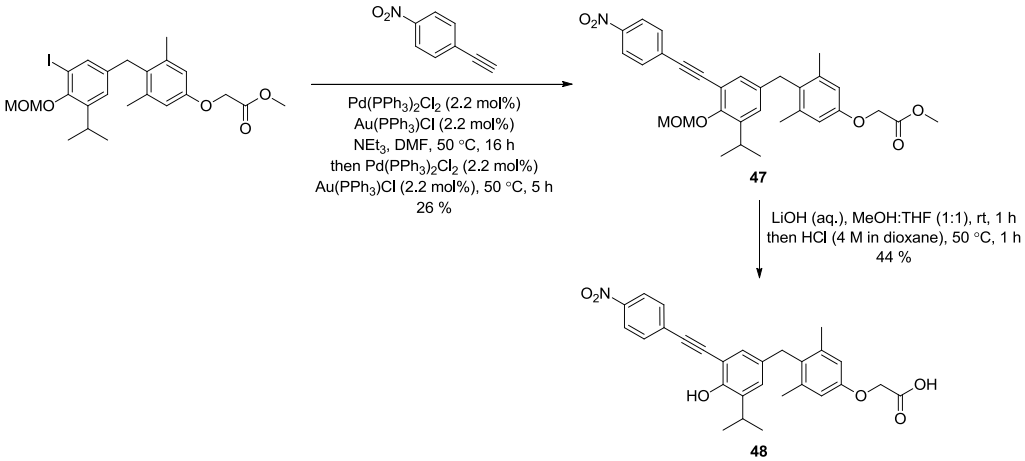

Scheme 19. Synthesis of NH-3 (**48**)

The linked binder **40**, Protac **44** and NH-3 (**48**) were submitted to the TR FRET and cellular assays, the results of which are outlined in Table 5. All the compounds were found to act as full antagonists, as previously reported for NH-3,[217] and as predicted for the corresponding linked binder and Protac. In the FRET assay, the linked binder **40** and Protac **44** were found to maintain the reported potency of NH-3 (TRα/β IC_{50} **40** = 198/46 nM, TRα/β IC_{50} **44** = 440/60 nM). The observed FRET potency of NH-3 itself (**48**) in this assay was lower than expected compared to literature values (TRα/β IC_{50} **48** = 502/775 nM), however this may be due to assay variability.

Table 5. Comparison of NH-3 based binders and corresponding Protac

Compound	Binding mode	TRα/β FRET IC_{50} antagonist mode (nM)[1]	TRβ Cell IC_{50} (nM)	Chrom LogD	Solubility (μM)[4]
40	Full antagonist	198/46	75[2]	4.8	≥478
44	Full antagonist	440/60	150[3]	4.8	≥508
48 (NH-3)	Full antagonist	502/775	50[3]	4.6	28

[1]Antagonist mode measured in the presence of 1 nM T_3 (TRα) or 3 nM T_3 (TRβ). [2]Measured in the presence of 5 nM T_3. [3]Measured in the presence of 1.5 nM T_3. [4]Solubility measured by CLND.

In the cellular assay, the linked binder and Protac effectively maintained the potency of NH-3, and also implies that the TR is engaged in cells (TRβ Cell IC_{50} **40** = 75 nM, **44** = 150 nM, **48** = 50 nM). NH-3 based Protac **44** was then submitted to the TRβ degradation assay, however this molecule showed no effect on TRβ levels, despite cellular target engagement.

3.6 Conclusions

In this chapter, the synthesis of a variety of TR-targeted Protacs was carried out, which proved to be cell permeable and demonstrated intracellular TR engagement. Despite this, no effect on TR protein levels were observed. It was thus considered that TR may not be a degradable target when recruiting VHL as an E3 ligase.

One possible explanation for lack of degradation observed is that, unlike ER and some other nuclear receptors, the TR/RXR heterodimer is permanently bound to DNA regardless of binding site occupancy.[211] This implies that, although degradation of nuclear-localised targets such as ER[189] and BRD4[130] has been demonstrated, degradation of DNA-bound proteins may not be possible. Another possibility is that the formation of the TR/RXR heterodimer sterically inhibits ubiquitin transfer. On the other hand, as RXR is exclusively nuclear, and nuclear-cytoplasmic shuttling of TR has been demonstrated in the literature (suggesting 10-15 % cytoplasmic localisation of TRβ),[241] it may be expected that free TR in both nuclear and cytoplasmic compartments should be degradable. Another unusual factor observed throughout the programme was that VHL potency was found to be lower than expected in all Protacs, which would reduce the efficiency of ternary complex formation.

In the absence of any observed TR degradation, no further work on this target was carried out and a novel strategy towards target selection was considered.

4. Promiscuous Kinase Protacs

4.1 Introduction

In previous chapters, target selection for a degradation approach has been guided by the potential of demonstrating novel target pharmacology. Despite considerable efforts, target degradation was not observed in both cases for various possible reasons. Following on from this, an orthogonal approach to target degradation was considered: rather than selecting a single target then assessing its degradability, an unselective Protac may degrade multiple targets simultaneously, potentially allowing multiple novel degradable targets to be identified. This approach may also give insight into the wider susceptibility of the proteome to Protac-mediated degradation and the scope of the approach in general.

Multiple potential approaches for selecting promiscuous binders were considered, for example, several studies have demonstrated proteome-wide profiling of proteins using molecules containing reactive warheads.[242] These warheads, such as epoxides and Michael acceptors, probe for reactive cysteines or serines. However, most of these reactive functional groups result in irreversible binding to the target, preventing the event-driven pharmacology possible using a Protac approach. Some warheads are also highly reactive, which may result in cell toxicity and incompatibility with the required E3 ligase binders. It was thought that use of a protein subclass selective molecule would allow simpler Protac design without high reactivity and irreversibility.

Initially, the kinase subclass of proteins was selected for this more promiscuous Protac approach. Modern kinase drug discovery often requires highly selective inhibition to avoid undesirable side effects mediated by off-target inhibition.[243] In contrast, in this case a lack of selectivity is preferable to give maximal coverage of the kinome. Protein kinases modulate intracellular processes by transfer of phosphate groups from adenosine triphosphate (ATP, Figure 87), and contain a highly conserved ATP binding site.[244]

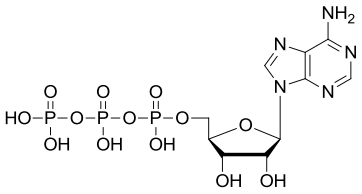

Figure 87. Structure of ATP

Direct elaboration of ATP could result in a highly unselective Protac since it does not exclusively bind to kinases; a vast array of non-kinase proteins have been reported to bind ATP.[245] However, an ATP-based Protac is likely to have poor cell permeability due to its highly charged nature.[246] The most prominent example of an unselective ATP-competitive kinase inhibitor is Staurosporine, a microbial alkaloid (Figure 88).[247,248] Though Staurosporine is highly unselective in its own right, analogues incorporating linkers have demonstrated relatively poor kinome-wide binding in cells.[249]

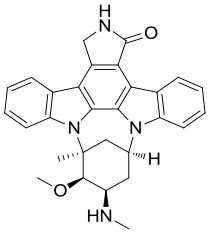

Figure 88. Broad spectrum natural product kinase inhibitor, Staurosporine

CTx-0294885 has been identified in the literature as a broad spectrum kinase inhibitor (Figure 89, left).[249,250] Within our laboratories, a modified version of this inhibitor with a pendant amine was synthesised which retained the pan-kinase selectivity (Figure 89, right), indicating a potential linking vector for modification into a Protac.[251]

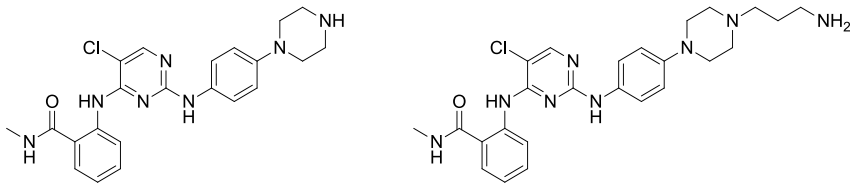

Figure 89. Broad spectrum kinase inhibitor (CTx-0294885, left), and linkable equivalent (right)

The kinase binding profile for the amine-modified kinase binder is indicated in Figure 90. The isolated binder engages 186 kinases with a pIC_{50} > 5, with little selectivity between kinase subsets.

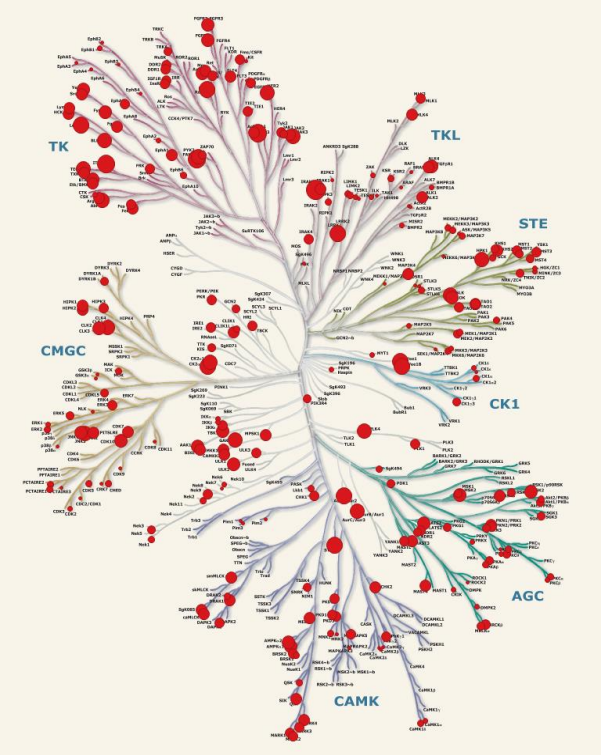

pIC_{50} range	5.0-6.0	6.0-7.0	7.0-8.3
No. of affected kinases	70	98	18

Figure 90. Kinome interaction tree for broad spectrum kinase inhibitor (top) and kinase potencies (bottom)

CTx-0294885 was selected for elaboration into the desired promiscuous kinase Protacs; a 4EG chain connecting the kinase and ligase binder was selected, taking into account that the same linker length was previously employed with Vandetanib-based Protacs and proved to be the most efficient (Section 2.5).[124] Thus, the synthesis of a series of Protacs based on the promiscuous binder was required, the general structure for which is presented in Figure 91.

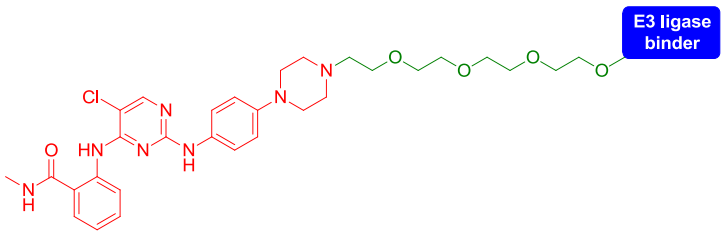

Figure 91. General structure of proposed promiscuous kinase Protacs

The nature of this experiment allows us not only to identify novel degradable targets, but also the effect of recruiting orthogonal E3 ligases. Beyond VHL, the ligase which has been regularly employed in previous chapters, the E3 ligase cereblon had been reported as a ligase amenable for recruitment by a Protac.[130,131] As the ligase had only been reported to demonstrate degradation for a small number of proteins (BRD2/3/4 and FKBP12), it was thought that conjugation to the promiscuous binder would allow rapid assessment of the wider applicability of this ligase. The IMiD lenalidomide was selected to recruit cereblon,[252] with a potential linking position available through the pendant aniline suggested by the co-crystal structure (see Section 1.3.3.2; Figure 92, left).[253]

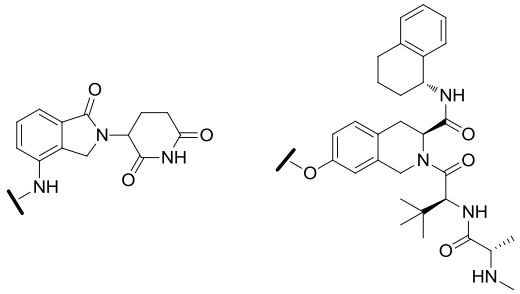

Figure 92. Further E3 ligase binders to be employed in this experiment with linking positions: lenalidomide, which recruits cereblon (left) and an IAP binder (right)

Protacs recruiting IAP as a ligase (also known as SNIPERs) have been reported to degrade multiple proteins, however this effect has exclusively been observed at high concentrations where degradation cannot be delineated from compound-related toxicity (Section 1.2). To explore whether IAP is indeed a valid ligase to recruit in a Protac, it was believed that a more selective IAP binder would be necessary. At the time of planning the experiment, a series of potent heterodimeric IAP antagonists have

been reported which, since they simultaneously engage two BIR domains of IAP, suggest a potential linking position for incorporation into a Protac (Figure 92, right).[254]

Following the synthesis of the Protacs, rather than assess effects on individual proteins by western blotting, a combination of MS strategies will be employed to assess both kinome-wide intracellular target engagement and proteome-wide effects on protein levels to allow identification of multiple degraded targets in a single experiment. The nature of these strategies to assess both protein binding and protein degradation will be outlined in greater detail in later sections.

4.2 Promiscuous Kinase Protac Synthesis

The synthesis of the promiscuous kinase Protacs was then carried out. First, an S_NAr reaction was performed between commercially available 2,4,5-trichloropyrimidine and 2-amino-*N*-methylbenzamide to give pyrimidine **49** in 97 % yield (Scheme 20. Displacement was observed selectively at the 4-position; the 5-position being disfavoured due to lack of electronic conjugation onto adjacent nitrogen atoms and the 2-position disfavoured due to repulsion between the nucleophile and the two adjacent nitrogen lone pairs. Another S_NAr reaction was then attempted between **49** and 1-Boc-4-(4-aminophenyl)piperazine, however no conversion to product was observed. A Buchwald reaction was then carried out as an alternative, to give Boc-protected binder **50** in 41 % yield, however, this strategy was deemed inadequate to generate sufficient material to continue the synthesis.

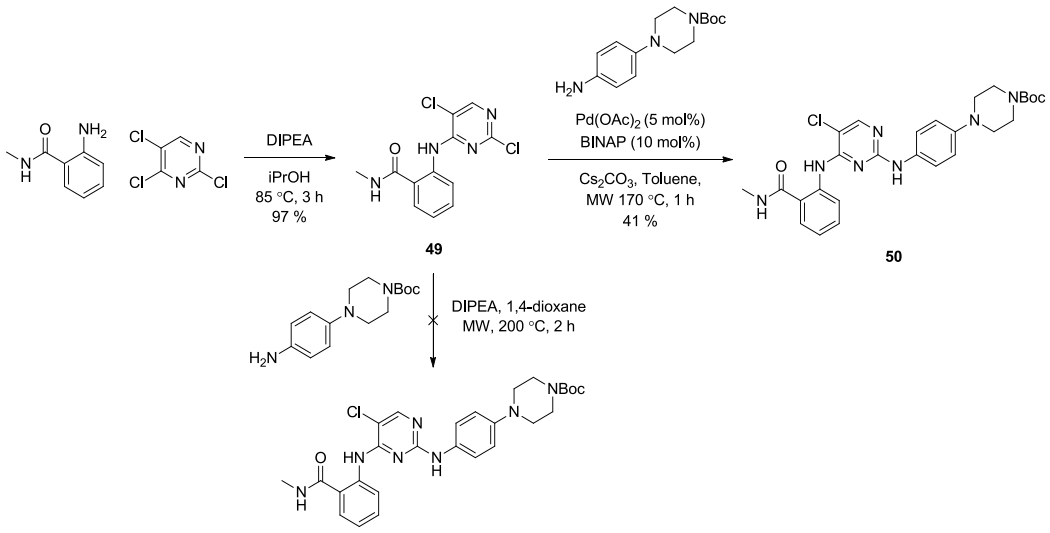

Scheme 20. Synthesis of Boc-protected binder **50**

It was thought that acid catalysis may promote the S_NAr reaction, however these conditions would be incompatible with the Boc protecting group of the required aniline. Accordingly, trifluoroacetamide was selected as a viable alternative protecting group for this developing route, hence the corresponding protected aniline was required. An S_NAr reaction was carried out between 1-fluoro-4-nitrobenzene and piperazine, then protected with trifluoroacetic anhydride to give protected nitroaryl **51** in 78 % yield (Scheme 21). This was then reduced under an atmosphere of hydrogen to give aniline **52** in 97 % yield.

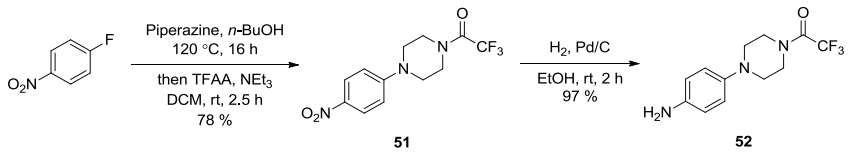

Scheme 21. Preparation of aniline **52**

An acid-catalysed S_NAr reaction was then carried out between pyrimidine **49** and aniline **52** to give the desired protected binder **53** in 84 % yield, then deprotection of the trifluoroacetamide group delivered piperazine **54** in 81 % yield (Scheme 22). After preparation of these compounds, a synthesis of **54** was reported in the literature making use of microwave and flow synthesis.[255] It is of note that the batch process carried out within this section demonstrates an overall superior yield to that reported, with an equal number of purifications.

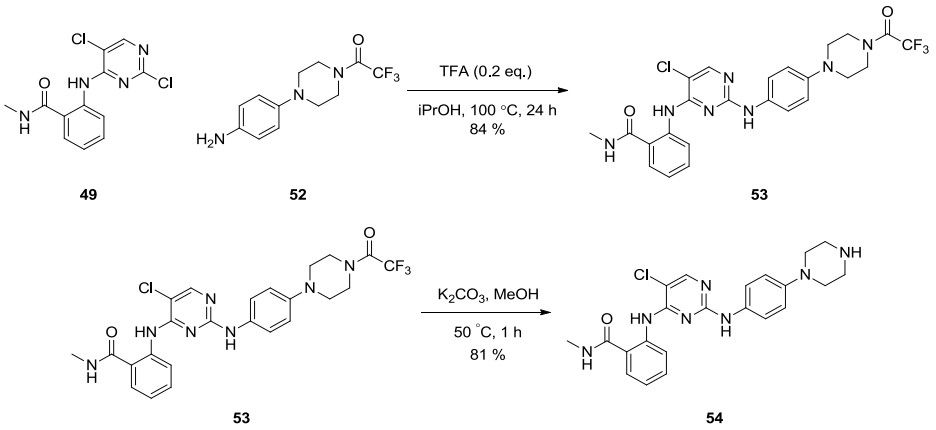

49 52 53 53 54

Scheme 22. Preparation of piperazine **54**

Linker attachment was then carried out (Scheme 23). Alkylation with a 4EG chloro-ester chain was first performed. Basic hydrolysis was then carried out to afford the corresponding acid **55** in 67 % yield over two steps. Similarly, alkylation with a 4EG bis-chloro ether was carried out to give chloride **56** in 35 % yield.

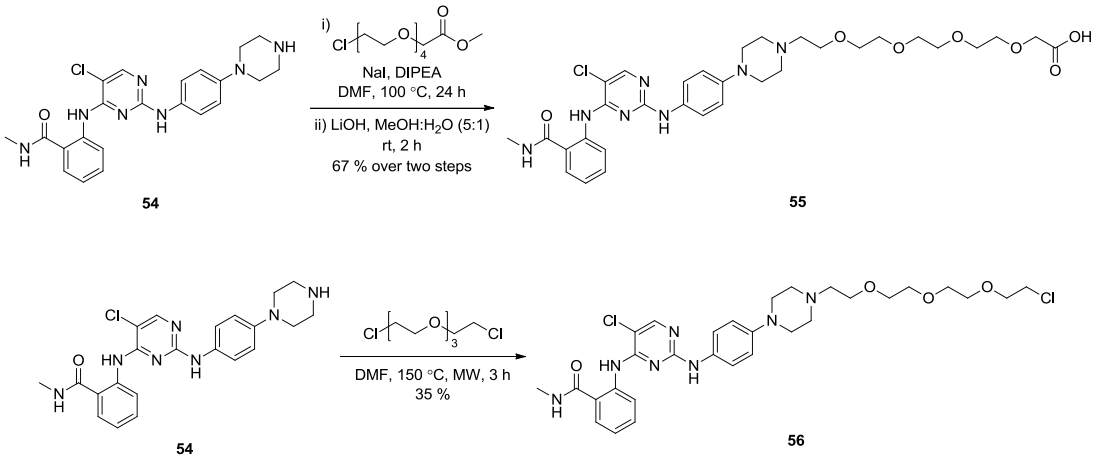

54 55 54 56

Scheme 23. Synthesis of linked kinase binders **55** and **56**

Acid **55** was then coupled to commercially available cereblon binder, Lenalidomide, to give cereblon Protac **57** in 32 % yield (Scheme 24). Further amide couplings were carried out with VHL amine and its enantiomer to give active VHL Protac **58** and its enantiomer **59** in 61 % and 89 % yield, respectively.

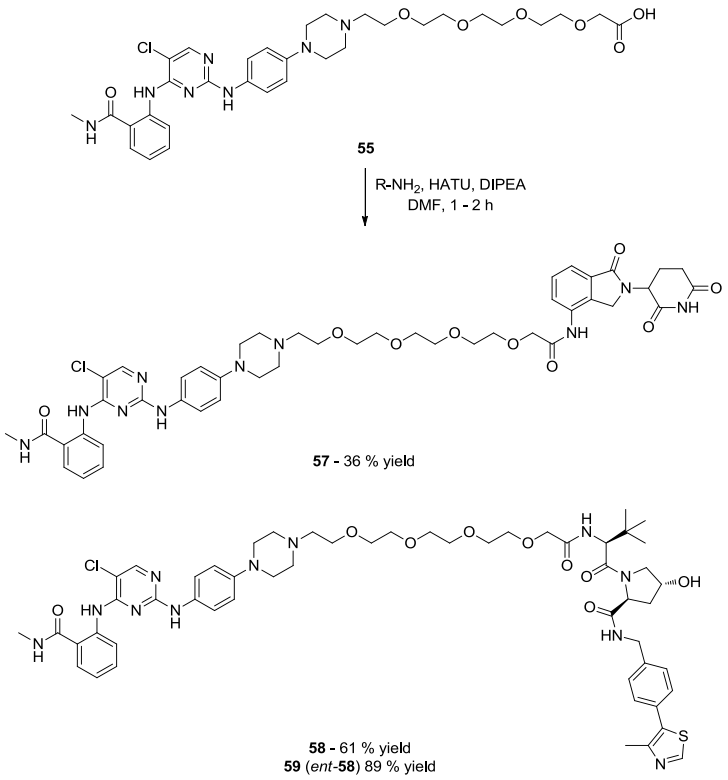

Scheme 24. Synthesis of promiscuous kinase cereblon Protac **57** and active and inactive VHL Protacs **58** and **59**

Chloro-linked compound **56** was alkylated with a phenol-linked IAP binder available within our laboratories to give IAP Protac **60** in 55 % yield (Scheme 25), assisted by sodium iodide to induce a Finkelstein reaction, with transient iodide displacement observed by LCMS.

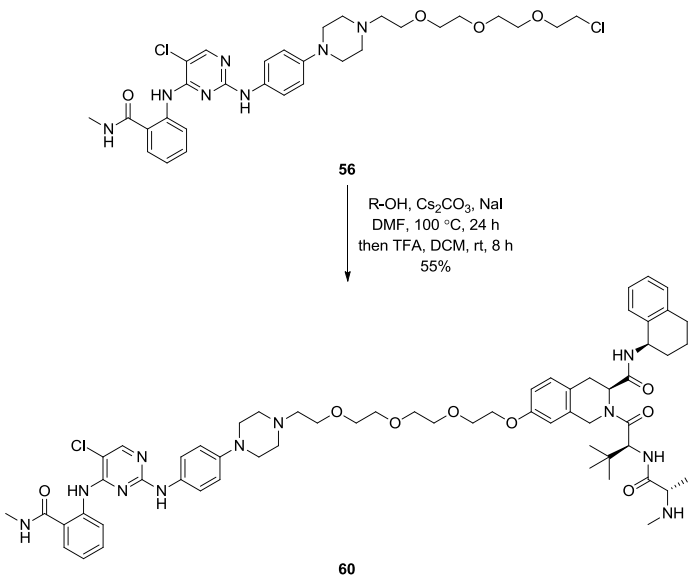

Scheme 25. Synthesis of promiscuous kinase IAP Protac **60**

4.3 Promiscuous Kinase Protac Properties

The physicochemical properties of the prepared Protacs were then assessed to determine their suitability for the expression proteomics study (Table 6). The cereblon and VHL Protacs **57**, **58** and **59** were found to have reasonable lipophilicities, with a measured chrom logD of 4.1 and 5.2 respectively, with moderate solubilities: 81 μM for cereblon and ~34 μM for both VHL Protacs. The IAP Protac **60** was found to be highly lipophilic with a measured chrom logD of 6.8. However, as the molecule retained some solubility (24 μM), it was deemed acceptable as a tool compound for this experiment. The VHL Protac **58** and its enantiomer **59** were found to be appropriately active and inactive, respectively, towards VHL.

Table 6. Physicochemical properties and biochemical data for promiscuous kinase Protacs

Compound no.	Ligase	Chrom LogD	Solubility (μM)[1]	VHL pIC_{50}	PΔC[2]
57	Cereblon	4.1	81	n/a	0.7
58	VHL	5.2	32	6.2	1.6
59	VHL (inactive)	5.2	38	<4	1.9
60	IAP	6.8	24	n/a	2.4

[1]Solubility measured by CLND [2]Cellular accumulation in HeLa cells

PΔC is an approximate measurement of the intracellular concentration of compounds.[256] HeLa cells are incubated with a sample of the compound (10 μM concentration), then the cells are lysed, extracted, and analysed by LCMS/MS to determine intracellular compound concentrations. PΔC describes the logarithmic ratio of concentration of compound in cells compared to a control sample. PΔC values in the region of 0-1 imply good slight accumulation in cells, and values greater than 1 indicate significant cellular accumulation. All promiscuous kinase Protacs displayed positive accumulation in cells, with increasing accumulation observed with increasing lipophilicity from cereblon Protac **57** to IAP Protac **60**.

A caveat to note regarding cellular accumulation data is that it does not distinguish between species present in the cell membrane and cytoplasm; positive cellular accumulation values may not reflect the true Protac intracellular free fraction in cells. While the compounds may be accumulating within cells, the more lipophilic Protacs are likely to be more highly protein bound and less free to engage the desired targets (for example, highly lipophilic compounds may be strongly associated with the cell membrane).

The Protacs were then submitted to a kinobead assay to determine whether their broad spectrum inhibition across the kinome was maintained.[257] Kinobead technology allows profiling of ATP competitive compounds in cells or lysates without compound or

protein modification, which gives a more accurate reflection of target binding in cells (compared to modified proteins used in typical cellular assays).[258] Broad spectrum kinase inhibitors affixed to beads compete with the compound of interest for kinase binding, the concentration dependence of which allows IC_{50} measurement across a large number of kinases (Figure 93).

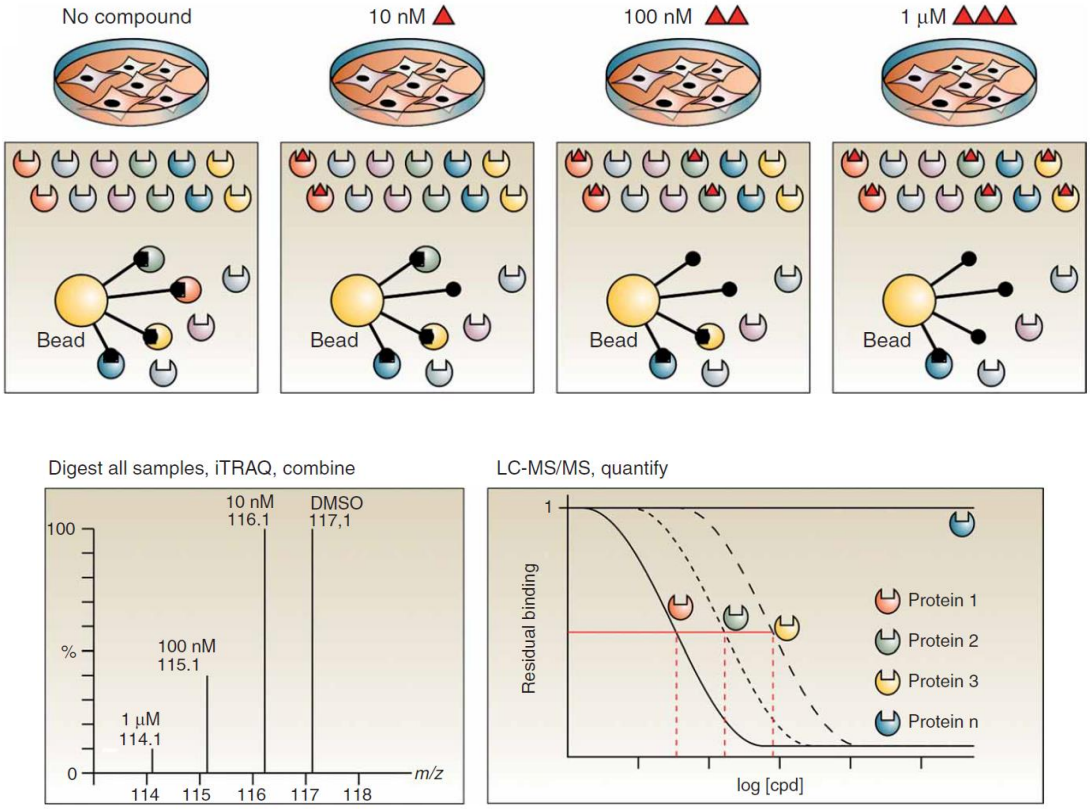

Figure 93.[258] Kinobead assay workflow

A cell lysate is treated with a range of compound concentrations. Proteins are captured by beads functionalised with broad spectrum kinase inhibitors; the free compound competes with the beads for protein binding (Figure 93, top). Proteins bound to beads are digested and labelled with isobaric tags (see Section 4.4) corresponding to the inhibitor concentration; all labelled digests are then combined and analysed by LCMS/MS (Figure 93, bottom left). If the free compound is more active at the target, less protein will have been bound to the bead, leading to a reduced MS signal. Hence, quantifying the decrease in signal intensity of labelled proteins compared to DMSO

control reflects competition of the free compound for each kinase, allowing IC_{50} determination for multiple targets (Figure 93, bottom right).

Each Protac was profiled in a mixed lysate of HEK293/K562/Placenta cells, and were found to mostly maintain broad spectrum kinase inhibition, though all Protacs tended to be one log unit less potent across the measured kinome than the parent promiscuous kinase binder (Figure 94). Activity was reduced compared to the parent binder for kinases with pIC_{50} = 5-6, though highly potent targets mostly maintained activity. Cereblon Protac **57** maintained the largest amount of kinase binding when compared to the parent promiscuous binder, while IAP Protac **60** was found to have reduced potency across a large number of targets, potentially caused by the high lipophilicity and lower solubility of the Protac. The overall properties of the designed Protacs were deemed appropriate for undertaking expression proteomics profiling, hence, these were advanced into the experiment.

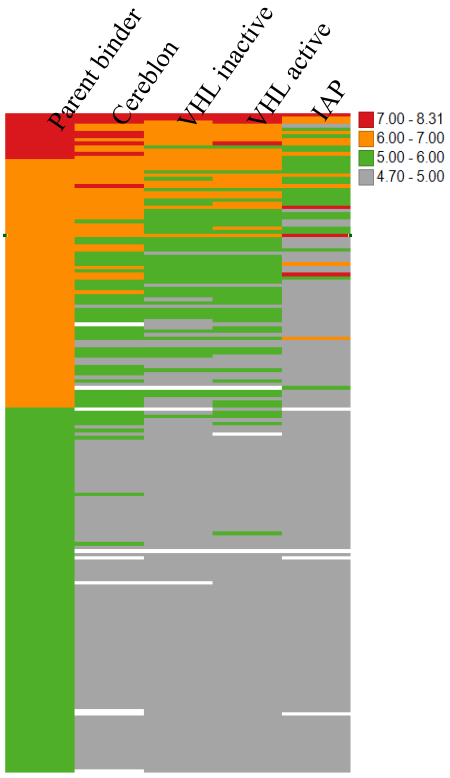

Figure 94. Kinobead profile of promiscuous kinase Protacs **57**-**60** plotted by ligase compared to the parent amine-linked binder

4.4 Expression Proteomics

Expression proteomics experiments were then carried out to quantify degradation induced by the promiscuous kinase Protacs at the proteome level.[124,257] In this case, an isobaric labelling strategy was used;[259] this approach allows labelling of peptides with a chemically indistinguishable, but isotopically unique tag to allow derivation of relative intracellular protein levels between treated and untreated states. Common examples of isobaric mass tags include tandem mass tagging (TMT)[260] and isobaric tags for relative and absolute quantification (iTRAQ).[261]

In this experiment, TMT isobaric reagents were employed, the structures of which are presented in Figure 95.[260] The TMT tag itself consists of a dimethylpiperazine reporter group and an amine-reactive *N*-hydroxysuccinimide (NHS) moiety. In order to keep the tags chemically identical, the two groups are separated by a linker which acts to counterbalance the molecular weight shift induced by the isotopic label. The structure of the tag allows six unique isotopomers, termed TMT 6-plex reagents as six samples can be uniquely tagged in multiplex. Further isotopomers with unique ^{13}C and ^{15}N enrichment patterns permit up to 10-fold multiplexing.[262,263]

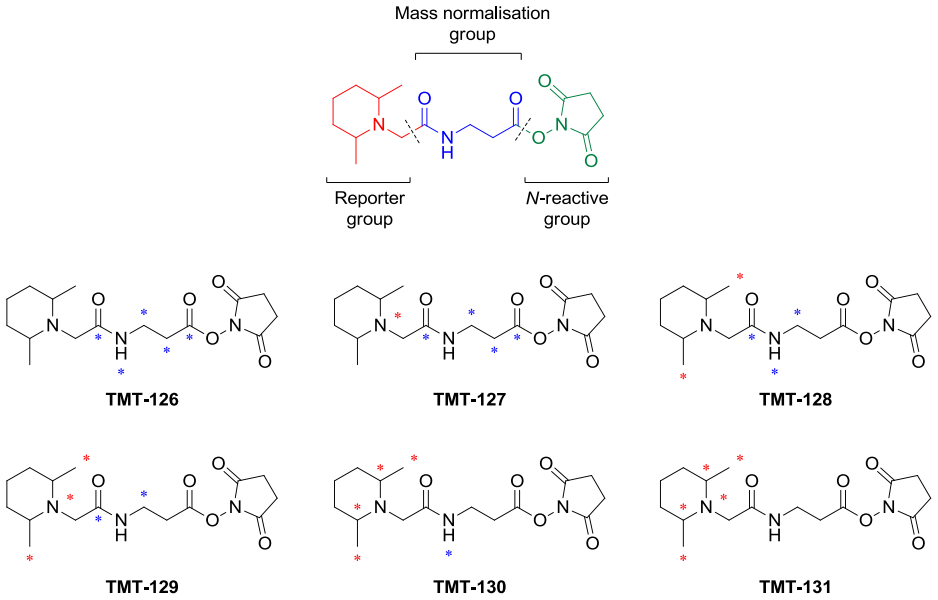

Figure 95. General structure of a TMT reagent (above) and isotopic labelling patterns of TMT 6-plex reagents (below; red = $^{13}C/^{15}N$ reporter isotope, blue = $^{13}C/^{15}N$ mass balancing isotope)

The NHS moiety of TMT isobaric mass tags allows labelling of the *N*-termini and lysine residues of peptides which, in turn, allows tagging of peptides directly derived from cell lysates (Figure 96). Following individual treatment of cell samples with stimuli, proteins are then extracted from cells, followed by reduction, alkylation and digestion to peptides. The individual peptide samples are then discretely labelled with distinct TMT tags and pooled at equal concentrations.

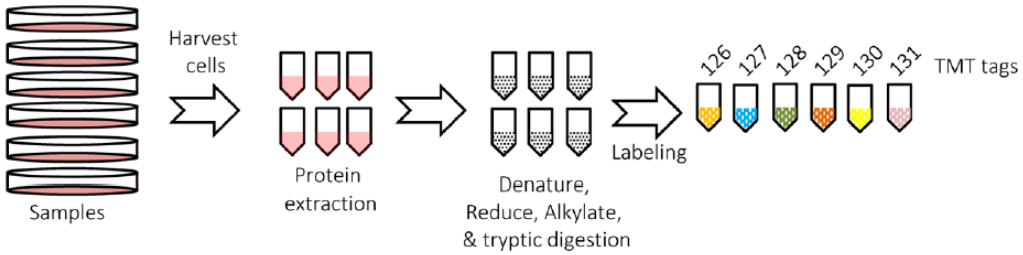

Figure 96.[264] TMT assay workflow

The differentially tagged peptide pools are then combined into one sample and analysed by LCMS/MS (Figure 97), allowing separation of distinct peptides which remain chemically indistinguishable. Following MS/MS, the specific fragmentation patterns of the individual peptides can be deconvoluted and correlated back to the parent proteins. Simultaneously, fragmentation of the TMT label occurs, resulting in release of distinct TMT reporter group ions between m/z = 126-131. The relative intensity of the reporter group ion indicates the relative amount of each peptide in the parent sample, which, by extension, allows relative quantification of protein in the cell sample.

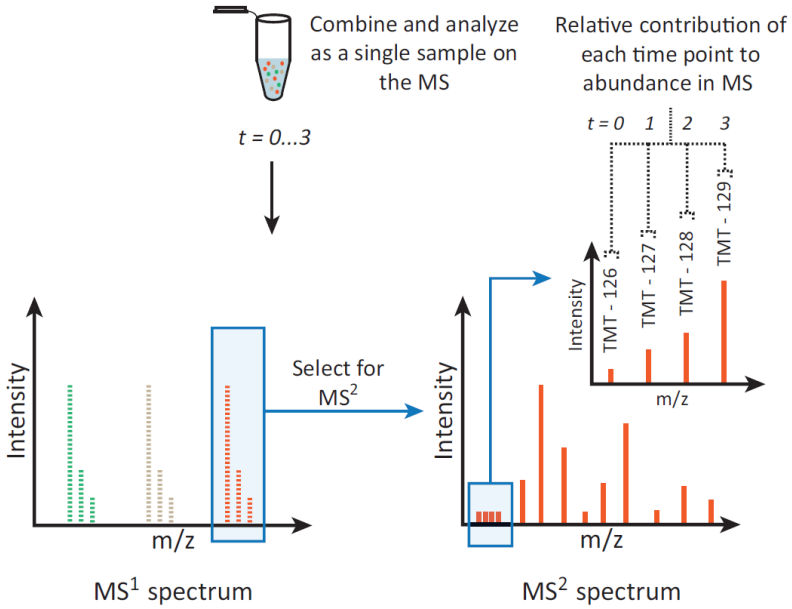

Figure 97.[265] Example MS readout from a TMT time course experiment

In this experiment, if individual protein levels are found to be significantly reduced in a treated sample compared to the untreated sample, and binding to the protein has also been observed through the previous kinobead experiments, this reduction in protein level is highly probable to be a Protac-mediated effect (Figure 98). Hence, by employing this technique, proteome-wide Protac profiling can be carried out in a single experiment, rather than numerous experiments profiling degradation of individual proteins by western blotting.

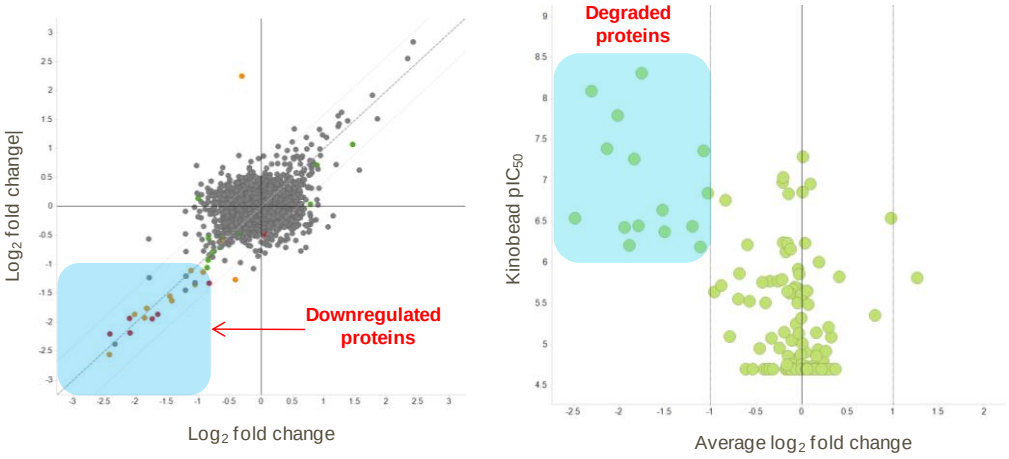

Figure 98. An active Protac should induce protein degradation (left), which, in combination with evidence of target engagement (kinobead pIC_{50}, right), results in identification of novel degradable targets

For this expression proteomics experiment, THP-1 cells were treated for 6 h or 24 h with 0.1 µM or 1 µM of each Protac in duplicate, then relative protein abundance was then analysed to a depth of >7000 quantified proteins, including >260 kinases. The resulting protein regulation is then plotted as fold change (log_2) of the two replicate experiments, the logarithmic scale producing a continuous spectrum of values independently of upregulation or downregulation.[266] For example, a protein degraded to approximately 20 % of the control sample corresponds to a log_2 (fold change) = -2.3. Statistically significant upregulation and downregulation is considered to be $|log_2$ fold change$| \geq 1$, i.e. 50 % target degradation.

4.4.1 Cereblon Protac Expression Proteomics

Incubation of promiscuous cereblon Protac **57** resulted in protein degradation at all concentrations and time points. At 0.1 µM concentration, the 6 h time point led to significant degradation of a number of proteins (Figure 99, top), while at the 24 h time point an increased number were observed (Figure 99, bottom), also downregulating other unengaged proteins which will be discussed in greater detail in later sections.

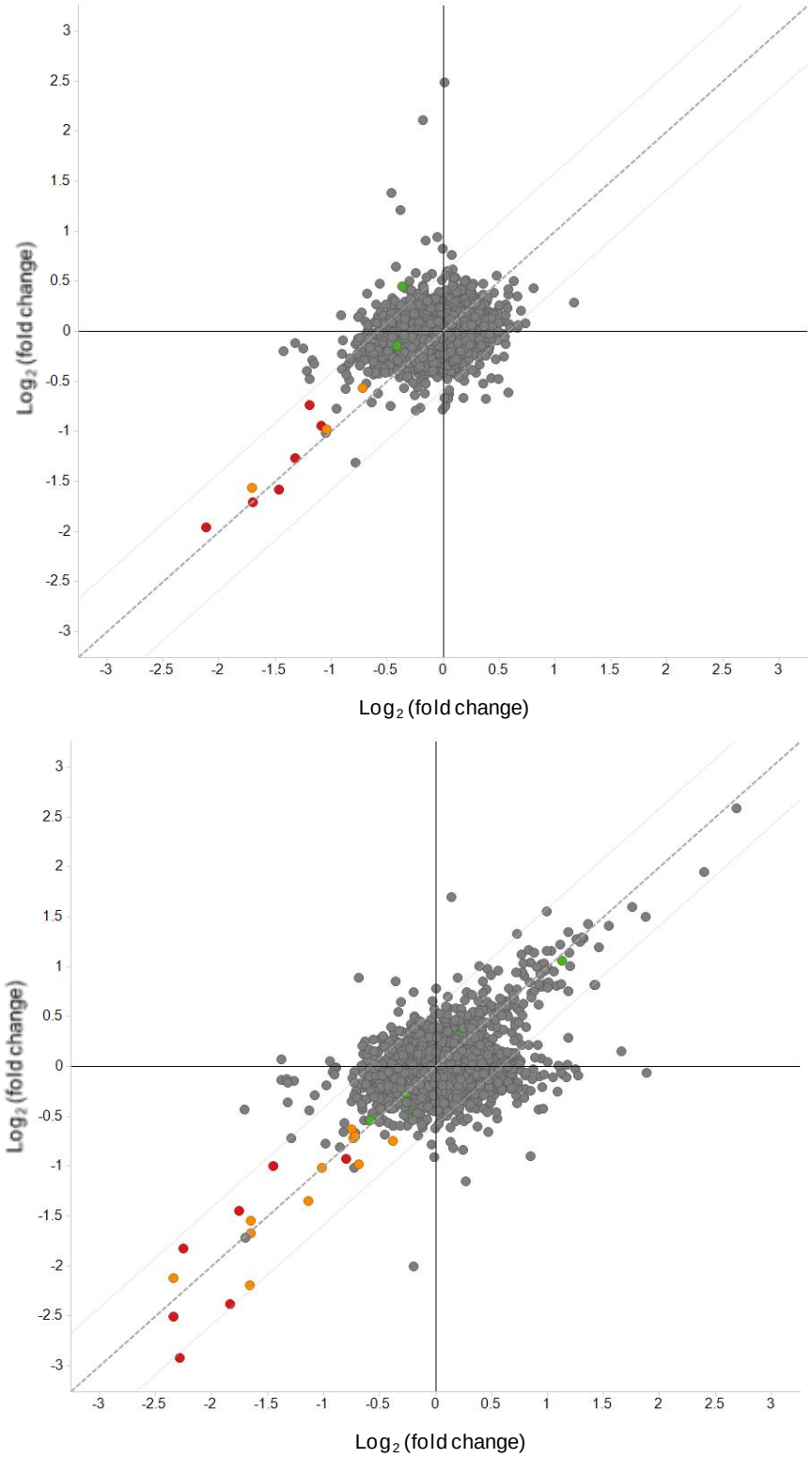

Figure 99. Expression proteomics following incubation with cereblon Protac **57** at 0.1 μM after 6 h (above) and 24 h (below). Points are coloured by kinobead pIC_{50} (red = 7.0-8.3, yellow = 6.0-7.0, green = 5.0-6.0, grey = <5.0).

Closer examination of the degraded kinases corresponding to actively engaged targets at 0.1 µM concentration of cereblon Protac **57** indicated significant degradation of 7 kinases at the 6 h time point (AAK1, AURKA, BTK, IRAK3, PTK2B, TEC and WEE1; Figure 100). After 24 h, 5 further kinases (AURKB, GAK, LATS1, PTK2 and RPS6KA1) were found to be degraded, totalling 12 proteins at this concentration (WEE1 was not found to be degraded).

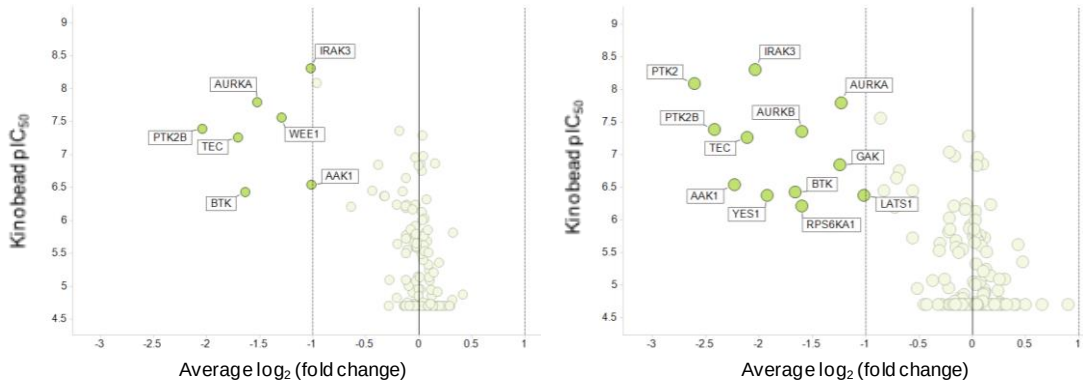

Figure 100. Significantly degraded targets by cereblon Protac **57** at 0.1 µM plotted against kinobead potency

At 1 µM concentration, a similar degradation profile was observed at the 6 h time point as with 0.1 µM concentration (Figure 101), with the majority the same proteins found to be degraded (excluding TEC which could not be quantified at this time point, Figure 102). At the 24 h time point, a total of 15 kinases were found to be degraded; with ABL1, MAPK9, PRKAA1 and RPS6KA3 degraded alongside all degraded proteins previously observed at this time point following incubation with 0.1 µM cereblon Protac (YES1 was not significantly degraded in this case).

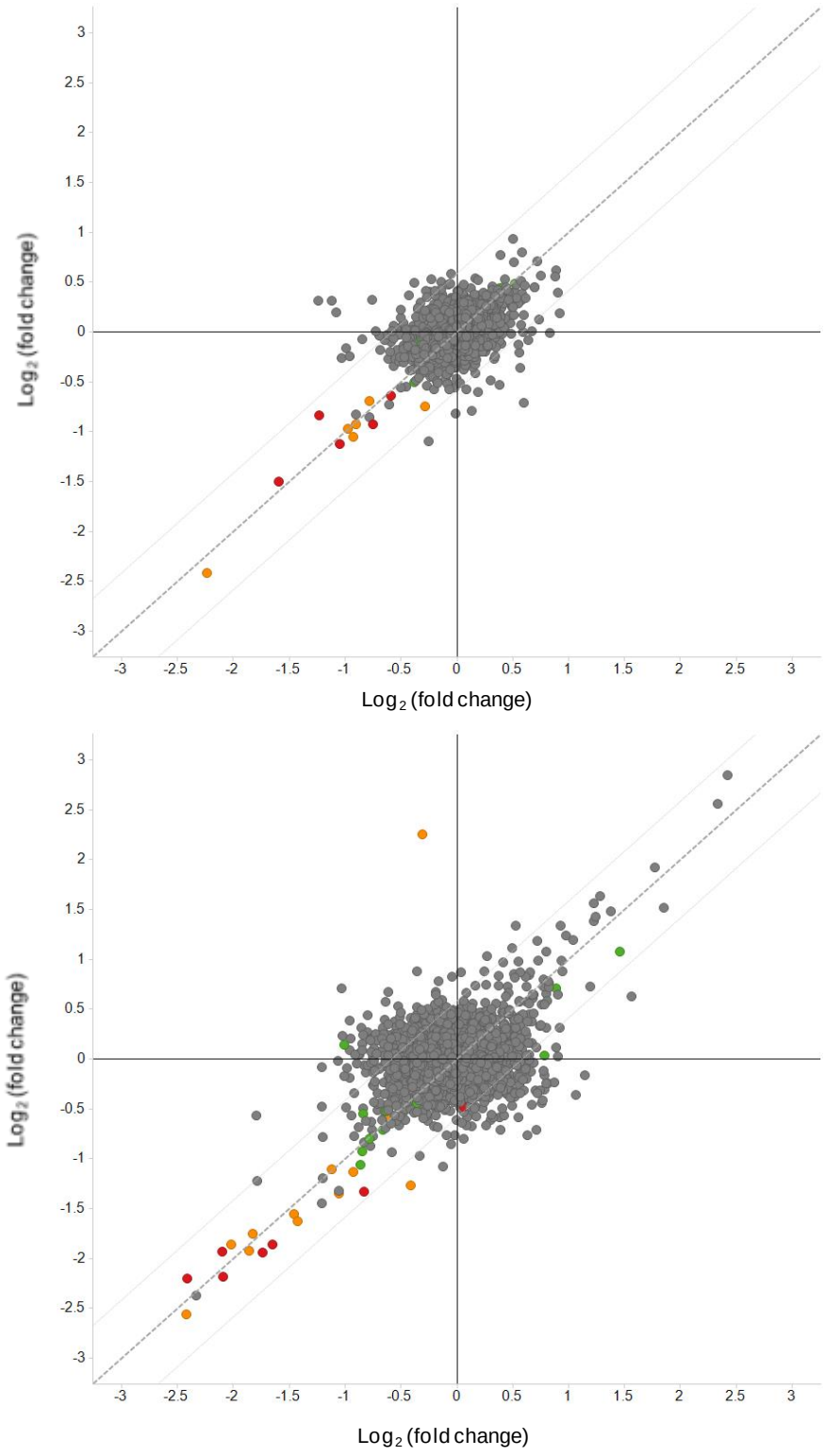

Figure 101. Expression proteomics following incubation with cereblon Protac **57** at 1 μM after 6 h (above) and 24 h (below). Points are coloured by kinobead pIC_{50} (red = 7.0-8.3, yellow = 6.0-7.0, green = 5.0-6.0, grey = <5.0).

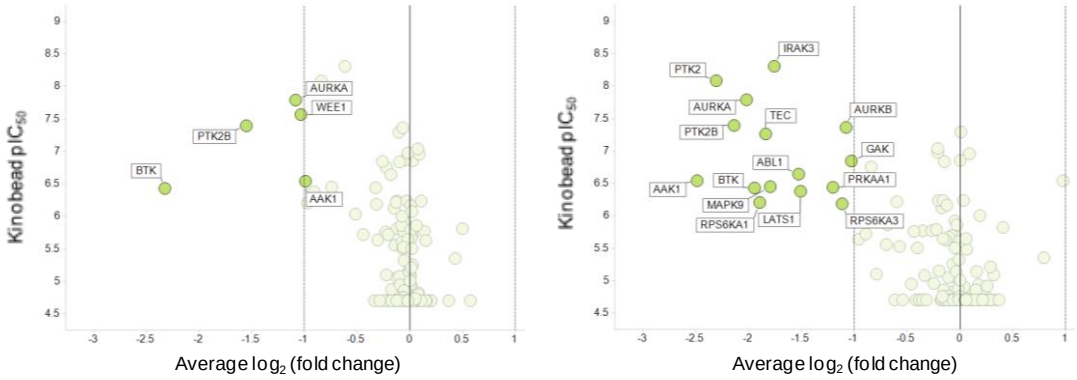

Figure 102. Significantly degraded targets by cereblon Protac **57** at 1 µM

The outcome of the expression proteomics indicates that recruitment of cereblon is a highly effective strategy for Protac-mediated degradation, with 50 % of quantified kinases found to be degraded (15/30 kinases both bound with pIC_{50} > 6 and degraded; Figure 103). For this ligase, a minimum pIC_{50} = 6 at the target binder appears to be necessary to induce protein degradation. Further interrogation of the data collected with this molecule will be outlined in upcoming sections.

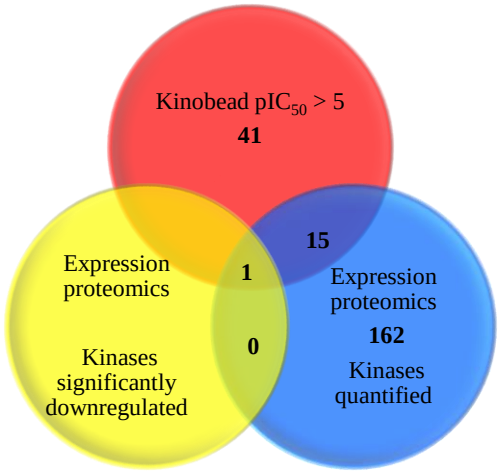

Figure 103. Comparison of engaged, quantified and degraded kinases following 24 h incubation with 1 µM cereblon Protac **57**

4.4.2 VHL Protac Expression Proteomics

Active VHL Protac **58** induced significantly less protein degradation across all concentrations; at the 6 h time point, no degradation was observed at both concentrations (Figure 104).

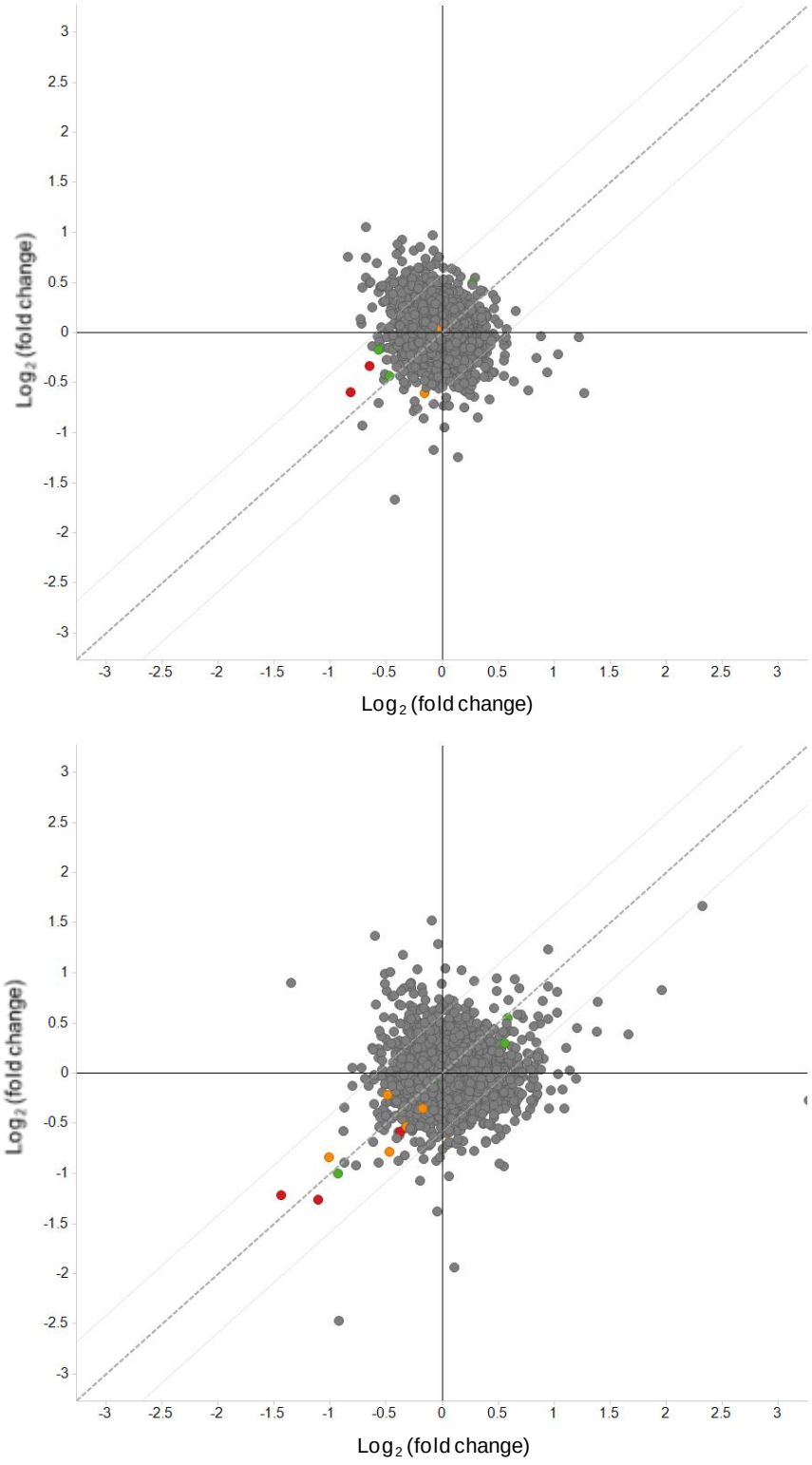

Figure 104. Expression proteomics following incubation with VHL Protac **58** at 0.1 μM after 6 h (above) and 24 h (below). Points are coloured by kinobead pIC_{50} (red = 7.0-8.3, yellow = 6.0-7.0, green = 5.0-6.0, grey = <5.0)

At the 24 h time point, incubation with Protac **58** led to modest degradation at both concentrations (Figure 105).

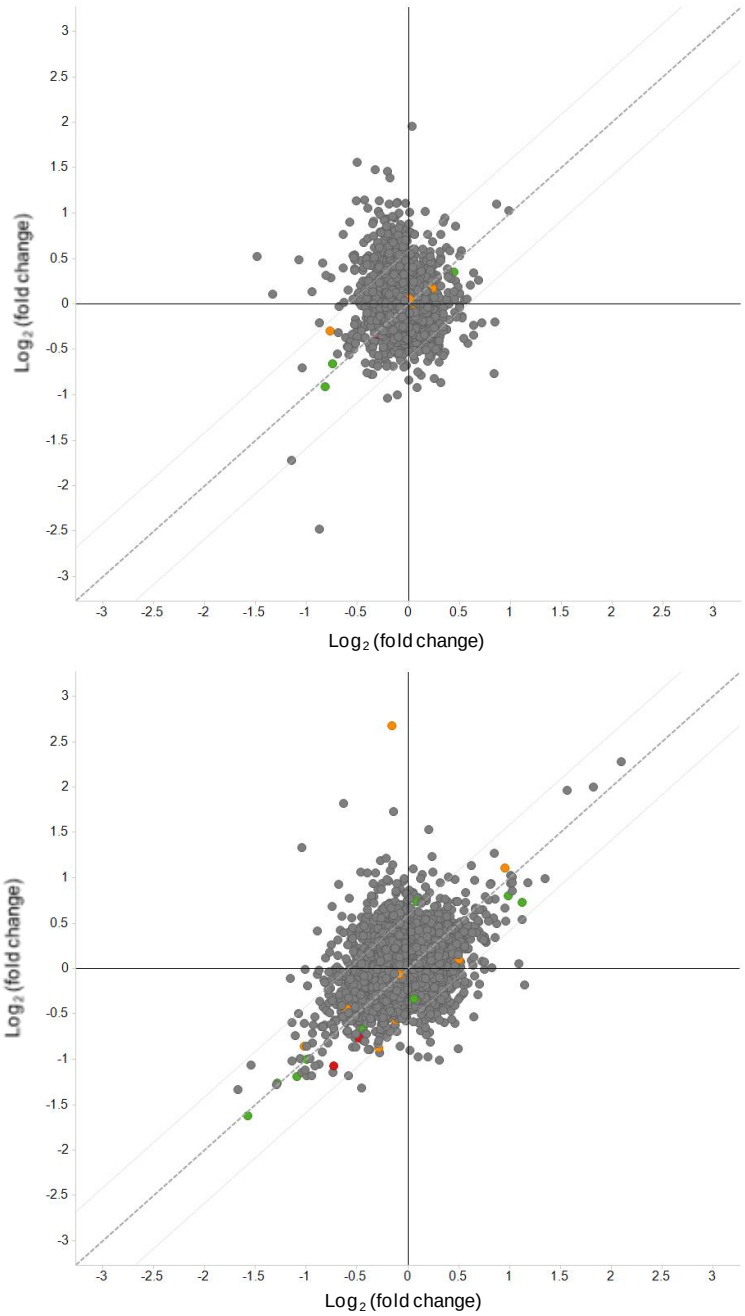

Figure 105. Expression proteomics following incubation with VHL Protac **58** at 1 µM after 6 h (above) and 24 h (below). Points are coloured by kinobead pIC_{50} (red = 7.0-8.3, yellow = 6.0-7.0, green = 5.0-6.0, grey = <5.0)

These results starkly contrast with results observed using cereblon Protac **57**, as some previously observed degradable kinases are not degraded by employing VHL despite target engagement. Degraded targets such as IRAK3 and PTK2 are potently engaged by the VHL Protac, suggesting that highly potent target binding may be necessary for VHL-mediated degradation. The observation that some weakly engaged kinases (pIC_{50} = 5-6) are degraded by this Protac implies that these targets may be particularly susceptible to degradation. This is similar to the case of degradation of MAPKAPK3 using a RIPK2-VHL Protac reported by our laboratories,[124] where unrelated kinase MAPKAPK3 was found to be degraded while not being significantly engaged by the Protac (K_d >3 μM). It is of note that the magnitude of degradation is also relatively weak compared to the corresponding cereblon Protac, with $|\log_2$ fold change| < 1.5 observed for the most potently inhibited targets.

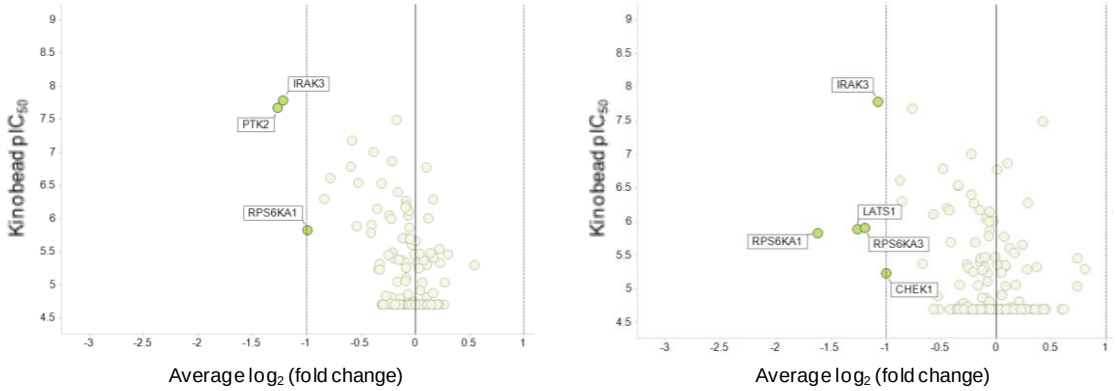

Figure 106. Significantly degraded targets by VHL Protac **58** after 24 h plotted against kinobead potency at 0.1 μM (left) and 1 μM (right)

Inactive VHL Protac **59** led to no protein degradation at all concentrations and time points. As this Protac does not recruit a ligase, the compound acts as an effective control for this experiment. The significance of the proteins upregulated in the presence of this Protac compared to Protacs with active ligase binders will be outlined in later sections.

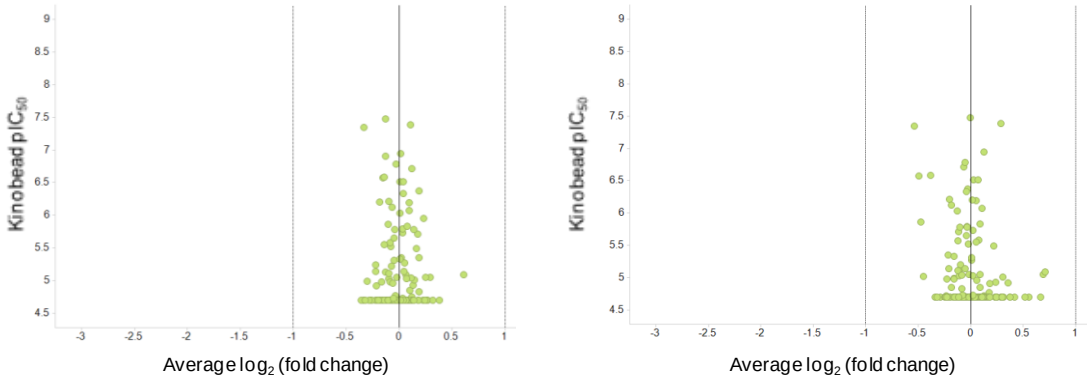

Figure 107. Lack of kinase degradation by inactive VHL Protac **59** at 0.1 μM (left) and 1 μM (right) plotted against kinobead potency after 24 h incubation

Based on the relative paucity of targets found to be degraded by active VHL Protac **58**, with ~5 % (1/21 kinases both bound with $pIC_{50} > 6$ and degraded at 1 μM, Figure 108) of engaged targets degraded compared to 50 % (15/30 kinases) with cereblon Protac **57**, it may also be possible that induced degradation employing VHL is slower or less effective than with other ligase binders. The apparent substrate specificity of VHL Protacs is reminiscent of observations by Crews and co-workers using Protacs targeting oncogenic BCR-ABL;[129] cereblon Protacs based on kinase inhibitor bosutinib were found to degrade both ABL and BCR-ABL, while the corresponding VHL Protac failed to degrade either protein despite target engagement. This, and data generated through this experiment, suggests that recruitment of VHL in isolation (disregarding other ligases such as cereblon) may be an imperfect strategy for demonstrating degradation of an empirically selected protein.

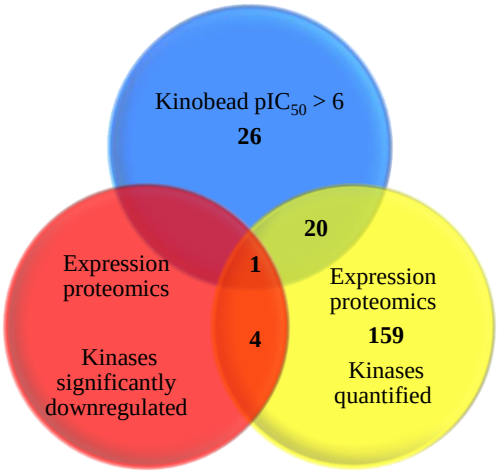

Figure 108. Comparison of engaged, quantified and degraded kinases following 24 h incubation with 1 μM VHL Protac **58**

4.4.3 IAP Protac Expression Proteomics

IAP Protac **60** was found to act as a moderately effective degrader across all concentrations and time points, influenced by its global weaker kinase potency (Figure 109). At the earlier 6 h time point, relatively few kinases were found to be degraded across both concentrations, while at 24 h, more significant protein degradation was observed, with maximal degradation at 1 μM concentration.

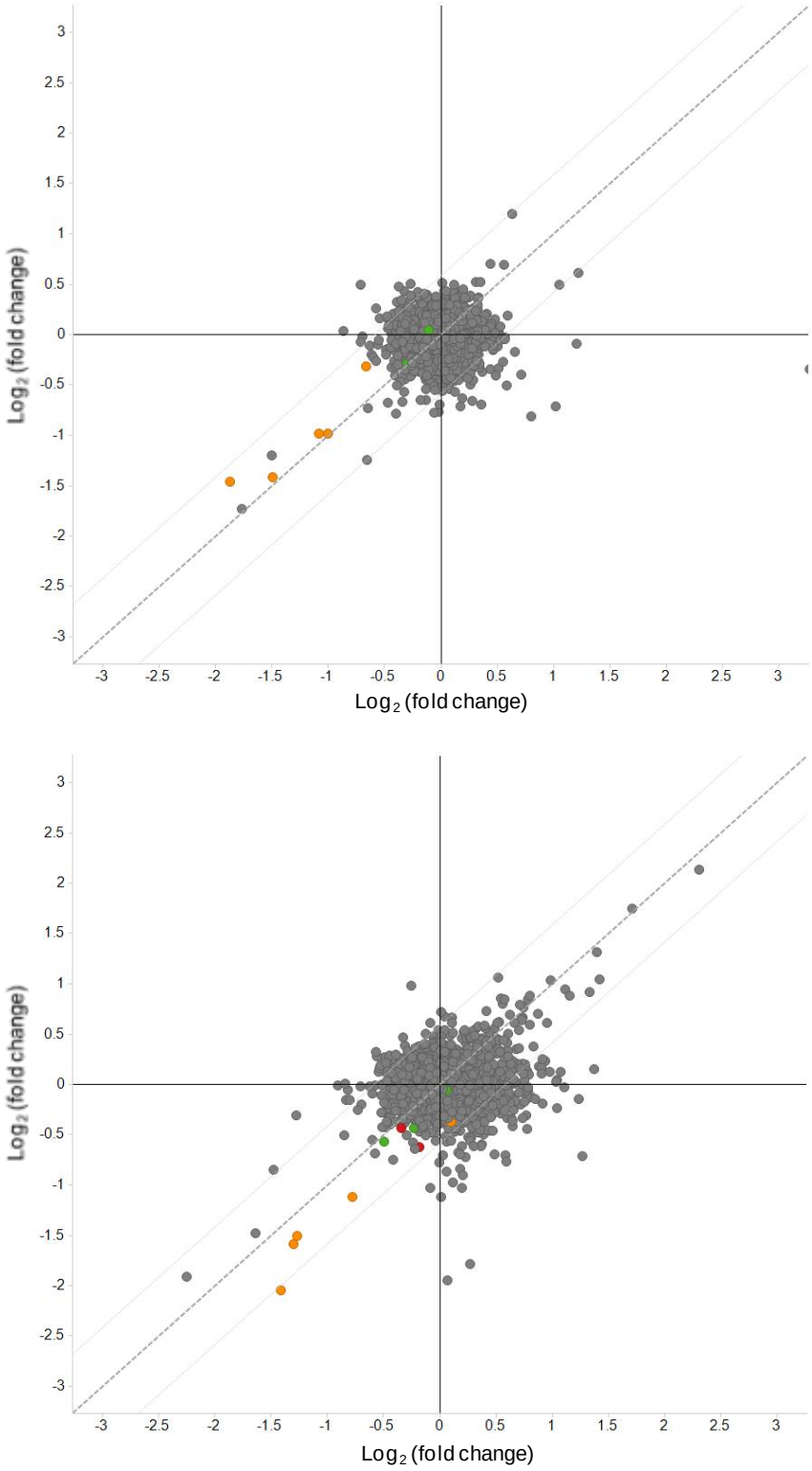

Figure 109. Expression proteomics following incubation with IAP Protac **60** at 0.1 µM after 6 h (above) and 24 h (below). Points are coloured by kinobead pIC_{50} (red = 7.0-8.3, yellow = 6.0-7.0, green = 5.0-6.0, grey = <5.0)

Following 0.1 μM incubation with IAP Protac **60**, kinases AURKA, GAK, PTK2B and TEC were found to be degraded at 6 h, with the same proteins also observed to be degraded at the 24 h time point (Figure 110).

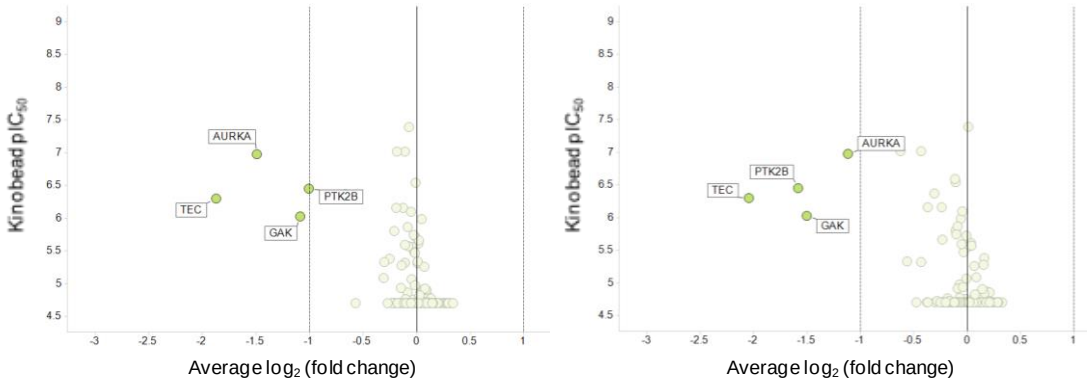

Figure 110. Degraded targets by IAP Protac **60** at 0.1 μM plotted against kinobead potency at 6 h (left) and 24 h (right)

A similar degradation profile was observed at the 6 h time point following 1 μM incubation (Figure 111), although TEC degradation not observed, potentially due to experimental variability. At the 24 h time point, further degradation of BTK, MAPK9, PTK2 and RPS6KA1 was observed, including degradation of the more weakly engaged targets (pIC_{50} = 5-6), presumably due to a greater number of target binding events over the longer time period.

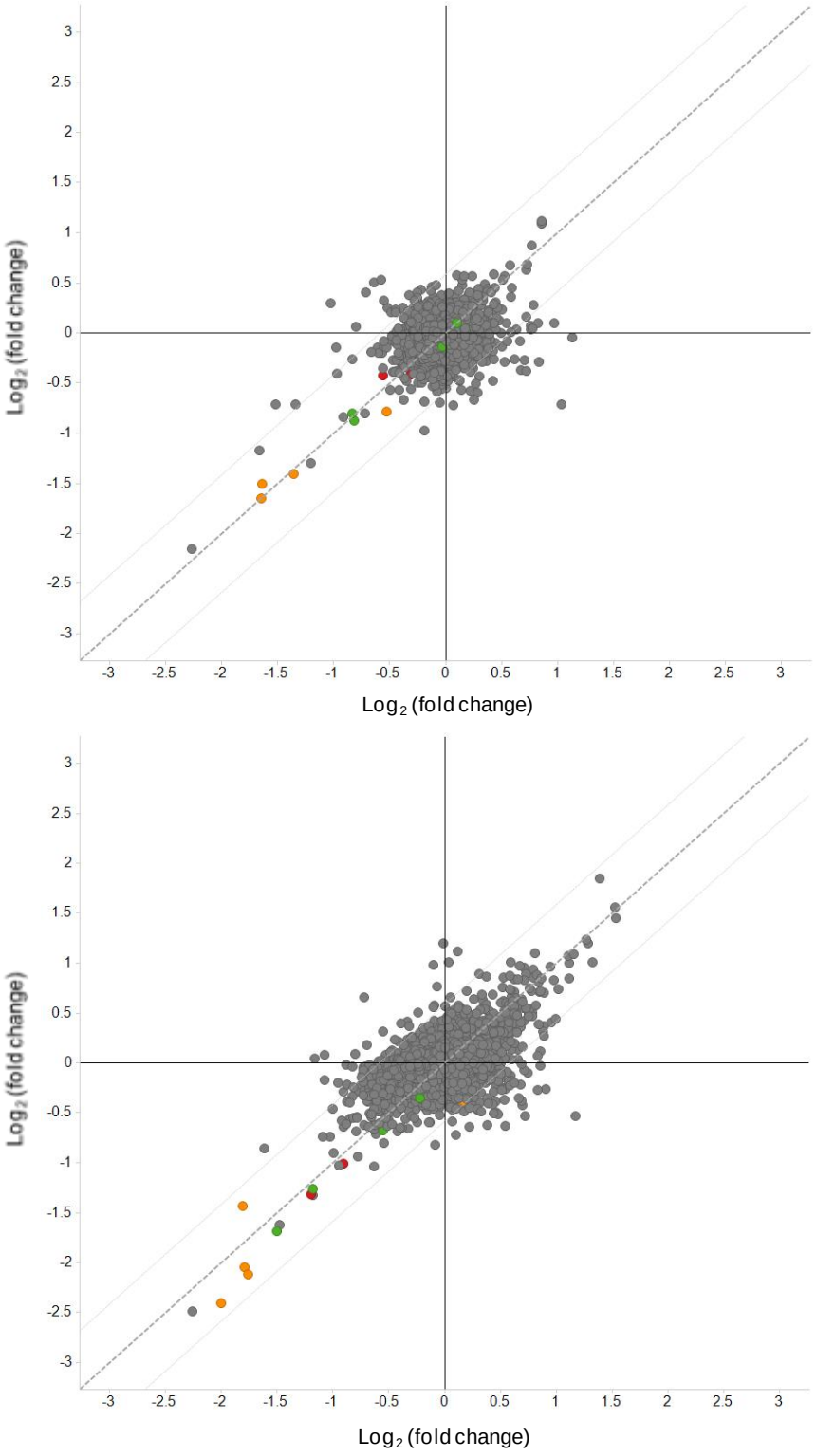

Figure 111. Expression proteomics following incubation with IAP Protac **60** at 1 μM after 6 h (above) and 24 h (below). Points are coloured by kinobead pIC_{50} (red = 7.0-8.3, yellow = 6.0-7.0, green = 5.0-6.0, grey = <5.0)

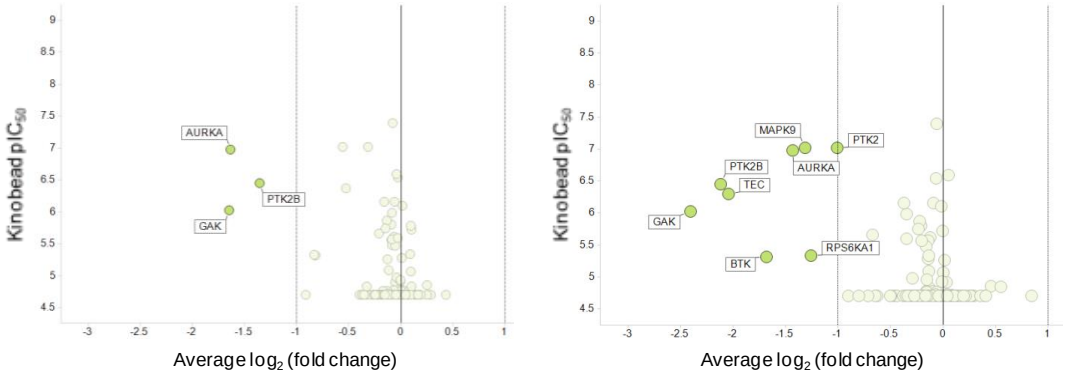

Figure 112. Degraded targets by IAP Protac **60** at 1 μM plotted against kinobead potency at 6 h (left) and 24 h (right)

The extent of IAP degradation with Protac **60** proves to be equally positive to that observed with cereblon Protac **57**, with 50 % of significantly engaged and quantified kinases degraded (6/12 kinases both bound with pIC_{50} > 6 and degraded; Figure 113) although the Protac employed in this experiment may be an imperfect tool molecule given its reduced levels of kinase binding. However, this experiment validates IAP as a widely applicable ligase for Protac-mediated degradation, a significant advantage of which is the large number of known IAP binders, allowing subtle modulation of Protac properties for potential optimisation.

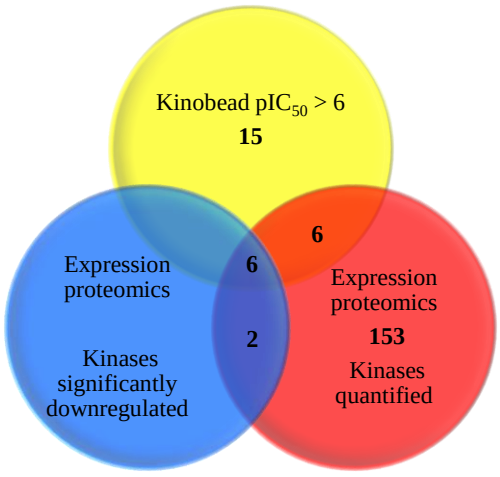

Figure 113. Comparison of engaged, quantified and degraded kinases following 24 h incubation with 1 μM IAP Protac **60**

4.5 Broader Considerations Following Expression Proteomics

4.5.1 Degraded Proteins

Following 24 h incubation with 1 μM Protac, the most significant protein degradation of kinases engaged with a $pIC_{50} \geq 6$ (in lysates) was observed. Few kinases were found to be degraded with target engagement below this concentration, suggesting that target engagement above this potency is typically necessary to observed protein degradation (with some exceptions). Cereblon Protac **57** was found to degrade 15 kinases (Figure 114), while IAP Protac **60** was found to degrade 8 kinases in total (Section 4.4.3), all of which correlated with those degraded by cereblon recruitment, hence further analysis will be carried out considering the cereblon Protac only.

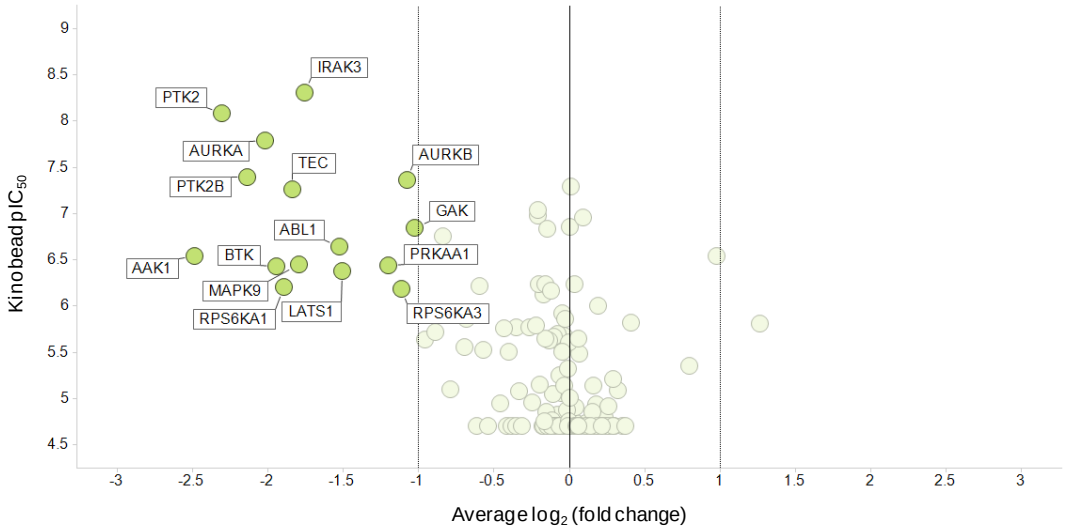

Figure 114. Proteins engaged with $pIC_{50} \geq 6$ and significantly degraded by cereblon Protac **57** after 24 h incubation at 1 μM

AAK1 was found to be degraded only when cereblon was recruited as a ligase, despite sufficient binding to induce degradation with all ligase partners (AAK1 pIC_{50} cereblon/VHL/IAP Protac = 6.54/6.15/5.60). This suggests that a potentially critical factor in target degradability may be the subcellular localisation of the protein. The vast majority of degraded kinases, ABL1,[267] AURKA/B,[268] BTK,[269] GAK,[270] IRAK3,[271] LATS1,[272] MAPK9,[273] PRKAA1,[274] PTK2,[275] PTK2B,[276] RPS6KA1/3,[277,278] and TEC,[279] are reported to localise in the nucleus or cytoplasm (Figure 114). This correlates with previously reported cases where proteins such as

BRD4 (localised in the nucleus) and RIPK2 (localised in the cytoplasm) have been shown to be degradable respectively.[124,130,131] However, AAK1 is reported to be associated with the cell membrane (though not a transmembrane protein),[280] potentially indicating that only cereblon recruitment allows degradation of proteins in this cellular subsection.

Across all of the expression proteomics experiments with active Protacs, IRAK3, PTK2, and RPS6KA1 were found to be degradable employing Protacs with each ligase binders. Degradation of IRAK3 and PTK2 correlate with high levels of target engagement (IRAK3 pIC_{50} cereblon/VHL = 8.31/7.79 (IAP unquantified); PTK2 pIC_{50} cereblon/VHL/IAP = 8.09/7.68/7.02), while RPS6KA1 degradation was observed despite relatively weak Protac binding in all cases (RPS6KA1 pIC_{50} cereblon/VHL/IAP Protac = 6.21/5.79/5.33). This suggests that this kinase is particularly susceptible to degradation, possibly in a similar manner to that of MAPKAPK3 by the RIPK2-VHL Protac developed within our laboratories.[124]

4.5.2 Undegraded Proteins with Protac Engagement

By combination of the expression proteomics experiment and kinobead data, kinases which were engaged yet undegraded can be identified. Protac-mediated degradation requires access to free lysine residues on which to transfer ubiquitin. Thus, the approach vector of the target protein and E3 ligase in ternary complex formation is likely to be highly relevant in induction of substrate degradation. These factors will, in turn, be influenced by the structure of the Protac and, specifically, factors such as length of the PEG chain and the manner in which the Protac exits the binding site of the target. As only one PEG chain length and binding site exit vector has been explored in this programme, these undegraded kinases cannot definitively be described as undegradable. Rather, these species can be considered to be unsusceptible to degradation by these particular Protacs. However, from subcellular localisations of these individual undegraded proteins, some possible rationalisation will be proposed.

As incubation with 1 μM Protac for 24 h resulted in most significant regulation, only these conditions will be considered. Also, as only cereblon and IAP Protacs resulted in significant degradation, the VHL Protac will not be analysed. As previously stated,

cereblon Protac **87** degraded 15/30 engaged proteins with a $pIC_{50} \geq 6$ after 24 h with 1 μM compound. Among the proteins engaged but not degraded included proteins known to localise to the cell membrane: AXL,[281] JAK2,[282] LCK,[283] STK10[284] and TGFBR1[285] (Figure 115). Other unregulated proteins included those reported to localise in the cytoplasm or nucleus: BCR,[267] CAMKK2,[286] CSNK2A1/2,[287] IRAK1,[288] KIAA1804,[289] MAP3K4,[274] RPS6KA4,[290] SLK[291] and TBK1.[292] It is notable that BCR was not degraded, though degradation of the oncogenic fusion BCR/ABL has been reported, potentially mediated by engagement of the ABL binding site.[129] Similarly, degradation of TBK1 has been demonstrated using a VHL Protac,[293] however is engaged yet undegraded by this Protac.

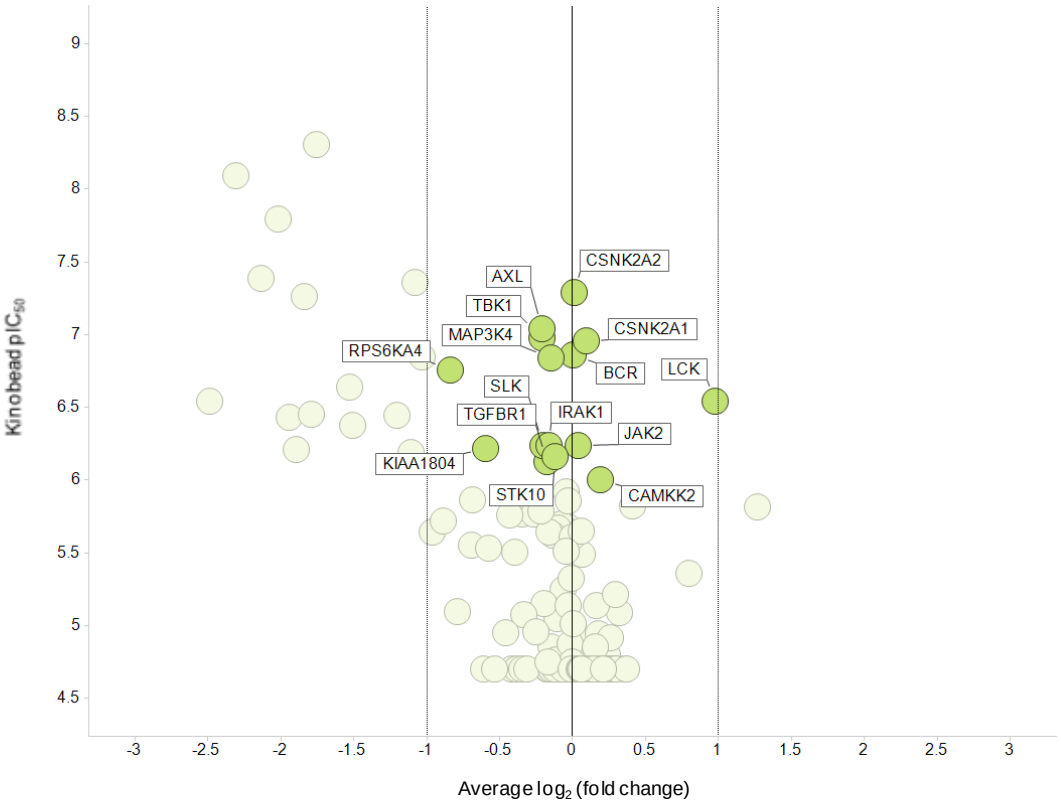

Figure 115. Proteins engaged with $pIC_{50} \geq 6$ but not degraded by cereblon Protac **57**

IAP Protac **60** also caused no degradation of AXL, CAMKK2 and TBK1, as previously discussed with cereblon Protac **57** (Figure 116). TAOK1 and TAOK3 were also unregulated, and localise in the cytoplasm and cytoplasm/cell membrane, respectively.[294] AURKB was not degraded by IAP Protac **60**, however was degraded

by cereblon Protac **57** (Figure 114), again indicating the variable effect of the recruited ligase on target protein degradation.

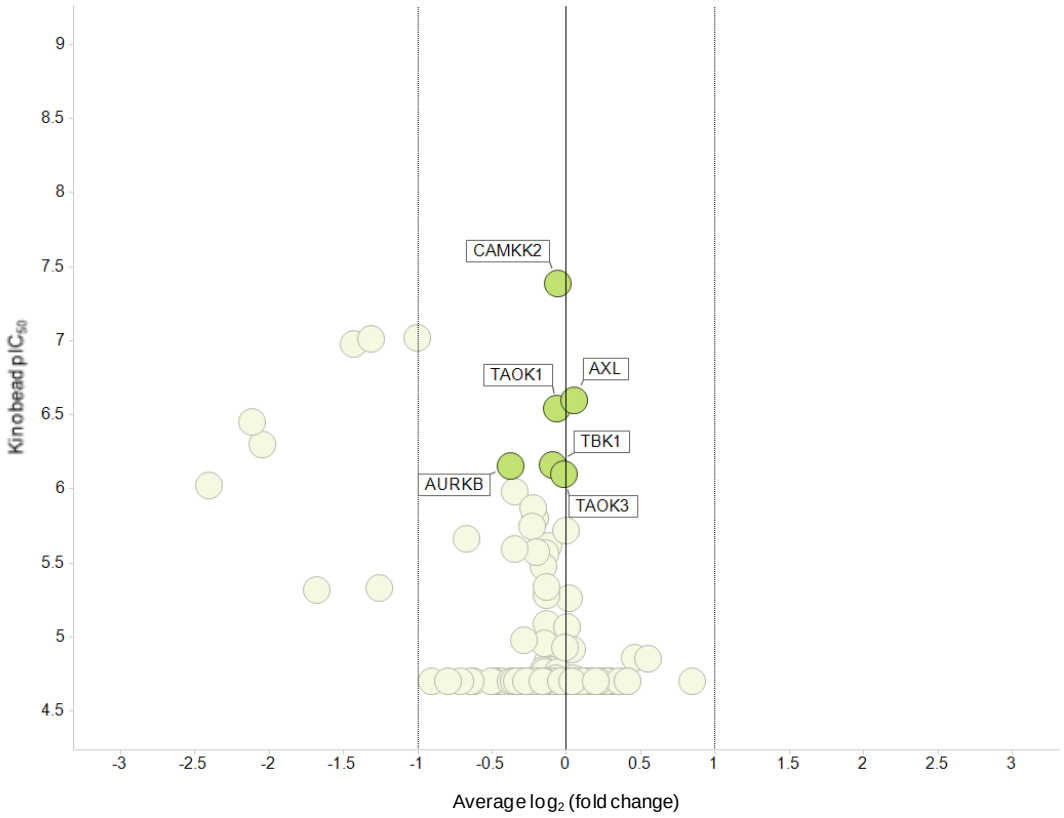

Figure 116. Proteins engaged with $pIC_{50} \geq 6$ but not degraded by IAP Protac **60**

As previously stated regarding degraded proteins, there may be potential issues with proteins associated with the cell membrane. In this case, 5/15 of the undegraded proteins were found to be membrane associated. However, the majority of undegraded proteins were found to be either cytoplasmic or nuclear. In these cases, the lack of observed degradation may be caused by a conformational mismatch between ligase and protein, or potentially a lack of available surface lysines onto which ubiquitin may be transferred.

4.5.3 Unexpected Upregulated or Downregulated Proteins

The outcome of the proteomics experiments also resulted in some unpredictable upregulation and downregulation of certain proteins; the 24 h time point and 1 µM concentration will be considered due to most significant protein regulation. A series of proteins, APOM, PLTP and POSTN, were found to be upregulated throughout all the proteomics experiments (Figure 117, Figure 118). As this effect is still observed in the presence of the inactive VHL Protac **59**, this suggests upregulation is driven by the kinase inhibitor alone, as the inactive Protac does not recruit a ligase.

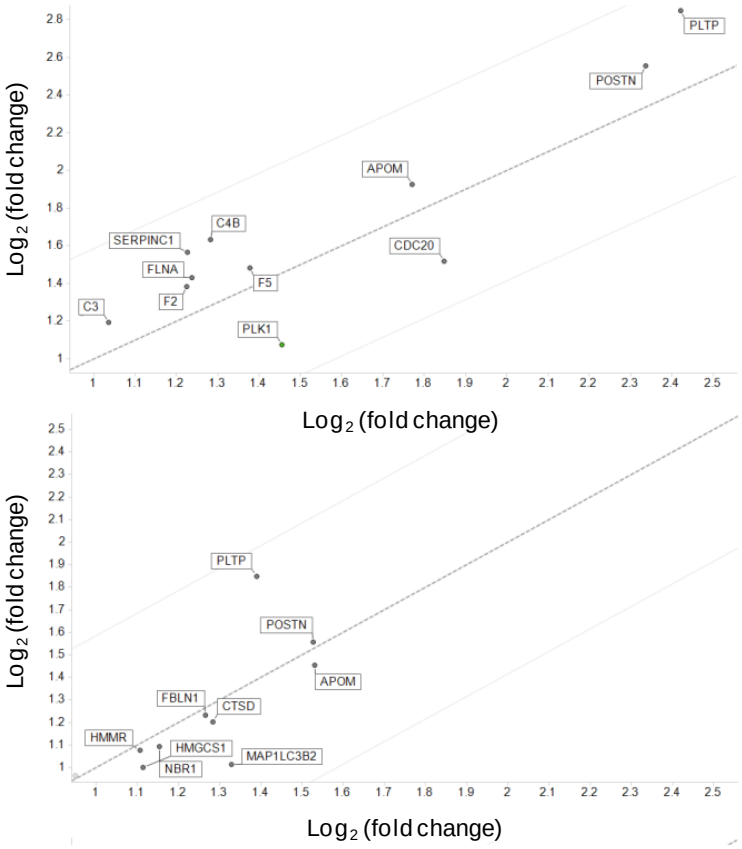

Figure 117. Significantly upregulated proteins after incubation with cereblon Protac (**57**, above) and IAP Protac (**60**, below) following 24 h incubation at 1 µM

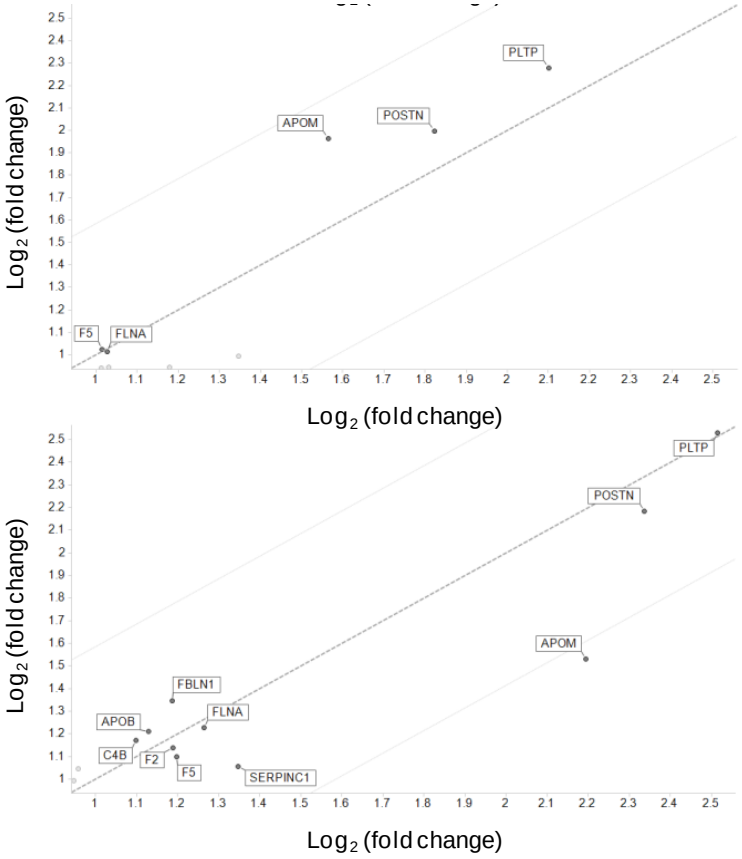

Figure 118. Significantly upregulated proteins after incubation with VHL active (**58**, above) and VHL inactive (**59**, below) Protacs following 24 h incubation at 1 μM

Similarly, certain proteins were found to be downregulated without observed target engagement, as determined by the kinobead experiments. Only cereblon and IAP Protacs were found to induce significant downregulation of unengaged targets, hence VHL Protacs will not be considered. It is notable that no unexpected downregulation was observed in the case of inactive VHL Protac **59**, indicating that kinase inhibition alone has no significant effect on intracellular protein levels.

The poorly characterised protein named YJ005_Human was found to be significantly downregulated by cereblon Protac **57** (Figure 119, top), although this protein has been suggested to be an isoform of AAK1,[295,296] previously shown to be degraded by cereblon Protac **57** exclusively (Section 4.5.1).

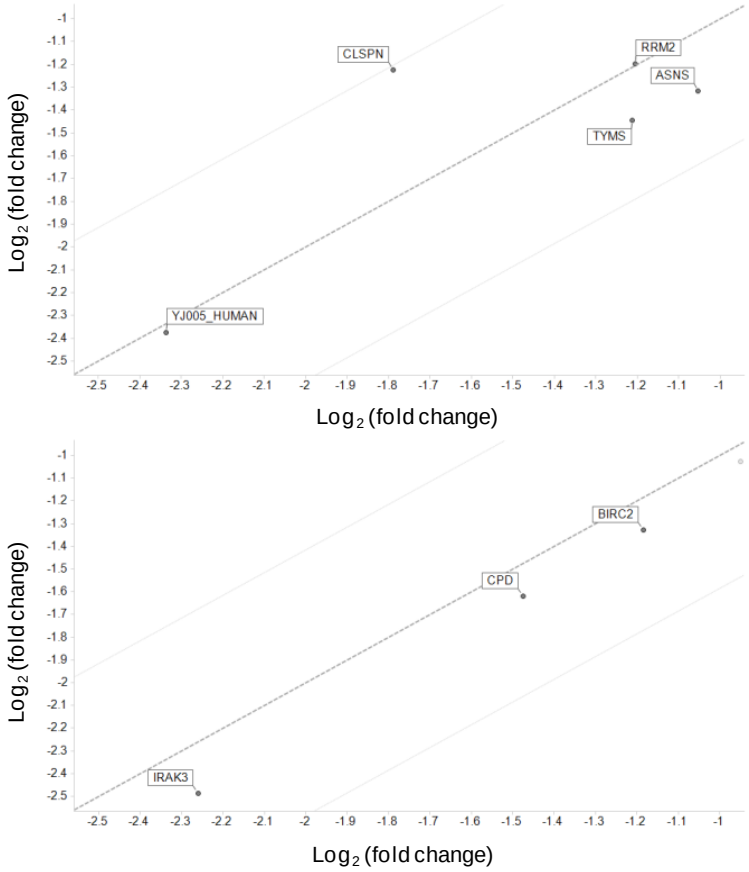

Figure 119. Significantly downregulated proteins after incubation with cereblon Protac **57** (top) and IAP Protac **60** (bottom) following 24 h incubation at 1 μM

The protein TYMS was found to be slightly downregulated by cereblon Protac **57**. TYMS is known to irreversibly binds uracil,[297] which in turn is a known binder of cereblon.[298] Employing lenalidomide to recruit cereblon in Protac **57** may also result in irreversible inhibition of TYMS, resulting in its downregulation in this experiment. CLSPN was also found to be downregulated by the cereblon Protac **57**. CLSPN is known to be ubiquitinated by anaphase-promoting complex (APC/C),[299] which is upregulated by CDC20,[300] which is itself found to be upregulated by Protac **57** (Figure 117).

Following incubation with IAP Protac **60**, BIRC2 was found to be downregulated (Figure 119, bottom). This protein is also known as cIAP1, degradation of which is to be expected as cIAP1 autoubiquitinates and degrades following Smac binding.[136] IRAK3 was degraded by IAP Protac **60**, a target for which kinobead data was not

recorded. However, since cereblon and VHL Protacs were both found to significantly engage and degrade IRAK3 (Section 4.5.1), this effect can be attributed to IAP-mediated degradation. The observed downregulation of CPD may be associated with an off-target effect of the Smac IAP inhibitor as downregulation was only observed with this Protac.

4.6 Observing Single Target Degradation

Following on from the expression proteomics experiments, it was thought that conformation of single target degradation by western blotting would correlate the degradation observed by through the MS approach. One of these proteins, Bruton's tyrosine kinase (BTK), was selected as a single protein to validate this. As only cereblon Protac **57** and IAP Protac **60** were found to degrade BTK by expression proteomics, degradation with VHL Protac **58** was not expected (Table 7).

Table 7. BTK-related properties of promiscuous kinase Protacs

Compound no.	Ligase	BTK cell pIC_{50}	BTK degrader?
57	Cereblon	6.43	✓
58	Active VHL	6.05	✕
60	IAP	5.32	✓

First, cereblon Protac **57** was incubated in THP-1 cells for 24 h across a range of concentrations, then BTK protein levels were monitored by western blotting.[301] Concentration-dependent degradation of BTK was observed, consistent with degradation observed by expression proteomics. Quantification of protein levels resulted in an approximate DC_{50} ~ 1 nM (Figure 120).

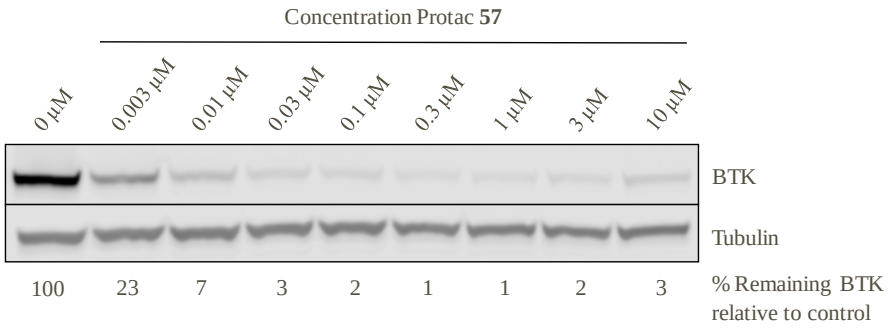

Figure 120. BTK degradation observed by western blotting with promiscuous cereblon Protac **57** after 24 h incubation in THP-1 cells (above); quantification of BTK protein levels (below)

Comparison of this DC_{50} to the cellular binding potency of the Protac demonstrates one of the benefits of a Protac-mediated approach. By kinobead experiments, it is known that the cereblon Protac **57** inhibits BTK with a pIC_{50} = 6.43 (i.e. 370 nM, Table 7). Thus, with a DC_{50} ~ 1 nM, this Protac induces degradation at a concentration 300 times below the level of BTK inhibition, indicative of the event-driven rather than absolute target occupancy required for efficient degradation.

As no significant degradation of BTK was observed by expression proteomics with VHL Protac **58**, the result was confirmed by western blotting (Figure 121), which also showed no significant knockdown of BTK.

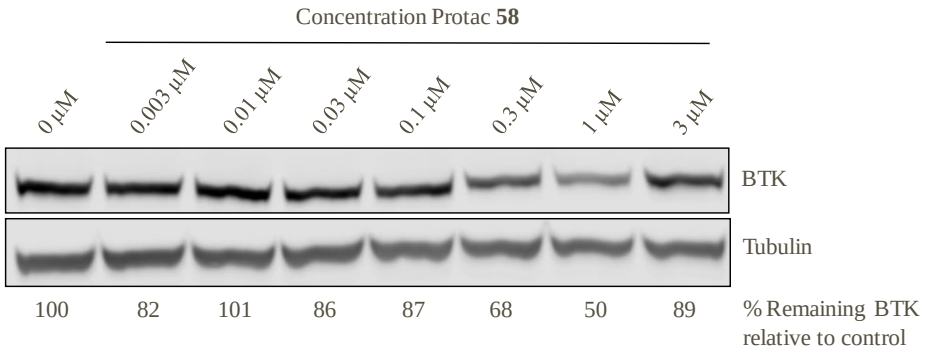

Figure 121. No significant BTK degradation is observed by western blotting with promiscuous VHL Protac **58** after 24 h incubation in THP-1 cells

Carrying out the same experiment using the IAP Protac **60** also resulted in concentration dependent BTK degradation, although to a lesser extent, with an observed DC_{50} ~ 300 nM (Figure 122). The higher DC_{50} observed with this Protac is consistent with the weaker degree of binding potency; by kinobead assay BTK pIC_{50} **60** = 5.32 (i.e. 4.8 µM, Table 7), correlating less potent target binding to less efficient degradation. In this case degradation is occurring 16 times below the inhibition concentration, again indicating the event-driven rather than occupancy-driven efficacy possible using a Protac approach.

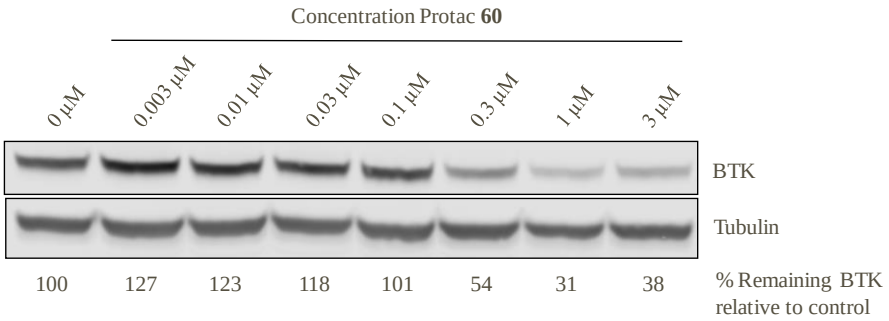

Figure 122. BTK degradation observed by western blotting with promiscuous IAP Protac **60** after 24 h incubation in THP-1 cells

To confirm that degradation observed in these cellular experiments is driven by degradation rather than a cytotoxic effect, cell viability experiments were carried out concomitantly (Figure 123). Across the relevant concentrations where degradation was observed (<10 µM), cellular viability was mostly maintained, indicating that the reduction in protein levels is not due to cytotoxicity. At 10 µM concentration, compound related cytotoxicity was observed with both VHL and IAP Protacs; in the case of IAP this may be caused by induction of apoptosis due to cIAP1 degradation.[302]

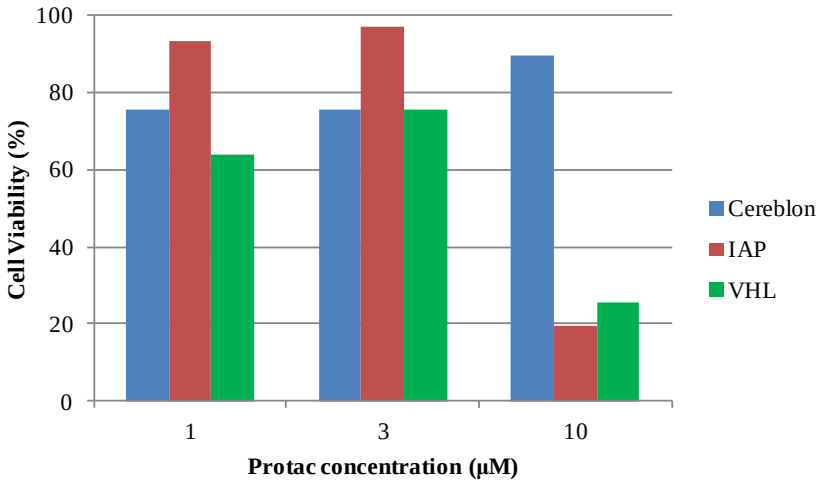

Figure 123. Viability of THP-1 cells following treatment with promiscuous kinase Protacs **57**, **58** and **60**

4.7 Conclusions

Protacs incorporating a promiscuous kinase binder based on inhibitor CTx-0294885 recruiting the ligases cereblon, VHL, and IAP were synthesised to assess the wider applicability of Protacs towards a targeted degradation approach. In total, 15 novel targets were found to be degraded by the promiscuous Protacs. Cereblon and IAP were found to be highly valuable ligases to recruit, as both Protacs demonstrated knockdown of at least 50 % of the targets significantly engaged by the respective Protacs, while recruitment of VHL demonstrated a more modest degree of protein degradation.

Following on from this experiment, it was found that degradation of newly identified targets captured in the expression proteomics experiment could be recapitulated by western blotting, with dose-dependent protein degradation observed. This approach also demonstrates the possibility for degradation selectivity in the absence of binding selectivity, and as concentrations required for effective degradation are often significantly lower than that required for inhibition.

In summary, before the commencement of this programme, only a small number of targets were known to be degradable (<10 in total). The promiscuous approach permitted rapid assessment of target degradability, and allowed highly efficient identification of a number of novel degradable targets. The outcomes also point

towards the critical matching of target protein to E3 ligase, and that proteins associated with the membrane may be more challenging targets for degradation than those residing in the cytoplasm or nucleus. Having identified BTK as a novel degradable target, development of selective BTK Protacs was then explored.

5. Bruton's Tyrosine Kinase Protacs

5.1 Bruton's Tyrosine Kinase

In the previous chapter, using a promiscuous approach towards identification of novel degradable targets, BTK was found to be a highly susceptible target towards Protac-mediated degradation upon recruitment of IAP or Cereblon as E3 ligases. In this chapter, this kinase will be assessed as a prototypical target for a Protac-based approach by pursuit of selective degradation.

5.1.1 Target Introduction

BTK is a tyrosine kinase primarily expressed in B cells and myeloid cells.[303] It is a member of the Tec kinase family which all share a similar global structure, consisting of a *N*-terminal pleckstrin homology (PH) domain, a proline-rich Tec homology (TH) domain, Src homology 3 (SH3) and SH2 domains, and a *C*-terminal kinase domain (Figure 124).[304]

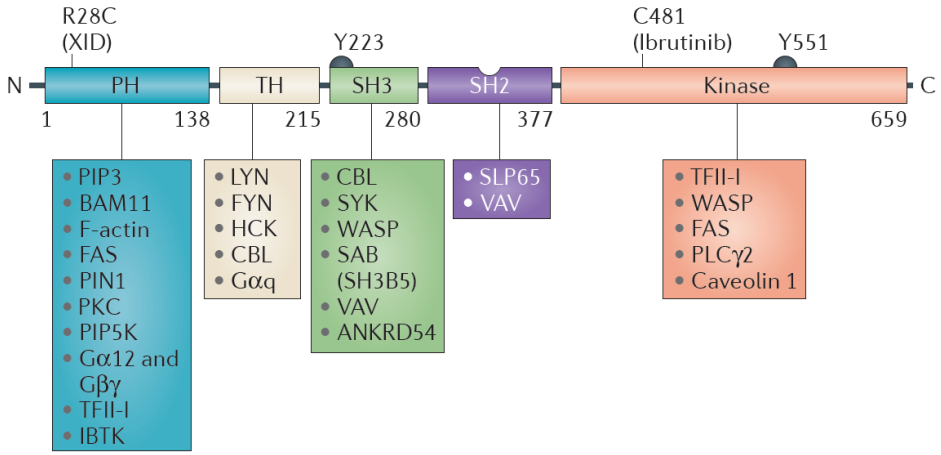

Figure 124.[305] Structure of BTK indicating interaction partners and critical residues

Mapping of the human *BTK* gene led to discovery that the chromosome region directly overlapped with the defective gene causing X-linked agammaglobulinemia (XLA),[306,307] a primary immunological deficiency (PID) first described by Bruton.[308] XLA severely impacts development and function of B cells, resulting in ~100 fold B cell reduction in peripheral blood lymphocytes,[309] and is the most common PID with

an incidence of 1:250,000. Due to this B cell deficiency, XLA patients are highly susceptible to recurrent bacterial infections in the respiratory or gastrointestinal tract.[310] Either null or point mutations in *BTK* directly cause XLA, with over 600 distinct inactivating mutations reported.[311] In mice, a single point mutation in the PH domain (R28C) causes X-linked immunodeficiency (xid) leading to abnormal B cell function.[312] This has a much less severe phenotype than XLA, but closely matches the phenotype observed in BTK knockout mice.[313,314]

Given the role of *BTK* in B cell development, it is unsurprising that BTK is a critical mediator in the B cell receptor (BCR) pathway (Figure 125).[315,316] Upstream activation of the BCR pathway by antigen presentation to the BCR begins a transphosphorylation cascade, first from the kinase LYN to spleen tyrosine kinase (SYK).[303,317] Although in its inactivated state BTK is generally a cytosolic protein, its activation first requires membrane association through an interaction between the PH domain and phosphatidylinositol (3,4,5)-trisphosphate (PIP_3). Upon membrane association, BTK is phosphorylated by SYK at Y551 in the kinase domain, followed by a subsequent autophosphorylation step, with phosphate transfer from Y551 to Y223 in the SH3 domain, inducing full activation of BTK.[318,319]

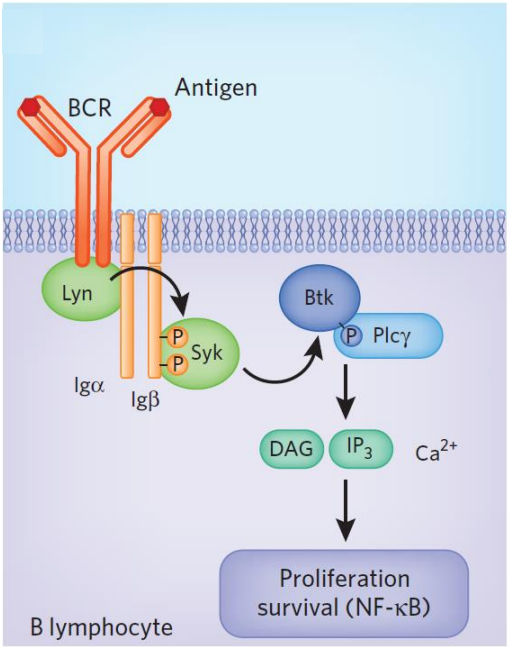

Figure 125.[320] Simplified representation of the BCR signalling pathway

Activation of BTK leads to subsequent phosphorylation of phospholipase C-γ (PLCγ),[321] which in turn leads to generation of inositol-1,4,5-trisphosphate (IP_3) and diacylglycerol (DAG), promoters of Ca^{2+} influx.[322] This Ca^{2+} influx causes activation of multiple intracellular pathways, including that of mitogen-activated protein kinase (MAPK),[323] and nuclear factor kappa-light-chain-enhancer of activated B cells (NF-κB),[324] which promote B cell proliferation and survival.

5.1.2 BTK Inhibition

The important role of BTK in B cell signalling has promoted intervention by small molecule inhibition. Indications targeted thus far have primarily focused on B cell malignancies or rheumatoid arthritis (RA), which are highly dependent on BCR signalling.[305,325] The possibility of therapeutic benefit for further autoimmune diseases such as lupus and multiple sclerosis through inhibition of BCR signalling have also been demonstrated preclinically.[326,327] BTK is overexpressed in many B cell leukemias and lymphomas, where the BCR pathway is constitutively active and required for tumour survival.[328–330] This suggests that blockade of BCR signalling through small molecule-mediated inhibition of BTK would inhibit progression of B cell associated tumours, hence this approach has been explored extensively in various cancers.

RA is a common autoimmune disease which causes severe and persistent joint inflammation, resulting in cartilage damage, joint destruction and, eventually, bone erosion.[331] Initiation of RA causes B cell activation, which causes disease progression. The anti-CD20 antibody rituximab, which selectivity depletes B cells, has demonstrated a beneficial clinical response in the treatment of RA.[332] Xid mice have been shown to be less susceptible to developing arthritis, as this loss of function BTK mutation drives an analogous, though indirect, B cell population depletion.[333] This suggests that inhibition of BTK kinase activity would mimic this phenotype and have potential therapeutic benefit in RA.

Given the opportunities available by modulation of BCR signalling, and a viable population of humans with loss of function BTK mutations (XLA patients), it is a particularly convincing target for modulation using small molecule inhibitors. Critical

advances in the field of BTK inhibitor discovery will be outlined in subsequent sections.

5.1.2.1 Ibrutinib

As previously stated, and used advantageously in Section 4, ATP binding sites of kinases are often highly conserved. Consequently, the generation of selective kinase inhibitors is highly challenging. As described in Section 1.1, covalent inhibition can also be a strategy for extending pharmacodynamic efficacy, as duration of action is dependent on resynthesis of the target protein. However, it can be also used as a strategy to gain kinase selectivity, as a covalent inhibitor can target unconserved amino acids proximal to the ATP binding site.[334–336]

In the case of BTK, the presence of a cysteine residue (C481) in the vicinity of the ATP binding site prompted the development of Ibrutinib (previously known as PCI-32765),[337] developed from a previously reported LCK inhibitor.[338] The pendant acrylamide residue incorporated into the inhibitor is in close proximity to C481 and acts as Michael acceptor, resulting in covalent inhibition of BTK (Figure 126). This compound was the first potent and selective tool for probing the effects BTK inhibition, though nine further kinases share an aligned cysteine residue (BLK, BMX, EGFR, ErbB2, ErbB4, ITK, JAK3, TEC and TXK) and the compound also reversibly inhibits various off-target kinases.[337] Although initially developed as a potential treatment for RA, Ibrutinib was found to demonstrate outstanding preclinical activity in a canine B cell non-Hodgkin lymphoma (NHL) model.[339]

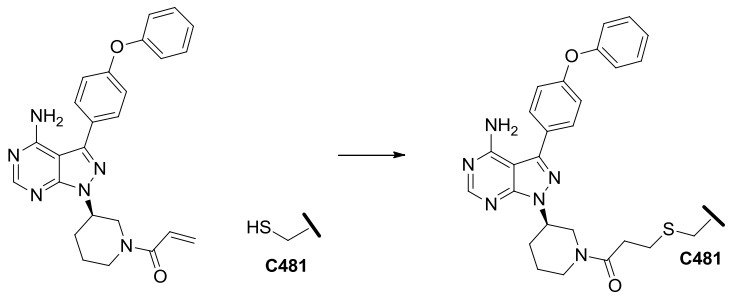

Figure 126. Ibrutinib irreversibly inhibits BTK by covalent binding to C481

Subsequent clinical development directly targeted various B-cell cancers, where positive efficacy as a monotherapy in chronic lymphocytic leukaemia (CLL),[340] mantle-cell lymphoma (MCL),[341] and Waldenstrom's macroglobulinaemia (WM)[342] were demonstrated, eventually leading to FDA approval for these indications (marketed as Imbruvica). International sales of Ibrutinib are expected to reach $9 billion by 2020.[343]

The oral PK profile of Ibrutinib is ideal for a covalent inhibitor, as it reaches maximal plasma concentrations within 1-2 h and is widely distributed while having a relatively short half-life of 4-6 h.[344] As high target exposure and BTK engagement are achieved rapidly, this limits exposure at reversible off-target kinases. In CLL patients, high target occupancy (>95 %) is achieved 4 h after dosing, with the extended PD effect allowing a once-daily dosing strategy to maintain pathway inhibition (420 mg/day in CLL).

Though Ibrutinib is mostly well tolerated,[340] it can cause multiple adverse events not observed in the XLA phenotype, associated with engagement of off-target kinases with aligned cysteines, such as bleeding, rash, diarrhoea, atrial fibrillation and major haemorrhage.[340,345,346] To maintain a clinical response and prevent disease progression, uninterrupted treatment is required, with discontinuation often leading to a poor prognosis for patients.[347,348]

As Ibrutinib has moved into the clinic and numbers of treated patients has increased, there are emerging issues with relapses caused by resistance mechanisms not observed in naïve patients.[349,350] The first and most prevalent resistance mechanism arises from a direct BTK C481S mutation, which has been observed in 5 % of CLL patients.[351] As C481 is critical for irreversible binding of Ibrutinib, duration of action and BTK occupancy are significantly reduced, resulting in a severely diminished pharmacological effect in patients and progression of disease.

The second mutation occurs downstream of BTK in PLCγ2 (see Figure 125).[352] A R665W mutation allows BCR signalling to bypass BTK in the phosphorylation cascade, causing redundancy of BTK inhibition. It is thought that the PLCγ2 mutation may cause conformational change which activates its catalytic function regardless of

phosphorylation, or acquires higher affinity for LYN or SYK and is phosphorylated directly (Figure 127).

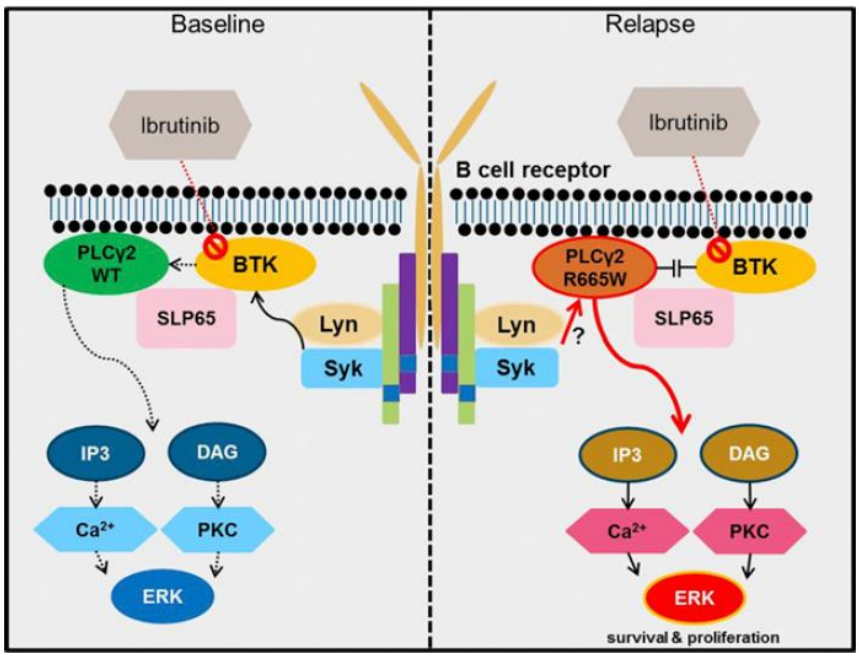

Figure 127.[352] Rationalisation of BTK-independent BCR signalling maintained by the PLCγ2 R665W mutation compared to typical BCR inhibition by Ibrutinib (SLP65 = B cell linker protein, PKC = Protein kinase C, ERK = Extracellular signal–regulated kinase)

5.1.2.2 Further Covalent Inhibitors

CC-292 (Figure 128) also covalently inhibits BTK through binding to C481, and shares a similar selectivity profile to Ibrutinib.[353] CC-292 was the first BTK inhibitor to be tested in patients with RA and is currently in phase II clinical trials for this indication. As indicated in Figure 129, following dosing with CC-292, PK and PD become uncoupled as target occupancy is maintained in the absence of free circulating drug, the profile expected for a covalent inhibitor.

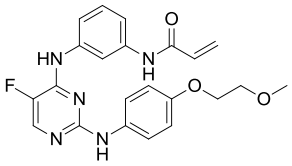

Figure 128. Structure of irreversible BTK inhibitor CC-292

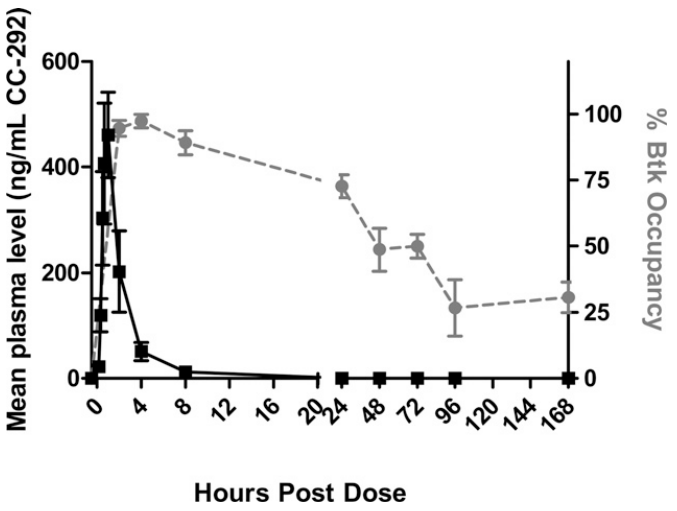

Figure 129.[353] Uncoupled PK/PD observed in healthy human volunteers following dosing with CC-292 (2 mg/kg). BTK occupancy is maintained in the absence of circulating drug, as indicated by mean plasma level

A second-generation covalent BTK inhibitor, Acalabrutinib (previously known as ACP-196, Figure 130), has been designed to improve on the safety and efficacy of Ibrutinib, with which it shares some structural similarity.[354] Acalabrutinib has a far superior selectivity profile to both Ibrutinib and CC-292, with increased selectivity over Tec family kinases and no covalent inhibition of EGFR, a key driver of adverse effects observed upon treatment with Ibrutinib. This inhibitor is currently Phase III clinical trials for CLL in direct comparison with Ibrutinib.[355]

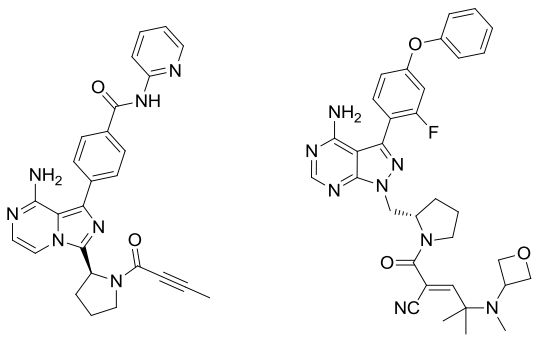

Figure 130. Second generation BTK inhibitor Acalabrutinib (left), and a lead reversible-covalent BTK inhibitor (right)

An alternative strategy to irreversible inhibition is reversible-covalent inhibition,[356] where a tuned electrophilic moiety is employed to retain the extended duration

accessible with a covalent inhibitor, whilst avoiding the associated toxicity risks (see Section 1.1). The covalent bond formed with the pendant cysteine group is reversible, as the presence of the nitrile increases the acidity of the cyanoacrylamide adduct, allowing slow retro-Michael elimination.

This reversible-covalent strategy has been applied to BTK,[357] with the potential for an improved safety profile over Ibrutinib as there is no permanent adduct formation with non-specific covalent off-target proteins and idiosyncratic toxicity issues are also avoided.[358] An exemplar reversible-covalent BTK inhibitor (Figure 130, right), has sustained BTK engagement *in vivo* ($t_{1/2}$ = 18 h) and is orally bioavailable.[357] Addition of steric hindrance and polarity *β*- to the cyanoacrylamide also result in increased kinome-wide selectivity, with reduced binding to kinases with aligned cysteine residues (including key off-target kinases EGFR and ITK). A further reversible covalent BTK inhibitor (PRN1008) is currently in Phase II clinical studies for treatment of autoimmune diseases.[359]

5.1.2.3 Reversible Inhibition

As identified in Section 5.1.2.1, issues with the current covalent approach to selective inhibition of BTK are the development of Ibrutinib resistance in treated patients caused by mutations of critical residues, and adverse events driven by covalent inhibition of off-target proteins. Although some recent developments in covalent space have aimed to address these issues, selective and reversible inhibition of BTK has also been targeted. The major advances in the field will be reviewed here, though a myriad of reversible BTK inhibitors have been disclosed by multiple sources in the patent literature.[359,360]

Development of a fully reversible BTK inhibitor required a *de novo* structural approach to access a pocket on the SH3 domain not targeted by previous covalent inhibitors.[361] This resulted in the identification of a novel inhibitor CGI-1746 (Figure 131, left), which is highly potent and outstandingly selective for BTK (Figure 131, right), with ~10^3 fold selectivity over the next most potently inhibited kinase BMX.

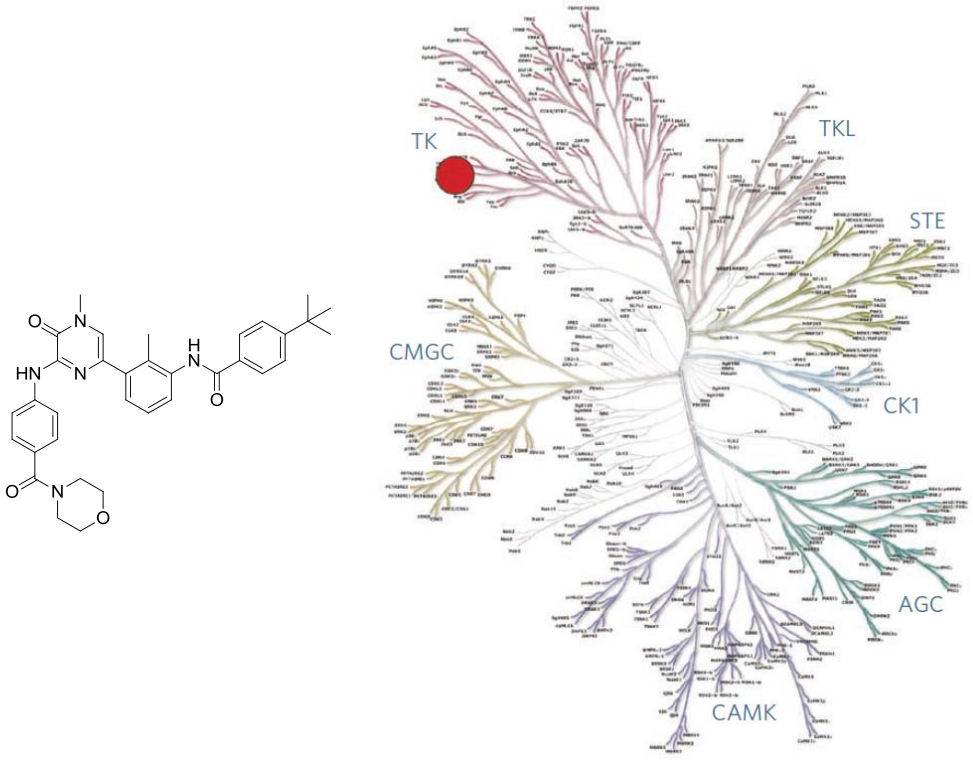

Figure 131.[361] Left: Structure of CGI-1746. Right: kinome tree indicating the high selectivity of CGI-1746 (BTK is the only kinase significantly inhibited at 1 μM concentration)

CGI-1746 proved to be efficacious in multiple models of inflammatory arthritis, inducing profound inhibition of pro-inflammatory cytokines (TNFα, IL-1β, IL-6),[361] however the compound was not considered to be a viable clinical candidate due to poor ADME properties.[362]

In an attempt to improve on the profile of CGI-1746 while retaining the high selectivity for BTK, the scaffold was further developed seeking to address high clearance attributed to the pendant *tert*-butyl group.[362] This led to the discovery of GDC-0834 (Figure 132, left), which was found to retain the high potency and selectivity of CGI-1746. Upon further investigation, a significant species difference in the rate of hydrolysis of the newly introduced thiophene amide was observed,[363] with substantially higher clearance by this pathway in humans than in other preclinical species. This resulted in the termination of GDC-0834, though further medicinal

chemistry efforts led to RN486 (Figure 132, right),[364] further description of which will be detailed in Section 5.3.

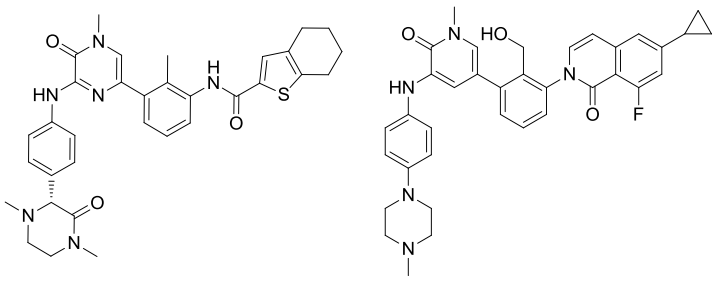

Figure 132. Reversible BTK inhibitors GDC-0834 (left) and RN486 (right)

A carbazole-based BTK inhibitor, BMS-935177, has been reported as a potent reversible inhibitor of BTK (Figure 134, left),[365] however this compound suffers from poorer kinase selectivity than other reversible inhibitors based on this scaffold, and also demonstrates poor aqueous solubility (<1 μg/mL) and high plasma protein binding (99.4 % in human serum). When profiled further in tolerability studies, the compound was found to have a poor therapeutic margin in multiple species, hence was not developed further.[366]

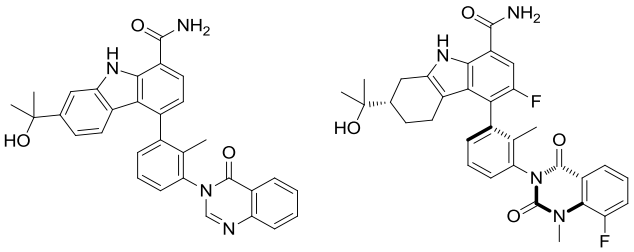

Figure 133. Structure of reversible BTK inhibitors; BMS-935177 (left) and BMS-986142 (right)

A further tetrahydrocarbazole inhibitor, BMS-986142, was developed to resolve these tolerability issues observed using BMS-935177.[366] BMS-986142 was developed as a fixed single atropisomer, which resulted in improved BTK potency and a more favourable selectivity profile, though common off-target kinases TEC and ITK are inhibited within a 25 fold selectivity window. This molecule has since progressed into Phase II clinical studies for treatment of RA.

A reversible BTK inhibitor with a similar core to the Ibrutinib scaffold has been reported (Figure 134, left) with increased binding affinity driven by hydrophobic interactions with the trifluoropyridine group in the back pocket of the ATP binding site.[367] The compound proved to be effective in a pre-clinical rat model of collagen-induced arthritis, though when compared to inhibitors based on the CGI-1746 core structure described in this section, the selectivity profile of this compound is relatively modest, with a narrow selectivity window over other Tec kinases.

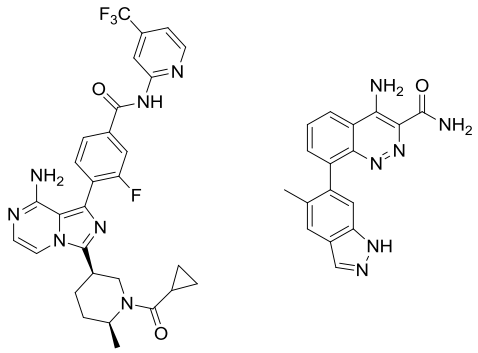

Figure 134. Further reversible BTK inhibitors

In order to avoid the often high molecular weight of both covalent and reversible inhibitors described above, a fragment based approach has been undertaken in order to maximise ligand efficiency (Figure 134, right).[368] This resulted in a potent lower molecular weight inhibitor, however the selectivity profile proved to be poor, with multiple kinases inhibited within a 10-fold concentration window.

5.1.3 Project Aims

As outlined above, BTK is a well-validated therapeutic target for multiple indications for which numerous inhibitors have been reported. Having previously identified BTK as a novel degradable target (Section 4.6), we sought to demonstrate the potential of the promiscuous approach as a target identification strategy. As it is known which ligase and linker length are able to degrade the target, a highly selective Protac could be developed from an entirely unselective species through minimal iterations. It may then be explored whether degradation of BTK could give a significant advantage over inhibition alone.

One application of a BTK Protac would be the opportunity to offer significantly decreased dose to achieve an effect equivalent to covalent inhibition. Whilst efficacy would also be driven by protein resynthesis, the catalytic nature of degradation would circumvent the considerable dose required to fully saturate target occupancy by covalent inhibition. Equally for current reversible BTK inhibitors, doses of ≥30 mg/kg have been shown to be required for efficacy in murine preclinical models.[366,369] This may result in tolerability issues and high, impractical dosing in humans, which a Protac would also be able to circumvent due to increased therapeutic index (TI). By use of a reversible inhibitor not dependent on binding to C481, this gives access to an increasing relapsed patient population of C481S mutant who do not respond to Ibrutinib treatment due to disrupted covalent binding.[351]

For a Protac, the overall selectivity profile of the parent inhibitor is likely to be more important than its absolute potency, as efficacy is less dependent on occupancy than a traditional inhibitor. As the vast majority of adverse events currently observed in the clinic are caused by inhibition of off-target kinases, such as EGFR for Ibrutinib,[354] again a Protac may be advantageous here. Highly selective reversible BTK ligands such as CGI-1746 or RN486, should translate into highly selective Protacs and effectively replicate exclusive BTK knockout.

From the proposed mechanism of Protac-mediated protein degradation, it would be expected that covalent inhibition of a target protein would be unfavourable, as irreversible binding to the target would prevent catalytic turnover. However, as covalent inhibitors for BTK are well described, this presented an opportunity to test this experimentally and determine whether covalent inhibition of the target protein allows Protac-mediated target degradation.

For less tractable targets, one strategy for ligand discovery is through the use of covalent inhibition, as this can allow traction to be gained on proteins which are challenging to target through binding affinity alone.[370] A notable example where this strategy has proved to be partially successful is the generation of covalent inhibitors for the undruggable oncogenic protein KRas (G12C mutant), which lacks a distinct binding pocket.[371,372] By assessment of cysteine ligandability, combined with

fragment-based ligand discovery, strategies for expansion of druggable space through covalent trapping have also been described.[370] Although these proteins may be ligandable, cysteine trapping may not induce a pharmacodynamic response; therefore, a Protac approach may be able to drive efficacy despite the lack of catalytic activity. By modification of Ibrutinib, it may be able to answer whether irreversible inhibition is tolerated in a Protac and allows protein degradation.

A further opportunity available with a selective BTK Protac is to probe poorly described biological functions of the protein. The reported role of BTK in activation of the NOD-like receptor protein 3 (NLRP3, also known as NALP3) inflammasome activation proved to be an interesting opportunity in this case.[373] The NLRP3 inflammasome is a ligandable, but as yet undruggable, intracellular complex responsible for generation of the potent pyrogen and pro-inflammatory mediator IL-1β (Figure 135).

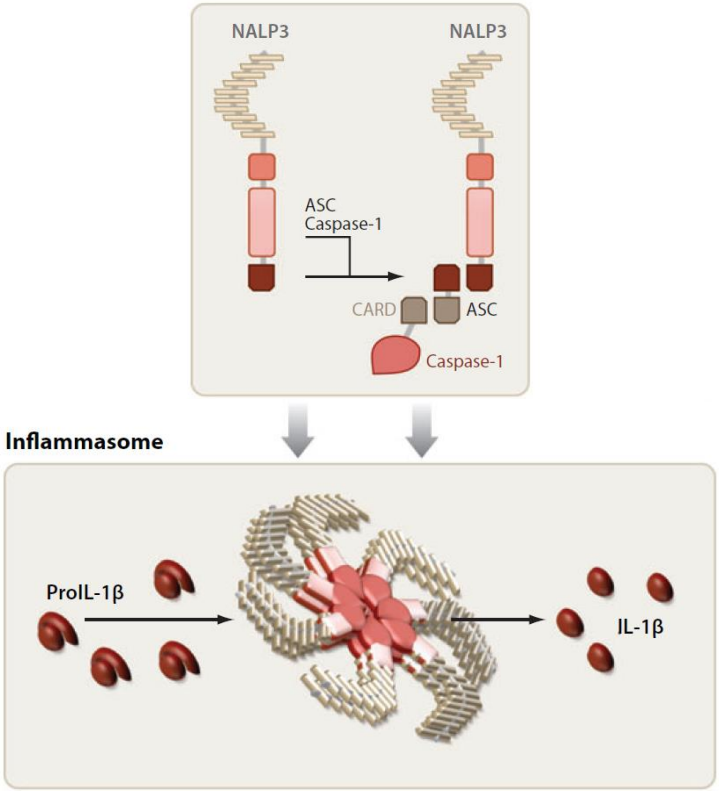

Figure 135.[374] NLRP3 (NALP3) inflammasome activation and formation, resulting in processing of pro-IL-β to IL-β

Once activated by a pathogen or intracellular damage, the NLRP3 protein forms a complex with the adaptor protein apoptosis-related speck-like protein containing a caspase recruitment domain (ASC), which, in turn, directly associates with procaspase-1.[375] Oligomerisation of these subunits leads to formation of a donut-shaped complex with an active caspase-1 core. This active complex cleaves pro-IL-1β to active IL-1β, and can also cause cell death by pyroptosis.[376] Due to the potential for blockade of this pro-inflammatory response, inhibition of NLRP3 has been implicated in several chronic inflammatory diseases, including Muckle–Wells syndrome, Alzheimer's disease, diabetes, and Parkinson's disease.[377,378]

It has been reported that both the xid mutation and BTK knockdown inhibit secretion of IL-1β following stimulation of NLRP3 assembly, which can be replicated through BTK inhibition.[373] BTK is thought to act as a scaffolding protein for NLRP3 and ASC, potentially through the kinase domain, with BTK-mediated phosphorylation of ASC resulting in activation of caspase-1. If this effect could be recapitulated using a BTK Protac, selective BTK degradation may be an attractive strategy to allow indirect inhibition of IL-1β, giving access to a variety of novel and valuable therapeutic indications through a known safe inhibition/knockout pathway.

One advantage of a Protac is that degradation of a protein can remove secondary functions independent of inhibition of its functional binding site. In the case of BTK, the high similarity of the XLA, inhibited, and kinase dead phenotypes suggests that degradation is unlikely to give additional novel pharmacology over inhibition. However, BTK does have some secondary functions independent of its kinase activity.

BTK can recruit phosphatidylinositol-4-phosphate 5-kinase (PIP5K) independently of its kinase activity; recruitment of PIP5K drives PIP_2 synthesis, stimulating PIP_3 production required for membrane recruitment of BTK.[379] As small molecule-mediated inhibition of BTK already prevents its catalytic function, a reduction in PIP_3 and reduced membrane recruitment is unlikely to add further pharmacology, apart from a potential reduction in PIP_2 synthesis, which may modulate another distinct pathway.

Though it was believed that selective reversible inhibition of BTK would give the most definitive understanding as to whether degradation demonstrates any supplementary benefit over inhibition, we sought first to explore the effect of covalent inhibition of BTK on Protac-induced degradation.

5.2 Covalent BTK Protacs

To probe the effect of covalency on Protac-induced degradation, the BTK inhibitor Ibrutinib was selected for elaboration into a covalent Protac. The design, synthesis, and profiling of Protacs based on this inhibitor will be outlined within this section.

5.2.1 Protac Design

First, an appropriate exit vector from the BTK binding site was required for conjugation of Ibrutinib to the E3 ligase. As there is no published crystal structure of Ibrutinib, a the crystal structure of a close reversible analogue is presented in Figure 136.[380] From this, it appears that the cyclopentyl analogue binds in a similar manner to Ibrutinib, due to the close proximity of the key C481 residue, and that the cyclopentyl group is the most solvent exposed vector, indicating a potential position for conjugation to the E3 ligase.

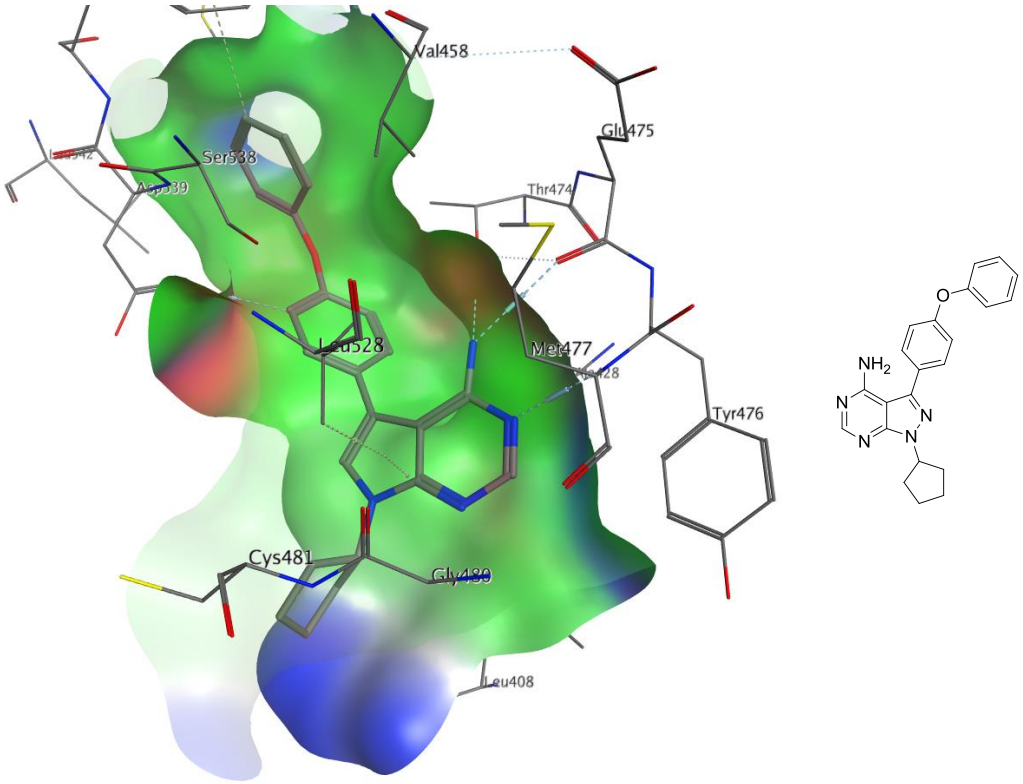

Figure 136.[380] Docked structure of reversible Ibrutinib analogue in the BTK kinase domain, indicating the proximity of C481 (surface coloured by pocket region; blue = solvent exposed, green = hydrophobic)

It was also known that the BODIPY fluorophore-tagged Ibrutinib probe PCI-33380 (Figure 137) potently and covalently inhibits BTK.[339] This molecule can be used to assess the degree of covalent occupancy of BTK in cells, as decreasing target occupancy results in increased labelling with the fluorescent tag. By knowledge of both the crystal structure and the fluorophore probe molecule, it was believed that linkage to the E3 ligase through a piperazine linker would be tolerated in the desired Ibrutinib-based Protacs.

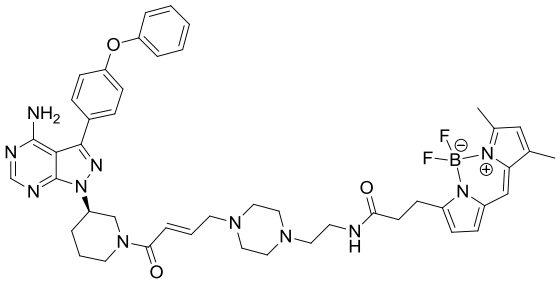

Figure 137. Structure of PCI-33380, a fluorescent probe employed to assess the degree of BTK target occupancy, suggesting solvent exposure accessible through a piperazine linker

As discussed in Section 4.6, the promiscuous IAP Protac used to degrade BTK was highly lipophilic, potentially limiting target exposure due to poor solubility. In order to compensate for this, it was thought that truncation of the IAP binder could improve the physiochemical properties of the following BTK Protacs. The IAP ligand indicated in Figure 138 was considered as a potential replacement,[381] as exchange of the tetrahydroisoquinoline used in the promiscuous kinase Protac for the aminoproline moiety results in removal of an aromatic ring and gain of an H-bond donor in the newly created amide.

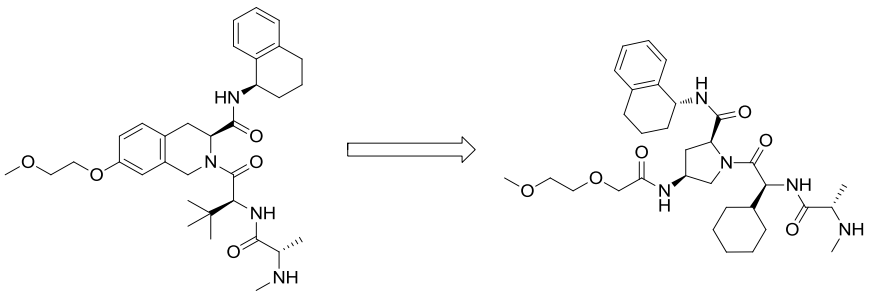

Figure 138. Truncation of IAP ligand in order to reduce lipophilicity

As previously, a 4EG linker was selected to link the target protein and ligase binders as this had proved to be sufficient to allow BTK degradation in the previous promiscuous kinase experiment. Combination of the proposed structural features gave the target Ibrutinib-based Protacs, this synthesis of which will be described in the subsequent section.

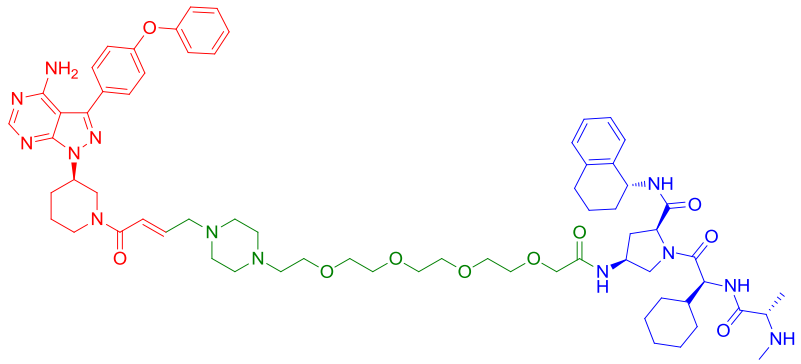

Figure 139. Structure of a proposed BTK Protac based on the inhibitor Ibrutinib

5.2.2 Covalent BTK Protac Synthesis

First, the BTK binding portion of the molecule was synthesised (Scheme 26). 4-Aminopyrazolo[3,4-*d*]pyrimidine was iodinated with NIS to give aryl iodide **61** in 60 % yield. Initially, a Suzuki reaction was carried out with (4-phenoxyphenyl)boronic acid to give pyrazolopyrimidine **62** in 64 % yield, then subsequent Mitsunobu reaction with (*S*)-*tert*-butyl 3-hydroxypiperidine-1-carboxylate and Boc deprotection gave piperidine **64** in 27 % yield. It was thought that the relatively poor yield observed for the Mitsunobu reaction was due to the poor solubility of intermediate **62**, so the steps were repeated in the opposite order. Mitsunobu reaction gave Boc piperidine **63** in 59 % yield and 90 % purity, then Suzuki reaction and deprotection afforded piperidine **64** in 92 % yield.

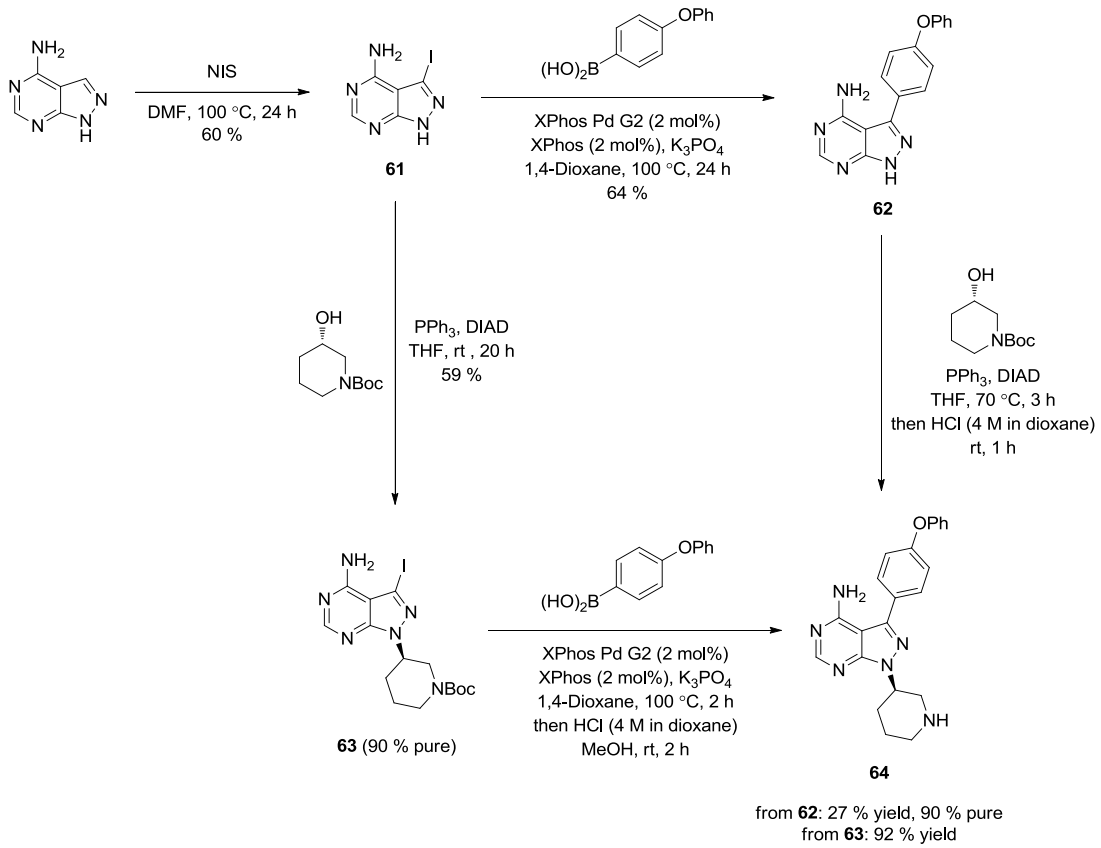

Scheme 26. Preparation of piperidine **64**

The synthesis of Ibrutinib was carried out to confirm that covalent inhibition does not affect BTK protein levels, a matter which has been disputed previously.[339,365] Therefore, an amide coupling was carried out using acryloyl chloride to give parent inhibitor Ibrutinib **65** in 38 % yield (Scheme 27).

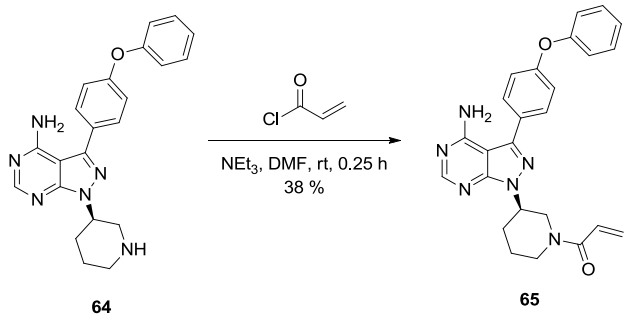

Scheme 27. Synthesis of Ibrutinib (**65**)

The IAP binder and linking fragment were then synthesised (Scheme 28). First, an amide coupling between a 4EG acid linker and a protected IAP binder both available within our laboratories,[125] was carried out to give IAP-4EG chloride **66** in 78 % yield. Then, a displacement with piperazine was carried out, followed by a second alkylation with 4-bromocrotonic acid to give acid **67** in 58 % yield over two steps.

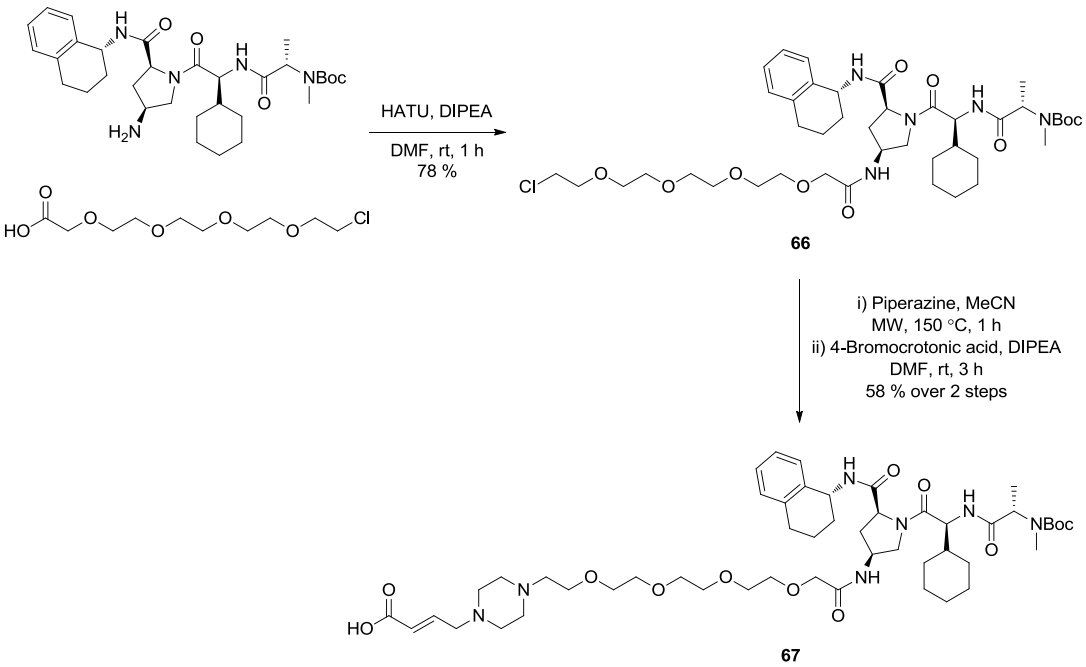

Scheme 28. Preparation of acid **67**

With piperidine **64** and IAP linking fragment **67** in hand, an amide coupling was carried out to give fully protected Protac **68** in 51 % yield and 80 % purity (Scheme 29). Acidic deprotection was then carried out to give acrylamide-containing BTK Protac **69** in 75 % yield.

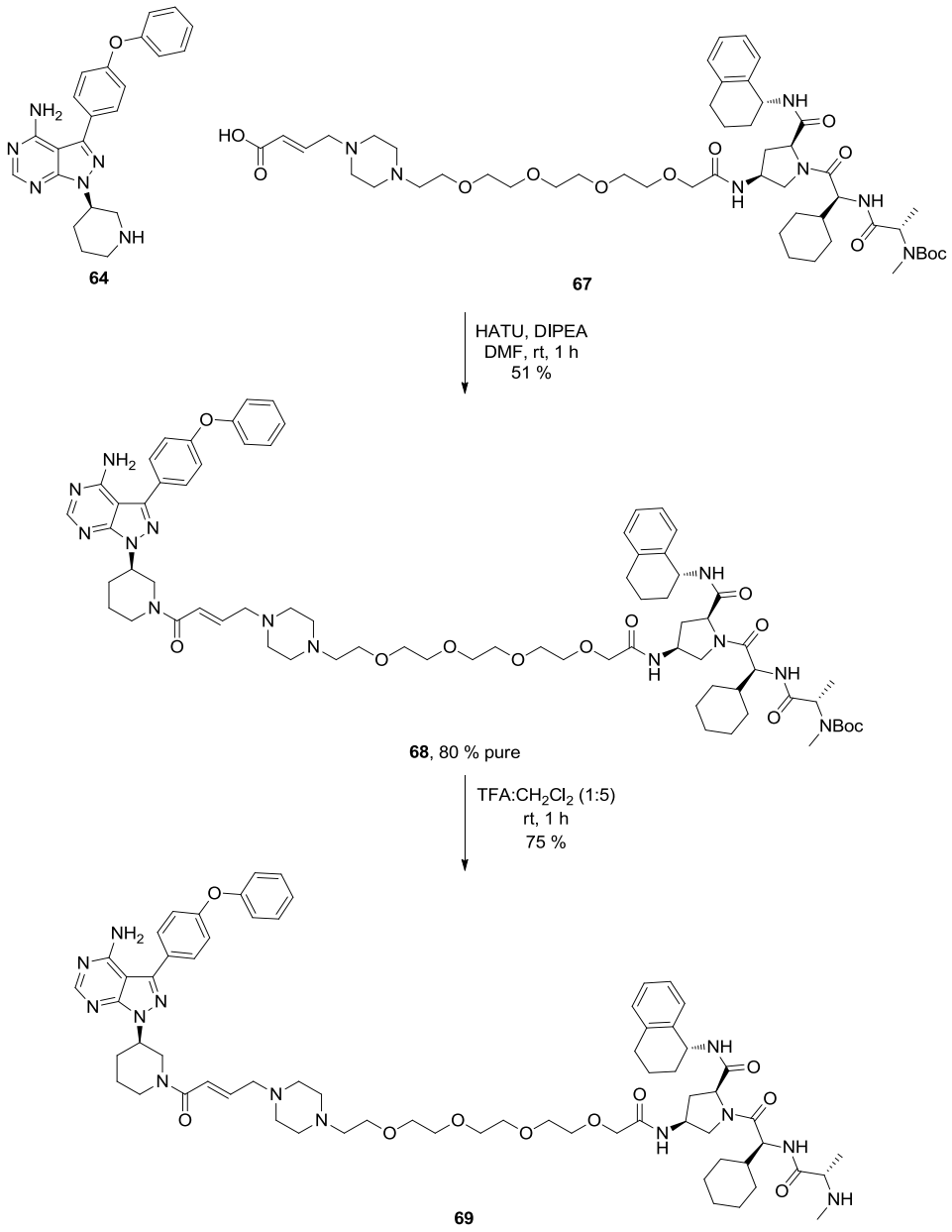

Scheme 29. Preparation of acrylamide-containing Ibrutinib Protac **69**

To confirm the effect of covalency on Protac induced degradation, removal of the cysteine-reactive acrylamide moiety was required. Hydrogenation of acrylamide **68** and subsequent Boc deprotection gave reduced BTK Protac **70** in 41 % yield over two steps (Scheme 30).

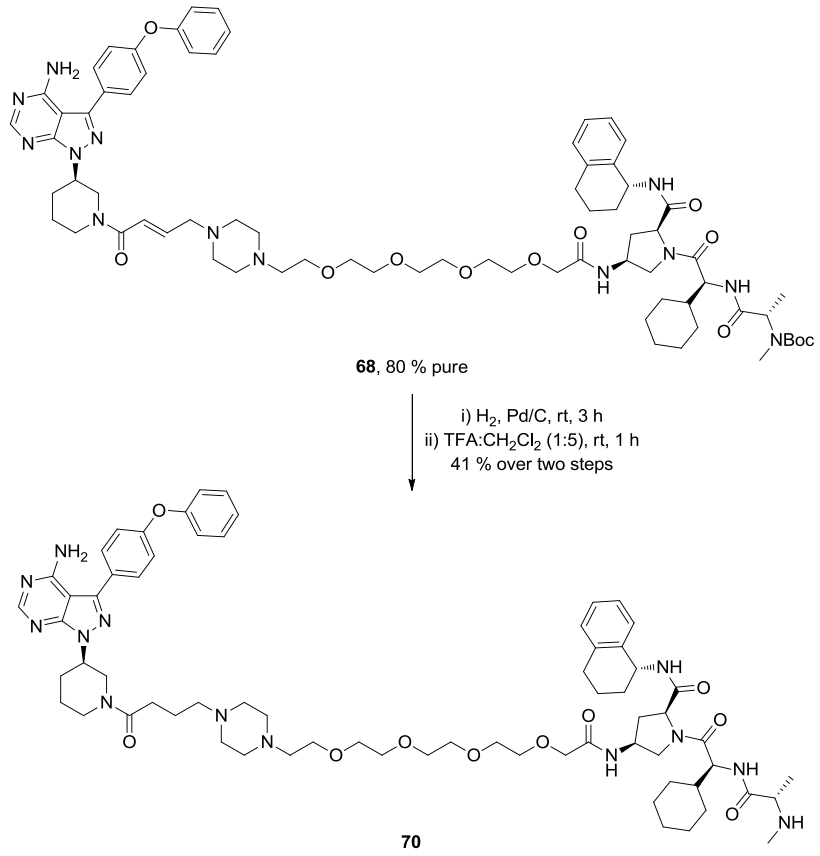

Scheme 30. Preparation of reduced acrylamide Protac **70**

5.2.3 Ibrutinib-IAP Protac Profiling

First, it was sought to confirm whether acrylamide-containing Protac **69** retained the fully covalent binding mode of the parent inhibitor **65**. Recombinant BTK was treated with binders **65**, **69** and **70** (10:1 inhibitor:protein) at room temperature then analysed by LCMS. Covalent modification is indicated by an increase in molecular weight, consistent with the molecular weight of the inhibitor, relative to a DMSO control sample. As expected, Ibrutinib (**65**) completely labelled recombinant BTK after 2 h incubation (Figure 140). Gratifyingly, acrylamide-containing Protac **69** also labelled BTK following 4 h incubation indicating that the Protac is covalently engaging BTK. A longer incubation time was required to demonstrate covalent binding than for Ibrutinib, implying that the substituted acrylamide in the Protac has reduced reactivity compared to the unsubstituted equivalent. Reduced acrylamide Protac **70**, caused no significant change to the observed mass following 4 h incubation, indicating that it is

a reversible binder. This also suggests that the acrylamide is critical for covalent binding and BTK C481 is likely to be the reactive residue, as it is for Ibrutinib.

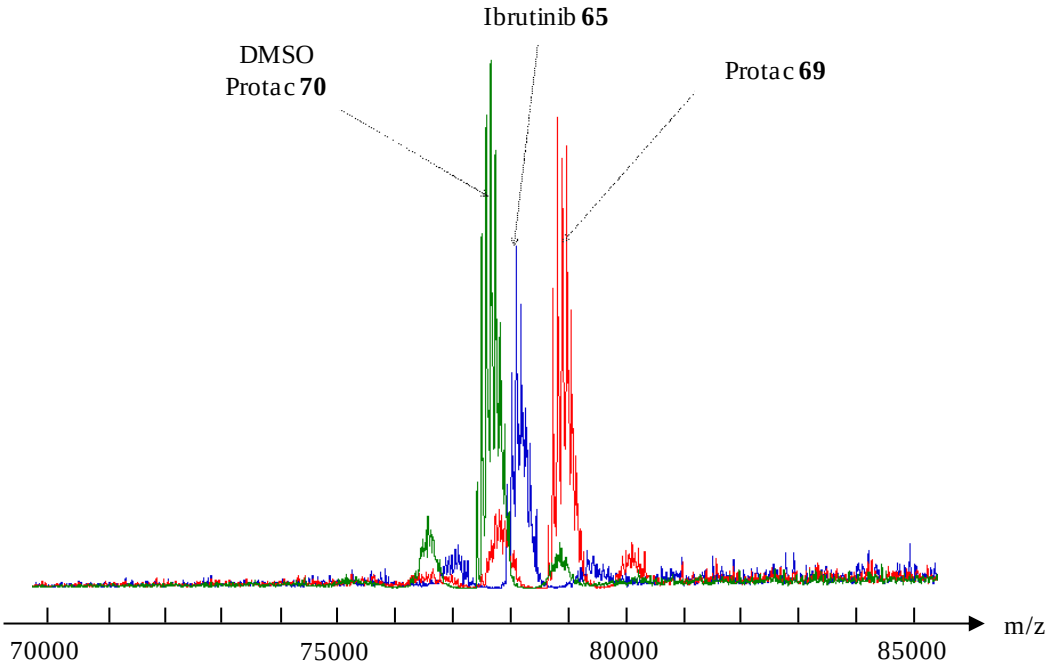

Figure 140. Incubation with Ibrutinib (**65**) and Protac **69** results in covalent modification of recombinant BTK, as observed by MS, whilst Protac **70** causes no covalent modification.

Biochemical binding data for Protacs **69** and **70** and parent binder of Ibrutinib (**65**) were then collected by Reaction Biology Corporation (Table 8). These were measured using a HotSpot™ radiometric filtration binding assay, where a radiolabelled γ-phosphate of ATP is transferred onto a peptide substrate, mediated by the kinase.[382] The phosphorylated substrate can then be separated by binding of the substrate to a filter and subsequent removal of unreacted ATP. Inhibition of the kinase inhibits substrate phosphorylation, resulting in a reduced radiometric signal.

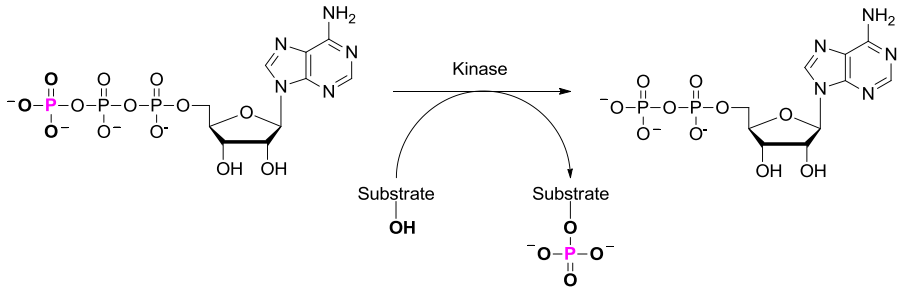

Figure 141. BTK binding assay

Assays profiling both BTK and mutant BTK(C481S) were available, and to attempt to distinguish between covalent and non-covalent binding for BTK, compounds were preincubated for 1 h before substrate addition. In the case of Ibrutinib (**65**) there is a significant difference (BTK/BTK(C481S) pIC_{50} = 9.4/8.1). The increased potency in the non-mutant protein supporting that covalent binding is occurring through C481S, as covalent binding occurring during the preincubation period allows increased inhibition of kinase activity. For BTK(C481S), only inhibition through reversible binding will be observed, therefore inhibition of kinase activity is reduced.

In the case of Protac **69**, no significant difference was observed between non-mutant and mutant BTK (BTK/BTK(C481S) pIC_{50} = 8.7/8.5), with a similar profile observed in the non-covalent equivalent Protac **70** (BTK/BTK(C481S) pIC_{50} = 8.6/8.8). The pre-incubation time appears to be insufficient to delineate between covalent and non-covalent binding, implying that covalent adduct formation is significantly slower upon substitution of the acrylamide. A longer preincubation before substrate addition would allow more time for covalent adduct formation to occur, and induce a more significant increase in observed potency.

Table 8. Ibrutinib-based BTK Protac properties

Compound no.	BTK pIC_{50}[1]	BTK C481S pIC_{50}[1]	Chrom LogD	Solubility (μM)[2]	PΔC[3]
65	9.4	8.1	5.0	48	-
69	8.7	8.5	5.4	168	1.9
70	8.6	8.8	5.1	188	1.8

[1]1 h preincubation before substrate addition, measured in the presence of 10 μM ATP [2]Solubility measured by CLND [3]Cellular accumulation in HeLa cells

In terms of physicochemical properties, Protacs **69** and **70** were found to have similar lipophilicity to the parent binder **65** and also improved solubility, presumably due to the addition of multiple H-bond acceptors. Positive cellular accumulation values were also demonstrated (PΔC = 1.8-1.9), indicating that the Protacs are likely to be cell penetrant. The compounds were then advanced into cellular experiments.

5.2.4 Covalent Inhibition Prevents IAP-Mediated Degradation of BTK

The synthesised BTK compounds were then profiled by western blotting to determine the effect on BTK protein levels in THP-1 cells, which were previously used in promiscuous binder experiments (Section 4).[301] First, it was confirmed that covalent inhibition with the parent binder Ibrutinib (**65**) had no effect on BTK protein levels (Figure 142). Though this result was consistent with reported data,[339] Ibrutinib and other covalent inhibitors have tentatively been described as a BTK degraders previously.[383]

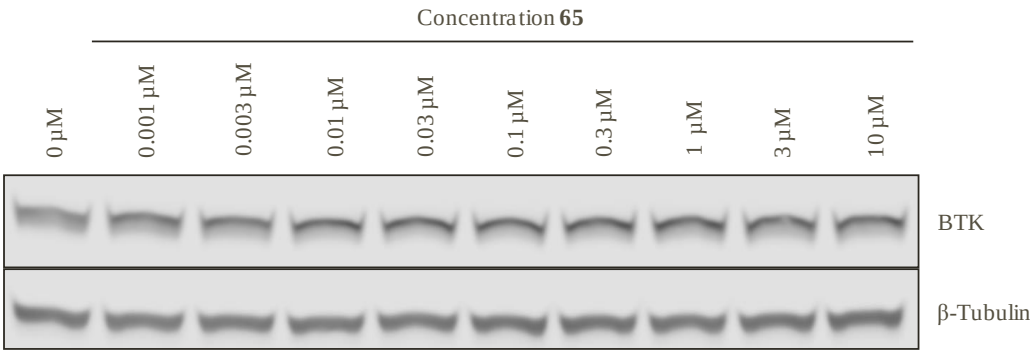

Figure 142. No BTK degradation is observed upon treatment with Ibrutinib (**65**) for 24 h in THP-1 cells

The effect of covalent Protac **69** on BTK protein levels was then tested (Figure 143, top), which surprisingly resulted in no degradation of BTK. Given the unusual effect observed with acrylamide Protac **69**, the reduced BTK Protac **70** was then profiled (Figure 143, bottom). In this case, BTK degradation was observed, with a $DC_{50} \approx 150$ nM and a $D_{max} > 95$ %. This suggested that covalent inhibition using a BTK Protac was somehow preventing its degradation. It was then sought to confirm whether BTK is being engaged in cells, as no target engagement would also result in no degradation.

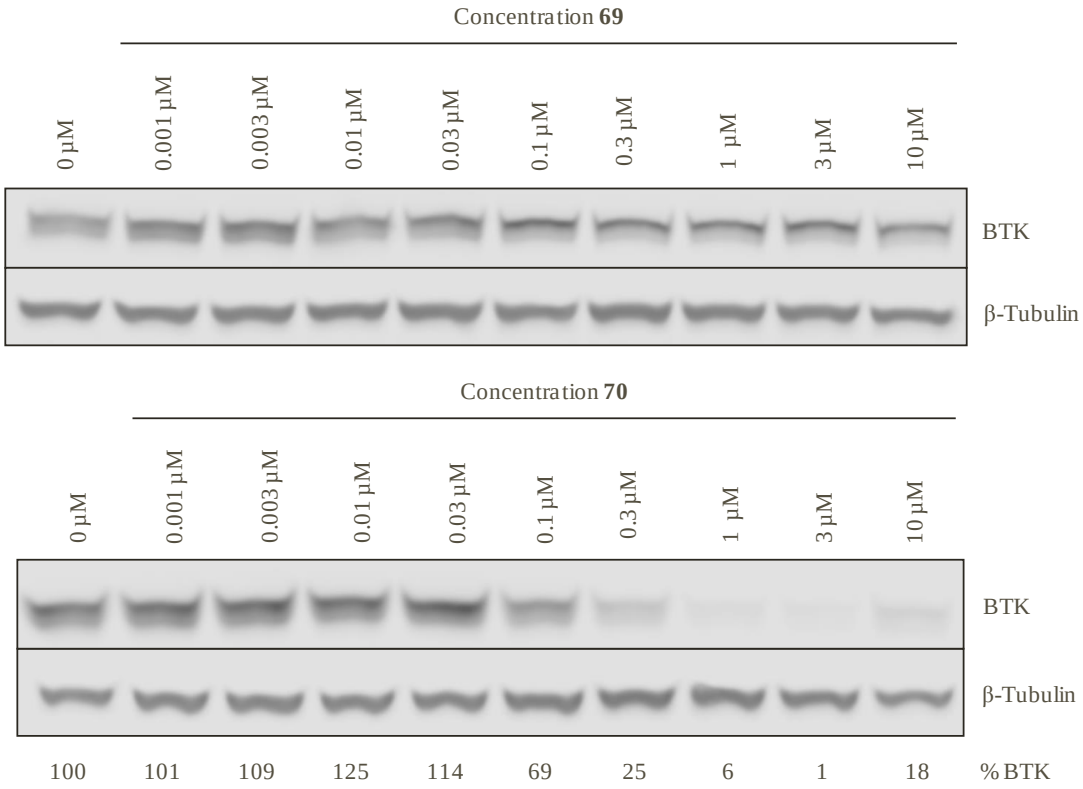

Figure 143. No BTK degradation is observed upon treatment with increasing concentrations of acrylamide-containing Protac **69** for 24 h in THP-1 cells (above); reduced acrylamide Protac **70** is an active degrader (below)

One approach for quantifying occupancy of the BTK binding site is by monitoring inhibition of autophosphorylation of BTK Y223. As stated previously, BCR pathway activation causes a phosphorylation cascade *via* LYN and SYK, resulting in phosphorylation of BTK Y551,[384] which is followed by an autophosphorylation event at Y223. Inhibition of the kinase domain of BTK is known to prevent this autophosphorylation event and directly correlates with binding site occupancy.[339,353]

To quantify the levels of phosphorylated Y223 (PY223) Ramos cells were employed, as these express an intact BCR pathway which can be strongly activated by stimulation with the BCR ligand anti-immunoglobin M (anti-IgM).[353] Ramos cells were treated with Ibrutinib (**65**) and BTK Protacs **69** and **70** for 16 h, then stimulated with anti-IgM. The samples were then probed for both BTK and PY223 BTK by western blot to compare total protein levels and degree of target engagement, including an unstimulated sample as a further control. As expected, treatment with Ibrutinib

resulted in potent inhibition of BTK PY223, and caused no BTK degradation (Figure 144).

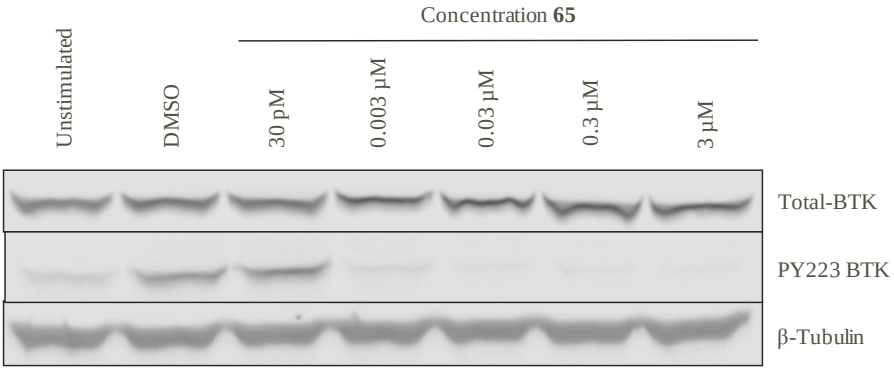

Figure 144. Ibrutinib (**65**) potently engages BTK with no effect on protein levels following 16 h treatment in Ramos cells

Interestingly, covalent Protac **69** was found to inhibit PY223, albeit at a higher concentration than that of Ibrutinib (Figure 145), but did not cause any effect on total protein levels. This suggests that the Protac is completely engaging BTK in cells, as PY223 is fully inhibited as higher concentrations (>300 nM), however the covalent inhibition through C481 is preventing protein degradation.

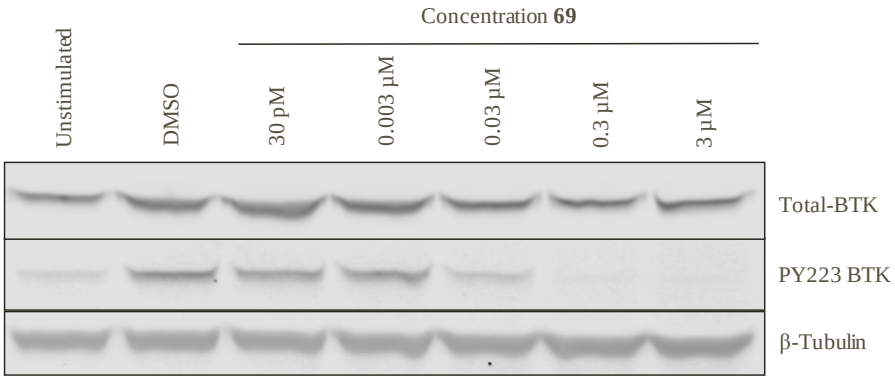

Figure 145. Irreversible Protac **69** engages BTK yet has no effect on protein levels following 16 h treatment in Ramos cells

Reversible Protac **70** was found to both engage and degrade BTK in Ramos cells (Figure 146), however the absolute degree of PY223 inhibition is likely to be confounded by the reduced protein levels caused by Protac-mediated BTK degradation. Protac **70** also appears to be a weaker inhibitor than Protac **69**, as a weaker

BTK PY223 signal is observed at 30 nM, presumably due to the additive effect of covalent binding.

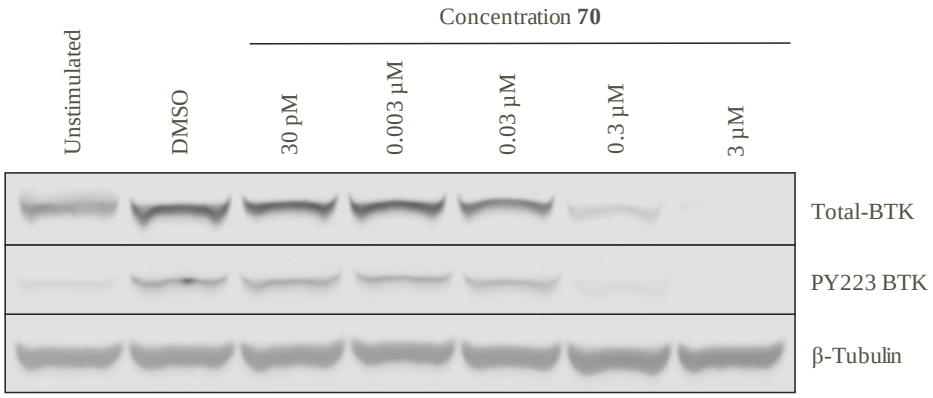

Figure 146. Reversible Protac **70** both engages and degrades BTK following 16 h treatment in Ramos cells

The fact that covalent Protac **69** is engaging BTK in cells but not causing protein degradation raised multiple questions as to why this effect occurs. An initial theory was that as Protac **69** is covalently inhibiting BTK, catalytic turnover of the Protac is inhibited, thus preventing any significant level of protein degradation. However, as complete inhibition of PY223 is observed at ~300 nM concentration (Figure 145), the binding site is completely occupied with Protac **69**. Therefore, as BTK is being quantitavely labelled with the IAP degron, stoichiometric BTK degradation would be expected at this concentration and above.

It was then considered that ubiquitin transfer between BTK and IAP may not be occurring in the presence of Protac **69** thus preventing degradation. However, given the high structural similarity between Protac **69** and **70**, BTK occupancy, exit vector and ternary complex formation will be almost identical with both Protacs. Given that ubiquitin transfer is likely to be occurring, as reversible Protac **70** is an active degrader, it is assumed that ubiquitination is also occurring with covalent Protac **69**.

It was then sought to confirm whether covalent Protac **69** was an active Protac, and lack of degradation was not caused by a compound stability issue in cells. Ibrutinib (**65**) is not a profoundly selective molecule and inhibits multiple kinases both reversibly and irreversibly.[339] Given that degradation of RIPK2 has previously been

demonstrated within our laboratories,[124] and that Ibrutinib reversibly engages RIPK2 (IC_{50} = 152 nM),[339] cell lysates generated from Protac-treated THP-1 cells in Figure 143 were reprobed for degradation of RIPK2 (Figure 147). Covalent Protac **69** was found to cause a minor reduction to RIPK2 levels, while reversible Protac **70** proved to be an active RIPK2 degrader (DC_{50} ~ 20 nM, D_{max} > 95 %).

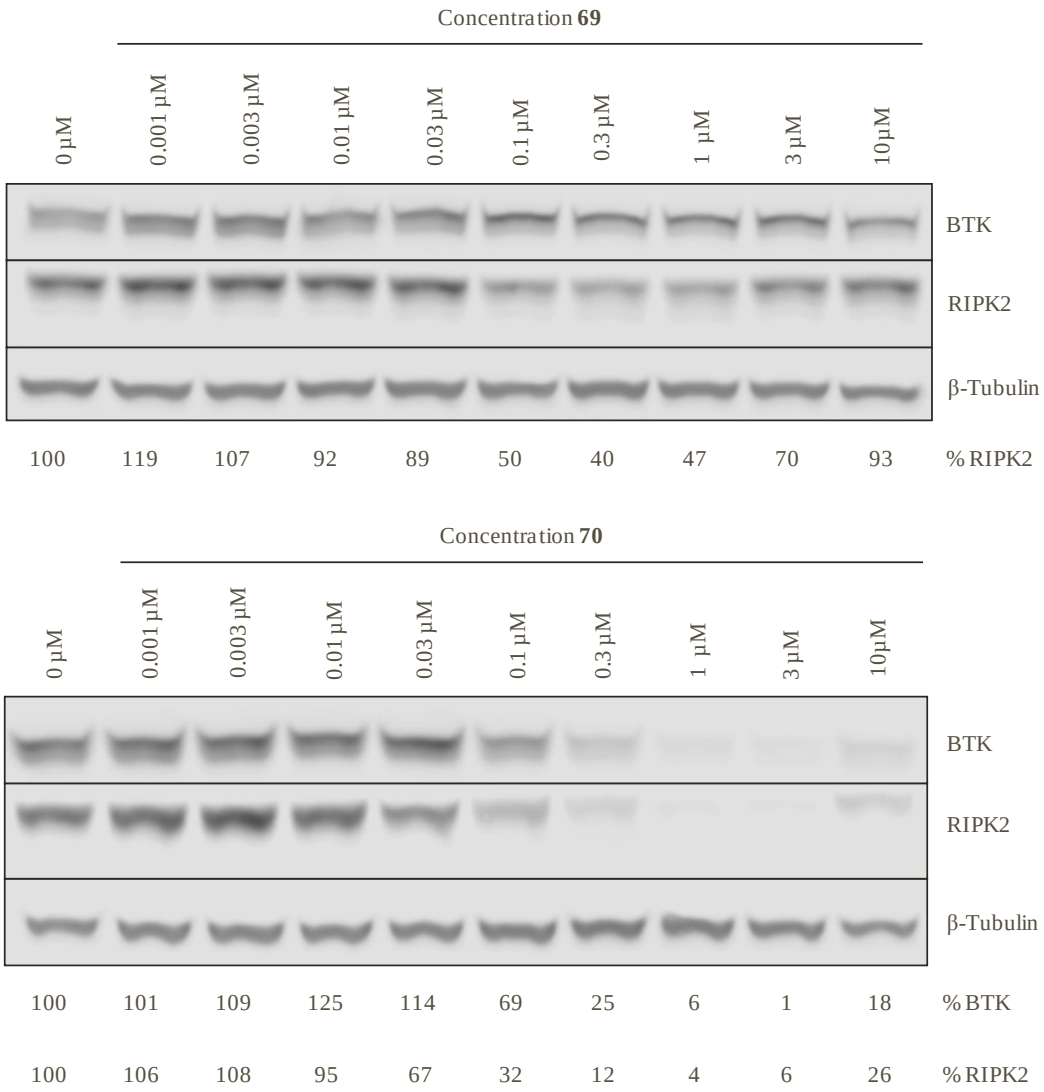

Figure 147. Comparing BTK and RIPK2 degradation following treatment with irreversible Protac **69** (top) and reversible Protac **70** (bottom) for 24 h in THP-1 cells

The reason for the modest degree of RIPK2 degradation with covalent Protac **69** was then considered. It is reported that treatment with Ibrutinib causes rapid covalent inhibition of BTK, with high active site occupancy (IC_{50} = 4 nM) following 1 h

treatment.[339] In the case of the covalent Protac **69**, this would also result in rapid sequestering of the Protac by BTK, resulting in a reduced amount of freely circulating Protac to engage and degrade reversible targets, such as RIPK2.

It was thought that pre-saturation of the BTK binding site with Ibrutinib (**65**), washout of Ibrutinib and subsequent Protac incubation would prevent this sequestering and result in more profound RIPK2 degradation by covalent Protac **69**. First, the concentration and time required for full pre-saturation of BTK was confirmed, based on previous reports on time and concentration required for complete inhibition.[339] Treatment with 100 nM Ibrutinib (**65**) for 2 h resulted in complete BTK PY223 inhibition, indicating full kinase binding site occupancy.

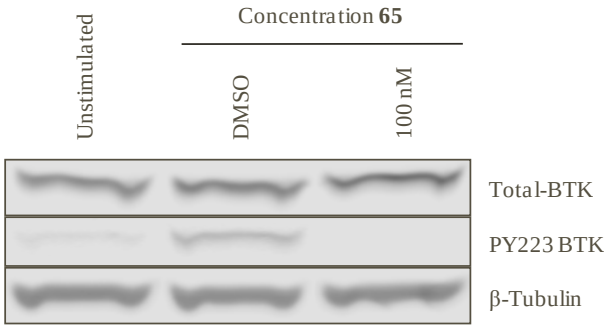

Figure 148. Complete inhibition of BTK PY223 following treatment with Ibrutinib (**65**) for 2 h in Ramos cells

The effect of pre-treatment with Ibrutinib (**65**) on degradation of RIPK2 with covalent Protac **69** was then profiled (Figure 149, left). Protac **69** was found to induce slightly more significant degradation than in the untreated case (Figure 147, top), though the observed D_{max} in each case is similar following quantification. The weaker degree of degradation with covalent Protac **69** may be due to incomplete washout of Ibrutinib, resulting in Protac competition with remaining Ibrutinib for binding to RIPK2, resulting in less complete degradation. Reversible Protac **70** was found to cause similar RIPK2 degradation in Ramos cells to that previously observed in THP-1 cells (Figure 149, right).

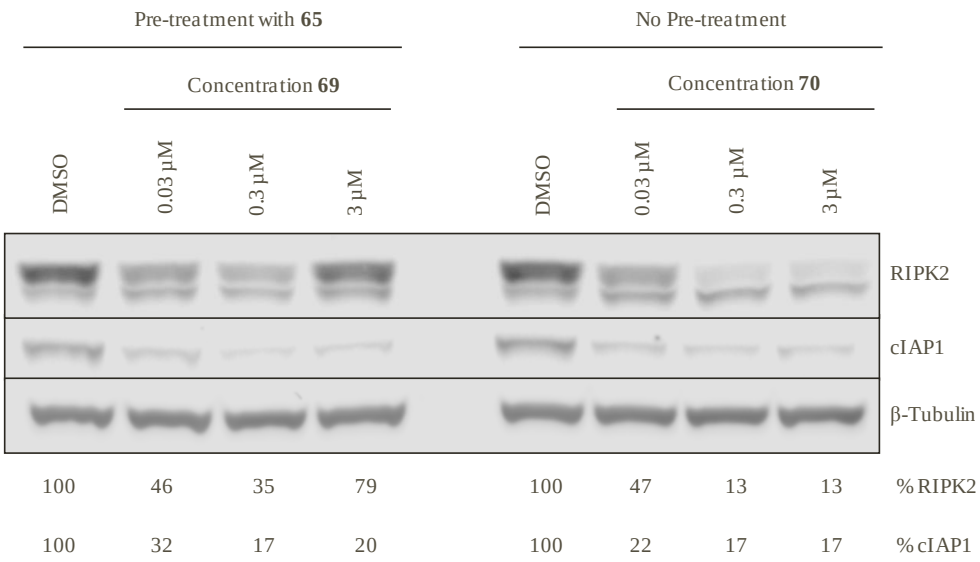

Figure 149. Left: Degradation of RIPK2 and cIAP1 in Ramos cells following 2 h pre-treatment with Ibrutinib (**65**, 100 nM) and subsequent washout, followed by treatment with covalent Protac **69** for 18 h. Right: Degradation of RIPK2 and cIAP1 in Ramos cells following treatment with reversible Protac **70** for 18 h

As inhibition of cIAP1 results in autoubiquitination and degradation, the effect of Protac treatment on cIAP1 level was quantified. As expected, Protac **70** was found to induce cIAP1 degradation. In the case of pre-treatment with Ibrutinib followed by incubation with Protac **69**, cIAP1 degradation was observed to a similar degree. This indicates that binding to cIAP1 is unchanged with either reversible or irreversible Protacs, and should be equally able to induce BTK degradation. Ideally, a sample with no Ibrutinib pre-treatment could be probed in this case, as cIAP1 degradation would confirm that binary complex formation is occurring between cIAP1 and the BTK-Protac covalent adduct.

It was then considered whether the observed effect of covalent inhibition was specific to combination of recruitment of IAP. As degradation of BTK had previously been demonstrated by recruitment of cereblon, exchange of the ligase binder incorporated into the Protac was then explored.

5.2.5 BTK-Cereblon Protacs

It was thought that the effect of covalent inhibition on induced degradation of BTK may be specific to recruitment of IAP; recruitment of an orthogonal ligase was considered to probe this. As it was known that BTK could be efficiently degraded by recruitment of cereblon (Section 4.6), an analogous Ibrutinib-cereblon Protac was prepared. Due to the chemical instability related to the cereblon binder, Protac assembly using click chemistry was targeted for ease of synthesis. First, an alkylation of 1-Boc-piperazine with 4-bromocrotonic acid was carried out to give acid **71** in 40 % yield (Scheme 31). An amide coupling was then carried out with piperidine **64** to give Boc-protected binder **72** in 79 % yield.

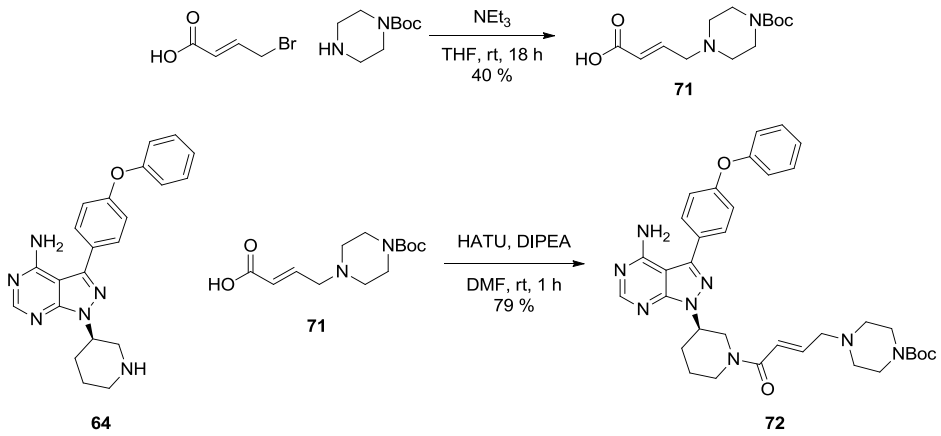

Scheme 31. Preparation of allylic piperazine **72**

To prepare an azide functionalised linker, tosylation of triethylene glycol was carried out to give ditosylate **73** in 95 % yield. Subsequent mono-displacement with sodium azide delivered linking fragment **74** in 63 % yield.

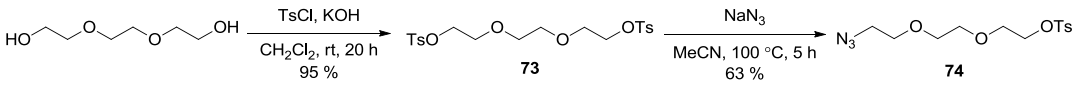

Scheme 32. Preparation of azide **74**

Deprotection of Boc piperazine **72** and subsequent alkylation with tosylate **74** gave acrylamide-azide **75** in 37 % yield over two steps (Scheme 33). A click reaction was

carried between **75** and a pomalidomide-based alkyne available within our laboratories[125] to give the desired acrylamide Protac **76** in 11 % yield.

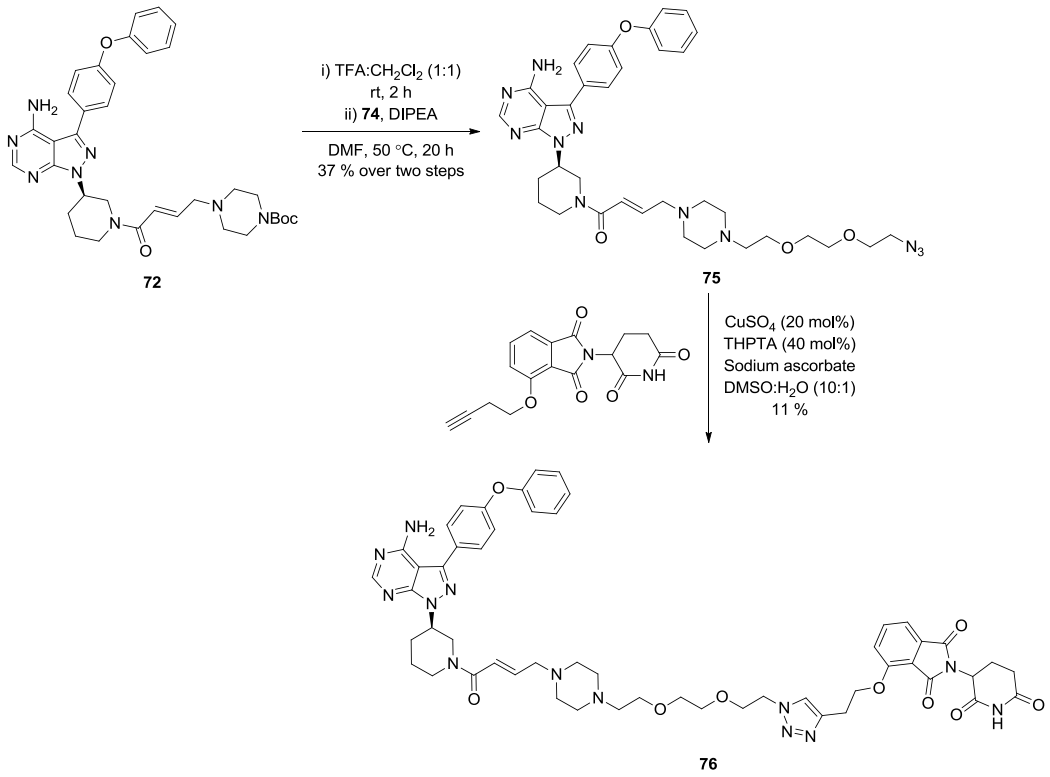

Scheme 33. Synthesis of acrylamide cereblon Protac **76**

For the corresponding reduced acrylamide Protac, acrylamide **72** was reduced under an atmosphere of hydrogen to give the required amide **77** in 77 % yield and 80 % purity (Scheme 34). Acid-mediated deprotection and piperazine alkylation gave azide **78** in 53 % yield over two steps, then click reaction with the previously described alkyne delivered Protac **79** in 74 % yield.

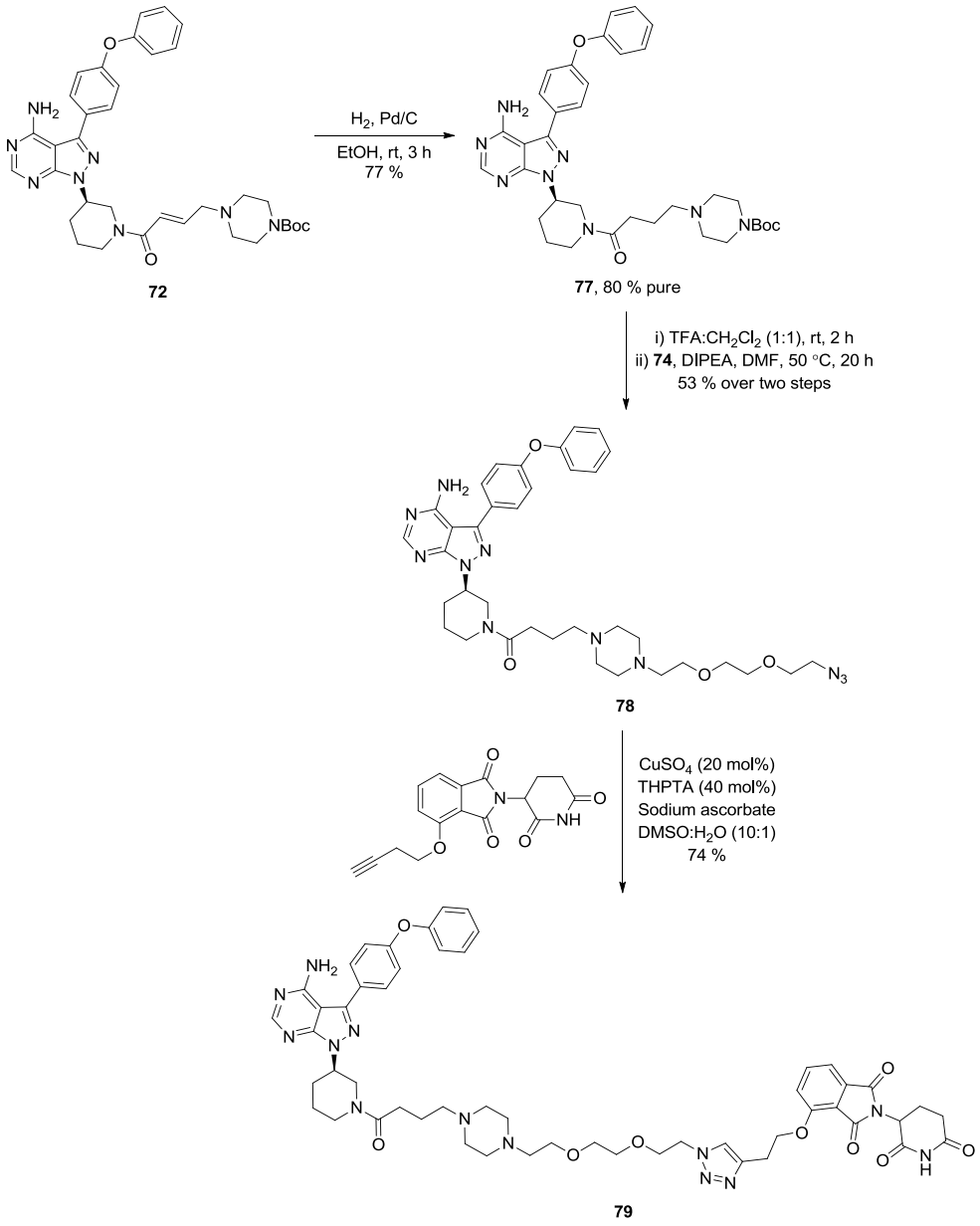

Scheme 34. Preparation of reduced BTK-cereblon Protac **79**

Protacs **76** and **79** were then directly profiled by western blotting (Figure 150).[301] As previously observed by Protac-mediated recruitment of IAP, acrylamide-containing cereblon Protac **76** demonstrated no degradation of BTK. Again, reduction of the acrylamide in Protac **79** restored BTK degradation, with a similar DC_{50} ~ 150 nM and D_{max} = 95 % as previously observed with Protac **70**.

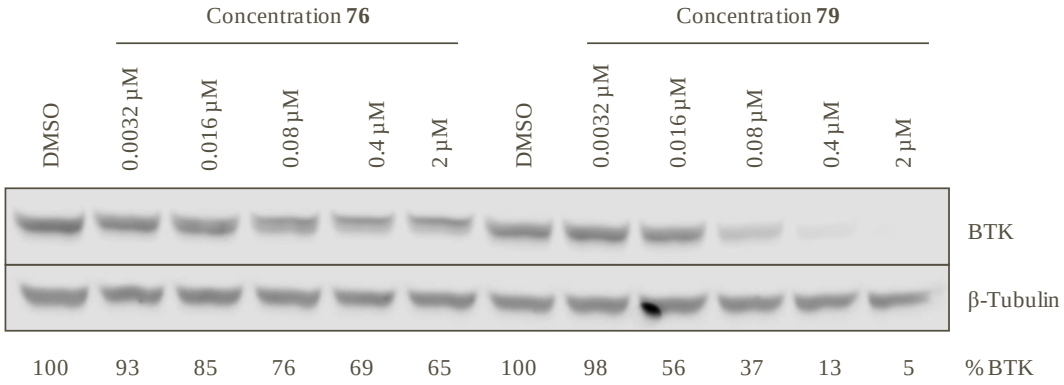

Figure 150. Western blotting using BTK-cereblon Protacs **76** and **79** following 18 h treatment in THP-1 cells

Given that no BTK degradation was observed upon recruitment of both IAP and cereblon, this suggests that the effect of covalent inhibition on BTK degradation is independent of recruited ligase. This suggests that the BTK-Protac covalent adduct itself is likely to be the reason behind the lack of observed degradation.

5.2.6 Reversible Covalent BTK Protac

As no BTK degradation was observed using covalent Protacs **69** and **76** while reversible Protacs **70** and **79** proved to be an active degraders, further exploration of the binding mode of this class of compounds was warranted. Particularly, reports of reversible covalent inhibition of BTK proved an attractive avenue to explore, as this would demonstrate whether tuning of the binding mode impacts degradation.[357] As a Protac based on this class of compounds would bind to BTK in the same manner as covalent Protac **69** through covalent cysteine attachment, then slowly dissociate, these compounds should be able to degrade BTK.

A report of a series of reversible covalent BTK inhibitors employed a close analogue of the binder used in the described Ibrutinib-based Protacs, and a particularly relevant example is displayed in Figure 151.[385] The availability of previously synthesised material related to this inhibitor from previous BTK Protac studies expedited exploration of this binding mode. Accordingly, the requisite synthesis was then performed.

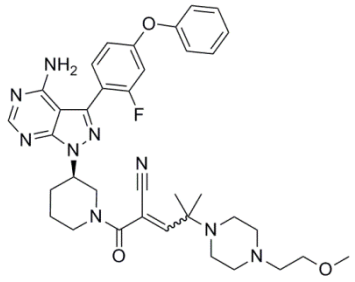

Figure 151. Example of a reversible covalent BTK inhibitor (BTK IC_{50} = 0.001 μM)

To replicate the cysteine-reactive cyanoacrylamide vector in the reversible covalent inhibitor shown in Figure 151, isobutyraldehyde was brominated to give α-bromoaldehyde **80** in 81 % yield (Scheme 35). Subsequent displacement with 1-Boc-piperazine delivered piperazinyl aldehyde **81** in 76 % yield. To incorporate the required nitrile group, piperidine **64** was coupled to cyanoacetic acid to give cyanoacetamide **82** in 81 % yield.

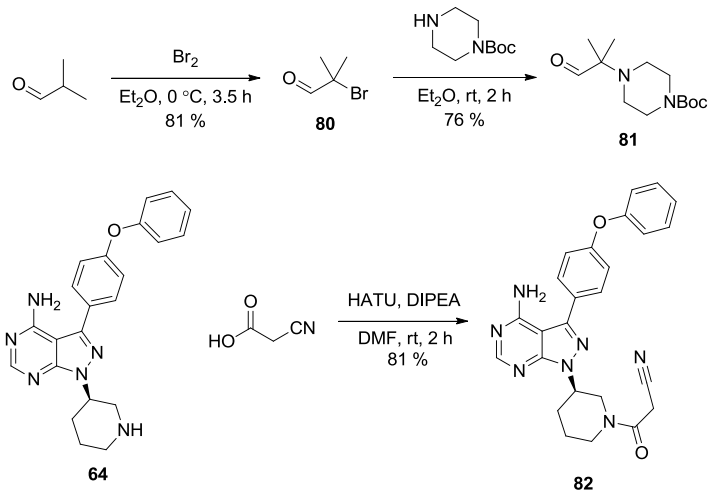

Scheme 35. Preparation of aldehyde **81** and cyanoacetamide **82**

Knoevenagel condensation of aldehyde **81** and cyanoacetamide **82** and subsequent acidic deprotection gave the required piperazine **83** as a mixture of geometric isomers in 88 % over two steps. This was then alkylated with chloride **66** and deprotected to give cyanoacrylamide Protac **84** over two steps, also as a mixture of geometric isomers.

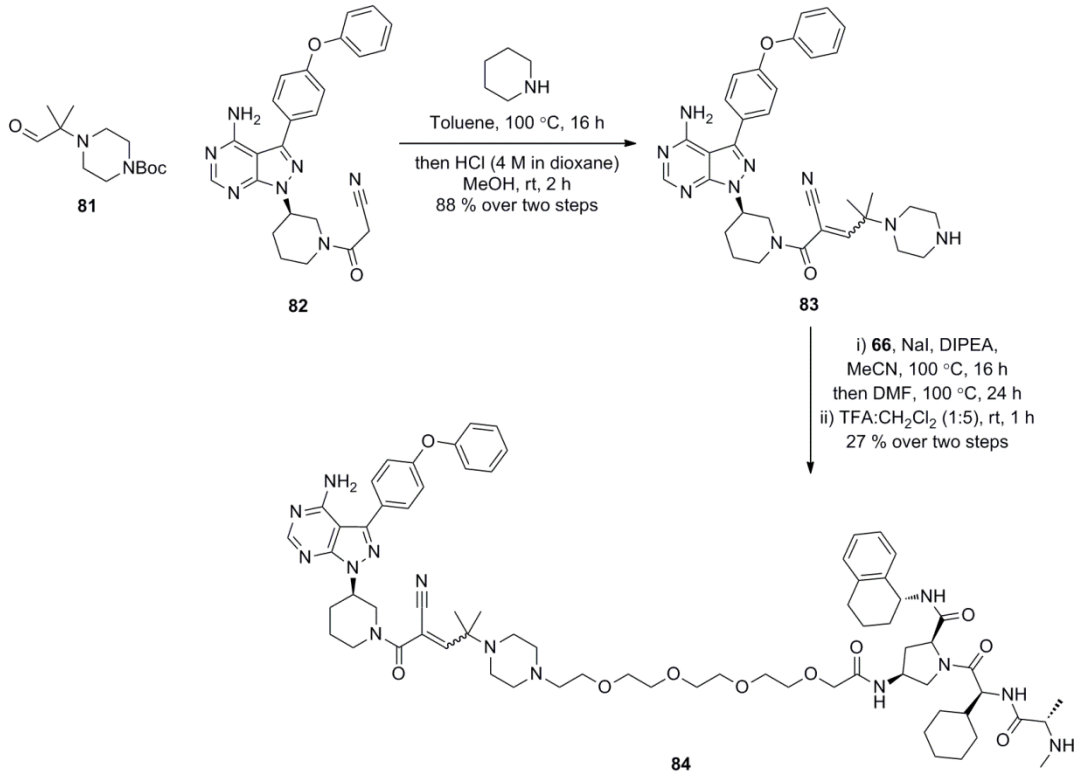

Scheme 36. Preparation of Protac **84**

Profiling of the cyanoacrylamide Protac **84** is outlined in Table 9. In the biochemical assay, a significant difference between BTK and BTK(C481S) was observed (BTK/BTK(C481S) pIC_{50} = 8.3/7.4), suggesting that C481 is contributing to binding as observed with Ibrutinib (BTK/BTK(C481S) pIC_{50} = 9.4/8.1) and that a covalent interaction is occurring. In terms of physicochemical properties, Protac **84** is significantly more lipophilic than the previous Ibrutinib-based IAP Protacs, presumably caused by the inclusion of the 1,1-dimethyl group proximal to the cyanoacrylamide, and this increased lipophilicity is reflected in the reduced solubility.

Table 9. Profiling of cyanoacrylamide Protac **84**

Compound no.	BTK pIC_{50}[1]	BTK C481S pIC_{50}[1]	Chrom LogD	Solubility (µM)[2]
84	8.3	7.4	6.2	53

[1]1 h preincubation before substrate addition, measured in the presence of 10 µM ATP [2]Solubility measured by CLND

Cyanoacrylamide Protac **84** was then profiled by western blotting in Ramos cells,[301] and was found to degrade BTK with a DC_{50} ~250 nM (Figure 152). The observed D_{max} = 69 % is lower than that observed with previous reversible Protac **70** (D_{max} > 95 %). One possible explanation for this is that there is a fraction of BTK still covalently inhibited by Protac **84** after the treatment time which remains undegradable, as previously observed with Protac **69**. However, due to the smaller range of concentrations tested using this Protac it is possible that the actual D_{max} may not have been observed.

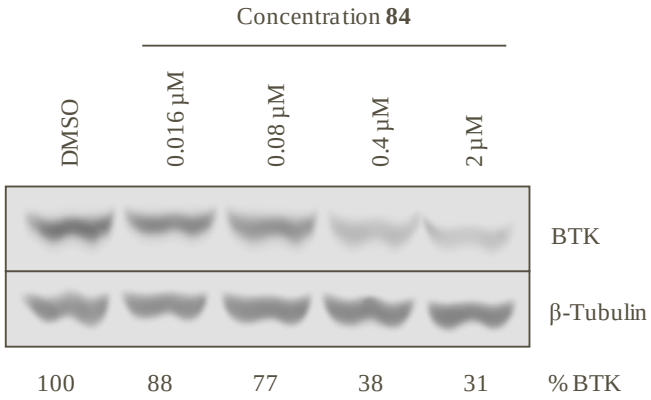

Figure 152. Cyanoacrylamide Protac **84** is an active BTK degrader following 18 h treatment in THP-1 cells.

While Protac **84** is clearly an active BTK degrader, whether its binding mode is indeed reversibly covalent remains unclear. Although the significant difference in potency observed in the biochemical binding assay suggests that C481 is involved in binding, attempts to carry out protein MS experiments did not demonstrate covalent modification of recombinant BTK. Therefore, the degradation profile demonstrated in Figure 152 may reflect a fully reversible degrader, with weaker BTK engagement as a result of higher lipophilicity (through increased non-specific protein binding). On the other hand, if Protac **84** is indeed binding in a reversible covalent manner, weaker and incomplete degradation may result from remaining covalent occupancy following the incubation period. Further investigation would be required to demonstrate whether reversible covalency is tolerated in a Protac.

5.2.7 Rationalising Effect of Covalency

Covalently inhibited BTK must be degradable, as the duration of action of covalent inhibitors such as Ibrutinib and CC-292 is limited by protein resynthesis.[339,353] It has been shown that upon blocking protein synthesis, mature covalently inhibited BTK is degraded by the proteasome, which can be rescued by proteasome inhibition.[383] Similarly, HaloProtacs are able to cause degradation of HaloTag-fused target proteins (Section 1.4.3).[155] In that case, the chloroalkane tether covalently inhibits the HaloTag protein, resulting in a fusion protein labelled with a VHL degron, much like BTK is covalently labelled with an IAP or cereblon degron in these cases.

BTK appears to be highly susceptible to protein degradation, however dissociation of the Protac before protein degradation appears to be critical to allow processing of the substrate by the proteasome. It is highly probable that BTK is ubiquitinated by Protac **69**, as the equivalent reversible Protac **70** permits its degradation. Therefore, covalent inhibition followed by ubiquitination would first result in a ubiquitinated BTK-Protac covalent adduct, which can then be recognised by the proteasome.

At this point, it is of interest to revisit how recognition and unfolding of ubiquitinated substrates by the proteasome occurs, as this is a possible explanation for the observed lack of degradation of the presumed BTK-Protac-ubiquitin adduct (Figure 153). As stated previously, ubiquitin transfer alone is not sufficient for proteasomal degradation, as the protein must also present an appropriate structurally disordered region to act as an initiation site for unfolding and proteolysis.[39] Binding of the polyubiquitin chain must first occur through a ubiquitin receptor, followed by presentation of the unstructured region and its pre-engagement in the narrow pore of the proteasomal channel. Structural rearrangement of the 19S lid allows pore opening and ubiquitin scanning allows increased engagement, followed by ubiquitin chain removal and proteolysis.

This process must be occurring with reversible Protac **70**, resulting in degradation by the standard proteasomal pathway. Therefore, the Protac appendage to the substrate generated upon incubation with covalent Protac **69** may interfere with either recognition or substrate acceptance by the proteasome, preventing degradation.

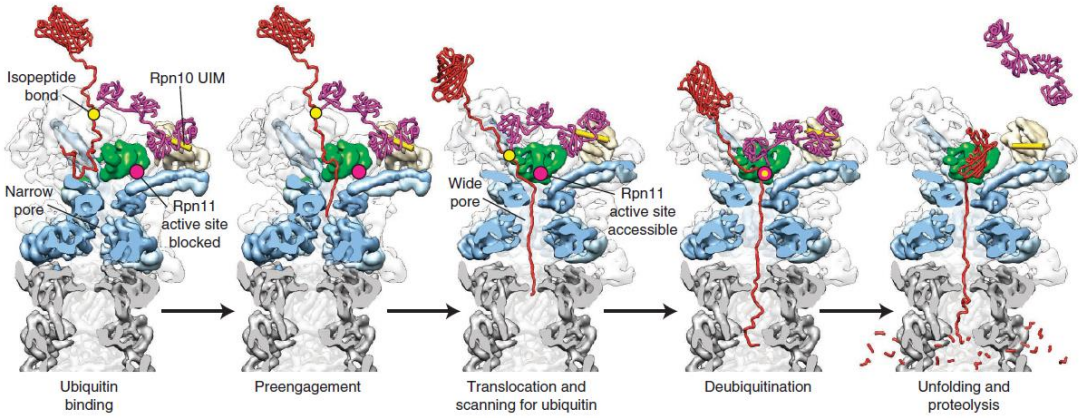

Figure 153.[386] Structural model of substrate degradation by the proteasome

As the BTK-Protac adduct formed with covalent Protac **69** is likely to be recruited to the proteasome as a result of polyubiquitination, one reason for the lack of degradation may be due to lack of presentation of the structurally disordered region required to initiate proteolysis. As the Protac itself is a considerable modification to the protein (1.2 kDa), it is possible that this blocks presentation of the unstructured region to the proteasome, preventing successful substrate engagement of the proteasome.

The presence of covalent Protac **69** may also prevent degradation since although the covalent modification of the protein allows recognition of the structurally disordered region, the extension of the Protac from the protein causes a steric clash with the 19S particle, preventing processing by the 20S particle and subsequent proteolysis. Recognition and pre-engagement of the structurally disordered region would cause ubiquitin dissociation. However, as the disordered region cannot be completely internalised, the substrate can dissociate and avoid proteolysis. This may cause partial proteasomal inhibition, which could account for the weaker RIPK2 degradation observed in the presence of covalent Protac **69** compared to reversible Protac **70**.

It may also be possible that the presence of the Protac modification simply hinders recognition of the ubiquitinated BTK-Protac substrate; hence, it cannot be recognised by the proteasome and no engagement or proteolysis can occur. Of course, it would be highly challenging to prove or disprove any of these proposed arguments due to the complex and dynamic nature of the proteasome, and the unknown ubiquitination site on BTK. However, further exploration of this phenomenon may allow greater

understanding of how substrates selectively targeted for degradation by Protacs are subjected to proteasomal degradation.

5.2.8 Conclusions

Having previously identified BTK as a novel degradable target using a promiscuous strategy, selective degradation of this target was first explored employing the covalent BTK inhibitor Ibrutinib. In this section, Protacs based on this inhibitor were synthesised, first recruiting IAP as an E3 ligase. Surprisingly, the covalent Protacs resulted in no degradation of BTK, despite intracellular target engagement. Reduction of the acrylamide moiety critical for irreversible binding resulted in a fully reversible Protac and allowed BTK degradation.

A similar Protac which binds through a reversible covalent mechanism also allowed BTK degradation, therefore Protac dissociation may be critical to allow processing of the BTK-Protac adduct by the proteasome. Due to the high structural similarity of the irreversible and reversible Protacs, it was thought the covalent protein-Protac adduct is likely to disrupt conventional engagement of the proteasome and prevent protein degradation. It has also been demonstrated that the effect of covalent inhibition on Protac-mediated degradation of BTK is independent of the recruited ligase, as exchange of the ligase binder cereblon results in the same overall profile. It is not yet known whether this is a general effect or specific for BTK, especially since analogous strategies such as HaloProtacs or hydrophobic tags both covalently inhibit and degrade their respective target proteins.

Although the use of a covalent inhibitor as a target protein binder proved to be ineffective in this experiment, it brings to attention the potential advantage of incorporation of a covalent ligase binder into a Protac. As covalent ligase inhibition would avoid the kinetic barrier to ternary complex formation, the ligase would be effectively reprogrammed as a degrader of the targeted protein through formation of binary complexes only. As duration would then be driven by resynthesis of the covalently inhibited ligase, and the potential for low ligase occupancy to drive efficacy, this would allow increasingly infrequent dosing strategies over standard Protacs.

Whilst the fully reversible Ibrutinib Protac **70** is an effective BTK degrader, it is not useful as a probe for selective degradation of BTK. Given the poor selectivity profile of the reduced form of Ibrutinib,[387] Protac **70** is also likely to be a fairly promiscuous degrader. For example, it has been shown that Protac **70** is a more efficient RIPK2 degrader than BTK. Therefore, to probe selective knockdown of BTK, a highly potent, reversible inhibitor of BTK was required for elaboration into a Protac.

5.3 Reversible BTK Protacs

As covalent inhibition of BTK does not promote Protac-mediated degradation, a selective, non-covalent ligand was required to probe whether degradation of BTK could demonstrate any significant advantage over inhibition. The selective BTK inhibitor RN486 was selected to investigate this, and the synthesis and profiling of a BTK degrader based upon this ligand will be described within this section.

5.3.1 RN486

In order to accurately attribute a degradation phenotype to exclusive knockdown of BTK, rather than a secondary target of the parent ligand (a potential issue with use of Ibrutinib-based Protacs described in Section 5.2), a highly selective fully reversible BTK ligand was required. RN486 is a potent and selective inhibitor of BTK (Figure 154),[364,369] developed from previously described reversible BTK inhibitors CGI-1746 and GDC-0834 (Section 5.1.2.3).

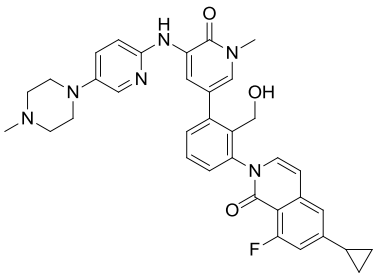

Figure 154. Structure of BTK inhibitor RN486

The selectivity profile of RN486 indicates that only 5 kinases are inhibited within a 10^3 fold selectivity window from a panel of 369 kinases (Table 10).[369] The nearest most potently inhibited kinase is SLK (139 fold selectivity), which has previously been observed to be inhibited but not degraded by promiscuous kinase Protacs (Section 4), indicating the potential for highly specific degradation using this ligand. RN486 also demonstrates high selectivity over kinases commonly inhibited by Ibrutinib, such as the Tec family, which should avoid any confounding effects mediated by Ibrutinib's secondary targets.

Table 10.[369] RN486 selectivity profile

Kinase	BTK	SLK	TEC	FGR	ITK	ABL1
K_d (μM)	0.00031	0.043	0.064	0.1	0.24	0.29
Fold selectivity	1	139	206	323	774	935

RN486 also has also demonstrated a favourable PK profile, with a $t_{1/2}$ = 9.8 h in rat upon IV administration, far superior to reversible BTK inhibitors CGI-1746 and GDC-0834, which both suffered from rapid clearance.[362] Hence, this inhibitor was deemed suitable for incorporation into the required BTK reversible Protac.

5.3.2 Protac Design

The aim of this experiment is to design a Protac with a highly selective profile to allow clear delineation between single target degradation and single target inhibition. The target Protac would preferably have favourable physicochemical properties to allow rapid lead optimisation if there is a clear therapeutic benefit to Protac intervention; hence these properties were designed *in silico* in advance of synthesis.

First, it was necessary to determine a potential linking position from the BTK inhibitor to the E3 ligase. The crystal structure of a close analogue of RN486 was employed to select an appropriate linking position to the E3 ligase (Figure 155).[364] The pendant ethyl piperazine was found to be highly solvent exposed and indicated a desirable linking position for conjugation to the E3 ligase. Minor extensions through the piperazinyl vector using oxetanes and azetidines have also been reported to be tolerated at BTK.[388]

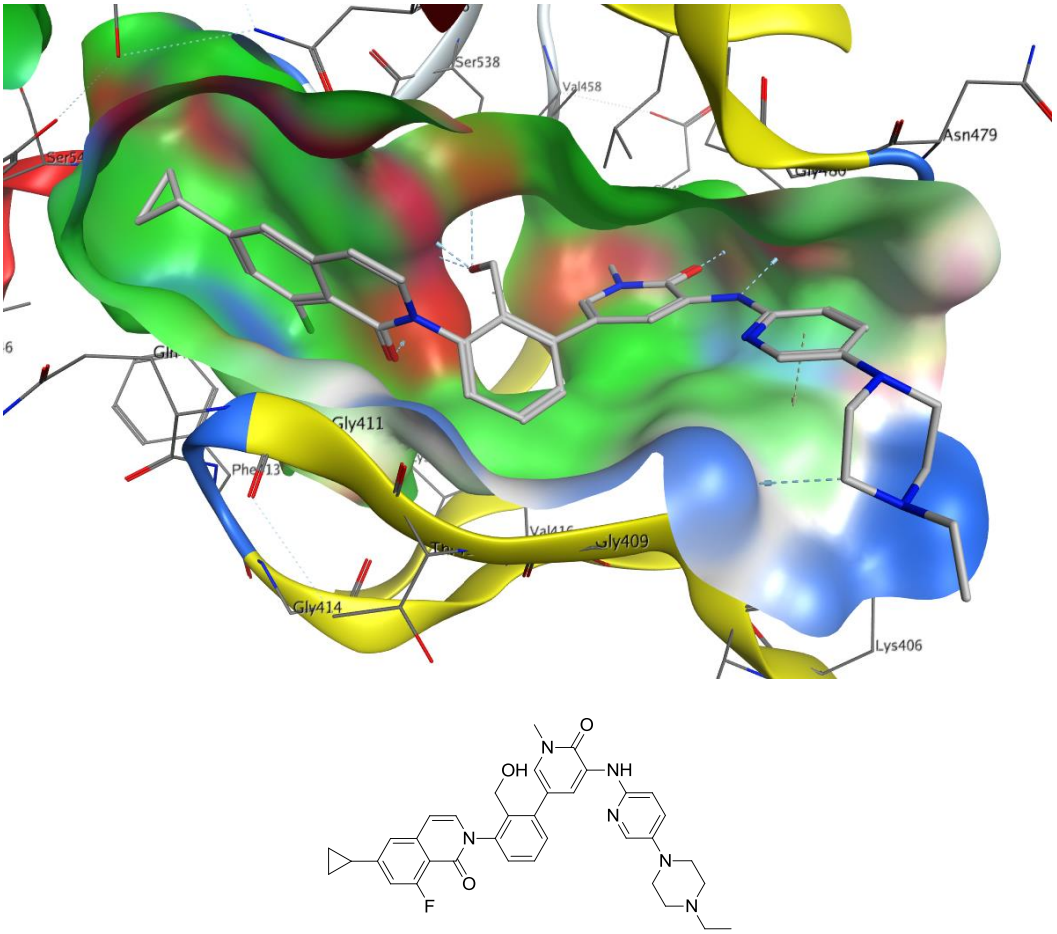

Figure 155.[364] Co-crystal structure of RN486 analogue and BTK (surface coloured by pocket region: blue = solvent exposed, green = hydrophobic, red = polar) PDB: 4OTR

A potential issue with use of RN486 is its reported poor aqueous solubility (0.6 μg/mL), likely to be driven by increased lipophilicity as a result of its relatively high aromatic ring count.[364] There is a reported 50 fold drop-off between biochemical FRET binding and human whole blood (HWB) potency, and whilst no lipophilicity measures have been reported for this compound, elevated lipophilicity may drive high protein binding and cause this potency reduction. To address this potential issue in the resulting Protac, a more polar ligase binder was considered to compensate for the lipophilic BTK inhibitor.

In this case, IAP was selected as the E3 ligase to recruit in the BTK Protac. Recruitment of cereblon was deemed to be inappropriate in this case due to potentially confounding effects on cytokines mediated by cereblon inhibition.[88] The short half-

life of the parent cereblon inhibitor and the potential teratogenic effects also disfavoured selection of this ligase. As VHL demonstrated no effect on BTK protein levels using promiscuous kinase Protacs (Section 4), this ligase was not selected. Upon referring to known IAP antagonists, it was thought that the most clinical IAP inhibitor LCL-161 may be a potential candidate for incorporation into the BTK Protac (see Section 1.3.3.3). Analysis of the crystal structure of a similar Smac mimetic to LCL-161 containing a cyclohexyl group indicated that this exit vector was likely to be tolerated as this region is highly solvent exposed (Figure 156).[389] LCL-161 was also selected not only due to its favourable safety profile,[390] but also its relatively low predicted lipophilicity when compared to IAP inhibitors incorporated into previous iterations of BTK Protacs (Figure 157).

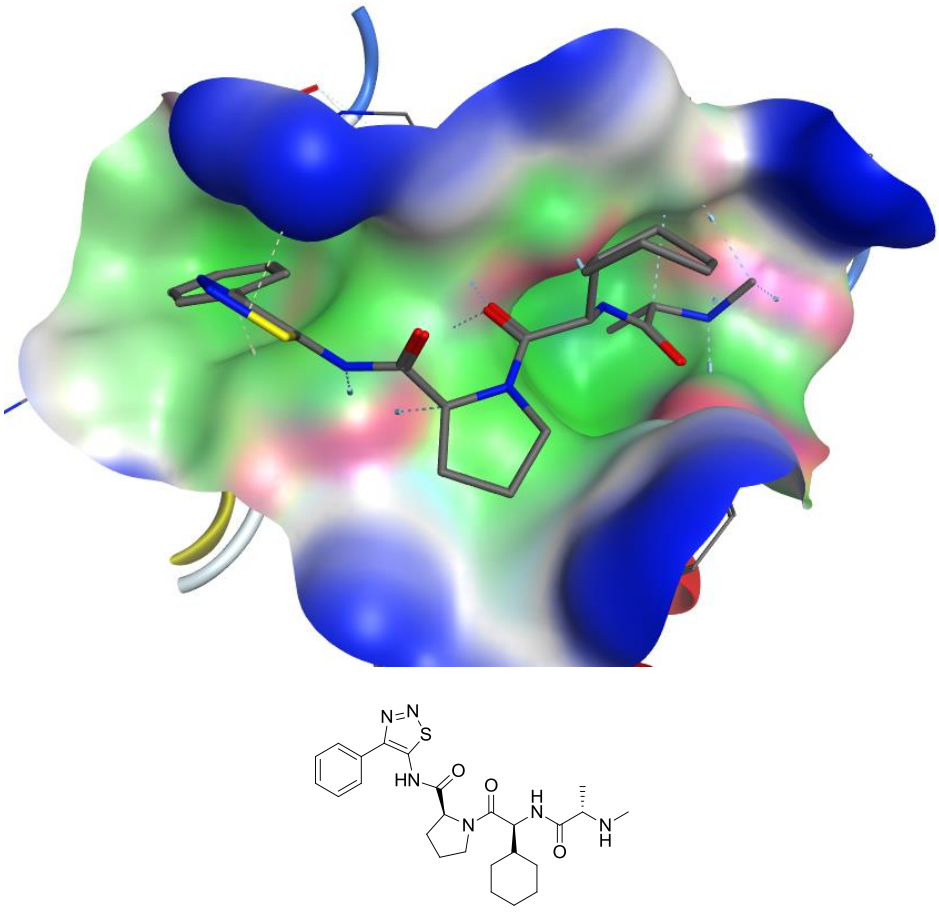

Figure 156.[362] Co-crystal structure of a Smac mimetic and cIAP1 BIR3 indicating solvent exposure through the cyclohexyl group (surface coloured by pocket region: blue = solvent exposed, green = hydrophobic, red = polar)

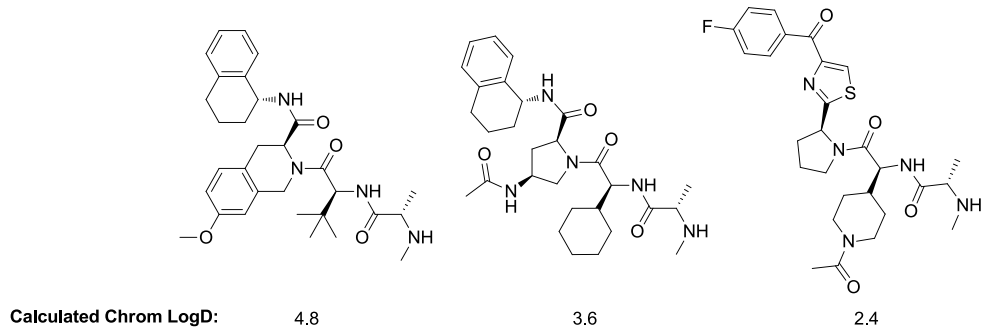

Figure 157. Reduced lipophilicity of IAP ligands compared to those incorporated in previous iterations of BTK Protacs (by calculated chrom logD)

As a 4EG linker had previously shown to induce degradation of BTK using promiscuous kinase IAP Protac **60** and reversible Ibrutinib Protac **70**, it was thought that retaining this linker length would be sufficient to allow degradation. By combination of these factors, the target Protac was identified (Figure 158), the synthesis and profiling of which will be outlined in subsequent sections.

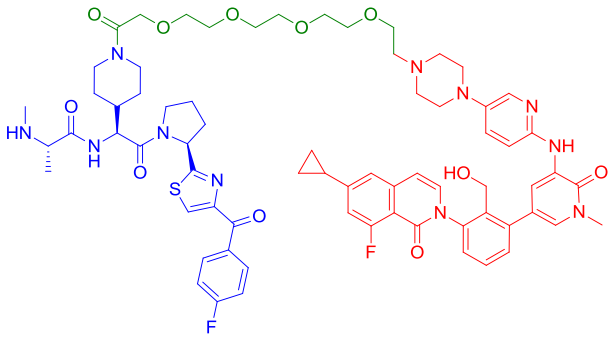

Figure 158. Target BTK-IAP Protac based on BTK ligand RN486

5.3.3 Protac Synthesis

The synthesis of the target RN486 Protac was then carried out. Retrosynthetic analysis of an appropriate linkable RN486 ligand is outlined in Figure 159. Previous syntheses of RN486 have been described, however these begin using a complex non-commercial starting material to assemble the desired cyclopropyl isoquinolone fragment.[364,388] Hence, an alternative route was sought for this fragment of the ligand. To achieve the desired substitution pattern, a Pomeranz-Fritsch reaction to assemble the

corresponding isoquinoline was considered, followed by oxidation to afford the isoquinolone.

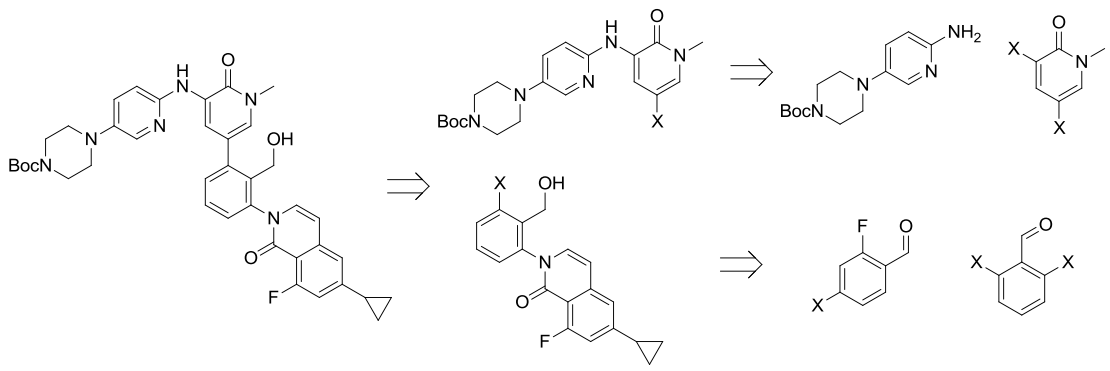

Figure 159. Retrosynthetic analysis of protected RN486 binder

First, a reductive amination was carried out between 4-bromo-2-fluorobenzaldehyde and aminoacetaldehyde dimethyl acetal using sodium borohydride, then the resulting amine directly protected with tosyl chloride to give acetal **85** in 94 % yield over two steps. Tosylation was carried out in this case to prevent tautomerisation to the corresponding imine under the subsequent cyclisation conditions, as it was thought that this would result in starting material decomposition or undesired side-reactions. A Pomeranz-Fritsch reaction mediated by $AlCl_3$ afforded isoquinoline **86** in 32 % yield and 90 % purity. It was thought that the relatively electron-poor aromatic ring may have hindered the cyclisation, resulting in the poor conversion to desired product.

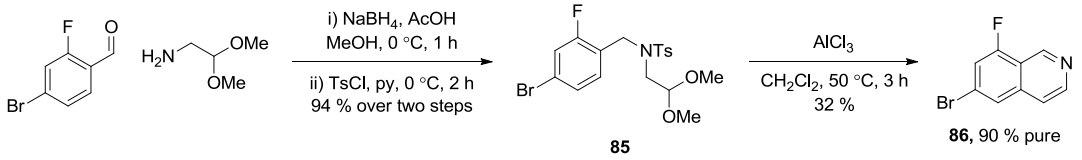

Scheme 37. Preparation of isoquinoline **86**

In an attempt to improve the yield of this cyclisation reaction, it was thought that addition of the more electron-donating cyclopropyl group first would allow cyclisation to occur more readily. However, upon subjecting the cyclopropyl substrate to the reaction conditions, a variety of side reactions occurred, including opening of the cyclopropane ring, resulting in only traces of the desired product.

For the subsequent Suzuki coupling step to insert the cyclopropyl group, early test reactions using cyclopropyl boronic acid as a coupling partner resulted in almost complete debromination of starting material. Following reports by Molander and co-workers, potassium cyclopropyl trifluoroborate was employed as an alternative to the boronic acid, which has been reported to have increased stability and less propensity to protodeborylate.[391] Thus, the Suzuki reaction delivered cyclopropyl isoquinoline **87** in 64 % yield (Scheme 38). Oxidation of isoquinoline **87** with *m*-CPBA gave isoquinoline *N*-oxide **88** in 90 % yield.

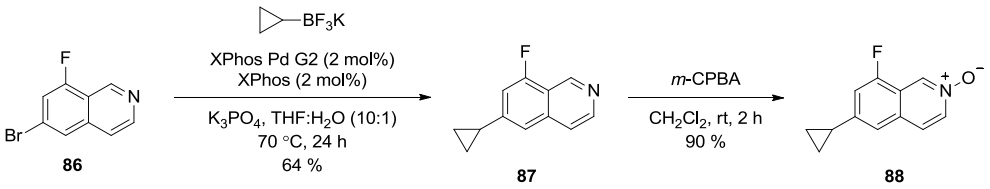

Scheme 38. Preparation of isoquinoline *N*-oxide **88**

Isoquinoline *N*-oxide **88** was then rearranged to isoquinolone **89** in 79 % yield following heating in acetic anhydride and subsequent hydrolysis (Scheme 39). A copper-catalysed amidation was then carried out in order to couple isoquinolone **89** to 2,6-dibromobenzaldehyde, which delivered aldehyde **90** in 51 % yield and 90 % purity. Subsequent reduction of aldehyde **90** using sodium borohydride gave alcohol **91** in 72 % yield.

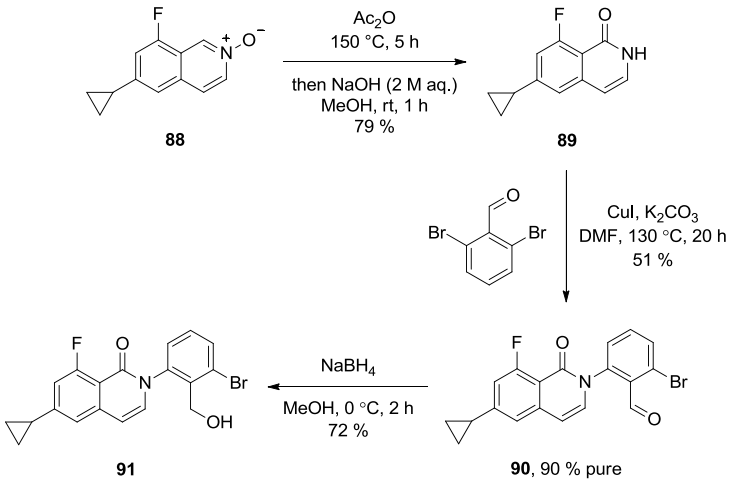

Scheme 39. Preparation of alcohol **91**

In order to synthesise the second portion of the binder, bromination of *N*-methyl-2-pyridone with NBS to give dibromo-*N*-methylpyridone **92** in 98 % yield (Scheme 40). Then, an S_NAr reaction was carried out between 5-bromo-2-nitropyridine and 1-Boc-piperazine to give nitropyrimidine **93** in 80 % yield. Hydrogenation afforded the corresponding aniline **94** in 75 % yield, which was then coupled to **92** to selectively give bromo-*N*-methylpyridone **94** in 89 % yield. In this case, selectivity between the two aryl bromides is presumably determined by proximity to the electron-withdrawing carbonyl group, resulting in faster oxidative addition at the proximal halide. Subsequent Miyaura borylation of aryl bromide **95** delivered boronic ester **96** in 78 % yield.

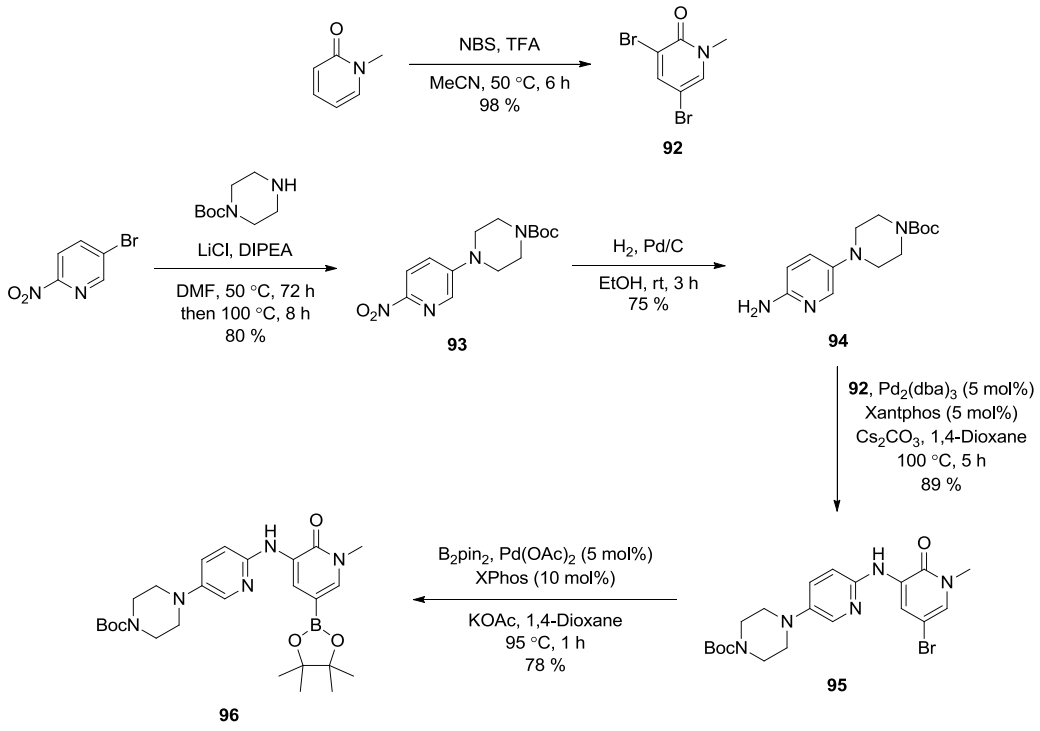

Scheme 40. Preparation of boronic ester **96**

Aryl bromide **91** and boronic ester **96** were then coupled to give the desired Boc-protected BTK binder **97** in 55 % yield (Scheme 41). The parent BTK inhibitor RN486 was then synthesised by Boc deprotection and subsequent reductive amination with formaldehyde to give inhibitor **98** in 40 % yield over two steps.

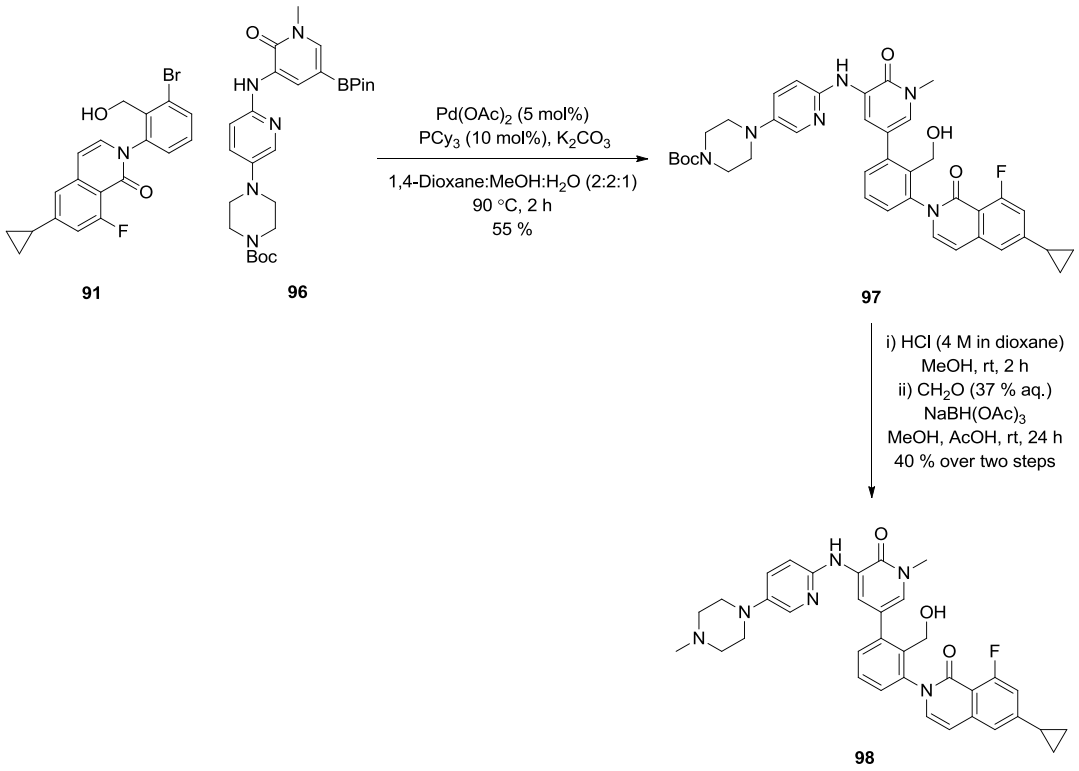

Scheme 41. Synthesis of Boc-protected RN486 **97** and parent BTK binder **98**

To synthesise the final Protac, Boc deprotection of **97** was carried out, followed by alkylation and hydrolysis to deliver acid **99** in 51 % yield over three steps. This was then coupled to an Fmoc-protected linkable LCL-161 analogue available within our laboratories[125] and deprotected to give the desired BTK Protac **100** in 46 % yield over two steps.

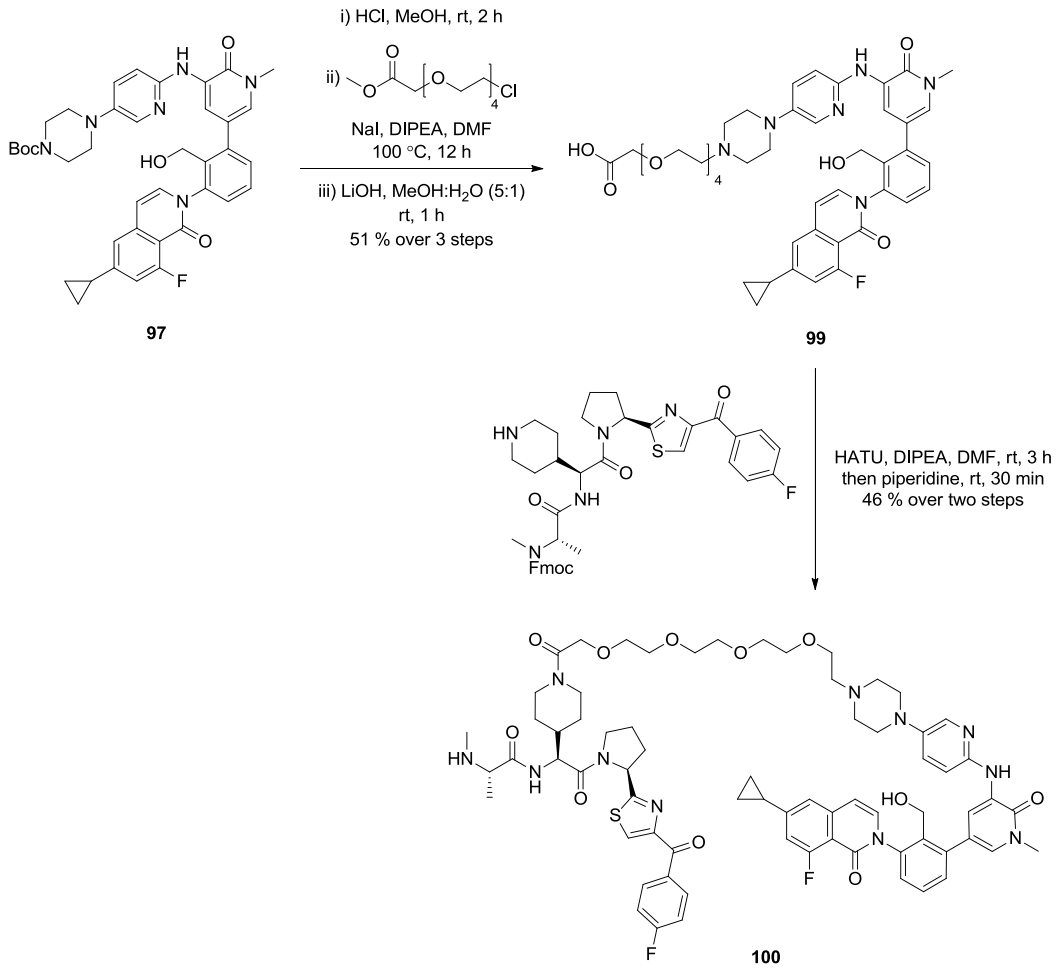

Scheme 42. Preparation of BTK Protac **100**

The isolated enzyme binding and physicochemical properties of the parent BTK inhibitor RN486 (**98**) and BTK Protac **100** were then profiled. BTK Protac **100** was found to maintain the potency of parent ligand RN486 (BTK pIC_{50} **98**/**100** = 8.4/7.9), and also proved to be potent in the BTK C481S mutant (BTK C481S pIC_{50} **98**/**100** = 9.5/8.9). As predicted, RN486 (**98**) was found to be relatively lipophilic (chrom logD = 4.7) with moderate solubility (60 μM). Employing an IAP antagonist predicted to be less lipophilic proved to be successful in this case, as direct elaboration of RN486 into a Protac had only a modest effect on its overall physicochemical profile. Protac **100** was considered suitable for further characterisation and was advanced into degradation experiments.

Table 11. RN486 compound properties

Compound	BTK pIC_{50}	BTK C481S pIC_{50}	Chrom LogD	Solubility (μM)[1]
98 (RN486)	8.4	9.5	4.7	60
100	7.9	8.9	5.1	56

[1]*Solubility measured by CLND*

5.3.4 Protac Profile

The effect of RN486 Protac **100** on BTK protein levels was then assessed by western blotting.[301] As expected, Protac **100** demonstrated dose-dependent degradation of BTK with an observed DC_{50} ~ 50 nM and a D_{max} = 90 % (Figure 160).[301] This is significantly improved from previous BTK degradation observed with promiscuous kinase IAP Protac **60** (BTK DC_{50} = 350 nM, D_{max} = 69 %).

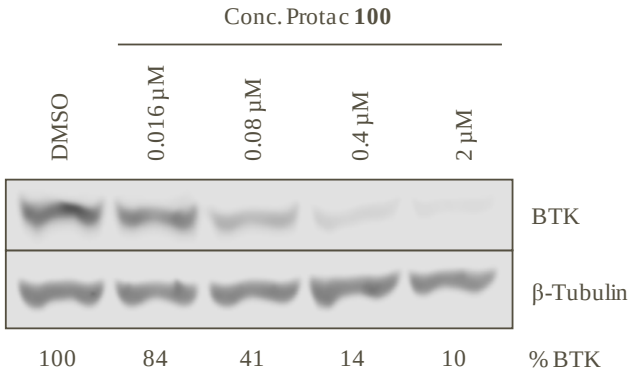

Figure 160. Protac **100** demonstrates dose-dependent degradation of BTK following 18 h treatment in THP-1 cells

As Protac **100** should retain the selectivity profile of the parent inhibitor (139 fold over SLK, which is not expected to degrade, and 200 fold selectivity over Tec),[369] BTK is likely to be the only protein significantly degraded at the observed DC_{50}, therefore, Protac **100** is likely to be a highly selective probe for BTK knockdown. It was then directly compared with Ibrutinib (**65**) to probe the reported effect of BTK inhibition on formation of the NLRP3 inflammasome.

Following the protocol employed by Itu and co-workers,[373] THP-1 cells were differentiated into macrophages, then treated overnight with increasing concentrations of Ibrutinib (**65**) and BTK Protac **100**.[301] The treated samples were then stimulated with aluminium hydroxide for 6 h, which triggers formation of the NLRP3 inflammasome,[392,393] resulting in processing of pro-IL-1β to IL-1β. Levels of IL-1β were then measured by an enzyme-linked immunosorbent assay (ELISA, Figure 161).[301] Inhibition of IL-1β is likely to be caused by compound-driven inhibition of NLRP3 activation.

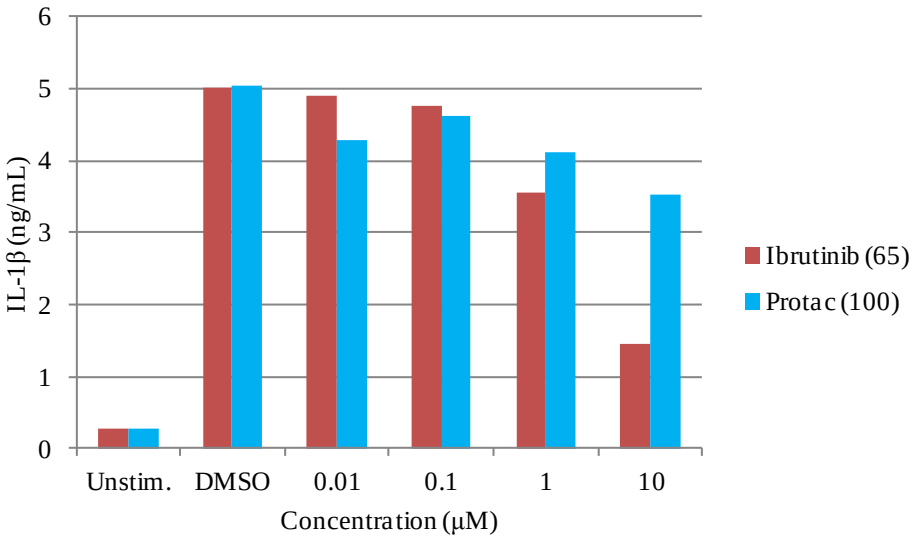

Figure 161. Effect on IL-1β levels as a result of NLRP3 inflammasome inactivation by Ibrutinib (**65**) and BTK Protac (**100**)

As expected, Ibrutinib (**65**) was found to reduce IL-1β levels at 10 μM concentration, consistent with data previously reported.[373] On the other hand, BTK Protac **100** was found to have no significant effect on IL-1β levels. Given the DC_{50} of the Protac is approximately 50 nM, it would be expected that inhibition of IL-1β would correlate directly with BTK protein levels; however, even when BTK is depleted to approximately 10 % at 1 μM concentration of Protac **100**, IL-1β levels are not significantly reduced (Figure 162). As NLRP3-mediated IL-1β inhibition does not appear to directly correlate with BTK protein levels, it is likely that BTK is not involved in inhibition of NLRP3 inflammasome activation. Given that Ibrutinib (**65**) is known to inhibit BTK autophosphorylation at nanomolar concentration (BTK

PY223 IC_{50} = 11 nM), and IL-1β inhibition *via* NLRP3 inflammasome inactivation occurs at concentrations above 1 μM, this suggests that the latter effect is likely to be mediated by a secondary target of Ibrutinib.

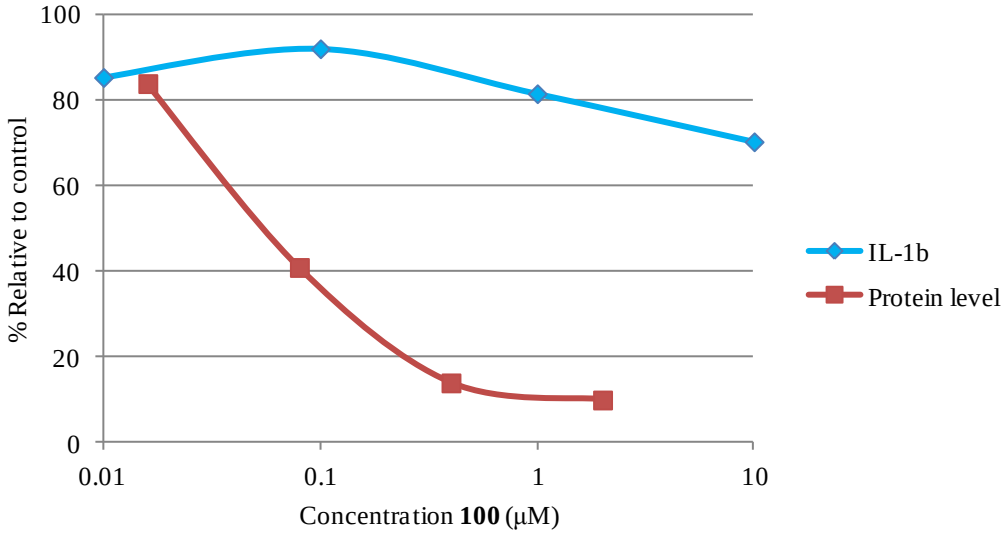

Figure 162. Relative comparison of IL-1β inhibition and BTK protein levels after treatment with Protac **100** (IL-1β is relative to DMSO control sample, protein level is relative to β-tubulin standard)

The major mode of action of small-molecule inhibitors of the NLRP3 inflammasome is by modification of cysteine residues using Michael acceptors.[394] The high concentrations of Ibrutinib (**65**) required to inhibit IL-1β secretion may simply result from unselective cysteine trapping of NLRP3. Indeed, a series α,β-unsaturated carbonyl compounds have been described as inhibitors of NLRP3 activity.[395] At 10 μM, Ibrutinib is known to be highly unselective and demonstrates highly promiscuous covalent inhibition.[358]

Another possibility for the observed inhibition of IL-1β using Ibrutinib rather than a BTK-selective Protac is inhibition of Tec, a secondary target of Ibrutinib. Tec has been reported to be required for activation and assembly of the non-canonical caspase-8 inflammasome,[396] which is known to promote NLRP3 inflammasome formation.[397] As inhibition of Tec is believed to inhibit caspase-8 inflammasome formation, this may also inhibit NLRP3 inflammasome formation. As the RN486 Protac is likely to have

increased selectivity for BTK over TEC compared to Ibrutinib (RN486 has 200 fold selectivity for BTK over TEC), though this effect may not be significant within the concentration range used in this experiment.

The results generated by selective BTK knockdown using Protac **100** compared to BTK inhibition using Ibrutinib (**65**) highlight the critical importance of selecting a high-quality chemical probe in order to directly relate biological function.[243,398] The conclusions previously drawn in the literature regarding the role of BTK in NLRP3 inflammasome activation highlight the potentially misleading conclusions that can be drawn from use of a poorly selective inhibitor or an inappropriate concentration range.

5.3.5 Conclusions

Having previously identified BTK as a novel degradable target using a promiscuous strategy (Section 4), a highly selective BTK Protac, based on the reversible inhibitor RN486, was targeted. This Protac was subsequently generated in 14 linear steps and demonstrated a DC_{50} ~ 50 nM and a D_{max} = 90 % in Ramos cells. As Protac **100** should retain the exquisite selectivity profile of the parent inhibitor, it is expected to be a highly selective probe for degradation of BTK.

Following reports highlighting the role of BTK in activation of the NLRP3 inflammasome, the effect of Protac-mediated BTK knockdown was compared to the described effects using Ibrutinib. Incubation with the BTK Protac at concentrations where protein levels were depleted >90 % resulted in no significant inhibition of NLRP3 inflammasome formation. As micromolar concentrations of Ibrutinib were required to demonstrate significant inhibition of IL-1β, it is believed that the effect observed with Ibrutinib is likely to be mediated by unselective cysteine modification through its reactive acrylamide, or through inhibition of one of the secondary targets of the inhibitor.

Having developed a selective BTK Protac, this brought into question whether a degrader could compete with other small molecule inhibitors in the field. In the oncology arena, where the Ibrutinib reigns as a single agent treatment, no reversible inhibitors have significantly progressed clinically. Almost certainly, the extended PD

efficacy available through covalent inhibition will be challenging to compete with through reversible occupancy. Though a BTK Protac would have the same PD profile as Ibrutinib, as efficacy in both cases is driven by protein resynthesis, it only has modest advantages over a covalent profile. If reducing dose was a priority for using a Protac approach through catalytic degradation, Ibrutinib has already shown to have no dose-limiting toxicity and high dosing is well tolerated.[344] If it was sought to reduce adverse events observed upon Ibrutinib treatment through an improved selectivity profile, covalent successor Acalabrutinib has already achieved this.[354] The only clear advantage a Protac may have in B cell cancers is efficacy in relapsed C481S mutant patients; however, competing PLCγ2 mutations causing BTK redundancy may complicate this further.[399]

Likewise as a treatment for RA, does a BTK degrader present a potential clinical opportunity? No BTK inhibitors have yet progressed beyond Phase II clinically, though efficacy in preclinical models is highly encouraging.[325] However, this bring into question as to whether a druggable kinase with pre-existing clinical inhibitors is the best target for a Protac approach. If a Protac is bringing completely novel pharmacology to a challenging target, or adding otherwise inaccessible duration of action, it is certainly an attractive prospect to pursue. However, given the crowded inhibitor landscape and active clinical pipeline targeting BTK, a Protac would not be much more than a "super-inhibitor" given its lack of additional pharmacology. If all BTK inhibitors were to fail in Phase II studies for efficacy in RA, then a BTK Protac would present an ideal opportunity to circumvent this. However, currently, there is no clinical need for this.

Despite this, the pathway undertaken in targeting BTK demonstrates the strength of the promiscuous approach detailed in previous sections to identify novel degradable targets (Section 4). In one step, a highly selective Protac has been developed from a pan-kinase degrader, and allowed decision making upon whether further interrogation of the target was required for pre-clinical development. This prompts investigation of promiscuous strategies in further target classes to allow less empirical target selection and increase expansion of the protein degradation field.

6. Conclusions

Targeted small-molecule induced protein degradation has recently emerged as a highly valuable drug discovery strategy with considerable potential, and the evolution of the technology through recent years has been reflected in the progression of this work. The key advantages and challenges of the technology have been presented; for example, the power of Protac catalysis in uncoupling of binding potency and induced degradation. However, the challenges presented by target selection have proved to be critical to the success or failure of a project.

The idea of empirical Protac target selection was inverted through the approach of non-selective target degradation, which led to the identification of multiple novel targets in druggable kinase space. With the knowledge that single target degradation is possible, Protacs targeting one of the identified kinases were able to be rapidly and effectively designed, allowing prosecution of the advantages of degradation over inhibition, whilst producing unexpected results as a result of binding mode. In most cases, serendipity is likely to be a flawed approach to selecting a target, as a high-value disease-relevant target should be determined *a priori*. However, the promiscuous kinase experiment gives confidence in the wider applicability of Protacs, as only a small number of targets have been identified to date.

This brings into perspective the future of Protacs as a drug discovery prospect. As explored here, target selection can be one of the most challenging aspects of the process, although the research described in this thesis may act as a guide for future target selection. On one hand, Protacs may stand alone as a platform for repurposing of inhibitors which have failed for efficacy reasons, such as low target exposure. However, the lucrative potential for targeting undruggable space using Protacs remains untapped, despite this being one of their most unique features. Novel hit-finding technologies such as encoded libraries may allow generation of affinity probes for these poorly tractable proteins in the future; indeed, as demonstrated through the promiscuous kinase Protac experiment in this thesis, only weak intracellular inhibition is required to demonstrate profound target degradation.

On a similar theme, the range of ligases known to be functional in Protacs is currently relatively limited, and each have their own advantages and disadvantages. Whilst cereblon has proved to be a fairly agnostic degrader based on the results detailed in this thesis, issues with on-target ligase pharmacology and ligand stability may hinder further clinical development. Similarly, recruitment of IAP, whilst having validated clinical inhibitors, may cause issues due to the potential for induction of apoptosis at high local concentrations of Protac. Although VHL has no relevant on-target ligase pharmacology, it has been shown in this thesis that the range of proteins it can degrade may be limited. Undoubtedly, in the future, novel E3 ligase inhibitors will be generated and incorporated into Protacs in a similar way as for the target protein binders themselves.

Protac-mediated protein degradation has now been demonstrated to be a reliable new pharmacologic paradigm allowing efficient and selective removal of proteins from within cells *in vivo*. The catalytic mechanism of action and absence of requirement for a functional inhibitor may offer substantial new opportunities for highly potent effects and modulation of hitherto inaccessible targets. Despite this potential, many areas still require further investigation before this approach can be evaluated in the clinic. Specifically, extensive knowledge of the *in vivo* effects around pharmacokinetics and safety must be gathered to assess suitability of any agents for clinical use. The increasing level of publication and investment from both academic and industrial groups will likely herald a further rapid increase in our knowledge in this area to allow us to better understand the optimal applications of Protacs. Will this represent a transformational example of breakthroughs in chemical biology directly leading to new therapeutics? The first data on safety and efficacy of a Protac in a clinical setting are eagerly awaited and will provide the initial steps towards answering this question.

7. Experimental Section

7.1 General Methods

All temperatures are in °C.

Nuclear Magnetic Resonance (NMR)

NMR spectra were recorded using a Bruker DPX400, DPX500, AV400, or AVIII600 (with cryoprobe). Chemical shifts (δ) are reported in parts per million (ppm) relative to tetramethylsilane and coupling constants (*J*) in Hz. The following abbreviations are used for multiplicities: s = singlet; br. s = broad singlet; d = doublet; t = triplet; q = quartet; spt = septet; m = multiplet; dd = doublet of doublets. If not specifically stated, the NMR experiments were run at 30 °C.

Liquid Chromatography Mass Spectroscopy (LCMS)

i) LCMS Method A

The analysis was conducted on an Acquity UPLC BEH C18 column (50 mm x 2.1 mm internal diameter 1.7 μm packing diameter) at 40 °C.

The solvents employed were:

A = 0.1 % v/v solution of formic acid in water.
B = 0.1 % v/v solution of formic acid in acetonitrile.

The gradient employed was as follows:

Time (min)	Flow rate (mL/min)	% A	% B
0	1	97	3
1.5	1	5	95
1.9	1	5	95
2.0	1	97	3

The UV detection was an averaged signal from wavelength of 210 nm to 350 nm and mass spectra were recorded on a Waters ZQ mass spectrometer using alternate-scan positive and negative mode electrospray ionisation (ES +ve and ES -ve).

ii) LCMS Method B

The analysis was conducted on an XBridge C18 column (50 mm x 4.6 mm internal diameter 3.5 μm packing diameter) at 30 °C. The solvents employed were:

A = 10 mM ammonium bicarbonate in water adjusted to pH 10 with ammonia solution
B = acetonitrile.

The typical gradient employed was as follows:

Time (min)	Flow rate (mL/min)	% A	% B
0	1	97	3
0.05	1	97	3
1.50	1	5	95
1.90	1	5	95
2.00	1	97	3

The UV detection was an averaged signal from wavelength of 210 nm to 350 nm and mass spectra were recorded on a Waters ZQ mass spectrometer using alternate-scan positive and negative mode electrospray ionisation (ES +ve and ES -ve).

High Resolution Mass Spectroscopy (HRMS)

ESI (+) high resolution mass spectra were obtained on a Micromass Q-Tof 2 hybrid quadrupole time-of-flight mass spectrometer, equipped with a Z-spray interface, over a mass range of 100 - 1500 Da, with a scan time of 0.9 s and an interscan delay of 0.1 s. Reserpine was used as the external mass calibrant ($[M + H]^+$ = 609.2812 Da). The Q-Tof 2 mass spectrometer was operated in W reflectron mode to give a resolution (FWHM) of 16000 - 20000. Ionisation was achieved with a spray voltage of 3.2 kV, a

cone voltage of 50 V, with cone and desolvation gas flows of 10-20 and 600 L/h, respectively. The source block and desolvation temperatures were maintained at 120 ºC and 250 ºC, respectively. The elemental composition was calculated using MassLynx v4.1 for the $[M + H]^+$ and the mass error quoted as ppm.

Mass Directed Auto-Preparative (MDAP)

"Mass directed automated preparative HPLC" (MDAP) was conducted on a system such as a Waters FractionLynx system comprising of a Waters 600 pump with extended pump heads, Waters 2700 autosampler, Waters 996 diode array and Gilson 202 fraction collector on an XBridge C18 column (100 mm x 30 mm i.d. 5 μm packing diameter) at ambient temperature, eluting with 10 mM ammonium bicarbonate in water adjusted to pH 10 with ammonia solution (solvent A) and acetonitrile (solvent B) using the appropriate elution gradient. The UV detection was a summed signal from wavelength of 210 nm to 350 nm. The mass spectra were recorded on a Waters ZQ spectrometer using electrospray positive and negative mode (ES +ve and ES -ve). The software used was MassLynx 3.5 with OpenLynx and FractionLynx option or using equivalent alternative systems. Similar systems using Sunfire C18 columns and gradient of solvents such as formic acid (or TFA) in water (solvent A) and acetonitrile (solvent B) were also employed.

Infrared

IR spectra were recorded from solid samples using a Perkin Elmer Spectrum One FTIR spectrometer fitted with a Perkin Elmer Universal ATR (attenuated total reflectance) sampling accessory. Absorption frequencies are reported in wavenumbers (cm^{-1}).

Melting point

Melting points were measured on a Stuart automatic melting point apparatus, SMP40.

Phase Separators

'Hydrophobic frits' refer to filtration tubes sold by Whatman.

Purification by Column Chromatography

Chromatography techniques are reported in column volumes (CV) of solvent and include either automated techniques (Flashmaster/Biotage) using pre-packed silica or reverse phase (C18) silica cartridges, or manual chromatography on pre-packed solid phase extraction (SPE) cartridges.

7.2 Experimental Data

7.2.1 ActR2B Compounds

3-Bromo-2-methoxypyridine (1)

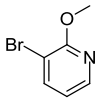

3-Bromo-2-chloropyridine (10.0 g, 52.0 mmol) was added to sodium methoxide (25 % in MeOH) (25 mL) and the reaction stirred at reflux for 2 h. In a separate flask, NaH_2PO_4 (12 g) was dissolved in water (100 mL) and CH_2Cl_2 (100 mL), then stirred and cooled with an ice bath. The reaction mixture was added slowly to the solution, the precipitate filtered and the phases separated. The aqueous phase was back-extracted with CH_2Cl_2 (100 mL), the organic phases combined, dried with $MgSO_4$, and evaporated *in vacuo* to give the required product (7.52 g, 77 % yield) as an orange liquid.

^{1}H NMR (400 MHz, DMSO-d_6) δ 8.17 (d, *J* = 4.9 Hz, 1H), 8.03 (d, *J* = 7.6 Hz, 1H), 6.95 (dd, *J* = 4.9, 7.6 Hz, 1H), 3.92 (s, 3H). **^{13}C NMR** (101 MHz, DMSO-d_6) δ 159.2, 145.8, 142.0, 118.5, 106.0, 54.1. **LCMS** (Method A) (ES +ve) *m/z* 188.1/190.1 $(M + H)^+$ Rt 0.92 min (90 % pure). **HRMS** (ES) calcd for C_6H_7BrNO, $(M + H)^+$ 187.9706, found 187.9706. Note: The compound is >95 % pure by NMR, however LCMS analysis shows 90 % purity. This may be due to the compound having a poor chromophore.

3-Bromo-5-iodo-2-methoxypyridine (2)

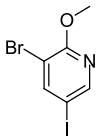

3-Bromo-2-methoxypyridine (7.10 g, 37.8 mmol) was dissolved in DCE (35 mL), then *N*-iodosuccinimide (12.5 g, 55.6 mmol) and TFA (8.00 mL, 104 mmol) were added and the reaction stirred at 60 ºC for 20 h. The reaction was quenched with an aqueous

solution (120 mL) containing Na_2CO_3 (15 g) and $Na_2S_2O_3$ (5 g). The phases were separated and the aqueous layer back-extracted with DCE (100 mL). The organic layers were pooled, dried using a hydrophobic frit, and evaporated *in vacuo*. The sample was purified by chromatography on silica using a 0-50 % EtOAc-cyclohexane gradient over 12 CV. The appropriate fractions were combined and evaporated *in vacuo* to give the required product (9.69 g, 82 % yield) as a white solid.

^{1}H NMR (400 MHz, $CDCl_3$) δ 8.25 (s, 1H), 8.03 (s, 1H), 3.97 (s, 3H). **^{13}C NMR** (101 MHz, $CDCl_3$) δ 159.6, 151.2, 148.2, 108.2, 81.3, 54.6. **LCMS** (Method A) (ES +ve) *m/z* 314.0 $(M + H)^+$ Rt 1.25 min (90 % pure). **HRMS** (ES) calcd for C_6H_6BrINO, $(M + H)^+$ 313.8672, found 313.8673. Note: The compound is >95 % pure by NMR, however LCMS analysis suggests 90 % purity. This may be due to the compound having a poor chromophore.

4-(5-Bromo-6-methoxypyridin-3-yl)-3-methylphenol (3)

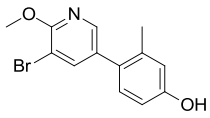

3-Bromo-5-iodo-2-methoxypyridine (5.00 g, 16.0 mmol) and (4-hydroxy-2-methylphenyl)boronic acid (2.42 g, 15.9 mmol) were dissolved in 1,4-dioxane (100 mL). A solution of sodium carbonate (2 M aq., 20 mL, 40 mmol) was added and the resulting reaction mixture stirred under nitrogen for 5 min. $Pd(dppf)Cl_2$ (0.876 g, 1.20 mmol) was added and the reaction was heated to 60 ºC under nitrogen for 3.5 h. The reaction was cooled to rt then diluted with EtOAc (100 mL) and brine (100 mL), the insoluble material filtered off, and the phases separated. The aqueous layer was washed with EtOAc (100 mL) then the organic layers were combined, dried using a hydrophobic frit, and evaporated *in vacuo*. The sample was purified by chromatography on silica using a 0-50 % EtOAc-cyclohexane gradient over 14 CV. The appropriate fractions were combined and evaporated *in vacuo* to give the required product (2.86 g, 61 % yield) as a light brown solid.

^{1}H NMR (400 MHz, $CDCl_3$) δ 8.03 (s, 1H), 7.78 (s, 1H), 7.06 (d, J = 8.3 Hz, 1H), 6.77 (s, 1H), 6.73 (d, J = 8.3 Hz, 1H), 4.92 (s, 1H), 4.06 (s, 3H), 2.24 (s, 3H). **^{13}C**

NMR (101 MHz, $CDCl_3$) δ 158.8, 155.4, 145.2, 142.6, 137.5, 131.8, 131.2, 129.3, 117.2, 113.0, 106.3, 54.6, 20.5 **LCMS** (Method A) (ES +ve) *m/z* 294.2/296.2 $(M + H)^+$ Rt 1.10 min (>95 % pure). **HRMS** (ES) calcd for $C_{13}H_{13}BrNO_2$, $(M + H)^+$ 294.0124, found 294.0127.

3-Bromo-2-methoxy-5-(4-(methoxymethoxy)-2-methylphenyl)pyridine (4)

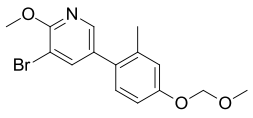

Sodium hydride (60 % w/w in mineral oil, 1.50 g, 62.5 mmol) was washed twice with cyclohexane (2 x 30 mL) under nitrogen and the solvent replaced with DMF (40 mL). 4-(5-Bromo-6-methoxypyridin-3-yl)-3-methylphenol (2.76 g, 9.38 mmol) was dissolved in DMF (30 mL) and was added to the reaction mixture dropwise at 0 ºC. After stirring for 5 min, chloromethyl methyl ether (1.43 mL, 18.8 mmol) was added dropwise at 0 ºC and then the reaction mixture was allowed to warm to room temperature. After 30 min, the reaction was quenched with water (60 mL) then diluted with EtOAc (60 mL) and the phases separated. The aqueous phase was back-extracted with further EtOAc (60 mL). The combined organic layers were washed with brine (60 mL), dried using a hydrophobic frit, and evaporated *in vacuo* to give the required product (3.22 g, 100 % yield) as a pale brown oil.

^{1}H NMR (400 MHz, DMSO-d_6) δ 8.07 - 8.13 (m, 1H), 7.97 - 8.02 (m, 1H), 7.15 (d, *J* = 8.3 Hz, 1H), 6.97 (s, 1H), 6.92 (d, *J* = 8.3 Hz, 1H), 5.21 (s, 2H), 3.96 (s, 3H), 3.38 (s, 3H), 2.21 (s, 3H). **^{13}C NMR** (101 MHz, DMSO-d_6) δ 158.1, 156.4, 145.3, 142.2, 136.8, 131.4, 130.9, 129.7, 117.9, 113.7, 105.5, 93.6, 55.5, 54.3, 20.2. **LCMS** (Method A) (ES +ve) *m/z* 338.3/340.3 $(M + H)^+$ Rt 1.33 min (>95 % pure). **HRMS** (ES) calcd for $C_{15}H_{17}BrNO_3$, $(M + H)^+$ 338.0386, found 338.0395.

2-(2-Methoxy-5-(4-(methoxymethoxy)-2-methylphenyl)pyridin-3-yl)benzo[*b*]thiophene-5-carbaldehyde (5)

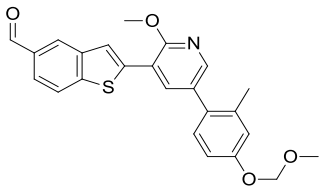

3-Bromo-2-methoxy-5-(4-(methoxymethoxy)-2-methylphenyl)pyridine (3.12 g, 9.23 mmol) and 2-(4,4,5,5-tetramethyl-1,3,2-dioxaborolan-2-yl)benzo[*b*]thiophene-5-carbaldehyde (4.04 g, 14.0 mmol) were dissolved in 1,4-dioxane (70 mL). Sodium carbonate (2 M aq., 11.5 mL, 23.1 mmol) was added and the resulting reaction stirred under nitrogen for 5 min. $Pd(dppf)Cl_2$ (1.05 g, 1.43 mmol) was added, then the reaction was heated to 90 ºC under nitrogen for 2.5 h. The reaction was cooled to rt, diluted with water (70 mL) and EtOAc (70 mL), filtered, and the phases separated. The aqueous layer was back-extracted with EtOAc (70 mL), then the organic layers were combined, dried using a hydrophobic frit, and evaporated *in vacuo*. The sample was purified by chromatography on silica using a 0-25 % EtOAc-cyclohexane gradient over 10 CV. The appropriate fractions were combined and evaporated *in vacuo* to give the required product (2.50 g, 65 % yield) as a yellow solid.

^{1}H NMR (400 MHz, DMSO-d_6) δ 10.10 (s, 1H), 8.40 (s, 1H), 8.29 (s, 1H), 8.17 - 8.23 (m, 3H), 7.84 (d, *J* = 8.3 Hz, 1H), 7.23 - 7.29 (m, 1H), 7.01 - 7.05 (m, 1H), 6.98 (d, *J* = 8.3 Hz, 1H), 5.24 (s, 2H), 4.11 (s, 3H), 3.41 (s, 3H), 2.29 (s, 3H). **^{13}C NMR** (101 MHz, DMSO-d_6) δ 192.8, 157.9, 156.3, 146.4, 145.1, 139.4, 139.0, 137.6, 136.9, 133.3, 130.9, 130.5, 130.5, 126.8, 123.6, 123.3, 122.9, 118.0, 115.4, 113.8, 93.7, 55.5, 53.9, 20.4. **LCMS** (Method A) (ES +ve) *m/z* 420.4 $(M + H)^+$ Rt 1.46 min (>95 % pure). **HRMS** (ES) calcd for $C_{24}H_{22}NO_4S$, $(M + H)^+$ 420.1264, found 420.1262.

(2-(2-Methoxy-5-(4-(methoxymethoxy)-2-methylphenyl)pyridin-3-yl)benzo[*b*]thiophen-5-yl)methanol (6)

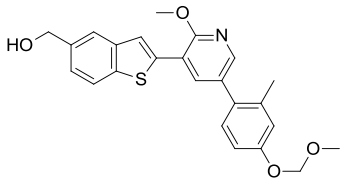

2-(2-Methoxy-5-(4-(methoxymethoxy)-2-methylphenyl)pyridin-3-yl)benzo[*b*]thiophene-5-carbaldehyde (266 mg, 0.634 mmol) was dissolved in methanol and THF (1:1 mixture, 6 mL) and cooled to 0 ºC. Sodium borohydride (52 mg, 1.4 mmol) was added and the reaction stirred at 0 ºC for 30 min. The reaction was quenched with water (6 mL), diluted with EtOAc (6 mL), and the phases separated. The aqueous layer was back-extracted with EtOAc (10 mL), then the organic layers were combined, dried using a hydrophobic frit, and evaporated *in vacuo* to give the required product (249 mg, 93 % yield) as a light brown gum.

^{1}H NMR (400 MHz, DMSO-d_6) δ 8.11 - 8.17 (m, 2H), 8.09 (s, 1H), 7.91 (d, *J* = 8.1 Hz, 1H), 7.79 (s, 1H), 7.32 (d, *J* = 8.3 Hz, 1H), 7.25 (d, *J* = 8.3 Hz, 1H), 7.03 (s, 1H), 6.97 (d, *J* = 8.3 Hz, 1H), 5.25 (t, *J* = 5.7 Hz, 1H), 5.23 (s, 2H), 4.61 (d, *J* = 5.7 Hz, 2H), 4.09 (s, 3H), 3.40 (s, 3H), 2.28 (s, 3H). **^{13}C NMR** (101 MHz, DMSO-d_6) δ 157.9, 156.3, 145.8, 139.5, 139.2, 137.8, 137.3, 137.2, 136.9, 130.9, 130.6, 130.5, 123.9, 123.3, 121.6, 121.2, 118.0, 116.1, 113.8, 93.7, 62.9, 55.5, 53.8, 20.4. **LCMS** (Method A) (ES +ve) *m/z* 422.4 $(M + H)^+$ Rt 1.30 min (>95 % pure). **HRMS** (ES) calcd for $C_{24}H_{24}NO_4S$, $(M + H)^+$ 422.1421, found 422.1421.

5-(4-Hydroxy-2-methylphenyl)-3-(5-(hydroxymethyl)benzo[*b*]thiophen-2-yl)pyridin-2(1*H*)-one (7)

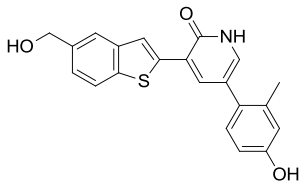

(2-(2-Methoxy-5-(4-(methoxymethoxy)-2-methylphenyl)pyridin-3-yl)benzo[*b*]thiophen-5-yl)methanol (196 mg, 0.465 mmol) was dissolved in THF (3 mL). HCl (6 M aq., 1.5 mL, 9.0 mmol) was added and the reaction stirred for 2 h. The reaction temperature was raised to 80 ºC and stirred for a further 1 h. The reaction was stopped and the solvents evaporated. The residue was dissolved in DMSO (1 mL) and purified by MDAP (formic acid modifier gradient). The solvent was dried under a stream of nitrogen to give the required product (33 mg, 19 % yield) as a yellow solid.

^{1}H NMR (400 MHz, DMSO-d_6) δ 12.22 (br. s, 1H), 9.45 (br. s, 1H), 8.18 (s, 1H), 8.09 (s, 1H), 7.86 (d, *J* = 8.3 Hz, 1H), 7.73 (s, 1H), 7.35 (s, 1H), 7.27 (d, *J* = 8.3 Hz, 1H), 7.09 (d, *J* = 8.3 Hz, 1H), 6.72 (s, 1H), 6.67 (d, *J* = 8.3 Hz, 1H), 5.22 (br. s, 1H), 4.60 (s, 2H), 2.24 (s, 3H) **^{13}C NMR** (151 MHz, DMSO-d_6) δ 159.1, 156.8, 139.1, 138.8, 138.4, 138.2, 136.6, 133.2, 130.7, 127.3, 123.4, 122.5, 121.5, 120.9, 120.8, 119.1, 117.0, 113.0, 63.0, 20.3. HMBC analysis indicated two overlapping quaternary carbons at 138.4 ppm. **LCMS** (Method A) (ES +ve) *m/z* 364.1 $(M + H)^+$ Rt 0.77 min (>95 % pure). **HRMS** (ES) calcd for $C_{21}H_{18}NO_3S$, $(M + H)^+$ 364.1002, found 364.1010. **IR** ν_{max} (neat) 3286, 3058, 3009, 2880, 1758, 1686, 1632, 1596, 1574 cm^{-1}. **MP** 268 – 270 ºC (decomposition).

1-(2-(2-Methoxy-5-(4-(methoxymethoxy)-2-methylphenyl)pyridin-3-yl)benzo[*b*]thiophen-5-yl)-2,5,8,11,14-pentaoxahexadecan-16-oic acid (8)

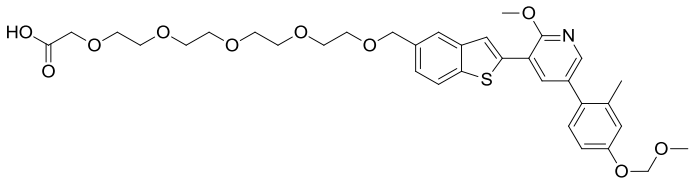

Sodium hydride (60 % w/w in mineral oil, 196 mg, 4.90 mmol) was washed twice with cyclohexane (2 x 2 mL) under nitrogen and the solvent replaced with DMF (2 mL). (2-(2-Methoxy-5-(4-(methoxymethoxy)-2-methylphenyl)pyridin-3-yl)benzo[*b*]thiophen-5-yl)methanol (512 mg, 1.22 mmol) was dissolved in DMF (3 mL), added to the reaction mixture and stirred for 5 min at rt until gas evolution ceased. *tert*-Butyl 14-(tosyloxy)-3,6,9,12-tetraoxatetradecan-1-oate (1.21 g, 2.62 mmol) was dissolved in DMF (2 mL) and added to the reaction mixture. After 3 h, further aliquots of *tert*-butyl 14-(tosyloxy)-3,6,9,12-tetraoxatetradecan-1-oate (720 mg, 1.56 mmol) and sodium hydride (60 % w/w in mineral oil, 117 mg, 2.93 mmol) were added and the reaction stirred at 90 ºC for 1 h. The reaction was quenched with MeOH (~1 mL) and the solvent evaporated *in vacuo*. The sample was loaded in DMSO and purified by reverse phase (C18) chromatography using a 10-90 % acetonitrile-water (ammonium bicarbonate modifier) gradient over 12 CV. The appropriate fractions were combined and evaporated *in vacuo* to give the acid product (520 mg, 65 % yield) as a pale yellow gum.

^{1}H NMR (400 MHz, $CDCl_3$) δ 8.08 (s, 1H), 7.90 (s, 1H), 7.87 (s, 1H), 7.78 (d, *J* = 8.3 Hz, 1H), 7.75 (s, 1H), 7.31 (d, *J* = 8.3 Hz, 1H), 7.18 (d, *J* = 8.3 Hz, 1H), 7.00 (s, 1H), 6.97 (d, *J* = 8.3 Hz, 1H), 5.22 (s, 2H), 4.66 (s, 2H), 4.15 (s, 3H), 3.98 (s, 2H), 3.56 - 3.69 (m, 16H), 3.52 (s, 3H), 2.31 (s, 3H). **^{13}C NMR** (101 MHz, $CDCl_3$) δ 174.55, 158.78, 156.79, 145.68, 140.31, 138.93, 138.55, 137.93, 137.31, 134.40, 131.32, 130.97, 130.66, 124.75, 123.44, 123.09, 121.89, 118.13, 116.92, 113.79, 94.34, 73.13, 70.26, 70.18, 70.13, 70.09, 69.99, 69.96, 69.76, 68.89, 56.00, 53.79, 20.71. Note that ^{13}C NMR data are reported to two decimal places to differentiate the signals. One carbon was not observed, however HSQC indicates a signal between δ 69.8-70.2. **LCMS** (Method A) (ES +ve) *m/z* 656.7 $(M + H)^+$ Rt 1.32 min (>95 % pure). **HRMS**

(ES) calcd for $C_{34}H_{42}NO_{10}S$, $(M + H)^+$ 656.2524, found 656.2526.

1-(2-(5-(4-Hydroxy-2-methylphenyl)-2-oxo-1,2-dihydropyridin-3-yl)benzo[*b*]thiophen-5-yl)-2,5,8,11,14-pentaoxahexadecan-16-oic acid (9)

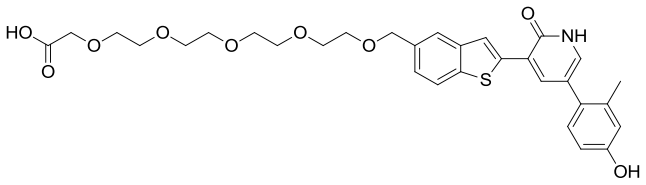

1-(2-(2-Methoxy-5-(4-(methoxymethoxy)-2-methylphenyl)pyridin-3-yl)benzo[*b*]thiophen-5-yl)-2,5,8,11,14-pentaoxahexadecan-16-oic acid (450 mg, 0.69 mmol) was dissolved in THF (7 mL), then HCl (6 M aq., 3.40 mL, 20.4 mmol) was added and the reaction stirred at 70 ºC for 6 h. The reaction was diluted with water (20 mL) and EtOAc (20 mL), then the pH adjusted to ~3 with $NaHCO_3$ (sat. aq.). The phases were separated, the aqueous phase washed with EtOAc (20 mL), then the organic layers were combined. The organic phase was back-extracted with brine (20 mL), dried using a hydrophobic frit then evaporated *in vacuo*. The sample was loaded in minimal MeOH and purified by reverse phase (C18) chromatography using a 10-90 % acetonitrile-water (+0.1 % formic acid modifier) gradient over 14 CV. The appropriate fractions were combined to give the required product (160 mg, 39 % yield, 80 % purity), which was used directly in the next reaction.

LCMS (Method A) (ES +ve) *m/z* 598.3 $(M + H)^+$ Rt 0.85 min (80 % pure).

(2*S*,4*R*)-1-((*S*)-18-(*tert*-Butyl)-1-(2-(5-(4-hydroxy-2-methylphenyl)-2-oxo-1,2-dihydropyridin-3-yl)benzo[*b*]thiophen-5-yl)-16-oxo-2,5,8,11,14-pentaoxa-17-azanonadecan-19-oyl)-4-hydroxy-*N*-(4-(4-methylthiazol-5-yl)benzyl)pyrrolidine-2-carboxamide (10a)

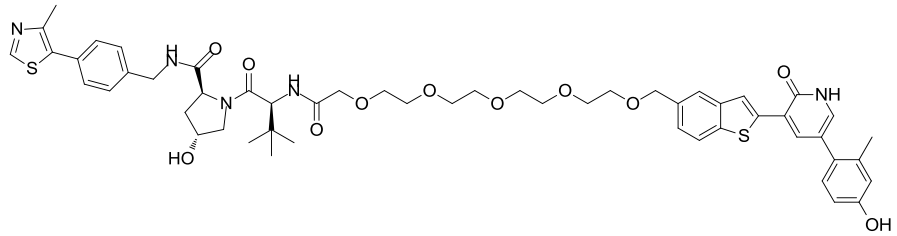

A mixture of 1-(2-(5-(4-hydroxy-2-methylphenyl)-2-oxo-1,2-dihydropyridin-3-yl)benzo[*b*]thiophen-6-yl)-2,5,8,11,14-pentaoxahexadecan-16-oic acid (71 mg, 0.12 mmol), (2*S*,4*R*)-1-((*S*)-2-amino-3,3-dimethylbutanoyl)-4-hydroxy-*N*-(4-(4-methylthiazol-5-yl)benzyl)pyrrolidine-2-carboxamide hydrochloride (71 mg, 0.15 mmol), and DIPEA (0.270 mL, 1.55 mmol) were stirred in DMF (0.8 mL). HATU (61 mg, 0.16 mmol) was added and the reaction stirred at rt for 3 h. Further aliquots of HATU (10 mg, 0.026 mmol) and DIPEA (0.10 mL, 0.57 mmol) were added and the reaction stirred for a further 2 h. The reaction mixture was then directly purified by MDAP (formic acid modifier gradient). The solvent was dried under a stream of nitrogen to give the required product (33 mg, 27 % yield) as a green oil.

^{1}H NMR (400 MHz, Methanol-d_4) δ 8.85 (s, 1H), 8.08 (s, 1H), 8.05 (s, 1H), 7.81 (d, *J* = 8.3 Hz, 1H), 7.79 (s, 1H), 7.35 - 7.46 (m, 4H), 7.30 - 7.34 (m, 2H), 7.08 (d, *J* = 8.3 Hz, 1H), 6.78 (s, 1H), 6.72 (d, *J* = 8.3 Hz, 1H), 4.41 - 4.82 (m, 6H), 4.29 - 4.38 (m, 1H), 4.00 - 4.10 (m, 2H), 3.85 - 3.93 (m, 1H), 3.77 - 3.84 (m, 1H), 3.54 - 3.75 (m, 16H), 2.44 - 2.49 (m, 3H), 2.27 (s, 3H), 2.19 - 2.25 (m, 1H), 2.05 - 2.14 (m, 1H), 1.05 (s, 9H). **^{13}C NMR** (101 MHz, Methanol-d_4) δ 174.47, 172.21, 171.81, 161.70, 158.61, 152.91, 149.13, 141.38, 141.13, 141.02, 140.33, 139.92, 138.50, 136.18, 134.00, 133.52, 132.06, 131.61, 130.46, 129.59, 129.13, 129.08, 126.00, 125.05, 124.15, 123.43, 123.11, 122.98, 118.40, 114.36, 74.34, 72.36, 71.74, 71.71, 71.69, 71.65, 71.53, 71.21, 71.18, 70.71, 60.95, 58.31, 58.22, 43.87, 39.07, 37.23, 27.13, 20.89, 16.01. Note that ^{13}C NMR data are reported to two decimal places to differentiate the signals. **LCMS** (Method B) (ES +ve) *m/z* 1010.5 $(M + H)^+$ Rt 0.97 min (>95 % pure).

HRMS (ES) calcd for $C_{53}H_{64}N_5O_{11}S_2$, $(M + H)^+$ 1010.404, found 1010.40. **IR** ν_{max} (neat) 3268, 2914, 1641, 1612, 1531, 1506, 1436 cm^{-1}.

(2*R*,4*S*)-1-((*R*)-18-(*tert*-Butyl)-1-(2-(5-(4-hydroxy-2-methylphenyl)-2-oxo-1,2-dihydropyridin-3-yl)benzo[*b*]thiophen-5-yl)-16-oxo-2,5,8,11,14-pentaoxa-17-azanonadecan-19-oyl)-4-hydroxy-*N*-(4-(4-methylthiazol-5-yl)benzyl)pyrrolidine-2-carboxamide (10b)

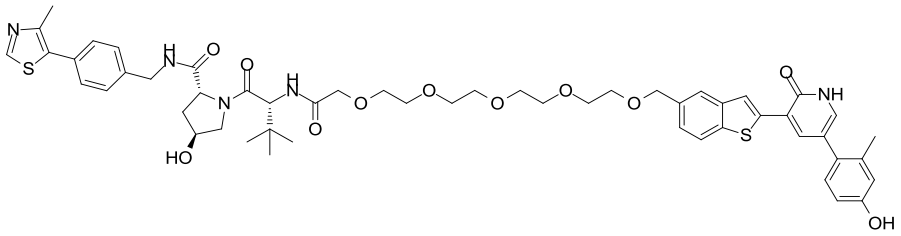

A mixture of 1-(2-(5-(4-hydroxy-2-methylphenyl)-2-oxo-1,2-dihydropyridin-3-yl)benzo[*b*]thiophen-6-yl)-2,5,8,11,14-pentaoxahexadecan-16-oic acid (71 mg, 0.12 mmol), (2*R*,4*S*)-1-((*R*)-2-amino-3,3-dimethylbutanoyl)-4-hydroxy-*N*-(4-(4-methylthiazol-5-yl)benzyl)pyrrolidine-2-carboxamide hydrochloride (74 mg, 0.16 mmol), and DIPEA (0.270 mL, 1.55 mmol) were stirred at rt in DMF (0.8 mL). HATU (63 mg, 0.17 mmol) was added and the reaction stirred at rt for 3 h. Further aliquots of HATU (10 mg, 0.026 mmol) and DIPEA (0.10 mL, 0.57 mmol) were added and the reaction stirred for a further 2 h. The reaction mixture was then directly purified by MDAP (formic acid modifier gradient). The solvent was removed under a stream of nitrogen to give the required product (37 mg, 31 % yield) as a green oil.

^{1}H NMR (400 MHz, Methanol-d_4) δ 8.85 (s, 1H), 8.09 (s, 1H), 8.05 (s, 1H), 7.82 (d, *J* = 8.3 Hz, 1H), 7.79 (s, 1H), 7.36 - 7.46 (m, 4H), 7.30 - 7.35 (m, 2H), 7.08 (d, *J* = 8.3 Hz, 1H), 6.77 (s, 1H), 6.72 (d, *J* = 8.3 Hz, 1H), 4.42 - 4.81 (m, 6H), 4.29 - 4.38 (m, 1H), 3.96 - 4.08 (m, 2H), 3.85 - 3.93 (m, 1H), 3.77 - 3.84 (m, 1H), 3.59 – 3.72 (m, 16H), 2.46 (s, 3H), 2.27 (s, 3H), 2.19 - 2.26 (m, 1H), 2.05 - 2.15 (m, 1H), 1.05 (s, 9H). **^{13}C NMR** (101 MHz, Methanol-d_4) δ 172.92, 170.67, 170.26, 160.17, 157.07, 151.37, 147.60, 139.85, 139.60, 139.48, 138.78, 138.38, 136.96, 134.64, 132.46, 131.97, 130.51, 130.06, 128.93, 128.05, 127.60, 127.53, 124.47, 123.52, 122.62, 121.89, 121.58, 121.44, 116.85, 112.81, 111.99, 72.80, 70.83, 70.20, 70.17, 70.11, 70.00,

69.67, 69.64, 69.17, 59.41, 56.76, 56.67, 42.32, 37.52, 35.69, 25.58, 19.34, 14.46. Note that ^{13}C NMR data are reported to two decimal places to differentiate the signals. **LCMS** (Method B) (ES +ve) *m/z* 1010.5 $(M + H)^+$ Rt 0.97 min (>95 % pure). **HRMS** (ES) calcd for $C_{53}H_{64}N_5O_{11}S_2$, $(M + H)^+$ 1010.4044, found 1010.40. **IR** ν_{max} (neat) 3267, 2871, 1642, 1612, 1505, 1436 cm^{-1}.

3-(5-(13-Chloro-2,5,8,11-tetraoxatridecyl)benzo[*b*]thiophen-2-yl)-2-methoxy-5-(4-(methoxymethoxy)-2-methylphenyl)pyridine (11)

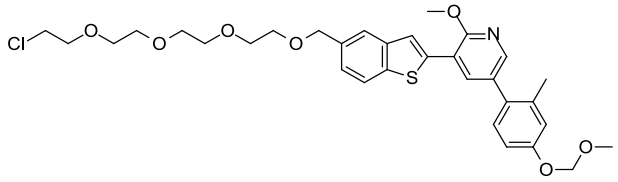

Sodium hydride (60 % w/w in mineral oil, 170 mg, 4.25 mmol) was washed twice with cyclohexane (2 x 10 mL) and the solvent replaced with DMF (5 mL). (2-(2-Methoxy-5-(4-(methoxymethoxy)-2-methylphenyl)pyridin-3-yl)benzo[*b*]thiophen-5-yl)methanol (422 mg, 1.00 mmol) was dissolved in DMF (5 mL) and added to the reaction mixture and left to stir for 5 min. 1-Chloro-2-(2-(2-(2-chloroethoxy)ethoxy)ethoxy)ethane (1.20 mL, 6.01 mmol) was added and the reaction stirred at rt for 1 h. A further aliquot of 1-chloro-2-(2-(2-(2-chloroethoxy)ethoxy)ethoxy)ethane (1.00 mL, 5.00 mmol) was added and the reaction stirred for a further 3 h. The reaction was diluted with water (10 mL) and EtOAc (10 mL) and the phases separated. The aqueous layer was back-extracted with EtOAc (10 mL) and the organic layers were combined, dried using a hydrophobic frit, and evaporated *in vacuo*. The sample was purified by chromatography on silica using a 0-50 % EtOAc-cyclohexane gradient over 40 min. The appropriate fractions were combined and evaporated *in vacuo* to give the required product (375 mg, 61 % yield) as a pale yellow oil.

^{1}H NMR (400 MHz, DMSO-d_6) δ 8.11 - 8.17 (m, 2H), 8.10 (s, 1H), 7.95 (d, *J* = 8.3 Hz, 1H), 7.81 (s, 1H), 7.33 (d, *J* = 8.3 Hz, 1H), 7.23 - 7.27 (m, 1H), 7.02 (s, 1H), 6.97 (d, *J* = 8.3 Hz, 1H), 5.23 (s, 2H), 4.61 (s, 2H), 4.09 (s, 3H), 3.62 - 3.70 (m, 4H), 3.52 - 3.60 (m, 12H), 3.40 (s, 3H), 2.28 (s, 3H). **^{13}C NMR** (101 MHz, DMSO-d_6) δ 157.92,

156.33, 145.89, 139.51, 138.45, 137.45, 137.38, 136.84, 135.07, 130.94, 130.60, 130.47, 124.63, 123.26, 122.50, 121.88, 118.01, 116.02, 113.80, 93.71, 72.01, 70.50, 69.82, 69.80, 69.78, 69.75, 69.65, 69.06, 55.51, 53.82, 43.51, 20.36. Note that ^{13}C NMR data are reported to two decimal places to differentiate the signals. **LCMS** (Method A) (ES +ve) *m/z* 616.6/618.6 $(M + H)^+$ Rt 1.50 min (>95 % pure). **HRMS** (ES) calcd for $C_{32}H_{39}ClNO_7S$, $(M + H)^+$ 616.2130, found 616.2130.

(2*S*,4*R*)-4-Hydroxy-*N*-(2-((1-(2-(2-methoxy-5-(4-(methoxymethoxy)-2-methylphenyl)pyridin-3-yl)benzo[*b*]thiophen-5-yl)-2,5,8,11-tetraoxatridecan-13-yl)oxy)-4-(4-methylthiazol-5-yl)benzyl)-1-((*S*)-3-methyl-2-(1-oxoisoindolin-2-yl)butanoyl)pyrrolidine-2-carboxamide (12a)

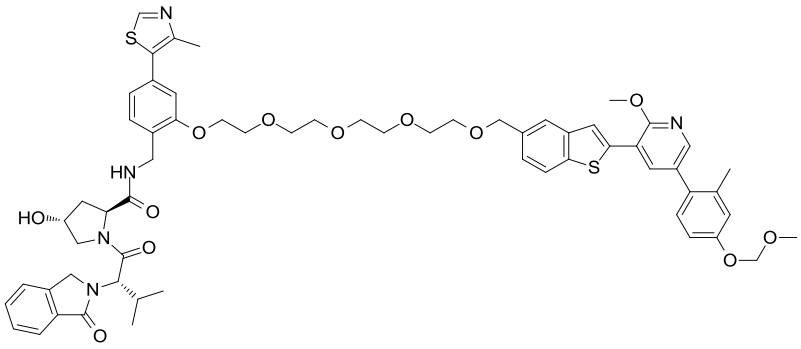

3-(5-(13-Chloro-2,5,8,11-tetraoxatridecyl)benzo[*b*]thiophen-2-yl)-2-methoxy-5-(4-(methoxymethoxy)-2-methylphenyl)pyridine (136 mg, 0.221 mmol), (2*S*,4*R*)-4-hydroxy-*N*-(2-hydroxy-4-(4-methylthiazol-5-yl)benzyl)-1-((*S*)-3-methyl-2-(1-oxoisoindolin-2-yl)butanoyl)pyrrolidine-2-carboxamide (83 mg, 0.15 mmol) and potassium carbonate (65 mg, 0.47 mmol) were dissolved in NMP (0.7 mL) and stirred at 120 ºC for 4 days. The reaction mixture was purified directly by MDAP (ammonium bicarbonate modifier gradient). The solvent was removed under a stream of nitrogen to give the required product which was impure by LCMS. The crude material was used directly in the next reaction (22 mg, 13 % yield).

LCMS (Method B) (ES +ve) *m/z* 1128.6 $(M + H)^+$ Rt 1.43 min (66 % pure).

(2*R*,4*S*)-4-Hydroxy-*N*-(2-((1-(2-(2-methoxy-5-(4-(methoxymethoxy)-2-methylphenyl)pyridin-3-yl)benzo[*b*]thiophen-5-yl)-2,5,8,11-tetraoxatridecan-13-yl)oxy)-4-(4-methylthiazol-5-yl)benzyl)-1-((*R*)-3-methyl-2-(1-oxoisoindolin-2-yl)butanoyl)pyrrolidine-2-carboxamide (12b)

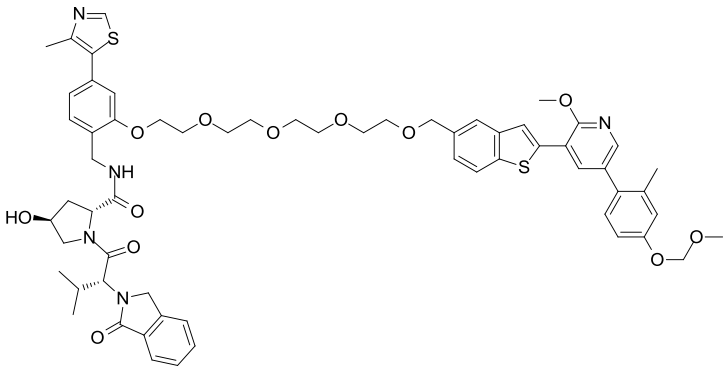

3-(5-(13-Chloro-2,5,8,11-tetraoxatridecyl)benzo[*b*]thiophen-2-yl)-2-methoxy-5-(4-(methoxymethoxy)-2-methylphenyl)pyridine (143 mg, 0.232 mmol) in NMP (1 mL) was added to (2*R*,4*S*)-4-hydroxy-*N*-(2-hydroxy-4-(4-methylthiazol-5-yl)benzyl)-1-((*R*)-3-methyl-2-(1-oxoisoindolin-2-yl)butanoyl)pyrrolidine-2-carboxamide (106 mg, 0.193 mmol) and potassium carbonate (80 mg, 0.58 mmol). The reaction was stirred at 90 ºC for 3 days. The reaction mixture was purified directly by MDAP (ammonium bicarbonate modifier gradient). The solvent was dried under a stream of nitrogen to give the required product (48 mg, 22 % yield) as a yellow oil.

^{1}H NMR (400 MHz, Methanol-d_4) δ 8.85 (s, 1H), 8.06 (s, 1H), 7.96 (s, 1H), 7.92 (s, 1H), 7.76 - 7.88 (m, 3H), 7.46 - 7.67 (m, 3H), 7.30 - 7.43 (m, 2H), 7.19 (d, *J* = 8.3 Hz, 1H), 6.94 - 7.06 (m, 4H), 5.24 (s, 2H), 4.37 - 4.73 (m, 8H), 4.08 - 4.20 (m, 5H), 3.95 - 4.03 (m, 1H), 3.81 - 3.93 (m, 3H), 3.59 - 3.77 (m, 16H), 3.51 (s, 3H), 2.47 (s, 3H), 2.30 (s, 3H), 0.80 - 1.08 (m, 6H). **^{13}C NMR** (101 MHz, Methanol-d_4) δ 172.59, 169.48, 169.15, 168.89, 158.58, 157.00, 156.67, 151.35, 147.70, 145.44, 142.35, 140.19, 139.00, 138.11, 137.57, 136.92, 134.82, 132.03, 131.77, 131.53, 131.07, 131.00, 130.92, 130.60, 128.74, 127.74, 126.89, 124.53, 123.23, 122.98, 122.94, 122.72, 121.40, 117.88, 116.77, 113.61, 112.33, 94.05, 72.70, 70.40, 70.21, 70.20, 70.17, 69.43, 69.35, 69.19, 67.91, 59.23, 58.68, 55.71, 54.83, 52.94, 48.45, 38.13, 37.67, 28.76, 19.51, 18.29, 17.62, 14.58. Note that ^{13}C NMR data are reported to two decimal

places to differentiate the signals. **LCMS** (Method A) (ES +ve) *m/z* 1128.5 $(M + H)^+$ Rt 1.43 min (>95 % pure). **HRMS** (ES) calcd for $C_{61}H_{70}N_5O_{12}S_2$, $(M + H)^+$ 1128.438, found 1128.440.

(2*S*,4*R*)-4-Hydroxy-*N*-(2-((1-(2-(5-(4-hydroxy-2-methylphenyl)-2-oxo-1,2-dihydropyridin-3-yl)benzo[*b*]thiophen-5-yl)-2,5,8,11-tetraoxatridecan-13-yl)oxy)-4-(4-methylthiazol-5-yl)benzyl)-1-((*S*)-3-methyl-2-(1-oxoisoindolin-2-yl)butanoyl)pyrrolidine-2-carboxamide (13a)

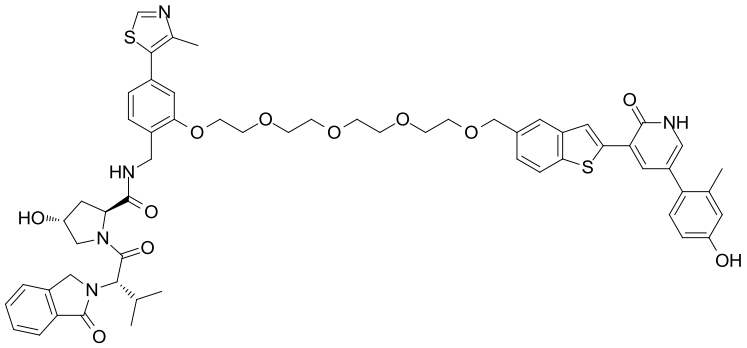

To a stirred solution of (2*S*,4*R*)-4-hydroxy-*N*-(2-((1-(2-(2-methoxy-5-(4-(methoxymethoxy)-2-methylphenyl)pyridin-3-yl)benzo[*b*]thiophen-5-yl)-2,5,8,11-tetraoxatridecan-13-yl)oxy)-4-(4-methylthiazol-5-yl)benzyl)-1-((*S*)-3-methyl-2-(1-oxoisoindolin-2-yl)butanoyl)pyrrolidine-2-carboxamide (73 mg, 0.057 mmol) in DMF (1.2 mL) was added HCl (4 M in dioxane, 0.5 mL, 2 mmol) and the reaction stirred at 50 ºC for 5 h. The solution was concentrated under nitrogen then purified directly by MDAP (ammonium bicarbonate modifier gradient) The solvent was dried under a stream of nitrogen to give the required product (38 mg, 63 % yield) as a yellow solid.

^{1}H NMR (600 MHz, Methanol-d_4) δ 8.82 (s, 1H), 8.04 (s, 1H), 8.00 (s, 1H), 7.77 - 7.78 (m, 1H), 7.75 - 7.77 (m, 2H), 7.56 - 7.61 (m, 1H), 7.50 - 7.53 (m, 1H), 7.45 - 7.50 (m, 1H), 7.37 (d, *J* = 7.7 Hz, 1H), 7.28 - 7.31 (m, 2H), 7.05 (d, *J* = 8.4 Hz, 1H), 6.97 (d, *J* = 7.7 Hz, 1H), 6.95 (s, 1H), 6.75 (s, 1H), 6.69 (d, *J* = 8.1 Hz, 1H), 4.52 - 4.64 (m, 4H), 4.37 - 4.49 (m, 4H), 4.09 - 4.14 (m, 2H), 3.94 - 3.99 (m, 1H), 3.82 - 3.88 (m, 3H), 3.57 - 3.71 (m, 14H), 2.45 (s, 3H), 2.25 (s, 3H), 2.15 - 2.21 (m, 1H), 2.01 - 2.07 (m, 1H), 0.78 - 1.05 (m, 6H). **^{13}C NMR** (151 MHz, Methanol-d_4) δ 174.22, 171.09, 170.75, 161.74, 158.65, 158.23, 152.91, 149.28, 143.95, 141.42, 141.15, 140.98, 139.91,

138.51, 136.26, 133.96, 133.63, 133.34, 133.08, 132.66, 132.06, 130.24, 129.30, 129.17, 128.45, 126.01, 125.10, 124.54, 124.51, 124.15, 123.47, 123.16, 122.95, 122.92, 118.41, 114.37, 113.89, 74.32, 71.97, 71.80, 71.79, 71.74, 71.02, 70.92, 70.75, 69.47, 60.82, 60.27, 57.27, 49.72, 39.68, 39.25, 30.33, 20.86, 19.84, 19.16, 16.11. Note that ^{13}C NMR data are reported to two decimal places to differentiate the signals. **LCMS** (Method B) (ES +ve) *m/z* 1070.3 $(M + H)^+$ Rt 1.04 min (>95 % pure). **HRMS** (ES) calcd for $C_{58}H_{64}N_5O_{11}S_2$, $(M + H)^+$ 1070.397, found 1070.401.

(2*R*,4*S*)-4-Hydroxy-*N*-(2-((1-(2-(5-(4-hydroxy-2-methylphenyl)-2-oxo-1,2-dihydropyridin-3-yl)benzo[*b*]thiophen-5-yl)-2,5,8,11-tetraoxatridecan-13-yl)oxy)-4-(4-methylthiazol-5-yl)benzyl)-1-((*R*)-3-methyl-2-(1-oxoisoindolin-2-yl)butanoyl)pyrrolidine-2-carboxamide (13b)

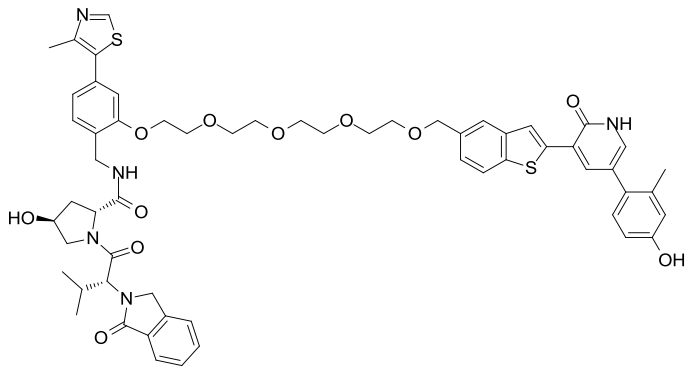

To a stirred solution of (2*R*,4*S*)-4-hydroxy-*N*-(2-((1-(2-(2-methoxy-5-(4-(methoxymethoxy)-2-methylphenyl)pyridin-3-yl)benzo[*b*]thiophen-5-yl)-2,5,8,11-tetraoxatridecan-13-yl)oxy)-4-(4-methylthiazol-5-yl)benzyl)-1-((*R*)-3-methyl-2-(1-oxoisoindolin-2-yl)butanoyl)pyrrolidine-2-carboxamide (47 mg, 0.042 mmol) in DMF (1.2 mL) was added HCl (4 M in dioxane, 0.5 mL, 2 mmol) and the reaction stirred at 50 ºC for 5 h. The solution was concentrated under a stream of nitrogen and then purified directly by MDAP (ammonium bicarbonate modifier gradient). The solvent was dried under a stream of nitrogen to give the required product (26 mg, 58 % yield) as a yellow solid.

^{1}H NMR (400 MHz, Methanol-d_4) δ 8.81 (s, 1H), 8.02 (s, 1H), 7.97 (s, 1H), 7.72 - 7.78 (m, 3H), 7.54 - 7.59 (m, 1H), 7.43 - 7.53 (m, 2H), 7.36 (d, *J* = 7.6 Hz, 1H), 7.24 - 7.30 (m, 2H), 7.03 (d, *J* = 8.3 Hz, 1H), 6.93 (s, 2H), 6.74 (s, 1H), 6.68 (d, *J* = 8.3 Hz,

1H), 4.52 - 4.63 (m, 4H), 4.36 - 4.49 (m, 4H), 4.06 - 4.13 (m, 2H), 3.94 - 4.00 (m, 1H), 3.78 - 3.89 (m, 3H), 3.54 - 3.71 (m, 14H), 2.43 (s, 3H), 2.23 (s, 3H), 2.13 - 2.20 (m, 1H), 2.03 (s, 1H), 0.77 - 1.05 (m, 6H). **^{13}C NMR** (101 MHz, Methanol-d_4) δ 174.21, 171.05, 170.73, 161.68, 158.62, 158.18, 152.91, 149.23, 143.92, 141.37, 141.09, 140.95, 139.89, 138.49, 136.21, 133.97, 133.61, 133.33, 133.03, 132.63, 132.05, 130.19, 129.29, 129.13, 128.41, 125.98, 125.04, 124.53, 124.50, 124.13, 123.43, 123.08, 122.95, 122.89, 118.41, 114.37, 113.82, 74.29, 71.94, 71.76, 71.71, 71.01, 70.89, 70.72, 69.42, 60.80, 60.24, 57.28, 50.00, 39.67, 39.26, 30.32, 20.89, 19.84, 19.17, 16.13. Note that ^{13}C NMR data are reported to two decimal places to differentiate the signals. Two coincident peaks at 71.76 ppm were resolved with more scans. **LCMS** (Method B) (ES +ve) *m/z* 1070.4 $(M + H)^+$ Rt 1.03 min (>95 % pure). **HRMS** (ES) calcd for $C_{58}H_{64}N_5O_{11}S_2$, $(M + H)^+$ 1070.397, found 1070.400. **IR** ν_{max} (neat) 3336, 3052, 2949, 1643, 1559, 1473, 1409 cm^{-1}.

7.2.2 TR Compounds

4-Bromo-2-isopropylphenol (14)

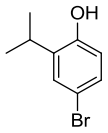

To a 250 mL flask connected to a nitrogen inlet and a sodium hydroxide trap was added 2-isopropylphenol (1.00 mL, 7.43 mmol) and CH_2Cl_2 (70 mL). Bromine (0.483 mL, 9.38 mmol) was then added dropwise over 1 h. The reaction vessel was purged with nitrogen to remove remaining HBr, then the mixture concentrated *in vacuo*. The sample was purified by chromatography on silica using a 0-100 % EtOAc-cyclohexane gradient over 60 min. The appropriate fractions were combined and evaporated *in vacuo* to give the required product (1.09 g, 68 % yield) as a pale brown oil.

^{1}H NMR (400 MHz, $CDCl_3$) δ 7.29 (s, 1H), 7.17 (d, *J* = 8.6 Hz, 1H), 6.64 (d, *J* = 8.6 Hz, 1H), 4.69 (s, 1H), 3.17 (spt, *J* = 6.9 Hz, 1H), 1.25 (d, *J* = 6.8 Hz, 6H). **LCMS** (Method A) (ES -ve) *m/z* 213.0/215.0 $(M - H)^-$ Rt 1.15 min (>95 % pure).

Consistent with literature data.[400]

4-Bromo-2-isopropyl-1-(methoxymethoxy)benzene (15)

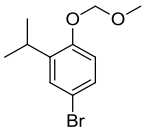

To a solution of sodium hydride (60 % w/w in mineral oil, 0.387 g, 9.68 mmol) was added to DMF (20 mL). 4-Bromo-2-isopropylphenol (0.886 g, 4.12 mmol) was then added and stirred until gas evolution ceased. Chloromethyl methyl ether (0.344 mL, 4.53 mmol) was added dropwise and the reaction stirred at rt for 10 min. The reaction was diluted with ether (40 mL) and water (40 mL). The phases were separated and the organic layer washed with brine (3 x 100 mL). The organic layer was dried using a hydrophobic frit, and evaporated *in vacuo*. The sample was purified by chromatography on silica using a 0-50 % EtOAc-cyclohexane gradient over 20 min.

The appropriate fractions were combined and evaporated *in vacuo* to give the required product (0.682 g, 64 % yield) as a colourless oil.

^{1}H NMR (400 MHz, $CDCl_3$) δ 7.31 (s, 1H), 7.23 (d, *J* = 8.8 Hz, 1H), 6.95 (d, *J* = 8.8 Hz, 1H), 5.18 (s, 2H), 3.49 (s, 3H), 3.31 (spt, *J* = 6.9 Hz, 1H), 1.22 (d, *J* = 6.8 Hz, 6H). **LCMS** (Method A) Rt 1.36 min (>95 % pure). Sample does not ionise by ES.

Consistent with literature data.[235]

(4-Bromo-3,5-dimethylphenoxy)triisopropylsilane (16)

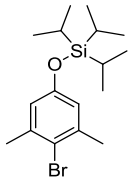

A solution of 4-bromo-3,5-dimethylphenol (501 mg, 2.49 mmol), triisopropylsilyl chloride (0.554 mL, 2.62 mmol), and imidazole (0.427 g, 6.27 mmol) in CH_2Cl_2 (5 mL) was stirred at rt for 16 h. The reaction was diluted with CH_2Cl_2 (10 mL), brine (10 mL), and water (10 mL) and the phases separated. The organic layer was dried using a hydrophobic frit, and evaporated *in vacuo*. The sample was purified by chromatography on silica using a 0-100 % EtOAc-cyclohexane gradient over 20 min. The appropriate fractions were combined and evaporated *in vacuo* to give the required product (848 mg, 95 % yield) as a colourless oil.

^{1}H NMR (400 MHz, $CDCl_3$) δ 6.62 (s, 2H), 2.35 (s, 6H), 1.19 - 1.30 (m, 3H), 1.11 (d, *J* = 7.3 Hz, 18H). **LCMS** (Method A) Rt 1.88 min (>95 % pure). Sample does not ionise by ES.

Consistent with literature data.[235]

2,6-Dimethyl-4-((triisopropylsilyl)oxy)benzaldehyde (17)

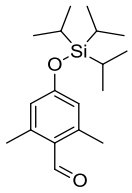

To a stirred solution of (4-bromo-3,5-dimethylphenoxy)triisopropylsilane (833 mg, 2.33 mmol) in THF (10 mL) at -78 ºC was added *n*-BuLi (2.5 M in hexanes, 1.12 mL, 2.80 mmol). The reaction mixture was stirred for 20 min at -78 ºC, then DMF (0.39 mL, 5.04 mmol) was added. The reaction was stirred at -78 ºC for 1 h and at rt for 30 min. The reaction was diluted with TBME (20 mL) and the organic phase washed with water (50 mL), acidified with HCl (1 M aq., 50 mL), and washed with brine (50 mL). The organic layer was dried using a hydrophobic frit, and evaporated *in vacuo*. The sample was purified by chromatography on silica using a 0-50 % EtOAc-cyclohexane gradient over 20 min. The appropriate fractions were combined and evaporated *in vacuo* to give the required product (527 mg, 74 % yield) as a colourless oil.

^{1}H NMR (400 MHz, $CDCl_3$) δ 10.48 (s, 1H), 6.57 (s, 2H), 2.58 (s, 6H), 1.23 - 1.35 (m, 3H), 1.12 (d, *J* = 6.8 Hz, 18H). **LCMS** (Method A) (ES +ve) *m/z* 307.2 $(M + H)^+$ Rt 1.72 min (>95 % pure).

Consistent with literature data.[235]

(2,6-Dimethyl-4-((triisopropylsilyl)oxy)phenyl)(3-isopropyl-4-methoxymethoxy)phenyl) methanol (18)

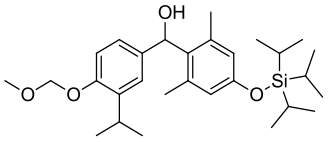

To a stirred solution of 4-bromo-2-isopropyl-1-(methoxymethoxy)benzene (8.99 g, 34.7 mmol) in THF (100 mL) at -78 ºC was added *n*-BuLi (2.5 M in hexanes, 27.8 mL, 69.4 mmol) and the mixture stirred for 30 min. A solution of 2,6-dimethyl-4-((triisopropylsilyl)oxy)benzaldehyde (11.7 g, 38.2 mmol) in THF (100 mL) was then

added and the reaction stirred at -78 ºC for 1 h, then at rt for 4 h. The reaction was diluted with EtOAc (200 mL) and water (200 mL) and the phases separated. The organic phase was washed with brine (2 x 200 mL), dried using a hydrophobic frit, and evaporated *in vacuo*. The sample was purified by chromatography on silica using a 0-10 % EtOAc-cyclohexane gradient over 14 CV. The appropriate fractions were combined and evaporated *in vacuo* to give the required product (10.4 g, 62 % yield) as a pale yellow oil.

^{1}H NMR (400 MHz, $CDCl_3$) δ 7.16 (s, 1H), 6.90 - 6.99 (m, 2H), 6.57 (s, 2H), 6.23 (s, 1H), 5.19 (s, 2H), 3.49 (s, 3H), 3.32 (spt, *J* = 6.9 Hz, 1H), 2.21 (s, 6H), 1.21 - 1.32 (m, 3H), 1.15 - 1.20 (m, 6H), 1.12 (d, *J* = 6.9 Hz, 18H). **LCMS** (Method B) (ES -ve) *m/z* 485.5 $(M - H)^-$ Rt 1.80 min (>95 % pure).

Consistent with literature data.[235]

Triisopropyl(4-(3-isopropyl-4-(methoxymethoxy)benzyl)-3,5-dimethylphenoxy)silane (19)

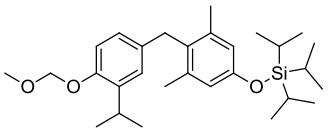

A solution of (2,6-dimethyl-4-((triisopropylsilyl)oxy)phenyl)(3-isopropyl-4-(methoxymethoxy)phenyl)methanol (5.48 g, 11.3 mmol) and 10 % Pd/C (0.350 g, 3.29 mmol) in ethanol (30 mL) and acetic acid (2.7 mL) was stirred under an atmosphere of hydrogen at rt for 24 h. The solution was filtered through a Celite pad, diluted with EtOAc (200 mL), and washed with sat. $NaHCO_3$ (3 x 50 mL). The organic layer was dried using a hydrophobic frit, and evaporated *in vacuo* to give the required product (4.97 g, 94 % yield).

^{1}H NMR (400 MHz, $CDCl_3$) δ 6.86 - 6.93 (m, 2H), 6.69 (d, *J* = 8.3 Hz, 1H), 6.60 (s, 2H), 5.16 (s, 2H), 3.91 (s, 2H), 3.48 (s, 3H), 3.28 (spt, *J* = 6.9 Hz, 1H), 2.18 (s, 6H), 1.22 - 1.32 (m, 3H), 1.16 (d, *J* = 6.8 Hz, 6H), 1.12 (d, *J* = 6.9 Hz, 18H). **LCMS** Not visible using Method A or B, however >95 % pure by NMR.

Consistent with literature data.[235]

4-(3-Iodo-5-isopropyl-4-(methoxymethoxy)benzyl)-3,5-dimethylphenol (20)

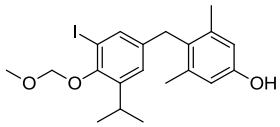

To a stirred solution of triisopropyl(4-(3-isopropyl-4-(methoxymethoxy)benzyl)-3,5-dimethylphenoxy)silane (4.97 g, 10.6 mmol) in THF (80 mL) and cyclohexane (40 mL) at -78 ºC was added *n*-BuLi (1.6 M in hexanes, 15 mL, 24 mmol), then the mixture warmed to rt. After 1.5 h, the mixture was cooled to -78 ºC then *N*-iodosuccinimide (3.56 g, 15.84 mmol) was added as a solution in THF (15 mL). The mixture was warmed to rt and stirred for an additional 6 h. The solution was diluted with EtOAc (150 mL) and water (150 mL) and the phases separated. The organic layer was washed with $Na_2S_2O_3$ (1 M aq., 3 x 150 mL), then the organic layer dried using a hydrophobic frit, and evaporated *in vacuo*.

The sample was dissolved in THF (15 mL), then TBAF (1 M in THF, 15 mL, 15 mmol) was added and the mixture stirred at rt for 1 h. The mixture was diluted with EtOAc (25 mL), then washed with water (2 x 25 mL) and brine (2 x 25 mL), then the organic phase dried using a hydrophobic frit, and evaporated *in vacuo* to give the required product (2.18 g, 23 % yield, 50 % pure) as a 1:1 mixture with TIPS-deprotected starting material. The sample was used directly in the next reactions.

LCMS (Method B) (ES -ve) *m/z* 439.3 $(M - H)^-$ Rt 1.44 min (50 % pure).

The yield of this reaction is correlated to the amount of required product in the impure sample.

4-(3-Isopropyl-4-(methoxymethoxy)-5-((4-methoxyphenyl)ethynyl)benzyl)-3,5-dimethylphenol (21)

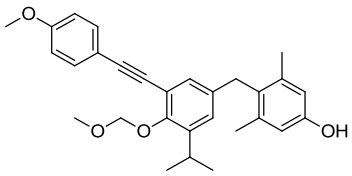

To a stirred solution of 1-ethynyl-4-methoxybenzene (16.0 µL, 0.16 mmol) in THF (1 mL) at -78 ºC was added LiHMDS (1 M in hexanes, 180 µL, 0.18 mmol) and the solution stirred for 30 min. 9-Methoxy-BBN (1 M in hexanes, 170 µL, 0.17 mmol) was added and the mixture stirred for a further 30 min. The mixture was then added to a solution of 4-(3-iodo-5-isopropyl-4-(methoxymethoxy)benzyl)-3,5-dimethylphenol (50 % pure, 60 mg, 0.082 mmol) and bis(triphenylphosphine)palladium(II) chloride (14 mg, 0.020 mmol) in THF (1 mL) and the reaction stirred at 50 ºC for 24 h. The mixture was diluted with EtOAc (5 mL) and water (5 mL) and the phases separated, then the aqueous layer was back-extracted with EtOAc (5 mL). The organic layers were pooled, washed with brine (10 mL), dried using a hydrophobic frit, filtered through a Celite pad, and evaporated *in vacuo*. The sample was dissolved in DMSO and purified by MDAP (ammonium bicarbonate modifier gradient). The solvent was evaporated *in vacuo* to give the required product (21 mg, 51 % yield, 90 % pure) as an orange oil.

^{1}H NMR (400 MHz, $CDCl_3$) δ 7.41 - 7.46 (m, 2H), 6.93 - 6.98 (m, 1H), 6.83 - 6.90 (m, 3H), 6.58 (s, 2H), 5.27 (s, 2H), 3.91 (s, 2H), 3.83 (s, 3H), 3.62 (s, 3H), 3.43 (spt, *J* = 6.8 Hz, 1H), 2.20 (s, 6H), 1.19 (d, *J* = 6.8 Hz, 6H). **LCMS** (Method B) (ES +ve) m/z 445.3 $(M + H)^+$ Rt 1.54 min (90 % pure).

***tert*-Butyl 14-(4-iodophenoxy)-3,6,9,12-tetraoxatetradecan-1-oate (22)**

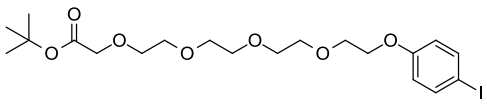

tert-Butyl 14-(tosyloxy)-3,6,9,12-tetraoxatetradecan-1-oate (4.05 g, 8.76 mmol), 4-iodophenol (2.12 g, 9.63 mmol) and cesium carbonate (5.89 g, 18.1 mmol) were

dissolved in DMF (40 mL) and stirred at rt for 24 h. The mixture was diluted with water (50 mL) and EtOAc (50 mL) and the phases separated. The aqueous layer was back-extracted with EtOAc (50 mL), then the organic layers were pooled, washed with LiCl (5 % aq., 3 x 100 mL), dried using a hydrophobic frit, and evaporated *in vacuo*. The sample purified by chromatography on silica using a 0-50 % EtOAc-cyclohexane gradient over 40 min. The appropriate fractions were combined and evaporated *in vacuo* to give the required product (4.06 g, 91 % yield) as a pale yellow oil.

^{1}H NMR (400 MHz, DMSO-d_6) δ 7.58 (d, J = 8.8 Hz, 2H), 6.80 (d, J = 8.8 Hz, 2H), 4.03 - 4.09 (m, 2H), 3.97 (s, 2H), 3.69 - 3.75 (m, 2H), 3.47 - 3.60 (m, 12H), 1.41 (s, 9H). **^{13}C NMR** (101 MHz, DMSO-d_6) δ 169.80, 158.85, 138.40, 117.77, 83.57, 81.08, 70.38, 70.33, 70.25, 70.19, 70.16, 69.26, 68.58, 67.75, 28.24. Note that ^{13}C NMR data are reported to two decimal places to differentiate the signals. One signal not resolved potentially due to overlapping frequencies of PEG chain carbons. **LCMS** (Method B) (ES +ve) *m/z* 528.2 $(M + NH_4)^+$ Rt 1.30 min (>95 % pure).

14-(4-Iodophenoxy)-3,6,9,12-tetraoxatetradecan-1-oic acid (23)

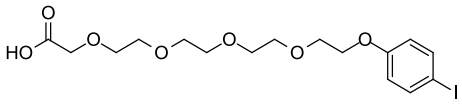

To a solution of *tert*-butyl 14-(4-iodophenoxy)-3,6,9,12-tetraoxatetradecan-1-oate (1.31 g, 2.57 mmol) in 1,4-dioxane (10 mL) was added HCl (4 M in dioxane, 6.5 mL, 26 mmol) and the reaction stirred at 50 ºC for 24 h. The mixture was diluted with CH_2Cl_2 (20 mL) and water (20 mL) and the phases separated. The organic layer was dried using a hydrophobic frit, and evaporated *in vacuo* to give the required product (979 mg, 84 % yield) as a white oil.

^{1}H NMR (400 MHz, $CDCl_3$) δ 7.52 - 7.57 (m, J = 9.0 Hz, 2H), 6.68 - 6.73 (m, J = 9.0 Hz, 2H), 4.14 (s, 2H), 4.08 - 4.12 (m, 2H), 3.83 - 3.89 (m, 2H), 3.64 - 3.77 (m, 12H). **^{13}C NMR** (101 MHz, $CDCl_3$) δ 171.8, 158.6, 138.2, 117.1, 82.9, 71.5, 70.9, 70.7, 70.4, 70.3, 70.2, 69.6, 69.1, 67.4. **LCMS** (Method B) (ES +ve) *m/z* 472.2 $(M + NH_4)^+$ Rt 0.76 min (>95 % pure).

***tert*-Butyl 2-(4-(3-ethynyl-5-isopropyl-4-(methoxymethoxy)benzyl)-3,5-dimethylphenoxy)acetate (24)**

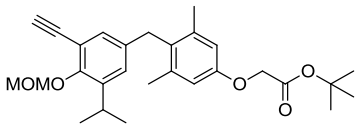

To a stirred solution of ethynyltrimethylsilane (0.235 mL, 1.65 mmol) in THF (5 mL) at -78 ºC was added LiHMDS (1 M in hexanes, 2.07 mL, 2.07 mmol) and the mixture stirred for 30 min. 9-Methoxy-BBN (1 M in hexanes, 1.74 mL, 1.74 mmol) was then added and stirred for a further 1 h at -78 ºC. The solution was added to a mixture of 4-(3-iodo-5-isopropyl-4-(methoxymethoxy)benzyl)-3,5-dimethylphenol (607 mg, 0.827 mmol, 60 % pure) and bis(triphenylphosphine)palladium(II) chloride (145 mg, 0.207 mmol) in THF (5 mL) and the mixture stirred at reflux for 22 h. The mixture was diluted with EtOAc (10 mL) then washed with water (20 mL) and brine (20 mL). The organic layer was filtered through Celite, dried using a hydrophobic frit, and evaporated *in vacuo*.

LCMS (Method B) (ES +ve) *m/z* 409.3 $(M + H)^+$ Rt 1.60 min (60 % pure).

The sample was dissolved in DMF (5 mL), then cesium carbonate (600 mg, 1.842 mmol) and *tert*-butyl bromoacetate (0.300 mL, 2.03 mmol) were added and the mixture stirred at 50 ºC for 42 h. The mixture was diluted with CH_2Cl_2 (25 mL) and washed with brine (2 x 25 mL) and water (2 x 25 mL). The organic layer was collected, dried using a hydrophobic frit, and evaporated *in vacuo*. The sample was dissolved THF (5 mL), then TBAF (1 M in THF, 0.745 mL, 0.745 mmol) was added and stirred for 10 min. The mixture was diluted with EtOAc (10 mL) and water (10 mL) and the phases separated. The organic layer was washed with brine (2 x 20 mL) and water (2 x 20 mL), then the organic layer collected, dried using a hydrophobic frit, and evaporated *in vacuo*. The sample dissolved in DMSO and purified by MDAP (ammonium bicarbonate modifier gradient). However, a close running impurity was also collected. The solvent was removed under a stream of nitrogen to give the crude product (185 mg, 60 % pure, 30 % yield) which was used directly in the next reaction.

LCMS (Method B) (ES +ve) *m/z* 470.3 $(M + NH_4)^+$ Rt 1.55 min (60 % pure).

Di-*tert*-butyl 2,2'-((((buta-1,3-diyne-1,4-diylbis(3-isopropyl-4-(methoxymethoxy)-5,1-phenylene))bis(methylene))bis(3,5-dimethyl-4,1-phenylene))bis(oxy))diacetate (25)

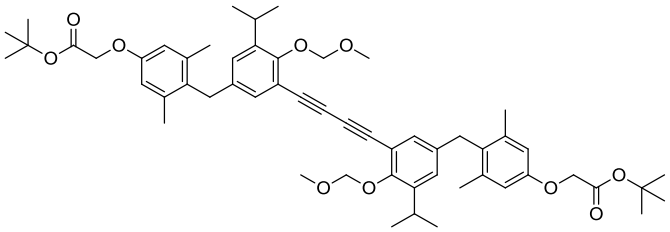

a) To a stirred solution of *tert*-butyl 2-(4-(3-ethynyl-5-isopropyl-4-(methoxymethoxy)benzyl)-3,5-dimethylphenoxy)acetate (8.6 mg, 0.011 mmol), 14-(4-iodophenoxy)-3,6,9,12-tetraoxatetradecan-1-oic acid (8.0 mg, 0.018 mmol) and triethylamine (10 µL, 0.072 mmol) in THF (0.5 mL) was added copper(I) iodide (1 mg, 5 µmol) and bis(triphenylphosphine)palladium(II) chloride (4 mg, 5 µmol) and the mixture stirred at rt for 16 h. LCMS analysis of the reaction mixture indicated the Glaser coupled product as a major peak.

b) To a stirred solution of 14-(4-iodophenoxy)-3,6,9,12-tetraoxatetradecan-1-oic acid (13 mg, 0.029 mmol) palladium(II) chloride (0.2 mg, 1 µmol) and pyrrolidine (15 µL, 0.15 mmol) in water (0.5 mL) was added *tert*-butyl 2-(4-(3-ethynyl-5-isopropyl-4-(methoxymethoxy)benzyl)-3,5-dimethylphenoxy)acetate (11 mg, 0.024 mmol) and the mixture stirred at rt for 5 h. LCMS analysis of the reaction mixture indicated the Glaser coupled product only.

LCMS (Method A) (ES +ve) *m/z* 925.9 $(M + Na)^+$ Rt 1.84 min.

14-(4-((5-(4-(2-(*tert*-Butoxy)-2-oxoethoxy)-2,6-dimethylbenzyl)-3-isopropyl-2-(methoxymethoxy)phenyl)ethynyl)phenoxy)-3,6,9,12-tetraoxatetradecan-1-oic acid (26)

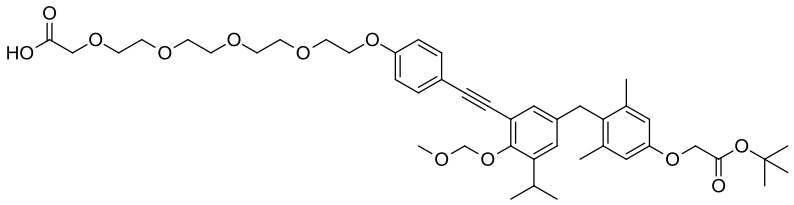

To a stirred solution of *tert*-butyl 2-(4-(3-ethynyl-5-isopropyl-4-(methoxymethoxy)benzyl)-3,5-dimethylphenoxy)acetate (150 mg, 60 % pure, 0.199 mmol) in THF (2 mL) at -78 ºC was added LiHMDS (1 M in hexanes, 0.80 mL, 0.80 mmol) and the mixture stirred for 15 min. 9-Methoxy-BBN (1 M in hexanes, 0.30 mL, 0.30 mmol) was added and the mixture allowed to stir for 1 h at -78 ºC. The mixture was transferred to a solution containing 14-(4-iodophenoxy)-3,6,9,12-tetraoxatetradecan-1-oic acid (135 mg, 0.298 mmol) and bis(triphenylphosphine)palladium(II) chloride (35 mg, 0.050 mmol) in THF (2 mL) which was stirred at 50 ºC for 3 h. The mixture was diluted with CH_2Cl_2 (10 mL) and water (10 mL), the pH adjusted to 4 with HCl (1 M aq.) and the phases separated. The aqueous layer was back-extracted with CH_2Cl_2 (10 mL), then the organic layers were pooled, dried using a hydrophobic frit, and evaporated *in vacuo*. The residue was dissolved in DMSO and purified by MDAP (formic acid modifier gradient). The solvent was evaporated *in vacuo* to give the required product (17 mg, 11 % yield) as a colourless oil.

^{1}H NMR (400 MHz, $CDCl_3$) δ 7.41 (d, *J* = 8.8 Hz, 2H), 6.93 (d, *J* = 2.2 Hz, 1H), 6.83 - 6.90 (m, 3H), 6.63 (s, 2H), 5.25 (s, 2H), 4.51 (s, 2H), 4.13 - 4.18 (m, 2H), 4.11 (s, 2H), 3.91 (s, 2H), 3.84 - 3.89 (m, 2H), 3.71 - 3.77 (m, 4H), 3.65 - 3.70 (m, 8H), 3.61 (s, 3H), 3.41 (spt, *J* = 6.9 Hz, 1H), 2.21 (s, 6H), 1.49 (s, 9H), 1.18 (d, *J* = 6.8 Hz, 6H). **LCMS** (Method B) (ES +ve) *m/z* 796.7 $(M + H)^+$ Rt 1.32 min (>95 % pure).

4-((Trimethylsilyl)ethynyl)phenol (27)

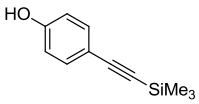

To a stirred solution of 4-iodophenol (3.30 g, 15.0 mmol), bis(triphenylphosphine)palladium (II) chloride (0.211 g, 0.300 mmol) and copper (I) iodide (0.057 g, 0.30 mmol) in triethylamine (40 mL) was added trimethylsilylacetylene (2.32 mL, 16.5 mmol) and the mixture stirred at 80 ºC for 2 h. The solution was cooled to rt, filtered through a Celite pad, and evaporated *in vacuo*. The sample was purified by chromatography on silica using a 0-100 % cyclohexane-TBME gradient over 14 CV. The appropriate fractions were combined and evaporated *in vacuo* to give the required product (2.62 g, 92 % yield) as a light brown solid.

^{1}H NMR (400 MHz, $CDCl_3$) δ 7.38 (d, *J* = 8.8 Hz, 2H), 6.77 (d, *J* = 8.8 Hz, 2H), 0.26 (s, 9H). **LCMS** (Method B) (ES -ve) *m/z* 189.1 $(M - H)^-$ Rt 1.28 min (>95 % pure).

Consistent with literature data.[235]

***tert*-Butyl 14-(4-ethynylphenoxy)-3,6,9,12-tetraoxatetradecan-1-oate (28)**

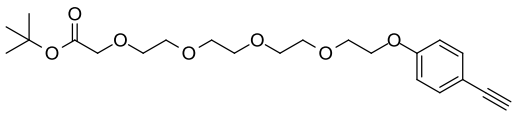

A solution of 4-((trimethylsilyl)ethynyl)phenol (2.42 g, 12.7 mmol), *tert*-butyl 14-(tosyloxy)-3,6,9,12-tetraoxatetradecan-1-oate (6.63 g, 14.3 mmol) and cesium carbonate (12.4 g, 38.1 mmol) in DMF (40 mL) was stirred at 50 ºC for 14 h. The mixture was diluted with EtOAc (50 mL) and washed with LiCl (5 % aq., 3 x 200 mL), then the organic phase collected, dried using a hydrophobic frit, and evaporated *in vacuo*. The residue was dissolved in THF (50 mL), then TBAF (1 M in THF, 15 mL, 15 mmol) added and stirred at rt for 20 h. The mixture was diluted with EtOAc (50 mL), then washed with brine (3 x 100 mL), and water (2 x 100 mL). The organic layer was dried using a hydrophobic frit, and evaporated *in vacuo*. The sample was purified by chromatography on silica using a 20-80 % EtOAc-cyclohexane gradient over 20

CV. The appropriate fractions were combined and evaporated *in vacuo* to give the required product (3.83 g, 74 % yield) as an orange oil.

^{1}H NMR (400 MHz, $CDCl_3$) δ 7.42 (d, *J* = 8.8 Hz, 2H), 6.86 (d, *J* = 8.8 Hz, 2H), 4.12 - 4.16 (m, 2H), 4.02 (s, 2H), 3.84 - 3.88 (m, 2H), 3.64 - 3.75 (m, 12H), 3.00 (s, 1H), 1.48 (s, 9H). **^{13}C NMR** (101 MHz, $CDCl_3$) δ 169.63, 159.18, 133.54, 114.61, 114.35, 83.64, 81.50, 75.77, 70.87, 70.74, 70.65, 70.62, 70.60, 69.62, 69.07, 67.50, 28.12. Note that ^{13}C NMR data are reported to two decimal places to differentiate the signals. One signal is not resolved due to overlapping frequencies of PEG chain carbons; confirmed by HMBC. **LCMS** (Method B) (ES +ve) *m/z* 426.4 $(M + NH_4)^+$ Rt 1.21 min (>95 % pure).

14-(4-Ethynylphenoxy)-3,6,9,12-tetraoxatetradecan-1-oic acid (29)

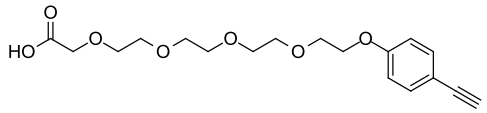

To a stirred solution of *tert*-butyl 14-(4-ethynylphenoxy)-3,6,9,12-tetraoxatetradecan-1-oate (590 mg, 1.44 mmol) in THF (5 mL) was added sodium hydroxide (2 M aq., 5 mL, 10 mmol) and the solution stirred at 50 ºC for 15 h. The solution was diluted with EtOAc (15 mL) and HCl (1 M aq., 10 mL), then the pH adjusted to 3 with further HCl (1 M aq.) and the phases separated. The aqueous layer was back-extracted with EtOAc (15 mL), then the organic layers were pooled, dried using a hydrophobic frit, and evaporated *in vacuo* to give the required product (355 mg, 70 % yield) as a brown oil.

^{1}H NMR (400 MHz, $CDCl_3$) δ 7.42 (d, *J* = 8.8 Hz, 2H), 6.87 (d, *J* = 8.8 Hz, 2H), 4.13 - 4.17 (m, 2H), 4.12 (s, 2H), 3.85 - 3.89 (m, 2H), 3.65 - 3.77 (m, 12H), 3.00 (s, 1H). **^{13}C NMR** (101 MHz, $CDCl_3$) δ 172.1, 159.0, 133.5, 114.6, 114.3, 83.6, 75.8, 71.2, 70.8, 70.5, 70.4, 70.3, 70.2, 69.6, 69.0, 67.3. **LCMS** (Method B) (ES -ve) *m/z* 351.3 $(M - H)^-$ Rt 0.69 min (>95 % pure). **HRMS** (ES) calcd for $C_{18}H_{24}O_7Na$, $(M + Na)^+$ 375.1420, found 375.1414.

14,14'-((Buta-1,3-diyne-1,4-diylbis(4,1-phenylene))bis(oxy))bis(3,6,9,12-tetraoxatetradecan-1-oic acid) (30)

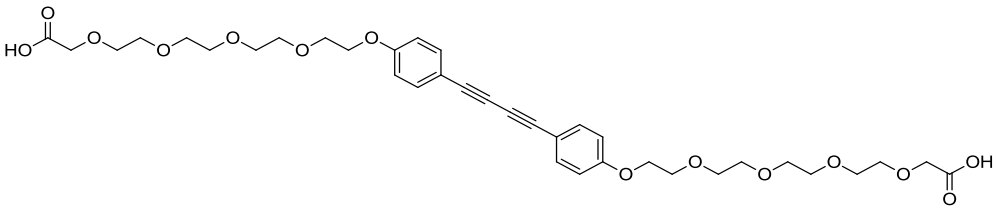

To a stirred solution of 14-(4-ethynylphenoxy)-3,6,9,12-tetraoxatetradecan-1-oic acid (21 mg, 0.060 mmol) and 4-(3-iodo-5-isopropyl-4-(methoxymethoxy)benzyl)-3,5-dimethylphenol (48 mg, 0.055 mmol) in triethylamine (0.50 mL, 3.6 mmol) was added copper(I) iodide (0.7 mg, 4 µmol) and bis(triphenylphosphine)palladium(II) chloride (2.5 mg, 4 µmol) and the mixture stirred at 50 ºC for 1 h. LCMS analysis of the reaction mixture indicated the Glaser coupled product only.

LCMS (Method B) (ES -ve) *m/z* 701.7 $(M - H)^-$ Rt 1.10 min.

14-(4-((5-(4-Hydroxy-2,6-dimethylbenzyl)-3-isopropyl-2-(methoxymethoxy)phenyl)ethynyl)phenoxy)-3,6,9,12-tetraoxatetradecan-1-oic acid (31)

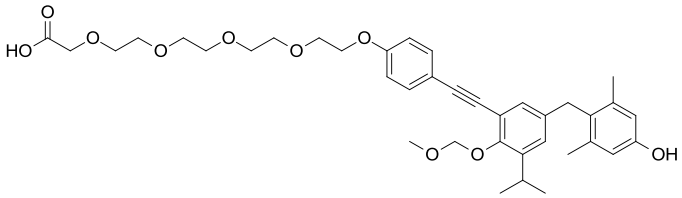

To a stirred solution of 4-(3-iodo-5-isopropyl-4-(methoxymethoxy)benzyl)-3,5-dimethylphenol (546 mg, 0.620 mmol, 50 % purity), bis(triphenylphosphine)palladium(II) chloride (22 mg, 0.031 mmol) and triethylamine (0.30 mL, 2.2 mmol) in DMF (5 mL) was added chloro(triphenylphosphine)gold(I) (16 mg, 0.032 mmol) followed by 14-(4-ethynylphenoxy)-3,6,9,12-tetraoxatetradecan-1-oic acid (255 mg, 0.724 mmol) and the mixture stirred at 80 ºC for 3 h. The mixture was diluted with EtOAc (15 mL) then filtered through a Celite pad. The filtrate was diluted with water (20 mL), then the pH adjusted to 3 with HCl (1 M aq.) and the phases separated. The organic layer was washed with LiCl (5 % aq., 3 x 100 mL), then dried using a hydrophobic frit, and evaporated *in vacuo*. The sample was loaded in acetonitrile and purified by reverse phase (C18) chromatography using

a 50-100 % acetonitrile-water (formic acid modifier) gradient over 18 CV. The appropriate fractions were combined and evaporated *in vacuo*, however this failed to completely separate the product. The sample was again loaded in acetonitrile and purified by reverse phase (C18) chromatography using a 50-100 % acetonitrile-water (+0.1 % ammonium bicarbonate modifier) gradient over 18 CV. The appropriate fractions were combined and acetonitrile removed *in vacuo*. The remaining aqueous solution was diluted with CH_2Cl_2 (100 mL) then the pH adjusted to 5 with HCl (1 M aq.) and the phases separated. The organic layer was collected and evaporated *in vacuo* to give the required product (141 mg, 34 % yield) as a yellow gum.

^{1}H NMR (400 MHz, $CDCl_3$) δ 7.38 (d, *J* = 8.8 Hz, 2H), 7.01 (s, 1H), 6.85 (d, *J* = 8.8 Hz, 2H), 6.75 (s, 1H), 6.59 (s, 2H), 5.24 (s, 2H), 4.09 - 4.14 (m, 2H), 3.98 (s, 2H), 3.89 (s, 2H), 3.80 - 3.84 (m, 2H), 3.59 - 3.72 (m, 15H), 3.42 (spt, *J* = 6.9 Hz, 1H), 2.17 (s, 6H), 1.20 (d, *J* = 6.8 Hz, 6H). **^{13}C NMR** (101 MHz, $CDCl_3$) δ 173.8, 158.7, 154.2, 153.6, 141.8, 138.4, 136.1, 132.8, 129.2, 128.2, 126.7, 116.7, 115.7, 115.0, 114.8, 99.7, 92.7, 85.7, 77.2, 70.5, 70.2, 70.1, 70.0, 69.9, 69.5, 67.4, 57.5, 33.7, 26.4, 23.4, 20.3. One signal is not resolved potentially due to overlapping frequencies of PEG chain carbons, as confirmed by HMBC. **LCMS** (Method A) (ES +ve) *m/z* 663.8 $(M + H)^+$ Rt 1.38 min (>95 % pure). **HRMS** (ES) calcd for $C_{38}H_{49}O_{10}$, $(M + H)^+$ 665.3326, found 665.3298.

2-(4-(4-Hydroxy-3-((4-(((*S*)-16-((2*S*,4*R*)-4-hydroxy-2-((4-(4-methylthiazol-5-yl)benzyl)carbamoyl)pyrrolidine-1-carbonyl)-17,17-dimethyl-14-oxo-3,6,9,12-tetraoxa-15-azaoctadecyl)oxy)phenyl)ethynyl)-5-isopropylbenzyl)-3,5-dimethylphenoxy)acetic acid (32)

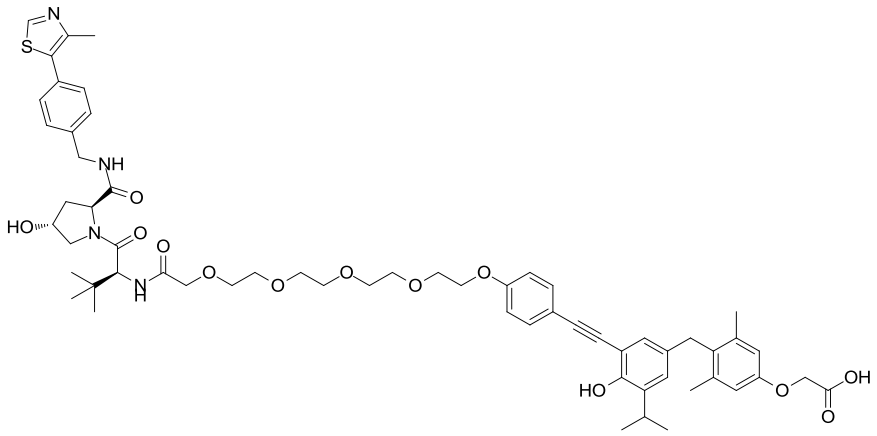

To a stirred solution of 14-(4-((5-(4-hydroxy-2,6-dimethylbenzyl)-3-isopropyl-2-(methoxymethoxy)phenyl)ethynyl)phenoxy)-3,6,9,12-tetraoxatetradecan-1-oic acid (77.1 mg, 0.116 mmol), (2*S*,4*R*)-1-((*S*)-2-amino-3,3-dimethylbutanoyl)-4-hydroxy-*N*-(4-(4-methylthiazol-5-yl)benzyl)pyrrolidine-2-carboxamide hydrochloride (61 mg, 0.13 mmol), and DIPEA (0.101 mL, 0.580 mmol) in DMF (2 mL) was added HATU (67 mg, 0.18 mmol) and the mixture stirred at rt for 2 h. The mixture was diluted with CH_2Cl_2 (5 mL) and water (5 mL) and the phases separated. The organic layer was dried using a hydrophobic frit, and concentrated under a stream of nitrogen. The sample was directly dissolved in DMF (2 mL), then *tert*-butyl bromoacetate (41 μL, 0.28 mmol) and cesium carbonate (90 mg, 0.28 mmol) were added and the mixture stirred at rt for 24 h. The mixture was diluted with CH_2Cl_2 (10 mL) and water (10 mL) and the phases separated. The aqueous layer was extracted with CH_2Cl_2 (3 x 10 mL) then the organic layers were combined, dried using a hydrophobic frit, and evaporated *in vacuo*. The sample was directly dissolved in 1,4-dioxane (2 mL) then HCl (4 M in dioxane, 0.70 mL, 2.8 mmol) was added the mixture stirred at 50 ºC for 72 h. Sodium hydroxide (2 M aq., 2.8 mL, 5.6 mmol) was then added and the mixture stirred at 50 ºC for a further 24 h. The mixture was diluted with CH_2Cl_2 (10 mL) and water (10 mL), the pH adjusted to 3 with HCl (1 M aq.), and the phases separated. The aqueous layer was back-extracted with CH_2Cl_2 (2 x 5 mL), then the organic layers were combined, dried

using a hydrophobic frit, and the solvent evaporated under a stream of nitrogen. The sample was purified directly by MDAP (formic acid modifier gradient). The solvent was removed under a stream of nitrogen to give the required product (25 mg, 16 % yield) as an off-white solid.

^{1}H NMR (400 MHz, Methanol-d_4) δ 8.83 (s, 1H), 7.75 (d, *J* = 8.8 Hz, 2H), 7.34 - 7.47 (m, 4H), 6.99 (d, *J* = 8.8 Hz, 2H), 6.79 - 6.89 (m, 3H), 6.68 (s, 2H), 4.67 (s, 1H), 4.62 (s, 2H), 4.52 - 4.59 (m, 1H), 4.46 - 4.50 (m, 1H), 4.29 - 4.37 (m, 1H), 4.12 - 4.18 (m, 2H), 4.05 (s, 2H), 4.01 (d, *J* = 3.2 Hz, 2H), 3.81 - 3.89 (m, 3H), 3.75 - 3.80 (m, 1H), 3.59 - 3.72 (m, 12H), 3.33 - 3.43 (m, 1H), 2.44 (s, 3H), 2.16 - 2.25 (m, 7H), 2.02 - 2.12 (m, 1H), 1.38 (d, *J* = 6.8 Hz, 6H), 1.02 (s, 9H). **^{13}C NMR** (101 MHz, Methanol-d_4) δ 174.49, 172.24, 171.80, 160.75, 157.71, 157.03, 152.93, 152.59, 149.18, 140.36, 139.73, 136.39, 132.80, 131.96, 131.64, 131.10, 130.51, 129.09, 127.35, 125.16, 122.67, 117.84, 116.17, 115.34, 113.55, 101.05, 72.46, 71.94, 71.80, 71.75, 71.63, 71.23, 71.20, 70.96, 68.89, 66.19, 60.95, 58.29, 58.23, 43.87, 39.07, 37.24, 35.25, 30.78, 27.12, 23.24, 20.77, 15.99. Note that ^{13}C NMR data are reported to two decimal places to differentiate the signals. Two signals are not resolved, likely to be acetylene carbons. **LCMS** (Method B) (ES +ve) *m/z* 1091.9 $(M + H)^+$ Rt 1.11 min (>95 % pure). **HRMS** (ES) calcd for $C_{60}H_{75}N_4O_{13}S$, $(M + H)^+$ 1091.5051, found 1091.5079. **IR** ν_{max} (neat) 3316, 2926, 2852, 1735, 1670, 1634, 1606, 1506, 1483, 1448 cm^{-1}. **MP** >250 °C (decomposition).

2-(4-(4-Hydroxy-3-((4-(((*R*)-16-((2*R*,4*S*)-4-hydroxy-2-((4-(4-methylthiazol-5-yl)benzyl)carbamoyl)pyrrolidine-1-carbonyl)-17,17-dimethyl-14-oxo-3,6,9,12-tetraoxa-15-azaoctadecyl)oxy)phenyl)ethynyl)-5-isopropylbenzyl)-3,5-dimethylphenoxy)acetic acid (33)

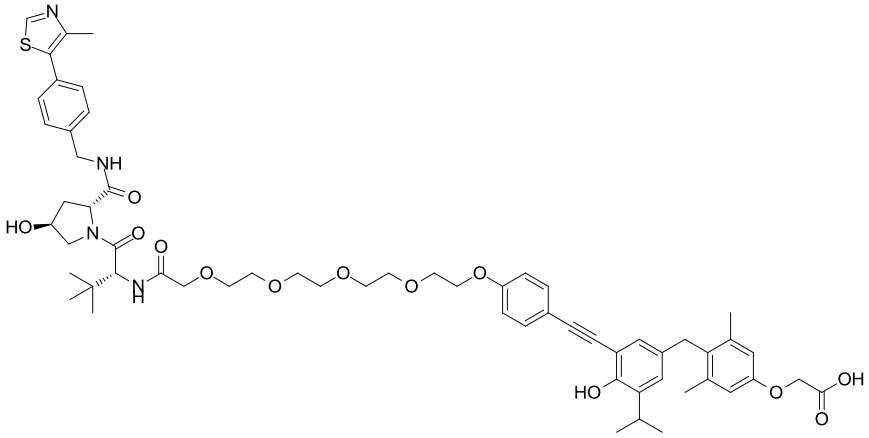

To a stirred solution of 14-(4-((5-(4-hydroxy-2,6-dimethylbenzyl)-3-isopropyl-2-(methoxymethoxy)phenyl)ethynyl)phenoxy)-3,6,9,12-tetraoxatetradecan-1-oic acid (63 mg, 0.094 mmol), (2*R*,4*S*)-1-((*R*)-2-amino-3,3-dimethylbutanoyl)-4-hydroxy-*N*-(4-(4-methylthiazol-5-yl)benzyl)pyrrolidine-2-carboxamide hydrochloride (50 mg, 0.11 mmol), and DIPEA (0.082 mL, 0.47 mmol) in DMF (2 mL) was added HATU (53 mg, 0.14 mmol) and the mixture stirred at rt for 2 h. The mixture was diluted with CH_2Cl_2 (5 mL) and water (5 mL) and the phases separated. The organic layer was dried using a hydrophobic frit, and evaporated *in vacuo*. The sample was directly dissolved in DMF (2 mL), then *tert*-butyl bromoacetate (37 µL, 0.25 mmol) and cesium carbonate (82 mg, 0.25 mmol) were added and the mixture stirred at rt for 24 h. The mixture was diluted with CH_2Cl_2 (10 mL) and water (10 mL) and the phases separated. The aqueous layer was extracted with CH_2Cl_2 (3 x 10 mL) then the organic layers were combined, dried using a hydrophobic frit, and evaporated *in vacuo*. The sample was directly dissolved in 1,4-dioxane (2 mL) then HCl (4 M in dioxane, 0.70 mL, 2.8 mmol) was added the mixture stirred at 50 ºC for 72 h. NaOH (2 M aq., 2.8 mL, 5.6 mmol) was then added and the mixture stirred at 50 ºC for a further 24 h. The mixture was diluted with CH_2Cl_2 (10 mL) and water (10 mL), the pH adjusted to 3 with HCl (1 M aq.) and the phases separated. The aqueous layer was back-extracted with CH_2Cl_2 (2 x 5 mL), then the organic layers were combined, dried using a hydrophobic frit, and

the solvent evaporated under a stream of nitrogen. The sample was purified by MDAP (formic acid modifier gradient). The solvent was removed under a stream of nitrogen to give the required product (19 mg, 14 % yield) as an off-white solid.

^{1}H NMR (400 MHz, Methanol-d_4) δ 8.83 (s, 1H), 7.75 (d, *J* = 8.8 Hz, 2H), 7.34 - 7.46 (m, 4H), 6.99 (d, *J* = 8.8 Hz, 2H), 6.79 - 6.90 (m, 3H), 6.68 (s, 2H), 4.67 (s, 1H), 4.60 (s, 2H), 4.52 - 4.58 (m, 1H), 4.47 - 4.51 (m, 1H), 4.29 - 4.37 (m, 1H), 4.12 - 4.18 (m, 2H), 4.05 (s, 2H), 4.01 (d, *J* = 2.9 Hz, 2H), 3.81 - 3.88 (m, 3H), 3.75 - 3.81 (m, 1H), 3.58 - 3.72 (m, 12H), 3.33 - 3.42 (m, 1H), 2.44 (s, 3H), 2.17 - 2.25 (m, 7H), 2.02 - 2.12 (m, 1H), 1.38 (d, *J* = 6.8 Hz, 6H), 1.02 (s, 9H). **^{13}C NMR** (101 MHz, Methanol-d_4) δ 174.49, 172.24, 171.80, 160.74, 157.76, 157.03, 152.92, 152.59, 149.17, 140.35, 139.70, 136.41, 132.79, 131.89, 131.64, 131.10, 130.50, 129.09, 127.35, 125.17, 122.67, 117.84, 116.17, 115.35, 113.55, 101.06, 89.94, 72.45, 71.93, 71.79, 71.74, 71.63, 71.23, 71.20, 70.96, 68.89, 66.37, 60.95, 58.30, 58.23, 43.88, 39.07, 37.23, 35.25, 30.78, 27.12, 23.24, 20.77, 15.99. Note that ^{13}C NMR data are reported to two decimal places to differentiate the signals. One signal is not resolved, likely to be an acetylene carbon. **LCMS** (Method B) (ES +ve) *m/z* 1092.0 $(M + H)^+$ Rt 1.11 min (>95 % pure). **HRMS** (ES) calcd for $C_{60}H_{75}N_4O_{13}S$, $(M + H)^+$ 1091.5051, found 1091.5079. **IR** ν_{max} (neat) 3112, 2924, 2852, 2161, 1735, 1634, 1606, 1506, 1445 cm^{-1}. **MP** >250 °C (decomposition).

***tert*-Butyl 2-(4-(3-iodo-5-isopropyl-4-(methoxymethoxy)benzyl)-3,5-dimethylphenoxy)acetate (34)**

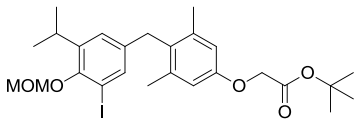

To a stirred solution of 4-(3-iodo-5-isopropyl-4-(methoxymethoxy)benzyl)-3,5-dimethylphenol (489 mg, 0.555 mmol, 50 % pure) and *tert*-butyl bromoacetate (0.123 mL, 0.833 mmol) in DMF (3 mL) was added cesium carbonate (540 mg, 1.66 mmol) and the mixture stirred at 50 ºC for 16 h. The solution was diluted with EtOAc (20 mL) and water (20 mL), then the phases were separated. The organic layer was washed with

brine (2 x 50 mL) then evaporated *in vacuo*. The crude product (648 mg, quantitative yield, 50 % pure) was used directly in the next reaction.

LCMS (Method B) (ES +ve) *m/z* 572.2 $(M + NH_4)^+$ Rt 1.70 min (50 % pure)

2-(2-(2-Methoxyethoxy)ethoxy)ethyl 4-methylbenzenesulfonate (35)

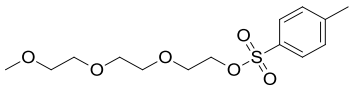

A solution of 2-(2-(2-methoxyethoxy)ethoxy)ethanol (3.00 g, 18.3 mmol), tosyl chloride (4.18 g, 21.9 mmol) and triethylamine (3.82 mL, 27.4 mmol) in CH_2Cl_2 (15 mL) was stirred at rt for 16 h. The solution was washed with $NaHCO_3$ (sat. aq., 2 x 100 mL) and evaporated *in vacuo*, then loaded in CH_2Cl_2 and purified by chromatography on silica using a 25-100 % EtOAc-cyclohexane gradient over 20 min. The appropriate fractions were combined and evaporated *in vacuo* to give the required product (4.68 g, 80 % yield) as an orange liquid.

^{1}H NMR (400 MHz, $CDCl_3$) δ 7.81 (d, *J* = 8.3 Hz, 2H), 7.35 (d, *J* = 8.3 Hz, 1H), 4.17 (t, *J* = 4.9 Hz, 2H), 3.69 (t, *J* = 4.9 Hz, 2H), 3.58 - 3.64 (m, 6H), 3.51 - 3.56 (m, 2H), 3.38 (s, 3H), 2.45 (s, 3H). **LCMS** (Method A) (ES +ve) *m/z* 319.1 $(M + H)^+$ Rt 0.95 min (>95 % pure).

Consistent with literature data.[401]

2-Bromo-5-nitrophenol (36)

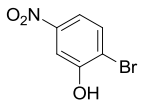

To a stirred solution of 1-bromo-2-methoxy-4-nitrobenzene (1.00 g, 4.31 mmol) in CH_2Cl_2 (10 mL) was added boron tribromide (1 M in CH_2Cl_2, 8.80 mL, 8.80 mmol) and the mixture stirred at rt for 16 h. The reaction was cooled to 0 ºC and slowly quenched with water (20 mL) then diluted with CH_2Cl_2 (10 mL) and the phases separated. The aqueous layer was back-extracted with CH_2Cl_2 (10 mL), then the organic layers were pooled, dried using a hydrophobic frit, and evaporated *in vacuo*.

The sample was loaded in CH_2Cl_2 and purified by chromatography on silica using a 0-50 % EtOAc-cyclohexane gradient over 60 min. The appropriate fractions were combined and evaporated *in vacuo* to give the required product (792 mg, 84 % yield) as a yellow powder.

^{1}H NMR (400 MHz, $CDCl_3$) δ 7.87 (s, 1H), 7.71 (d, *J* = 8.6 Hz, 1H), 7.66 (d, *J* = 8.6 Hz, 1H), 5.91 (br. s., 1H). **LCMS** (Method A) (ES +ve) *m/z* 216.0/218.0 $(M + H)^+$ Rt 0.94 min (>95 % pure).

Consistent with literature data.[402]

1-Bromo-2-(2-(2-(2-methoxyethoxy)ethoxy)ethoxy)-4-nitrobenzene (37)

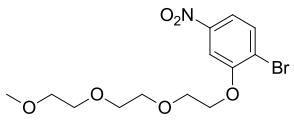

A solution of 2-bromo-5-nitrophenol (250 mg, 1.15 mmol), 2-(2-(2-methoxyethoxy)ethoxy)ethyl 4-methylbenzenesulfonate (421 mg, 1.32 mmol) and cesium carbonate (768 mg, 2.36 mmol) in DMF (5 mL) was stirred at rt for 20 h. The mixture was diluted with EtOAc (10 mL) and water (10 mL), then the pH adjusted to 7 with HCl (1 M aq.) and the phases separated. The organic phase was washed with LiCl (1 M aq., 2 x 50 mL), then dried using a hydrophobic frit and evaporated *in vacuo*. The sample was loaded in CH_2Cl_2 and purified by chromatography on silica using a 0-50 % EtOAc-cyclohexane gradient over 40 min. The appropriate fractions were combined and evaporated *in vacuo* to give the required product (289 mg, 62 % yield, 90 % pure) as a yellow oil.

^{1}H NMR (400 MHz, $CDCl_3$) δ 7.81 (d, *J* = 2.2 Hz, 1H), 7.73 (d, *J* = 2.2 Hz, 1H), 7.72 (s, 1H), 4.28 - 4.34 (m, 2H), 3.94 - 4.00 (m, 2H), 3.78 - 3.83 (m, 2H), 3.64 - 3.73 (m, 4H), 3.53 - 3.58 (m, 2H), 3.38 (s, 3H). **LCMS** (Method B) (ES +ve) *m/z* 364.1/366.1 $(M + H)^+$ Rt 1.11 min (90 % purity).

1-Ethynyl-2-(2-(2-(2-methoxyethoxy)ethoxy)ethoxy)-4-nitrobenzene (38)

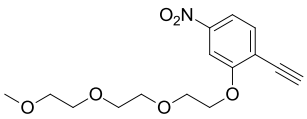

To a stirred solution of 1-bromo-2-(2-(2-(2-methoxyethoxy)ethoxy)ethoxy)-4-nitrobenzene (287 mg, 0.788 mmol), bis(triphenylphosphine)palladium(II) chloride (11 mg, 0.016 mmol), copper(I) iodide (4 mg, 0.02 mmol) and triethylamine (0.330 mL, 2.36 mmol) in THF (2 mL) was added trimethylsilylacetylene (0.180 mL, 1.28 mmol) and the mixture stirred at 50 °C for 1 h. The reaction mixture was diluted with EtOAc (10 mL) and water (10 mL), then filtered through Celite and the phases separated. The organic layer was dried using a hydrophobic frit and evaporated *in vacuo*. The sample was loaded in CH_2Cl_2 and purified on chromatography on silica using a 0-50 % EtOAc-cyclohexane gradient over 40 min. The appropriate fractions were combined and evaporated *in vacuo*. TBAF (1 M in THF, 1 mL, 1 mmol) was added to the sample and the mixture stirred at rt for 15 min. The reaction mixture was concentrated *in vacuo* then purified by chromatography on silica using a 0-100 % EtOAc-cyclohexane gradient over 15 min. The appropriate fractions were combined and evaporated *in vacuo* to give the required product (166 mg, 68 % yield) as a dark brown oil.

^{1}H NMR (400 MHz, $CDCl_3$) δ 7.77 - 7.83 (m, 2H), 7.58 (d, *J* = 8.8 Hz, 1H), 4.27 - 4.34 (m, 2H), 3.92 - 3.98 (m, 2H), 3.76 - 3.83 (m, 2H), 3.63 - 3.72 (m, 4H), 3.49 - 3.59 (m, 3H), 3.38 (s, 3H). **^{13}C NMR** (101 MHz, $CDCl_3$) δ 160.41, 148.51, 134.25, 118.69, 115.68, 107.23, 85.90, 78.31, 71.96, 71.20, 70.73, 70.61, 69.42, 69.36, 59.02. Note that ^{13}C NMR data are reported to two decimal places to differentiate the signals. **LCMS** (Method B) (ES +ve) *m/z* 327.1 $(M + NH_4)^+$ Rt 1.04 min (>95 % pure). **HRMS** (ES) calcd for $C_{15}H_{20}NO_6$, $(M + H)^+$ 310.1291, found 310.1280.

tert-Butyl 2-(4-(3-isopropyl-5-((2-(2-(2-(2-methoxyethoxy)ethoxy)ethoxy)-4-nitrophenyl)ethynyl)-4-(methoxymethoxy)benzyl)-3,5-dimethylphenoxy)acetate (39)

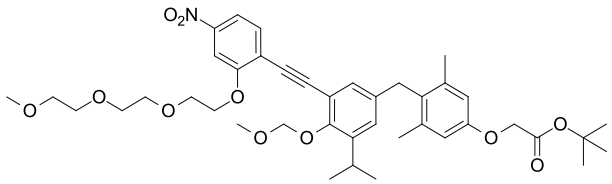

To a stirred solution of *tert*-butyl 2-(4-(3-iodo-5-isopropyl-4-(methoxymethoxy)benzyl)-3,5-dimethylphenoxy)acetate (100 mg, 90 µmol, 50 % pure), bis(triphenylphosphine)palladium(II) chloride (2.0 mg, 2.9 µmol), chloro(triphenylphosphine)gold(I) (1.5 mg, 3.0 µmol) and triethylamine (50 µL, 0.36 mmol) in DMF (1 mL) was added a solution of 1-ethynyl-2-(2-(2-(2-methoxyethoxy)ethoxy)ethoxy)-4-nitrobenzene (33 mg, 0.11 mmol) in DMF (0.5 mL) and the solution stirred at 80 °C for 4 h. The mixture was diluted with EtOAc (10 mL) and water (10 mL) and the phases separated. The aqueous layer was back-extracted with EtOAc (10 mL) then the organic layers combined, dried using a hydrophobic frit, and evaporated *in vacuo*. The sample was loaded in DMSO and purified by MDAP (ammonium bicarbonate modifier gradient). The solvent was removed under a stream of nitrogen to give the required product (37 mg, 56 % yield) as a brown oil.

^{1}H NMR (400 MHz, $CDCl_3$) δ 7.78 - 7.84 (m, 2H), 7.57 (d, *J* = 9.0 Hz, 1H), 7.00 (s, 1H), 6.88 (s, 1H), 6.61 - 6.67 (m, 2H), 5.32 (s, 2H), 4.52 (s, 2H), 4.31 (t, *J* = 4.8 Hz, 2H), 3.90 - 3.97 (m, 4H), 3.70 - 3.76 (m, 2H), 3.58 - 3.65 (m, 7H), 3.48 - 3.53 (m, 2H), 3.44 (spt, *J* = 6.8 Hz, 1H), 3.34 (s, 3H), 2.22 (s, 6H), 1.50 (s, 9H), 1.18 (d, *J* = 6.9 Hz, 6H). **^{13}C NMR** (101 MHz, $CDCl_3$) δ 168.2, 159.5, 156.1, 154.3, 147.8, 142.0, 138.4, 135.8, 133.3, 129.8, 129.5, 127.5, 120.1, 115.8, 114.2, 107.0, 100.0, 96.0, 87.8, 82.2, 71.9, 71.0, 70.7, 70.5, 69.3, 69.1, 65.7, 58.9, 57.5, 33.8, 28.0, 26.4, 23.6, 23.3, 20.5. **LCMS** (Method B) (ES +ve) *m/z* 753.7 $(M + NH_4)^+$ Rt 1.69 min (>95 % pure).

2-(4-(4-Hydroxy-3-isopropyl-5-((2-(2-(2-(2-methoxyethoxy)ethoxy)ethoxy)-4-nitrophenyl)ethynyl)benzyl)-3,5-dimethylphenoxy)acetic acid (40)

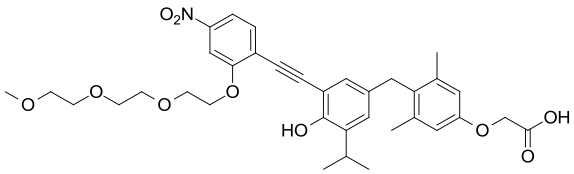

To a stirred solution of *tert*-butyl 2-(4-(3-isopropyl-5-((2-(2-(2-(2-methoxyethoxy)ethoxy)ethoxy)-4-nitrophenyl)ethynyl)-4-(methoxymethoxy)benzyl)-3,5-dimethylphenoxy)acetate (38 mg, 52 µmol) in DMF (1 mL) was added HCl (4 M in dioxane, 200 µL, 0.8 mmol) and stirred at 50 °C for 4 h. NaOH (2 M aq., 0.8 mL, 1.6 mmol) was added and the solution stirred at 50 °C for 18 h. The mixture was diluted with CH_2Cl_2 (10 mL) and water (10 mL), the pH adjusted to 3 with HCl (1 M aq.) then the phases were separated. The aqueous layer was back-extracted with CH_2Cl_2 (3 x 10 mL) then the organic layers were combined, dried using a hydrophobic frit, and evaporated *in vacuo*. The samples were dissolved in DMSO and purified by MDAP (formic acid modifier gradient). The solvent was removed under a stream of nitrogen to give the required product (5.8 mg, 18 % yield) as a yellow oil.

^{1}H NMR (400 MHz, $CDCl_3$) δ 7.85 (d, *J* = 8.3 Hz, 1H), 7.79 (s, 1H), 7.55 (d, *J* = 8.3 Hz, 1H), 7.03 (s, 1H), 6.64 - 6.72 (m, 3H), 4.68 (s, 2H), 4.31 - 4.39 (m, 2H), 3.94 - 4.01 (m, 2H), 3.91 (s, 2H), 3.75 - 3.82 (m, 2H), 3.66 - 3.73 (m, 2H), 3.59 - 3.65 (m, 2H), 3.48 - 3.55 (m, 2H), 3.36 (s, 3H), 3.29 (spt, *J* = 6.8 Hz, 1H), 2.24 (s, 6H), 1.24 (d, *J* = 6.8 Hz, 6H). **^{13}C NMR** (101 MHz, $CDCl_3$) δ 171.3, 158.9, 155.5, 153.3, 147.8, 138.7, 134.5, 131.6, 131.3, 130.5, 128.5, 126.3, 119.4, 116.2, 114.2, 108.3, 106.5, 94.6, 91.1, 71.8, 70.9, 70.6, 70.4, 69.1, 69.1, 65.0, 59.0, 33.6, 27.5, 22.3, 20.5. **LCMS** (Method B) (ES -ve) *m/z* 634.8 $(M - H)^-$ Rt 1.08 min (>95 % pure). **HRMS** (ES) calcd for $C_{35}H_{42}NO_{10}$ $(M + H)^+$ 636.2809, found 636.2801. **IR** ν_{max} (neat) 2921, 2852, 2193, 1979, 1742, 1604, 1520, 1378 cm^{-1}. **MP** >250 °C (decomposition).

tert-Butyl 14-(2-bromo-5-nitrophenoxy)-3,6,9,12-tetraoxatetradecan-1-oate (41)

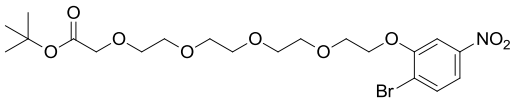

To a stirred solution of 2-bromo-5-nitrophenol (250 mg, 1.15 mmol) and *tert*-butyl 14-(tosyloxy)-3,6,9,12-tetraoxatetradecan-1-oate (740 mg, 1.60 mmol) in DMF (5 mL) was added cesium carbonate (780 mg, 2.39 mmol) and the mixture stirred at rt for 72 h. The mixture was diluted with EtOAc (20 mL) and water (20 mL), the pH adjusted to 7 with HCl (1 M aq.), then the phases were separated. The aqueous layer was back-extracted with EtOAc (2 x 20 mL) then the organic layers were combined, dried using a hydrophobic frit, and evaporated *in vacuo*. The sample was dissolved in DMSO and purified by reverse phase (C18) chromatography using a 30-95 % acetonitrile-water (ammonium bicarbonate modifier) gradient over 14 CV. The appropriate fractions were combined and evaporated *in vacuo* to give the required product (444 mg, 69 % yield, 90 % pure) as a yellow oil.

^{1}H NMR (400 MHz, $CDCl_3$) δ 7.78 - 7.81 (m, 1H), 7.68 - 7.77 (m, 2H), 4.31 (t, *J* = 4.6 Hz, 2H), 4.02 (s, 2H), 3.96 (t, *J* = 4.6 Hz, 2H), 3.75 - 3.82 (m, 2H), 3.65 - 3.73 (m, 10H), 1.48 (s, 9H). **LCMS** (Method B) (ES +ve) *m/z* 525.4/527.3 $(M + NH_4)^+$ Rt 1.29 min (90 % pure).

14-(2-Ethynyl-5-nitrophenoxy)-3,6,9,12-tetraoxatetradecan-1-oic acid (42)

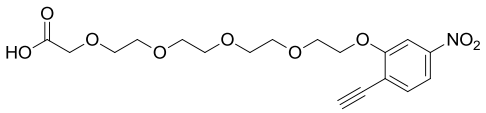

To a stirred solution of *tert*-butyl 14-(2-bromo-5-nitrophenoxy)-3,6,9,12-tetraoxatetradecan-1-oate (438 mg, 0.775 mmol) in triethylamine (10 mL) was added bis(triphenylphosphine)palladium(II) chloride (12 mg, 17 μmol) and copper(I) iodide (4 mg, 21 μmol), followed by trimethylsilylacetylene (0.200 mL, 1.43 mmol). The mixture was stirred at 90 °C for 2 h. The solution was diluted with EtOAc (20 mL) and water (20 mL), filtered through Celite, then the phases were separated. The aqueous layer was back extracted with EtOAc (2 x 20 mL), then the organic layers combined

and evaporated *in vacuo*. The sample was directly dissolved in THF (10 mL) and NaOH (2 M aq., 10 mL, 20 mmol) and the mixture stirred at rt for 18 h. The mixture was diluted with EtOAc (20 mL) and water (20 mL), the pH adjusted to 3 with HCl (1 M aq.), then the phases were separated. The aqueous layer was back-extracted with EtOAc (20 mL) then the organic layers combined and evaporated *in vacuo*. The sample was dissolved in methanol and purified by reverse phase (C18) chromatography using a 5-70 % acetonitrile-water (formic acid modifier) gradient over 12 CV. The appropriate fractions were combined and evaporated *in vacuo* to give the required product (234 mg, 76 % yield), as a yellow oil.

^{1}H NMR (400 MHz, $CDCl_3$) δ 7.78 - 7.84 (m, 2H), 7.59 (d, *J* = 9.0 Hz, 1H), 4.30 - 4.35 (m, 2H), 4.15 (s, 2H), 3.93 - 4.00 (m, 2H), 3.78 - 3.84 (m, 2H), 3.73 - 3.78 (m, 2H), 3.65 - 3.72 (m, 8H), 3.53 (s, 1H). **^{13}C NMR** (101 MHz, $CDCl_3$) δ 173.9, 154.2, 148.7, 134.3, 131.2, 115.7, 107.2, 86.0, 71.5, 71.2, 70.7, 70.5, 70.3, 70.1, 69.4, 69.3, 69.1. One signal is not observed, likely to be an acetylene carbon. **LCMS** (Method A) (ES -ve) *m/z* $(M - H)^-$ Rt 0.92 min (>95 % pure).

14-(2-((5-(4-(2-(*tert*-Butoxy)-2-oxoethoxy)-2,6-dimethylbenzyl)-3-isopropyl-2-(methoxymethoxy)phenyl)ethynyl)-5-nitrophenoxy)-3,6,9,12-tetraoxatetradecan-1-oic acid (43)

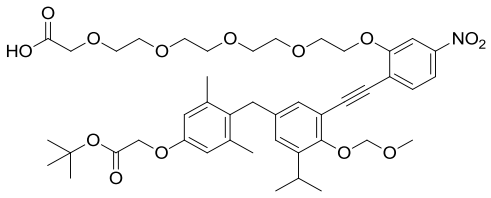

To a stirred solution of *tert*-butyl 2-(4-(3-iodo-5-isopropyl-4-(methoxymethoxy)benzyl)-3,5-dimethylphenoxy)acetate (243 mg, 0.219 mmol) and triethylamine (0.10 mL, 0.717 mmol) in DMF (2 mL) was added bis(triphenylphosphine)palladium(II) chloride (3 mg, 4 µmol) and chloro(triphenylphosphine)gold(I) (3 mg, 6 µmol), followed by 14-(2-ethynyl-5-nitrophenoxy)-3,6,9,12-tetraoxatetradecan-1-oic acid (100 mg, 0.252 mmol) and the mixture stirred at 80 °C for 14 h. The mixture was diluted with EtOAc (20 mL) and water (20 mL) and the pH adjusted to 3 with HCl (1 M aq.) and the phases separated.

The aqueous layer was back-extracted with EtOAc (2 x 20 mL) then the organic layers combined and evaporated *in vacuo*. The sample was loaded in methanol and purified by reverse phase (C18) chromatography using a 30-100 % acetonitrile-water (ammonium bicarbonate modifier) gradient over 14 CV. The appropriate fractions were combined and evaporated *in vacuo* to give the required product (88 mg, 49 % yield) as a dark brown oil.

^{1}H NMR (400 MHz, $CDCl_3$) δ 7.79 - 7.85 (m, 2H), 7.57 (d, *J* = 8.8 Hz, 1H), 7.00 (s, 1H), 6.87 (s, 1H), 6.64 (s, 2H), 5.32 (s, 2H), 4.52 (s, 2H), 4.32 (t, *J* = 4.8 Hz, 2H), 4.11 (s, 2H), 3.91 - 3.95 (m, 4H), 3.69 - 3.77 (m, 4H), 3.57 - 3.67 (m, 11H), 3.43 (spt, *J* = 6.9 Hz, 1H), 2.22 (s, 6H), 1.50 (s, 9H), 1.19 (d, *J* = 6.9 Hz, 6H). Exchangeable acid proton not observed. **^{13}C NMR** (101 MHz, $CDCl_3$) δ 173.25, 165.77, 159.45, 154.27, 142.05, 138.41, 135.83, 133.27, 129.78, 129.49, 127.57, 120.08, 118.58, 115.91, 114.26, 107.18, 105.58, 103.48, 99.95, 95.96, 85.18, 82.23, 71.35, 71.08, 70.59, 70.47, 70.22, 70.08, 69.31, 69.12, 69.08, 65.71, 57.52, 33.78, 28.06, 26.40, 23.31, 20.55. Note that ^{13}C NMR data are reported to two decimal places to differentiate the signals. **LCMS** (Method B) (ES -ve) *m/z* 822.9 $(M - H)^-$ Rt 1.30 min (>95 % pure). **HRMS** (ES) calcd for $C_{44}H_{57}NO_{14}Na$ $(M + Na)^+$ 846.3677, found 846.3669.

2-(4-(4-Hydroxy-3-((2-(((*S*)-16-((2*S*,4*R*)-4-hydroxy-2-((4-(4-methylthiazol-5-yl)benzyl)carbamoyl)pyrrolidine-1-carbonyl)-17,17-dimethyl-14-oxo-3,6,9,12-tetraoxa-15-azaoctadecyl)oxy)-4-nitrophenyl)ethynyl)-5-isopropylbenzyl)-3,5-dimethylphenoxy)acetic acid (44)

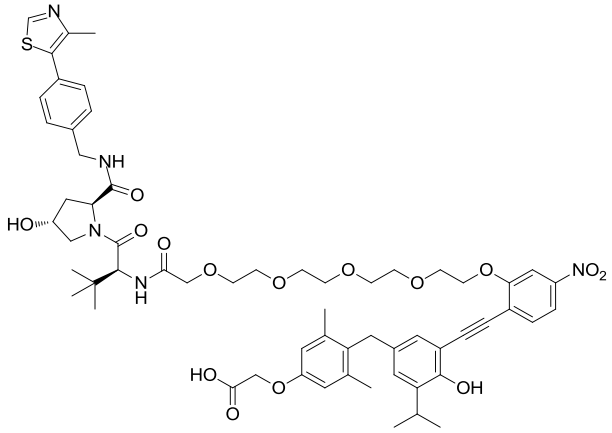

To a stirred solution of (2*S*,4*R*)-1-((*S*)-2-amino-3,3-dimethylbutanoyl)-4-hydroxy-*N*-(4-(4-methylthiazol-5-yl)benzyl)pyrrolidine-2-carboxamide hydrochloride (26 mg, 0.056 mmol), 14-(2-((5-(4-(2-(*tert*-butoxy)-2-oxoethoxy)-2,6-dimethylbenzyl)-3-isopropyl-2-(methoxymethoxy)phenyl)ethynyl)-5-nitrophenoxy)-3,6,9,12-tetraoxatetradecan-1-oic acid (42 mg, 0.051 mmol), and DIPEA (27 µL, 0.15 mmol) in DMF (1 mL) was added HATU (29 mg, 0.076 mmol) and the mixture stirred at rt for 1 h. The mixture was diluted with CH_2Cl_2 (10 mL) and water (10 mL) and the pH adjusted to 3 with HCl (1 M aq.), then the phases were separated. The aqueous layer was back-extracted with CH_2Cl_2 (3 x 10 mL) then the organic layers combined and evaporated *in vacuo*. The sample was directly dissolved in DMF (1 mL), then HCl (4 M in dioxane, 0.30 mL, 1.2 mmol) was added and the mixture stirred for 50 °C for 5 h. NaOH (2 M aq., 1.30 mL, 2.60 mmol) was then added and the mixture stirred at 50 °C for 16 h. The mixture was diluted with CH_2Cl_2 (10 mL) and water (10 mL), then the pH adjusted to 3 with HCl (1 M aq.) The aqueous layer was back-extracted with CH_2Cl_2 (5 x 10 mL), then the organic layers were combined, dried using a hydrophobic frit, and evaporated *in vacuo*. The sample was dissolved in DMSO and purified by MDAP (formic acid modifier gradient). The solvent was removed under a stream of nitrogen to give the required product (10.5 mg, 18 % yield) as a bright yellow oil.

^{1}H NMR (400 MHz, $CDCl_3$) δ 8.72 (s, 1H), 7.82 (d, *J* = 8.4 Hz, 1H), 7.77 (s, 1H), 7.53 (d, *J* = 8.3 Hz, 1H), 7.29 - 7.36 (m, 4H), 7.04 (s, 1H), 6.68 (s, 1H), 6.65 (s, 2H), 4.71 (t, *J* = 7.9 Hz, 1H), 4.62 (s, 2H), 4.46 - 4.59 (m, 3H), 4.27 - 4.35 (m, 2H), 4.06 - 4.12 (m, 1H), 3.87 - 4.02 (m, 6H), 3.69 - 3.74 (m, 1H), 3.51 - 3.65 (m, 11H), 3.28 (spt, *J* = 6.9 Hz, 1H), 2.44 - 2.53 (m, 4H), 2.22 (s, 6H), 2.08 - 2.17 (m, 1H), 1.27 (s, 2H), 1.23 (d, *J* = 6.8 Hz, 6H), 0.93 (s, 9H). **^{13}C NMR** (101 MHz, $CDCl_3$) δ 171.3, 170.8, 168.9, 166.7, 158.9, 157.5, 153.2, 150.6, 148.1, 147.8, 139.7, 138.4, 138.2, 134.5, 131.7, 131.6, 130.6, 130.2, 129.4, 128.7, 128.1, 126.5, 119.4, 116.2, 114.2, 108.3, 106.6, 100.9, 94.5, 71.0, 70.9, 70.5, 70.4, 70.3, 70.2, 69.1, 65.3, 58.6, 57.3, 56.8, 43.2, 36.0, 34.9, 33.6, 29.3, 27.5, 26.4, 22.4, 20.6, 15.8. Two signals are not resolved, potentially due to overlapping frequencies of PEG chain carbons. **LCMS** (Method B) (ES -ve) *m/z* 1135.3 $(M - H)^-$ Rt 1.10 min (>95 % pure). **HRMS** (ES) calcd for $C_{60}H_{74}N_5O_{15}S$, $(M + H)^+$ 1136.4902, found 1136.4918.

***tert*-Butyl 2-(4-(3-isopropyl-4-(methoxymethoxy)-5-((4-nitrophenyl)ethynyl)benzyl)-3,5-dimethylphenoxy)acetate (45)**

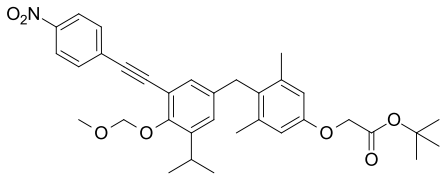

To a stirred solution of *tert*-butyl 2-(4-(3-iodo-5-isopropyl-4-(methoxymethoxy)benzyl)-3,5-dimethylphenoxy)acetate (100 mg, 90 µmol, 50 % pure), bis(triphenylphosphine)palladium(II) chloride (4 mg, 6 µmol) and triethylamine (40 µl, 0.29 mmol) in DMF (1 mL) was chloro(triphenylphosphine)gold(I) (4 mg, 8 µmol), then 1-ethynyl-4-nitrobenzene (13 mg, 90 µmol) was added and the mixture stirred at 80 °C for 20 h. The mixture was diluted with EtOAc (10 mL) and water (10 mL), then filtered through Celite and the phases separated. The aqueous layer was back-extracted with EtOAc (10 mL), then the organic layers combined and then evaporated *in vacuo*. The sample was dissolved in DMSO and purified by MDAP (ammonium bicarbonate modifier gradient). The solvent was removed under a stream of nitrogen to give the required product (12 mg, 23 % yield) as a yellow oil.

^{1}H NMR (400 MHz, $CDCl_3$) δ 8.21 (d, *J* = 8.8 Hz, 2H), 7.63 (d, *J* = 8.8 Hz, 2H), 7.05 (s, 1H), 6.86 (s, 1H), 6.65 (s, 2H), 5.24 (s, 2H), 4.52 (s, 2H), 3.94 (s, 2H), 3.62 (s, 3H), 3.41 (spt, *J* = 6.8 Hz, 1H), 2.22 (s, 6H), 1.51 (s, 9H), 1.20 (d, *J* = 6.8 Hz, 6H). **^{13}C NMR** (101 MHz, $CDCl_3$) δ 168.3, 156.1, 154.2, 146.9, 142.2, 138.4, 136.1, 132.1, 130.3, 129.7, 129.4, 127.9, 123.6, 115.5, 114.3, 100.0, 92.5, 90.9, 82.2, 65.7, 57.6, 33.8, 28.1, 26.5, 23.3, 20.5. **LCMS** (Method B) (ES +ve) *m/z* 591.5 $(M + NH_4)^+$ Rt 1.70 min (>95 % pure).

***tert*-Butyl 2-(4-((7-isopropyl-2-(4-nitrophenyl)benzofuran-5-yl)methyl)-3,5-dimethylphenoxy)acetate (46)**

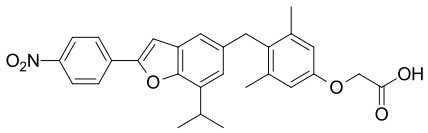

To a stirred solution of *tert*-butyl 2-(4-(3-isopropyl-4-(methoxymethoxy)-5-((4-nitrophenyl)ethynyl)benzyl)-3,5-dimethylphenoxy)acetate (12 mg, 21 μmol) in DMF (1 mL) was added HCl (4 M in dioxane, 0.1 mL, 0.4 mmol) and stirred for at 50 °C for 4 h. NaOH (2 M aq., 0.4 mL, 0.8 mmol) was then added and the reaction stirred at 50 °C for 20 h. The mixture was diluted with CH_2Cl_2 (10 mL) and water (10 mL), the pH adjusted to 3 with HCl (1 M aq.), then the phases were separated. The aqueous layer was back-extracted with CH_2Cl_2 (2 x 5 mL), then the organic layers were combined, dried using a hydrophobic frit, and evaporated *in vacuo*. The residue was dissolved in DMSO and purified by MDAP (formic acid modifier gradient). The solvent was removed under a stream of nitrogen to give the product (6.6 mg, 67 % yield) as a bright yellow solid.

^{1}H NMR (400 MHz, $CDCl_3$) δ 8.29 (d, *J* = 8.8 Hz, 2H), 7.95 (d, *J* = 8.8 Hz, 2H), 7.08 (s, 1H), 7.01 (s, 1H), 6.87 (s, 1H), 6.70 (s, 2H), 4.69 (s, 2H), 4.08 (s, 2H), 3.45 (spt, *J* = 6.8 Hz, 1H), 2.25 (s, 6H), 1.44 (d, *J* = 6.9 Hz, 6H). **^{13}C NMR** (101 MHz, $CDCl_3$) δ 169.4, 156.0, 152.8, 152.2, 147.0, 138.7, 136.6, 135.5, 132.2, 130.4, 128.7, 124.9, 124.3, 123.6, 117.1, 114.2, 105.3, 68.7, 34.3, 29.3, 22.6, 20.5. **LCMS** (Method A) (ES -ve) *m/z* 472.3 $(M - H)^-$ Rt 1.62 min (>95 % pure).

Methyl 2-(4-(3-isopropyl-4-(methoxymethoxy)-5-((4-nitrophenyl)ethynyl)benzyl)-3,5-dimethylphenoxy)acetate (47)

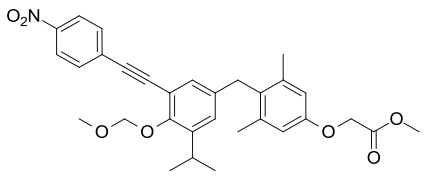

To a stirred solution of methyl 2-(4-(3-iodo-5-isopropyl-4-(methoxymethoxy)benzyl)-3,5-dimethylphenoxy)acetate (90 mg, 0.18 mmol), bis(triphenylphosphine)palladium(II) chloride (3 mg, 4 µmol), chloro(triphenylphosphine)gold(I) (2 mg, 4 µmol) and triethylamine (100 µl, 0.717 mmol) in DMF (2 mL) was added 1-ethynyl-4-nitrobenzene (31 mg, 0.21 mmol) and the mixture stirred at 50 °C for 16 h. Further bis(triphenylphosphine)palladium(II) chloride (3 mg, 4 µmol), chloro(triphenylphosphine)gold(I) (2 mg, 4 µmol) and 1-ethynyl-4-nitrobenzene (31 mg, 0.21 mmol) and the mixture stirred at 50 °C for a further 5 h. The mixture was diluted with EtOAc (10 mL) and water (10 mL) and filtered through Celite, then the phases were separated. The aqueous layer was back-extracted with EtOAc (10 mL), then the organic layers were combined and evaporated *in vacuo*. The sample was purified by chromatography on silica using a 0-10 % EtOAc-cyclohexane gradient over 12 CV. The appropriate fractions were combined and evaporated *in vacuo* to give the required product (25 mg, 26 % yield) as a red oil.

^{1}H NMR (400 MHz, $CDCl_3$) δ 8.21 (d, *J* = 9.0 Hz, 2H), 7.63 (d, *J* = 8.8 Hz, 2H), 7.06 (s, 1H), 6.85 (s, 1H), 6.66 (s, 2H), 5.23 (s, 2H), 4.65 (s, 2H), 3.94 (s, 2H), 3.83 (s, 3H), 3.62 (s, 3H), 3.41 (spt, *J* = 6.9 Hz, 1H), 2.23 (s, 6H), 1.21 (d, *J* = 6.8 Hz, 6H) **LCMS** (Method B) (ES +ve) *m/z* 549.5 $(M + NH_4)^+$ Rt 1.61 min (>95 % pure).

Consistent with literature data.[217]

2-(4-(4-Hydroxy-3-isopropyl-5-((4-nitrophenyl)ethynyl)benzyl)-3,5-dimethylphenoxy)acetic acid (48)

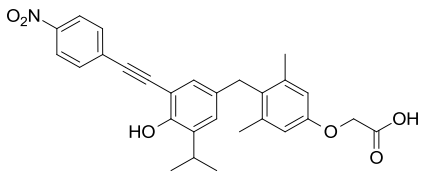

To a stirred solution of methyl 2-(4-(3-isopropyl-4-(methoxymethoxy)-5-((4-nitrophenyl)ethynyl)benzyl)-3,5-dimethylphenoxy)acetate (25 mg, 47 μmol) in MeOH (1 mL) and THF (1 mL) was added a solution of LiOH (50 mg, 2 mmol) in water (0.2 mL) and the mixture stirred at rt for 1 h. The reaction mixture was evaporated *in vacuo*, then the sample dissolved in 1,4-dioxane (5 mL), HCl (4 M in dioxane, 1 mL, 4 mmol) was added and the mixture stirred at 50 °C for 1 h. The mixture was diluted with EtOAc (10 mL) and water (10 mL), then the pH adjusted to 3 with $NaHCO_3$ (sat. aq.) and the phases were separated. The aqueous layer was back-extracted with EtOAc (2 x 10 mL), then the organic layers combined and evaporated *in vacuo*. The sample was dissolved in DMSO and purified by MDAP (formic acid modifier gradient). The solvent was evaporated *in vacuo* to give the required product (10 mg, 44 % yield) as a yellow solid.

^{1}H NMR (400 MHz, $CDCl_3$) δ 8.21 (d, *J* = 8.8 Hz, 2H), 7.64 (d, *J* = 8.8 Hz, 2H), 7.03 (s, 1H), 6.72 (s, 1H), 6.67 (s, 2H), 4.62 (s, 2H), 3.89 (s, 2H), 3.27 (spt, *J* = 6.9 Hz, 1H), 2.21 (s, 6H), 1.23 (d, *J* = 6.9 Hz, 6H). **LCMS** (Method B) (ES -ve) *m/z* 472.4 $(M - H)^-$ Rt 1.45 min (>95 % pure).

Consistent with literature data.[217]

7.2.3 Promiscuous Kinase Compounds

2-((2,5-Dichloropyrimidin-4-yl)amino)-*N*-methylbenzamide (49)

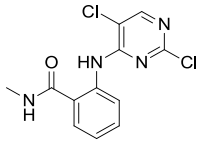

A solution of 2,4,5-trichloropyrimidine (1.25 mL, 10.9 mmol), 2-amino-N-methylbenzamide (2.00 g, 13.3 mmol) and DIPEA (2.30 mL, 13.2 mmol) in *i*-PrOH (40 mL) was heated at 85 °C for 3 h. The mixture was cooled to rt, then the resulting solid separated by filtration and washed with *i*-PrOH (3 x 20 mL). The solid was dried under vacuum to give the required product (3.14 g, 97 % yield) as a white solid.

^{1}H NMR (400 MHz, DMSO-d_6) δ 12.17 (s, 1H), 8.85 (s, 1H), 8.52 (d, J = 8.4 Hz, 1H), 8.48 (s, 1H), 7.81 (d, J = 8.1 Hz, 1H), 7.56 - 7.64 (m, 1H), 7.19 - 7.26 (m, 1H), 2.81 (d, J = 4.6 Hz, 3H). **LCMS** (Method A) (ES +ve) *m/z* 296.9/298.9 $(M + H)^+$ Rt 1.04 min (>95 % pure).

Consistent with literature data.[403]

***tert*-Butyl 4-(4-((5-chloro-4-((2-(methylcarbamoyl)phenyl)amino)pyrimidin-2-yl)amino)phenyl)piperazine-1-carboxylate (50)**

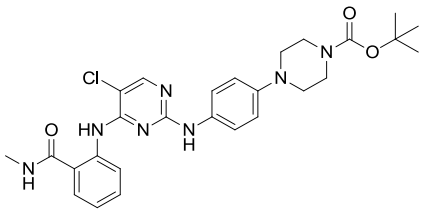

To a stirred solution of 2-((2,5-dichloropyrimidin-4-yl)amino)-*N*-methylbenzamide (522 mg, 1.76 mmol), *tert*-butyl 4-(4-aminophenyl)piperazine-1-carboxylate (536 mg, 1.93 mmol), BINAP (109 mg, 0.176 mmol) and cesium carbonate (1.72 g, 5.27 mmol) in toluene (8 mL) was added palladium(II) acetate (20 mg, 0.088 mmol) and the mixture heated in the microwave at 170 °C for 1 h. The mixture was filtered through Celite, diluted with EtOAc (100 mL) and water (100 mL) and filtered, then the phases

were separated. The aqueous phase was back-extracted with EtOAc (2 x 100 mL), then the organic layers were combined, dried using a hydrophobic frit and evaporated *in vacuo*. The sample was loaded in DMSO and purified by reverse phase (C18) chromatography using a 30-95 % acetonitrile-water (formic acid modifier) gradient over 14 CV. The appropriate fractions were combined and evaporated *in vacuo* to give the required product (383 mg, 41 % yield) as a brown solid.

^{1}H NMR (400 MHz, DMSO-d_6) δ 11.58 (s, 1H), 9.21 (s, 1H), 8.67 - 8.82 (m, 2H), 8.17 (s, 1H), 7.75 (d, J = 8.0 Hz, 1H), 7.44 - 7.55 (m, 3H), 7.13 (t, J = 7.6 Hz, 1H), 6.91 (d, J = 9.0 Hz, 2H), 3.45 - 3.50 (m, 4H), 3.00 - 3.06 (m, 4H), 2.81 (d, J = 4.4 Hz, 3H), 1.91 (s, 9H). **LCMS** (Method A) (ES +ve) *m/z* 538.5 $(M + H)^+$ Rt 1.16 min (>95 % pure).

Consistent with literature data.[255]

2,2,2-Trifluoro-1-(4-(4-nitrophenyl)piperazin-1-yl)ethanone (51)

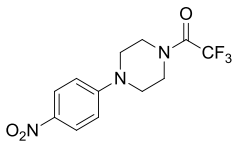

A solution of 1-chloro-4-nitrobenzene (3.00 g, 19.04 mmol) and piperazine (4.92 g, 57.1 mmol) in 1-butanol (30 mL) was heated at 120 °C for 16 h. The reaction mixture was evaporated *in vacuo*, then the resulting solid dissolved in HCl (2 M aq., 50 mL). The solution was washed with EtOAc (2 x 50 mL), then the pH adjusted to ~10 with NaOH (50 % aq.). The aqueous layer was then extracted with EtOAc (3 x 100 mL), then the organic layers were combined, washed with brine, dried over $MgSO_4$, filtered, then evaporated *in vacuo* to give a bright yellow solid. The solid was transferred to a three-necked flask and dissolved in CH_2Cl_2 (100 mL), then triethylamine (5.3 mL, 38 mmol) was added, then a stream of nitrogen was passed through the flask into an NaOH scrubber. A solution of trifluoroacetic anhydride (3.30 mL, 23.4 mmol) was dissolved in CH_2Cl_2 (100 mL) and added dropwise to the amine solution over 2 h, then the mixture stirred for a further 30 min. The solution was diluted with CH_2Cl_2 (100 mL) and water (200 mL), then the phases were separated. The aqueous layer was back-

extracted with CH_2Cl_2 (200 mL), then the organic layers were combined and evaporated *in vacuo*. The resulting solid was dissolved in CH_2Cl_2 and purified on silica using a 20-40 % EtOAc-cyclohexane gradient over 8 CV. The appropriate fractions were combined and evaporated *in vacuo* to give the required product (4.48 g, 78% yield) as a yellow powder.

^{1}H NMR (400 MHz, $CDCl_3$) δ 8.18 (d, *J* = 9.4 Hz, 2H), 6.88 (d, *J* = 9.4 Hz, 2H), 3.78 - 3.93 (m, 4H), 3.47 - 3.55 (m, 4H). **^{13}C NMR** (101 MHz, $CDCl_3$) δ 155.6 (q, *J* = 35.9 Hz), 154.1, 139.7, 125.9, 116.3 (d, *J* = 288.3 Hz), 113.5, 47.3, 46.7, 44.9, 42.7. Multiple signals observed corresponding to piperazine carbons, potentially caused by a locked confirmation induced by the trifluoroacetamide. **^{19}F NMR** (376 MHz, $CDCl_3$) δ -69.0. **LCMS** (Method A) (ES +ve) *m/z* 304.2 $(M + H)^+$ Rt 1.06 min (>95 % pure). **HRMS** (ES) calcd for $C_{12}H_{13}F_3N_3O_3$, $(M + H)^+$ 304.0904, found 304.0916.

1-(4-(4-Aminophenyl)piperazin-1-yl)-2,2,2-trifluoroethanone (52)

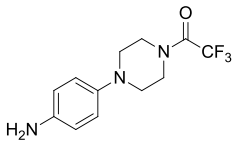

To a flask containing 2,2,2-trifluoro-1-(4-(4-nitrophenyl)piperazin-1-yl)ethanone (4.00 g, 13.2 mmol) and Pd/C (10 % w/w, 0.420 g, 3.95 mmol) was added EtOH (80 mL) and the mixture stirred under an atmosphere of hydrogen for 2 h. The reaction mixture was passed through Celite, then evaporated *in vacuo* to give the required product (3.69 g, 97 % yield) as a pale orange gum. The sample was used directly in the next reaction without further purification

^{1}H NMR (400 MHz, $CDCl_3$) δ 6.81 (d, *J* = 8.8 Hz, 1H), 6.66 (d, *J* = 8.8 Hz, 2H), 3.82 (t, *J* = 5.1 Hz, 2H), 3.74 (t, *J* = 4.9 Hz, 2H), 3.51 (br. s., 2H), 3.06 (t, *J* = 4.9 Hz, 4H). **^{19}F NMR** (376 MHz, $CDCl_3$) δ -68.7. **LCMS** (Method A) (ES +ve) *m/z* 274.3 $(M + H)^+$ Rt 0.43 min (>95 % pure).

2-((5-Chloro-2-((4-(4-(2,2,2-trifluoroacetyl)piperazin-1-yl)phenyl)amino)pyrimidin-4-yl)amino)-*N*-methylbenzamide (53)

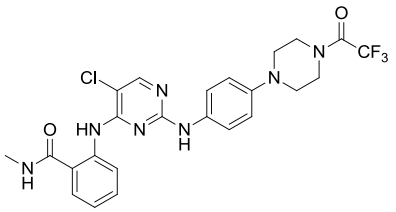

To a stirred slurry of 2-((2,5-dichloropyrimidin-4-yl)amino)-*N*-methylbenzamide (3.80 g, 12.8 mmol) and 1-(4-(4-aminophenyl)piperazin-1-yl)-2,2,2-trifluoroethanone (3.69 g, 12.8 mmol) in *i*-PrOH (100 mL) was added TFA (0.2 mL, 2.60 mmol) then the mixture stirred at 100 °C for 24 h. The solution was concentrated *in vacuo*, then diluted with EtOAc (200 mL), water (200 mL) and $NaHCO_3$ (sat. aq., 50 mL), then the phases were separated. The aqueous layer was back-extracted with EtOAc (2 x 100 mL), then the organic layers were combined, dried over $MgSO_4$, filtered and evaporated *in vacuo*. The resulting solid was triturated with boiling TBME (2 x 50 mL), then dried to give the required product (5.72 g, 84 % yield) as an off-white solid.

^{1}H NMR (400 MHz, DMSO-d_6) δ 11.65 (s, 1H), 9.30 (s, 1H), 8.67 - 8.81 (m, 2H), 8.17 (s, 1H), 7.75 (d, *J* = 8.0 Hz, 1H), 7.41 - 7.62 (m, 3H), 7.14 (t, *J* = 7.6 Hz, 1H), 6.93 (d, *J* = 9.0 Hz, 2H), 3.65 - 3.79 (m, 6H), 3.18 (t, *J* = 5.1 Hz, 4H), 2.81 (d, *J* = 4.4 Hz, 3H). **^{19}F NMR** (376 MHz, DMSO-d_6) δ -68.0. **LCMS** (Method A) (ES +ve) *m/z* 534.4 $(M + H)^+$ Rt 1.07 min (>95 % pure). **HRMS** (ES) calcd for $C_{24}H_{24}ClF_3N_7O_2$, $(M + H)^+$ 534.1627, found 534.1636.

2-((5-Chloro-2-((4-(piperazin-1-yl)phenyl)amino)pyrimidin-4-yl)amino)-*N*-methylbenzamide (54)

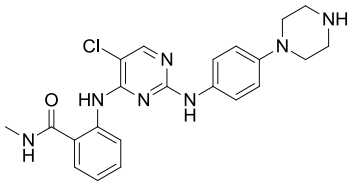

To a stirred solution of 2-((5-chloro-2-((4-(4-(2,2,2-trifluoroacetyl)piperazin-1-yl)phenyl)amino)pyrimidin-4-yl)amino)-*N*-methylbenzamide (5.60 g, 10.5 mmol) in MeOH (100 mL) was added potassium carbonate (2.17 g, 15.7 mmol) and the mixture stirred at 50 °C for 1 h. The mixture was poured into EtOAc (200 mL) and water (200 mL), then the pH adjusted to 2 with HCl (25 % aq.). The organic layer was decanted, then the aqueous layer basified to pH 12 with NaOH (50 % aq.). The resulting precipitate was separated by filtration, washed with water, azeotropically dried with toluene (3 x 100 mL) then further under vacuum to give the required product (3.72 g, 81 % yield) as an off-white solid.

^{1}H NMR (400 MHz, Methanol-d_4) δ 8.69 (d, J = 8.3 Hz, 1H), 8.01 (s, 1H), 7.64 (d, J = 7.8 Hz, 1H), 7.34 - 7.50 (m, 3H), 7.10 (t, J = 7.6 Hz, 1H), 6.96 (d, J = 8.9 Hz, 2H), 3.15 - 3.21 (m, 4H), 3.08 - 3.14 (m, 4H), 2.92 (s, 3H). **LCMS** (Method A) (ES +ve) *m/z* 438.2/440.2 $(M + H)^+$ Rt 0.99 min (indicates 80 % purity, NMR indicates >95 %)

Consistent with literature data.[255]

14-(4-(4-((5-Chloro-4-((2-(methylcarbamoyl)phenyl)amino)pyrimidin-2-yl)amino)phenyl)piperazin-1-yl)-3,6,9,12-tetraoxatetradecan-1-oic acid (55)

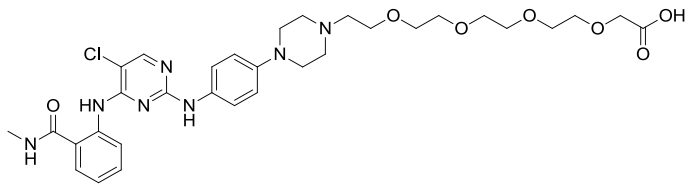

A solution of 2-((5-chloro-2-((4-(piperazin-1-yl)phenyl)amino)pyrimidin-4-yl)amino)-*N*-methylbenzamide (150 mg, 0.343 mmol), methyl 14-chloro-3,6,9,12-tetraoxatetradecanoate (117 mg, 0.411 mmol), sodium iodide (52 mg, 0.347 mmol) and DIPEA (0.179 mL, 1.03 mmol) in DMF (2.5 mL) was heated at 100 °C for 24 h. The mixture was diluted with *n*-BuOH (15 mL) and water (30 mL), then the phases were separated. The aqueous solution was back-extracted with *n*-BuOH (15 mL), then the organic layers were combined and evaporated *in vacuo*.

The residue was dissolved in MeOH (5 mL), then a solution of LiOH (82 mg, 3.43 mmol) in water (1 mL) was added and the mixture stirred at rt for 2 h. The reaction mixture was evaporated *in vacuo*, then dissolved in minimal DMSO and purified by reverse phase (C18) chromatography using a 0-50 % acetonitrile-water (+0.1 % ammonium bicarbonate modifier) gradient over 12 CV. The appropriate fractions were combined and evaporated *in vacuo* to give the required product (153 mg, 67 % yield) as a gold solid.

^{1}H NMR (400 MHz, DMSO-d_6) δ 11.60 (s, 1H), 9.21 (s, 1H), 8.67 - 8.81 (m, 2H), 8.16 (s, 1H), 7.75 (d, J = 7.8 Hz, 1H), 7.41 - 7.56 (m, 3H), 7.08 - 7.16 (m, 1H), 6.91 (d, J = 9.3 Hz, 2H), 4.01 (s, 2H), 3.62 - 3.73 (m, 3H), 3.49 - 3.62 (m, 13H), 3.15 - 3.24 (m, 4H), 2.90 - 2.97 (m, 4H), 2.81 (d, J = 4.4 Hz, 3H). **^{13}C NMR** (101 MHz, DMSO-d_6) δ 171.58, 168.89, 162.95, 157.95, 154.90, 154.55, 150.03, 139.41, 132.72, 131.44, 127.90, 121.74, 121.22, 120.47, 116.03, 108.52, 69.80, 69.73, 69.62, 69.61, 67.59, 55.97, 52.14, 48.56, 47.49, 26.27. Note that ^{13}C NMR data are reported to two decimal places to differentiate the signals. Two signals are not resolved potentially due to overlapping frequencies of PEG chain carbons. **LCMS** (Method A) (ES +ve) *m/z* 672.6

$(M + H)^+$ Rt 0.59 min (>95 % pure). **HRMS** (ES) calcd for $C_{32}H_{43}ClN_7O_7$, $(M + H)^+$ 672.2907, found 672.2953.

2-((5-Chloro-2-((4-(4-(2-(2-(2-chloroethoxy)ethoxy)ethyl)piperazin-1-yl)phenyl)amino)pyrimidin-4-yl)amino)-*N*-methylbenzamide (56)

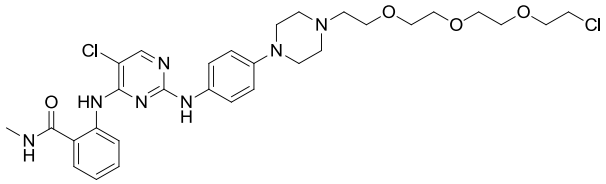

A solution of 2-((5-Chloro-2-((4-(piperazin-1-yl)phenyl)amino)pyrimidin-4-yl)amino)-*N*-methylbenzamide (258 mg, 0.589 mmol) and 1-chloro-2-(2-(2-(2-chloroethoxy)ethoxy)ethoxy)ethane (0.346 mL, 1.767 mmol) in DMF (3 mL) was heated in the microwave at 150 °C for 3 h. The mixture was diluted with EtOAc (20 mL) and NaHCO3 (sat. aq., 20 mL), then the phases were separated. The aqueous layer was back-extracted with EtOAc (2 x 20 mL), then the organic layers were combined, washed with brine (50 mL), dried using a hydrophobic frit and evaporated *in vacuo*. The sample was loaded in CH_2Cl_2 and purified on silica using a 0-15% MeOH-CH_2Cl_2 gradient over 14 CV. The appropriate fractions were combined and evaporated *in vacuo* to give the required product (130 mg, 35 % yield) as a brown solid.

^{1}H NMR (400 MHz, $CDCl_3$) δ 11.06 (s, 1H), 8.66 (d, *J* = 8.6 Hz, 1H), 8.05 (s, 1H), 7.46 (d, *J* = 7.8 Hz, 1H), 7.35 - 7.43 (m, 3H), 7.00 - 7.07 (m, 1H), 6.98 (s, 1H), 6.90 (d, *J* = 8.8 Hz, 2H), 6.29 (d, *J* = 4.6 Hz, 1H), 3.76 (t, *J* = 5.9 Hz, 2H), 3.60 - 3.73 (m, 12H), 3.14 - 3.22 (m, 4H), 3.01 (d, *J* = 4.9 Hz, 3H), 2.63 - 2.75 (m, 6H). **^{13}C NMR** (101 MHz, $CDCl_3$) δ 169.6, 158.2, 155.7, 154.5, 147.6, 139.7, 131.9, 131.7, 126.6, 122.3, 122.2, 122.0, 121.4, 116.7, 106.2, 71.4, 70.7, 70.6, 70.4, 69.0, 57.8, 53.6, 49.8, 42.7, 26.9. One signal is not resolved potentially due to overlapping frequencies of PEG chain carbons. **LCMS** (Method A) (ES +ve) *m/z* 632.6/634.5 $(M + H)^+$ Rt 0.69 min (>95 % pure). **HRMS** (ES) calcd for $C_{30}H_{40}Cl_2N_7O_4$, $(M + H)^+$ 632.2513, found 632.2549.

14-(4-(4-((5-Chloro-4-((2-(methylcarbamoyl)phenyl)amino)pyrimidin-2-yl)amino)phenyl)piperazin-1-yl)-*N*-(2-(2,6-dioxopiperidin-3-yl)-1-oxoisoindolin-4-yl)-3,6,9,12-tetraoxatetradecan-1-amide, formic acid salt (57)

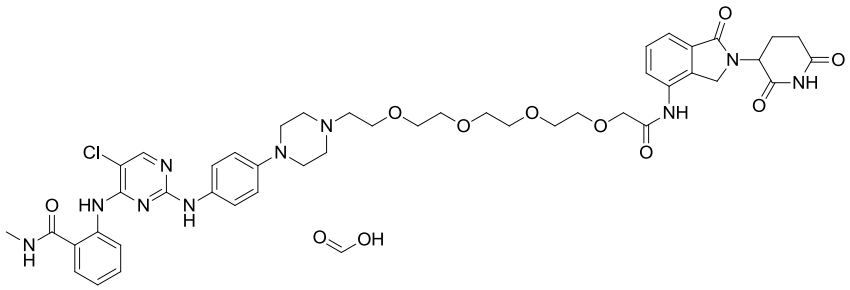

To a stirred solution of 14-(4-(4-((5-chloro-4-((2-(methylcarbamoyl)phenyl)amino)pyrimidin-2-yl)amino)phenyl)piperazin-1-yl)-3,6,9,12-tetraoxatetradecanoic acid (109 mg, 0.162 mmol), 3-(4-amino-1-oxoisoindolin-2-yl)piperidine-2,6-dione (46.2 mg, 0.178 mmol) and DIPEA (85 µL, 0.49 mmol) in DMF (1.5 mL) was added HATU (74.0 mg, 0.195 mmol) and the mixture stirred at rt for 1 h. The reaction mixture was directly purified by MDAP (formic acid modifier gradient), then the appropriate fractions concentrated under a stream of nitrogen to give the required product (57 mg, 37 % yield) as a yellow solid.

^{1}H NMR (400 MHz, DMSO-d_6) δ 11.61 (s, 1H), 11.02 (s, 1H), 9.67 (s, 1H), 9.20 (s, 1H), 8.65 - 8.83 (m, 2H), 7.72 - 7.78 (m, 2H), 7.42 - 7.60 (m, 5H), 7.12 (t, J = 7.5 Hz, 1H), 6.88 (d, J = 9.3 Hz, 2H), 5.15 (dd, J = 5.1, 13.4 Hz, 1H), 4.30 - 4.46 (m, 1H), 4.14 (s, 2H), 3.43 - 3.74 (m, 15H), 3.04 - 3.14 (m, 4H), 2.85 - 2.98 (m, 1H), 2.81 (d, J = 4.6 Hz, 3H), 2.55 - 2.71 (m, 7H), 2.36 (m, 1H), 1.96 - 2.05 (m, 1H). **^{13}C NMR** (101 MHz, DMSO-d_6) δ 172.84, 171.00, 168.94, 168.43, 167.76, 163.19, 158.02, 154.92, 154.61, 146.37, 139.46, 134.82, 132.89, 132.73, 132.28, 131.48, 128.64, 127.93, 126.32, 121.76, 121.30, 120.46, 119.75, 115.77, 104.33, 70.42, 69.96, 69.85, 69.75, 69.71, 69.65, 69.63, 67.80, 56.90, 52.91, 51.53, 48.61, 46.42, 31.21, 26.32, 22.59. Note that ^{13}C NMR data are reported to two decimal places to differentiate the signals. **LCMS** (Method A) (ES +ve) *m/z* 913.3 $(M + H)^+$ Rt 0.60 min (>95 % pure). **HRMS** (ES) calcd for $C_{45}H_{54}ClN_{10}O_9$, $(M + H)^+$ 913.3758, found 913.3761. **IR** ν_{max} (neat) 2865, 1689, 1600, 1559, 1512, 1448, 1414 cm^{-1}. **MP** >250 °C (decomposition).

(2*S*,4*R*)-1-((*S*)-2-(*tert*-Butyl)-17-(4-(4-((5-chloro-4-((2-(methylcarbamoyl)phenyl)amino) pyrimidin-2-yl)amino)phenyl)piperazin-1-yl)-4-oxo-6,9,12,15-tetraoxa-3-azaheptadecan-1-oyl)-4-hydroxy-*N*-(4-(4-methylthiazol-5-yl)benzyl)pyrrolidine-2-carboxamide (58)

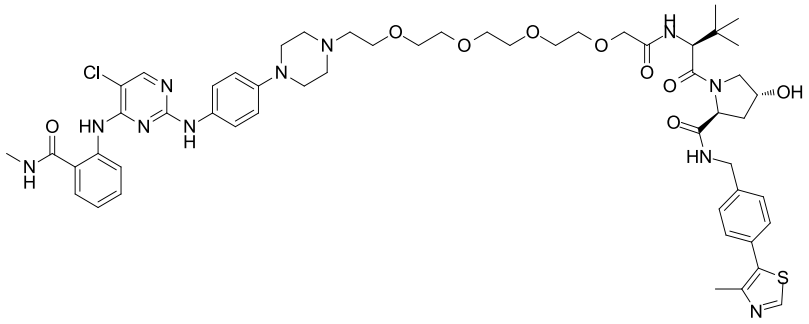

To a stirred solution of 14-(4-(4-((5-chloro-4-((2-(methylcarbamoyl)phenyl)amino)pyrimidin-2-yl)amino)phenyl)piperazin-1-yl)-3,6,9,12-tetraoxatetradecan-1-oic acid (58 mg, 0.086 mmol), (2*S*,4*R*)-1-((*S*)-2-amino-3,3-dimethylbutanoyl)-4-hydroxy-*N*-(4-(4-methylthiazol-5-yl)benzyl)pyrrolidine-2-carboxamide hydrochloride (48 mg, 0.10 mmol), and DIPEA (75 µL, 0.43 mmol) in DMF (0.7 mL) was added HATU (46 mg, 0.12 mmol) and the mixture stirred at rt for 1 h. The reaction mixture was directly purified by MDAP (ammonium bicarbonate modifier gradient), then the appropriate fractions were evaporated *in vacuo* to give the required product (57 mg, 61 % yield) as a yellow solid.

^{1}H NMR (400 MHz, Methanol-d_4) δ 10.04 (s, 1H), 8.12 (br. s., 1H), 7.77 (d, J = 7.8 Hz, 1H), 7.48 - 7.60 (m, 5H), 7.42 (d, J = 8.8 Hz, 2H), 7.27 - 7.33 (m, 1H), 7.22 (d, J = 8.8 Hz, 2H), 4.67 (s, 1H), 4.35 - 4.64 (m, 5H), 3.77 - 4.05 (m, 12H), 3.65 - 3.75 (m, 14H), 3.49 - 3.54 (m, 2H), 2.93 (s, 3H), 2.61 (s, 3H), 2.23 - 2.33 (m, 1H), 2.01 - 2.13 (m, 1H), 1.04 (s, 9H). **^{13}C NMR** (101 MHz, DMSO-d_6) δ 174.56, 172.19, 171.86, 170.89, 158.61, 156.92, 142.85, 142.15, 141.43, 138.34, 137.84, 133.17, 130.75, 130.59, 129.61, 129.26, 127.90, 127.26, 126.67, 124.43, 124.34, 119.19, 119.03, 115.01, 108.14, 72.40, 72.35, 71.80, 71.65, 71.60, 71.53, 71.49, 71.20, 65.69, 61.03, 58.44, 58.30, 57.44, 53.23, 43.74, 39.29, 37.09, 27.14, 27.04, 13.13. Note that ^{13}C NMR data are reported to two decimal places to differentiate the signals. One signal is

not observed, potentially due to overlapping signals of PEG chain carbons. **LCMS** (Method B) (ES +ve) *m/z* 1084.5 $(M + H)^+$ Rt 1.14 min (>95 % pure). **HRMS** (ES) calcd for $C_{54}H_{71}ClN_{11}O_9S$, $(M + H)^+$ 1084.4845, found 1084.4813. **IR** ν_{max} (neat) 3269, 2919, 1632, 1601, 1513, 1448, 1415 cm^{-1}. **MP** >250 °C (decomposition).

(2*R*,4*S*)-1-((*R*)-2-(*tert*-Butyl)-17-(4-(4-((5-chloro-4-((2-(methylcarbamoyl)phenyl)amino) pyrimidin-2-yl)amino)phenyl)piperazin-1-yl)-4-oxo-6,9,12,15-tetraoxa-3-azaheptadecan-1-oyl)-4-hydroxy-*N*-(4-(4-methylthiazol-5-yl)benzyl)pyrrolidine-2-carboxamide (59)

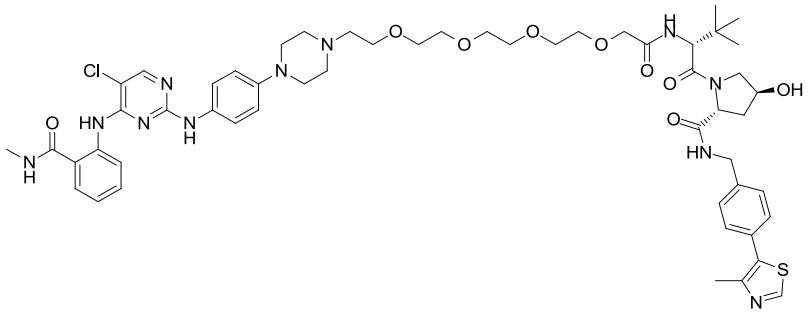

To a stirred solution of 14-(4-(4-((5-chloro-4-((2-(methylcarbamoyl)phenyl)amino)pyrimidin-2-yl)amino)phenyl)piperazin-1-yl)-3,6,9,12-tetraoxatetradecan-1-oic acid (20.3 mg, 0.030 mmol), (2*R*,4*S*)-1-((*R*)-2-amino-3,3-dimethylbutanoyl)-4-hydroxy-*N*-(4-(4-methylthiazol-5-yl)benzyl)pyrrolidine-2-carboxamide hydrochloride (17 mg, 0.036 mmol) and DIPEA (40 µl, 0.229 mmol) in DMF (0.7 mL) was added HATU (16 mg, 0.042 mmol) and the mixture stirred at rt for 2 h. The solution was purified directly by MDAP (formic acid modifier gradient), then the appropriate fractions were combined and dried under a stream of nitrogen to give the required product (29 mg, 89 % yield) as a yellow solid.

^{1}H NMR (400 MHz, Methanol-d_4) δ 10.02 (s, 1H), 8.10 (s, 1H), 7.77 (d, *J* = 7.8 Hz, 1H), 7.50 - 7.60 (m, 5H), 7.40 (d, *J* = 8.8 Hz, 2H), 7.26 - 7.35 (m, 1H), 7.19 (d, *J* = 8.8 Hz, 2H), 4.67 (s, 1H), 4.36 - 4.63 (m, 5H), 3.76 - 4.08 (m, 12H), 3.63 - 3.76 (m, 14H), 3.47 - 3.53 (m, 2H), 2.93 (s, 3H), 2.60 (s, 3H), 2.22 - 2.31 (m, 1H), 2.01 - 2.13 (m, 1H), 1.04 (s, 9H). **^{13}C NMR** (101 MHz, Methanol-d_4) δ 174.58, 172.21, 171.90, 170.97, 158.69, 156.89, 142.85, 142.21, 141.42, 138.36, 137.85, 133.15, 130.77,

130.64, 129.62, 129.24, 127.94, 127.39, 126.66, 124.56, 124.39, 119.09, 119.04, 114.96, 108.17, 72.37, 71.81, 71.67, 71.64, 71.56, 71.49, 71.22, 71.20, 65.58, 61.05, 58.44, 58.32, 57.45, 53.31, 43.76, 39.29, 37.13, 27.13, 27.03, 13.10. Note that ^{13}C NMR data are reported to two decimal places to differentiate the signals. One signal is not observed, potentially due to overlapping signals of PEG chain carbons. **LCMS** (Method A) (ES +ve) *m/z* 543.2 $([M + 2H]/2)^+$ Rt 0.76 min (>95 % pure). Note: ionisation pattern is weak. **HRMS** (ES) calcd for $C_{54}H_{71}ClN_{11}O_9S$, $(M + H)^+$ 1084.4845, found 1084.4853. **IR** ν_{max} (neat) 3265, 3053, 2922, 1631, 1601, 1513, 1447, 1415 cm^{-1}. **MP** >250 °C (decomposition).

(*S*)-7-(2-(2-(2-(2-(4-(4-((5-Chloro-4-((2-(methylcarbamoyl)phenyl)amino)pyrimidin-2-yl)amino)phenyl)piperazin-1-yl)ethoxy)ethoxy)ethoxy)ethoxy)-2-((*S*)-3,3-dimethyl-2-((*S*)-2-(methylamino)propanamido)butanoyl)-*N*-((*R*)-1,2,3,4-tetrahydronaphthalen-1-yl)-1,2,3,4-tetrahydroisoquinoline-3-carboxamide (60)

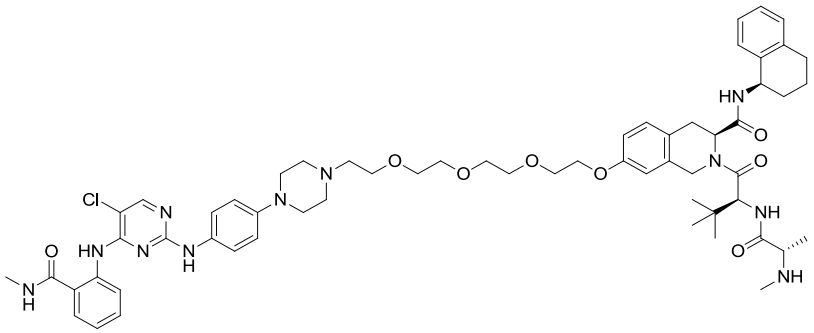

A solution of 2-((5-chloro-2-((4-(4-(2-(2-(2-(2-chloroethoxy)ethoxy)ethoxy)ethyl)piperazin-1-yl)phenyl)amino)pyrimidin-4-yl)amino)-*N*-methylbenzamide (66.0 mg, 0.104 mmol), *tert*-butyl ((*S*)-1-(((*S*)-1-((*S*)-7-hydroxy-3-(((*R*)-1,2,3,4-tetrahydronaphthalen-1-yl)carbamoyl)-3,4-dihydroisoquinolin-2(1*H*)-yl)-3,3-dimethyl-1-oxobutan-2-yl)amino)-1-oxopropan-2-yl)(methyl)carbamate (78.0 mg, 0.125 mmol), sodium iodide (15.6 mg, 0.104 mmol) and cesium carbonate (51.0 mg, 0.157 mmol) in DMF (1.5 mL) was stirred at 100 °C for 24 h. The reaction mixture was partitioned between CH_2Cl_2 (10 mL) and water (10 mL), then the phases were separated. The aqueous layer was back-extracted with CH_2Cl_2 (2 x 5 mL), then the organic layers were combined and evaporated *in vacuo*.

The residue was dissolved in minimal DMSO and purified by reverse phase (C18) chromatography using a 45-95 % acetonitrile-water (+0.1 % ammonium bicarbonate modifier) gradient over 14 CV. The appropriate fractions were combined and evaporated *in vacuo*, then the residue directly dissolved in CH_2Cl_2 (1.5 mL). TFA (150 µL, 1.95 mmol) was added, then the mixture left to stand for 8 h. The reaction mixture was evaporated *in vacuo*, then the sample was loaded in minimal MeOH and purified by SPE on an aminopropyl functionalised silica cartridge (Biotage Isolute NH_2) eluting with MeOH (20 mL). The eluent was dried under a stream of nitrogen to give the required product (64 mg, 55 % yield) as a beige solid.

^{1}H NMR (400 MHz, DMSO-d_6, T = 120 °C) δ 11.26 (br. s., 1H), 8.59 - 8.80 (m, 2H), 8.31 (br. s., 1H), 8.09 (s, 1H), 7.73 (d, *J* = 7.8 Hz, 1H), 7.37 - 7.46 (m, 3H), 6.99 - 7.14 (m, 6H), 6.77 - 6.90 (m, 4H), 4.83 - 4.96 (m, 2H), 4.11 (t, *J* = 5.0 Hz, 2H), 3.78 (t, *J* = 5.1 Hz, 2H), 3.54 - 3.67 (m, 11H), 3.08 - 3.12 (m, 4H), 2.83 - 3.04 (m, 11H), 2.65 - 2.79 (m, 2H), 2.55 - 2.64 (m, 6H), 2.20 (s, 3H), 1.78 - 1.89 (m, 2H), 1.58 - 1.74 (m, 2H), 1.13 (d, *J* = 6.8 Hz, 3H), 1.03 (br. s., 9H). **^{13}C NMR** (101 MHz, DMSO-d_6, T = 120 °C) δ 170.30, 168.38, 157.88, 156.76, 154.68, 153.87, 153.84, 146.40, 136.34, 131.58, 130.42, 127.67, 127.43, 127.09, 125.79, 124.94, 123.69, 123.54, 121.34, 120.99, 120.88, 115.13, 115.00, 113.22, 111.80, 105.18, 70.14, 69.56, 69.41, 69.39, 69.24, 68.58, 68.04, 67.24, 58.75, 58.67, 56.73, 53.85, 53.57, 52.92, 52.62, 52.51, 48.62, 46.36, 33.28, 29.99, 29.08, 28.10, 25.80, 25.73, 25.47, 19.41, 17.85. Note that ^{13}C NMR data are reported to two decimal places to differentiate the signals. Three signals are not observed potentially due to overlapping signals of PEG chain carbons. **LCMS** (Method B) (ES +ve) *m/z* 1116.4 $(M + H)^+$ Rt 1.35 min (>95 % pure). **HRMS** (ES) calcd for $C_{60}H_{79}ClN_{11}O_8$, $(M + H)^+$ 1116.5801, found 1116.5811. **IR** ν_{max} (neat) 3306, 2926, 1642, 1601, 1561, 1506, 1447, 1414 cm^{-}1. **MP** >250 °C (decomposition).

7.2.4 BTK Compounds

3-Iodo-1*H*-pyrazolo[3,4-d]pyrimidin-4-amine (61)

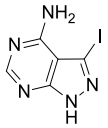

A suspension of 1*H*-pyrazolo[3,4-d]pyrimidin-4-amine (2.50 g, 18.5 mmol) and NIS (4.99 g, 22.2 mmol) in DMF (20 mL) was heated at 100 °C for 24 h. The reaction mixture was poured into water (400 mL) and the solution filtered. The precipitate was collected, washed with EtOH (2 x 50 mL) and dried to give the required product (2.88 g, 60 % yield) as a beige solid.

^{1}H NMR (400 MHz, DMSO-d_6) δ 13.79 (br. s., 1H), 8.17 (s, 1H), 3.30 (br. s., 2H). **LCMS** (Method B) (ES +ve) *m/z* 262.0 $(M + H)^+$ Rt 0.44 min (>95 % pure).

Consistent with literature data.[404]

3-(4-Phenoxyphenyl)-1*H*-pyrazolo[3,4-d]pyrimidin-4-amine (62)

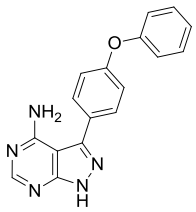

To a degassed solution of 3-iodo-1*H*-pyrazolo[3,4-d]pyrimidin-4-amine (2.88 g, 11.0 mmol) (4-phenoxyphenyl)boronic acid (2.83 g, 13.2 mmol) and potassium phosphate (7.03 g, 33.1 mmol) in 1,4-dioxane (100 mL) was added XPhos (0.105 g, 0.221 mmol) and XPhos Pd G2 (0.174 g, 0.221 mmol) then the mixture stirred at 100 °C for 24 h. The reaction mixture was poured into water (500 mL), and the resulting precipitate separated by filtration. The precipitate was washed with water (2 x 50 mL) and EtOH (2 x 50 mL). The solid was triturated with ice-cold EtOAc (50 mL) and dried to give the required product (2.15 g, 64 % yield) as a brown solid.

^{1}H NMR (400 MHz, DMSO-d_6) δ 8.21 (s, 1H), 7.66 (d, *J* = 8.8 Hz, 2H), 7.43 (t, *J* =

8.0 Hz, 2H), 7.10 - 7.21 (m, 5H). **LCMS** (Method B) (ES +ve) *m/z* 304.1 $(M + H)^+$ Rt 0.91 min (>95 % pure).

Consistent with literature data.[404]

(*R*)-*tert*-Butyl 3-(4-amino-3-iodo-1*H*-pyrazolo[3,4-d]pyrimidin-1-yl)piperidine-1-carboxylate (63)

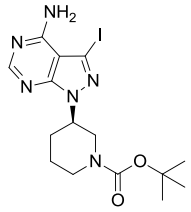

To a stirred solution of 3-iodo-1*H*-pyrazolo[3,4-d]pyrimidin-4-amine (2.04 g, 7.82 mmol) and triphenylphosphine (3.07 g, 11.7 mmol) in THF (200 mL) was added DIAD (2.28 mL, 11.7 mmol) and (*S*)-*tert*-butyl 3-hydroxypiperidine-1-carboxylate (2.36 g, 11.7 mmol), then the mixture stirred at rt for 20 h. The mixture was evaporated *in vacuo*, then loaded in CH_2Cl_2 and purified on silica using a 0-80 % EtOAc-CH_2Cl_2 gradient over 14 CV. The appropriate fractions were combined and evaporated *in vacuo* to give the required product (2.26 g, 59 % yield, 90 % purity) as a white solid.

^{1}H NMR (400 MHz, DMSO-d_6, T = 120 °C) δ 8.23 (s, 1H), 6.81 (br. s., 2H), 4.55 - 4.72 (m, 1H), 4.04 (d, *J* = 12.8 Hz, 1H), 3.76 - 3.89 (m, 1H), 3.30 - 3.46 (m, 1H), 2.94 - 3.09 (m, 1H), 2.03 - 2.28 (m, 2H), 1.85 - 2.00 (m, 1H), 1.50 - 1.67 (m, 1H), 1.41 (s, 9H). **LCMS** (Method A) (ES +ve) *m/z* 445.2 $(M + H)^+$ Rt 1.01 min (90 % pure).

Consistent with literature data.[405]

(*R*)-3-(4-phenoxyphenyl)-1-(piperidin-3-yl)-1I-pyrazolo[3,4-d]pyrimidin-4-amine (64)

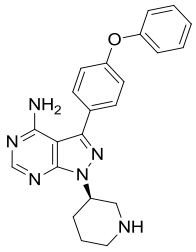

Method 1: Employing **62** as starting material

To a stirred suspension of (*S*)-*tert*-butyl 3-hydroxypiperidine-1-carboxylate (1.99 g, 9.89 mmol) and triphenylphosphine (polymer bound, 4 g, 12 mmol) was added DIAD (1.92 mL, 9.87 mmol) dropwise, then the mixture stirred at rt for 5 min. 3-(4-Phenoxyphenyl)-1*H*-pyrazolo[3,4-d]pyrimidin-4-amine (1.50 g, 4.95 mmol) was then added and the mixture heated at 70 °C for 3 h. The mixture was passed through Celite, then the remaining resin washed with CH_2Cl_2 (100 mL) and MeOH (100 mL). The filtrate was evaporated *in vacuo*, then directly loaded in CH_2Cl_2 and purified by chromatography on silica using a 30-60 % EtOAc-cyclohexane gradient over 14 CV. The appropriate fractions were combined and evaporated *in vacuo*, then the residue treated with HCl (4 M in dioxane, 12.4 mL, 49.5 mmol) and the mixture stirred at rt for 1 h. The reaction mixture was evaporated *in vacuo*, then purified by SPE using a sulfonic acid (SCX) cartridge eluting with MeOH (200 mL), followed by ammonia (2 M in MeOH, 200 mL). The ammonia-containing fractions were evaporated *in vacuo*, then minimal EtOAc was added to the residue. The resulting white precipitate was removed by filtration, then the filtrate evaporated *in vacuo* to give the required product (562 mg, 27 % yield, 90 % purity) as a yellow solid.

LCMS (Method B) (ES +ve) *m/z* 387.4 $(M + H)^+$ Rt 1.07 min (90 % pure).

Method 2: Employing **63** as starting material

To a stirred solution of (*R*)-*tert*-butyl 3-(4-amino-3-iodo-1*H*-pyrazolo[3,4-d]pyrimidin-1-yl)piperidine-1-carboxylate (471 mg, 0.954 mmol), (4-phenoxyphenyl)boronic acid (245 mg, 1.15 mmol) and XPhos (9.0 mg, 0.019 mmol)

in 1,4-dioxane (10 mL) was added a solution of potassium phosphate (405 mg, 1.908 mmol) in water (1 mL), then the mixture degassed (3 cycles vacuum/nitrogen). XPhos Pd G2 (15 mg, 0.019 mmol) was added, the mixture degassed again, then the mixture stirred at 100 ºC for 2 h. The mixture was passed through Celite and diluted with EtOAc (50 mL) and water (50 mL), then the phases were separated. The aqueous layer was back-extracted with EtOAc (50 mL), then the organic layers were combined, dried using a hydrophobic frit and evaporated *in vacuo*. The residue was dissolved in MeOH (5 mL), then treated with HCl (4 M in dioxane, 5 mL, 20 mmol) and the mixture stirred at rt for 2 h. The mixture was evaporated *in vacuo*, then purified by SPE using a sulfonic acid (SCX) cartridge using a MeOH (200 mL), followed by ammonia (2 M in MeOH, 100 mL). The ammonia-containing fractions were combined and evaporated *in vacuo* to give the required product (338 mg, 92 % yield) as a off-white solid.

1H NMR (400 MHz, DMSO-d_6) δ 8.23 (s, 1H), 7.65 (d, *J* = 8.6 Hz, 2H), 7.43 (dd, *J* = 7.6, 8.6 Hz, 2H), 7.08 - 7.22 (m, 5H), 4.61 - 4.74 (m, 1H), 3.08 (dd, *J* = 3.0, 11.8 Hz, 1H), 2.84 - 3.01 (m, 2H), 2.42 - 2.48 (m, 1H), 1.93 - 2.20 (m, 2H), 1.76 (d, *J* = 12.8 Hz, 1H), 1.47 - 1.64 (m, 1H). Exchangeable amine protons not observed. **LCMS** (Method A) (ES +ve) *m/z* 387.2 $(M + H)^+$ Rt 0.63 min (>95 % pure).

Consistent with literature data.[406]

(*R*)-1-(3-(4-Amino-3-(4-phenoxyphenyl)-1*H*-pyrazolo[3,4-d]pyrimidin-1-yl)piperidin-1-yl)prop-2-en-1-one (65)

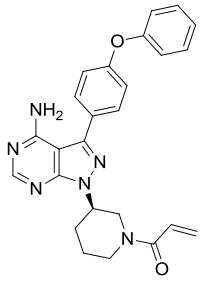

To a stirred solution of (*R*)-3-(4-phenoxyphenyl)-1-(piperidin-3-yl)-1*H*-pyrazolo[3,4-d]pyrimidin-4-amine (12 mg, 0.031 mmol) and triethylamine (0.013 mL, 0.093 mmol) in DMF (0.5 mL) was added acryloyl chloride (3.0 µl, 0.037 mmol) dropwise, then the mixture stirred at rt for 15 min. The mixture was concentrated under a stream of

nitrogen, then the residue dissolved in minimal DMSO and purified by MDAP (formic acid modifier gradient). The appropriate fractions were combined and dried under a stream of nitrogen to give the required product (5.2 mg, 38 % yield) as a white solid.

^{1}H NMR (400 MHz, DMSO-d_6) δ 8.26 (s, 1H), 7.66 (d, *J* = 8.1 Hz, 2H), 7.40 - 7.47 (m, 2H), 7.10 - 7.21 (m, 5H), 6.81 - 6.91 (m, 0.5H), 6.65 - 6.77 (m, 0.5H), 6.00 - 6.19 (m, 0.5H), 5.70 (d, *J* = 10.3 Hz, 0.5H), 5.59 (d, *J* = 9.8 Hz, 0.5H), 4.62 - 4.78 (m, 1H), 4.55 (d, *J* = 10.8 Hz, 1H), 4.21 (br. s., 1H), 4.07 (d, *J* = 11.6 Hz, 0.5H), 3.71 (t, *J* = 11.2 Hz, 0.5H), 3.15 - 3.25 (m, 1H), 3.02 (t, *J* = 11.0 Hz, 0.5H), 2.20 - 2.31 (m, 1H), 2.14 (m, 1H), 1.88 - 1.99 (m, 1H), 1.51 - 1.67 (m, 1H). **LCMS** (Method A) (ES +ve) *m/z* 441.2 $(M + H)^+$ Rt 1.01 min (>95 % pure).

Consistent with literature data.[404]

***tert*-Butyl ((*S*)-1-(((S)-2-((2*S*,4*S*)-4-(14-chloro-3,6,9,12-tetraoxatetradecanamido)-2-(((*R*)-1,2,3,4-tetrahydronaphthalen-1-yl)carbamoyl)pyrrolidin-1-yl)-1-cyclohexyl-2-oxoethyl)amino)-1-oxopropan-2-yl)(methyl)carbamate (66)**

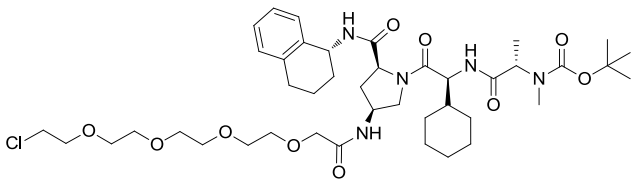

To a stirred solution of 14-chloro-3,6,9,12-tetraoxatetradecan-1-oic acid (111 mg, 0.411 mmol) and HATU (169 mg, 0.445 mmol) in DMF (3 mL) was added DIPEA (0.180 mL, 1.028 mmol) and the mixture stirred at rt for 10 min. *tert*-Butyl ((*S*)-1-(((*S*)-2-((2*S*,4*S*)-4-amino-2-(((*R*)-1,2,3,4-tetrahydronaphthalen-1-yl)carbamoyl)pyrrolidin-1-yl)-1-cyclohexyl-2-oxoethyl)amino)-1-oxopropan-2-yl)(methyl)carbamate (200 mg, 0.343 mmol) was added and the mixture stirred at rt for 1 h. The reaction mixture was concentrated under a stream of nitrogen, then the mixture directly purified by MDAP (ammonium bicarbonate modifier gradient). The appropriate fractions were collected and acetonitrile removed *in vacuo*, then the aqueous solution extracted with CH_2Cl_2 (50 mL). The organic layer was evaporated *in vacuo* to give the required product (224 mg, 78 % yield) as a colourless gum.

^{1}H NMR (400 MHz, DMSO-d_6) δ 8.44 (d, *J* = 8.8 Hz, 1H), 8.34 (d, *J* = 8.3 Hz, 1H), 7.32 (d, *J* = 7.6 Hz, 1H), 7.05 - 7.20 (m, 4H), 4.91 - 5.00 (m, 1H), 4.40 - 4.50 (m, 1H), 4.28 - 4.39 (m, 2H), 4.08 (q, *J* = 5.4 Hz, 1H), 3.96 - 4.04 (m, 1H), 3.90 (s, 2H), 3.64 - 3.72 (m, 4H), 3.44 - 3.62 (m, 13H), 3.18 (d, *J* = 5.4 Hz, 2H), 2.73 - 2.78 (m, 4H), 2.34 - 2.44 (m, 1H), 1.56 - 1.93 (m, 12H), 1.40 (s, 7H), 1.10 - 1.27 (m, 6H), 0.88 - 1.07 (m, 2H). **^{13}C NMR** (101 MHz, DMSO-d_6) δ 171.11, 171.06, 169.81, 168.99, 137.28, 136.88, 128.47, 128.31, 126.60, 125.57, 78.93, 70.51, 70.40, 69.95, 69.77, 69.72, 69.62, 69.58, 58.52, 54.83, 52.88, 48.55, 47.38, 46.71, 43.48, 34.23, 29.98, 29.73, 28.71, 28.63, 27.98, 25.83, 25.75, 25.54, 20.24. Note that ^{13}C NMR data are reported to two decimal places to differentiate the signals. Carbamate C=O not observed, but indicated by HMBC. Two further signals are not resolved potentially due to overlapping frequencies of PEG chain carbons. **LCMS** (Method B) (ES -ve) *m/z* 834.5 $(M - H)^+$ Rt 1.36 min (>95 % pure). **HRMS** (ES) calcd for $C_{42}H_{67}ClN_5O_{10}$, $(M + H)^+$ 836.4571, found 836.4571.

(*E*)-4-(4-(14-(((3*S*,5*S*)-1-((*S*)-2-((*S*)-2-((*tert*-Butoxycarbonyl)(methyl)amino)propanamido)-2-cyclohexylacetyl)-5-(((R)-1,2,3,4-tetrahydronaphthalen-1-yl)carbamoyl)pyrrolidin-3-yl)amino)-14-oxo-3,6,9,12-tetraoxatetradecyl)piperazin-1-yl)but-2-enoic acid (67)

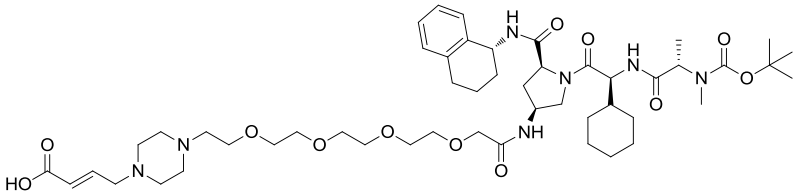

To a stirred solution of *tert*-butyl ((*S*)-1-(((*S*)-2-((2*S*,4*S*)-4-(14-chloro-3,6,9,12-tetraoxatetradecanamido)-2-(((*R*)-1,2,3,4-tetrahydronaphthalen-1-yl)carbamoyl)pyrrolidin-1-yl)-1-cyclohexyl-2-oxoethyl)amino)-1-oxopropan-2-yl)(methyl)carbamate (526 mg, 0.629 mmol) in acetonitrile (5 mL) was added piperazine (433 mg, 5.03 mmol), then the mixture heated in the microwave at 150 °C for 1 h. The solution was poured into CH_2Cl_2 (100 mL) and water (100 mL), the pH adjusted to ~8 with HCl (2 M aq.), then the phases were separated. The aqueous layer was back-extracted with CH_2Cl_2 (2 x 50 mL), then the organic layers were combined,

dried using a hydrophobic frit and evaporated *in vacuo*. The residue was directly dissolved in DMF (5 mL), then DIPEA (0.329 mL, 1.89 mmol) was added, followed by 4-bromocrotonic acid (125 mg, 0.755 mmol), then the mixture stirred at rt for 3 h. The reaction mixture was concentrated under a stream of nitrogen, then directly purified by reverse phase (C18) chromatography using a 15-55 % acetonitrile-water (+0.1 % ammonium bicarbonate modifier) gradient over 14 CV. The appropriate fractions were combined and evaporated *in vacuo* to give the required product (351 mg, 58 % yield) as a white solid.

^{1}H NMR (400 MHz, DMSO-d_6, T = 120 °C) δ 7.99 (br. s., 2H), 7.32 (br. s., 1H), 7.00 - 7.19 (m, 5H), 6.74 (dt, *J* = 6.1, 15.7 Hz, 1H), 5.90 (d, *J* = 15.7 Hz, 1H), 4.98 (q, *J* = 6.5 Hz, 1H), 4.37 - 4.60 (m, 5H), 3.90 (s, 2H), 3.44 - 3.59 (m, 14H), 3.09 (dd, *J* = 1.6, 6.0 Hz, 2H), 2.67 - 2.83 (m, 7H), 2.38 - 2.49 (m, 11H), 1.55 - 2.00 (m, 15H), 0.91 - 1.32 (m, 11H). Exchangeable acid proton not observed. **^{13}C NMR** (101 MHz, DMSO-d_6, T = 120 °C) δ 170.41, 170.39, 169.45, 168.35, 165.90, 154.55, 149.36, 143.65, 136.41, 131.20, 127.75, 127.62, 125.92, 124.95, 122.99, 78.73, 70.02, 69.77, 69.42, 69.36, 69.32, 69.18, 69.12, 67.99, 58.25, 57.58, 56.66, 54.19, 53.34, 52.52, 52.44, 52.17, 47.30, 46.49, 29.42, 29.10, 28.44, 28.13, 27.30, 25.19, 25.14, 24.92, 19.45, 13.72. Note that ^{13}C NMR data are reported to two decimal places to differentiate the signals. **LCMS** (Method A) (ES +ve) *m/z* 970.8 $(M + H)^+$ Rt 0.90 min (>95 % pure). **HRMS** (ES) calcd for $C_{50}H_{80}N_7O_{12}$, $(M + H)^+$ 970.5860, found 970.5824.

***tert*-Butyl ((*S*)-1-(((*S*)-2-((2*S*,4*S*)-4-(14-(4-((*E*)-4-((*R*)-3-(4-amino-3-(4-phenoxyphenyl)-1*H*-pyrazolo[3,4-d]pyrimidin-1-yl)piperidin-1-yl)-4-oxobut-2-en-1-yl)piperazin-1-yl)-3,6,9,12-tetraoxatetradecanamido)-2-(((*R*)-1,2,3,4-tetrahydronaphthalen-1-yl)carbamoyl)pyrrolidin-1-yl)-1-cyclohexyl-2-oxoethyl)amino)-1-oxopropan-2-yl)(methyl)carbamate (68)**

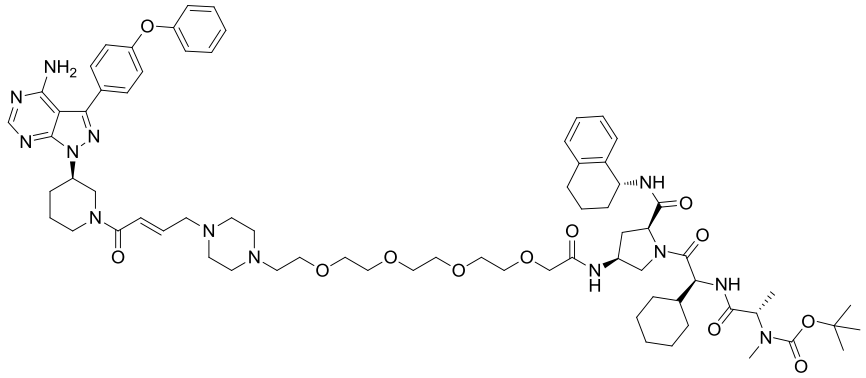

To a stirred solution of (*E*)-4-(4-(14-(((3*S*,5*S*)-1-((*S*)-2-((*S*)-2-((*tert*-butoxycarbonyl)(methyl)amino)propanamido)-2-cyclohexylacetyl)-5-(((*R*)-1,2,3,4-tetrahydronaphthalen-1-yl)carbamoyl)pyrrolidin-3-yl)amino)-14-oxo-3,6,9,12-tetraoxatetradecyl)piperazin-1-yl)but-2-enoic acid (148 mg, 0.153 mmol), (*R*)-3-(4-phenoxyphenyl)-1-(piperidin-3-yl)-1*H*-pyrazolo[3,4-d]pyrimidin-4-amine (65 mg, 0.17 mmol) and DIPEA (0.133 mL, 0.763 mmol) in DMF (1 mL) was added HATU (70 mg, 0.18 mmol) and the mixture stirred at rt for 1 h. The reaction mixture was directly purified by reverse phase (C18) chromatography eluting with a 45-95 % acetonitrile-water (+0.1 % ammonium bicarbonate modifier) gradient, however the product failed to elute. The column was washed with MeOH (1 CV), then appropriate fractions were combined and evaporated *in vacuo*. The residue was partitioned between CH_2Cl_2 (20 mL) and water (20 mL), then the phases were separated using a hydrophobic frit. The organic layer was concentrated under a stream of nitrogen to give the required product (130 mg, 51 % yield, 80 % purity) as an orange solid.

LCMS (Method B) (ES +ve) *m/z* 670.4 $([M + 2H]/2)^+$ Rt 1.39 min (80 % pure).

(2*S*,4*S*)-4-(14-(4-((*E*)-4-((*R*)-3-(4-Amino-3-(4-phenoxyphenyl)-1*H*-pyrazolo[3,4-d]pyrimidin-1-yl)piperidin-1-yl)-4-oxobut-2-en-1-yl)piperazin-1-yl)-3,6,9,12-tetraoxatetradecanamido)-1-((*S*)-2-cyclohexyl-2-((*S*)-2-(methylamino)propanamido)acetyl)-*N*-((*R*)-1,2,3,4-tetrahydronaphthalen-1-yl)pyrrolidine-2-carboxamide (69)

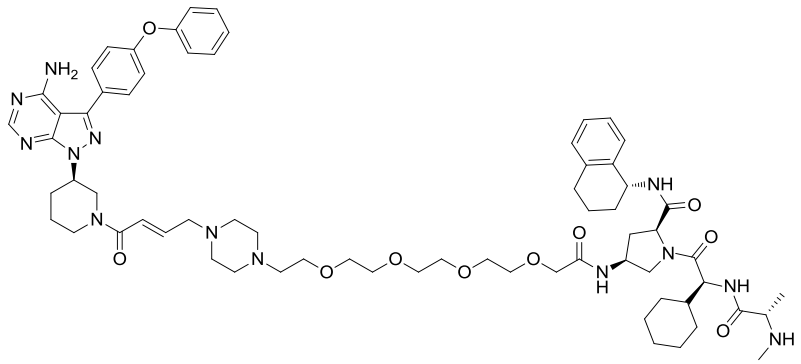

To a stirred solution of *tert*-butyl ((*S*)-1-(((*S*)-2-((2*S*,4*S*)-4-(14-(4-((*E*)-4-((*R*)-3-(4-amino-3-(4-phenoxyphenyl)-1*H*-pyrazolo[3,4-d]pyrimidin-1-yl)piperidin-1-yl)-4-oxobut-2-en-1-yl)piperazin-1-yl)-3,6,9,12-tetraoxatetradecanamido)-2-(((*R*)-1,2,3,4-tetrahydronaphthalen-1-yl)carbamoyl)pyrrolidin-1-yl)-1-cyclohexyl-2-oxoethyl)amino)-1-oxopropan-2-yl)(methyl)carbamate (43 mg, 0.026 mmol, 80 % pure) in CH_2Cl_2 (0.5 mL) was added TFA (0.1 mL, 1.3 mmol) and the mixture stirred at rt for 1 h. The mixture was concentrated under a stream of nitrogen, then dissolved in minimal MeOH and purified by MDAP (ammonium bicarbonate modifier gradient), then the appropriate fractions concentrated under a stream of nitrogen to give the required product (24 mg, 75 % yield) as a white solid.

^{1}H NMR (400 MHz, DMSO-d_6, T = 120 °C) δ 8.26 (s, 1H), 7.89 - 8.09 (m, 2H), 7.68 (d, *J* = 8.8 Hz, 2H), 7.58 (br. s., 1H), 7.43 (t, *J* = 8.1 Hz, 2H), 7.26 - 7.38 (m, 1H), 7.02 - 7.23 (m, 7H), 6.49 - 6.61 (m, 1H), 6.40 - 6.49 (m, 2H), 4.98 (q, *J* = 6.5 Hz, 1H), 4.75 (spt, *J* = 4.7 Hz, 1H), 4.39 - 4.54 (m, 3H), 4.33 (d, *J* = 11.7 Hz, 1H), 3.96 - 4.09 (m, 2H), 3.90 (s, 2H), 3.45 - 3.68 (m, 15H), 3.22 (ddd, *J* = 3.2, 10.6, 13.7 Hz, 1H), 2.96 - 3.07 (m, 3H), 2.66 - 2.81 (m, 4H), 2.13 - 2.49 (m, 16H), 1.83 - 2.05 (m, 4H), 1.55 - 1.82 (m, 9H), 0.93 - 1.32 (m, 8H). Exchangeable amine protons not observed. **^{13}C NMR** (101 MHz, DMSO-d_6, T = 120 °C) δ 171.46, 170.51, 170.47, 169.78, 168.36,

164.93, 164.31, 157.66, 156.86, 155.92, 154.91, 153.79, 142.57, 139.99, 136.40, 129.36, 129.32, 127.75, 127.64, 125.92, 125.00, 123.10, 122.29, 118.39, 118.33, 97.35, 70.03, 69.78, 69.42, 69.36, 69.32, 69.18, 69.12, 67.99, 58.73, 58.00, 56.68, 53.69, 52.44, 52.29, 52.14, 50.90, 46.49, 33.39, 29.11, 28.57, 28.45, 28.13, 27.44, 27.36, 25.74, 25.24, 25.12, 24.91, 19.43, 18.02. Note that ^{13}C NMR data are reported to two decimal places to differentiate the signals. Two signals not resolved, potentially due to overlapping peaks or temperature-related broadening. **LCMS** (Method B) (ES +ve) *m/z* 1239.4 $(M + H)^+$ Rt 1.23 min (>95 % pure). **HRMS** (ES) calcd for $C_{67}H_{92}N_{13}O_{10}$, $(M + H)^+$ 1238.7085, found 1238.7082. **IR** ν_{max} (neat) 3300, 2926, 2854, 1626, 1587, 1565, 1520, 1484, 1437 cm^{-1}. **MP** >250 °C (decomposition).

(2*S*,4*S*)-4-(14-(4-(4-((*R*)-3-(4-Amino-3-(4-phenoxyphenyl)-1*H*-pyrazolo[3,4-d]pyrimidin-1-yl)piperidin-1-yl)-4-oxobutyl)piperazin-1-yl)-3,6,9,12-tetraoxatetradecanamido)-1-((*S*)-2-cyclohexyl-2-((*S*)-2-(methylamino)propanamido)acetyl)-*N*-((*R*)-1,2,3,4-tetrahydronaphthalen-1-yl)pyrrolidine-2-carboxamide (70)

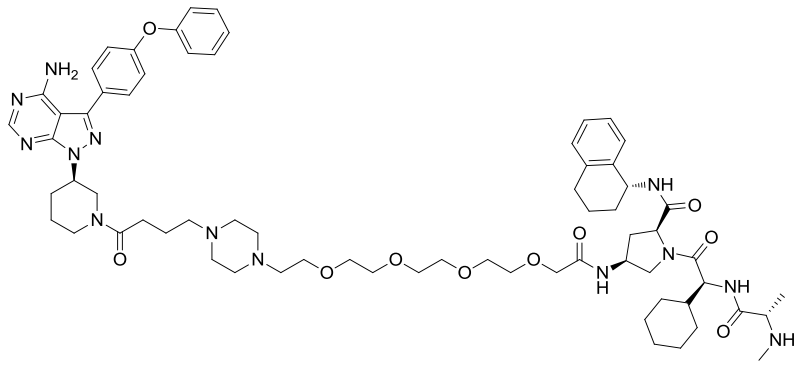

A solution of *tert*-butyl ((*S*)-1-(((*S*)-2-((2*S*,4*S*)-4-(14-(4-((*E*)-4-((*R*)-3-(4-amino-3-(4-phenoxyphenyl)-1*H*-pyrazolo[3,4-d]pyrimidin-1-yl)piperidin-1-yl)-4-oxobut-2-en-1-yl)piperazin-1-yl)-3,6,9,12-tetraoxatetradecanamido)-2-(((*R*)-1,2,3,4-tetrahydronaphthalen-1-yl)carbamoyl)pyrrolidin-1-yl)-1-cyclohexyl-2-oxoethyl)amino)-1-oxopropan-2-yl)(methyl)carbamate (50 mg, 0.030 mmol, 80 % pure) and Pd/C (10 % w/w, 32 mg, 0.030 mmol) in EtOH (2 mL) was stirred under an atmosphere of hydrogen for 3 h. The reaction mixture was passed through a pad of Celite, then the pad washed with MeOH and the solution evaporated *in vacuo*. The

residue was directly dissolved in CH_2Cl_2 (5 mL) then TFA (1 mL) was added and the mixture stirred at rt for 1 h. The mixture was evaporated *in vacuo*, then dissolved in minimal MeOH and purified by MDAP (ammonium bicarbonate modifier gradient). The appropriate fractions were combined and dried under a stream of nitrogen to give the required product (15 mg, 41 % yield) as a white solid.

^{1}H NMR (400 MHz, DMSO-d_6, T = 120 °C) δ 8.26 (s, 1H), 7.89 - 8.09 (m, 2H), 7.68 (d, *J* = 8.8 Hz, 2H), 7.51 - 7.64 (m, 1H), 7.43 (t, *J* = 8.1 Hz, 2H), 7.27 - 7.37 (m, 1H), 7.00 - 7.22 (m, 7H), 6.36 - 6.52 (m, 1H), 4.98 (q, *J* = 6.6 Hz, 1H), 4.73 (spt, *J* = 4.8 Hz, 1H), 4.39 - 4.55 (m, 3H), 4.23 - 4.37 (m, 1H), 4.04 (br. s., 2H), 3.90 (s, 2H), 3.45 - 3.66 (m, 15H), 2.96 - 3.12 (m, 5H), 2.66 - 2.84 (m, 3H), 2.13 - 2.47 (m, 18H), 1.83 - 2.00 (m, 4H), 1.56 - 1.82 (m, 11H), 0.96 - 1.26 (m, 8H). Exchangeable amine protons not observed. **^{13}C NMR** (101 MHz, DMSO-d_6, T = 120 °C) δ 171.12, 170.45, 170.37, 169.32, 168.35, 166.98, 166.59, 164.01, 157.65, 156.86, 155.91, 154.90, 153.77, 142.57, 136.40, 129.35, 129.32, 127.74, 127.64, 125.92, 124.98, 123.10, 118.39, 118.33, 97.35, 70.02, 69.77, 69.41, 69.35, 69.31, 69.17, 69.12, 67.99, 58.71, 58.21, 56.74, 56.60, 53.65, 52.57, 52.41, 52.20, 46.49, 33.38, 29.66, 29.10, 28.69, 28.13, 27.40, 27.37, 25.74, 25.24, 25.12, 24.91, 21.78, 19.44, 18.01. Note that ^{13}C NMR data are reported to two decimal places to differentiate the signals. Two signals are not observed, potentially due to overlapping peaks or temperature-related broadening. **LCMS** (Method B) (ES +ve) *m/z* 1240.7 $(M + H)^+$ Rt 1.25 min (>95 % pure). **HRMS** (ES) calcd for $C_{67}H_{94}N_{13}O_{10}$, $(M + H)^+$ 1240.7241, found 1240.7149. **IR** ν_{max} (neat) 3297, 2927, 2854, 1626, 1587, 1565, 1520, 1490, 1437 cm^{-1}. **MP** >250 °C (decomposition).

(*E*)-4-(4-(*tert*-Butoxycarbonyl)piperazin-1-yl)but-2-enoic acid (71)

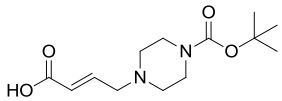

To a stirred solution of *tert*-butyl piperazine-1-carboxylate (2.25 g, 12.1 mmol) and triethylamine (5.05 mL, 36.2 mmol) in THF (20 mL) at 0 °C was added (*E*)-4-bromobut-2-enoic acid (2.39 g, 14.5 mmol) dropwise, then the mixture stirred at rt for

18 h. The reaction mixture was filtered and the precipitate washed with THF (50 mL). The filtrate was evaporated, then loaded in minimal CH_2Cl_2 and purified on silica using a 0-15 % MeOH-CH_2Cl_2 gradient over 12 CV. The appropriate fractions were combined and evaporated *in vacuo* to give the required product (1.33 g, 40 % yield) as a white solid.

^{1}H NMR (400 MHz, DMSO-d_6) δ 12.28 (br. s., 1H), 6.73 (dt, *J* = 6.0, 15.6 Hz, 1H), 5.91 (d, *J* = 15.6 Hz, 1H), 3.28 - 3.34 (m, 4H), 3.11 (dd, *J* = 1.5, 6.1 Hz, 2H), 2.27 - 2.37 (m, 4H), 1.39 (s, 9H). **^{13}C NMR** (101 MHz, DMSO-d_6) δ 167.2, 154.3, 145.1, 124.2, 79.2, 58.6, 52.9, 43.9 (br.), 28.5. **LCMS** (Method B) (ES +ve) *m/z* 271.2 $(M + H)^+$ Rt 0.56 min (>95 % pure). **HRMS** (ES) calcd for $C_{13}H_{23}N_2O_4$, $(M + H)^+$ 271.1652, found 271.1655.

(*R*,*E*)-*tert*-Butyl 4-(4-(3-(4-amino-3-(4-phenoxyphenyl)-1*H*-pyrazolo[3,4-d]pyrimidin-1-yl)piperidin-1-yl)-4-oxobut-2-en-1-yl)piperazine-1-carboxylate (72)

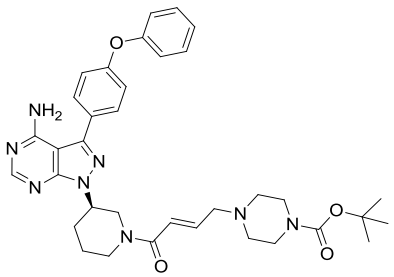

To a stirred solution of (*R*)-3-(4-phenoxyphenyl)-1-(piperidin-3-yl)-1*H*-pyrazolo[3,4-d]pyrimidin-4-amine (237 mg, 0.613 mmol), (*E*)-4-(4-(*tert*-butoxycarbonyl)piperazin-1-yl)but-2-enoic acid (199 mg, 0.736 mmol) and DIPEA (0.540 mL, 3.09 mmol) in DMF (8 mL) was added HATU (280 mg, 0.736 mmol) and the mixture stirred at rt for 1 h. The mixture was diluted with CH_2Cl_2 (50 mL) and brine (150 mL), then the phases were separated. The aqueous layer was back-extracted with CH_2Cl_2 (50 mL), then the organic layers were combined, dried using a hydrophobic frit and evaporated *in vacuo*. The sample was loaded in minimal DMSO and purified by reverse phase (C18) chromatography using a 35-85 % (+0.1 % ammonium bicarbonate modifier) gradient over 12 CV. The appropriate fractions were combined and acetonitrile removed *in*

vacuo, then the aqueous slurry extracted with CH_2Cl_2 (2 x 30 mL) to give the required product (308 mg, 79 % yield) as a yellow solid.

^{1}H NMR (400 MHz, DMSO-d_6, T =120 °C) δ 8.26 (s, 1H), 7.68 (d, *J* = 8.6 Hz, 2H), 7.43 (t, *J* = 8.0 Hz, 2H), 7.10 - 7.21 (m, 5H), 6.48 - 6.60 (m, 2H), 6.46 (br. s., 2H), 4.71 - 4.80 (m, 1H), 4.28 - 4.39 (m, 1H), 4.03 (dt, *J* = 3.8, 13.2 Hz, 1H), 3.52 - 3.63 (m, 1H), 3.29 - 3.35 (m, 4H), 3.21 (ddd, *J* = 3.3, 10.6, 13.5 Hz, 1H), 3.08 (d, *J* = 5.4 Hz, 2H), 2.29 - 2.39 (m, 5H), 2.14 - 2.24 (m, 1H), 2.00 (dt, *J* = 4.1, 13.3 Hz, 1H), 1.57 - 1.70 (m, 1H), 1.42 (s, 9H). **^{13}C NMR** (101 MHz, DMSO-d_6, T =120 °C) δ 165.3, 158.8, 158.0, 157.0, 156.0, 154.9, 154.5, 143.7, 140.6, 130.5, 130.4, 128.7, 124.2, 123.8, 119.5, 119.4, 98.4, 79.2, 59.0, 53.4, 52.9, 44.0, 29.7, 28.7, 26.8, 24.3. One piperazinyl signal is not observed, potentially due to temperature-related broadening. **LCMS** (Method A) (ES +ve) *m/z* 639.3 $(M + H)^+$ Rt 0.82 min (>95 % pure). **HRMS** (ES) calcd for $C_{35}H_{43}N_8O_4$, $(M + H)^+$ 639.3407, found 639.3403.

(Ethane-1,2-diylbis(oxy))bis(ethane-2,1-diyl) bis(4-methylbenzenesulfonate) (73)

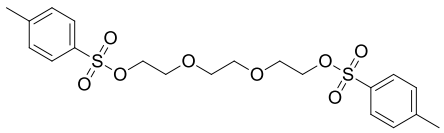

To a stirred solution of triethylene glycol (3.00 mL, 22.5 mmol) and tosyl chloride (8.57 g, 45.0 mmol) in CH_2Cl_2 (25 mL) was added KOH (10.1 g, 180 mmol) portionwise at 0 °C. The mixture was stirred left to stir at rt for 20 h, then diluted with CH_2Cl_2 (150 mL) and water (200 mL). The phases were separated, then the aqueous layer was back-extracted with CH_2Cl_2 (150 mL). The organic layers were combined, dried using a hydrophobic frit and evaporated *in vacuo*, then the residue triturated with ice-cold cyclohexane (20 mL) to give the required product (9.80 g, 95 % yield) as a white solid.

^{1}H NMR (400 MHz, $CDCl_3$) δ 7.80 (d, *J* = 8.3 Hz, 4H), 7.35 (d, *J* = 8.3 Hz, 4H), 4.15 (t, *J* = 4.6 Hz, 4H), 3.66 (t, *J* = 4.6 Hz, 4H), 3.53 (s, 4H), 2.45 (s, 6H). **LCMS** (Method A) (ES +ve) *m/z* 476.1 $(M + NH_4)^+$ Rt 1.20 min (>95 % pure).

Consistent with literature data.[407]

2-(2-(2-Azidoethoxy)ethoxy)ethyl 4-methylbenzenesulfonate (74)

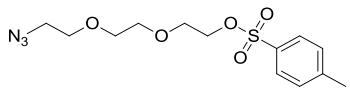

To a stirred solution of (ethane-1,2-diylbis(oxy))bis(ethane-2,1-diyl) bis(4-methylbenzenesulfonate) (5.94 g, 13.0 mmol) in acetonitrile (50 mL) was added sodium azide (337 mg, 5.18 mmol) and the mixture stirred at 100 °C for 5 h. The mixture was concentrated *in vacuo*, then diluted with CH_2Cl_2 (100 mL) and NaOH (2 M aq., 100 mL) and the phases separated. The aqueous layer was back-extracted with CH_2Cl_2 (2 x 50 mL), then the organic layers were combined, dried using a hydrophobic frit and evaporated *in vacuo*. The sample was loaded in CH_2Cl_2 and purified on silica using a 30-50 % EtOAc-cyclohexane gradient over 10 CV. The appropriate fractions were combined and evaporated *in vacuo* to give the required product (1.07 g, 63 % yield) as a colourless oil.

^{1}H NMR (400 MHz, $CDCl_3$) δ 7.81 (d, *J* = 8.3 Hz, 2H), 7.35 (d, *J* = 7.8 Hz, 2H), 4.18 (t, *J* = 4.9 Hz, 2H), 3.71 (t, *J* = 4.9 Hz, 2H), 3.65 (t, *J* = 4.9 Hz, 2H), 3.61 (s, 4H), 3.37 (t, *J* = 5.0 Hz, 2H), 2.46 (s, 3H). **LCMS** (Method A) (ES +ve) *m/z* 347.1 $(M + NH_4)^+$ Rt 1.08 min (>95 % pure).

Consistent with literature data.[408]

(*R*,*E*)-1-(3-(4-Amino-3-(4-phenoxyphenyl)-1*H*-pyrazolo[3,4-d]pyrimidin-1-yl)piperidin-1-yl)-4-(4-(2-(2-(2-azidoethoxy)ethoxy)ethyl)piperazin-1-yl)but-2-en-1-one (75)

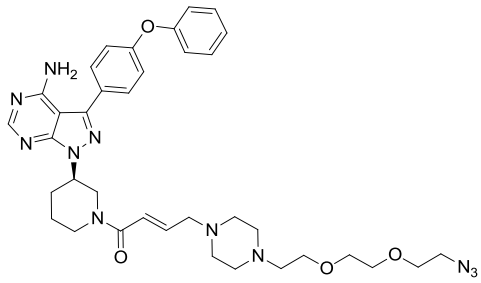

To a stirred solution of *tert*-butyl (*R*,*E*)-4-(4-(3-(4-amino-3-(4-phenoxyphenyl)-1*H*-pyrazolo[3,4-d]pyrimidin-1-yl)piperidin-1-yl)-4-oxobut-2-en-1-yl)piperazine-1-carboxylate (83 mg, 0.13 mmol) in CH_2Cl_2 (0.5 mL) was added TFA (0.5 mL) then the mixture stirred at rt for 2 h. The reaction mixture was directly purified by SPE on a sulfonic acid (SCX) cartridge eluting with MeOH (50 mL), followed by ammonia (2 M in MeOH, 50 mL). The ammonia-containing fractions were combined and evaporated *in vacuo*. The residue was directly dissolved in a solution of 2-(2-(2-azidoethoxy)ethoxy)ethyl 4-methylbenzenesulfonate (52.0 mg, 0.158 mmol) in DMF (1.5 mL), then the mixture was stirred at 50 °C for 20 h. The mixture was concentrated under a stream of nitrogen, then directly purified by reverse phase (C18) chromatography using a 10-50 % acetonitrile-water (+0.1 % formic acid modifier) gradient over 12 CV. The appropriate fractions were combined, then acetonitrile was removed *in vacuo*. The aqueous solution was extracted with CH_2Cl_2 (2 x 10 mL), then the organic layers were combined and concentrated under a stream of nitrogen to give (33 mg, 37 % yield) as a white solid.

^{1}H NMR (400 MHz, DMSO-d_6) δ 8.26 (s, 1H), 7.68 (d, *J* = 8.6 Hz, 1H), 7.38 - 7.47 (m, 2H), 7.07 - 7.25 (m, 5H), 6.36 - 6.60 (m, 4H), 4.76 (spt, *J* = 4.7 Hz, 1H), 4.33 (d, *J* = 11.5 Hz, 1H), 3.96 - 4.06 (m, 1H), 3.47 - 3.68 (m, 9H), 3.39 (t, *J* = 5.0 Hz, 2H), 3.17 - 3.26 (m, 1H), 3.05 (d, *J* = 5.9 Hz, 2H), 2.27 - 2.53 (m, 11H), 2.14 - 2.24 (m, 1H), 1.94 - 2.05 (m, 1H), 1.54 - 1.70 (m, 1H). **^{13}C NMR** (101 MHz, DMSO-d_6) δ 164.29, 157.64, 156.85, 155.90, 154.89, 153.78, 142.55, 139.93, 129.34, 129.30, 127.63, 123.07, 122.32, 118.38, 118.31, 97.34, 69.34, 69.17, 68.51, 68.01, 57.98, 56.65, 52.42,

52.28, 52.10, 49.83, 28.55, 23.17. Note that ^{13}C NMR data are reported to two decimal places to differentiate the signals. Two piperazine signals are not observed, potentially due to slow ring inversion. **LCMS** (Method A) (ES +ve) *m/z* 696.5 $(M + H)^+$ Rt 0.77 min (indicates 80 % purity, NMR indicates >95 %). **HRMS** (ES) calcd for $C_{36}H_{46}N_{11}O_4$, $(M + H)^+$ 696.3729, found 696.3710.

4-(2-(1-(2-(2-(2-(4-((*E*)-4-((*R*)-3-(4-amino-3-(4-phenoxyphenyl)-1*H*-pyrazolo[3,4-d]pyrimidin-1-yl)piperidin-1-yl)-4-oxobut-2-en-1-yl)piperazin-1-yl)ethoxy)ethoxy)ethyl)-1*H*-1,2,3-triazol-4-yl)ethoxy)-2-(2,6-dioxopiperidin-3-yl)isoindoline-1,3-dione (76)

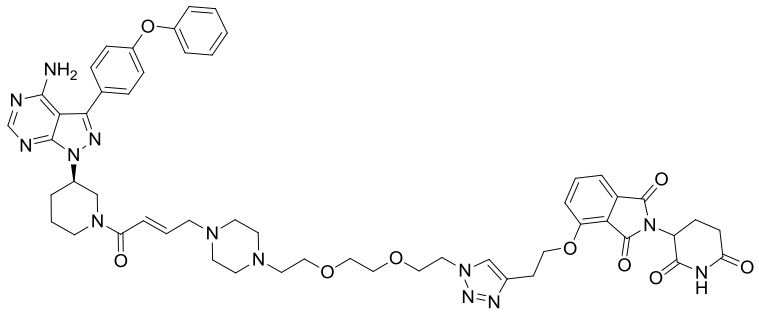

To a stirred solution of (*R*,*E*)-1-(3-(4-amino-3-(4-phenoxyphenyl)-1*H*-pyrazolo[3,4-d]pyrimidin-1-yl)piperidin-1-yl)-4-(4-(2-(2-(2-azidoethoxy)ethoxy)ethyl)piperazin-1-yl)but-2-en-1-one (38.5 mg, 0.055 mmol) and 4-(but-3-yn-1-yloxy)-2-(2,6-dioxopiperidin-3-yl)isoindoline-1,3-dione (19 mg, 0.058 mmol) in DMSO (1 mL) was added a solution of tris(3-hydroxypropyltriazolylmethyl)amine (9.6 mg, 0.022 mmol) and sodium ascorbate (11.0 mg, 0.056 mmol) in water (0.1 mL), then $CuSO_4$ (1.8 mg, 0.011 mmol) was added and the mixture stirred at rt for 24 h. The reaction mixture was directly loaded on silica and purified using a 0-20 % MeOH-CH_2Cl_2 gradient over 14 CV. The appropriate fractions were combined and evaporated in vacuo to give the required product (6.5 mg, 11 % yield) as a white solid.

^{1}H NMR (600 MHz, DMSO-d_6) δ 11.13 (br. s., 1H), 8.26 (s, 1H), 8.05 (br. s., 1H), 7.78 - 7.85 (m, 1H), 7.63 - 7.70 (m, 2H), 7.54 (t, *J* = 7.9 Hz, 1H), 7.41 - 7.48 (m, 4H), 7.10 - 7.22 (m, 6H), 6.40 - 6.70 (m, 2H), 5.10 (dd, *J* = 5.3, 12.7 Hz, 1H), 4.27 - 4.77 (m, 7H), 3.98 - 4.19 (m, 2H), 3.76 - 3.83 (m, 2H), 3.44 - 3.65 (m, 8H), 3.05 - 3.21 (m, 2H), 2.82 - 2.96 (m, 2H), 2.57 - 2.63 (m, 1H), 1.85 - 2.45 (m, 14H), 1.52 - 1.65 (m,

1H). **^{13}C NMR** (151 MHz, DMSO-d_6) δ 172.75, 170.49, 169.87, 166.77, 165.38, 162.44, 158.18, 157.11, 157.08, 156.29, 156.26, 155.65, 155.60, 153.99, 153.88, 143.35, 143.24, 143.18, 142.87, 137.08, 133.20, 130.11, 130.05, 130.00, 127.92, 127.87, 123.96, 123.77, 123.48, 119.87, 118.94, 116.31, 115.44, 97.41, 97.32, 73.00, 72.19, 69.79, 69.48, 69.45, 68.65, 67.91, 57.44, 56.74, 54.90, 52.63, 52.05, 49.83, 49.36, 49.26, 48.76, 47.05, 46.53, 45.35, 44.95, 41.11, 32.98, 30.94, 29.90, 29.59, 29.40, 25.38, 24.61, 23.49, 22.01. Sample is a mixture of inseparable diastereomers, all signals are reported for diagnostic purposes only. Note that ^{13}C NMR data are reported to two decimal places to differentiate the signals. **LCMS** (Method A) (ES +ve) *m/z* 511.9 $([M + 2H]/2)^+$ Rt 0.78 min (>95 % pure). **HRMS** (ES) calcd for $C_{53}H_{60}N_{13}O_9$, $(M + H)^+$ 1022.4637, found 1022.4608. **IR** ν_{max} (neat) 3330, 2931, 1771, 1709, 1614, 1587, 1564, 1520, 1490 cm^{-1}. **MP** >250 °C (decomposition).

(*R*)-*tert*-Butyl 4-(4-(3-(4-amino-3-(4-phenoxyphenyl)-1*H*-pyrazolo[3,4-d]pyrimidin-1-yl)piperidin-1-yl)-4-oxobutyl)piperazine-1-carboxylate (77)

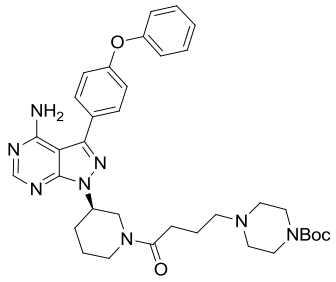

A solution of *tert*-butyl (*R*,*E*)-4-(4-(3-(4-amino-3-(4-phenoxyphenyl)-1*H*-pyrazolo[3,4-d]pyrimidin-1-yl)piperidin-1-yl)-4-oxobut-2-en-1-yl)piperazine-1-carboxylate (81.0 mg, 0.127 mmol) and Pd/C (10 % w/w, 34 mg, 0.032 mmol) in EtOH (1.5 mL) was stirred under an atmosphere of hydrogen for 3 h. The mixture was filtered through Celite, then the pad washed with MeOH and the organics evaporated *in vacuo* to give the required product (78 mg, 77 % yield, 80 % purity) as a grey solid. The sample was used directly in the next reaction without further purification.

LCMS (Method A) (ES +ve) *m/z* 641.6 $([M + H])^+$ Rt 0.87 min (80 % pure).

(*R*)-1-(3-(4-Amino-3-(4-phenoxyphenyl)-1*H*-pyrazolo[3,4-d]pyrimidin-1-yl)piperidin-1-yl)-4-(4-(2-(2-(2-azidoethoxy)ethoxy)ethyl)piperazin-1-yl)butan-1-one (78)

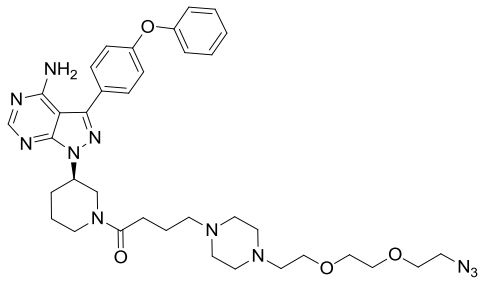

To a stirred solution of *tert*-butyl (*R*)-4-(4-(3-(4-amino-3-(4-phenoxyphenyl)-1*H*-pyrazolo[3,4-d]pyrimidin-1-yl)piperidin-1-yl)-4-oxobutyl)piperazine-1-carboxylate (70.0 mg, 0.109 mmol) in CH_2Cl_2 (0.5 mL) was added TFA (0.5 mL) then the mixture stirred at rt for 2 h. The reaction mixture was directly purified by SPE on a sulfonic acid (SCX) cartridge eluting with MeOH (50 mL), followed by ammonia (2 M in MeOH, 50 mL). The ammonia-containing fractions were combined and evaporated *in vacuo*. The residue was directly dissolved in a solution of 2-(2-(2-azidoethoxy)ethoxy)ethyl 4-methylbenzenesulfonate (43.2 mg, 0.131 mmol) in DMF (1.5 mL) then the mixture stirred at 50 °C for 20 h. The mixture was concentrated under a stream of nitrogen, then directly purified by MDAP (ammonium bicarbonate modifier gradient). The appropriate fractions were combined and dried under a stream of nitrogen to give the required product (40 mg, 53 % yield) as a white solid.

^{1}H NMR (400 MHz, DMSO-d_6) δ 8.26 (s, 1H), 7.68 (d, *J* = 8.8 Hz, 2H), 7.39 - 7.46 (m, 2H), 7.09 - 7.21 (m, 5H), 6.45 (br. s., 2H), 4.68 - 4.79 (m, 1H), 4.31 (br. s., 1H), 3.97 - 4.10 (m, 1H), 3.61 - 3.66 (m, 2H), 3.48 - 3.61 (m, 7H), 3.38 (t, *J* = 5.1 Hz, 2H), 3.08 (t, *J* = 10.9 Hz, 2H), 2.25 - 2.48 (m, 15H), 2.13 - 2.22 (m, 1H), 1.91 - 2.01 (m, 1H), 1.63 - 1.73 (m, 2H). **^{13}C NMR** (101 MHz, DMSO-d_6) δ 170.35, 157.65, 156.86, 155.91, 154.90, 153.77, 142.57, 129.34, 129.31, 127.64, 123.08, 118.38, 118.33, 97.35, 69.34, 69.17, 68.52, 68.03, 56.72, 56.58, 52.56, 52.41, 52.20, 49.83, 29.65, 28.68, 23.27, 21.77. Note that ^{13}C NMR data are reported to two decimal places to differentiate the signals. Two piperazine signals not observed, potentially due to slow ring inversion. **LCMS** (Method A) (ES +ve) *m/z* 698.5 $(M + H)^+$ Rt 0.72 min (>95 % pure). **HRMS**

(ES) calcd for $C_{36}H_{48}N_{11}O_4$, $(M + H)^+$ 698.3885, found 698.3859.

4-(2-(1-(2-(2-(2-(4-(4-((*R*)-3-(4-Amino-3-(4-phenoxyphenyl)-1*H*-pyrazolo[3,4-d]pyrimidin-1-yl)piperidin-1-yl)-4-oxobutyl)piperazin-1-yl)ethoxy)ethoxy)ethyl)-1*H*-1,2,3-triazol-4-yl)ethoxy)-2-(2,6-dioxopiperidin-3-yl)isoindoline-1,3-dione (79)

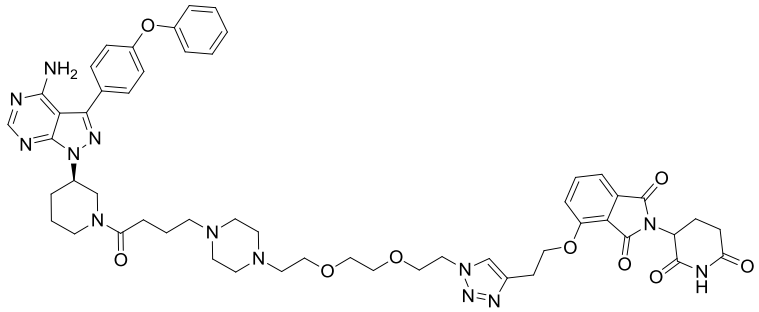

To a stirred solution of (*R*)-1-(3-(4-amino-3-(4-phenoxyphenyl)-1*H*-pyrazolo[3,4-d]pyrimidin-1-yl)piperidin-1-yl)-4-(4-(2-(2-(2-azidoethoxy)ethoxy)ethyl)piperazin-1-yl)butan-1-one (43.5 mg, 0.062 mmol) and 4-(but-3-yn-1-yloxy)-2-(2,6-dioxopiperidin-3-yl)isoindoline-1,3-dione (21.4 mg, 0.0660 mmol) in DMSO (1 mL) was added a solution of tris(3-hydroxypropyltriazolylmethyl)amine (10.8 mg, 25.0 μmol) and sodium ascorbate (12.4 mg, 63.0 μmol) in water (0.1 mL), then $CuSO_4$ (2.0 mg, 0.013 mmol) was added and the mixture stirred at rt for 24 h. The reaction mixture was directly loaded on silica and purified using a 0-20 % MeOH-CH_2Cl_2 gradient over 14 CV. The appropriate fractions were combined and evaporated *in vacuo* to give the required product (47 mg, 74 % yield) as a white solid.

^{1}H NMR (600 MHz, DMSO-d_6) δ 11.12 (s, 1H), 8.25 (d, *J* = 11.4 Hz, 1H), 8.02 - 8.07 (m, 3H), 7.78 - 7.84 (m, 1H), 7.63 - 7.68 (m, 2H), 7.54 (t, *J* = 8.4 Hz, 1H), 7.41 - 7.48 (m, 3H), 7.09 - 7.21 (m, 5H), 5.06 - 5.12 (m, 1H), 4.59 - 4.80 (m, 2.5H), 4.38 - 4.54 (m, 8H), 4.22 (d, *J* = 12.8 Hz, 0.5H), 4.04 (d, *J* = 11.0 Hz, 0.5H), 3.87 (d, *J* = 13.9 Hz, 0.5H), 3.79 (m, 2H), 3.56 - 3.65 (m, 4H), 3.47 - 3.51 (m, 2H), 3.38 - 3.45 (m, 7H), 3.06 - 3.19 (m, 3H), 2.81 - 2.93 (m, 2H), 2.56 - 2.63 (m, 2H), 1.83 - 2.15 (m, 7H), 1.46 - 1.75 (m, 2H). **^{13}C NMR** (151 MHz, DMSO-d_6) δ 172.75, 170.49, 169.87, 166.77, 165.38, 162.44, 158.18, 157.11, 157.08, 156.29, 156.26, 155.65, 155.60, 153.99, 153.88, 143.35, 143.24, 143.18, 142.87, 137.08, 133.20, 130.11, 130.05, 130.00,

127.92, 127.87, 123.96, 123.77, 123.48, 119.87, 118.94, 116.31, 115.44, 97.41, 97.32, 73.00, 72.19, 69.79, 69.48, 69.45, 68.65, 67.91, 57.44, 56.74, 54.90, 52.63, 52.05, 49.83, 49.36, 49.26, 48.76, 47.05, 46.53, 45.35, 44.95, 41.11, 32.98, 30.94, 29.90, 29.59, 29.40, 25.38, 24.61, 23.49, 22.01. Sample is a mixture of inseparable diastereomers, all signals are reported for diagnostic purposes only. Note that ^{13}C data is reported to two decimal places to differentiate the signals. **LCMS** (Method A) (ES +ve) *m/z* 512.9 $([M + 2H]/2)^+$ Rt 0.75 min (>95 % pure). **HRMS** (ES) calcd for $C_{53}H_{62}N_{13}O_9$, $(M + H)^+$ 1024.4793, found 1024.4778. **IR** ν_{max} (neat) 2912, 1709, 1614, 1587, 1520, 1455 cm^{-1}. **MP** >250 °C (decomposition).

2-Bromo-2-methylpropanal (80)

To an ice-cooled solution of isobutyraldehyde (1.86 mL, 20.38 mmol) in Et_2O (7 mL) was added bromine (1.00 mL, 19.4 mmol) dropwise over 30 min, then the mixture stirred at 0 °C for 3 h. The solution was washed with ice water (2 x 10 mL), then the solvent removed under partial vacuum (100 mbar, rt) to give the required product (2.38 g, 81 % yield) as a colourless, volatile liquid which was used directly in the next reaction.

^{1}H NMR (400 MHz, $CDCl_3$) δ 9.39 (s, 1H), 1.82 (s, 6H).

Consistent with literature data.[409]

***tert*-Butyl 4-(2-methyl-1-oxopropan-2-yl)piperazine-1-carboxylate (81)**

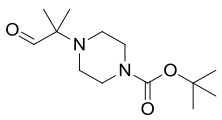

To a stirred solution of 2-bromo-2-methylpropanal (2.02 g, 13.4 mmol) in Et_2O (40 mL) was added *tert*-butyl piperazine-1-carboxylate (7.47 g, 40.1 mmol) and the mixture stirred at rt for 2 h, after which time a white precipitate was evolved. The suspension was filtered and the precipitate washed with Et_2O (2 x 50 mL), then the filtrate was washed with water (2 x 50 mL), dried using a hydrophobic frit and

evaporated *in vacuo*. The sample was loaded in CH_2Cl_2 and purified on silica using a 0-10 % MeOH-CH_2Cl_2 gradient over 10 CV. The appropriate fractions were combined and evaporated *in vacuo* to give an oil, which solidified upon standing in air gave the required product (2.61 g, 76 % yield) as a white solid.

^{1}H NMR (400 MHz, $CDCl_3$) δ 9.43 (s, 1H), 3.45 (t, *J* = 5.1 Hz, 4H), 2.43 (t, *J* = 5.1 Hz, 4H), 1.46 (s, 9H), 1.09 (s, 6H). **^{13}C NMR** (101 MHz, $CDCl_3$) δ 204.5, 154.6, 79.7, 65.3, 46.4, 44.2 (br.), 28.4, 17.2. **LCMS** Compound has no chromophore.

(*R*)-3-(3-(4-Amino-3-(4-phenoxyphenyl)-1*H*-pyrazolo[3,4-d]pyrimidin-1-yl)piperidin-1-yl)-3-oxopropanenitrile (82)

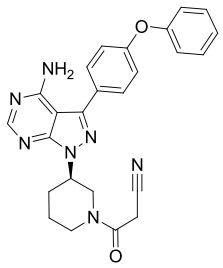

To a stirred solution of (R)-3-(4-phenoxyphenyl)-1-(piperidin-3-yl)-1H-pyrazolo[3,4-d]pyrimidin-4-amine (250 mg, 0.647 mmol), 2-cyanoacetic acid (66.0 mg, 0.776 mmol) and DIPEA (0.339 mL, 1.941 mmol) in DMF (3 mL) was added HATU (295 mg, 0.776 mmol), then the mixture stirred at rt for 2 h. The mixture was diluted with EtOAc (20 mL) and water (20 mL), then the phases were separated. The aqueous layer was back-extracted with EtOAc (2 x 10 mL), then the organic layers were combined, washed with brine (50 mL), and evaporated in vacuo. The sample was loaded in DMSO and purified by reverse phase (C18) chromatography using a 20-80 % acetonitrile-water (+0.1 % ammonium bicarbonate modifier) gradient over 14 CV. The appropriate fractions were combined, then acetonitrile removed in vacuo. The aqueous slurry was extracted with CH_2Cl_2 (3 x 50 mL), then the organic layers combined, dried using a hydrophobic frit, and evaporated in vacuo to give the required product (237 mg, 81 % yield) as a white solid.

^{1}H NMR (400 MHz, $CDCl_3$) δ 8.32 - 8.40 (m, 1H), 7.60 - 7.69 (m, 2H), 7.35 - 7.44 (m, 2H), 7.13 - 7.22 (m, 3H), 7.06 - 7.12 (m, 2H), 5.50 - 5.84 (m, 2H), 4.84 - 4.97 (m,

1H), 4.63 - 4.74 (m, 0.5H), 4.21 - 4.31 (m, 0.5H), 3.86 - 3.94 (m, 1H), 3.70 - 3.80 (m, 0.5H), 3.53 - 3.66 (m, 2H), 3.45 - 3.53 (m, 0.5H), 3.26 - 3.39 (m, 0.5H), 3.13 - 3.23 (m, 0.5H), 2.44 - 2.56 (m, 0.5H), 2.22 - 2.43 (m, 1.5H), 1.63 - 2.14 (m, 2H). Mixture of rotamers that do not resolve at T = 120 °C in DMSO. **^{13}C NMR** (101 MHz, $CDCl_3$) δ 160.52, 160.15, 158.74, 158.57, 157.92, 157.85, 156.31, 156.20, 156.00, 155.86, 154.43, 144.17, 144.04, 129.97, 129.94, 129.86, 127.68, 127.36, 124.13, 124.05, 123.95, 119.61, 119.54, 119.45, 119.09, 113.83, 113.69, 98.71, 98.55, 52.95, 52.02, 50.27, 46.63, 46.40, 42.83, 29.80, 29.30, 25.09, 25.04, 24.55, 23.14. As the sample is a mixture of rotamers; all observed signals are reported for diagnostic purposes only. Note that ^{13}C NMR data are reported to two decimal places to differentiate the signals. **LCMS** (Method B) (ES +ve) *m/z* 454.2 $(M + H)^+$ Rt 1.07 min (>95 % pure). **HRMS** (ES) calcd for $C_{25}H_{24}N_7O_2$, $(M + H)^+$ 454.1986, found 454.1986.

(*R*)-2-(3-(4-Amino-3-(4-phenoxyphenyl)-1*H*-pyrazolo[3,4-d]pyrimidin-1-yl)piperidine-1-carbonyl)-4-methyl-4-(piperazin-1-yl)pent-2-enenitrile (83)

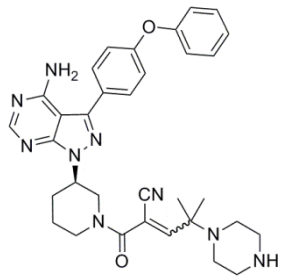

To a stirred solution of (*R*)-3-(3-(4-amino-3-(4-phenoxyphenyl)-1*H*-pyrazolo[3,4-d]pyrimidin-1-yl)piperidin-1-yl)-3-oxopropanenitrile (175 mg, 0.386 mmol) and *tert*-butyl 4-(2-methyl-1-oxopropan-2-yl)piperazine-1-carboxylate (297 mg, 1.16 mmol) in toluene (4 mL) was added piperidine (0.191 mL, 1.93 mmol) then the mixture stirred at 100 °C for 16 h. The mixture was poured into EtOAc (50 mL) and water (50 mL), then the phases were separated. The aqueous layer was back-extracted with EtOAc (2 x 20 mL), then the organic layers were combined, dried using a hydrophobic frit and evaporated *in vacuo*. The sample was loaded in CH_2Cl_2 and purified by chromatography on silica using a 0-5 % MeOH-CH_2Cl_2 (+0.1 % triethylamine) gradient over 12 CV. The appropriate fractions were combined and evaporated in vacuo, then HCl (4 M in dioxane, 2 mL) was added and the mixture stirred at rt for 2

h. The reaction mixture was directly purified by SPE on sulfonic acid (SCX) cartridge eluting with MeOH (100 mL), followed by ammonia (2 M in MeOH, 100 mL). The ammonia-containing fractions were combined and evaporated *in vacuo* to give the required product (201 mg, 88 % yield) as a gold solid.

^{1}H NMR (400 MHz, DMSO-d_6, T = 120 °C) δ 8.20-8.30 (m, 1H), 7.62-7.73 (m, 2H), 7.37-7.47 (m, 2H), 7.02-7.26 (m, 6H), 6.46 (br. s., 2H). Spectrum in non-aromatic region is highly complex and peaks are too broad or poorly resolved to accurately identify. Sample is insoluble in alternative NMR solvents. **^{13}C NMR** (101 MHz, DMSO-d_6, T = 120 °C) δ 159.60, 159.28, 158.98, 158.77, 158.66, 158.03, 158.00, 157.88, 157.02, 156.98, 156.95, 156.11, 156.05, 154.93, 154.89, 143.83, 130.47, 130.45, 130.41, 130.39, 129.22, 128.66, 128.63, 128.61, 128.50, 125.61, 124.20, 124.19, 124.16, 122.37, 119.49, 119.46, 119.44, 119.42, 119.38, 116.41, 113.43, 98.55, 52.92, 52.84, 50.45, 50.28, 43.90, 43.58, 30.72, 29.62, 29.56, 29.47, 29.39, 29.29, 22.72, 22.62. Sample is a mixture of geometric isomers, all observed signals are reported for diagnostic purposes only. Significant peak broadening is observed at both 30 °C and 120 °C. **LCMS** (Method B) (ES +ve) *m/z* 592.3 $(M + H)^+$ Rt 1.08 min (>95 % pure). **HRMS** (ES) calcd for $C_{33}H_{38}N_9O_2$ $(M + H)^+$ 592.3148, found 592.3145.

(2*S*,4*S*)-4-(14-(4-(5-((*R*)-3-(4-Amino-3-(4-phenoxyphenyl)-1*H*-pyrazolo[3,4-d]pyrimidin-1-yl)piperidin-1-yl)-4-cyano-2-methyl-5-oxopent-3-en-2-yl)piperazin-1-yl)-3,6,9,12-tetraoxatetradecanamido)-1-((*S*)-2-cyclohexyl-2-((*S*)-2-(methylamino)propanamido)acetyl)-*N*-((*R*)-1,2,3,4-tetrahydronaphthalen-1-yl)pyrrolidine-2-carboxamide (84)

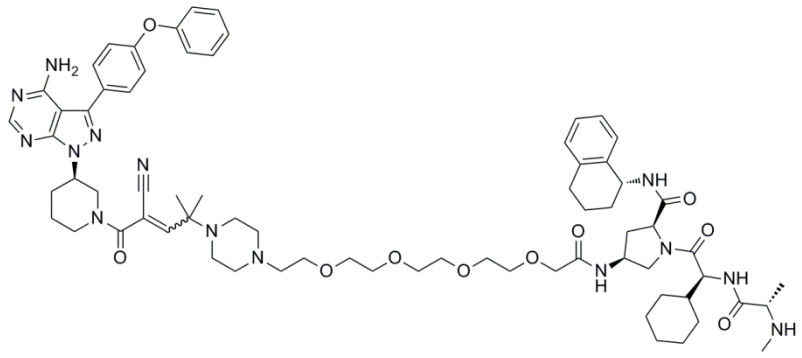

A solution of (*R*)-2-(3-(4-amino-3-(4-phenoxyphenyl)-1*H*-pyrazolo[3,4-d]pyrimidin-1-yl)piperidine-1-carbonyl)-4-methyl-4-(piperazin-1-yl)pent-2-enenitrile (100 mg, 0.169 mmol), *tert*-butyl ((*S*)-1-(((*S*)-2-((2*S*,4*S*)-4-(14-chloro-3,6,9,12-tetraoxatetradecanamido)-2-(((*R*)-1,2,3,4-tetrahydronaphthalen-1-yl)carbamoyl)pyrrolidin-1-yl)-1-cyclohexyl-2-oxoethyl)amino)-1-oxopropan-2-yl)(methyl)carbamate (170 mg, 0.203 mmol), DIPEA (89 µL, 0.510 mmol) and sodium iodide (25 mg, 0.167 mmol) in acetonitrile (2 mL) was stirred at 100 °C for 16 h. DMF (1 mL) was added and mixture was heated at 100 °C for a further 24 h. The reaction mixture was diluted with EtOAc (10 mL) and water (10 mL), then the phases were separated. The aqueous layer was back-extracted with EtOAc (3 x 5 mL), then the organic layers were combined and evaporated *in vacuo*. The sample was loaded in DMSO and purified by reverse phase (C18) chromatography using a 50-95 % acetonitrile-water (+0.1 % ammonium bicarbonate modifier) gradient over 16 CV. The appropriate fractions were combined and evaporated *in vacuo*. The residue was directly dissolved in CH_2Cl_2 (5 mL), then treated with TFA (1 mL) and the mixture stirred at rt for 1 h. The mixture was concentrated *in vacuo*, then dissolved in minimal MeOH and purified by MDAP (ammonium bicarbonate modifier gradient). The solvent was removed under a stream of nitrogen to give the required product (58 mg, 27 % yield) as a white solid.

^{1}H NMR (400 MHz, DMSO-d_6) δ 8.26 (t, *J* = 4.6 Hz, 1H), 7.99 (br. s., 1 H), 7.64 - 7.73 (m, 2H), 7.51 - 7.63 (m, 1H), 7.43 (t, *J* = 7.6 Hz, 2H), 7.27 - 7.36 (m, 1H), 7.01 - 7.24 (m, 7H), 6.33 - 6.56 (m, 1H), 4.98 (d, *J* = 6.6 Hz, 1H), 4.73 - 4.92 (m, 1H), 4.37 - 4.56 (m, 3H), 4.13 - 4.26 (m, 1H), 4.04 (br. s., 1H), 3.82 - 3.95 (m, 2H), 3.30 - 3.78 (m, 16H), 2.86 - 3.16 (m, 14H), 2.69 - 2.84 (m, 2H), 2.55 - 2.66 (m, 1H), 2.28 - 2.48 (m, 8H), 2.20 - 2.28 (m, 3H), 1.54 - 2.19 (m, 14H), 0.95 - 1.25 (m, 11H). **^{13}C NMR** (151 MHz, DMSO-d_6) δ 174.85, 171.58, 170.46, 169.50, 162.89, 162.35, 158.67, 157.65, 157.63, 156.76, 156.72, 156.11, 154.47, 143.78, 137.76, 137.37, 130.58, 130.51, 128.97, 128.89, 128.38, 128.32, 127.11, 126.10, 124.28, 124.25, 119.48, 119.43, 97.84, 72.75, 70.92, 70.45, 70.30, 70.21, 70.10, 70.07, 68.76, 60.74, 59.59, 59.01, 57.68, 55.55, 54.68, 53.38, 47.88, 47.21, 46.39, 45.50, 34.72, 30.21, 29.91, 29.21, 28.45, 26.36, 26.24, 26.02, 23.90, 22.61, 20.70, 19.57, 17.29. Sample is a mixture of geometric isomers, all observed signals are reported for diagnostic purposes only. **LCMS** (Method B) (ES +ve) *m/z* 646.7 $([M + 2H]/2)^+$ Rt 1.32 min (>95 % pure). **HRMS** (ES) calcd for $C_{70}H_{95}N_{14}O_{10}$, $(M + H)^+$ 1291.7356, found 1291.7339. **IR** ν_{max} (neat) 3302, 2926, 1639, 1586, 1565, 1520, 1489, 1438 cm^{-1}. **MP** >250 °C (decomposition).

_N_-(4-Bromo-2-fluorobenzyl)-_N_-(2,2-dimethoxyethyl)-4-methylbenzenesulfonamide (85)

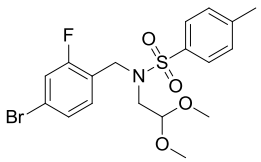

A solution of 4-bromo-2-fluorobenzaldehyde (24.1 g, 119 mmol) and aminoacetaldehyde dimethyl acetal (14.2 mL, 130 mmol) in MeOH (200 mL) and AcOH (5 mL) was stirred for 1 h, then cooled to 0 °C. Sodium borohydride (8.98 g, 237 mmol) was added portionwise over 30 min, then the mixture was stirred at rt for a further 30 min. MeOH was removed *in vacuo*, then EtOAc (250 mL) and NaOH (2 M aq., 250 mL) added and the phases were separated. The aqueous layer was back-extracted with EtOAc (100 mL), then the organic layers were combined, dried using a hydrophobic frit and evaporated *in vacuo* to give a gold oil. The residue was directly dissolved in CH_2Cl_2 (200 mL), then cooled to 0 °C and treated with pyridine (20 mL). TsCl (27.2 g, 142 mmol) was added portionwise and the mixture was stirred at 0 °C for 2 h. NaOH (2 M aq., 300 mL) was added, then the phases were separated. The aqueous layer was back-extracted with CH_2Cl_2 (2 x 50 mL), then the organic layers were combined and washed with $CuSO_4$ (10 % aq., 2 x 500 mL) and EDTA (0.01 M, 200 mL) and evaporated *in vacuo*. The sample was loaded in CH_2Cl_2 and purified by chromatography on silica using a 15-30 % EtOAc-cyclohexane gradient over 6 CV. The appropriate fractions were combined and evaporated *in vacuo* to give the required product (49.6 g, 94 % yield) as a pale yellow oil.

^{1}H NMR (400 MHz, DMSO-d_6) δ 7.72 (d, J = 8.3 Hz, 2H), 7.33 - 7.51 (m, 5H), 4.37 (s, 2H), 4.29 (t, J = 5.3 Hz, 1H), 3.19 (d, J = 5.3 Hz, 2H), 3.12 (s, 6H), 2.40 (s, 3H). **^{13}C NMR** (101 MHz, DMSO-d_6) δ 159.86 (d, $J_{C\text{-}F}$ = 250.2 Hz), 143.41, 135.87, 131.85 (d, $J_{C\text{-}F}$ = 5.1 Hz), 129.78, 127.35 (d, $J_{C\text{-}F}$ = 3.7 Hz), 126.97, 123.84 (d, $J_{C\text{-}F}$ = 13.9 Hz), 120.61 (d, $J_{C\text{-}F}$ = 9.5 Hz), 118.36 (d, $J_{C\text{-}F}$ = 24.9 Hz), 102.83, 53.84, 50.27, 46.06, 20.93. Note that ^{13}C NMR data are reported to two decimal places to differentiate the signals. **^{19}F NMR** (376 MHz, DMSO-d_6) δ -115.2 (m). **LCMS** (Method A) (ES +ve) *m/z* 469.9 $(M + Na)^+$ Rt 1.39 min (>95 % pure). **HRMS** Does not align, potentially

due to an unusual ionisation pattern as observed by LCMS.

6-Bromo-8-fluoroisoquinoline (86)

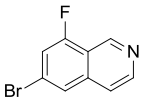

To a stirred solution of *N*-(4-bromo-2-fluorobenzyl)-*N*-(2,2-dimethoxyethyl)-4-methylbenzenesulfonamide (49.6 g, 111 mmol) was added $AlCl_3$ (44.5 g, 333 mmol) and the mixture stirred at 50 °C for 3 h. The mixture was slowly poured onto ice (1 L), then filtered and the phases were separated. The aqueous layer was back-extracted with CH_2Cl_2 (2 x 100 mL), then the organic layers were combined, washed with NaOH (2 M aq., 400 mL), and evaporated *in vacuo*. The sample was loaded in CH_2Cl_2 and purified by chromatography on silica using a 10-30 % EtOAc-cyclohexane gradient over 16 CV. The appropriate fractions were combined and evaporated *in vacuo* to give the required product (9.04 g, 32 % yield, 90 % purity) as a brown solid.

^{1}H NMR (400 MHz, DMSO-d_6) δ 9.41 (s, 1H), 8.64 (d, *J* = 5.9 Hz, 1H), 8.12 (s, 1H), 7.85 (d, *J* = 5.6 Hz, 1H), 7.74 (dd, *J* = 1.5, 10.0 Hz, 1H). **LCMS** (Method A) (ES +ve) *m/z* 226.0/228.0 $(M + H)^+$ Rt 0.91 min (90 % pure).

6-Cyclopropyl-8-fluoroisoquinoline (87)

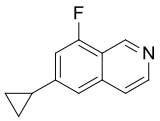

To a solution of 6-bromo-8-fluoroisoquinoline (2.20 g, 8.76 mmol), potassium cyclopropyl trifluoroborate (1.56 g, 10.5 mmol) and XPhos (0.084 g, 0.175 mmol) in THF (50 mL) was added a solution of K_3PO_4 (3.72 g, 17.52 mmol) in water (5 mL) then the solution was degassed (3 cycles vacuum/nitrogen). XPhos Pd G2 (0.138 g, 0.175 mmol) was added, the mixture degassed again, then the mixture stirred at 70 °C for 24 h The mixture was passed through Celite, diluted with EtOAc (75 mL) and water (75 mL), then the phases were separated. The aqueous layer was back-extracted with EtOAc (25 mL), then the organic layers were combined, washed with brine (100 mL),

dried using a hydrophobic frit and evaporated *in vacuo*. The sample was loaded in CH_2Cl_2 and purified by chromatography on silica using a 0-40 % EtOAc-cyclohexane gradient over 14 CV, however this failed to completely separate the product. The appropriate fractions were combined and evaporated *in vacuo*, then the residue loaded in DMSO and purified by reverse phase (C18) chromatography using a 0-30 % acetonitrile-water (+0.1 % formic acid modifier) for 10 CV, then 40 % acetonitrile-water for a further 3 CV. The appropriate fractions were combined and acetonitrile removed *in vacuo*, then the solution extracted with EtOAc (3 x 100 mL) and the organic layers combined and evaporated *in vacuo* to give the required product (1.05 g, 64 % yield) as a colourless oil.

^{1}H NMR (400 MHz, $CDCl_3$) δ 9.42 (s, 1H), 8.53 (d, J = 5.9 Hz, 1H), 7.55 (d, J = 5.9 Hz, 1H), 7.31 (s, 1H), 6.91 (dd, J = 1.5, 11.5 Hz, 1H), 2.02 - 2.12 (m, 1H), 1.09 - 1.17 (m, 2H), 0.83 - 0.89 (m, 2H). **^{13}C NMR** (101 MHz, $CDCl_3$) δ 163.9, 159.3 (d, J_{C-F} = 256.0 Hz), 148.5 (d, J_{C-F} = 7.3 Hz), 145.8 (d, J_{C-F} = 5.1 Hz), 143.8, 137.1 (d, J_{C-F} = 4.4 Hz), 119.4 (d, J_{C-F} = 2.9 Hz), 118.1 (d, J_{C-F} = 4.4 Hz), 109.4 (d, J_{C-F} = 19.1 Hz), 16.1 (d, J_{C-F} = 2.2 Hz), 10.2. **^{19}F NMR** (376 MHz, $CDCl_3$) δ -123.7 (d, J_{C-F} = 10.4 Hz). **LCMS** (Method A) (ES +ve) *m/z* 188.1 $(M + H)^+$ Rt 0.62 min (>95 % pure). **HRMS** (ES) calcd for $C_{12}H_{11}FN$, $(M + H)^+$ 188.0870, found 188.0866.

6-Cyclopropyl-8-fluoroisoquinoline 2-oxide (88)

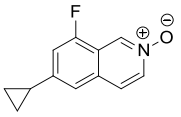

To a stirred solution of 6-cyclopropyl-8-fluoroisoquinoline (919 mg, 4.91 mmol) in CH_2Cl_2 (25 mL) was added *m*-CPBA (1.32 g, 5.89 mmol) portionwise, then the mixture stirred at rt for 2 h. The mixture was concentrated *in vacuo*, then EtOAc (100 mL), water (50 mL) and K_2CO_3 (sat. aq., 50 mL) were added and the phases were separated. The aqueous layer was back-extracted with EtOAc (50 mL), then the organic layers were combined and evaporated *in vacuo* to give the required product (895 mg, 90 % yield) as a pale yellow solid.

^{1}H NMR (400 MHz, DMSO-d_6) δ 8.73 (s, 1H), 8.16 (dd, J = 1.7, 7.1 Hz, 1H), 7.87

(dd, *J* = 1.2, 7.1 Hz, 1H), 7.54 (s, 1H), 7.25 (dd, *J* = 1.5, 12.2 Hz, 1H), 2.11 (s, 1H), 1.03 - 1.12 (m, 2H), 0.82 - 0.90 (m, 2H). **^{19}F NMR** (376 MHz, DMSO-d_6) δ -122.9 (d, J_{C-F} = 13.9 Hz). **LCMS** (Method A) (ES +ve) *m/z* 204.1 $(M + H)^+$ Rt 0.72 min (>95 % pure).

6-Cyclopropyl-8-fluoroisoquinolin-1(2*H*)-one (89)

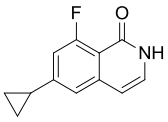

A solution of 6-cyclopropyl-8-fluoroisoquinoline 2-oxide (890 mg, 4.38 mmol) in acetic anhydride (10 mL, 106 mmol) was stirred at 150 °C for 5 h. The mixture was concentrated *in vacuo*, then the residue dissolved in MeOH (20 mL) and treated with NaOH (2 M aq., 20 mL), then the mixture stirred at rt for 1 h. MeOH was removed *in vacuo*, then the suspension was diluted with water (50 mL) and extracted twice with *n*-BuOH (2 x 50 mL). The organic layers were combined, dried using a hydrophobic frit and evaporated *in vacuo*. The residue was dissolved in DMSO, then purified by reverse phase (C18) chromatography using a 5-55 % acetonitrile-water (+0.1 % ammonium bicarbonate modifier) gradient over 14 CV. The appropriate fractions were combined, then acetonitrile removed *in vacuo*. The solution was extracted with *n*-BuOH (2 x 50 mL), then the organic layers were combined and evaporated *in vacuo* to give the required product (706 mg, 79 % yield) as a red/brown solid.

^{1}H NMR (400 MHz, DMSO-d_6) δ 11.16 (br. s., 1H), 7.15 (d, *J* = 1.2 Hz, 1H), 7.12 (d, *J* = 7.1 Hz, 1H), 6.86 (dd, *J* = 1.5, 13.2 Hz, 1H), 6.41 (dd, *J* = 2.2, 7.1 Hz, 1H), 1.94 - 2.07 (m, 1H), 1.00 - 1.08 (m, 2H), 0.77 - 0.85 (m, 2H). **^{13}C NMR** (101 MHz, DMSO-d_6) δ 162.2 (d, J_{C-F} = 259.7 Hz), 159.6 (d, J_{C-F} = 4.4 Hz), 151.3 (d, J_{C-F} = 9.5 Hz), 141.1 (d, J_{C-F} = 1.5 Hz), 130.7, 118.7 (d, J_{C-F} = 3.7 Hz), 112.9 (d, J_{C-F} = 6.6 Hz), 110.5 (d, J_{C-F} = 22.0 Hz), 104.3 (d, J_{C-F} = 2.9 Hz), 15.8 (d, J_{C-F} = 1.5 Hz), 10.9. **^{19}F NMR** (376 MHz, DMSO-d_6) δ -112.02 (d, J_{C-F} = 13.9 Hz). **LCMS** (Method A) (ES +ve) *m/z* 204.1 $(M + H)^+$ Rt 0.81 min (>95 % pure). **HRMS** (ES) calcd for $C_{12}H_{11}FNO$, $(M + H)^+$ 204.0819, found 204.0836.

2-Bromo-6-(6-cyclopropyl-8-fluoro-1-oxoisoquinolin-2(1H)-yl)benzaldehyde (90)

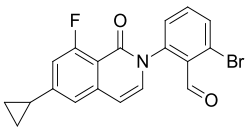

To a degassed solution of 6-cyclopropyl-8-fluoroisoquinolin-1(2*H*)-one (248 mg, 1.22 mmol), 2,6-dibromobenzaldehyde (483 mg, 1.83 mmol) and K_2CO_3 (337 mg, 2.44 mmol) in DMF (10 mL) was added CuI (116 mg, 0.610 mmol), the solution degassed (3 cycles vacuum/nitrogen), then heated at 130 °C for 20 h. The mixture was diluted with EtOAc (50 mL) and water (100 mL), then the phases were separated. The aqueous layer was back-extracted with EtOAc (2 x 50 mL), then the organic layers were combined, washed with brine (200 mL), dried using a hydrophobic frit and evaporated *in vacuo*. The sample was loaded in CH_2Cl_2 and purified on silica using a 0-35% EtOAc-cyclohexane gradient over 14 CV. The appropriate fractions were combined and evaporated *in vacuo* to give the required product (269 mg, 51 % yield, 90 % pure) as an orange solid. The sample was used directly in the next reaction without further purification.

^{1}H NMR (400 MHz, DMSO-d_6) δ 10.06 (s, 1H), 7.91 (dd, *J* = 0.9, 8.2 Hz, 1H), 7.71 (t, *J* = 7.9 Hz, 1H), 7.52 (d, *J* = 7.6 Hz, 1H), 7.41 (d, *J* = 7.6 Hz, 1H), 7.26 (d, *J* = 1.5 Hz, 1H), 6.99 (dd, *J* = 1.5, 13.4 Hz, 1H), 6.57 - 6.66 (m, 1H), 2.03 - 2.11 (m, 1H), 1.07 - 1.13 (m, 2H), 0.84 - 0.90 (m, 2H). **^{19}F NMR** (376 MHz, DMSO-d_6) δ -110.9 (d, $J_{C\text{-}F}$ = 10.4 Hz). **LCMS** (Method A) (ES +ve) *m/z* 386.2/388.2 $(M + H)^+$ Rt 1.16 min (>95 % pure).

2-(3-Bromo-2-(hydroxymethyl)phenyl)-6-cyclopropyl-8-fluoroisoquinolin-1(2*H*)-one (91)

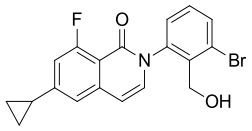

To a stirred solution of 2-bromo-6-(6-cyclopropyl-8-fluoro-1-oxoisoquinolin-2(1*H*)-yl)benzaldehyde (266 mg, 0.620 mmol, 90 % purity) in MeOH (5 mL) at 0 °C was added $NaBH_4$ (47.0 mg, 1.24 mmol) portionwise, then the mixture stirred at 0 °C for 2 h. NH_4Cl (sat. aq., 2 mL) was added, the mixture diluted with water (20 mL) and CH_2Cl_2 (20 mL), then the phases were separated. The aqueous layer was back-extracted with CH_2Cl_2 (10 mL), then the organic layers were combined, dried using a hydrophobic frit and evaporated *in vacuo*. The sample was loaded in CH_2Cl_2 and purified on silica using a 0-2 % MeOH-CH_2Cl_2 gradient over 18 CV, however this failed to completely separate the product. The appropriate fractions were combined and evaporated *in vacuo*, then the residue was loaded in DMSO and purified by reverse phase (C18) chromatography using a 35-50 % acetonitrile-water (+0.1 % ammonium bicarbonate modifier) gradient for 3 CV, then held at 50 % for 2 CV, then 50-85 % for 3 CV. The appropriate fractions were combined and evaporated *in vacuo* to give the required product (173 mg, 72 % yield) as a pale yellow solid.

^{1}H NMR (400 MHz, DMSO-d_6) d 7.76 (dd, J = 1.3, 7.9 Hz, 1H), 7.40 (t, J = 7.8 Hz, 1H), 7.35 (dd, J = 1.2, 7.8 Hz, 1H), 7.29 (d, J = 7.3 Hz, 1H), 7.26 (d, J = 1.2 Hz, 1H), 6.99 (dd, J = 1.5, 13.2 Hz, 1H), 6.59 (dd, J = 2.0, 7.3 Hz, 1H), 4.90 (t, J = 5.1 Hz, 1H), 4.49 (dd, J = 4.9, 11.7 Hz, 1H), 4.28 (dd, J = 5.1, 11.7 Hz, 1H), 2.01 - 2.13 (m, 1H), 1.04 - 1.14 (m, 2H), 0.87 (dd, J = 2.1, 4.8 Hz, 2H). **^{13}C NMR** (101 MHz, DMSO-d_6) δ 161.9 (d, $J_{C\text{-}F}$ = 260.4 Hz), 158.2 (d, $J_{C\text{-}F}$ = 4.4 Hz), 151.9 (d, $J_{C\text{-}F}$ = 10.3 Hz), 141.8, 140.0, 137.7, 134.6, 133.2, 130.1, 128.5, 125.0, 118.4 (d, $J_{C\text{-}F}$ = 2.2 Hz), 111.8 (d, $J_{C\text{-}F}$ = 5.9 Hz), 110.8 (d, $J_{C\text{-}F}$ = 22.0 Hz), 104.3 (d, $J_{C\text{-}F}$ = 2.2 Hz), 59.4, 15.4 (d, $J_{C\text{-}F}$ = 1.5 Hz), 10.7. Only clearly resolved ^{13}C-^{19}F couplings are reported. **^{19}F NMR** (376 MHz, DMSO-d_6) δ -111.0 (d, $J_{C\text{-}F}$ = 13.9 Hz). **LCMS** (Method A) (ES +ve) *m/z* 388.0/390.0

$(M + H)^+$ Rt 1.08 min (>95 % pure). **HRMS** (ES) calcd for $C_{19}H_{16}BrFNO_2$, $(M + H)^+$ 388.0343, found 388.0343.

3,5-Dibromo-1-methylpyridin-2(1H)-one (92)

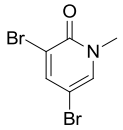

To a stirred solution of *N*-methyl-2-pyridone (0.90 mL, 9.17 mmol) and NBS (3.92 g, 22.0 mmol) in acetonitrile (10 mL) was added TFA (3.53 mL, 45.9 mmol) and the mixture stirred at 50 °C for 6 h. The mixture was diluted with EtOAc (100 mL), K_2CO_3 (1 M aq., 50 mL) and water (50 mL), then the phases were separated. The aqueous layer was back-extracted with EtOAc (2 x 50 mL), then the organic layers were combined, washed with $Na_2S_2O_3$ (10 % aq., 100 mL) and NaOH (2 M aq., 100 mL) dried using a hydrophobic frit and evaporated *in vacuo* to give the required product (2.41 g, 98 % yield) as a white solid.

^{1}H NMR (400 MHz, $CDCl_3$) δ 7.80 (d, *J* = 2.2 Hz, 1H), 7.44 (d, *J* = 2.4 Hz, 1H), 3.61 (s, 3H). **LCMS** (Method A) (ES +ve) *m/z* 265.9/267.9 $(M + H)^+$ Rt 0.70 min (>95 % pure).

Consistent with literature data.[410]

***tert*-Butyl 4-(6-nitropyridin-3-yl)piperazine-1-carboxylate (93)**

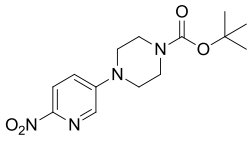

A solution of 5-bromo-2-nitropyridine (1.38 g, 6.80 mmol), *tert*-butyl piperazine-1-carboxylate (1.39 g, 7.46 mmol), LiCl (0.288 g, 6.80 mmol) and DIPEA (1.8 mL, 10.3 mmol) in DMF (10 mL) was stirred at 50 °C for 72 h. The temperature was increased to 100 °C and the mixture stirred for a further 8 h. The solution was diluted with water (80 mL)and left to stand overnight. The resulting precipitate was separated by filtration, then dissolved in CH_2Cl_2 and purified on silica using a 0-50 % EtOAc-

cyclohexane gradient for 8 CV, then 50 % EtOAc for a further 2CV. The appropriate fractions were combined and evaporated *in vacuo* to give the required product (1.67 g, 80 % yield) as a yellow solid.

^{1}H NMR (400 MHz, $CDCl_3$) δ 8.19 (d, *J* = 9.0 Hz, 1H), 8.14 (d, *J* = 3.0 Hz, 1H), 7.22 (dd, *J* = 3.0, 9.0 Hz, 1H), 3.62 - 3.68 (m, 4H), 3.43 - 3.50 (m, 4H), 1.50 (s, 9H). **LCMS** (Method A) (ES +ve) *m/z* 309.1 $(M + H)^+$ Rt 1.00 min (>95 % pure).

Consistent with literature data.[411]

***tert*-Butyl 4-(6-aminopyridin-3-yl)piperazine-1-carboxylate (94)**

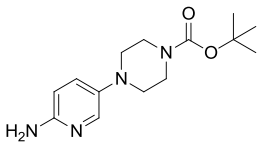

A suspension of *tert*-butyl 4-(6-nitropyridin-3-yl)piperazine-1-carboxylate (1.33 g, 4.31 mmol) and Pd/C (10 % wt, 0.918 g, 0.863 mmol) in EtOH (20 mL) was stirred under an atmosphere of hydrogen for 3 h. The reaction mixture was passed through Celite and evaporated *in vacuo*, however some residual Pd visibly remained. The solution was passed through a silica plug eluting with 8:2 CH_2Cl_2:MeOH, then the eluent was collected and evaporated *in vacuo* to give the required product (903 mg, 75 % yield) as a grey solid. The sample was used directly in the next reaction.

^{1}H NMR (400 MHz, DMSO-d_6) δ 7.62 (d, *J* = 2.9 Hz, 1H), 7.17 (dd, *J* = 2.9, 8.8 Hz, 1H), 6.40 (d, *J* = 8.8 Hz, 1H), 5.42 (s, 2H), 3.39 - 3.46 (m, 4H), 2.81 - 2.90 (m, 4H), 1.41 (s, 9H). **LCMS** (Method A) (ES +ve) *m/z* 279.2 $(M + H)^+$ Rt 0.52 min (>95 % pure).

Consistent with literature data.[412]

tert-Butyl 4-(6-((5-bromo-1-methyl-2-oxo-1,2-dihydropyridin-3-yl)amino)pyridin-3-yl)piperazine-1-carboxylate (95)

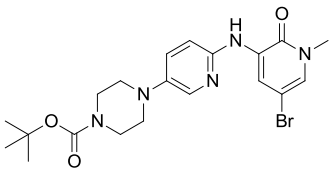

To a stirred solution of *tert*-butyl 4-(6-aminopyridin-3-yl)piperazine-1-carboxylate (953 mg, 3.42 mmol) in 1,4-dioxane (20 mL) was added 3,5-dibromo-1-methylpyridin-2(1*H*)-one (1.10 g, 4.11 mmol), Xantphos (396 mg, 0.685 mmol) and Cs_2CO_3 (2.23 g, 6.85 mmol) then the solution degassed (3 cycles vacuum/nitrogen). $Pd_2(dba)_3$ (157 mg, 0.171 mmol) was added, then the solution degassed (3 cycles), then heated at 100 °C for 5 h. The mixture was poured into EtOAc (150 mL) and water (150 mL), filtered through Celite, then the phases were separated. The aqueous layer was back-extracted with EtOAc (100 mL), then the organic layers were combined, dried using a hydrophobic frit and evaporated *in vacuo*. The sample was loaded in CH_2Cl_2 and purified on silica eluting with 20:1 CH_2Cl_2:MeOH for 8 CV. The appropriate fractions were combined and evaporated *in vacuo* to give the required product (1.42 g, 89 % yield) as a pale brown solid.

^{1}H NMR (400 MHz, DMSO-d_6) δ 8.57 (d, *J* = 2.4 Hz, 1H), 8.54 (s, 1H), 7.95 (d, *J* = 3.0 Hz, 1H), 7.44 (d, *J* = 2.4 Hz, 1H), 7.40 (dd, *J* = 3.0, 9.1 Hz, 1H), 7.26 (d, *J* = 9.1 Hz, 1H), 3.51 (s, 3H), 3.42 - 3.48 (m, 4H), 2.99 - 3.06 (m, 4H), 1.42 (s, 9H). **^{13}C NMR** (101 MHz, DMSO-d_6) δ 156.0, 153.7, 148.5, 141.1, 134.3, 132.1, 127.6, 126.6, 116.4, 113.4, 97.8, 78.9, 49.0, 37.0, 28.0. One piperazine carbon is not observed but visible by HSQC, potentially due to slow ring inversion. **LCMS** (Method A) (ES +ve) *m/z* 464.1/466.1 $(M + H)^+$ Rt 1.21 min (>95 % pure). **HRMS** (ES) calcd for $C_{20}H_{27}BrN_5O_3$, $(M + H)^+$ 464.1292, found 464.1286.

tert-Butyl 4-(6-((1-methyl-2-oxo-5-(4,4,5,5-tetramethyl-1,3,2-dioxaborolan-2-yl)-1,2-dihydropyridin-3-yl)amino)pyridin-3-yl)piperazine-1-carboxylate (96)

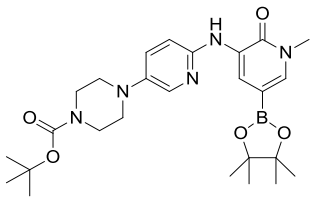

To an oven-dried flask containing *tert*-butyl 4-(6-((5-bromo-1-methyl-2-oxo-1,2-dihydropyridin-3-yl)amino)pyridin-3-yl)piperazine-1-carboxylate (500 mg, 1.08 mmol), bis(pinacolato)diboron (383 mg, 1.51 mmol), palladium(II) acetate (12.1 mg, 0.054 mmol), XPhos (51.3 mg, 0.108 mmol) and potassium acetate (528 mg, 5.38 mmol) was added 1,4-dioxane (8 mL), then the mixture degassed (3 cycles vacuum/nitrogen) and heated to 95 °C for 1 h. The mixture was filtered through Celite, then the pad washed with CH_2Cl_2 and the filtrate evaporated *in vacuo*. The sample was dissolved in minimal dioxane (~4 mL), then heated to 90 ºC. Hexane (10 mL) was added, resulting in precipitate formation. The mixture was cooled to rt, then left to stand in the fridge overnight. The remaining solvent was decanted and the precipitate dried to give the required product (428 mg, 78 % yield) as a dark brown solid.

^{1}H NMR (400 MHz, DMSO-d_6) δ 8.45 (d, *J* = 1.7 Hz, 1H), 8.21 (s, 1H), 7.91 (d, *J* = 2.9 Hz, 1H), 7.48 (d, *J* = 1.7 Hz, 1H), 7.37 (dd, *J* = 2.9, 9.0 Hz, 1H), 7.16 (d, *J* = 9.0 Hz, 1H), 3.55 (s, 3H), 3.43 - 3.49 (m, 4H), 2.99 - 3.05 (m, 4H), 1.42 (s, 9H), 1.28 (s, 12H). **^{13}C NMR** (101 MHz, DMSO-d_6) δ 157.9, 153.8, 149.2, 140.6, 135.9, 134.5, 130.7, 127.8, 117.5, 112.9, 83.5, 81.3, 78.9, 49.2, 37.1, 28.0, 24.6, 24.4. **LCMS** (Method A) (ES +ve) *m/z* 512.4 $(M + H)^+$ Rt 1.15 min (indicates 70 % purity, however the boronic ester is likely to be unstable to the aqueous acid LCMS method. NMR indicates >95 % purity). **HRMS** (ES) calcd for $C_{26}H_{39}BN_5O_5$, $(M + H)^+$ 512.3039, found 512.3040.

tert-Butyl 4-(6-((5-(3-(6-cyclopropyl-8-fluoro-1-oxoisoquinolin-2(1*H*)-yl)-2-(hydroxymethyl)phenyl)-1-methyl-2-oxo-1,2-dihydropyridin-3-yl)amino)pyridin-3-yl)piperazine-1-carboxylate (97)

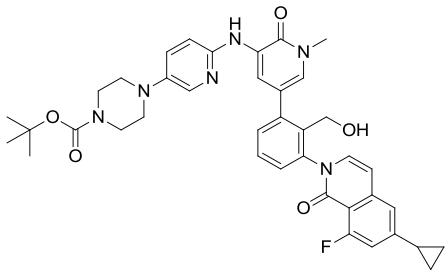

To a vial containing 2-(3-bromo-2-(hydroxymethyl)phenyl)-6-cyclopropyl-8-fluoroisoquinolin-1(2H)-one (190 mg, 0.489 mmol), *tert*-butyl 4-(6-((1-methyl-2-oxo-5-(4,4,5,5-tetramethyl-1,3,2-dioxaborolan-2-yl)-1,2-dihydropyridin-3-yl)amino)pyridin-3-yl)piperazine-1-carboxylate (375 mg, 0.734 mmol) and tricyclohexylphosphine (14 mg, 0.049 mmol) was added 1,4-dioxane (2 mL), MeOH (2 mL) and a solution of potassium carbonate (135 mg, 0.979 mmol) in water (1 mL). The solution was degassed (3 cycles vacuum/nitrogen) then the mixture was stirred at 90 °C for 2 h. The mixture was poured into water (50 mL), then the resulting precipitate separated by filtration and washed with water (50 mL). The precipitate was dissolved in CH_2Cl_2 (50 mL), then filtered again. The sample was loaded in DMSO and purified by reverse phase (C18) chromatography using a 45-95% acetonitrile-water (+0.1 % ammonium bicarbonate modifier) gradient over 12 CV. The appropriate fractions were combined and evaporated *in vacuo* to give the required product (185 mg, 55 % yield) as a pale purple solid.

^{1}H NMR (400 MHz, DMSO-d_6) δ 8.57 (d, J = 2.2 Hz, 1H), 8.38 (s, 1H), 7.88 (d, J = 2.9 Hz, 1H), 7.52 (t, J = 7.8 Hz, 1H), 7.43 (d, J = 7.8 Hz, 1H), 7.30 - 7.39 (m, 4H), 7.26 (s, 1H), 7.22 (d, J = 9.0 Hz, 1H), 6.98 (d, J = 13.3 Hz, 1H), 6.59 (d, J = 7.5 Hz, 1H), 4.68 - 4.79 (m, 1H), 4.32 (d, J = 11.0 Hz, 1H), 4.21 (d, J = 11.0 Hz, 1H), 3.59 (s, 3H), 3.44 (t, J = 4.8 Hz, 4H), 2.99 (t, J = 4.9 Hz, 4H), 2.03 - 2.12 (m, 1H), 1.41 (s, 9H), 1.06 - 1.13 (m, 2H), 0.84 - 0.90 (m, 1H). **^{13}C NMR** (101 MHz, DMSO-d_6) δ 161.9 (d, J_{C-F} = 257.5 Hz), 160.6, 158.4 (d, J_{C-F} = 5.1 Hz), 156.5, 153.7, 151.6 (d, J_{C-F} = 9.5 Hz), 149.0, 141.5, 140.7, 140.3, 140.1, 135.9, 135.2, 134.6, 130.6, 128.6, 128.1, 127.8,

127.7, 126.7, 118.3 (d, J_{C-F} = 3.7 Hz), 118.0, 116.7, 112.9, 111.9 (d, J_{C-F} = 5.9 Hz), 110.7 (d, J_{C-F} = 22.0 Hz), 104.0 (d, J_{C-F} = 3.7 Hz), 78.9, 56.9, 49.2, 37.3, 28.0, 15.4, 10.6 (d, J_{C-F} = 3.7 Hz). One piperazine carbon is not observed but visible by HSQC, potentially due to slow ring inversion. Only clearly resolved ^{13}C-^{19}F couplings are reported.**^{19}F NMR** (376 MHz, DMSO-d_6) δ -111.1 (d, J_{C-F} = 10.4 Hz). **LCMS** (Method B) (ES +ve) *m/z* 693.3 $(M + H)^+$ Rt 1.35 min (>95 % pure). **HRMS** (ES) calcd for $C_{39}H_{42}FN_6O_5$, $(M + H)^+$ 693.3195, found 693.3241.

6-Cyclopropyl-8-fluoro-2-(2-(hydroxymethyl)-3-(1-methyl-5-((5-(4-methylpiperazin-1-yl)pyridin-2-yl)amino)-6-oxo-1,6-dihydropyridin-3-yl)phenyl)isoquinolin-1(2*H*)-one (98)

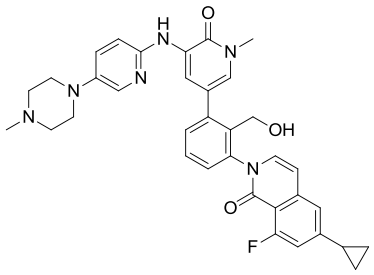

To a stirred solution of *tert*-butyl 4-(6-((5-(3-(6-cyclopropyl-8-fluoro-1-oxoisoquinolin-2(1*H*)-yl)-2-(hydroxymethyl)phenyl)-1-methyl-2-oxo-1,2-dihydropyridin-3-yl)amino)pyridin-3-yl)piperazine-1-carboxylate (13 mg, 0.019 mmol) in MeOH (1 mL) was added HCl (4 M in dioxane, 1 mL) and the mixture stirred at rt for 2 h. The solution was concentrated to dryness under a stream of nitrogen, then the residue was dissolved in MeOH (1 mL) and treated with formaldehyde (38% aq., 14 µL, 0.19 mmol) and $NaBH(OAc)_3$ (40 mg, 0.19 mmol). The mixture was stirred at rt for 24 h, after which the reaction mixture was directly purified by MDAP (ammonium bicarbonate modifier gradient). The appropriate fractions were combined and evaporated *in vacuo* to give the required product (4.5 mg, 40 % yield) as a white solid.

^{1}H NMR (400 MHz, DMSO-d_6) δ 8.55 (d, *J* = 2.3 Hz, 1H), 8.34 (s, 1H), 7.85 (d, *J* = 3.0 Hz, 1H), 7.49 - 7.55 (m, 1H), 7.43 (dd, *J* = 1.3, 7.8 Hz, 1H), 7.29 - 7.37 (m, 4H), 7.26 (d, *J* = 1.5 Hz, 1H), 7.20 (d, *J* = 9.1 Hz, 1H), 6.98 (dd, *J* = 1.5, 13.3 Hz, 1H), 6.59

(dd, *J* = 2.0, 7.3 Hz, 1H), 4.32 (d, *J* = 11.3 Hz, 1H), 4.21 (d, *J* = 11.3 Hz, 1H), 3.59 (s, 3H), 3.00 - 3.06 (m, 4H), 2.40 - 2.45 (m, 4H), 2.20 (s, 3H), 2.03 - 2.11 (m, 1H), 1.06 - 1.13 (m, 2H), 0.83 - 0.90 (m, 2H). **^{19}F NMR** (376 MHz, DMSO-d_6) δ -111.1 (d, $J_{C\text{-}F}$ = 12.2 Hz). **LCMS** (Method B) (ES +ve) *m/z* 607.2 $(M + H)^+$ Rt 1.12 min (>95 % pure).

Consistent with literature data.[364,388]

14-(4-(6-((5-(3-(6-Cyclopropyl-8-fluoro-1-oxoisoquinolin-2(1*H*)-yl)-2-(hydroxymethyl)phenyl)-1-methyl-2-oxo-1,2-dihydropyridin-3-yl)amino)pyridin-3-yl)piperazin-1-yl)-3,6,9,12-tetraoxatetradecan-1-oic acid (99)

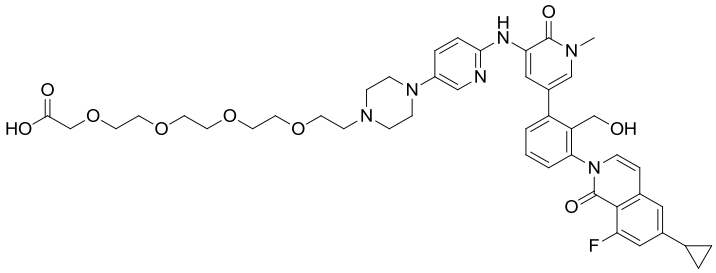

To a stirred solution of *tert*-butyl 4-(6-((5-(3-(6-cyclopropyl-8-fluoro-1-oxoisoquinolin-2(1*H*)-yl)-2-(hydroxymethyl)phenyl)-1-methyl-2-oxo-1,2-dihydropyridin-3-yl)amino)pyridin-3-yl)piperazine-1-carboxylate (58 mg, 0.084 mmol) in MeOH (0.5 mL) was added HCl (4 M in dioxane, 0.5 mL) and the mixture stirred at rt for 2 h. The mixture was neutralised with $NaHCO_3$ (sat. aq.), and diluted with water (10 mL), then the precipitate collected by filtration and dried under a stream of nitrogen. The sample was dissolved in a solution of methyl 14-chloro-3,6,9,12-tetraoxatetradecanoate (29 mg, 0.102 mmol) and DIPEA (0.044 mL, 0.25 mmol) in DMF (1.5 mL), then sodium iodide (12.5 mg, 0.083 mmol) was added and the mixture stirred at 100 °C for 12 h. The mixture was diluted with *n*-BuOH (10 mL) and water (20 mL), then the phases were separated. The aqueous layer was back-extracted with *n*-BuOH (10 mL), then the organic layers were combined, washed with brine and evaporated *in vacuo*. The residue was dissolved in MeOH (5 mL) then a solution of LiOH (20 mg, 0.84 mmol) in water (1 mL) was added and the mixture stirred at rt for 1 h. The mixture was evaporated *in vacuo*, then the sample was loaded in DMSO and

purified by reverse phase (C18) chromatography using a 0-60 % acetonitrile-water (+0.1 % ammonium bicarbonate modifier) gradient over 14 CV. The appropriate fractions were combined and evaporated *in vacuo* to give the required product (35 mg, 51 % yield) as an orange solid.

^{1}H NMR (400 MHz, DMSO-d_6) δ 8.55 (d, J = 2.3 Hz, 1H), 8.33 (s, 1H), 7.84 (d, J = 3.0 Hz, 1H), 7.49 - 7.55 (m, J = 7.8 Hz, 1H), 7.43 (dd, J = 1.1, 7.7 Hz, 1H), 7.29 - 7.37 (m, 4H), 7.26 (d, J = 1.3 Hz, 1H), 7.20 (d, J = 9.1 Hz, 1H), 6.97 (dd, J = 1.4, 13.2 Hz, 1H), 6.59 (dd, J = 2.0, 7.3 Hz, 1H), 4.84 (br. s., 1H), 4.31 (d, J = 11.1 Hz, 1H), 4.20 (d, J = 11.3 Hz, 1H), 3.50 - 3.60 (m, 19H), 2.98 - 3.06 (m, 4H), 2.52 - 2.56 (m, 6H), 2.02 - 2.12 (m, 1H), 1.06 - 1.12 (m, 2H), 0.83 - 0.89 (m, 2H). **^{13}C NMR** (101 MHz, DMSO-d_6) δ 172.47, 162.40 (d, $J_{C\text{-}F}$ = 257.5 Hz), 158.89 (d, $J_{C\text{-}F}$ = 4.4 Hz), 157.05, 152.14 (d, $J_{C\text{-}F}$ = 9.5 Hz), 148.97, 142.04, 141.43, 140.90, 140.67, 136.41, 135.69, 134.31, 131.16, 130.95, 129.13, 128.30, 127.38, 127.08, 118.79 (d, $J_{C\text{-}F}$ = 3.7 Hz), 118.54, 116.99, 113.31, 112.46 (d, $J_{C\text{-}F}$ = 5.9 Hz), 111.16 (d, $J_{C\text{-}F}$ = 21.3 Hz), 104.47 (d, $J_{C\text{-}F}$ = 3.7 Hz), 70.22, 70.17, 70.11, 69.95, 69.24, 68.77, 57.66, 57.44, 53.46, 49.40, 37.85, 15.89, 11.12 (d, $J_{C\text{-}F}$ = 3.7 Hz). Note that ^{13}C NMR data are reported to two decimal places to differentiate the signals. Two signals are not observed, potentially due to overlapping frequencies of PEG chain carbons. Only clearly resolved ^{13}C-^{19}F couplings are reported. **^{19}F NMR** (376 MHz, DMSO-d_6) δ -111.1 (d, $J_{C\text{-}F}$ = 10.4 Hz). **LCMS** (Method B) (ES +ve) *m/z* 827.3 $(M + H)^+$ Rt 0.85 min (>95 % pure). **HRMS** (ES) calcd for $C_{44}H_{52}FN_6O_9$, $(M + H)^+$ 827.3774, found 827.3773.

(*S*)-*N*-((*S*)-1-(1-(14-(4-(6-((5-(3-(6-Cyclopropyl-8-fluoro-1-oxoisoquinolin-2(1*H*)-yl)-2-(hydroxymethyl)phenyl)-1-methyl-2-oxo-1,2-dihydropyridin-3-yl)amino)pyridin-3-yl)piperazin-1-yl)-3,6,9,12-tetraoxatetradecan-1-oyl)piperidin-4-yl)-2-((*S*)-2-(4-(4-fluorobenzoyl)thiazol-2-yl)pyrrolidin-1-yl)-2-oxoethyl)-2-(methylamino)propanamide (100)

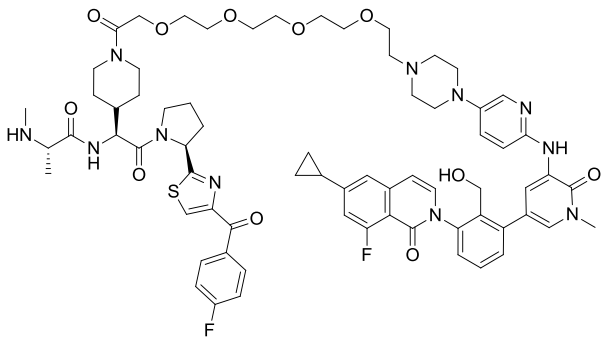

To a stirred solution of 14-(4-(6-((5-(3-(6-cyclopropyl-8-fluoro-1-oxoisoquinolin-2(1*H*)-yl)-2-(hydroxymethyl)phenyl)-1-methyl-2-oxo-1,2-dihydropyridin-3-yl)amino)pyridin-3-yl)piperazin-1-yl)-3,6,9,12-tetraoxatetradecanoic acid (34.5 mg, 0.042 mmol), (9*H*-fluoren-9-yl)methyl ((*S*)-1-(((*S*)-2-((*S*)-2-(4-(4-fluorobenzoyl)thiazol-2-yl)pyrrolidin-1-yl)-2-oxo-1-(piperidin-4-yl)ethyl)amino)-1-oxopropan-2-yl)(methyl)carbamate hydrochloride (35 mg, 0.046 mmol) and DIPEA (36.0 µL, 0.209 mmol) in DMF (1 mL) was added HATU (18 mg, 0.047 mmol) and the mixture stirred at rt for 3 h. The solution was treated with piperidine (83 µL, 0.83 mmol), stirred at rt for a further 30 min. The mixture was concentrated under a stream of nitrogen, then directly purified by MDAP (ammonium bicarbonate modifier gradient) to give the required product (25 mg, 46 % yield) as a yellow solid.

^{1}H NMR (600 MHz, DMSO-d_6) δ 8.56 (d, *J* = 2.2 Hz, 1H), 8.50 (s, 1H), 8.34 (s, 1H), 8.24 (d, *J* = 5.9 Hz, 2H), 7.85 (d, *J* = 2.9 Hz, 1H), 7.49 - 7.56 (m, 1H), 7.28 - 7.47 (m, 8H), 7.26 (s, 1H), 7.20 (d, *J* = 8.8 Hz, 1H), 6.98 (dd, *J* = 1.1, 13.2 Hz, 1H), 6.59 (dd, *J* = 1.7, 7.5 Hz, 1H), 5.40 (dd, *J* = 2.9, 8.1 Hz, 1H), 4.73 - 4.77 (m, 1H), 4.55 (d, *J* = 5.9 Hz, 1H), 4.33 (d, *J* = 9.5 Hz, 1H), 4.19 - 4.24 (m, 1H), 4.07 (br. s., 2H), 3.65 - 3.88 (m, 3H), 3.59 (s, 3H), 3.47 - 3.55 (m, 15H), 2.94 - 3.06 (m, 5H), 2.72 - 2.89 (m, 1H), 2.52 - 2.56 (m, 4H), 2.35 - 2.46 (m, 1H), 2.28 (d, *J* = 8.4 Hz, 1H), 2.14 - 2.22 (m, 4H), 1.95 - 2.12 (m, 5H), 1.60 (t, *J* = 12.1 Hz, 2H), 1.01 - 1.27 (m, 8H), 0.85 - 0.89 (m, 2H).

^{13}C NMR (151 MHz, DMSO-d_6) δ 185.05, 175.06, 173.41, 170.62, 167.32, 165.37 (d, J_{C-F} = 253.2 Hz), 162.41 (d, J_{C-F} = 260.9 Hz), 158.89 (d, J_{C-F} = 4.4 Hz), 157.05, 152.96, 152.14 (d, J_{C-F} = 10.0 Hz), 148.98, 142.04, 141.43, 140.90, 140.67, 136.40, 135.69, 134.31, 133.92 (d, J_{C-F} = 2.2 Hz), 133.56 (d, J_{C-F} = 7.7 Hz), 131.16, 130.95, 130.25 (d, J_{C-F} = 4.4 Hz), 129.13, 128.31, 127.38, 127.09, 118.79, 118.52, 116.99, 115.95 (d, J_{C-F} = 22.1 Hz), 113.32, 112.46 (d, J_{C-F} = 5.5 Hz), 111.16 (d, J_{C-F} = 22.1 Hz), 104.46, 70.26, 70.23, 70.20, 70.14, 70.07, 69.90, 69.85, 68.84, 59.59, 58.76, 57.69, 57.43, 53.89, 53.49, 49.44, 47.59, 38.41, 37.86, 34.74, 32.06, 24.58, 19.52, 15.90, 11.13 (d, J_{C-F} = 5.5 Hz). Note that ^{13}C NMR data are reported to two decimal places to differentiate the signals. Two signals are not resolved, potentially due to overlapping frequencies of PEG chain carbons. Only clearly resolved ^{13}C-^{19}F couplings are reported. **^{19}F NMR** (376 MHz, DMSO-d_6) δ -105.8 (m, 1F), -111.1 (d, J_{C-F} = 13.0 Hz, 1F). **LCMS** (Method B) (ES +ve) *m/z* 655.9 $([M + 2H]/2)^+$ Rt 1.18 min (>95 % pure). **HRMS** (ES) calcd for $C_{69}H_{82}F_2N_{11}O_{11}S$, $(M + H)^+$ 1310.5884, found 1310.5863. **IR** ν_{max} (neat) 3338, 2925, 1646, 1597, 1578, 1497, 1469 cm^{-1}. **MP** >250 °C (decomposition).

7.3 Protein MS Data

General Procedure:

Recombinant BTK (70 %, 0.1 ug/µL, buffered aqueous glycerol solution, 24.75 µL) was then added (0.25 µL of 1 mM DMSO stock solution), then left to incubate at room temperature. After the appropriate reaction time, the solution was quenched with formic acid solution (10 % aq., 75 µL). The solution was transferred to 96 well plate, then the analysis conducted using an Agilent 6224/6230 TOF LCMS system. The appropriate LC peak was deconvoluted within a 50-100 kDa range to give the required MS spectrum.

MS Spectra:

i) Treatment with DMSO and compound **65**, incubation time = 2 h.

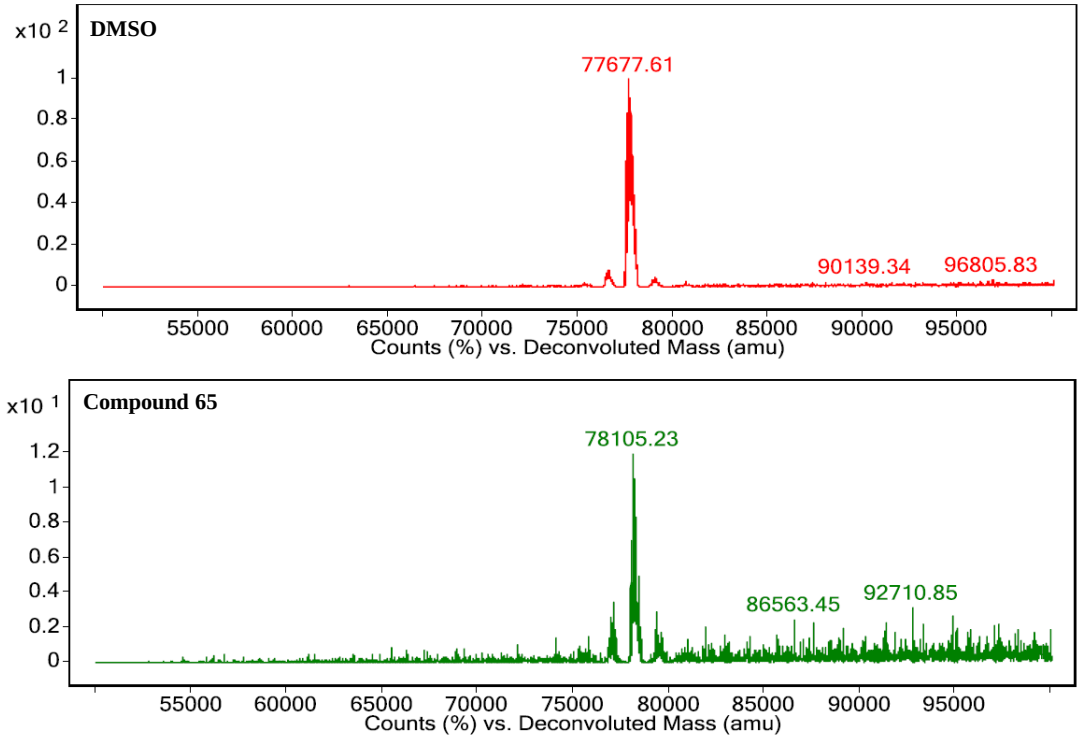

ii) Treatment with compound **69** and **70**, incubation time = 4 h.

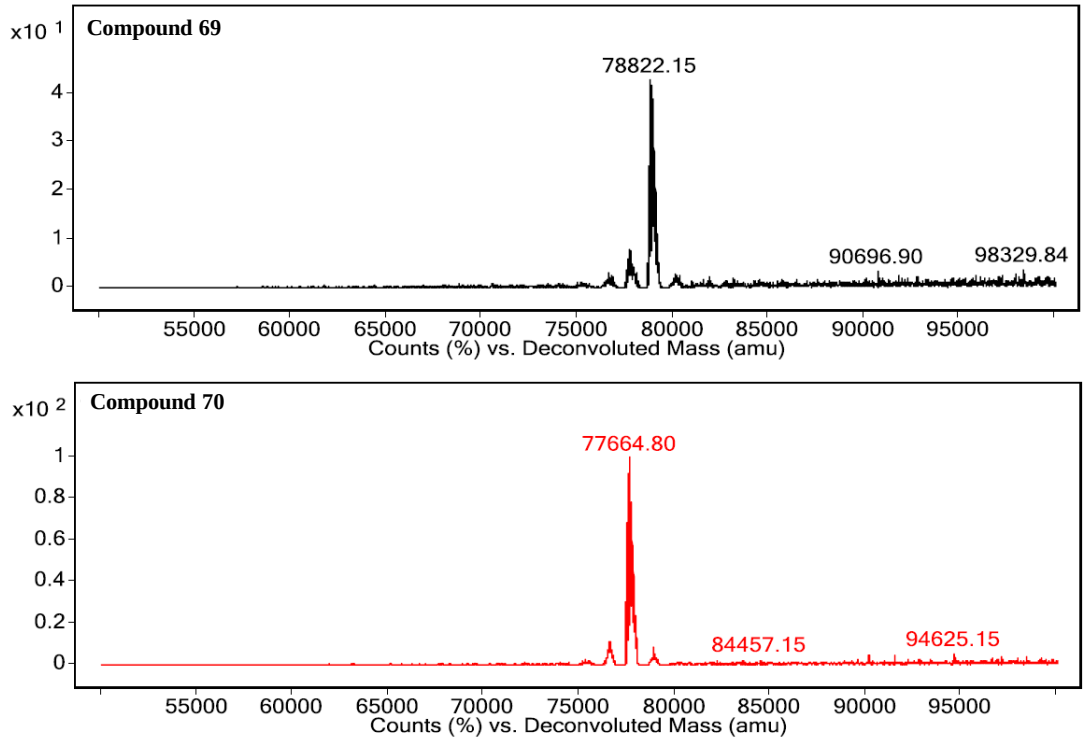

Spectral peaks observed:

		Compound		
Peak	**DMSO**	**65**	**69**	**70**
1	N/A	N/A	78743.1	77427.5
2	77513.4	77982.0	78822.2	77504.7
3	77595.1	78030.2	78842.5	77584.8
4	77677.6	78061.2	78861.2	77664.8
5	77725.0	78105.2	78904.5	77691.3
6	77746.0	78128.4	78921.4	77711.5
7	77769.2	78186.6	78982.1	77743.0
8	77784.7	78211.4	79001.9	77784.5
9	77825.5	78229.4	79061.6	77821.8
10	77847.4	78283.5	79080.7	77846.7
11	77907.0	78374.0	N/A	N/A

Observed Mass Shift, Determination of Binding Mode:

	Mass shift relative to DMSO		
Compound	**65**	**69**	**70**
Peak 1	N/A	N/A	N/A
Peak 2	468.6	1308.7	8.74
Peak 3	435.1	1247.4	10.3
Peak 4	383.6	1183.6	12.81
Peak 5	380.2	1179.5	33.68
Peak 6	382.4	1175.3	34.5
Peak 7	417.5	1213.0	26.12
Peak 8	426.6	1217.1	0.28
Peak 9	403.9	1236.1	3.76
Peak 10	436.1	1233.4	0.69
Peak 11	466.9	N/A	N/A
Significant change from DMSO	Y	Y	N
Mean mass shift	420.1	1221.6	14.5
Inhibitor MW	428.2	1238.5	1240.5
Covalent binding	Y	Y	N

N/A = Peak not detected

8. References

(1) Grimwood, S.; Hartig, P. R. *Pharmacol. Ther.* **2009**, *122*, 281–301.

(2) Morgan, P.; Van Der Graaf, P. H.; Arrowsmith, J.; Feltner, D. E.; Drummond, K. S.; Wegner, C. D.; Street, S. D. A. *Drug Discov. Today* **2012**, *17*, 419–424.

(3) Rask-Andersen, M.; Almén, M. S.; Schiöth, H. B. *Nat. Rev. Drug Discov.* **2011**, *10*, 579–590.

(4) Copeland, R. A.; Pompliano, D. L.; Meek, T. D. *Nat. Rev. Drug Discov.* **2006**, *5*, 730–739.

(5) Copeland, R. A. *Nat. Rev. Drug Discov.* **2016**, *15*, 87–95.

(6) Cusack, K. P.; Wang, Y.; Hoemann, M. Z.; Marjanovic, J.; Heym, R. G.; Vasudevan, A. *Bioorg. Med. Chem. Lett.* **2015**, *25*, 2019–2027.

(7) Cambridge, S. B.; Gnad, F.; Nguyen, C.; Bermejo, J. L.; Krüger, M.; Mann, M. *J. Proteome Res.* **2011**, *10*, 5275–5284.

(8) Yen, H.-C. S.; Xu, Q.; Chou, D. M.; Zhao, Z.; Elledge, S. J. *Science* **2008**, *322*, 918–923.

(9) Barf, T.; Kaptein, A. *J. Med. Chem.* **2012**, *55*, 6243–6262.

(10) Uetrecht, J. *Chem. Res. Toxicol.* **2008**, *21*, 84–92.

(11) Uetrecht, J. *Chem. Res. Toxicol.* **2009**, *22*, 24–34.

(12) Burnett, J. C.; Rossi, J. J. *Chem. Biol.* **2012**, *19*, 60–71.

(13) Melnikova, I. *Nat. Rev. Drug Discov.* **2007**, *6*, 863–864.

(14) Bennett, C. F.; Swayze, E. E. *Annu. Rev. Pharmacol. Toxicol.* **2010**, *50*, 259–293.

(15) Bobbin, M. L.; Rossi, J. J. *Annu. Rev. Pharmacol. Toxicol.* **2016**, *56*, 103–122.

(16) Lecker, S. H.; Goldberg, A. L.; Mitch, W. E. *J. Am. Soc. Nephrol.* **2006**, *17*, 1807–1819.

(17) Rock, K. L.; Gramm, C.; Rothstein, L.; Clark, K.; Stein, R.; Dick, L.; Hwang, D.; Goldberg, A. L. *Cell* **1994**, *78*, 761–771.

(18) Baehrecke, E. H. *Nat. Rev. Mol. Cell Biol.* **2005**, *6*, 505–510.

(19) Hershko, A.; Ciechanover, A. *Annu. Rev. Biochem.* **1992**, *61*, 761–807.

(20) Ciechanover, A. *Cell* **1994**, *79*, 13–21.

(21) Hershko, A. *Angew. Chem. Int. Ed.* **2005**, *44*, 5932–5943.

(22) Buckley, D. L.; Crews, C. M. *Angew. Chem. Int. Ed.* **2014**, *53*, 2312–2330.

(23) Jackson, P. K.; Eldridge, A. G.; Freed, E.; Furstenthal, L.; Hsu, J. Y.; Kaiser, B. K.; Reimann, J. D. R. *Trends Cell Biol.* **2000**, *10*, 429–439.

(24) Weissman, A. M.; Shabek, N.; Ciechanover, A. *Nat. Rev. Mol. Cell Biol.* **2011**, *12*, 605–620.

(25) Zaaroor-Regev, D.; de Bie, P.; Scheffner, M.; Noy, T.; Shemer, R.; Heled, M.; Stein, I.; Pikarsky, E.; Ciechanover, A. *Proc. Natl. Acad. Sci. U. S. A.* **2010**, *107*, 6788–6793.

(26) Maccario, H.; Ciechanover, A.; Kolch, W.; Kholodenko, B. N.; Nguyen, L. K.; Mun, J. *PLoS Comput Biol* **2011**, *7*, 1–11.

(27) Sorkin, A.; Goh, L. K. *Exp. Cell Res.* **2009**, *315*, 683–696.

(28) Weake, V. M.; Workman, J. L. *Mol. Cell* **2008**, *29*, 653–663.

(29) Zhou, W.; Wang, X.; Rosenfeld, M. G. *Int. J. Biochem. Cell Biol.* **2009**, *41*, 12–15.

(30) Komander, D. *Biochem. Soc. Trans.* **2009**, *37*, 937–953.

(31) Chau, V.; Tobias, J. W.; Bachmair, A.; Marriott, D.; Ecker, D. J.; Gonda, D. K.; Varshavsky, A. *Science* **1989**, *243*, 1576–1583.

(32) Thrower, J. S.; Hoffman, L.; Rechsteiner, M.; Pickart, C. M. *EMBO J.* **2000**, *19*, 94–102.

(33) Lu, Y.; Lee, B.-H.; King, R. W.; Finley, D.; Kirschner, M. W. *Science* **2015**, *348*, 1250834.

(34) Braten, O.; Livneh, I.; Ziv, T.; Admon, A.; Kehat, I.; Caspi, L. H.; Gonen, H.; Bercovich, B.; Godzik, A.; Jahandideh, S.; Jaroszewski, L.; Sommer, T.; Kwon, Y. T.; Guharoy, M.; Tompa, P.; Ciechanover, A. *Proc. Natl. Acad. Sci. U. S. A.* **2016**, *113*, 4639–4647.

(35) Bedford, L.; Lowe, J.; Dick, L. R.; Mayer, R. J.; Brownell, J. E. *Nat. Rev. Drug Discov.* **2011**, *10*, 29–46.

(36) Cohen, P.; Tcherpakov, M. *Cell* **2010**, *143*, 686–693.

(37) Marques, A. J.; Palanimurugan, R.; Matias, A. C.; Ramos, P. C.; Dohmen, R. J. *Chem. Rev.* **2009**, *109*, 1509–1536.

(38) Chen, S.; Wu, J.; Lu, Y.; Ma, Y.-B.; Lee, B.-H.; Yu, Z.; Ouyang, Q.; Finley, D. J.; Kirschner, M. W.; Mao, Y. *Proc. Natl. Acad. Sci. U. S. A.* **2016**, *113*, 12991–12996.

(39) Aufderheide, A.; Unverdorben, P.; Baumeister, W.; Förster, F. *FEBS Lett.* **2015**, *589*, 2552–2560.

(40) Yu, H.; Kago, G.; Yellman, C. M.; Matouschek, A. *EMBO J.* **2016**, 1–15.

(41) Yao, T.; Cohen, R. E. *Nature* **2002**, *419*, 403–407.

(42) Verma, R.; Aravind, L.; Oania, R.; McDonald, W. H.; Yates, J. R.; Koonin, E. V; Deshaies, R. J. *Science* **2002**, *298*, 611–615.

(43) Bhattacharyya, S.; Yu, H.; Mim, C.; Matouschek, A. *Nat. Rev. Mol. Cell Biol.* **2014**, *15*, 122–133.

(44) Groll, M.; Huber, R. *Biochim. Biophys. Acta - Mol. Cell Res.* **2004**, *1695*, 33–44.

(45) Vincenz, L.; Jäger, R.; O'Dwyer, M.; Samali, A. *Mol. Cancer Ther.* **2013**, *12*,

831–843.

(46) Moreau, P.; Richardson, P. G.; Cavo, M.; Orlowski, R. Z.; San Miguel, J. F.; Palumbo, A.; Harousseau, J.-L. *Blood* **2012**, *120*, 947–959.

(47) Kisselev, A. F.; Van Der Linden, W. A.; Overkleeft, H. S. *Chem. Biol.* **2012**, *19*, 99–115.

(48) Palombella, V. J.; Rando, O. J.; Goldberg, A. L.; Maniatis, T. *Cell* **1994**, *78*, 773–785.

(49) Lindsten, K.; Menendez-Benito, V.; Masucci, M. G.; Dantuma, N. P. *Nat. Biotechnol.* **2003**, *21*, 897–902.

(50) Kouroukis, T. C.; Baldassarre, F. G.; Haynes, A. E.; Imrie, K.; Reece, D. E.; Cheung, M. C. *Curr. Oncol.* **2014**, *21*, 573–603.

(51) Robak, T. *Futur. Oncol.* **2015**, *11*, 2807–2818.

(52) Groll, M.; Berkers, C. R.; Ploegh, H. L.; Ovaa, H. *Structure* **2006**, *14*, 451–456.

(53) Arastu-Kapur, S.; Anderl, J. L.; Kraus, M.; Parlati, F.; Shenk, K. D.; Lee, S. J.; Muchamuel, T.; Bennett, M. K.; Driessen, C.; Ball, A. J.; Kirk, C. J. *Clin. Cancer Res.* **2011**, *17*, 2734–2743.

(54) Kupperman, E.; Lee, E. C.; Cao, Y.; Bannerman, B.; Fitzgerald, M.; Berger, A.; Yu, J.; Yang, Y.; Hales, P.; Bruzzese, F.; Liu, J.; Blank, J.; Garcia, K.; Tsu, C.; Dick, L.; Fleming, P.; Yu, L.; Manfredi, M.; Rolfe, M.; Bolen, J. *Cancer Res.* **2010**, *70*, 1970–1980.

(55) Piva, R.; Ruggeri, B.; Williams, M.; Costa, G.; Tamagno, M.; Ferrero, D.; Giai, V.; Coscia, M.; Peola, S.; Massaia, M.; Pezzoni, G.; Allievi, C.; Pescalli, N.; Cassin, M.; Giovine, S. Di; Nicoli, P.; De Feudis, P.; Strepponi, I.; Roato, M.; Ferracini, R.; Bussolati, B.; Camussi, G.; Jones-Bolin, S.; Hunter, K.; Zhao, H.; Neri, A.; Palumbo, A.; Berkers, C.; Ovaa, H.; Bernareggi, A.; Inghirami, G. *Blood* **2008**, *111*, 2765–2775.

(56) Shirley, M. *Drugs* **2016**, *76*, 405–411.

(57) Hanada, M.; Sugawara, K.; Kaneta, K.; Toda, S.; Nishiyama, Y.; Tomita, K.; Yamamoto, H.; Konishi, M.; Oki, T. *J. Antibiot.* **1992**, *45*, 1746–1752.

(58) Meng, L.; Mohan, R.; Kwok, B. H.; Elofsson, M.; Sin, N.; Crews, C. M. *Proc. Natl. Acad. Sci. U. S. A.* **1999**, *96*, 10403–10408.

(59) Groll, M.; Kim, K. B.; Kairies, N.; Huber, R.; Crews, C. M. *J. Am. Chem. Soc.* **2000**, *122*, 1237–1238.

(60) Kortuem, K. M.; Stewart, A. K. *Blood* **2013**, *121*, 893–897.

(61) Zhou, H.-J.; Aujay, M.; Bennett, M.; Dajee, M.; Demo, S.; Fang, Y.; Ho, M.; Jiang, J.; Kirk, C.; Laidig, G.; Lewis, E. *J. Med. Chem.* **2009**, *52*, 3028–3038.

(62) Hochstrasser, M. *Nat. Cell Biol.* **2000**, *2*, 153–157.

(63) Da Silva, S. R.; Paiva, S. L.; Lukkarila, J. L.; Gunning, P. T. *J. Med. Chem.* **2013**, *56*, 2165–2177.

(64) Saha, A.; Deshaies, R. J. *Mol. Cell* **2008**, *32*, 21–31.

(65) Soucy, T. A.; Smith, P. G.; Milhollen, M. A.; Berger, A. J.; Gavin, J. M.; Adhikari, S.; Brownell, J. E.; Burke, K. E.; Cardin, D. P.; Critchley, S.; Cullis, C. A.; Doucette, A.; Garnsey, J. J.; Gaulin, J. L.; Gershman, R. E.; Lublinsky, A. R.; McDonald, A.; Mizutani, H.; Narayanan, U.; Olhava, E. J.; Peluso, S.; Rezaei, M.; Sintchak, M. D.; Talreja, T.; Thomas, M. P.; Traore, T.; Vyskocil, S.; Weatherhead, G. S.; Yu, J.; Zhang, J.; Dick, L. R.; Claiborne, C. F.; Rolfe, M.; Bolen, J. B.; Langston, S. P. *Nature* **2009**, *458*, 732–736.

(66) Swords, R. T.; Erba, H. P.; Deangelo, D. J.; Bixby, D. L.; Altman, J. K.; Maris, M.; Hua, Z.; Blakemore, S. J.; Faessel, H.; Sedarati, F.; Dezube, B. J.; Giles, F. J.; Medeiros, B. C. *Br. J. Haematol.* **2015**, *169*, 534–543.

(67) Ceccarelli, D. F.; Tang, X.; Pelletier, B.; Orlicky, S.; Xie, W.; Plantevin, V.; Neculai, D.; Chou, Y. C.; Ogunjimi, A.; Al-Hakim, A.; Varelas, X.; Koszela, J.; Wasney, G. A.; Vedadi, M.; Dhe-Paganon, S.; Cox, S.; Xu, S.; Lopez-Girona, A.; Mercurio, F.; Wrana, J.; Durocher, D.; Meloche, S.; Webb, D. R.; Tyers, M.; Sicheri, F. *Cell* **2011**, *145*, 1075–1087.

(68) Huang, H.; Ceccarelli, D. F.; Orlicky, S.; St-Cyr, D. J.; Ziemba, A.; Garg, P.; Plamondon, S.; Auer, M.; Sidhu, S.; Marinier, A.; Kleiger, G.; Tyers, M.; Sicheri, F. *Nat. Chem. Biol.* **2014**, *10*, 156–163.

(69) Tobergte, D. R.; Curtis, S. *J. Chem. Inf. Model.* **2013**, *53*, 1689–1699.

(70) Landré, V.; Rotblat, B.; Melino, S.; Bernassola, F.; Melino, G. *Oncotarget* **2014**, *5*, 7988–8013.

(71) Kaelin Jr, W. G. *Nat. Rev. Cancer* **2008**, *8*, 865–873.

(72) Semenza, G. L. *Trends Mol. Med.* **2001**, *7*, 345–350.

(73) Hon, W.-C.; Wilson, M. I.; Harlos, K.; Claridge, T. D. W.; Schofield, C. J.; Pugh, C. W.; Maxwell, P. H.; Ratcliffe, P. J.; Stuart, D. I.; Jones, E. Y. *Nature* **2002**, *417*, 975–978.

(74) Muchnik, E.; Kaplan, J. *Expert Opin. Investig. Drugs* **2011**, *20*, 645–656.

(75) Buckley, D. L.; Gustafson, J. L.; Van-Molle, I.; Roth, A. G.; Tae, H. S.; Gareiss, P. C.; Jorgensen, W. L.; Ciulli, A.; Crews, C. M. *Angew. Chem. Int. Ed.* **2012**, *51*, 11463–11467.

(76) Van Molle, I.; Thomann, A.; Buckley, D. L.; So, E. C.; Lang, S.; Crews, C. M.; Ciulli, A. *Chem. Biol.* **2012**, *19*, 1300–1312.

(77) Buckley, D. L.; Van Molle, I.; Gareiss, P. C.; Tae, H. S.; Michel, J.; Noblin, D. J.; Jorgensen, W. L.; Ciulli, A.; Crews, C. M. *J. Am. Chem. Soc.* **2012**, *134*, 4465–4468.

(78) Crews, C. M.; Buckley, D.; Ciulli, A.; Jorgensen, W.; Gareiss, P. C.; Van Molle, I.; Gustafson, J.; Tae, H.-S.; Michel, J.; Hoyer, D. W.; Roth, A. G.; Harling, J. D.; Smith, I. E. D.; Miah, A. H.; Campos, S. A.; Le, J. Compounds & Methods for the Enhanced Degradation of Targeted Proteins & Other Polypeptides By an E3 Ubiquitin Ligase. WO2013/106643A2, 2013.

(79) Galdeano, C.; Gadd, M. S.; Soares, P.; Scaffidi, S.; Van Molle, I.; Birced, I.; Hewitt, S.; Dias, D. M.; Ciulli, A. *J. Med. Chem.* **2014**, *57*, 8657–8663.

(80) Van Molle, I.; Ciulli, A. University of Cambridge, Unpublished results.

(81) Miller, M. T.; Strömland, K. *Teratology* **1999**, *60*, 306–321.

(82) Melchert, M.; List, A. *Int. J. Biochem. Cell Biol.* **2007**, *39*, 1489–1499.

(83) Knobloch, J.; Rüther, U. *Cell Cycle* **2008**, *7*, 1121–1127.

(84) Ito, T.; Ando, H.; Suzuki, T.; Ogura, T.; Hotta, K.; Imamura, Y.; Yamaguchi, Y.; Handa, H. *Science* **2010**, *327*, 1345–1350.

(85) Gandhi, A. K.; Kang, J.; Havens, C. G.; Conklin, T.; Ning, Y.; Wu, L.; Ito, T.; Ando, H.; Waldman, M. F.; Thakurta, A.; Klippel, A.; Handa, H.; Daniel, T. O.; Schafer, P. H.; Chopra, R. *Br. J. Haematol.* **2014**, *164*, 811–821.

(86) Krönke, J.; Udeshi, N. D.; Narla, A.; Grauman, P.; Hurst, S. N.; McConkey, M.; Svinkina, T.; Heckl, D.; Comer, E.; Li, X.; Ciarlo, C.; Hartman, E.; Munshi, N.; Schenone, M.; Schreiber, S. L.; Carr, S. A.; Ebert, B. L. *Science* **2014**, *1*, 301–306.

(87) Lu, G.; Middleton, R. E.; Sun, H.; Naniong, M.; Ott, C. J.; Mitsiades, C. S.; Wong, K.-K.; Bradner, J. E.; Kaelin, W. G. *Science* **2014**, *343*, 305–309.

(88) Corral, L. G.; Haslett, P. A.; Muller, G. W.; Chen, R.; Wong, L. M.; Ocampo, C. J.; Patterson, R. T.; Stirling, D. I.; Kaplan, G. *J. Immunol.* **1999**, *163*, 380–386.

(89) Fischer, E. S.; Böhm, K.; Lydeard, J. R.; Yang, H.; Stadler, M. B.; Cavadini, S.; Nagel, J.; Serluca, F.; Acker, V.; Lingaraju, G. M.; Tichkule, R. B.; Schebesta, M.; Forrester, W. C.; Schirle, M.; Hassiepen, U.; Ottl, J.; Hild, M.; Beckwith, R. E. J.; Harper, J. W.; Jenkins, J. L.; Thomä, N. H. *Nature* **2014**, *512*, 49–53.

(90) Huang, X.; Dixit, V. M. *Cell Res.* **2016**, *26*, 484–498.

(91) Krönke, J.; Fink, E. C.; Hollenbach, P. W.; MacBeth, K. J.; Hurst, S. N.; Udeshi, N. D.; Chamberlain, P. P.; Mani, D. R.; Man, H. W.; Gandhi, A. K.; Svinkina, T.; Schneider, R. K.; McConkey, M.; Järås, M.; Griffiths, E.; Wetzler, M.; Bullinger, L.; Cathers, B. E.; Carr, S. A.; Chopra, R.; Ebert, B. L. *Nature* **2015**, *523*, 183–188.

(92) Matyskiela, M. E.; Lu, G.; Ito, T.; Pagarigan, B.; Lu, C.; Miller, K.; Fang, W.; Wang, N.; Nguyen, D.; Houston, J.; Carmel, G.; Tran, T.; Riley, M.; Nosaka, L. Al; Lander, G. C.; Gaidarova, S.; Xu, S.; Ruchelman, A. L.; Handa, H.; Carmichael, J.; Daniel, T. O. *Nature* **2016**, *535*, 252–257.

(93) Salvesen, G. S.; Duckett, C. S. *Nat. Rev. Mol. Cell Biol.* **2002**, *3*, 401–410.

(94) Gyrd-Hansen, M.; Meier, P. *Nat. Rev. Cancer* **2010**, *10*, 561–574.

(95) Vaux, D. L.; Silke, J. *Nat. Rev. Mol. Cell Biol.* **2005**, *6*, 287–297.

(96) Varfolomeev, E.; Vucic, D. *Cell Cycle* **2008**, *7*, 1511–1521.

(97) Shiozaki, E. N.; Chai, J.; Rigotti, D. J.; Riedl, S. J.; Li, P.; Srinivasula, S. M.;

Alnemri, E. S.; Fairman, R.; Shi, Y. *Mol. Cell* **2003**, *11*, 519–527.

(98) Scott, F. L.; Denault, J.; Riedl, S. J.; Shin, H.; Renatus, M.; Salvesen, G. S. *EMBO J.* **2005**, *24*, 645 LP-655.

(99) Wang, C.-Y.; Mayo, M. W.; Korneluk, R. G.; Goeddel, D. V; Baldwin, A. S. *Science* **1998**, *281*, 1680–1683.

(100) Du, C.; Fang, M.; Li, Y.; Li, L.; Wang, X. *Cell* **2000**, *102*, 33–42.

(101) Verhagen, A. M.; Ekert, P. G.; Pakusch, M.; Silke, J.; Connolly, L. M.; Reid, G. E.; Moritz, R. L.; Simpson, R. J.; Vaux, D. L. *Cell* **2000**, *102*, 43–53.

(102) Wu, G.; Chai, J.; Suber, T. L.; Wu, J.-W.; Du, C.; Wang, X.; Shi, Y. *Nature* **2000**, *408*, 1008–1012.

(103) Gao, Z.; Tian, Y.; Wang, J.; Yin, Q.; Wu, H.; Li, Y.-M.; Jiang, X. *J. Biol. Chem.* **2007**, *282*, 30718–30727.

(104) Temesgen, S.; Welsh, K.; Lober, T.; Togo, S. H.; Zapata, J. M.; Reed, J. C. *J. Biol. Chem.* **2006**, *281*, 1080–1090.

(105) Buetow, L.; Huang, D. T. *Nat. Rev. Mol. Cell Biol.* **2016**, *17*, 626–642.

(106) Tamm, I.; Kornblau, S. M.; Segall, H.; Krajewski, S.; Welsh, K.; Kitada, S.; Scudiero, D. A.; Tudor, G.; Qui, Y. H.; Monks, A.; Andreeff, M.; Reed, J. C. *Clin. Cancer Res.* **2000**, *6*, 1796–1803.

(107) Fulda, S.; Vucic, D. *Nat. Rev. Drug Discov.* **2012**, *11*, 109–124.

(108) Bai, L.; Smith, D. C.; Wang, S. *Pharmacol. Ther.* **2014**, *144*, 82–95.

(109) Varfolomeev, E.; Blankenship, J. W.; Wayson, S. M.; Fedorova, A. V; Kayagaki, N.; Garg, P.; Zobel, K.; Dynek, J. N.; Elliott, L. O.; Wallweber, H. J. A.; Flygare, J. A.; Fairbrother, W. J.; Deshayes, K.; Dixit, V. M.; Vucic, D. *Cell* **2007**, *131*, 669–681.

(110) Varfolomeev, E.; Alicke, B.; Elliott, J. M.; Zobel, K.; West, K.; Wong, H.; Scheer, J. M.; Ashkenazi, A.; Gould, S. E.; Fairbrother, W. J.; Vucic, D. *J. Biol. Chem.* **2009**, *284*, 34553–34560.

(111) Corson, T. W.; Aberle, N.; Crews, C. M. *ACS Chem. Biol.* **2008**, *3*, 677–692.

(112) Sakamoto, K. M.; Kim, K. B.; Kumagai, A.; Mercurio, F.; Crews, C. M.; Deshaies, R. J. *Proc. Natl. Acad. Sci. U. S. A.* **2001**, *98*, 8554–8559.

(113) Raina, K.; Crews, C. M. *J. Biol. Chem.* **2010**, *285*, 11057–11060.

(114) Schneekloth Jr., J. S.; Crews, C. M. *ChemBioChem* **2005**, *6*, 40–46.

(115) Tinworth, C.; Lithgow, H.; Churcher, I. *Med. Chem. Commun.* **2016**.

(116) Douglass, E. F.; Miller, C. J.; Sparer, G.; Shapiro, H.; Spiegel, D. A. *J. Am. Chem. Soc.* **2013**, *135*, 6092–6099.

(117) Sakamoto, K. M.; Kim, K. B.; Verma, R.; Ransick, A.; Stein, B.; Crews, C. M.; Deshaies, R. J. *Mol. Cell. Proteomics* **2003**, *2*, 1350–1358.

(118) Bargagna-Mohan, P.; Baek, S. H.; Lee, H.; Kim, K.; Mohan, R. *Bioorg. Med. Chem. Lett.* **2005**, *15*, 2724–2727.

(119) Schneekloth Jr., J. S.; Fonseca, F. N.; Koldobskiy, M.; Mandal, A.; Deshaies, R.; Sakamoto, K.; Crews, C. M. *J. Am. Chem. Soc.* **2004**, *126*, 3748–3754.

(120) Cyrus, K.; Wehenkel, M.; Choi, E. Y.; Han, H. J.; Lee, H.; Swanson, H.; Kim, K. B. *Mol Biosyst* **2011**, *7*, 359–364.

(121) Lee, H.; Puppala, D.; Choi, E. Y.; Swanson, H.; Kim, K. B. *ChemBioChem* **2007**, *8*, 2058–2062.

(122) Puppala, D.; Lee, H.; Kim, K. B.; Swanson, H. I. *Mol. Pharmacol.* **2008**, *73*, 1064–1071.

(123) Lipinski, C. A.; Lombardo, F.; Dominy, B. W.; Feeney, P. J. *Adv. Drug Deliv. Rev.* **1997**, *23*, 3–25.

(124) Bondeson, D. P.; Mares, A.; Smith, I. E. D.; Ko, E.; Campos, S.; Miah, A. H.; Mulholland, K. E.; Routly, N.; Buckley, D. L.; Gustafson, J. L.; Zinn, N.; Grandi, P.; Shimamura, S.; Bergamini, G.; Faelth-Savitski, M.; Bantscheff, M.; Cox, C.; Gordon, D. A.; Willard, R. R.; Flanagan, J. J.; Casillas, L. N.; Votta, B. J.; den Besten, W.; Famm, K.; Kruidenier, L.; Carter, P. S.; Harling, J. D.; Churcher, I.; Crews, C. M. *Nat. Chem. Biol.* **2015**, *11*, 611–617.

(125) Protein Degradation DPU, GlaxoSmithKline.

(126) Zengerle, M.; Chan, K.-H.; Ciulli, A. *ACS Chem. Biol.* **2015**, *10*, 1770–1777.

(127) Hughes, S.; Bassi, I. Z. GlaxoSmithKline, Unpublished results.

(128) Raina, K.; Lu, J.; Qian, Y.; Altieri, M.; Gordon, D.; Rossi, A. M. K.; Wang, J.; Chen, X.; Dong, H.; Siu, K.; Winkler, J. D.; Crew, A. P.; Crews, C. M.; Coleman, K. G. *Proc. Natl. Acad. Sci. U. S. A.* **2016**, *113*, 7124–7129.

(129) Lai, A. C.; Toure, M.; Hellerschmied, D.; Salami, J.; Jaime-Figueroa, S.; Ko, E.; Hines, J.; Crews, C. M. *Angew. Chem. Int. Ed.* **2016**, *55*, 807–810.

(130) Winter, G. E.; Buckley, D. L.; Paulk, J.; Roberts, J. M.; Souza, A.; Dhe-Paganon, S.; Bradner, J. E. *Science* **2015**, *348*, 1376–1381.

(131) Lu, J.; Qian, Y.; Altieri, M.; Dong, H.; Wang, J.; Raina, K.; Hines, J.; Winkler, J. D.; Crew, A. P.; Coleman, K.; Crews, C. M. *Chem. Biol.* **2015**, *22*, 755–763.

(132) Reist, M.; Carrupt, P.-A.; Francotte, E.; Testa, B. *Chem. Res. Toxicol.* **1998**, *11*, 1521–1528.

(133) Jacques, V.; Czarnik, A. W.; Judge, T. M.; Ploeg, L. H. T. Van Der; Dewitt, S. H.; Jacques, V.; Czarnik, A. W.; Judge, T. M.; Ploeg, L. H. T. Van Der; Dewitt, S. H. *Proc. Natl. Acad. Sci.* **2015**, *112*, 1471–1479.

(134) Hoffmann, M.; Kasserra, C.; Reyes, J.; Schafer, P.; Kosek, J.; Capone, L.; Parton, A.; Kim-Kang, H.; Surapaneni, S.; Kumar, G. *Cancer Chemother. Pharmacol.* **2013**, *71*, 489–501.

(135) Doak, B. C.; Over, B.; Giordanetto, F.; Kihlberg, J. *Chem. Biol.* **2014**, *21*, 1115–1142.

(136) Sekine, K.; Takubo, K.; Kikuchi, R.; Nishimoto, M.; Kitagawa, M.; Abe, F.; Nishikawa, K.; Tsuruo, T.; Naito, M. *J. Biol. Chem.* **2008**, *283*, 8961–8968.

(137) Mathé, G. *Biomed. Pharmacother.* **1991**, *45*, 49–54.

(138) Okuhira, K.; Ohoka, N.; Sai, K.; Nishimaki-Mogami, T.; Itoh, Y.; Ishikawa, M.; Hashimoto, Y.; Naito, M. *FEBS Lett.* **2011**, *585*, 1147–1152.

(139) Itoh, Y.; Ishikawa, M.; Kitaguchi, R.; Sato, S.; Naito, M.; Hashimoto, Y. *Bioorg. Med. Chem.* **2011**, *19*, 3229–3241.

(140) Itoh, Y.; Kitaguchi, R.; Ishikawa, M.; Naito, M.; Hashimoto, Y. *Bioorg. Med. Chem.* **2011**, *19*, 6768–6778.

(141) Demizu, Y.; Okuhira, K.; Motoi, H.; Ohno, A.; Shoda, T.; Fukuhara, K.; Okuda, H.; Naito, M.; Kurihara, M. *Bioorg. Med. Chem. Lett.* **2012**, *22*, 1793–1796.

(142) Okuhira, K.; Demizu, Y.; Hattori, T.; Ohoka, N.; Shibata, N.; Nishimaki-Mogami, T.; Okuda, H.; Kurihara, M.; Naito, M. *Cancer Sci.* **2013**, *104*, 1492–1498.

(143) Wade, M.; Li, Y.-C.; Wahl, G. M. *Nat. Rev. Cancer* **2013**, *13*, 83–96.

(144) Vousden, K. H.; Lu, X. *Nat. Rev. Cancer* **2002**, *2*, 594–604.

(145) Stiewe, T. *Nat. Rev. Cancer* **2007**, *7*, 165–167.

(146) Toledo, F.; Wahl, G. M. *Nat. Rev. Cancer* **2006**, *6*, 909–923.

(147) Brown, C. J.; Lain, S.; Verma, C. S.; Fersht, A. R.; Lane, D. P. *Nat. Rev. Cancer* **2009**, *9*, 862–873.

(148) Haupt, Y.; Maya, R.; Kazaz, A.; Oren, M. *Nature* **1997**, *387*, 296–299.

(149) Kubbutat, M. H.; Vousden, K. H. *Mol. Cell. Biol.* **1997**, *17*, 460–468.

(150) Vassilev, L. T. *Trends Mol. Med.* **2007**, *13*, 23–31.

(151) Vassilev, L. T.; Vu, B. T.; Craves, B.; Carvajal, D.; Podlaski, F.; Filipovic, Z.; Kong, N.; Kammlott, U.; Lukacs, C.; Klein, C.; Fotouhi, N.; Liu, E. A. *Science* **2004**, *303*, 844–848.

(152) Schneekloth, A. R.; Pucheault, M.; Tae, H. S.; Crews, C. M. *Bioorg. Med. Chem. Lett.* **2008**, *18*, 5904–5908.

(153) Zhao, Y.; Aguilar, A.; Bernard, D.; Wang, S. *J. Med. Chem.* **2015**, *58*, 1038–1052.

(154) Los, G. V.; Encell, L. P.; McDougall, M. G.; Hartzell, D. D.; Karassina, N.; Zimprich, C.; Wood, M. G.; Learish, R.; Friedman Ohana, R.; Urh, M.; Simpson, D.; Mendez, J.; Zimmerman, K.; Otto, P.; Vidugiris, G.; Zhu, J.; Darzins, A.; Klaubert, D. H.; Bulleit, R. F.; Wood, K. V. *ACS Chem. Biol.* **2008**, *3*, 373–382.

(155) Buckley, D. L.; Raina, K.; Darricarrere, N.; Hines, J.; Gustafson, J. L.; Smith, I. E.; Miah, A. H.; Harling, J. D.; Crews, C. M. *ACS Chem. Biol.* **2015**, *10*, 1831–1837.

(156) Tae, H. S.; Sundberg, T. B.; Neklesa, T. K.; Noblin, D. J.; Gustafson, J. L.; Roth, A. G.; Raina, K.; Crews, C. M. *ChemBioChem* **2012**, *13*, 538–541.

(157) Tomoshige, S.; Hashimoto, Y.; Ishikawa, M. *Bioorg. Med. Chem.* **2016**, *24*, 3144–3148.

(158) Wakeling, A. E.; Dukes, M.; Bowler, J. *Am. Assoc. Cancer Res.* **1991**, *5*, 3867–3873.

(159) Wittmann, B. M.; Sherk, A.; McDonnell, D. P. *Cancer Res.* **2007**, *67*, 9549–9560.

(160) van Kruchten, M.; de Vries, E. G.; Glaudemans, A. W.; van Lanschot, M. C.; van Faassen, M.; Kema, I. P.; Brown, M.; Schröder, C. P.; de Vries, E. F.; Hospers, G. A. *Cancer Discov.* **2015**, *5*, 72–81.

(161) Lai, A.; Kahraman, M.; Govek, S.; Nagasawa, J.; Bonnefous, C.; Julien, J.; Douglas, K.; Sensintaffar, J.; Lu, N.; Lee, K. J.; Aparicio, A.; Kaufman, J.; Qian, J.; Shao, G.; Prudente, R.; Moon, M. J.; Joseph, J. D.; Darimont, B.; Brigham, D.; Grillot, K.; Heyman, R.; Rix, P. J.; Hager, J. H.; Smith, N. D. *J. Med. Chem.* **2015**, *58*, 4888–4904.

(162) Citri, A.; Alroy, I.; Lavi, S.; Rubin, C.; Xu, W.; Grammatikakis, N.; Patterson, C.; Neckers, L.; Fry, D. W.; Yarden, Y. *EMBO J.* **2002**, *21*, 2407–2417.

(163) Peltonen, K.; Colis, L.; Liu, H.; Trivedi, R.; Moubarek, M.; Moore, H.; Bai, B.; Rudek, M.; Bieberich, C.; Laiho, M. *Cancer Cell* **2014**, *25*, 77–90.

(164) Bill, A.; Hall, M. L.; Borawski, J.; Hodgson, C.; Jenkins, J.; Piechon, P.; Popa, O.; Rothwell, C.; Tranter, P.; Tria, S.; Wagner, T.; Whitehead, L.; Gaither, L. A. *J. Biol. Chem.* **2014**, *289*, 11029–11041.

(165) Neklesa, T. K.; Tae, H. S.; Schneekloth, A. R.; Stulberg, M. J.; Corson, T. W.; Sundberg, T. B.; Raina, K.; Holley, S. A.; Crews, C. M. *Nat. Chem. Biol.* **2011**, *7*, 538–543.

(166) Xie, T.; Lim, S. M.; Westover, K. D.; Dodge, M. E.; Ercan, D.; Ficarro, S. B.; Udayakumar, D.; Gurbani, D.; Tae, H. S.; Riddle, S. M.; Sim, T.; Marto, J. A.; Jänne, P. A.; Crews, C. M.; Gray, N. S. *Nat. Chem. Biol.* **2014**, *10*, 1006–1012.

(167) Wegele, H.; Müller, L.; Buchner, J. In *Reviews of Physiology, Biochemistry and Pharmacology*; Springer: Berlin, Heidelberg, 2004; Vol. 151, pp 1–44.

(168) Gustafson, J. L.; Neklesa, T. K.; Cox, C. S.; Roth, A. G.; Buckley, D. L.; Tae, H. S.; Sundberg, T. B.; Stagg, D. B.; Hines, J.; McDonnell, D. P.; Norris, J. D.; Crews, C. M. *Angew. Chem. Int. Ed.* **2015**, *54*, 9659–9662.

(169) Long, M. J. C.; Gollapalli, D. R.; Hedstrom, L. *Chem. Biol.* **2012**, *19*, 629–637.

(170) Shi, Y.; Long, M. J. C.; Rosenberg, M. M.; Li, S.; Kobjack, A.; Lessans, P.; Coffey, R. T.; Hedstrom, L. *ACS Chem. Biol.* **2016**, *11*, 3328–3337.

(171) Lee, S. J.; McPherron, A. C. *Proc. Natl. Acad. Sci. U. S. A.* **2001**, *98*, 9306–9311.

(172) McPherron, A. C.; Lawler, A. M.; Lee, S.-J. *Nature* **1997**, *387*, 83–90.

(173) Welle, S.; Bhatt, K.; Pinkert, C. A.; Tawil, R.; Thornton, C. A. *Am. J. Physiol.*

Endocrinol. Metab. **2007**, *292*, 985–991.

(174) Zimmers, T. A.; Davies, M. V; Koniaris, L. G.; Haynes, P.; Esquela, A. F.; Tomkinson, K. N.; McPherron, A. C.; Wolfman, N. M.; Lee, S.-J. *Science* **2002**, *296*, 1486–1488.

(175) Durieux, A. C.; Amirouche, A.; Banzet, S.; Koulmann, N.; Bonnefoy, R.; Pasdeloup, M.; Mouret, C.; Bigard, X.; Peinnequin, A.; Freyssenet, D. *Endocrinology* **2007**, *148*, 3140–3147.

(176) Carnac, G.; Vernus, B.; Bonnieu, A. *Curr. Genomics* **2007**, *8*, 415–422.

(177) De Caestecker, M. *Cytokine Growth Factor Rev.* **2004**, *15*, 1–11.

(178) Joulia-Ekaza, D.; Cabello, G. *Curr. Opin. Pharmacol.* **2007**, *7*, 310–315.

(179) Rebbapragada, A.; Benchabane, H.; Wrana, J. L.; Celeste, A. J.; Attisano, L. *Mol. Cell. Biol.* **2003**, *23*, 7230–7242.

(180) Attisano, L.; Wrana, J. L.; Montalvo, E.; Massagué, J. *Mol. Cell. Biol.* **1996**, *16*, 1066–1073.

(181) Willis, S. A.; Zimmerman, C. M.; Li, L. I.; Mathews, L. S. *Mol. Endocrinol.* **1996**, *10*, 367–379.

(182) Ohsawa, Y.; Okada, T.; Nishimatsu, S.; Ishizaki, M.; Suga, T.; Fujino, M.; Murakami, T.; Uchino, M.; Tsuchida, K.; Noji, S.; Hinohara, A.; Shimizu, T.; Shimizu, K.; Sunada, Y. *Lab. Invest.* **2012**, *92*, 1100–1114.

(183) Anderton, M. J.; Mellor, H. R.; Bell, A.; Sadler, C.; Pass, M.; Powell, S.; Steele, S. J.; Roberts, R. R. A.; Heier, A. *Toxicol. Pathol.* **2011**, *39*, 916–924.

(184) Smith, G. K.; Turnbull, P. S.; Rheault, T. R.; Stanley, T. B.; Barrett, G.; Billin, A. N.; Carter, L.; Christie, J.; Creech, K. L.; Ellis, B.; Gampe, R. T.; Gurley, S. A.; Hightower, K. E.; Jensen, T. C.; Kadwell, S.; Merrihew, R. V; Orband-Miller, L. A.; Nartey, E.; Price, D. J.; Schaller, L. T.; Shen, Y.; Smith, D. M.; Taylor, D.; Waitt, G. M.; Wang, L.; Wang, R. H. GlaxoSmithKline, Unpublished results.

(185) Castanet, A. S.; Colobert, F.; Broutin, P. E. *Tetrahedron Lett.* **2002**, *43*, 5047–5048.

(186) Miyaura, N.; Suzuki, A. *Chem. Rev.* **1995**, *95*, 2457–2483.

(187) Stille, J. K.; Lau, K. S. *Acc. Chem. Res.* **1977**, *10*, 434–442.

(188) Ishiyama, T.; Nobuta, Y.; Hartwig, J. F.; Miyaura, N. *Chem. Commun.* **2003**, 2924–2925.

(189) Campos, S.; Miah, A. H.; Smith, I. E. D.; Harling, J. D. GlaxoSmithKline, Unpublished results.

(190) Carpino, L. A. *J. Am. Chem. Soc.* **1993**, *115*, 4397–4398.

(191) Towbin, H.; Staehelin, T.; Gordon, J. *Proc. Natl. Acad. Sci. U. S. A.* **1979**, *76*, 4350–4354.

(192) Rybicki, E. P.; von Wechmar, M. B. *J. Virol. Methods* **1982**, *5*, 267–278.

(193) Dennis-Sykes, C. A.; Miller, W. J.; McAleer, W. J. *J. Biol. Stand.* **1985**, *13*, 309–314.

(194) Mares, A.; Mulholland, K.; Liang, H. GlaxoSmithKline performed western blotting.

(195) Carlomagno, F.; Vitagliano, D.; Guida, T.; Ciardiello, F.; Tortora, G.; Vecchio, G.; Ryan, A. J.; Fontanini, G.; Fusco, A.; Santoro, M. *Cancer Res.* **2002**, *62*, 7284–7290.

(196) McCarthy, J. V.; Ni, J.; Dixit, V. M. *J. Biol. Chem.* **1998**, *273*, 16968–16975.

(197) Holmes, K.; Roberts, O. L.; Thomas, A. M.; Cross, M. J. *Cell. Signal.* **2007**, *19*, 2003–2012.

(198) MacGurn, J. A.; Hsu, P.-C.; Emr, S. D. *Annu. Rev. Biochem.* **2012**, *81*, 231–259.

(199) Evans, R. M. *Science* **1988**, *240*, 889–895.

(200) Mangelsdorf, D. J.; Thummel, C.; Beato, M.; Herrlich, P.; Schütz, G.; Umesono, K.; Blumberg, B.; Kastner, P.; Mark, M.; Chambon, P.; Evans, R. M. *Cell* **1995**, *83*, 835–839.

(201) Ribeiro, R. C.; Kushner, P. J.; Baxter, J. D. *Annu. Rev. Med.* **1995**, *46*, 443–453.

(202) Lazar, M. A. *Endocr. Rev.* **1993**, *14*, 184–193.

(203) Koenig, R. J.; Warne, R. L.; Brent, G. A.; Harney, J. W.; Larsen, P. R.; Moore, D. D. *Proc. Natl. Acad. Sci. U. S. A.* **1988**, *85*, 5031–5035.

(204) Hodin, R. A.; Lazar, M. A.; Chin, W. W. *J. Clin. Invest.* **1990**, *85*, 101–105.

(205) Hodin, R. A.; Lazar, M. A.; Wintman, B. I.; Darling, D. S.; Koenig, R. J.; Larsen, P. R.; Moore, D. D.; Chin, W. W. *Science* **1989**, *244*, 76–79.

(206) Mitsuhashi, T.; Tennyson, G. E.; Nikodem, V. M. *Proc. Natl. Acad. Sci. U. S. A.* **1988**, *85*, 5804–5808.

(207) Malm, J.; Färnegårdh, M.; Grover, G. J.; Ladenson, P. W. *Curr. Med. Chem.* **2009**, *16*, 3258–3266.

(208) Steinmetz, A. C. U.; Renaud, J.; Moras, D. *Annu. Rev. Biochem.* **1999**, *68*, 559–581.

(209) Bourguet, W.; Germain, P.; Gronemeyer, H. *Trends Pharmacol. Sci.* **2000**, *21*, 381–388.

(210) Glass, C. K.; Rosenfeld, M. G. *Genes Dev.* **2000**, *14*, 121–141.

(211) Yen, P. M. *Physiol. Rev.* **2001**, *81*, 1097–1142.

(212) Feng, W.; Ribeiro, R. C.; Wagner, R. L.; Nguyen, H.; Apriletti, J. W.; Fletterick, R. J.; Baxter, J. D.; Kushner, P. J.; West, B. L. *Science* **1998**, *280*, 1747–1749.

(213) Webb, P.; Nguyen, N.-H.; Chiellini, G.; Yoshihara, H. A. I.; Cunha Lima, S. T.; Apriletti, J. W.; Ribeiro, R. C. J.; Marimuthu, A.; West, B. L.; Goede, P.;

Mellstrom, K.; Nilsson, S.; Kushner, P. J.; Fletterick, R. J.; Scanlan, T. S.; Baxter, J. D. *J. Steroid Biochem. Mol. Biol.* **2002**, *83*, 59–73.

(214) Jorgensen, E. C. In *Hormonal Peptides and Proteins, vol. VI*; Li, C. H., Ed.; Academic Press: New York, 1978; pp 107–204.

(215) Chiellini, G.; Apriletti, J. W.; Yoshihara, H. A.; Baxter, J. D.; Ribeiro, R. C.; Scanlan, T. S. *Chem. Biol.* **1998**, *5*, 299–306.

(216) Malm, J.; Grover, G. J.; Färnegårdh, M. *Mini Rev. Med. Chem.* **2007**, *7*, 79–86.

(217) Nguyen, N.-H.; Apriletti, J. W.; Cunha Lima, S. T.; Webb, P.; Baxter, J. D.; Scanlan, T. S. *J. Med. Chem.* **2002**, *45*, 3310–3320.

(218) Yoshihara, H. A.; Apriletti, J. W.; Baxter, J. D.; Scanlan, T. S. *Bioorg. Med. Chem. Lett.* **2001**, *11*, 2821–2825.

(219) Koehler, K.; Gordon, S.; Brandt, P.; Carlsson, B.; Bäcksbro-Saeidi, A.; Apelqvist, T.; Agback, P.; Grover, G. J.; Nelson, W.; Grynfarb, M.; Färnegårdh, M.; Rehnmark, S.; Malm, J. *J. Med. Chem.* **2006**, *49*, 6635–6637.

(220) Lim, W.; Nguyen, N.-H.; Yang, H. Y.; Scanlan, T. S.; Furlow, J. D. *J. Biol. Chem.* **2002**, *277*, 35664–35670.

(221) Grover, G.; Dunn, C.; Nguyen, N. *J. Pharmacol. Exp. Ther.* **2007**, *322*, 385–390.

(222) Meanwell, N. A. *Chem. Res. Toxicol.* **2011**, *24*, 1420–1456.

(223) Chiellini, G.; Nguyen, N. H.; Apriletti, J. W.; Baxter, J. D.; Scanlan, T. S. *Bioorg. Med. Chem.* **2002**, *10*, 333–346.

(224) Bowler, J.; Lilley, T. J.; Pittam, J. D.; Wakeling, A. E. *Steroids* **1989**, *54*, 71–99.

(225) Wakeling, A. E.; Bowler, J. *J. Endocrinol.* **1987**, *112*, R7–R10.

(226) Mandel, S. J.; Brent, G. A.; Larsen, P. R. *Ann. Intern. Med.* **1993**, *119*, 492–502.

(227) Utiger, R. D. In *Endocrinology and Metabolism*; McGraw-Hill, Ed.; New York, 1995; pp 435–519.

(228) Weetman, A. P. *N. Engl. J. Med.* **2000**, *343*, 1236–1248.

(229) Lubin, E.; Cooper, D. S. *N. Engl. J. Med.* **2005**, *352*, 905–917.

(230) Ruf, J.; Carayon, P. *Arch. Biochem. Biophys.* **2006**, *445*, 269–277.

(231) Kota, S. K.; Meher, L. K.; Kota, S. K.; Jammula, S.; Modi, K. D. *Indian J. Endocrinol. Metab.* **2013**, *17*, 326–328.

(232) Blomfield, G. W.; Jones, J. C.; Macgregor, A. G.; Miller, H.; Wayne, E. J.; Weetch, R. S. *Br. Med. J.* **1955**, *2*, 1223–1229.

(233) Kocher, A. *Proc. R. Soc. Med.* **1912**, *5*, 89–96.

(234) Phenex Pharmaceuticals AG.

(235) Chiellini, G.; Nguyen, N. H.; Yoshihara, H. A. I.; Scanlan, T. S. *Bioorg. Med. Chem. Lett.* **2000**, *10*, 2607–2611.

(236) Siemsen, P.; Livingston, R. C.; Diederich, F. *Angew. Chem. Int. Ed.* **2000**, *39*, 2632–2657.

(237) Liang, B.; Dai, M.; Chen, J.; Yang, Z. *J. Org. Chem.* **2005**, *70*, 391–393.

(238) Panda, B.; Sarkar, T. *Synthesis* **2013**, *45*, 817–829.

(239) Bleicher, L.; Aparicio, R.; Nunes, F. M.; Martinez, L.; Gomes Dias, S. M.; Figueira, A. C. M.; Santos, M. A. M.; Venturelli, W. H.; da Silva, R.; Donate, P. M.; Neves, F. A.; Simeoni, L. A.; Baxter, J. D.; Webb, P.; Skaf, M. S.; Polikarpov, I. *BMC Struct. Biol.* **2008**, *8*, 8.

(240) Synthesised by Manchester Organics.

(241) Baumann, C. T.; Maruvada, P.; Hager, G. L.; Yen, P. M. *J. Biol. Chem.* **2001**, *276*, 11237–11245.

(242) Lee, J. S.; Yoo, Y. H.; Yoon, C. N. *BMB Rep.* **2014**, *47*, 149–157.

(243) Uitdehaag, J. C. M.; Verkaar, F.; Alwan, H.; De Man, J.; Buijsman, R. C.; Zaman, G. J. R. *Br. J. Pharmacol.* **2012**, *166*, 858–876.

(244) Manning, G.; Whyte, D. B.; Martinez, R.; Hunter, T.; Sudarsanam, S.; Hunter, T.; Lander, E. S.; Rubin, G. M.; Manning, G.; Plowman, G.; Hunter, T.; Sudarsanam, S.; Venter, J. C.; Hunter, T.; Plowman, G. D.; Blume-Jensen, P.; Hunter, T.; Hunter, T.; Cohen, P.; Yamaguchi, H.; Matsushita, M.; Nairn, A. C.; Kuriyan, J.; Rickert, P.; Hanks, S. K.; Hunter, T.; Crump, J. G.; Zhen, M.; Jin, Y.; Bargmann, C. I.; Sasakura, Y.; Ogasawara, M.; Makabe, K. W.; McLysaght, A.; Hokamp, K.; Wolfe, K. H.; Gu, X.; Wang, Y.; Gu, J.; Abi-Rached, L.; Gilles, A.; Shiina, T.; Pontarotti, P.; Inoko, H.; Spring, J.; How, G. F.; Venkatesh, B.; Brenner, S.; Knuutila, S.; Zervas, C. G.; Brown, N. H.; Morrison, D. K.; Kroiher, M.; Miller, M. A.; Steele, R. E.; Xu, B.; Chen, M.; Chinkers, M.; Garbers, D. L.; Li, Y.; Spangenberg, O.; Paarmann, I.; Konrad, M.; Lavie, A.; Tabuchi, K.; Biederer, T.; Butz, S.; Sudhof, T. C.; Tanaka, H.; Lopez-Borges, S.; Lazo, P. A.; Seeley, T. W.; Wang, L.; Zhen, J. Y.; Abe, Y.; Frodin, M.; Jensen, C. J.; Merienne, K.; Gammeltoft, S.; Emanuel, B. S.; Shaikh, T. H.; Cormand, B.; Diaz, A.; Grinberg, D.; Chabas, A.; Vilageliu, L.; Gaozza, E.; Baker, S. J.; Vora, R. K.; Reddy, E. P.; Bork, P. *Science* **2002**, *298*, 1912–1934.

(245) Adachi, J.; Kishida, M.; Watanabe, S.; Hashimoto, Y.; Fukamizu, K.; Tomonaga, T. *J. Proteome Res.* **2014**, *13*, 5461–5470.

(246) Fouda, A. E.; Pflum, M. K. H. *Angew. Chem. Int. Ed.* **2015**, *54*, 9618–9621.

(247) Meggio, F.; Donella Deana, A.; Ruzzene, M.; Brunati, A. M.; Cesaro, L.; Guerra, B.; Meyer, T.; Mett, H.; Fabbro, D.; Furet, P.; Dobrowolska, G.; Pinna, L. A. *Eur. J. Biochem.* **1995**, *234*, 317–322.

(248) Tanramluk, D.; Schreyer, A.; Pitt, W. R.; Blundell, T. L. *Chem. Biol. Drug Des.* **2009**, *74*, 16–24.

(249) Médard, G.; Pachl, F.; Ruprecht, B.; Klaeger, S.; Heinzlmeir, S.; Helm, D.;

Qiao, H.; Ku, X.; Wilhelm, M.; Kuehne, T.; Wu, Z.; Dittmann, A.; Hopf, C.; Kramer, K.; Kuster, B. *J. Proteome Res.* **2015**, *14*, 1574–1586.

(250) Zhang, L.; Holmes, I. P.; Hochgräfe, F.; Walker, S. R.; Ali, N. A.; Humphrey, E. S.; Wu, J.; Silva, M. De; Kersten, W. J. A.; Connor, T.; Falk, H.; Allan, L.; Street, I. P.; Bentley, J. D.; Pilling, P. A.; Monahan, B. J.; Peat, T. S.; Daly, R. J. *J. Proteome Res.* **2013**, *12*, 3104–3116.

(251) Performed by Cellzome AG.

(252) Lopez-Girona, A.; Mendy, D.; Ito, T.; Miller, K.; Gandhi, A. K.; Kang, J.; Karasawa, S.; Carmel, G.; Jackson, P.; Abbasian, M.; Mahmoudi, A.; Cathers, B.; Rychak, E.; Gaidarova, S.; Chen, R.; Schafer, P. H.; Handa, H.; Daniel, T. O.; Evans, J. F.; Chopra, R. *Leukemia* **2012**, *26*, 2326–2335.

(253) Chamberlain, P. P.; Lopez-Girona, A.; Miller, K.; Carmel, G.; Pagarigan, B.; Chie-Leon, B.; Rychak, E.; Corral, L. G.; Ren, Y. J.; Wang, M.; Riley, M.; Delker, S. L.; Ito, T.; Ando, H.; Mori, T.; Hirano, Y.; Handa, H.; Hakoshima, T.; Daniel, T. O.; Cathers, B. E. *Nat. Struct. Mol. Biol.* **2014**, *21*, 1–8.

(254) Perez, H. L.; Chaudhry, C.; Emanuel, S. L.; Fanslau, C.; Fargnoli, J.; Gan, J.; Kim, K. S.; Lei, M.; Naglich, J. G.; Traeger, S. C.; Vuppugalla, R.; Wei, D. D.; Vite, G. D.; Talbott, R. L.; Borzilleri, R. M. *J. Med. Chem.* **2015**, *58*, 1556–1562.

(255) Russell, C.; Lin, A. J. S.; Hains, P.; Simone, M. I.; Robinson, P. J.; Mccluskey, A. *RSC Adv.* **2015**, *5*, 93433–93437.

(256) Gordon, L. J.; Allen, M.; Artursson, P.; Hann, M. M.; Leavens, B. J.; Mateus, A.; Readshaw, S.; Valko, K.; Wayne, G. J.; West, A. *J. Biomol. Screen.* **2016**, *21*, 156–164.

(257) Zinn, N. Cellzome AG carried out kinobead and expression proteomics experiments.

(258) Bantscheff, M.; Eberhard, D.; Abraham, Y.; Bastuck, S.; Boesche, M.; Hobson, S.; Mathieson, T.; Perrin, J.; Raida, M.; Rau, C.; Reader, V.; Sweetman, G.; Bauer, A.; Bouwmeester, T.; Hopf, C.; Kruse, U.; Neubauer, G.; Ramsden, N.; Rick, J.; Kuster, B.; Drewes, G. *Nat. Biotechnol.* **2007**, *25*, 1035–1044.

(259) Thompson, A.; Schäfer, J.; Kuhn, K.; Kienle, S.; Schwarz, J.; Schmidt, G.; Neumann, T.; Hamon, C. *Anal. Chem.* **2003**, *75*, 1895–1904.

(260) Dayon, L.; Hainard, A.; Licker, V.; Turck, N.; Kuhn, K.; Hochstrasser, D. F.; Burkhard, P. R.; Sanchez, J.-C. *Anal. Chem.* **2008**, *80*, 2921–2931.

(261) Ross, P. L.; Huang, Y. N.; Marchese, J. N.; Williamson, B.; Parker, K.; Hattan, S.; Khainovski, N.; Pillai, S.; Dey, S.; Daniels, S.; Purkayastha, S.; Juhasz, P.; Martin, S.; Bartlet-Jones, M.; He, F.; Jacobson, A.; Pappin, D. J. *Mol. Cell. Proteomics* **2004**, *3*, 1154–1169.

(262) McAlister, G. C.; Huttlin, E. L.; Haas, W.; Ting, L.; Jedrychowski, M. P.; Rogers, J. C.; Kuhn, K.; Pike, I.; Grothe, R. A.; Blethrow, J. D.; Gygi, S. P. *Anal. Chem.* **2012**, *84*, 7469–7478.

(263) Werner, T.; Becher, I.; Sweetman, G.; Doce, C.; Savitski, M. M.; Bantscheff, M. *Anal. Chem.* **2012**, *84*, 7188–7194.

(264) Rauniyar, N.; Yates, J. R. *J. Proteome Res.* **2014**, *13*, 5293–5309.

(265) Hughes, C.; Krijgsveld, J. *Trends Biotechnol.* **2012**, *30*, 668–676.

(266) Quackenbush, J. *Nat. Genet.* **2002**, *32*, 496–501.

(267) Wetzler, M.; Talpaz, M.; Van Etten, R. A.; Hirsh-Ginsberg, C.; Beran, M.; Kurzrock, R. *J. Clin. Invest.* **1993**, *92*, 1925–1939.

(268) Fu, J.; Bian, M.; Liu, J.; Jiang, Q.; Zhang, C. *Proc. Natl. Acad. Sci. U. S. A.* **2009**, *106*, 6939–6944.

(269) Mohamed, A. J.; Vargas, L.; Nore, B. F.; Bäckesjö, C.-M.; Christensson, B.; Smith, C. I. E. *J. Biol. Chem.* **2000**, *275*, 40614–40619.

(270) Greener, T.; Zhao, X.; Nojima, H.; Eisenberg, E.; Greene, L. E. *J. Biol. Chem.* **2000**, *275*, 1365–1370.

(271) Su, J.; Xie, Q.; Wilson, I.; Li, L. *Cell. Signal.* **2007**, *19*, 1596–1601.

(272) Nishiyama, Y.; Hirota, T.; Morisaki, T.; Hara, T.; Marumoto, T.; Iida, S. I.; Makino, K.; Yamamoto, H.; Hiraoka, T.; Kitamura, N.; Saya, H. *FEBS Lett.* **1999**, *459*, 159–165.

(273) Hu, D.; Bi, X.; Fang, W.; Han, A.; Yang, W. *PLoS One* **2009**, *4*, 13–15.

(274) Abell, A. N.; Johnson, G. L. *J. Biol. Chem.* **2005**, *280*, 35793–35796.

(275) Zheng, C.; Xing, Z.; Bian, Z. C.; Guo, C.; Akbay, A.; Warner, L.; Guan, J. L. *J. Biol. Chem.* **1998**, *273*, 2384–2389.

(276) Chieffi, P.; Barchi, M.; Di Agostino, S.; Rossi, P.; Tramontano, D.; Geremia, R. *Mol. Reprod. Dev.* **2003**, *65*, 330–335.

(277) Chen, R. H.; Sarnecki, C.; Blenis, J. *Mol. Cell. Biol.* **1992**, *12*, 915–927.

(278) Chaturvedi, D.; Poppleton, H. M.; Stringfield, T.; Barbier, A.; Patel, T. B. *Mol. Cell. Biol.* **2006**, *26*, 4586–4600.

(279) Kane, L. P.; Watkins, S. C. *J. Biol. Chem.* **2005**, *280*, 21949–21954.

(280) Conner, S. D.; Schmid, S. L. *J. Cell Biol.* **2002**, *156*, 921–929.

(281) Craven, R. J.; Xu, L.; Weiner, T. M.; Fridell, Y. W.; Dent, G. A.; Srivastava, S.; Varnum, B.; Liu, E. T.; Cance, W. G. *Int. J. Cancer* **1995**, *60*, 791–797.

(282) Behrmann, I.; Smyczek, T.; Heinrich, P. C.; Schmitz-Van De Leur, H.; Komyod, W.; Giese, B.; Müller-Newen, G.; Haan, S.; Haan, C. *J. Biol. Chem.* **2004**, *279*, 35486–35493.

(283) Ley, S. C.; Marsh, M.; Bebbington, C. R.; Proudfoot, K.; Jordan, P. *J. Cell Biol.* **1994**, *125*, 639–649.

(284) Belkina, N. V; Liu, Y.; Hao, J.-J.; Karasuyama, H.; Shaw, S. *Proc. Natl. Acad. Sci. U. S. A.* **2009**, *106*, 4707–4712.

(285) Gilboa, L.; Wells, R. G.; Lodish, H. F.; Henis, Y. I. *J. Cell Biol.* **1998**, *140*,

767–777.

(286) Cao, W.; Sohail, M.; Liu, G.; Koumbadinga, G. A.; Lobo, V. G.; Xie, J. *RNA Biol.* **2011**, *8*, 1061–1072.

(287) Faust, M.; Montenarh, M. *Cell Tissue Res.* **2000**, *301*, 329–340.

(288) Su, J.; Richter, K.; Zhang, C.; Gu, Q.; Li, L. *Mol. Immunol.* **2007**, *44*, 900–905.

(289) Kashuba, V. I.; Grigorieva, E. V; Kvasha, S. M.; Pavlova, T. V; Zabarovsky, E. R. *Genomics Insights* **2011**, 1.

(290) Pierrat, B.; Correia, J. S.; Mary, J. L.; Tomás-Zuber, M.; Lesslauer, W. *J. Biol. Chem.* **1998**, *273*, 29661–29671.

(291) Jaberi, A.; Hooker, E.; Guillemette, J.; Papillon, J.; Kristof, A. S.; Cybulsky, A. V. *BBA Mol. Cell Res.* **2015**, *1853*, 2539–2552.

(292) Kuai, J.; Wooters, J.; Hall, J. P.; Rao, V. R.; Nickbarg, E.; Li, B.; Chatterjee-Kishore, M.; Qiu, Y.; Lin, L. L. *J. Biol. Chem.* **2004**, *279*, 53266–53271.

(293) Crew, A. P. Targeted Protein Degradation of Pathological Proteins. Cambridge Healthtech Institute, Discovery on Target Meeting, 2015.

(294) Yustein, J. T.; Xia, L.; Kahlenburg, J. M.; Robinson, D.; Templeton, D.; Kung, H.-J. *Oncogene* **2003**, *22*, 6129–6141.

(295) Deloukas, P.; Earthrowl, M. E.; Grafham, D. V; Rubenfield, M.; French, L.; Steward, C. A.; Sims, S. K.; Jones, M. C.; Searle, S.; Scott, C. *Nature* **2004**, *429*, 375–381.

(296) Ota, T.; Suzuki, Y.; Nishikawa, T.; Otsuki, T.; Sugiyama, T.; Irie, R.; Wakamatsu, A.; Hayashi, K.; Sato, H.; Nagai, K.; Kimura, K.; Makita, H.; Sekine, M.; Obayashi, M.; Nishi, T.; Shibahara, T.; Tanaka, T.; Ishii, S.; Yamamoto, J.; Saito, K.; Kawai, Y.; Isono, Y.; Nakamura, Y.; Nagahari, K.; Murakami, K.; Yasuda, T.; Iwayanagi, T.; Wagatsuma, M.; Shiratori, A.; Sudo, H.; Hosoiri, T.; Kaku, Y.; Kodaira, H.; Kondo, H.; Sugawara, M.; Takahashi, M.; Kanda, K.; Yokoi, T.; Furuya, T.; Kikkawa, E.; Omura, Y.; Abe, K.; Kamihara, K.; Katsuta, N.; Sato, K.; Tanikawa, M.; Yamazaki, M.; Ninomiya, K.; Ishibashi, T.; Yamashita, H.; Murakawa, K.; Fujimori, K.; Tanai, H.; Kimata, M.; Watanabe, M.; Hiraoka, S.; Chiba, Y.; Ishida, S.; Ono, Y.; Takiguchi, S.; Watanabe, S.; Yosida, M.; Hotuta, T.; Kusano, J.; Kanehori, K.; Takahashi-Fujii, A.; Hara, H.; Tanase, T.; Nomura, Y.; Togiya, S.; Komai, F.; Hara, R.; Takeuchi, K.; Arita, M.; Imose, N.; Musashino, K.; Yuuki, H.; Oshima, A.; Sasaki, N.; Aotsuka, S.; Yoshikawa, Y.; Matsunawa, H.; Ichihara, T.; Shiohata, N.; Sano, S.; Moriya, S.; Momiyama, H.; Satoh, N.; Takami, S.; Terashima, Y.; Suzuki, O.; Nakagawa, S.; Senoh, A.; Mizoguchi, H.; Goto, Y.; Shimizu, F.; Wakebe, H.; Hishigaki, H.; Watanabe, T.; Sugiyama, A.; Takemoto, M.; Kawakami, B.; Yamazaki, M.; Watanabe, K.; Kumagai, A.; Itakura, S.; Fukuzumi, Y.; Fujimori, Y.; Komiyama, M.; Tashiro, H.; Tanigami, A.; Fujiwara, T.; Ono, T.; Yamada, K.; Fujii, Y.; Ozaki, K.; Hirao, M.; Ohmori, Y.; Kawabata, A.; Hikiji, T.; Kobatake, N.; Inagaki, H.; Ikema, Y.; Okamoto, S.; Okitani, R.; Kawakami, T.; Noguchi, S.; Itoh, T.; Shigeta,

K.; Senba, T.; Matsumura, K.; Nakajima, Y.; Mizuno, T.; Morinaga, M.; Sasaki, M.; Togashi, T.; Oyama, M.; Hata, H.; Watanabe, M.; Komatsu, T.; Mizushima-Sugano, J.; Satoh, T.; Shirai, Y.; Takahashi, Y.; Nakagawa, K.; Okumura, K.; Nagase, T.; Nomura, N.; Kikuchi, H.; Masuho, Y.; Yamashita, R.; Nakai, K.; Yada, T.; Nakamura, Y.; Ohara, O.; Isogai, T.; Sugano, S. *Nat. Genet.* **2004**, *36*, 40–45.

(297) Shahrokni, A.; Rajebi, M. R.; Saif, M. W. *Clin. Colorectal Cancer* **2009**, *8*, 231–234.

(298) Boichenko, I.; Deiss, S.; Bär, K.; Hartmann, M. D.; Hernandez Alvarez, B. *J. Med. Chem.* **2016**, *59*, 770–774.

(299) Zhang, D.; Zaugg, K.; Mak, T. W.; Elledge, S. J. *Cell* **2006**, *126*, 529–542.

(300) Camasses, A.; Bogdanova, A.; Shevchenko, A.; Zachariae, W. *Mol. Cell* **2003**, *12*, 87–100.

(301) Hughes, S.; Bassi, I. Z. GlaxoSmithKline performed biological experiments.

(302) Vince, J. E.; Wong, W. W. L.; Khan, N.; Feltham, R.; Chau, D.; Ahmed, A. U.; Benetatos, C. A.; Chunduru, S. K.; Condon, S. M.; McKinlay, M.; Brink, R.; Leverkus, M.; Tergaonkar, V.; Schneider, P.; Callus, B. A.; Koentgen, F.; Vaux, D. L.; Silke, J. *Cell* **2007**, *131*, 682–693.

(303) Satterthwaite, A. B.; Li, Z.; Witte, O. N. *Semin. Immunol.* **1998**, *10*, 309–316.

(304) Bradshaw, J. M. *Cell. Signal.* **2010**, *22*, 1175–1184.

(305) Hendriks, R. W.; Yuvaraj, S.; Kil, L. P. *Nat. Rev. Cancer* **2014**, *14*, 219–232.

(306) Tsukada, S.; Saffran, D. C.; Rawlings, D. J.; Parolini, O.; Allen, R. C.; Klisak, I.; Sparkes, R. S.; Kubagawa, H.; Mohandas, T.; Quan, S.; Belmont, J. W.; Cooper, M. D.; Conley, M. E.; Witte, O. N. *Cell* **1993**, *72*, 279–290.

(307) Vetrie, D.; Vorechovsky, I.; Sideras, P.; Holland, J.; Davies, A.; Flinter, F.; Hammarstrom, L.; Kinnon, C.; Levinsky, R.; Bobrow, M.; Smith, C. I. E.; Bentley, D. R. *Nature* **1993**, *361*, 226–233.

(308) Bruton, O. C. *Pediatrics* **1952**, *9*, 722–728.

(309) Conley, M. E. *J. Immunol.* **1985**, *134*, 3070–3074.

(310) Lederman, H. M.; Winkelstein, J. A. *Medicine (Baltimore).* **1985**, *64*, 145–156.

(311) Conley, M. E.; Dobbs, A. K.; Farmer, D. M.; Kilic, S.; Paris, K.; Grigoriadou, S.; Coustan-Smith, E.; Howard, V.; Campana, D. *Annu. Rev. Immunol.* **2009**, *27*, 199–227.

(312) Rawlings, D. J.; Saffran, D. C.; Tsukuda, S.; Largaespada, D. A.; Grimaldi, J. C.; Cohen, L.; Mohr, R. N.; Bazan, J. F.; Howard, M.; Copeland, N. G. *Science* **1993**, *261*, 358–361.

(313) Khan, W. N.; Alt, F. W.; Gerstein, R. M.; Malynn, B. A.; Larsson, I.; Rathbun, G.; Davidson, L.; Müller, S.; Kantor, A. B.; Herzenberg, L. A.; Rosen, F. S.; Sideras, P. *Immunity* **1995**, *3*, 283–299.

(314) Kerner, J. D.; Appleby, M. W.; Mohr, R. N.; Chien, S.; Rawlings, D. J.; Maliszewski, C. R.; Witte, O. N.; Perlmutte, R. M. *Immunity* **1995**, *3*, 301–312.

(315) Aoki, Y.; Isselbacher, K. J.; Pillai, S. *Proc. Natl. Acad. Sci. U. S. A.* **1994**, *91*, 10606–10609.

(316) de Weers, M.; Brouns, G. S.; Hinshelwood, S.; Kinnon, C.; Schuurman, R. K.; Hendriks, R. W.; Borst, J. *J. Biol. Chem.* **1994**, *269*, 23857–23860.

(317) Khan, W. N. *Immunol. Res.* **2001**, *23*, 147–156.

(318) Park, H.; Wahl, M. I.; Afar, D. E. H.; Turck, C. W.; Rawlings, D. J.; Tam, C.; Scharenberg, A. M.; Kinet, J.-P.; Witte, O. N. *Immunity* **1996**, *4*, 515–525.

(319) Rawlings, D. J.; Scharenberg, A. M.; Park, H.; Wahl, M. I.; Lin, S.; Kato, R. M.; Fluckiger, A.-C.; Witte, O. N.; Kinet, J.-P. *Science* **1996**, *271*, 822–825.

(320) Hendriks, R. W. *Nat. Chem. Biol.* **2011**, *7*, 4–5.

(321) Humphries, L. A.; Dangelmaier, C.; Sommer, K.; Kipp, K.; Kato, R. M.; Griffith, N.; Bakman, I.; Turk, C. W.; Daniel, J. L.; Rawlings, D. J. *J. Biol. Chem.* **2004**, *279*, 37651–37661.

(322) Fluckiger, A.; Li, Z.; Kato, R. M.; Wahl, M. I.; Ochs, H. D.; Longnecker, R.; Kinet, J.; Witte, O. N.; Scharenberg, A. M.; Rawlings, D. J. *EMBO J.* **1998**, *17*, 1973–1985.

(323) Jiang, A.; Craxton, A.; Kurosaki, T.; Clark, E. A. *J. Exp. Med.* **1998**, *188*, 1297–1306.

(324) Kurosaki, T. *Annu. Rev. Immunol.* **1999**, *17*, 555–592.

(325) Whang, J. A.; Chang, B. Y. *Drug Discov. Today* **2014**, *19*, 1200–1204.

(326) Favas, C.; Isenberg, D. A. *Nat. Rev. Rheumatol.* **2009**, *512*, 711–716.

(327) Hauser, S. L.; Waubant, E.; Arnold, D. L.; Vollmer, T.; Antel, J.; Fox, R. J.; Bar-Or, A.; Panzara, M.; Sarkar, N.; Agarwal, S.; Langer-Gould, A.; Smith, C. H. *N. Engl. J. Med.* **2008**, *358*, 676–688.

(328) de Weers, M.; Verschuren, M. C. M.; Kraakman, M. E. M.; Mensink, R. G. J.; Schuurman, R. K. B.; van Dongen, J. J. M.; Hendriks, R. W. *Eur. J. Immunol.* **1993**, *23*, 3109–3114.

(329) Katz, F. E.; Lovering, R. C.; Bradley, L. A.; Rigley, K. P.; Brown, D.; Cotter, F.; Chessells, J. M.; Levinsky, R. J.; Kinnon, C. *Leukemia* **1994**, *8*, 574–577.

(330) Davis, R. E.; Ngo, V. N.; Lenz, G.; Tolar, P.; Young, R. M.; Romesser, P. B.; Kohlhammer, H.; Lamy, L.; Zhao, H.; Yang, Y.; Xu, W.; Shaffer, A. L.; Wright, G.; Xiao, W.; Powell, J.; Jiang, J.; Thomas, C. J.; Rosenwald, A.; Ott, G.; Muller-Hermelink, H. K.; Gascoyne, R. D.; Connors, J. M.; Johnson, N. A.; Rimsza, L. M.; Campo, E.; Jaffe, E. S.; Wilson, W. H.; Delabie, J.; Smeland, E. B.; Fisher, R. I.; Braziel, R. M.; Tubbs, R. R.; Cook, J. R.; Weisenburger, D. D.; Chan, W. C.; Pierce, S. K.; Staudt, L. M. *Nature* **2010**, *463*, 88–92.

(331) McInnes, I. B.; Schett, G. *N. Engl. J. Med.* **2011**, *365*, 2205–2219.

(332) Edwards, J. C. W.; Szczepański, L.; Szechiński, J.; Filipowicz-Sosnowska, A.; Emery, P.; Close, D. R.; Stevens, R. M.; Shaw, T. *N. Engl. J. Med.* **2004**, *350*, 2572–2581.

(333) Jannson, L.; Holmdahl, R. *Clin. Exp. Immunol.* **1993**, *94*, 459–465.

(334) Potashman, M. H.; Duggan, M. E. *J. Med. Chem.* **2009**, *52*, 1231–1246.

(335) Smith, A. J. T.; Zhang, X.; Leach, A. G.; Houk, K. N. *J. Med. Chem.* **2009**, *52*, 225–233.

(336) Liu, Q.; Sabnis, Y.; Zhao, Z.; Zhang, T.; Buhrlage, S. J.; Jones, L. H.; Gray, N. S. *Chem. Biol.* **2013**, *20*, 146–159.

(337) Pan, Z.; Scheerens, H.; Li, S. J.; Schultz, B. E.; Sprengeler, P. A.; Burrill, L. C.; Mendonca, R. V.; Sweeney, M. D.; Scott, K. C. K.; Grothaus, P. G.; Jeffery, D. A.; Spoerke, J. M.; Honigberg, L. A.; Young, P. R.; Dalrymple, S. A.; Palmer, J. T. *ChemMedChem* **2007**, *2*, 58–61.

(338) Burchat, A. F.; Calderwood, D. J.; Hirst, G. C.; Holman, N. J.; Johnston, D. N.; Munschauer, R.; Tometzki, G. B. *Bioorg. Med. Chem. Lett.* **2000**, *10*, 2171–2174.

(339) Honigberg, L. A.; Smith, A. M.; Sirisawad, M.; Verner, E.; Loury, D.; Chang, B.; Li, S.; Pan, Z.; Thamm, D. H.; Miller, R. A.; Buggy, J. J. *Proc. Natl. Acad. Sci. U. S. A.* **2010**, *107*, 13075–13080.

(340) Byrd, J. C.; Furman, R. R.; Coutre, S. E.; Flinn, I. W.; Burger, J. A.; Blum, K. A.; Grant, B.; Sharman, J. P.; Coleman, M.; Wierda, W. G.; Jones, J. A.; Zhao, W.; Heerema, N. A.; Johnson, A. J.; Sukbuntherng, J.; Chang, B. Y.; Clow, F.; Hedrick, E.; Buggy, J. J.; James, D. F.; O'Brien, S. *N. Engl. J. Med.* **2013**, *369*, 32.

(341) Wang, M. L.; Rule, S.; Martin, P.; Goy, A.; Auer, R.; Kahl, B. S.; Jurczak, W.; Advani, R. H.; Romaguera, J. E.; Williams, M. E.; Barrientos, J. C.; Chmielowska, E.; Radford, J.; Stilgenbauer, S.; Dreyling, M.; Jedrzejczak, W. W.; Johnson, P.; Spurgeon, S. E.; Li, L.; Zhang, L.; Newberry, K.; Ou, Z.; Cheng, N.; Fang, B.; McGreivy, J.; Clow, F.; Buggy, J. J.; Chang, B. Y.; Beaupre, D. M.; Kunkel, L. A.; Blum, K. A. *N. Engl. J. Med.* **2013**, *369*, 507–516.

(342) Treon, S. P.; Tripsas, C. K.; Meid, K.; Warren, D.; Varma, G.; Green, R.; Argyropoulos, K. V.; Yang, G.; Cao, Y.; Xu, L.; Patterson, C. J.; Rodig, S.; Zehnder, J. L.; Aster, J. C.; Harris, N. L.; Kanan, S.; Ghobrial, I.; Castillo, J. J.; Laubach, J. P.; Hunter, Z. R.; Salman, Z.; Li, J.; Cheng, M.; Clow, F.; Graef, T.; Palomba, M. L.; Advani, R. H. *N. Engl. J. Med.* **2015**, *372*, 1430–1440.

(343) Garber, K. *Nat. Rev. Drug Discov.* **2014**, *13*, 162–164.

(344) Advani, R. H.; Buggy, J. J.; Sharman, J. P.; Smith, S. M.; Boyd, T. E.; Grant, B.; Kolibaba, K. S.; Furman, R. R.; Rodriguez, S.; Chang, B. Y.; Sukbuntherng, J.; Izumi, R.; Hamdy, A.; Hedrick, E.; Fowler, N. H. *J. Clin. Oncol.* **2013**, *31*, 88–94.

(345) Byrd, J. C.; Brown, J. R.; O'Brien, S.; Barrientos, J. C.; Kay, N. E.; Reddy, N. M.; Coutre, S.; Tam, C. S.; Mulligan, S. P.; Jaeger, U.; Devereux, S.; Barr, P. M.; Furman, R. R.; Kipps, T. J.; Cymbalista, F.; Pocock, C.; Thornton, P.; Caligaris-Cappio, F.; Robak, T.; Delgado, J.; Schuster, S. J.; Montillo, M.; Schuh, A.; de Vos, S.; Gill, D.; Bloor, A.; Dearden, C.; Moreno, C.; Jones, J. J.; Chu, A. D.; Fardis, M.; McGreivy, J.; Clow, F.; James, D. F.; Hillmen, P. *N. Engl. J. Med.* **2014**, *371*, 213–223.

(346) O'Brien, S.; Furman, R. R.; Coutre, S. E.; Sharman, J. P.; Burger, J. A.; Blum, K. A.; Grant, B.; Richards, D. A.; Coleman, M.; Wierda, W. G.; Jones, J. A.; Zhao, W.; Heerema, N. A.; Johnson, A. J.; Izumi, R.; Hamdy, A.; Chang, B. Y.; Graef, T.; Clow, F.; Buggy, J. J.; James, D. F.; Byrd, J. C. *Lancet Oncol.* **2016**, *15*, 48–58.

(347) Jain, P.; Keating, M.; Wierda, W.; Estrov, Z. *Blood* **2015**, *125*, 2062–2068.

(348) Maddocks, K. J.; Ruppert, A. S.; Lozanski, G.; Heerema, N. A.; Zhao, W.; Abruzzo, L.; Lozanski, A.; Davis, M.; Gordon, A.; Smith, L.; Mantel, R.; Jones, J.; Flynn, J.; Jaglowski, S. M.; Andritsos, L. A.; Awan, F.; Blum, K. A.; Grever, M. R.; Johnson, A. J.; Byrd, J. C.; Woyach, J. A. *JAMA Oncol.* **2015**, *1*, 80–87.

(349) Woyach, J. A.; Furman, R. R.; Liu, T.-M.; Ozer, H. G.; Zapatka, M.; Ruppert, A. S.; Xue, L.; Li, D. H.-H.; Steggerda, S. M.; Versele, M.; Dave, S. S.; Zhang, J.; Yilmaz, A. S.; Jaglowski, S. M.; Blum, K. A.; Lozanski, A.; Lozanski, G.; James, D. F.; Barrientos, J. C.; Lichter, P.; Stilgenbauer, S.; Buggy, J. J.; Chang, B. Y.; Johnson, A. J.; Byrd, J. C. *N. Engl. J. Med.* **2014**, *370*, 2286–2294.

(350) Famà, R.; Bomben, R.; Rasi, S.; Dal Bo, M.; Ciardullo, C.; Monti, S.; Rossi, F.; D'Agaro, T.; Zucchetto, A.; Gattei, V.; Gaidano, G.; Rossi, D. *Blood* **2014**, *124*, 3831–3833.

(351) Cheng, S.; Guo, A.; Lu, P.; Ma, J.; Coleman, M.; Wang, Y. L. *Leukemia* **2015**, *29*, 895–900.

(352) Liu, T.-M. M.; Woyach, J. A.; Zhong, Y.; Lozanski, A.; Lozanski, G.; Dong, S.; Strattan, E.; Lehman, A.; Zhang, X.; Jones, J. A.; Flynn, J.; Andritsos, L. A.; Maddocks, K.; Jaglowski, S. M.; Blum, K. A.; Byrd, J. C.; Dubovsky, J. A.; Johnson, A. J. *Blood* **2015**, *126*, 61–68.

(353) Evans, E. K.; Tester, R.; Aslanian, S.; Karp, R.; Sheets, M.; Labenski, M. T.; Witowski, S. R.; Lounsbury, H.; Chaturvedi, P.; Mazdiyasni, H.; Zhu, Z.; Nacht, M.; Freed, M. I.; Petter, R. C.; Dubrovskiy, A.; Singh, J.; Westlin, W. F. *J. Pharmacol. Exp. Ther.* **2013**, *346*, 219–228.

(354) Wu, J.; Zhang, M.; Liu, D. *J. Hematol. Oncol.* **2016**, *9*, 21.

(355) Byrd, J. C.; Harrington, B.; O'Brien, S.; Jones, J. A.; Schuh, A.; Devereux, S.; Chaves, J.; Wierda, W. G.; Awan, F. T.; Brown, J. R.; Hillmen, P.; Stephens, D. M.; Ghia, P.; Barrientos, J. C.; Pagel, J. M.; Woyach, J.; Johnson, D.; Huang, J.; Wang, X.; Kaptein, A.; Lannutti, B. J.; Covey, T.; Fardis, M.; McGreivy, J.; Hamdy, A.; Rothbaum, W.; Izumi, R.; Diacovo, T. G.; Johnson, A. J.; Furman, R. R.; O'Brien, S.; Jones, J. A.; Schuh, A.; Devereux, S.;

Chaves, J.; Wierda, W. G.; Awan, F. T.; Brown, J. R.; Hillmen, P.; Stephens, D. M.; Ghia, P.; Barrientos, J. C.; Pagel, J. M.; Woyach, J.; Johnson, D.; Huang, J.; Wang, X.; Kaptein, A.; Lannutti, B. J.; Covey, T.; Fardis, M.; McGreivy, J.; Hamdy, A.; Rothbaum, W.; Izumi, R.; Diacovo, T. G.; Johnson, A. J.; Furman, R. R. *N. Engl. J. Med.* **2016**, *374*, 323–332.

(356) Serafimova, I. M.; Pufall, M. A.; Krishnan, S.; Duda, K.; Cohen, M. S.; Maglathlin, R. L.; McFarland, J. M.; Miller, R. M.; Frödin, M.; Taunton, J. *Nat. Chem. Biol.* **2012**, *8*, 471–476.

(357) Bradshaw, J. M.; McFarland, J. M.; Paavilainen, V. O.; Bisconte, A.; Tam, D.; Phan, V. T.; Romanov, S.; Finkle, D.; Shu, J.; Patel, V.; Ton, T.; Li, X.; Loughhead, D. G.; Nunn, P. A.; Karr, D. E.; Gerritsen, M. E.; Oliver Funk, J.; Owns, T. D.; Verner, E.; Bradmeld, K. A.; Kill, R. J.; Goldstein, D. M.; Taunton. *Nat. Chem. Biol.* **2015**, *11*, 525–531.

(358) Lanning, B. R.; Whitby, L. R.; Dix, M. M.; Douhan, J.; Gilbert, A. M.; Hett, E. C.; Johnson, T. O.; Joslyn, C.; Kath, J. C.; Niessen, S.; Roberts, L. R.; Schnute, M. E.; Wang, C.; Hulce, J. J.; Wei, B.; Whiteley, L. O.; Hayward, M. M.; Cravatt, B. F. *Nat. Chem. Biol.* **2014**, *10*, 760–767.

(359) Norman, P. *Expert Opin. Investig. Drugs* **2016**, *3784*, 1–9.

(360) Lou, Y.; Owens, T. D.; Kuglstatter, A.; Kondru, R. K.; Goldstein, D. M. *J. Med. Chem.* **2012**, *55*, 4539–4550.

(361) Di Paolo, J. A.; Huang, T.; Balazs, M.; Barbosa, J.; Barck, K. H.; Bravo, B. J.; Carano, R. A.; Darrow, J.; Davies, D. R.; DeForge, L. E.; Diehl, L.; Ferrando, R.; Gallion, S. L.; Giannetti, A. M.; Gribling, P.; Hurez, V.; Hymowitz, S. G.; Jones, R.; Kropf, J. E.; Lee, W. P.; Maciejewski, P. M.; Mitchell, S. A.; Rong, H.; Staker, B. L.; Whitney, J. A.; Yeh, S.; Young, W. B.; Yu, C.; Zhang, J.; Reif, K.; Currie, K. S. *Nat. Chem. Biol.* **2011**, *7*, 41–50.

(362) Young, W. B.; Barbosa, J.; Blomgren, P.; Bremer, M. C.; Crawford, J. J.; Dambach, D.; Gallion, S.; Hymowitz, S. G.; Kropf, J. E.; Lee, S. H.; Liu, L.; Lubach, J. W.; Macaluso, J.; Maciejewski, P.; Maurer, B.; Mitchell, S. A.; Ortwine, D. F.; Di Paolo, J.; Reif, K.; Scheerens, H.; Schmitt, A.; Sowell, C. G.; Wang, X.; Wong, H.; Xiong, J.-M.; Xu, J.; Zhao, Z.; Currie, K. S. *Bioorg. Med. Chem. Lett.* **2015**, *25*, 1333–1337.

(363) Liu, L.; Halladay, J. S.; Shin, Y.; Wong, S.; Coraggio, M.; La, H.; Baumgardner, M.; Le, H.; Gopaul, S.; Boggs, J.; Kuebler, P.; Davis, J. C.; Liao, X. C.; Lubach, J. W.; Deese, A.; Sowell, C. G.; Currie, K. S.; Young, W. B.; Khojasteh, S. C.; Hop, C. E. C. A.; Wong, H. *Drug Metab. Dispos.* **2011**, *39*, 1840–1849.

(364) Lou, Y.; Han, X.; Kuglstatter, A.; Kondru, R. K.; Sweeney, Z. K.; Soth, M.; Mcintosh, J.; Litman, R.; Suh, J.; Kocer, B.; Davis, D.; Park, J.; Frauchiger, S.; Dewdney, N.; Zecic, H.; Taygerly, J. P.; Sarma, K.; Hong, J.; Hill, R. J.; Gabriel, T.; Goldstein, D. M.; Owens, T. D. *J. Med. Chem.* **2015**, *58*, 512–516.

(365) De Lucca, G. V.; Shi, Q.; Liu, Q.; Batt, D. G.; Beaudoin Bertrand, M.; Rampulla, R.; Mathur, A.; Discenza, L.; D'Arienzo, C.; Dai, J.; Obermeier, M.; Vickery, R.; Zhang, Y.; Yang, Z.; Marathe, P.; Tebben, A. J.;

Muckelbauer, J. K.; Chang, C. J.; Zhang, H.; Gillooly, K.; Taylor, T.; Pattoli, M. A.; Skala, S.; Kukral, D. W.; McIntyre, K. W.; Salter-Cid, L.; Fura, A.; Burke, J. R.; Barrish, J. C.; Carter, P. H.; Tino, J. A. *J. Med. Chem.* **2016**, *59*, 7915–7935.

(366) Watterson, S. H.; De Lucca, G. V; Shi, Q.; Langevine, C. M.; Liu, Q.; Batt, D. G.; Beaudoin Bertrand, M.; Gong, H.; Dai, J.; Yip, S.; Li, P.; Sun, D.; Wu, D.-R.; Wang, C.; Zhang, Y.; Traeger, S. C.; Pattoli, M. A.; Skala, S.; Cheng, L.; Obermeier, M. T.; Vickery, R.; Discenza, L. N.; D'Arienzo, C. J.; Zhang, Y.; Heimrich, E.; Gillooly, K. M.; Taylor, T. L.; Pulicicchio, C.; McIntyre, K. W.; Galella, M. A.; Tebben, A. J.; Muckelbauer, J. K.; Chang, C.; Rampulla, R.; Mathur, A.; Salter-Cid, L.; Barrish, J. C.; Carter, P. H.; Fura, A.; Burke, J. R.; Tino, J. A. *J. Med. Chem.* **2016**, *59*, 9173–9200.

(367) Liu, J.; Guiadeen, D.; Krikorian, A.; Gao, X.; Wang, J.; Boga, S. B.; Alhassan, A.-B.; Yu, Y.; Vaccaro, H.; Liu, S.; Yang, C.; Wu, H.; Cooper, A.; Man, J. De; Kaptein, A.; Maloney, K.; Hornak, V.; Gao, Y.-D.; Fischmann, T. O.; Raaijmakers, H.; Vu-Pham, D.; Presland, J.; Mansueto, M.; Xu, Z.; Leccese, E.; Zhang-Hoover, J.; Knemeyer, I.; Garlisi, C. G.; Bays, N.; Stivers, P.; Brandish, P. E.; Hicks, A.; Kim, R.; Kozlowski, J. A. *ACS Med. Chem. Lett.* **2016**, *7*, 198–203.

(368) Smith, C. R.; Dougan, D. R.; Komandla, M.; Kanouni, T.; Knight, B.; Lawson, J. D.; Sabat, M.; Taylor, E. R.; Vu, P.; Wyrick, C. *J. Med. Chem.* **2015**, *58*, 5437–5444.

(369) Xu, D.; Kim, Y.; Postelnek, J.; Vu, M. D.; Hu, D. Q.; Liao, C.; Bradshaw, M.; Hsu, J.; Zhang, J.; Pashine, A.; Srinivasan, D.; Woods, J.; Levin, A.; O'Mahony, A.; Owens, T. D.; Lou, Y.; Hill, R. J.; Narula, S.; DeMartino, J.; Fine, J. S. *J. Pharmacol. Exp. Ther.* **2012**, *341*, 90–103.

(370) Backus, K. M.; Correia, B. E.; Lum, K. M.; Forli, S.; Horning, B. D.; González-Páez, G. E.; Chatterjee, S.; Lanning, B. R.; Teijaro, J. R.; Olson, A. J.; Wolan, D. W.; Cravatt, B. F. *Nature* **2016**, *534*, 570–574.

(371) Ostrem, J. M.; Peters, U.; Sos, M. L.; Wells, J. A.; Shokat, K. M. *Nature* **2013**, *503*, 548–551.

(372) Patricelli, M. P.; Janes, M. R.; Li, L. S.; Hansen, R.; Peters, U.; Kessler, L. V.; Chen, Y.; Kucharski, J. M.; Feng, J.; Ely, T.; Chen, J. H.; Firdaus, S. J.; Babbar, A.; Ren, P.; Liu, Y. *Cancer Discov.* **2016**, *6*, 316–329.

(373) Ito, M.; Shichita, T.; Okada, M.; Komine, R.; Noguchi, Y.; Yoshimura, A.; Morita, R. *Nat. Commun.* **2015**, *6*, 7360.

(374) Martinon, F.; Mayor, A.; Tschopp, J. *Annu. Rev. Immunol.* **2009**, *27*, 229–265.

(375) Martinon, F.; Burns, K.; Tschopp, J. *Mol. Cell* **2002**, *10*, 417–426.

(376) Lamkanfi, M. *Nat. Rev. Immunol.* **2011**, *11*, 213–220.

(377) Guo, H.; Callaway, J. B.; Ting, J. P.-Y. *Nat. Med.* **2015**, *21*, 677–687.

(378) Ozaki, E.; Campbell, M.; Doyle, S. L. *J. Inflamm. Res.* **2015**, *8*, 15–27.

(379) Saito, K.; Tolias, K. F.; Saci, A.; Koon, H. B.; Humphries, L. A.; Scharenberg,

A.; Rawlings, D. J.; Kinet, J. P.; Carpenter, C. L. *Immunity* **2003**, *19*, 669–678.

(380) Marcotte, D. J.; Liu, Y.-T.; Arduini, R. M.; Hession, C. A.; Miatkowski, K.; Wildes, C. P.; Cullen, P. F.; Hong, V.; Hopkins, B. T.; Mertsching, E.; Jenkins, T. J.; Romanowski, M. J.; Baker, D. P.; Silvian, L. F. *Protein Sci.* **2010**, *19*, 429–439.

(381) Mischke, S. G. Dimeric Compounds. WO2014090709A1, 2014.

(382) Ma, H.; Deacon, S.; Horiuchi, K. *Expert Opin. Drug Discov.* **2008**, *3*, 607–621.

(383) Wu, H.; Wang, W.; Liu, F.; Weisberg, E. L.; Tian, B.; Chen, Y.; Li, B.; Wang, A.; Wang, B.; Zhao, Z.; McMillin, D. W.; Hu, C.; Li, H.; Wang, J.; Liang, Y.; Buhrlage, S. J.; Liang, J.; Liu, J.; Yang, G.; Brown, J. R.; Treon, S. P.; Mitsiades, C. S.; Griffin, J. D.; Liu, Q.; Gray, N. S. *ACS Chem. Biol.* **2014**, *9*, 1086–1091.

(384) Watanabe, D.; Hashimoto, S.; Ishiai, M.; Matsushita, M.; Baba, Y.; Kishimoto, T.; Kurosaki, T.; Tsukada, S. *J. Biol. Chem.* **2001**, *276*, 38595–38601.

(385) Owens, T.; Verner, E. Pyrazolopyrimidine Compounds as Kinase Inhibitors. WO2014/039899A1, 2014.

(386) Matyskiela, M. E.; Lander, G. C.; Martin, A. *Nat. Struct. Mol. Biol.* **2013**, *20*, 781–788.

(387) Johnson, A. R.; Kohli, P. B.; Katewa, A.; Gogol, E.; Belmont, L. D.; Choy, R.; Penuel, E.; Burton, L.; Eigenbrot, C.; Yu, C.; Ortwine, D. F.; Bowman, K.; Franke, Y.; Tam, C.; Estevez, A.; Mortara, K.; Wu, J.; Li, H.; Lin, M.; Bergeron, P.; Crawford, J. J.; Young, W. B. *ACS Chem. Biol.* **2016**, *11*, 2897–2907.

(388) Zhao, X.; Xin, M.; Huang, W.; Ren, Y.; Jin, Q.; Tang, F.; Jiang, H.; Wang, Y.; Yang, J.; Mo, S.; Xiang, H. *Bioorg. Med. Chem.* **2015**, *23*, 348–364.

(389) Hashimoto, K.; Saito, B.; Miyamoto, N.; Oguro, Y.; Tomita, D.; Shiokawa, Z.; Asano, M.; Kakei, H.; Taya, N.; Kawasaki, M.; Sumi, H.; Yabuki, M.; Iwai, K.; Yoshida, S.; Yoshimatsu, M.; Aoyama, K.; Kosugi, Y.; Kojima, T.; Morishita, N.; Dougan, D. R.; Snell, G. P.; Imamura, S.; Ishikawa, T. *J. Med. Chem.* **2013**, *56*, 1228–1246.

(390) Infante, J. R.; Dees, E. C.; Olszanski, A. J.; Dhuria, S. V; Sen, S.; Cameron, S.; Cohen, R. B. *J. Clin. Oncol.* **2014**, *32*, 3103–3110.

(391) Molander, G. A.; Gormisky, P. E. *J. Org. Chem.* **2008**, *73*, 7481–7485.

(392) Li, H.; Willingham, S. B.; Ting, J. P.-Y.; Re, F. *J. Immunol.* **2008**, *181*, 17–21.

(393) Franchi, L.; Núñez, G. *Eur. J. Immunol.* **2008**, *38*, 2085–2089.

(394) Baldwin, A. G.; Brough, D.; Freeman, S. *J. Med. Chem.* **2016**, *59*, 1691–1710.

(395) Cocco, M.; Garella, D.; Di Stilo, A.; Borretto, E.; Stevanato, L.; Giorgis, M.; Marini, E.; Fantozzi, R.; Miglio, G.; Bertinaria, M. *J. Med. Chem.* **2014**, *57*,

10366–10382.

(396) Zwolanek, F.; Riedelberger, M.; Stolz, V.; Jenull, S.; Istel, F.; Köprülü, A. D.; Ellmeier, W.; Kuchler, K. *PLoS Pathog.* **2014**, *10*, e1004525.

(397) Gurung, P.; Kanneganti, T. D. *Am. J. Pathol.* **2015**, *185*, 17–25.

(398) Arrowsmith, C. H.; Audia, J. E.; Austin, C.; Baell, J.; Bennett, J.; Blagg, J.; Bountra, C.; Brennan, P. E.; Brown, P. J.; Bunnage, M. E.; Buser-Doepner, C.; Campbell, R. M.; Carter, A. J.; Cohen, P.; Copeland, R. A.; Cravatt, B.; Dahlin, J. L.; Dhanak, D.; Edwards, A. M.; Frye, S. V; Gray, N.; Grimshaw, C. E.; Hepworth, D.; Howe, T.; Huber, K. V. M.; Jin, J.; Knapp, S.; Kotz, J. D.; Kruger, R. G.; Lowe, D.; Mader, M. M.; Marsden, B.; Mueller-Fahrnow, A.; Müller, S.; O'Hagan, R. C.; Overington, J. P.; Owen, D. R.; Rosenberg, S. H.; Roth, B.; Ross, R.; Schapira, M.; Schreiber, S. L.; Shoichet, B.; Sundström, M.; Superti-Furga, G.; Taunton, J.; Toledo-Sherman, L.; Walpole, C.; Walters, M. A.; Willson, T. M.; Workman, P.; Young, R. N.; Zuercher, W. J. *Nat. Chem. Biol.* **2015**, *11*, 536–541.

(399) Zhang, S. Q.; Smith, S. M.; Zhang, S. Y.; Lynn Wang, Y. *Br. J. Haematol.* **2015**, *170*, 445–456.

(400) Erion, M. D.; Boyer, S. H.; Jiang, H. Novel phosphorus-containing thyromimetics. WO2005051298 A2, 2005.

(401) Guo, Z.; Tong, W.-L.; Chan, M. C. W. *Chem. Commun.* **2014**, *50*, 1711–1714.

(402) Hudson, S. A.; McLean, K. J.; Surade, S.; Yang, Y.-Q.; Leys, D.; Ciulli, A.; Munro, A. W.; Abell, C. *Angew. Chem. Int. Ed.* **2012**, *51*, 9311–9316.

(403) Ward, R. A.; Anderton, M. J.; Ashton, S.; Bethel, P. A.; Box, M.; Butterworth, S.; Colclough, N.; Chorley, C. G.; Chuaqui, C.; Cross, D. A. E.; Dakin, L. A.; Debreczeni, J. É.; Eberlein, C.; Finlay, M. R. V; Hill, G. B.; Grist, M.; Klinowska, T. C. M.; Lane, C.; Martin, S.; Orme, J. P.; Smith, P.; Wang, F.; Waring, M. J. *J. Med. Chem.* **2013**, *56*, 7025–7048.

(404) Overkleeft, H. S.; Liu, N.; Hoogendoorn, S.; van der Kar, B.; Kaptein, A.; Barf, T.; Driessen, C.; Filippov, D.; van der Marel, G. A.; van der Stelt, M. *Org. Biomol. Chem.* **2015**, *13*, 5147–5157.

(405) Zapf, C. W.; Gerstenberger, B. S.; Xing, L.; Limburg, D. C.; Anderson, D. R.; Caspers, N.; Han, S.; Aulabaugh, A.; Kurumbail, R.; Shakya, S.; Li, X.; Spaulding, V.; Czerwinski, R. M.; Seth, N.; Medley, Q. G. *J. Med. Chem.* **2012**, *55*, 10047–10063.

(406) Li, X.; Wang, A.; Yu, K.; Qi, Z.; Chen, C.; Wang, W.; Hu, C.; Wu, H.; Wu, J.; Zhao, Z.; Liu, J.; Zou, F.; Wang, L.; Wang, B.; Wang, W.; Zhang, S.; Liu, J.; Liu, Q. *J. Med. Chem.* **2015**, *58*, 9625–9638.

(407) Bonger, K. M.; van den Berg, R. J. B. H. N.; Heitman, L. H.; IJzerman, A. P.; Oosterom, J.; Timmers, C. M.; Overkleeft, H. S.; van der Marel, G. A. *Bioorg. Med. Chem.* **2007**, *15*, 4841–4856.

(408) Rokka, J.; Snellman, A.; Zona, C.; La Ferla, B.; Nicotra, F.; Salmona, M.; Forloni, G.; Haaparanta-Solin, M.; Rinne, J. O.; Solin, O. *Bioorg. Med. Chem.*

2014, *22*, 2753–2762.

(409) Lee, J.-J.; Yang, F.-Z.; Lin, Y.-F.; Chang, Y.-C.; Yu, K.-H.; Chang, M.-C.; Lee, G.-H.; Liu, Y.-H.; Wang, Y.; Liu, S.-T.; Chen, J.-T. *Dalt. Trans.* **2008**, 5945–5956.

(410) Messaoudi, S.; Brion, J.-D.; Alami, M. *Adv. Synth. Catal.* **2010**, *352*, 1677–1687.

(411) Toogood, P. L.; Harvey, P. J.; Repine, J. T.; Sheehan, D. J.; VanderWel, S. N.; Zhou, H.; Keller, P. R.; McNamara, D. J.; Sherry, D.; Zhu, T.; Brodfuehrer, J.; Choi, C.; Barvian, M. R.; Fry, D. W. *J. Med. Chem.* **2005**, *48*, 2388–2406.

(412) Chekal, B. P.; Ide, N. D. Solid Forms of a Selective CDK4/6 Inhibitor. WO2014/128588A1, 2014.